Inaugural - Dissertation

zur Erlangung der Doktorwürde der
Naturwissenschaftlich-Mathematischen Gesamtfakultät der
Ruprecht–Karls-Universität
Heidelberg

vorgelegt von
Manuel Hodecker, Master of Science Chemie
aus Bruchsal

Tag der mündlichen Prüfung: 29.04.2020

Development and Application of Hermitian Methods for Molecular Properties and Excited Electronic States

Manuel Hodecker

im März 2020

Gutachter:

Prof. Dr. Andreas Dreuw

Prof. Dr. Oriol Vendrell

Meinen Eltern

"Lasciate ogni speranza, voi ch'entrate!"

Dante Alighieri,
Inferno III, 9

Abstract

In many parts of physics, chemistry, biology, or material science, excited electronic states, accessible via the interaction of atoms or molecules with electromagnetic radiation, play an essential role. Experimental spectra, however, generally provide only indirect information on molecular structure and dynamics. Thus, a theoretical description of excitation energies and transition strengths is crucial for a comprehensive understanding of light-induced processes.

In this dissertation, the theory, implementation, and application of several Hermitian methods to calculate the properties mentioned above are described. If excitation energies are obtained by diagonalization of a non-Hermitian secular matrix, both left and right eigenvectors need to be calculated to obtain spectral intensities and other properties. In this case, the eigenvectors are not orthogonal to each other, and the energy may become complex. Hermiticity is thus a very desirable property since none of the aforementioned problems occurs. Thus, several approaches based on the algebraic-diagrammatic construction (ADC) scheme, as well as the related unitary coupled-cluster (UCC) method, are presented. Within these methods, one-electron properties such as dipole moments are available via the so-called intermediate state representation (ISR) approach, which corresponds to an expectation value of the respective one-electron operator with the wave function.

The ISR formalism is also used to derive explicit working equations for the second-order ADC scheme, which is based on a ground state described by Møller–Plesset (MP) perturbation theory. This implies that ADC inherits all weaknesses from the underlying MP model. For the ADC(2) scheme, merely the first-order MP wave function is required, which contains only doubly-excited determinants for a Hartree–Fock reference. Due to the form of the first-order doubles amplitudes, several cancellations occur in the singles block of the ADC(2) matrix. In order to remedy the breakdown of MP2, the first-order doubles amplitudes from MP are replaced by the ones obtained from a coupled-cluster (CC) calculation, which are formally correct through infinite order.

The resulting schemes, referred to as CC-ADC(2), are applied to several sets of small to medium-sized molecular systems, where generally minor improvements in excitation energies compared to the standard ADC(2) scheme can be observed. For the ozone molecule, which is known to be a difficult test case for quantum-chemical methods, the experimental first excitation energy is 1.6 eV; standard ADC(2) is far off with 2.14 eV, and CCD-ADC(2) yields 1.59 eV. Excited-state potential energy curves along the dissociation of the nitrogen molecule calculated with ADC(2) break down at around 2 Å due to the failure of MP2. The CCD-ADC(2) curves remain reasonable up to about 3.5 Å.

The CC-ADC(2) methods are successively extended to the calculation of static dipole polarizabilities. It is shown that the correlation amplitudes play a more important role in the modified transition moments than in the ADC secular matrix itself, and consistent

improvement is obtained for static polarizabilities with the CC-ADC schemes compared to standard ADC, particularly for aromatic systems like benzene or pyridine, which had proven difficult cases for standard ADC. Specifically, the CC-ADC(2) schemes yield significantly better results than the ADC(3/2) scheme, at a computational cost amounting to only 1% of the latter.

The ISR derivation can also be carried out with a CC wave function correct through first order instead of the MP one. However, having converged CCD amplitudes instead of the first-order MP ones, the aforementioned cancellations in the second-order singles block do not occur. Hence, the final matrix elements differ between CCD-ADC(2) and this scheme referred to as CCD-ISR(2). As the expansion of the UCC similarity-transformed Hamiltonian does not truncate naturally, it needs to be truncated manually, usually by using arguments from MP perturbation theory. The UCC2 doubles amplitudes correspond to those from LCCD, but the secular matrix elements depend on the treatment of the similarity-transformed Hamiltonian is treated. By employing the Baker–Campbell–Hausdorff expansion, the second-order singles block is equivalent to CCD-ISR(2), but by employing the Bernoulli expansion, the matrix elements are equivalent to CCD-ADC(2), with differences only in the correlation amplitudes. In a strict perturbation-theoretical framework, all methods turn out to be identical. All different Hermitian second-order methods have been implemented and tested on a set of small molecules, where it turned out that the differences in excitation energies between the methods are small whenever the systems are well described by means of perturbation theory.

The Bernoulli UCC scheme is further extended to third order, where excitation energies and oscillator strengths on medium-sized organic molecules as well as ground- and excited-state dipole moments are reported for the first time. While vertical excitation energies of the UCC3 scheme are similar to those obtained with ADC(3), significant improvements can be observed for the dipole moments in the ground and excited states. Furthermore, this UCC scheme is applied to the electron propagator, and ionization potentials of the IP-UCC2 and IP-UCC3 schemes of selected amino acids are reported for the first time.

Apart from expectation values, molecular properties can be calculated as derivatives of the energy with respect to a perturbation connected to the observable. The two approaches are only equivalent if the Hellmann–Feynman theorem is fulfilled. By using explicit working equations, the relationship between the two approaches is investigated with a focus on orbital relaxation for all standard quantum-chemical methods, in particular MP and ADC. It is shown that for MP2 the expectation value is very close to the orbital-relaxed property. In contrast, for ADC(1) the expectation value includes no orbital relaxation and for ADC(2) only a small fraction. With ADC(3) eigenvectors, on the other hand, the ISR gets closer to the relaxed values, but only for singly-excited states. Numerical investigations underline all the theoretical predictions.

Zusammenfassung

In vielen Bereichen der Physik, Chemie, Biologie oder Materialwissenschaft spielen elektronisch angeregte Zustände, die durch die Wechselwirkung von Atomen oder Molekülen mit elektromagnetischer Strahlung zugänglich sind, eine wichtige Rolle. Experimentelle Spektren liefern im Allgemeinen jedoch nur indirekte Informationen über molekulare Struktur und Dynamik, weshalb eine akkurate theoretische Beschreibung von Eigenschaften wie Anregungsenergien und Übergangswahrscheinlichkeiten entscheidend für ein umfassendes Verständnis von photophysikalischen und photochemischen Prozessen ist.

In dieser Dissertation wird die Theorie, Implementierung und Anwendung verschiedener hermitescher Methoden zur Berechnung der oben genannten Eigenschaften beschrieben. Wenn Anregungsenergien durch Diagonalisierung einer nicht-hermiteschen Matrix erhalten werden, müssen sowohl rechte als auch linke Eigenvektoren berechnet werden, um spektrale Intensitäten und andere molekulare Eigenschaften zu erhalten, die Eigenvektoren sind nicht orthogonal zueinander, und die Energie selbst kann komplex werden, insbesondere in der Nähe von konischen Durchschneidungen. Hermizität ist daher eine sehr wünschenswerte Eigenschaft, da in diesem Fall keine der genannten Probleme auftreten. In dieser Arbeit werden deshalb hermitesche Methoden betrachtet, insbesondere werden verschiedene Ansätze auf Basis des algebraisch-diagrammatischen Konstruktionsverfahrens (ADC) sowie unitäres *coupled cluster* (UCC) vorgestellt. Im Rahmen dieser Methoden sind elektronische Einteilcheneigenschaften wie Dipolmomente über die sogenannte *intermediate state representation* (ISR) zugänglich, die einem Erwartungswert des jeweiligen Einteilchenoperators mit der Wellenfunktion entspricht.

Der ISR-Formalismuns wird auch verwendet, um explizite Gleichungen für das ADC-Schema in zweiter Ordnung herzuleiten, welches auf einer Beschreibung des Grundzustandes durch Møller–Plesset (MP) Störungstheorie beruht. Letzteres impliziert, dass ADC alle Schwächen der Störungstheorie des zugrunde liegenden MP-Modells erbt. Für das ADC(2)-Schema ist nur die MP-Wellenfunktionskorrektur erster Ordnung notwendig, welche bei einer Hartree–Fock (HF) -Referenz nur doppelt angeregte Determinanten enthält. Aufgrund der Form der *doubles* Amplituden erster Ordnung lässt sich der Teil zweiter Ordnung der ADC(2)-Matrix deutlich vereinfachen, da sich bestimmte Terme gegeneinander kürzen. Um das Versagen von MP2 zu beheben, wurden die Amplituden erster Ordnung durch diejenigen ersetzt, die durch eine *coupled cluster* (CC) Rechnung erhalten wurden, bei der die Amplituden formal in unendlicher Ordnung korrekt sind.

Die resultierenden Schemata, CC-ADC(2) genannt, wird auf einige kleine bis mittelgroße molekulare Systeme angewendet, wobei im Allgemeinen geringfügige Verbesserungen der Anregungsenergien im Vergeich zum Standard-ADC(2)-Schema beobachtet werden. Für das Ozonmolekül, welches bekanntermaßen ein schwieriger Testfall für quantenchemische Methoden ist, beträgt die experimentelle erste Anregungsenergie 1.6 eV, ADC(2) ist

mit 2.14 eV weit davon enternt, mit CCD-ADC(2) wurden 1.59 eV erhalten. Potentialkurven in angeregten Zuständen entlang der Dissoziation des Stickstoffmoleküls, welche mit ADC(2) berechnet werden, sind aufgrund des Versagens von MP2 ab 2 Å nicht mehr sinnvoll, jene mit CCD-ADC(2) jedoch bis über 3.5 Å. Dieses bessere Verhalten kann große Vorteile bei der theoretischen Beschreibung photochemischer Reaktionen haben.

Die CC-ADC(2)-Methoden werden anschließend zur Berechnung der statischen Dipol-Polarisierbarkeit erweitert. Hierbei waren insbesondere aromatische System wie Benzol nur schlecht durch Standard-ADC-Methoden beschrieben worden. Es wird gezeigt, dass die Korrelationsamplituden in den modifizierten Übergangsmomenten eine größere Rolle spielen als in der ADC-Säkularmatrix selbst und dass mit den CC-ADC-Varianten konsistente Verbesserungen der statischen Polarisierbarkeit verglichen mit Standard-ADC-Methoden erhalten werden, besonders für aromatische Systeme wie Benzol oder Pyridin. Insbesondere liefern die CC-ADC(2)-Methoden signifikant bessere Ergebnisse als das ADC(3/2)-Schema, bei einem Rechenaufwand von nur etwa 1% des Letzteren.

Die ISR-Herleitung kann auch mit einer CC-Wellenfunktion, welche bis zur ersten Ordnung korrekt ist, durchgeführt werden. Jedoch treten die oben genannten Vereinfachungen nicht mehr auf, wenn man konvergierte CCD-Amplituden anstelle der MP-Amplituden erster Ordnung verwendet, sodass sich die Matrixelemente von CCD-ADC(2) und der CCD-ISR(2) genannten Methode etwas unterscheiden. Da die Entwicklung des ähnlichkeitstransformierten Hamilton-Operators in UCC-Theorie nicht natürlich abbricht, muss sie "von Hand" abgeschnitten werden, was normalerweise unter Verwendung von Argumenten aus MP-Störungstheorie geschieht. Bis zur zweiten Ordnung entsprechen die *doubles* Amplituden denen des linearisierten CCD-Modells. Die Elemente der UCC2-Säkularmatrix hängen jedoch davon ab, wie der ähnlichkeitstransformierte Hamilton-Operator behandelt wird. Bei Verwendung der Baker–Campbell–Hausdorff (BCH) Expansion ist der Block zweiter Ordnung äquivalent zu CCD-ISR(2), bei Verwendung der sogenannten Bernoulli-Expansion jedoch zu CCD-ADC(2). Die Unterschiede liegen nur in den jeweiligen Korrelationsamplituden. In einem strengen störungstheoretischen Rahmen erweisen sich jedoch alle Methoden als identisch. Die genannten hermitschen Methoden zweiter Ordnung wurden im Q-Chem-Programmpaket implementiert und auf eine Reihe kleiner Moleküle angewendet, wobei sich herausstellt, dass die Unterschiede in den Anregungsenergien zwischen den Methoden immer dann gering sind, wenn die Systeme gut durch Störungstheorie beschrieben werden.

Das auf der Bernoulli-Expansion basierte Schema wird anschließend bis zur dritten Ordnung erweitert, und es werden zum ersten Mal Anregungsenergien und Oszillatorstärken von mittelgroßen organischen Molekülen sowie Dipolmomente im Grundzustand und angeregten Zuständen berichtet. Während die vertikalen Anregungsenergien von UCC3 ähnlich zu denen von ADC(3) sind, können zum Teil signifikante Verbesserungen bei den Dipolmomenten beobachtet werden. Darüber hinaus wird dieses UCC-Schema erstmals auf den Elektronenpropagator zur Berechnung von Ionisationspotentialen angewendet,

und es werden Ergebnisse von ausgewählten Aminosäuren mit IP-UCC2 und IP-UCC3 angegeben, wobei ebenfalls einige Verbesserungen im Vergleich zu IP-ADC beobachtet werden können.

Abgesehen von Erwartungswerten können molekulare Eigenschaften auch als Ableitungen der Energie in Bezug auf eine Störung, welche mit der physikalischen Observablen verknüpft ist, berechnet werden. Die zwei Ansätze sind nur dann äquivalent, wenn das Hellmann–Feynman-Theorem erfüllt ist, die Methode also vollständig variationell ist. Durch Verwendung expliziter Gleichungen wird die Beziehung der beiden Ansätze mit einem besonderen Fokus auf Orbitalrelaxation für alle gängigen quantenchemischen Methoden untersucht, insbesondere MP und ADC. Es wird gezeigt, dass der Erwartungswert bei MP2 ähnlicher der orbitalrelaxierten Eigenschaft ist, wohingegen für ADC(1) der Erwartungswert keine Orbitalrelaxation beinhaltet, und für ADC(2) nur einen Bruchteil. Mit ADC(3)-Eigenvektoren liegen die ISR dagegen näher an den relaxierten Werten, da hier die doppel angeregten Konfigurationen vollständig gekoppelt sind. Numerische Untersuchungen unterstreichen alle theoretischen Vorhersagen.

Contents

Abbreviations

ADC	algebraic-diagrammatic construction
AO	atomic orbital
BCH	Baker–Campbell–Hausdorff (expansion)
Bn	Bernoulli (expansion)
BO	Born–Oppenheimer (approximation)
CC	coupled cluster
CCD	coupled cluster doubles
CCLR	coupled cluster linear response
CCSD	coupled cluster singles and doubles
CCPPA	coupled-cluster polarization propagator approximation
CI	configuration interaction
CIS	configuration interaction singles
CISD	configuration interaction singles and doubles
DFT	density functional theory
DIIS	direct inversion in the iterative subspace
DMABN	dimethylamino benzonitrile
DOSD	dipole oscillator strength distribution
EA	electron affinity
ECO	excitaton class orthogonalized
EOM	equation of motion
eV	electronvolt
FCI	full configuration interaction
GBT	generalized Brillouin theorem
GS	Gram–Schmidt
HF	Hartree–Fock
IP	ionization potential
IP-ADC	algebraic-diagrammatic construct for ionization potentials
IP-UCC	unitary coupled cluster for ionization potentials
ISC	intersystem crossing
ISR	intermediate state representation
KS	Kohn–Sham

LCCD	linearized coupled cluster doubles
LHS	left-hand side
LR	linear response
MBPT	many-body perturbation theory
MO	molecular orbital
MP	Møller–Plesset (perturbation theory)
ON	occupation number
rel	(orbital) relaxed
RHS	right-hand side
RI	resolution-of-the-identity
RMS	root mean square (deviation)
RPA	random phase approximation
RS	Rayleigh–Schrödinger (perturbation theory)
SCF	self-consistent field
SOC	spin-orbit coupling
SOPPA	second-order polarization propagator approximation
TBE	theoretical best estimate
TDHF	time-dependent Hartree–Fock
TDDFT	time-dependent density functional theory
UCC	unitary coupled cluster
unrel	(orbital) unrelaxed
VCC	variational coupled cluster
w.r.t.	with respect to
XCC	expectation-value coupled cluster
xc	exchange-correlation
ZPVA	zero-point vibrational averaging

Chapter 1

Introduction

Excited electronic states play a significant role in many fields of natural and material sciences. In organic electronics, for instance, a detailed knowledge about the photophysical and photochemical behavior of molecules is vital to develop and improve solar cells or organic light-emitting diodes.[1–4] Since experimental optical spectra of molecular systems generally provide only indirect information on molecular structure or dynamics, their theoretical description is often indispensable for a comprehensive understanding of photochemical processes and thus a very active research field.

In the absence of external radiation, molecules are in their electronic ground state, usually denoted by S_0. By shining light on a sample, molecules can absorb photons while undergoing a transition to some higher, so-called excited state. The electronic transition is usually accompanied by excitations of vibrational and rotational degrees of freedom, but the latter are often ignored in the theoretical description. The excited electronic state normally has a finite lifetime and can undergo several decay processes, such as internal conversion, intersystem crossing, fluorescence or phosphorescence, and charge or energy transfers.[5] From a simple theoretical perspective, an electron is excited from an occupied molecular orbital (MO) to an unoccupied (or virtual) one during the excitation. However, this simple MO picture is often not accurate and sufficient to correctly describe electronic processes when molecules absorb light, and hence many more elaborate methods for the description of electronic excitations have been developed over the last decades.

The most widely used method to calculate electronically excited states, especially for large molecules, is time-dependent density functional theory (TDDFT) in its linear response formalism.[6–8] However, since approximate exchange-correlation functionals with often unpredictable errors need to be employed in practical calculations, TDDFT can hardly be considered a "black-box" method. Methodologies with predictable errors that

---

Parts of this chapter have already been published in

- M. Hodecker, D. R. Rehn, A. Dreuw, "Hermitian Second-Order Methods for Excited Electronic States: Unitary Coupled Cluster in Comparison with Algebraic-Diagrammatic Construction Schemes", *The Journal of Chemical Physics*, **2020**, *152*, 094106.

can be improved systematically are thus desirable. The most prominent and successful approaches from wave-function theory are those based on a coupled-cluster (CC) parameterization of the electronic ground state,[9–11] mainly the equation-of-motion coupled-cluster (EOM-CC)[12–15] and coupled-cluster linear response (CCLR) theories.[16–19] In spite of their conceptual differences, both EOM-CC and CCLR yield identical excitation energies and can be viewed as biorthogonal representations (BCC) of the (shifted) Hamiltonian in terms of correlated excited states (CES) obtained from the CC ground state and an associated set of biorthogonal states corresponding essentially to excited determinants used in configuration interaction (CI) theory.[20,21] This BCC representation generates a non-Hermitian secular matrix whose eigenvalues correspond to excitation energies, but due to the non-symmetric nature of the representation, both left and right eigenvectors are needed to calculate spectral intensities and other properties.[13,21] Further undesirable properties arising due to lack of Hermiticity are that the eigenvectors of the secular matrix are not orthogonal to each other and that the excitation energies may become complex, in particular close to conical intersections.[22,23]

Hermitian excited-state theories are thus preferable since none of the problems mentioned before occur. The classical Hermitian excited-state method is CI, but lack of size consistency[24] is the main reason why single-reference, correlated and truncated CI schemes do not find widespread application anymore. A method that is both size consistent and also the most compact is the algebraic-diagrammatic construction scheme (ADC) for the polarization propagator.[25–28] Compact means that only very modest configuration spaces need to be taken into account for excitation energies to be consistent through a specific order in perturbation theory. ADC has originally been derived in the context of many-body Green's functions or propagators using diagrammatic perturbation theory.[25,26] However, a different, more elegant derivation route is offered via the so-called intermediate state representation (ISR).[28,29] This rather general approach does not only yield excitation energies and transition moments like the classical propagator approach, but also provides access to the excited-state wave function and thus to excited-state properties and state-to-state transition moments.[27–30] The ISR used in the ADC scheme for the polarization propagator is related to the BCC representation mentioned above, but the correlated excited states are orthonormalized in a specific manner, thus preserving the aforementioned properties of the propagator method such as compactness and size consistency.[20,31] Furthermore, the resulting secular matrix is Hermitian, and hence the eigenvalues are guaranteed to be real, and the eigenvectors are mutually orthogonal.

While the CES are formally obtained from the *exact* ground state, in practical applications for ADC-ISR schemes, the latter is replaced by the well-known expansion from Møller–Plesset perturbation theory (MP).[24,32,33] This gives rise to a hierarchy of approximations termed ADC(n) that are consistent through a specific order n in perturbation theory. The perturbation-theoretical description of the ground state, however, generally corresponds to the greatest weakness of the ADC methods since MP is well

known to fail in several cases, for instance, when a bond is stretched.[24] Coupled-cluster schemes are more stable than MP in this respect because of their iterated, self-consistent ground state.[15] A central goal of this work has been to overcome this deficiency.

However, there have also been significant efforts within the framework of coupled-cluster theory to obtain Hermitian (excited-state) methods. The two most important examples are the expectation-value or variational coupled-cluster approach (VCC),[34–36] and the closely related unitary coupled-cluster (UCC) ansatz.[37–39] The main disadvantage of the two approaches compared to traditional CC theory is that their expansions do not truncate naturally, and the working equations cannot be cast into closed-form expressions. Hence, the corresponding expansions need to be truncated manually, and several truncation schemes have been used, most often by employing arguments from perturbation theory.[37] Most of the resulting schemes have been applied exclusively to the ground-state energy and molecular ground-state properties.[34–37,40–47] Contrary to some claims in the literature, VCC and UCC do not yield identical results through all orders.[48] More recently, they have also been applied to the calculation of excited states via the time-dependent (TD) linear response formalism[49,50] and the time-independent polarization propagator approach.[51] Furthermore, the working equations of the second-order unitary scheme TD-UCC[2] were shown to be equivalent to the ones of the ADC(2) method,[50] whereas the ones from TD-VCC[2] following a variational VCC ansatz differ from ADC(2).[49] Similarly, the working equations of the UCC-based polarization propagator approach through third order (UCC3) have recently been shown to be equivalent to the ADC(3) scheme,[51] a fact that has been exploited in the course of this work.

In the scope of my dissertation, I developed several new Hermitian excited-state methods that can be regarded to connect ADC with CC theories, implemented them into a development version of the `adcman` module,[52] which is part of the Q-Chem program package,[53] and tested them on small to medium-sized molecules. The first approach has been inspired by work by Geertsen and Oddershede on the second-order polarization propagator approximation (SOPPA), a method closely related to ADC(2), where they replaced the MP correlation coefficients by CC amplitudes to obtain the coupled-cluster polarization propagator approximation (CCPPA).[54,55] In the same spirit, I replaced the MP coefficients by converged CCD amplitudes to obtain the CCD-ADC(2) scheme. This scheme, however, is closely related to a second-order unitary coupled-cluster method, denoted UCC2, which I also implemented in two different variants. Here, the ground state corresponds essentially to the linearized coupled-cluster doubles (LCCD) scheme. For both methods, two different variants exist that differ slightly in the elements of the secular matrix but are identical in a strict perturbation-theoretical framework. I investigated and explained the exact relationship among all those methods, implemented, and tested them. Analogous to the work of Sauer with his SOPPA(CCSD) method,[56] the CCD-ADC family of methods has also been applied to the calculation of static dipole polarizabilities, where significant and consistent improvements compared to standard

ADC could be observed. The UCC method has also been implemented in its third-order variant termed UCC3, not only for the calculation of excitation energies, but also for other one-electron properties such as dipole moments, both in the electronic ground and excited states as well as ionization potentials.

In general, molecular properties can be calculated in two different ways, the first being the expectation value of the corresponding operator with the wave function, and the second the derivative of the energy with respect to a perturbation connected to the observable. The two approaches do not yield identical results whenever the Hellmann–Feynman theorem is not fulfilled, which is the case for non-fully variational methods.[57] I investigated the exact relationship between the two approaches from a theoretical point of view for all standard quantum-chemical methods, with a particular focus on orbital-relaxation effects in methods based on perturbation theory like MP and ADC, and performed numerical tests to verify the theoretical predictions.

In this thesis, I want to present the (CC-)ADC and UCC methods and the results I obtained with the implementations. The theoretical aspects and quantum-chemical methods are introduced in Chapter 2, starting with the formalism of second quantization (Section 2.1), and a brief discussion of Hartree–Fock theory and correlation methods in Sections 2.2 and 2.3. Perturbation theory is presented in more detail in Section 2.4, followed by the algebraic-diagrammatic construction scheme and intermediate state representations in Section 2.5. Coupled-cluster theory is discussed in more detail in Section 2.6, in particular the diagrammatic formalism for the explicit derivation of working equations, since it is employed for the derivation of the UCC schemes. Eventually, general aspects of molecular properties are discussed in Section 2.7. Chapter 3 presents a thorough discussion of unitary coupled-cluster theory, starting with a general ISR approach and the Bernoulli expansion for the similarity-transformed Hamiltonian, followed by a derivation of the second- and third-order schemes UCC2 and UCC3, respectively, for ground and excited states. Successively, their connection to ADC methods is outlined, and the calculation of ground- and excited-state properties is discussed. Chapter 4 presents all different Hermitian second-order methods that I implemented, first from a theoretical point of view, and then I discuss the results for excitation energies obtained with these methods. Next, in Chapter 5, I take a turn away from electronic excitation energies and discuss the influence of the ground-state correlation amplitudes on static dipole polarizabilities calculated with ADC. In the following Chapter 6, I turn back to UCC and present its third-order implementation in more detail, followed by results for excitation energies as well as ground- and excited-state dipole moments. Due to the general similarity between ADC and UCC, I was also able to implement a UCC-based scheme for the electron propagator through third order and present some computational results for ionization potentials of amino acids. Chapter 7 goes back to fundamental theory at first and contrasts two different approaches for the calculation of one-electron properties, expectation values and energy derivatives. A focus is put on the inclusion

of orbital-relaxation effects in the two approaches, first by regarding explicit working equations and then by confirming the theoretical predictions with numerical results. Another turn towards the more applied field of computational chemistry is done in Chapter 8, where I present my results of a computational study in collaboration with experimental organic chemists in order to explain the surprising photophysical behavior of azaacenes. Here, an additional double bond drastically alters the emission properties, turning the molecule from highly fluorescent to almost non-fluorescent at all. A conclusion of my work and an outlook on future projects are given in Chapter 9.

Finally, I would like to mention that many parts of this dissertation have already been published in peer-reviewed journals. The respective article is always given as a footnote in the chapter. Further projects that I have been involved with, mainly in collaboration with experimentalists, are not included. However, the relevant publications I co-authored are listed along with the ones included in this thesis on page 247.

Chapter 2

Theoretical Methods

Most quantum-chemical calculations seek to solve the electronic, time-independent Schrödinger equation [57–61]

$$\hat{H}|\Psi_n\rangle = E_n|\Psi_n\rangle\,, \tag{2.1}$$

where $|\Psi_n\rangle$ is the wave function of electronic state n with corresponding energy E_n, and $\hat{H}$ is the electronic Hamiltonian operator that consists of kinetic and potential energy contributions. In atomic units, it is given by

$$\hat{H} = \hat{T}_\mathrm{e} + \hat{V}_\mathrm{ne} + \hat{V}_\mathrm{ee} = -\frac{1}{2}\sum_{i=1}^{N}\nabla_i^2 + \sum_i\sum_K \frac{Z_K}{r_{iK}} + \sum_{i>j}\frac{1}{r_{ij}}\,, \tag{2.2}$$

where the first sum on the right-hand side (RHS) is the kinetic energy operator of the N electrons, ∇ is the nabla operator, the second part is the potential energy of the interaction between the electrons i and the nuclei K with charge numbers $\{Z_K\}$, and the last double sum is the electron-electron repulsion operator, where $r_{ij} = |\mathbf{r}_j - \mathbf{r}_i|$ is the distance between electrons i and j.

Within the Born–Oppenheimer (BO) or adiabatic approximation, [57,62] the electronic Schrödinger equation is solved for a fixed geometry of the nuclei and hence the nuclear-nuclear repulsion energy

$$V_\mathrm{nn} = \sum_{K>L}\frac{Z_K Z_L}{R_{KL}}\,, \tag{2.3}$$

where $R_{KL} = |\mathbf{R}_L - \mathbf{R}_K|$ is the distance between nuclei K and L, is constant. Thus, it can be added to the electronic energy to yield the total energy of the molecule.

Before several approximation schemes for solving the electronic Schrödinger equation are discussed, a convenient formalism for many-electron systems is introduced.

2.1 Second Quantization

The following description of the formalism of second quantization closely follows Refs. 33 and 24.

Let $\{\phi_p(\mathbf{x})\}$ be a basis of M orthonormal **spin orbitals**, where the coordinates $\mathbf{x}$ collectively stand for the spatial coordinates $\mathbf{r}$ and the spin coordinate σ of the electron.[33] A **Slater determinant** is an anti-symmetrized product of an arbitrary number of spin orbitals. For instance, the normalized Slater determinant of a system containing N electrons may be written as

$$|\phi_{p_1}\phi_{p_2}\cdots\phi_{p_N}| = \frac{1}{\sqrt{N!}}\begin{vmatrix} \phi_{p_1}(\mathbf{x}_1) & \phi_{p_2}(\mathbf{x}_1) & \cdots & \phi_{p_N}(\mathbf{x}_1) \\ \phi_{p_1}(\mathbf{x}_2) & \phi_{p_2}(\mathbf{x}_2) & \cdots & \phi_{p_N}(\mathbf{x}_2) \\ \vdots & \vdots & \ddots & \vdots \\ \phi_{p_1}(\mathbf{x}_N) & \phi_{p_2}(\mathbf{x}_N) & \cdots & \phi_{p_N}(\mathbf{x}_N) \end{vmatrix} . \tag{2.4}$$

In a somewhat different manner one may introduce an abstract linear vector space, usually called **Fock space**, where each determinant is represented by a so-called *occupation number* (ON) *vector* $|\mathbf{k}\rangle$,

$$|\mathbf{k}\rangle = |k_1, k_2, \ldots, k_M\rangle\,,\ k_p = \begin{cases} 1 & \phi_p \text{ occupied} \\ 0 & \phi_p \text{ unoccupied} \end{cases} . \tag{2.5}$$

Hence, the **occupation number** k_p is 1 if ϕ_p is present in the determinant and 0 if not. The inner product between two ON vectors $|\mathbf{k}\rangle$ and $|\mathbf{m}\rangle$ is defined as

$$\langle\mathbf{k}|\mathbf{m}\rangle = \delta_{\mathbf{k},\mathbf{m}} = \prod_{p=1}^{M} \delta_{k_p m_p}\,, \tag{2.6}$$

which is consistent with the overlap of two Slater determinants that contain the same number of electrons. The definition in Eq. (2.6) also has a well-defined (zero) overlap between states with different electron numbers. In a given spin-orbital basis there is a one-to-one mapping between Slater determinants and the ON vectors in Fock space,[33] which is why much of the terminology is the same in both cases and they are treated equivalently in the following, as long as their differentiation is not of importance.

2.1.1 Creation and Annihilation Operators

In the formalism of second quantization, all operators can be constructed from a set of creation and annihilation operators. The **creation operator** $\hat{a}_p^\dagger$ is defined by

$$\hat{a}_p^\dagger|k_1, k_2, \ldots, 0_p, \ldots, k_M\rangle = \Gamma_p\,|k_1, k_2, \ldots, 1_p, \ldots, k_M\rangle\,, \tag{2.7}$$

where the phase factor

$$\Gamma_p = \prod_{l=1}^{p-1} (-1)^{k_l} \tag{2.8}$$

is equal to $+1$ if there is an even number of electrons in the spin orbitals $q < p$, i.e. to the left of p in the ON vector, or -1 if there is an odd number of electrons in these spin orbitals, that is necessary to be consistent with the definition of operators in first quantization and to fulfill the antisymmetry requirement. For Slater determinants this can correspondingly be written as

$$\hat{a}_q^\dagger |\phi_{p_1} \phi_{p_2} \cdots \phi_{p_N}| = |\phi_q \phi_{p_1} \phi_{p_2} \cdots \phi_{p_N}| = \Gamma_q |\phi_{p_1} \phi_{p_2} \cdots \phi_q \cdots \phi_{p_N}| \,, \tag{2.9}$$

which means that one creates an orbital in the first column of the determinant, which then by exchanging columns yields the respective prefactor. However, if the corresponding orbital has already been occupied, the operation yields zero,

$$\hat{a}_p^\dagger |k_1, k_2, \ldots, 1_p, \ldots, k_M\rangle = 0 \,, \tag{2.10}$$

which is in line with the Pauli exclusion principle. Due to the phase factor Γ_p, the order in which in the creation operators are applied is of importance,

$$\hat{a}_p^\dagger \hat{a}_q^\dagger |k_1, \ldots, 0_p, 0_q, \ldots, k_M\rangle = \hat{a}_p^\dagger \Gamma_q |k_1, \ldots, 0_p, 1_q, \ldots, k_M\rangle = |k_1, \ldots, 1_p, 1_q, \ldots, k_M\rangle \tag{2.11a}$$

$$\hat{a}_q^\dagger \hat{a}_p^\dagger |k_1, \ldots, 0_p, 0_q, \ldots, k_M\rangle = \hat{a}_q^\dagger \Gamma_p |k_1, \ldots, 1_p, 0_q, \ldots, k_M\rangle = -|k_1, \ldots, 1_p, 1_q, \ldots, k_M\rangle \,, \tag{2.11b}$$

where different signs must occur since there is one more electron before q in Eq. (2.11b). Adding the two above equations leads to the **anti-commutation relation** for creation operators[24]

$$\{\hat{a}_p^\dagger, \hat{a}_q^\dagger\} = \hat{a}_p^\dagger \hat{a}_q^\dagger + \hat{a}_q^\dagger \hat{a}_p^\dagger = 0 \,. \tag{2.12}$$

The adjoint of the creation operator $\hat{a}_p^\dagger$ is the annihilation (or destruction) operator $\hat{a}_p$ that removes and electron from the respective orbital ϕ_p, corresponding to

$$\hat{a}_p |k_1, k_2, \ldots, 1_p, \ldots, k_M\rangle = \Gamma_p |k_1, k_2, \ldots, 0_p, \ldots, k_M\rangle \tag{2.13a}$$

$$\hat{a}_p |k_1, k_2, \ldots, 0_p, \ldots, k_M\rangle = 0 \,. \tag{2.13b}$$

The annihilation operators can be shown to obey the anti-commutation relation[24]

$$\{\hat{a}_p, \hat{a}_q\} = \hat{a}_p \hat{a}_q + \hat{a}_q \hat{a}_p = 0 \,. \tag{2.14}$$

Analogously, it can be shown that the combination of creation and annihilation operators obeys the anti-commutation relation[24]

$$\{\hat{a}_p^\dagger, \hat{a}_q\} = \hat{a}_p^\dagger \hat{a}_q + \hat{a}_q \hat{a}_p^\dagger = \delta_{pq}\,. \tag{2.15}$$

2.1.2 Representation of Operators

As stated at the beginning of the last subsection, in the formalism of second quantization all operators are expressed in terms of creation and annihilation operators, possibly including a prefactor (or amplitude) in front of them. One- and two-particle operators $\hat{f}$ and $\hat{g}$ are given as[24]

$$\hat{f} = \sum_{pq} f_{pq}\, \hat{a}_p^\dagger \hat{a}_q \tag{2.16}$$

and

$$\hat{g} = \frac{1}{2} \sum_{pqrs} g_{pqrs}\, \hat{a}_p^\dagger \hat{a}_q^\dagger \hat{a}_s \hat{a}_r\,, \tag{2.17}$$

respectively, where prefactors are matrix elements of the first-quantized operators

$$\hat{f}_\mathrm{c} = \sum_{i=1}^{N} \hat{f}_\mathrm{c}(\mathbf{x}_i) \tag{2.18}$$

$$\hat{g}_\mathrm{c} = \frac{1}{2} \sum_{i \neq j} \hat{g}_\mathrm{c}(\mathbf{x}_i, \mathbf{x}_j) \tag{2.19}$$

within the basis of spin-orbitals

$$f_{pq} = \langle \phi_p | \hat{f}_\mathrm{c} | \phi_q \rangle = \int \phi_p^*(\mathbf{x}) \hat{f}_\mathrm{c} \phi_q(\mathbf{x}) \mathrm{d}\mathbf{x} \tag{2.20}$$

$$g_{pqrs} = \langle \phi_p \phi_q | \hat{g}_\mathrm{c} | \phi_r \phi_s \rangle = \iint \phi_p^*(\mathbf{x}_1) \phi_q^*(\mathbf{x}_2) \hat{g}_\mathrm{c} \phi_r(\mathbf{x}_1) \phi_s(\mathbf{x}_2) \mathrm{d}\mathbf{x}_1 \mathrm{d}\mathbf{x}_2\,. \tag{2.21}$$

2.1.3 Normal-Ordered Operators and Wick's Theorem

Definition: *A normal-ordered string of second-quantization operators is one in which all annihilation operators stand on the right of all creation operators.*[63,64]

"Normal ordering" of such strings provides a bookkeeping system which helps identifying non-zero matrix elements of second-quantized operators. For example, the arbitrary string of annihilation and creation operators, $\hat{A} = \hat{a}_p \hat{a}_q^\dagger \hat{a}_r \hat{a}_s^\dagger$, can be written in equivalent form by moving the two annihilation operators to the right and applying the

anticommutation relations as

$$\begin{aligned}\hat{A} &= \hat{a}_p\hat{a}_q^\dagger\hat{a}_r\hat{a}_s^\dagger \\ &= \delta_{pq}\hat{a}_r\hat{a}_s^\dagger - \hat{a}_q^\dagger\hat{a}_p\hat{a}_r\hat{a}_s^\dagger \\ &= \delta_{pq}\delta_{rs} - \delta_{pq}\hat{a}_s^\dagger\hat{a}_r - \delta_{rs}\hat{a}_q^\dagger\hat{a}_p + \hat{a}_q^\dagger\hat{a}_p\hat{a}_s^\dagger\hat{a}_r \\ &= \delta_{pq}\delta_{rs} - \delta_{pq}\hat{a}_s^\dagger\hat{a}_r - \delta_{rs}\hat{a}_q^\dagger\hat{a}_p + \delta_{ps}\hat{a}_q^\dagger\hat{a}_r - \hat{a}_q^\dagger\hat{a}_s^\dagger\hat{a}_p\hat{a}_r\,.\end{aligned} \tag{2.22}$$

The first term in the final rearrangement contains only Kronecker delta functions, and the next three terms contain operator strings of reduced length. Furthermore, all operator strings in the final equation are normal-ordered according to the above definition. Evaluating the quantum-mechanical expectation value of this operator with respect to the **true vacuum state** $|\mathrm{vac}\rangle$, i.e. the state that contains no electrons, one obtains

$$\langle\mathrm{vac}|\hat{A}|\mathrm{vac}\rangle = \langle\mathrm{vac}|\delta_{pq}\delta_{rs}|\mathrm{vac}\rangle = \delta_{pq}\delta_{rs}\,, \tag{2.23}$$

where it was assumed that the vacuum state is normalized, $\langle\mathrm{vac}|\mathrm{vac}\rangle = 1$. Hence, the only term of $\hat{A}$ in Eq. (2.22) that produces a non-zero result is the one containing no second-quantized operators; all others involve application of an annihilation operator on $|\mathrm{vac}\rangle$ to the right. The definition of normal-ordered operators can also help to evaluate matrix elements involving determinants other than $|\mathrm{vac}\rangle$ on the left and the right. However, since it is more convenient and elegant, Wick's theorem is explained for this purpose in the following.

Using the anticommutation relations of second-quantized operators, an arbitrary string of annihilation and creation operators can be written as a linear combination of normal-ordered strings (most of which contain reduced numbers of operators) multiplied by Kronecker delta functions. These reduced terms can be viewed as arising from so-called *contractions* between operator pairs. A **contraction** between two operators $\hat{A}$ and $\hat{B}$ is defined as

$$\overbrace{\hat{A}\hat{B}} = \hat{A}\hat{B} - \{\hat{A}\hat{B}\}_\mathrm{v}\,, \tag{2.24}$$

where the notation $\{\hat{A}\hat{B}\}_\mathrm{v}$ indicates the **normal-ordered form** of the pair with respect to the true vacuum. The contraction between the operators is simply the original ordering minus the normal-ordered pair. For example, the contraction between two creation or two annihilation operators is zero because they are already normal-ordered:

$$\overbrace{\hat{a}_p\hat{a}_q} = \hat{a}_p\hat{a}_q - \{\hat{a}_p\hat{a}_q\}_\mathrm{v} = \hat{a}_p\hat{a}_q - \hat{a}_p\hat{a}_q = 0 \tag{2.25}$$

$$\overbrace{\hat{a}_p^\dagger\hat{a}_q^\dagger} = \hat{a}_p^\dagger\hat{a}_q^\dagger - \{\hat{a}_p^\dagger\hat{a}_q^\dagger\}_\mathrm{v} = \hat{a}_p^\dagger\hat{a}_q^\dagger - \hat{a}_p^\dagger\hat{a}_q^\dagger = 0\,. \tag{2.26}$$

Additionally, a third combination in which $\hat{A}$ is a creation operator and $\hat{B}$ is an annihilation operator is also zero, since the string is already normal-ordered:

$$\hat{a}_p^\dagger \hat{a}_q = \hat{a}_p^\dagger \hat{a}_q - \{\hat{a}_p^\dagger \hat{a}_q\}_\mathrm{v} = \hat{a}_p^\dagger \hat{a}_q - \hat{a}_p^\dagger \hat{a}_q = 0\,. \tag{2.27}$$

The final combination, where $\hat{A}$ is an annihilation operator and $\hat{B}$ is a creation operator, is not zero, due to the anticommutation relations,

$$\hat{a}_p \hat{a}_q^\dagger = \hat{a}_p \hat{a}_q^\dagger - \{\hat{a}_p \hat{a}_q^\dagger\}_\mathrm{v} = \hat{a}_p \hat{a}_q^\dagger + \hat{a}_q^\dagger \hat{a}_p = \delta_{pq}\,, \tag{2.28}$$

where the correct sign must be maintained when the operators in braces are reordered. **Wick's theorem**[63,64] provides a recipe by which an arbitrary string of annihilation and creation operators, $\hat{A}\hat{B}\hat{C}\cdots\hat{X}\hat{Y}\hat{Z}$, may be written as a linear combination of normal-ordered strings. Schematically, Wick's theorem is

$$\begin{aligned}\hat{A}\hat{B}\hat{C}\cdots\hat{X}\hat{Y}\hat{Z} = \{&\hat{A}\hat{B}\hat{C}\cdots\hat{X}\hat{Y}\hat{Z}\}_\mathrm{v} \\ &+ \sum_{\text{singles}} \{\hat{A}\hat{B}\cdots\hat{X}\hat{Y}\hat{Z}\}_\mathrm{v} \\ &+ \sum_{\text{doubles}} \{\hat{A}\hat{B}\hat{C}\cdots\hat{X}\hat{Y}\hat{Z}\}_\mathrm{v} \\ &+ \cdots\,,\end{aligned} \tag{2.29}$$

where the limits ("singles", "doubles", etc.) refer to the number of pairwise contractions included in the summation. If this theorem is applied to the operator $\hat{A}$ from the last section, one obtains

$$\hat{A} = \{\hat{a}_p\hat{a}_q^\dagger\hat{a}_r\hat{a}_s^\dagger\}_\mathrm{v} + \{\hat{a}_p\hat{a}_q^\dagger\hat{a}_r\hat{a}_s^\dagger\}_\mathrm{v} + \{\hat{a}_p\hat{a}_q^\dagger\hat{a}_r\hat{a}_s^\dagger\}_\mathrm{v} + \{\hat{a}_p\hat{a}_q^\dagger\hat{a}_r\hat{a}_s^\dagger\}_\mathrm{v} + \{\hat{a}_p\hat{a}_q^\dagger\hat{a}_r\hat{a}_s^\dagger\}_\mathrm{v}\,, \tag{2.30}$$

where only non-zero contractions have been included [see Eqs. (2.25)–(2.28)]. The evaluation of pairwise contractions may introduce sign changes because the string of operators must be permuted to bring the pair together before the contraction can be evaluated. If the number of permutations is *even*, the sign is *positive*, if the number is *odd*, the sign is *negative*. For example,

$$\{\hat{A}\hat{B}\hat{C}\hat{D}\}_\mathrm{v} = \{\hat{A}\hat{D}\hat{B}\hat{C}\}_\mathrm{v} \tag{2.31a}$$

$$\{\hat{A}\hat{B}\hat{C}\hat{D}\}_\mathrm{v} = -\{\hat{A}\hat{C}\hat{B}\hat{D}\}_\mathrm{v}\,. \tag{2.31b}$$

Evaluating the contractions above for the operator $\hat{A}$ gives

$$\begin{aligned}\hat{A} &= \{\hat{a}_p\hat{a}_q^\dagger\hat{a}_r\hat{a}_s^\dagger\}_\mathrm{v} + \delta_{pq}\{\hat{a}_r\hat{a}_s^\dagger\}_\mathrm{v} + \delta_{ps}\{\hat{a}_q^\dagger\hat{a}_r\}_\mathrm{v} + \delta_{rs}\{\hat{a}_p\hat{a}_q^\dagger\}_\mathrm{v} + \delta_{pq}\delta_{rs} \\ &= -\hat{a}_q^\dagger\hat{a}_s^\dagger\hat{a}_p\hat{a}_r - \delta_{pq}\hat{a}_s^\dagger\hat{a}_r + \delta_{ps}\hat{a}_q^\dagger\hat{a}_r - \delta_{rs}\hat{a}_q^\dagger\hat{a}_p + \delta_{pq}\delta_{rs}\,,\end{aligned} \tag{2.32}$$

which is identical to the result obtained using the anticommutation relations in Eq. (2.22). Remembering that any matrix element of an operator may be written as a vacuum expectation value by writing its left- and right-hand determinants as operator strings acting on $|\text{vac}\rangle$, the composite string of creation and annihilation operators may then be rewritten using Wick's theorem as an expansion of normal-ordered strings. However, only the "fully contracted" terms survive, i.e. the ones where no creation/annihilation operator remains uncontracted, like the last term in Eq. (2.30). All other terms give a zero result, by construction. Thus, if one wants to evaluate an expectation value of a string of second-quantized operators with the vacuum state, one only needs to consider all possible full contractions.

2.1.4 The Fermi Vacuum and the Particle-Hole Formalism

In many-electron theories of quantum chemistry it is more convenient to deal with the N-electron reference determinant $|\Phi_0\rangle$, rather than the true vacuum state, $|\text{vac}\rangle$, since the use of normal-ordered strings would be extremely tedious if one had to include the complete set of operators required to generate $|\Phi_0\rangle$ from the true vacuum,[9]

$$|\Phi_0\rangle = \hat{a}_1^\dagger \hat{a}_2^\dagger \cdots \hat{a}_N^\dagger |\text{vac}\rangle \tag{2.33a}$$

$$\langle\Phi_0| = \langle\text{vac}|\hat{a}_N \ldots \hat{a}_2 \hat{a}_1 \,. \tag{2.33b}$$

A different definition of normal ordering relative to the reference state $|\Phi_0\rangle$, also called the "Fermi vacuum", is that *all q-annihilation operators lie to the right of all q-creation operators.*

For the definition of q-annihilation and q-creation operators, the so-called "particle-hole formalism" is used. Here, the one-electron states occupied in $|\Phi_0\rangle$ are referred to as *hole states*, whereas those unoccupied in $|\Phi_0\rangle$ are referred to as *particle states.* This nomenclature is due to the fact that a "hole" is created when an originally occupied state is acted upon by an annihilation operator such as $\hat{a}_i$, whereas a "particle" is created when an originally unoccupied state is acted upon by a creation operator such as $\hat{a}_a^\dagger$.[9] Therefore, operators that create or destroy holes and particles are referred to as *quasiparticle* (or just *q-particle*) construction operators. Hence, q-annihilation operators are those that annihilate holes and particles (e.g. $\hat{a}_i^\dagger$ and $\hat{a}_a$) and q-creation operators are those that create holes and particles (e.g. $\hat{a}_i$ and $\hat{a}_a^\dagger$). From now on simple braces without a subscript $\{\cdots\}$ are used to denote normal-order with respect to the Fermi vacuum.

Using the definition of a contraction, Eq. (2.24), for all possible combinations of q-particle creation and annihilation operators yields the following rules for contractions

$$\hat{a}_p^\dagger \hat{a}_q^\dagger = 0 \qquad \hat{a}_p \hat{a}_q = 0 \tag{2.34a}$$

$$\hat{a}_a \hat{a}_i^\dagger = 0 \qquad \hat{a}_i^\dagger \hat{a}_a = 0 \tag{2.34b}$$

$$\hat{a}_i \hat{a}_j^\dagger = 0 \qquad \hat{a}_a^\dagger \hat{a}_b = 0 \tag{2.34c}$$

$$\hat{a}_i^\dagger \hat{a}_j = \delta_{ij} \qquad \hat{a}_a \hat{a}_b^\dagger = \delta_{ab} \tag{2.34d}$$

With these rules, in principle all kinds of operator matrix elements can be evaluated in the following sections.

2.2 Hartree–Fock Theory

The most fundamental method and usually the starting point for more accurate calculations in quantum chemistry is the **Hartree–Fock** (HF) method. Essentially, a single determinant $|\Phi\rangle$ is chosen as the ansatz for the wave function and by using the variational principle the orbitals in it are varied until an energy minimum is reached.[24] This is why it is often also referred to as the **self-consistent field** (SCF).

2.2.1 Parameterization of the Wave Function

The energy calculated as the expectation value of the Hamiltonian with respect to a trial Slater determinant $|\tilde{\Phi}\rangle$ is given as

$$E[\tilde{\Phi}] = \langle \tilde{\Phi} | \hat{H} | \tilde{\Phi} \rangle \,, \tag{2.35}$$

where the electronic Hamiltonian $\hat{H}$ is split into a one-electron part $\hat{h}$, a two-electron part $\hat{W}$ and the nuclear repulsion V_{nn} from Eq. (2.3),

$$\hat{H} = \hat{h} + \hat{W} + V_{\mathrm{nn}} = \sum_{pq} h_{pq}\, \hat{a}_p^\dagger \hat{a}_q + \frac{1}{2} \sum_{pqrs} \langle pq|rs\rangle\, \hat{a}_p^\dagger \hat{a}_q^\dagger \hat{a}_s \hat{a}_r + V_{\mathrm{nn}} \,. \tag{2.36}$$

The one- and two-electron integrals are defined as

$$h_{pq} = -\frac{1}{2} \int \phi_p^*(\mathbf{x}) \nabla^2 \phi_q(\mathbf{x})\, \mathrm{d}\mathbf{x} - \sum_K \int \phi_p^*(\mathbf{x}) \frac{Z_K}{|\mathbf{r} - \mathbf{R}_K|} \phi_q \, \mathrm{d}\mathbf{x} \tag{2.37}$$

$$\langle pq|rs\rangle = \iint \phi_p^*(\mathbf{x}_1) \phi_q^*(\mathbf{x}_2) \frac{1}{r_{12}} \phi_r(\mathbf{x}_1) \phi_s(\mathbf{x}_2)\, \mathrm{d}\mathbf{x}_1 \mathrm{d}\mathbf{x}_2 \,. \tag{2.38}$$

The energy minimum can be found by rotating the orbitals using unitary transformations $\mathbf{U}$.[33] For unitary matrices the equality $\mathbf{U}^\dagger = \mathbf{U}^{-1}$ holds. However, unitary

matrices can be written as the exponential of an anti-Hermitian matrix $\boldsymbol{\kappa}$, for which $\boldsymbol{\kappa}^\dagger = -\boldsymbol{\kappa}$ holds. The unitary transformation of the orbitals can thus be written as a MacLaurin series of the expontential of an anti-Hermitian operator $\hat{\kappa}$

$$e^{-\hat{\kappa}}|\tilde{\Phi}\rangle = \sum_{n=0}^{\infty} \frac{(-1)^n}{n!} \hat{\kappa}^n |\tilde{\Phi}\rangle \,, \tag{2.39}$$

where $\hat{\kappa}$ is a one-electron operator, that is also called the **orbital rotation** operator, and with $\boldsymbol{\kappa} = \{\kappa_{pq}\}$

$$\hat{\kappa} = \sum_{p>q} \kappa_{pq} (\hat{a}_p^\dagger \hat{a}_q - \hat{a}_q^\dagger \hat{a}_p) = \sum_{p>q} \kappa_{pq} \hat{E}_{pq}^- \,. \tag{2.40}$$

2.2.2 Electronic Gradient and Hessian

The excitation operator $\hat{E}_{pq}^- = \hat{E}_{pq} - \hat{E}_{qp} = \hat{a}_p^\dagger \hat{a}_q - \hat{a}_q^\dagger \hat{a}_p$ in principle mixes all kinds of orbitals, occupied with occupied or virtual and correspondingly virtual with any kind. However, the only nonzero contribution is when occupied orbitals are mixed with virtual ones.[33] The expectation value of the Hamiltonian (2.35) can then be expanded as a function of $\boldsymbol{\kappa}$ around $\boldsymbol{\kappa} = \mathbf{0}$ as

$$E(\boldsymbol{\kappa}) = E^{(0)} + \boldsymbol{\kappa}^{\mathrm{T}} \mathbf{E}^{(1)} + \frac{1}{2} \boldsymbol{\kappa}^{\mathrm{T}} \mathbf{E}^{(2)} \boldsymbol{\kappa} + \dots \,, \tag{2.41}$$

where the column vector $\mathbf{E}^{(1)}$ is called the **electronic gradient** and the matrix $\mathbf{E}^{(2)}$ is the **electronic Hessian**.[33] On the other hand, one can insert the transformed determinants (2.39) into the energy expectation value (2.35) to yield

$$E(\hat{\kappa}) = \langle \tilde{\Phi} | e^{\hat{\kappa}} \hat{H} e^{-\hat{\kappa}} | \tilde{\Phi} \rangle = \langle \tilde{\Phi} | \big(1 + \hat{\kappa} + \frac{1}{2}\hat{\kappa}^2 + \dots\big) \hat{H} \big(1 - \hat{\kappa} + \frac{1}{2}\hat{\kappa}^2 - \dots\big) | \tilde{\Phi} \rangle \,, \tag{2.42}$$

which can be reordered in powers of the operator $\hat{\kappa}$ and written in terms of a **Baker–Campbell–Hausdorff** (BCH) expansion as[33]

$$E(\hat{\kappa}) = \langle \tilde{\Phi} | \hat{H} | \tilde{\Phi} \rangle + \langle \tilde{\Phi} | [\hat{\kappa}, \hat{H}] | \tilde{\Phi} \rangle + \frac{1}{2} \langle \tilde{\Phi} | [\hat{\kappa}, [\hat{\kappa}, \hat{H}]] | \tilde{\Phi} \rangle + \dots \,. \tag{2.43}$$

This expansion can be compared with the MacLaurin series of the energy (2.41) and one finds the following expressions for the electronic energy, gradient, and Hessian as[33]

$$E^{(0)} = E(\mathbf{0}) = \langle \tilde{\Phi} | \hat{H} | \tilde{\Phi} \rangle \tag{2.44}$$

$$E_{pq}^{(1)} = \left. \frac{\partial E(\boldsymbol{\kappa})}{\partial \kappa_{pq}} \right|_{\boldsymbol{\kappa}=\mathbf{0}} = \langle \tilde{\Phi} | [\hat{E}_{pq}^-, \hat{H}] | \tilde{\Phi} \rangle \tag{2.45}$$

$$E_{pqrs}^{(2)} = \left. \frac{\partial^2 E(\boldsymbol{\kappa})}{\partial \kappa_{pq} \partial \kappa_{rs}} \right|_{\boldsymbol{\kappa}=\mathbf{0}} = \frac{1}{2}(1 + \hat{P}_{pq,rs}) \langle \tilde{\Phi} | [\hat{E}_{pq}^-, [\hat{E}_{rs}^-, \hat{H}]] | \tilde{\Phi} \rangle \,, \tag{2.46}$$

where $\hat{P}_{pq,rs}$ permutes the index pairs pq and rs to make the electronic Hessian symmetric. The electronic gradient, on the other hand, is antisymmetric ($E^{(1)}_{pq} = -E^{(1)}_{qp}$) due to the antisymmetry of the excitation operator $\hat{E}^{-}_{pq}$.

2.2.3 Brillouin's Theorem

By expanding the commutator in Eq. (2.45) one can see that the electronic gradient vanishes whenever p and q belong to the same orbital space. The only nonzero contribution is when p and q belong to different spaces, which can also be called the only nonredundant orbital rotations. However, since an energy minimum is sought in the SCF procedure, the gradient has to vanish. Thus, the variational condition for HF can be written as

$$0 \stackrel{!}{=} \langle\tilde{\Phi}|[\hat{E}_{ai}, \hat{H}]|\tilde{\Phi}\rangle = -\langle\tilde{\Phi}|\hat{H}\hat{a}^{\dagger}_{a}\hat{a}_{i}|\tilde{\Phi}\rangle\,, \tag{2.47}$$

which means that the HF determinant does not couple to singly-excited determinants. This result is known as **Brillouin's theorem**.[24,33] More generally, the HF variational conditions can be written in the form

$$\langle\Phi_0|\hat{H}\hat{E}_{pq}|\Phi_0\rangle = \langle\Phi_0|\hat{H}\hat{E}_{qp}|\Phi_0\rangle\,, \tag{2.48}$$

which means that the converged HF state $|\Phi_0\rangle$ is in perfect balance between excitations and deexcitations, a result which is known as the *generalized Brillouin theorem* (GBT).[33]

2.2.4 The Fock Operator and the HF Energy

In order to uniquely define the wave function, other constraints apart from the variational condition are introduced, which leads to an effective one-particle operator called the **Fock operator** $\hat{F}$ that is constructed from the spin-orbitals that are eigenfunctions of the Hermitian Fock operator.[33] The matrix elements f_{pq} of the Fock operator $\hat{F}$ can be shown to be of the following form,

$$f_{pq} = h_{pq} + \sum_{i}\langle pi||qi\rangle\,, \tag{2.49}$$

where the notation for antisymmetrized two-electron integrals was introduced as

$$\langle pq||rs\rangle = \langle pq|rs\rangle - \langle pq|sr\rangle\,. \tag{2.50}$$

Since the matrix elements depend on the occupied spin orbitals ϕ_i, an iterative procedure for the solution of the HF problem has to be applied. The orbitals that diagonalize the Fock matrix are called the **canonical orbitals**,

$$f_{pp} = h_{pp} + \sum_{i}\langle pi||pi\rangle = \varepsilon_p\,, \tag{2.51}$$

where the eigenvalue of the Fock operator ε_p is called the **orbital energy**. The integral $\langle ij|ij\rangle$ is called **Coulomb integral** since it represents the quantum analogue of the classical repulsion energy of an interacting charge cloud, whereas the **exchange integral** $\langle ij|ji\rangle$, that arises due to the indistuingishability of the electrons, has no classical analogue.[24]

The Fock operator $\hat{F}$ can now be written as a sum of single-particle Fock operators $\hat{f}_i$ which consist of the respective one-electron part $\hat{h}$ and the Coulomb and exchange operators $\hat{J}$ and $\hat{K}$, respectively,

$$\hat{f}_i = \hat{h}_i + \hat{J}_i - \hat{K}_i \,. \tag{2.52}$$

The Hartree–Fock energy E_0^{HF} is given as the expectation value of the Hamiltonian with respect to the HF determinant $|\Phi_0\rangle$ consisting of the N orbitals with the lowest energy ε_i,

$$E_0^{\mathrm{HF}} = \langle\Phi_0|\hat{H}|\Phi_0\rangle = \sum_i h_{ii} + \frac{1}{2}\sum_{ij}\langle ij||ij\rangle = \sum_i \varepsilon_i - \frac{1}{2}\sum_{ij}\langle ij||ij\rangle \,. \tag{2.53}$$

As can be seen in Eq. (2.53), the HF energy is not equal to the sum of occupied orbital energies, since each orbital energy already includes the interaction of electron i with all others, but the expectation value of the Fock operator gives this result, $\langle\Phi_0|\hat{F}|\Phi_0\rangle = \sum_i \varepsilon_i$. The orbital energies are well suited for a description of the ionization or electron attachment process, the ionization potential (IP) for instance within HF is equal to the negative of the respective orbital energy, $E_i^{\mathrm{IP}} = -\varepsilon_i$. This result, which will later prove to be correct through first order in perturbation theory, is known as **Koopmans' theorem**.[24,65]

Even though Hartree–Fock yields most part of the total energy, it is not accurate enough to describe or predict physical or chemical processes in a way comparable to experiment. The remaining part of the electronic interaction beyond the mean-field approach as described by the effective one-particle Fock operator is called **electron correlation**, and several methods exist to recover parts of it. The most important ones are summarized in the next section.

2.3 Electron Correlation Methods

The Hartree–Fock method described in Section 2.2 describes only the average interaction of an electron with all others. The remaining part is called **electron correlation**, and the difference in energy (for a given one-particle basis set) compared to the fully interacting system, according to Löwdin,[66] is the **correlation energy** E_0^{corr} defined as

$$E_0^{\text{corr}} = E_0^{\text{exact}} - E_0^{\text{HF}} \,. \tag{2.54}$$

Since the approximation within Hartree–Fock consists of using only a single determinant, all post-HF methods expand the many-electron wave function in $|\Phi_0\rangle$ and additional determinants. Consequently, their difference lies in the evaluation of the correlation energy and the most important ones are briefly discussed in the following.

2.3.1 Configuration Interaction

Configuration interaction (CI) constitutes the conceptually simplest method to include electron correlation.[24,33,57,67] Here, a linear expansion for the ground-state wave function $|\Psi_0^{\text{CI}}\rangle$ is chosen starting from the HF determinant $|\Phi_0\rangle$ and determinants created thereof by replacing one or more occupied orbitals $i, j, \ldots$ with unoccupied (or virtual) ones $a, b, \ldots$, denoted by $|\Phi_{ij\ldots}^{ab\cdots}\rangle$. By employing excitation operators $\hat{C}^{\text{CI}} = \hat{C}_1^{\text{CI}} + \hat{C}_2^{\text{CI}} + \ldots + \hat{C}_N^{\text{CI}}$ of the form

$$\hat{C}_1^{\text{CI}} = \sum_{ia} c_i^a \, \hat{a}_a^\dagger \hat{a}_i \tag{2.55}$$

$$\hat{C}_2^{\text{CI}} = \frac{1}{4} \sum_{ijab} c_{ij}^{ab} \, \hat{a}_a^\dagger \hat{a}_b^\dagger \hat{a}_j \hat{a}_i \,, \tag{2.56}$$

and so on, where the amplitudes $\{c_i^a, c_{ij}^{ab}, \ldots\}$ need to be determined, the wave-function ansatz can be written as

$$\begin{aligned} |\Psi_0^{\text{CI}}\rangle &= |\Phi_0\rangle + \hat{C}_1^{\text{CI}}|\Phi_0\rangle + \hat{C}_2^{\text{CI}}|\Phi_0\rangle + \ldots \\ &= |\Phi_0\rangle + \sum_{ia} c_i^a |\Phi_i^a\rangle + \frac{1}{4} \sum_{ijab} c_{ij}^{ab} |\Phi_{ij}^{ab}\rangle + \ldots \,, \end{aligned} \tag{2.57}$$

where so-called **intermediate normalization** was chosen, $\langle \Phi_0 | \Psi_0^{\text{CI}} \rangle = 1$.

The wave-function ansatz (2.57) can be plugged into the electronic Schrödinger equation (2.1) and solved by employing the variational principle. This is done by representing the Hamiltonian $\hat{H}$ within the determinant basis and diagonalizing the resulting matrix $\mathbf{H}$. If the operator $\hat{C}^{\text{CI}}$ is not truncated, which is referred to as **full configuration interaction** (FCI), the numerically exact solution of the Schrödinger equation within a given one-particle basis set is obtained. This is only feasible for small systems with medium-sized basis sets, thus in practice the excitation manifold needs

to be truncated. Including only single and double excitations, $\hat{C}^{\mathrm{CI}} = \hat{C}_1^{\mathrm{CI}} + \hat{C}_2^{\mathrm{CI}}$, the approach is referred to as CISD. However, truncated CI schemes lack a property termed **size consistency**,[24,68] which essentially means that the calculated correlation energy does not scale properly with the system size. This is why nowadays CI methods do not find widespread application anymore. The only exception being the CI singles (CIS) method, which is size consistent due to Brillouin's theorem, but therefore also does not improve the ground-state description beyond HF. Yet, it is a very effective and cheap approach towards electronically excited states.[69]

2.3.2 Coupled Cluster

The flaw of CI not being size consistent can be traced back to the linear ansatz for the wave function[9,33]

$$|\Psi_0^{\mathrm{CI}}\rangle = \big(1 + \sum_{\mu} \hat{C}_\mu^{\mathrm{CI}}\big)|\Phi_0\rangle\,, \tag{2.58}$$

where μ runs over all included excitation classes. The proper, size-consistent form of the wave function would be a product[33]

$$|\Psi_0^{\mathrm{CC}}\rangle = \Big[\prod_{\mu}(1 + \hat{T}_\mu)\Big]|\Phi_0\rangle\,, \tag{2.59}$$

where the so-called **cluster operator** $\hat{T} = \hat{T}_1 + \hat{T}_2 + \ldots + \hat{T}_N$ is an excitation operator analogous to $\hat{C}^{\mathrm{CI}}$

$$\hat{T}_1 = \sum_{ia} t_i^a\, \hat{a}_a^\dagger \hat{a}_i = \sum_{ia} t_i^a\, \hat{E}_{ai} \tag{2.60}$$

$$\hat{T}_2 = \frac{1}{4}\sum_{ijab} t_{ij}^{ab}\, \hat{a}_a^\dagger \hat{a}_b^\dagger \hat{a}_j \hat{a}_i = \frac{1}{4}\sum_{ijab} t_{ij}^{ab}\, \hat{E}_{ai}\, \hat{E}_{bj}\,, \tag{2.61}$$

and the amplitudes $\{t_i^a, t_{ij}^{ab}, \ldots\}$ need to be determined. This ansatz for the wave function is referred to as **coupled cluster** (CC).[9–11,15,70] Since the cluster operators $\hat{T}_n$ commute and $\hat{E}_{ai}^2 = 0$, the wave-function ansatz (2.59) can also be written as

$$|\Psi_0^{\mathrm{CC}}\rangle = e^{\hat{T}}|\Phi_0\rangle\,. \tag{2.62}$$

This exponential ansatz is at the very heart of coupled-cluster theory.[9] More details on CC are discussed in Section 2.6 (page 34). A third approach based on perturbation theory is discussed in Section 2.4 (page 20).

2.3.3 Density Functional Theory

Another method that is formally closely related to Hartree–Fock, is **density functional theory** (DFT).[57,71,72] Its foundations have been laid by Hohenberg and Kohn[73] and

by Kohn and Sham.[74] Although its origins are quite different, the Kohn–Sham (KS) approach to DFT is very similar to Hartree–Fock theory. It can be regarded as an effective one-particle theory where the nonlocal exchange operator $\hat{K}$ from HF is replaced by a local exchange-correlation (xc) potential $\hat{v}_{\mathrm{xc}}$, that artificially incorporates both exchange and correlation effects.[75,76] The resulting KS operator $\hat{F}^{\mathrm{KS}}$ is thus given as

$$\hat{F}^{\mathrm{KS}} = \hat{h} + \hat{J} + \hat{v}_{\mathrm{xc}} \,. \tag{2.63}$$

The remaining machinery of KS-DFT is exactly identical to the one of HF, hence both are usually summarized as self-consistent field (SCF) methods. Due to its low computational cost but relatively accurate results, DFT is currently the most popular method in computational chemistry. However, since it cannot be systematically improved (in contrast to CI or CC theories), DFT cannot be regarded as a "black-box" method and thus has to be handled with care. A kind of evidence for this is the plethora of existing density functionals, that often depend on a number of empirical parameters.[57,76]

2.4 Perturbation Theory

Perturbation theory[24,57,77] assumes that a system similar to the one of interest is known and that the full system can be described by only slightly changing or "perturbing" the simpler one. This perturbation may be for instance an external field or the remaining two-electron interaction, as will be discussed later in this section. Mathematically this means that the total Hamiltonian of a system is formally divided into two parts

$$\hat{H} = \hat{H}_0 + \hat{H}_1 \,, \tag{2.64}$$

where $\hat{H}_1$ is called the perturbation, that needs to be small compared to the unperturbed system. The Schrödinger equation with the total Hamiltonian cannot be solved, but it is assumed that the solutions of a unperturbed system are known,

$$\hat{H}_0 |\Psi_n^{(0)}\rangle = E_n^{(0)} |\Psi_n^{(0)}\rangle \,, \tag{2.65}$$

where the eigenfunctions $|\Psi_n^{(0)}\rangle$ of $\hat{H}_0$ form a complete orthonormal set.

2.4.1 Rayleigh–Schrödinger Perturbation Theory

Within Rayleigh–Schrödinger (RS) perturbation theory, in order to obtain a numerical solution of the perturbation problem, a parameter λ is introduced in the Hamiltonian

$$\hat{H} = \hat{H}_0 + \lambda \hat{H}_1 \,. \tag{2.66}$$

When $\lambda = 0$, the perturbation is formally switched off, for $\lambda = 1$ it is "turned on". Now the exact eigenvalues E_n and the eigenfunctions $|\Psi_n\rangle$ of the full Hamiltonian $\hat{H}$ are expanded in a Taylor series in λ according to

$$E_n = E_n^{(0)} + \lambda E_n^{(1)} + \lambda^2 E_n^{(2)} + \ldots = \sum_{k=0}^{\infty} \lambda^k E_n^{(k)} \tag{2.67}$$

$$|\Psi_n\rangle = |\Psi_n^{(0)}\rangle + \lambda |\Psi_n^{(1)}\rangle + \lambda^2 |\Psi_n^{(2)}\rangle + \ldots = \sum_{k=0}^{\infty} \lambda^k |\Psi_n^{(k)}\rangle \,. \tag{2.68}$$

As defined by Eq. (2.65), the unperturbed system is described by the orthonormal set of functions $|\Psi_n^{(0)}\rangle$ with corresponding energies $E_n^{(0)}$. The wave-function corrections for the interacting system in Eq. (2.68) are chosen to be orthogonal with respect to $|\Psi_n^{(0)}\rangle$, which corresponds to the use of intermediate normalization, $\langle \Psi_n^{(0)} | \Psi_n \rangle = 1$.

Now the partitioning of the Hamiltonian (2.66) and the expansions for the energy (2.67) and wave function (2.68) are introduced into the Schrödinger equation (2.1) and ordered by powers of the parameter λ,

$$\begin{aligned}
\hat{H}_0 |\Psi_n^{(0)}\rangle &= E_0^{(0)} |\Psi_n^{(0)}\rangle \\
\hat{H}_0 |\Psi_n^{(1)}\rangle + \hat{H}_1 |\Psi_n^{(0)}\rangle &= E_n^{(0)} |\Psi_n^{(1)}\rangle + E_n^{(1)} |\Psi_n^{(0)}\rangle \\
\hat{H}_0 |\Psi_n^{(2)}\rangle + \hat{H}_1 |\Psi_n^{(1)}\rangle &= E_n^{(0)} |\Psi_n^{(2)}\rangle + E_n^{(1)} |\Psi_n^{(1)}\rangle + E_n^{(2)} |\Psi_n^{(0)}\rangle \\
&\vdots \\
\hat{H}_0 |\Psi_n^{(k)}\rangle + \hat{H}_1 |\Psi_n^{(k-1)}\rangle &= \sum_{i=0}^{k} E_n^{(i)} |\Psi_n^{(k-i)}\rangle \,.
\end{aligned} \tag{2.69}$$

Projecting the equations (2.69) on the zeroth-order wave function yields the equations for the corresponding energy corrections $E_n^{(k)}$, which by exploiting intermediate normalization and the fact that $\hat{H}_0$ is a Hermitian operator gives[24]

$$\begin{aligned}
E_n^{(0)} &= \langle \Psi_n^{(0)} | \hat{H}_0 | \Psi_n^{(0)} \rangle \\
E_n^{(1)} &= \langle \Psi_n^{(0)} | \hat{H}_1 | \Psi_n^{(0)} \rangle \\
E_n^{(2)} &= \langle \Psi_n^{(0)} | \hat{H}_1 | \Psi_n^{(1)} \rangle \\
E_n^{(3)} &= \langle \Psi_n^{(0)} | \hat{H}_1 | \Psi_n^{(2)} \rangle \,,
\end{aligned} \tag{2.70}$$

and so on. Since the eigenfunctions of the unperturbed Hamiltonian form a complete orthonormal basis, the wave-function corrections $|\Psi_n^{(k)}\rangle$ can be expanded in this basis,

$$|\Psi_n^{(k)}\rangle = \sum_i c_{n,i}^{(k)} |\Psi_i^{(0)}\rangle = \sum_i |\Psi_i^{(0)}\rangle \langle \Psi_i^{(0)} | \Psi_n^{(k)} \rangle \,, \tag{2.71}$$

where the expansion coefficients are determined by projecting Eqs. (2.69) on the respective zeroth-order eigenstates, $c_{n,i}^{(k)} = \langle \Psi_i^{(0)} | \Psi_n^{(k)} \rangle$. For example, the first-order coefficients are

obtained by projecting the first-order equation of (2.69) onto $\langle\Psi_m^{(0)}|$ (where $m \neq n$), which yields

$$c_{n,m}^{(1)} = \langle\Psi_m^{(0)}|\Psi_n^{(1)}\rangle = \frac{\langle\Psi_m^{(0)}|\hat{H}_1|\Psi_n^{(0)}\rangle}{E_n^{(0)} - E_m^{(0)}}\,. \tag{2.72}$$

Analogously, in second order one obtains

$$c_{n,m}^{(2)} = \langle\Psi_m^{(0)}|\Psi_n^{(2)}\rangle = \frac{\langle\Psi_m^{(0)}|\hat{H}_1|\Psi_n^{(1)}\rangle}{E_n^{(0)} - E_m^{(0)}} - E_n^{(1)}\frac{\langle\Psi_m^{(0)}|\hat{H}_1|\Psi_n^{(0)}\rangle}{\left(E_n^{(0)} - E_m^{(0)}\right)^2}\,. \tag{2.73}$$

2.4.2 Møller–Plesset Perturbation Theory

A special case of RS perturbation theory that is used frequently in quantum chemistry for the electronic ground state is the so-called Møller–Plesset (MP) perturbation theory.[24,32,33] Here, the unperturbed Hamiltonian $\hat{H}_0$ is the Fock operator $\hat{F}$, and the perturbation $\hat{H}_1$ is the difference between the full Hamiltonian (2.2) of the system and the Fock operator. MPn denotes the approximation where the ground-state energy is expanded consistently through order n in perturbation theory. By using the relationship between the Fock matrix and the one-particle elements (2.49) as well as the antisymmetrized two-electron integrals (2.50), the electronic Hamiltonian $\hat{H}$ can be written as

$$\hat{H} = \underbrace{\sum_{pq} f_{pq}\,\hat{a}_p^\dagger\hat{a}_q - \sum_{pqk}\langle pk||qk\rangle\,\hat{a}_p^\dagger\hat{a}_q}_{=\sum_{pq} h_{pq}\hat{a}_p^\dagger\hat{a}_q} + \frac{1}{4}\sum_{pqrs}\langle pq||rs\rangle\,\hat{a}_p^\dagger\hat{a}_q^\dagger\hat{a}_s\hat{a}_r\,, \tag{2.74}$$

where the nuclear repulsion V_{nn} is neglected from now on. For any converged HF solution Brillouin's theorem, which can now be written as

$$\langle\Phi_0|\hat{H}|\Phi_i^a\rangle = \langle\Phi_i^a|\hat{H}|\Phi_0\rangle = 0\,, \tag{2.75}$$

is fulfilled and the Fock operator is thus block diagonal,

$$\hat{F} = \sum_{ij} f_{ij}\,\hat{a}_i^\dagger\hat{a}_j + \sum_{ab} f_{ab}\,\hat{a}_a^\dagger\hat{a}_b\,, \tag{2.76}$$

whereas in the so-called *canonical* orbital basis it is fully diagonal, meaning that $f_{pq} = \varepsilon_p\,\delta_{pq}$, which further simplifies the Fock operator to

$$\hat{F} = \sum_{p} \varepsilon_p\,\hat{a}_p^\dagger\hat{a}_p\,. \tag{2.77}$$

From Eq. (2.74) the perturbation operator $\hat{H}_1$ can be identified, which is often called the **fluctuation potential** $\hat{V}$,[33]

$$\hat{V} = -\sum_{pqk} \langle pk||qk\rangle \, \hat{a}_p^\dagger \hat{a}_q + \frac{1}{4} \sum_{pqrs} \langle pq||rs\rangle \, \hat{a}_p^\dagger \hat{a}_q^\dagger \hat{a}_s \hat{a}_r \,. \tag{2.78}$$

The zeroth-order wave function is the HF ground state, $|\Psi_0^{(0)}\rangle = |\Phi_0\rangle$, and the corrections are expanded in the basis of excited determinants $|\Phi_{ij\ldots}^{ab\cdots}\rangle = \hat{a}_a^\dagger \hat{a}_b^\dagger \cdots \hat{a}_j \hat{a}_i |\Phi_0\rangle$, since all of them are eigenfunctions of the Fock operator $\hat{F}$. Thus, the wave-function correction for each order n is written in a CI-like expansion as

$$|\Psi_0^{(n)}\rangle = \sum_{ia} t_{ia}^{(n)} |\Phi_i^a\rangle + \frac{1}{4} \sum_{ijab} t_{ijab}^{(n)} |\Phi_{ij}^{ab}\rangle + \ldots \,, \tag{2.79}$$

where the expansion coefficients $t_\mu^{(n)}$ are determined as described in Section 2.4.1. For lower perturbation orders the expansion is not N-fold, but truncates to only modest excitation levels.[9,24,78]

The zeroth- and first-order energy contributions may be calculated by inserting the HF wave function into the corresponding expressions of Eqs. (2.70) and employing Wick's theorem as

$$E_0^{(0)} = \langle \Phi_0 | \hat{F} | \Phi_0 \rangle = \sum_{pq} f_{pq} \langle \Phi_0 | \hat{a}_p^\dagger \hat{a}_q | \Phi_0 \rangle = \sum_{ij} f_{ij} \delta_{ij} = \sum_i f_{ii} = \sum_i \varepsilon_i \,, \tag{2.80}$$

where the contraction only yields a nonzero result if both p and q are occupied indices, see Eq. (2.34d), and the last equation holds for canonical orbitals. The first-order correction can be evaluated as

$$\begin{aligned} E_0^{(1)} = \langle \Phi_0 | \hat{V} | \Phi_0 \rangle &= -\sum_{pqj} \langle pj||qj\rangle \langle \Phi_0 | \hat{a}_p^\dagger \hat{a}_q | \Phi_0 \rangle \\ &\quad + \frac{1}{4} \sum_{pqrs} \langle pq||rs\rangle \langle \Phi_0 | \hat{a}_p^\dagger \hat{a}_q^\dagger \hat{a}_s \hat{a}_r + \hat{a}_p^\dagger \hat{a}_q^\dagger \hat{a}_s \hat{a}_r | \Phi_0 \rangle \\ &= -\sum_{ij} \langle ij||ij\rangle + \frac{1}{2} \sum_{ij} \langle ij||ij\rangle = -\frac{1}{2} \sum_{ij} \langle ij||ij\rangle \,, \end{aligned} \tag{2.81}$$

where again the only surviving contractions are those, where all orbital indices are occupied ones. Hence, the Hartree–Fock energy (2.53) is the sum of the zeroth- and first-order MP contributions, $E_0^{\mathrm{HF}} = E_0^{(0)} + E_0^{(1)}$.

Therefore, the first correction to the HF energy comes at second order, for which the first-order correction to the wave function $|\Psi_0^{(1)}\rangle$ is required. The necessary first-order correlation coefficients $\{t_{ia}^{(1)}, t_{ijab}^{(1)}, \ldots\}$ can be obtained by projecting the first-order equation onto the respective excited determinants, which is not done here since it is very tedious especially for higher orders, but postponed to a later point in the discussion

of coupled-cluster theory (Section 2.6), where the MP coefficients arise as finite-order approximations to the CC amplitudes.

It is mentioned, though, that by employing the same technique as for the evaluation of the energy contributions above, it can be shown that the first-order singles vanish, $t_{ia}^{(1)} = 0$, as long as Brillouin's theorem (2.75) is fulfilled. The only contributions to the first-order wave function come from doubly-excited determinants, where the necessary matrix element can be evaluated as $\langle \Phi_{ij}^{ab} | \hat{V} | \Phi_0 \rangle = \langle ab||ij \rangle$. The first-order doubles amplitudes and wave-function correction are thus given as

$$t_{ijab}^{(1)} = -t_{abij}^{(1)*} = \frac{\langle \Phi_{ij}^{ab} | \hat{V} | \Phi_0 \rangle}{E_0^{(0)} - E_{\Phi_{ij}^{ab}}^{(0)}} = \frac{\langle ab||ij \rangle}{\varepsilon_i + \varepsilon_j - \varepsilon_a - \varepsilon_b} \tag{2.82}$$

$$|\Psi_0^{(1)}\rangle = \frac{1}{4} \sum_{ijab} \frac{\langle ab||ij \rangle}{\varepsilon_i + \varepsilon_j - \varepsilon_a - \varepsilon_b} |\Phi_{ij}^{ab}\rangle = \frac{1}{4} \sum_{ijab} t_{ijab}^{(1)} |\Phi_{ij}^{ab}\rangle \,. \tag{2.83}$$

Triply- and higher-excited determinants cannot contribute to $|\Psi_0^{(1)}\rangle$ because of the Slater–Condon rules.[24] The second-order energy contribution can thus be evaluated as

$$E_0^{(2)} = \langle \Phi_0 | \hat{V} | \Psi_0^{(1)} \rangle = \frac{1}{4} \sum_{ijab} t_{ijab}^{(1)} \langle \Phi_0 | \hat{V} | \Phi_{ij}^{ab} \rangle = \frac{1}{4} \sum_{ijab} t_{ijab}^{(1)} \langle ij||ab \rangle \,, \tag{2.84}$$

and the total MP2 energy is thus given as $E_0^{\mathrm{MP2}} = E_0^{\mathrm{HF}} + E_0^{(2)}$. I now turn the attention to a method for the calculation of electronically excited states based on MP perturbation theory, where the terms derived above are needed.

2.5 Algebraic-Diagrammatic Construction

The **algebraic-diagrammatic construction** scheme (ADC) is a method to calculate generalized excitation energies originally derived in the framework of Green's functions or propagator theory.[25–28,79–83] Depending on the kind of the propagator, different spectroscopic properties are obtained. For instance, ADC for the *polarization propagator* yields electronic excitation energies,[25–27,84–86] whereas ADC for the *electron propagator* yields ionization potentials and electron affinities.[28,82,87–90]

Within the original derivation, however, no excited-state wave function was available and only the excitation energy and transition moments could be calculated from the poles and corresponding residues of the propagator, respectively. This drawback has

Parts of Section 2.5 have already been published in

- M. Hodecker, D. R. Rehn, A. Dreuw, "Hermitian Second-Order Methods for Excited Electronic States: Unitary Coupled Cluster in Comparison with Algebraic-Diagrammatic Construction Schemes", *The Journal of Chemical Physics*, **2020**, *152*, 094106.

been overcome later by an algebraic approach commonly referred to as the **intermediate state representation** (ISR).[20,27–29,91] In the following, first some general aspects of intermediate state representations are discussed, then the procedure is carried out explicitly taking the example of the ADC scheme for the polarization propagator.

2.5.1 General Considerations of Intermediate State Representations

In the context of intermediate state representations,[20,28–31,91–93] excitation energies of an N-electron system are obtained by solving the secular equation of the shifted Hamiltonian or excitation energy operator $\hat{H} - E_0$ represented within an orthonormal basis of intermediate states (IS) $\{|\tilde{\Psi}_J\rangle\}$

$$M_{IJ} = \langle\tilde{\Psi}_I|\hat{H} - E_0|\tilde{\Psi}_J\rangle = \langle\tilde{\Psi}_I|\hat{H}|\tilde{\Psi}_J\rangle - E_0\delta_{IJ}\,. \tag{2.85}$$

The corresponding secular equation is a Hermitian eigenvalue problem

$$\mathbf{MX} = \mathbf{X\Omega}\,, \quad \mathbf{X}^\dagger\mathbf{X} = \mathbf{1}\,, \tag{2.86}$$

where $\mathbf{X}$ is the column matrix of eigenvectors $\mathbf{X}_n$ and $\mathbf{\Omega}$ is the diagonal matrix of eigenvalues ω_n that correspond to excitation energies, $\omega_n = E_n - E_0$.

Ground- to excited-state transition moments $x_n = \langle\Psi_n|\hat{D}|\Psi_0\rangle$, where $\hat{D}$ is a suitable transition operator, usually the dipole operator, can be calculated from an eigenvector as $x_n = \mathbf{X}_n^\dagger\,\tilde{\mathbf{F}}$, where the so-called *modified transition moments* $\tilde{\mathbf{F}}$ were introduced,[20] whose elements are given by

$$\tilde{F}_I = \langle\tilde{\Psi}_I|\hat{D}|\Psi_0\rangle\,. \tag{2.87}$$

A common starting point for intermediate state representations is the set of so-called correlated excited states (CES)

$$|\Psi_J^0\rangle = \hat{C}_J|\Psi_0\rangle\,, \tag{2.88}$$

which are obtained by applying "physical" excitation operators to the correlated ground state $|\Psi_0\rangle$. For different kinds of propagators, for which different properties are obtained, these operators take a different form, for instance excitation energies from the polarization propagator (PP), ionization potentials (IP) and electron affinities (EA) from the electron propagator:

$$\text{PP:} \qquad \{\hat{C}_J\} = \{\hat{a}_a^\dagger\hat{a}_i; \hat{a}_a^\dagger\hat{a}_i\hat{a}_b^\dagger\hat{a}_j, a<b, i<j; \dots\} \tag{2.89a}$$

$$\text{IP:} \qquad \{\hat{C}_J\} = \{\hat{a}_i; \hat{a}_a^\dagger\hat{a}_i\hat{a}_j, i<j; \dots\} \tag{2.89b}$$

$$\text{EA:} \qquad \{\hat{C}_J\} = \{\hat{a}_a^\dagger, \hat{a}_a^\dagger\hat{a}_b^\dagger\hat{a}_i, a<b; \dots\}\,. \tag{2.89c}$$

As usual, the indices $i, j, \dots$ stand for occupied orbitals in the reference $|\Phi_0\rangle$, whereas $a, b, \dots$ stand for unoccupied (virtual) ones and $p, q, \dots$ for the general case. Capital

Latin subscripts are used as a shorthand notation for strings of single-particle indices, $J \equiv (a, b, c, \ldots; i, j, k, \ldots)$. The excitation operators in $\hat{C}_J$ can obviously be decomposed into different classes referred to as μ-hole-μ-particle (μh-μp), $\mu = 1, 2, \ldots, N$, in the PP case according to the number μ of creation and annihilation operators. Analogously, this holds for IP, EA and other cases. The class of an excitation J will be denoted by $[J]$. The ground state represents a zeroth excitation class with $[J] = 0$.[20]

The different classes of excitation operators also lead to a decomposition of the matrix $\mathbf{M}$ into different blocks, according to the different classes of intermediate states. Taking only p-h and 2p-2h configurations into account, $\mathbf{M}$ has the following structure:

$$\begin{pmatrix} \mathbf{M}_{\mathrm{SS}} & \mathbf{M}_{\mathrm{SD}} \\ \mathbf{M}_{\mathrm{DS}} & \mathbf{M}_{\mathrm{DD}} \end{pmatrix} = \begin{pmatrix} \{\langle \tilde{\Psi}_i^a | \hat{H} - E_0 | \tilde{\Psi}_j^b \rangle\} & \{\langle \tilde{\Psi}_i^a | \hat{H} - E_0 | \tilde{\Psi}_{jk}^{bc} \rangle\} \\ \{\langle \tilde{\Psi}_{ij}^{ab} | \hat{H} - E_0 | \tilde{\Psi}_k^c \rangle\} & \{\langle \tilde{\Psi}_{ij}^{ab} | \hat{H} - E_0 | \tilde{\Psi}_{kl}^{cd} \rangle\} \end{pmatrix}, \tag{2.90}$$

where $\mathbf{M}_{\mathrm{SS}}$ is the so-called singles-singles block, $\mathbf{M}_{\mathrm{DD}}$ the doubles-doubles block and $\mathbf{M}_{\mathrm{SD}} = \mathbf{M}_{\mathrm{DS}}^{\dagger}$ are the coupling blocks.

The correlated excited states (2.88) are in general not orthonormal. However, a direct symmetrical orthonormalization of the CES would generate a representation of $\hat{H} - E_0$ that is neither compact nor separable,[20] which means that the properties obtained in this way would not be size consistent. Instead, a Gram–Schmidt (GS) procedure is employed, as described in more detail in the literature.[29,31] So-called **excitation class orthogonalized** (ECO) intermediate states $|\tilde{\Psi}_J\rangle$ may be constructed recursively as follows:[20]

1. Assume the IS $|\tilde{\Psi}_K\rangle$ of classes $1, 2, \ldots, \nu - 1$ have been constructed. Then the CES $|\Psi_J^0\rangle$ of class $[J] = \nu$ are orthogonalized to all intermediate states $|\tilde{\Psi}_K\rangle$ of the lower classes $[K] < \nu$ according to

$$|\Psi_J^{\#}\rangle = |\Psi_J^0\rangle - \sum_{\substack{K \\ [K]<[J]}} |\tilde{\Psi}_K\rangle\langle\tilde{\Psi}_K|\Psi_J^0\rangle\,. \tag{2.91}$$

2. The "precursor" states $|\Psi_J^{\#}\rangle$ of class ν are then orthonormalized symmetrically among each other via

$$|\tilde{\Psi}_I\rangle = \sum_{\substack{J \\ [J]=[I]}} |\Psi_J^{\#}\rangle S_{IJ}^{-\frac{1}{2}}\,. \tag{2.92}$$

Here, $\mathbf{S}$ is the overlap matrix of the precursor states, $S_{IJ} = \langle\Psi_I^{\#}|\Psi_J^{\#}\rangle$. As an example, let us consider the construction of the intermediate p-h states.[30] In the first step, the precursor states are obtained by orthogonalization of the correlated excited states with respect to the ground state:

$$|\Psi_{ai}^{\#}\rangle = |\Psi_{ai}^0\rangle - |\Psi_0\rangle\langle\Psi_0|\Psi_{ai}^0\rangle = \hat{a}_a^{\dagger}\hat{a}_i|\Psi_0\rangle - |\Psi_0\rangle\langle\Psi_0|\hat{a}_a^{\dagger}\hat{a}_i|\Psi_0\rangle\,. \tag{2.93}$$

In the second step, the intermediate states are obtained by Löwdin orthogonalization via

$$|\tilde{\Psi}_i^a\rangle = \sum_{jb} |\Psi_{bj}^{\#}\rangle S_{ia,bj}^{-\frac{1}{2}}\,, \tag{2.94}$$

where the overlap matrix of the precursor states is given by

$$S_{ia,bj} = \langle\Psi_0|\hat{a}_i^\dagger \hat{a}_a \hat{a}_b^\dagger \hat{a}_j|\Psi_0\rangle - \langle\Psi_0|\hat{a}_i^\dagger \hat{a}_a|\Psi_0\rangle\langle\Psi_0|\hat{a}_b^\dagger \hat{a}_j|\Psi_0\rangle\,. \tag{2.95}$$

An ISR derivation of the algebraic-diagrammatic construction scheme for the polarization propagator through second order is summarized in the following subsection, where the reader is referred to Ref. 94 for more details.

2.5.2 ADC Scheme for the Polarization Propagator

In the algebraic-diagrammatic construction scheme for the polarization propagator,[25–30] an ISR based on the ECO states (Section 2.5.1) with physical excitation operators (2.89a) is employed, but the exact ground state $|\Psi_0\rangle$ and its energy E_0 are replaced by perturbation expansions,

$$|\Psi_0\rangle = |\Psi_0^{(0)}\rangle + |\Psi_0^{(1)}\rangle + |\Psi_0^{(2)}\rangle + \dots \tag{2.96}$$

$$E_0 = E_0^{(0)} + E_0^{(1)} + E_0^{(2)} + \dots\,, \tag{2.97}$$

assuming the Møller–Plesset partitioning of the Hamiltonian into the (zeroth order) Fock operator and the (first order) perturbation, $\hat{H} = \hat{H}_0 + \hat{H}_1$, see Section 2.4.2 (page 22). Then the zeroth-order wave function is the Hartree–Fock determinant, $|\Psi_0^{(0)}\rangle = |\Phi_0\rangle$. Thus, the ADC secular matrix (2.85) is expanded in a series as well,

$$\mathbf{M} = \mathbf{M}^{(0)} + \mathbf{M}^{(1)} + \mathbf{M}^{(2)} + \dots\,. \tag{2.98}$$

Taking all terms up to a certain order n into account, the so-called ADC(n) scheme is obtained. However, not all blocks of the ADC matrix have to be expanded through the highest order n. Taking only singly (S) excited p-h and doubly (D) excited 2p-2h configurations into account, the ADC eigenvalue problem can be written in the form

$$\begin{pmatrix} \mathbf{M}_{\mathrm{SS}} & \mathbf{M}_{\mathrm{SD}} \\ \mathbf{M}_{\mathrm{DS}} & \mathbf{M}_{\mathrm{DD}} \end{pmatrix} \begin{pmatrix} \mathbf{X}_{\mathrm{S}} \\ \mathbf{X}_{\mathrm{D}} \end{pmatrix} = \omega \begin{pmatrix} \mathbf{X}_{\mathrm{S}} \\ \mathbf{X}_{\mathrm{D}} \end{pmatrix}\,, \tag{2.99}$$

where $\mathbf{X}_{\mathrm{S}}$ is the singles (p-h) and $\mathbf{X}_{\mathrm{D}}$ the doubles (2p-2h) part of the ADC eigenvector, and the matrix decomposition is given by Eq. (2.90). Carrying out the matrix-vector

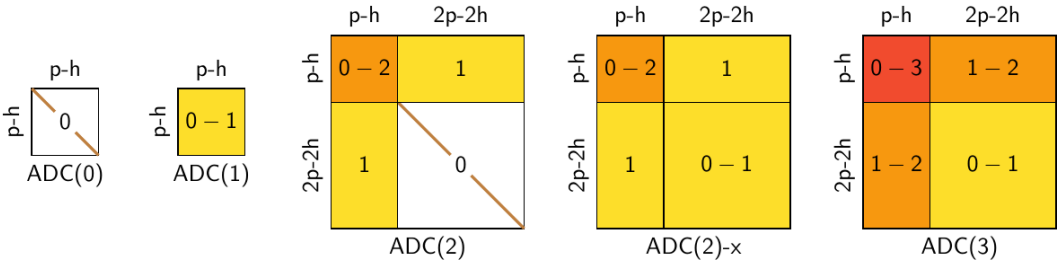

FIGURE 2.1: Structure of the ADC(n) matrix at different orders n. The numbers indicate the orders of perturbation theory used to expand the corresponding block.

multiplications, Eq. (2.99) can be equivalently written as a system of linear equations,

$$\mathbf{M}_{\mathrm{SS}}\,\mathbf{X}_{\mathrm{S}} + \mathbf{M}_{\mathrm{SD}}\,\mathbf{X}_{\mathrm{D}} = \omega\,\mathbf{X}_{\mathrm{S}} \tag{2.100a}$$

$$\mathbf{M}_{\mathrm{DS}}\,\mathbf{X}_{\mathrm{S}} + \mathbf{M}_{\mathrm{DD}}\,\mathbf{X}_{\mathrm{D}} = \omega\,\mathbf{X}_{\mathrm{D}}\,, \tag{2.100b}$$

the doubles part (2.100b) can be solved for $\mathbf{X}_{\mathrm{D}}$ to obtain $\mathbf{X}_{\mathrm{D}} = (\omega\mathbf{1} - \mathbf{M}_{\mathrm{DD}})^{-1}\mathbf{M}_{\mathrm{DS}}\mathbf{X}_{\mathrm{S}}$, which can be plugged into Eq. (2.100a), yielding an energy-dependent eigenvalue equation in the singles space only,

$$\left[\mathbf{M}_{\mathrm{SS}} + \mathbf{M}_{\mathrm{SD}}\,(\omega\mathbf{1} - \mathbf{M}_{\mathrm{DD}})^{-1}\,\mathbf{M}_{\mathrm{DS}}\right]\mathbf{X}_{\mathrm{S}} = \omega\,\mathbf{X}_{\mathrm{S}}\,, \tag{2.101}$$

from which the order relations of the different matrix blocks can be explained as follows. The leading contributions of $\mathbf{M}_{\mathrm{SS}}$ and $\mathbf{M}_{\mathrm{DD}}$, and thus also of $(\omega\mathbf{1} - \mathbf{M}_{\mathrm{DD}})^{-1}$, are of zeroth order, whereas the leading contributions of $\mathbf{M}_{\mathrm{SD}}$ and $\mathbf{M}_{\mathrm{DS}}$ are of first order. Hence, if excited states dominated by single excitations are desired to be correct through, say, second order, then $\mathbf{M}_{\mathrm{SS}} + \mathbf{M}_{\mathrm{SD}}\,(\omega\mathbf{1} - \mathbf{M}_{\mathrm{DD}})^{-1}\,\mathbf{M}_{\mathrm{DS}}$ needs to be correct through this order, meaning that $\mathbf{M}_{\mathrm{SS}}$ needs to be correct through second order, $\mathbf{M}_{\mathrm{SD}}$ and $\mathbf{M}_{\mathrm{DS}}$ through first order, whereas $\mathbf{M}_{\mathrm{DD}}$ only needs to be correct through zeroth order. Expanding $\mathbf{M}_{\mathrm{DD}}$ through first order would lead to a third-order term, since the coupling blocks are at least first order. For the same reason, expanding the coupling blocks through second order would lead to terms that are at least of third order and are thus neglected in a second-order scheme. A consistent third-order method requires each block one order higher in perturbation theory, i.e. the singles-singles block through third oder, the coupling blocks through second order and the doubles-doubles block through first order. This result is depicted schematically in Figure 2.1 for ADC(n) schemes up to third order. ADC(2)-x represents an *ad hoc* extension of ADC(2), where the first-order terms in the doubles-doubles block from ADC(3) are taken into account.

More explicitly, the matrix elements of a corresponding order $n = k + l + m$ can be obtained via

$$M_{IJ}^{(n)}\lambda^{k+l+m} = \sum_{k+l+m=n}\sum_{KL}\lambda^k\left(S_{IK}^{-\frac{1}{2}}\right)^{(k)}\lambda^l\left(\langle\Psi_K^0|\hat{H}-E_0|\Psi_L^0\rangle\right)^{(l)}\lambda^m\left(S_{LJ}^{-\frac{1}{2}}\right)^{(m)}, \tag{2.102}$$

where the auxiliary index $\lambda = 1$ was used to identify expressions with the same order of perturbation theory and the first sum indicates that summation over indices k, l, m with the restriction to $k + l + m = n$. Hence, ADC matrix elements can be derived by considering the perturbation expansion of the overlap matrix $\mathbf{S}$ and the Hamiltonian matrix in the basis of the precursor states $|\Psi_J^\#\rangle$. Thus, the p-h precursor states are considered first, which are expanded analogously as

$$|\Psi_{ai}^{\#(n)}\rangle\lambda^n = \hat{a}_a^\dagger\hat{a}_i|\Psi_0^{(n)}\rangle\lambda^n - \sum_{k+l+m=n}|\Psi_0^{(k)}\rangle\langle\Psi_0^{(l)}|\hat{a}_a^\dagger\hat{a}_i|\Psi_0^{(m)}\rangle\lambda^{k+l+m}, \tag{2.103}$$

which in zeroth order are excited HF determinants:

$$|\Psi_{ai}^{\#(0)}\rangle = \hat{a}_a^\dagger\hat{a}_i|\Phi_0\rangle - |\Phi_0\rangle\underbrace{\langle\Phi_0|\hat{a}_a^\dagger\hat{a}_i|\Phi_0\rangle}_{=0} = \hat{a}_a^\dagger\hat{a}_i|\Phi_0\rangle = |\Phi_i^a\rangle. \tag{2.104}$$

The first-order term reduces to

$$|\Psi_{ia}^{\#(1)}\rangle = \hat{a}_a^\dagger\hat{a}_i|\Psi_0^{(1)}\rangle - \left(|\Psi_0^{(1)}\rangle\underbrace{\langle\Phi_0|\hat{a}_a^\dagger\hat{a}_i|\Phi_0\rangle}_{=0} + |\Psi_0^{(0)}\rangle\underbrace{\left(\langle\Psi_0|\hat{a}_a^\dagger\hat{a}_i|\Psi_0\rangle\right)^{(1)}}_{=\rho_{ai}^{(1)}=0}\right) = \hat{a}_a^\dagger\hat{a}_i|\Psi_0^{(1)}\rangle, \tag{2.105}$$

where the first-order correction to the wave function $|\Psi_0^{(1)}\rangle$ is a sum of doubly-excited determinants according to Eq. (2.83) and the first-order p-h CES are thus triply-excited determinants.[94] The second-order term is given by

$$|\Psi_{ai}^{\#(2)}\rangle = \hat{a}_a^\dagger\hat{a}_i|\Psi_0^{(2)}\rangle - |\Psi_0^{(0)}\rangle\underbrace{\left(\langle\Psi_0|\hat{a}_a^\dagger\hat{a}_i|\Psi_0\rangle\right)^{(2)}}_{=\rho_{ai}^{(2)}} = \hat{a}_a^\dagger\hat{a}_i|\Psi_0^{(2)}\rangle - \rho_{ai}^{(2)}|\Phi_0\rangle, \tag{2.106}$$

where $\boldsymbol{\rho}^{(2)}$ is the second-order correction to the ground-state one-particle density matrix.[52,95,96]

2.5.2.1 Overlap Matrix

Following the same procedure, the perturbation expansion of the overlap matrix $\mathbf{S}$ can be shown to be diagonal in zeroth order $S_{IJ}^{(0)} = \langle\Phi_0|\hat{C}_I^\dagger\hat{C}_J|\Phi_0\rangle = \delta_{IJ}$ whereas the first-order contribution vanishes, $S_{IJ}^{(1)} = 0$. The second-order part is only needed for the p-h/p-h

block, the elements of which can be evaluated as[94]

$$\begin{aligned} S^{(2)}_{ia,bj} = \frac{1}{4}\delta_{ij}\delta_{ab}\sum_{klcd}|t^{(1)}_{klcd}|^2 - \frac{1}{2}\delta_{ab}\sum_{kcd} t^{(1)}_{ikcd}t^{(1)*}_{jkcd} \\ - \frac{1}{2}\delta_{ij}\sum_{klc} t^{(1)}_{klac}t^{(1)*}_{klbc} + \sum_{kc} t^{(1)}_{ikac}t^{(1)*}_{jkbc}\,. \end{aligned} \tag{2.107}$$

However, for the construction of the intermediate states in Eq. (2.94), the inverse square root $\mathbf{S}^{-\frac{1}{2}}$ is needed and not $\mathbf{S}$ itself. For this, $\mathbf{S}$ can be reformulated as

$$S_{IJ} = \delta_{IJ} + S^{(2)}_{IJ} + \mathcal{O}(3)\,, \tag{2.108}$$

where $\mathcal{O}(3)$ stands for all terms of third and higher orders. Thus, $\mathbf{S}$ in principle has the form

$$\mathbf{S}(\mathbf{x}) = \mathbf{1} + \mathbf{x} \tag{2.109}$$

with $\mathbf{x} = \mathbf{S}^{(2)} + \mathcal{O}(3)$, such that $\mathbf{S}^{-\frac{1}{2}}(\mathbf{x}) = (\mathbf{1}+\mathbf{x})^{-\frac{1}{2}}$, which can be expanded in a Taylor series around $\mathbf{x} = \mathbf{0}$. With the first derivative $\left(\mathbf{S}^{-\frac{1}{2}}(\mathbf{x})\right)' = -\frac{1}{2}(\mathbf{1}+\mathbf{x})^{-\frac{3}{2}}$, the series is thus given by

$$\begin{aligned} \mathbf{S}^{-\frac{1}{2}}(\mathbf{x}) &= \mathbf{S}^{-\frac{1}{2}}(\mathbf{0}) + \left(\mathbf{S}^{-\frac{1}{2}}(\mathbf{0})\right)'(\mathbf{x}-\mathbf{0}) + \ldots \\ &= \mathbf{1} - \frac{1}{2}\mathbf{x} + \ldots \\ &= \mathbf{1} - \frac{1}{2}\left(\mathbf{S}^{(2)} + \mathcal{O}(3)\right) + \ldots \end{aligned} \tag{2.110}$$

Thus, $\mathbf{S}^{-\frac{1}{2}}$ is finally given as

$$S^{-\frac{1}{2}}_{IJ} = \delta_{IJ} - \frac{1}{2}S^{(2)}_{IJ} + \mathcal{O}(3)\,. \tag{2.111}$$

2.5.2.2 Precursor Matrix

Now the matrix representation of the shifted Hamiltonian $\hat{H} - E_0$ in the basis of the precursor states is discussed, where again the standard MP partitioning $\hat{H} = \hat{H}_0 + \lambda\hat{H}_1$ is assumed. The so-called precursor matrix $\mathbf{M}^{\#}$ has the form

$$\begin{aligned} M^{\#(n)}_{IJ}\lambda^n &= \langle\Psi^{\#(k)}_I|\lambda^k(\hat{H}_0 + \lambda\hat{H}_1 - \lambda^l E^{(l)}_0)\lambda^m|\Psi^{\#(m)}_J\rangle \\ &= \langle\Psi^{\#(k)}_I|\hat{H}_0|\Psi^{\#(m)}_J\rangle\lambda^{k+m} + \langle\Psi^{\#(k)}_I|\hat{H}_1|\Psi^{\#(m)}_J\rangle\lambda^{k+m+1} \\ &\quad - (S_{IJ}E_0)^{(n)}\lambda^n\,, \end{aligned} \tag{2.112}$$

where the summations over k, l, m to yield all terms with order n is tacitly assumed. Up to second order, $\mathbf{M}^{\#}$ is given by[94]

$$M_{IJ}^{\#(0)} = \langle\Phi_0|\hat{C}_I^\dagger \hat{H}_0 \hat{C}_J|\Phi_0\rangle - \delta_{IJ}E_0^{(0)} \tag{2.113a}$$

$$M_{IJ}^{\#(1)} = \langle\Phi_0|\hat{C}_I^\dagger \hat{H}_1 \hat{C}_J|\Phi_0\rangle - \delta_{IJ}E_0^{(1)} \tag{2.113b}$$

$$\begin{aligned} M_{IJ}^{\#(2)} = {} & \langle\Psi_0^{(1)}|\hat{C}_I^\dagger \hat{H}_1 \hat{C}_J|\Psi_0^{(0)}\rangle + \langle\Psi_0^{(0)}|\hat{C}_I^\dagger \hat{H}_1 \hat{C}_J|\Psi_0^{(1)}\rangle + \langle\Psi_0^{(1)}|\hat{C}_I^\dagger \hat{H}_0 \hat{C}_J|\Psi_0^{(1)}\rangle \\ & - \delta_{IJ}E_0^{(2)} - S_{IJ}^{(2)}E_0^{(0)}\,, \end{aligned} \tag{2.113c}$$

where the MP energy contributions $E_0^{(0)}$ and $E_0^{(2)}$ are given in Eqs. (2.80) and (2.84), respectively.

2.5.2.3 Explicit Expressions for ADC(2)

Explicit expressions for the elements of the ADC(2) matrix have originally been derived diagramatically.[25] However, they can also be obtained via the ISR approach[94] by employing Wick's theorem with the expressions from MP perturbation theory for the wave function and energy as well as the overlap matrix and precursor states derived above. For a more detailed derivation, where many contractions are carried out explicitly, I refer the reader to Ref. 94 or 97. However, the same matrix elements are derived more conveniently in a diagrammatic UCC approach in Chapter 3 (page 59).

Zeroth and First Order. In zeroth order, Eq. (2.102) simplifies to

$$\begin{aligned} M_{IJ}^{(0)} &= \sum_{KL} \big(S_{IK}^{-\frac{1}{2}}\big)^{(0)} M_{KL}^{\#(0)} \big(S_{LJ}^{-\frac{1}{2}}\big)^{(0)} \\ &= \langle\Phi_0|\hat{C}_I^\dagger \hat{H}_0 \hat{C}_J|\Phi_0\rangle - \delta_{IJ}E_0^{(0)} \\ &= \sum_p \varepsilon_p \langle\Phi_0|\hat{C}_I^\dagger \hat{a}_p^\dagger \hat{a}_p \hat{C}_J|\Phi_0\rangle - \delta_{IJ}E_0^{(0)}\,, \end{aligned} \tag{2.114}$$

which yields orbital-energy differences on the diagonal of the p-h/p-h and 2p-2h/2p-2h blocks:

$$M_{ia,jb}^{(0)} = (\varepsilon_a - \varepsilon_i)\delta_{ab}\delta_{ij} \tag{2.115a}$$

$$M_{iajb,kcld}^{(0)} = (\varepsilon_a + \varepsilon_b - \varepsilon_i - \varepsilon_j)\delta_{ac}\delta_{bd}\delta_{ik}\delta_{jl}\,. \tag{2.115b}$$

Similarly, the first-order term is given by

$$\begin{aligned} M_{IJ}^{(1)} &= \sum_{KL} \big(S_{IK}^{-\frac{1}{2}}\big)^{(0)} M_{KL}^{\#(1)} \big(S_{LJ}^{-\frac{1}{2}}\big)^{(0)} \\ &= \langle\Phi_0|\hat{C}_I^\dagger \hat{H}_1 \hat{C}_J|\Phi_0\rangle - \delta_{IJ}E_0^{(1)}\,, \end{aligned} \tag{2.116}$$

which, after evaluating the matrix element of $\hat{H}_1$, yields for the p-h/p-h block[94]

$$M^{(1)}_{ia,jb} = E^{(1)}_0 \delta_{ab}\delta_{ij} - \langle aj||bi\rangle - E^{(1)}_0 \delta_{ab}\delta_{ij} = -\langle aj||bi\rangle \,, \tag{2.117}$$

whereas for the p-h/2p-2h and 2p-2h/p-h coupling blocks one obtains

$$M^{(1)}_{ia,kcld} = \langle kl||id\rangle\delta_{ac} - \langle kl||ic\rangle\delta_{ad} - \langle al||cd\rangle\delta_{ik} + \langle ak||cd\rangle\delta_{il} \tag{2.118a}$$

$$M^{(1)}_{iajb,kc} = \langle kb||ij\rangle\delta_{ac} - \langle ka||ij\rangle\delta_{bc} - \langle ab||cj\rangle\delta_{ik} + \langle ab||ci\rangle\delta_{jk} \,. \tag{2.118b}$$

Second Order. Second-order terms are only required for the p-h/p-h block. A more detailed derivation will be presented in Chapter 4 (page 91). Here, only the final result is presented, which can be written as

$$\begin{aligned} M^{(2)}_{ia,bj} = {} & \frac{1}{2}\sum_{kc}\left[\langle ac||ik\rangle\, t^{(1)*}_{jkbc} + \langle jk||bc\rangle\, t^{(1)}_{ikac}\right] \\ & - \frac{1}{4}\delta_{ab}\sum_{kcd}\left[\langle cd||ik\rangle\, t^{(1)*}_{jkcd} + \langle jk||cd\rangle\, t^{(1)}_{ikcd}\right] \\ & - \frac{1}{4}\delta_{ij}\sum_{klc}\left[\langle ac||kl\rangle\, t^{(1)*}_{klbc} + \langle kl||bc\rangle\, t^{(1)}_{klac}\right] , \end{aligned} \tag{2.119}$$

and mentioned, that the same results are obtained in a unitary coupled-cluster approach through second order as presented in Section 3.3 (page 67).

2.5.3 Intermediate State Representation of a General One-Particle Operator

Having solved the Hermitian eigenvalue problem (2.86), the ISR offers advantages over classical propagator approaches by offering direct access to excited-state and transition properties. For this, the exact excited-state wave function is expanded in the complete basis of intermediate states,

$$|\Psi_n\rangle = \sum_I |\tilde{\Psi}_I\rangle\langle\tilde{\Psi}_I|\Psi_n\rangle = \sum_I X_{I,n}|\tilde{\Psi}_I\rangle \,, \tag{2.120}$$

where the expansion coefficients $X_{I,n} = \langle\tilde{\Psi}_I|\Psi_n\rangle$ are given by the elements of an ADC eigenvector $\mathbf{X}_n$. This expansion can be plugged into the expectation value of an arbitrary operator $\hat{D}$ to calculate the corresponding physical observable D_n in electronic state n as

$$D_n = \langle\Psi_n|\hat{D}|\Psi_n\rangle = \sum_{IJ} X^*_{I,n}\,\langle\tilde{\Psi}_I|\hat{D}|\tilde{\Psi}_J\rangle\, X_{J,n} = \mathbf{X}^\dagger_n\,\tilde{\mathbf{B}}\,\mathbf{X}_n \,, \tag{2.121}$$

where $\tilde{B}_{IJ} = \langle\tilde{\Psi}_I|\hat{D}|\tilde{\Psi}_J\rangle$ is the matrix representation of the operator $\hat{D}$ in the IS basis. State-to-state transition moments T_{mn} can analogously be obtained by employing different vectors $m \neq n$ on the left and right side,

$$T_{mn} = \langle\Psi_m|\hat{D}|\Psi_n\rangle = \mathbf{X}_m^\dagger\,\tilde{\mathbf{B}}\,\mathbf{X}_n \tag{2.122}$$

Another approach to molecular properties D_n consists of calculating the derivative of the energy E_n with respect to a perturbation connected to the observable, which does not necessarily yield the same result as the expectation value for approximate methods. The relationship between the two approaches is investigated in detail in Chapter 7 (page 143).

Consequently, the only task is to determine the matrix representation $\tilde{\mathbf{B}}$ of the operator $\hat{D}$ in the IS basis, which can be decomposed into its ground- and excited-state contributions as $\tilde{B}_{IJ} = D_0\delta_{IJ} + B_{IJ}$, where $D_0 = \langle\Psi_0|\hat{D}|\Psi_0\rangle$ is the ground-state expectation value and hence $B_{IJ} = \langle\tilde{\Psi}_I|\hat{D} - D_0|\tilde{\Psi}_J\rangle$, analogous to the ADC matrix $\mathbf{M}$. Following the perturbation expansion of the intermediate states, the ISR matrix $\mathbf{B}$ is also expanded in a series,

$$\mathbf{B} = \mathbf{B}^{(0)} + \mathbf{B}^{(1)} + \mathbf{B}^{(2)} + \ldots. \tag{2.123}$$

Exploiting the form of a general one-particle operator in second quantization, $\hat{D} = \sum_{pq} d_{pq}\,\hat{a}_p^\dagger\hat{a}_q$, the above equations can be rewritten in terms of excited-state or state-to-state one-particle density matrices $\boldsymbol{\rho}_n$ or $\boldsymbol{\rho}_{mn}$, respectively,

$$D_n = \langle\Psi_n|\hat{D}|\Psi_n\rangle = \sum_{pq} d_{pq} \underbrace{\sum_{IJ} X_{I,n}^*\,\langle\tilde{\Psi}_I|\hat{a}_p^\dagger\hat{a}_q|\tilde{\Psi}_J\rangle\,X_{J,n}}_{=\rho_{n,pq}} = \sum_{pq} d_{pq}\,\rho_{n,pq} \tag{2.124}$$

$$T_{mn} = \langle\Psi_m|\hat{D}|\Psi_n\rangle = \sum_{pq} d_{pq} \underbrace{\sum_{IJ} X_{I,n}^*\,\langle\tilde{\Psi}_I|\hat{a}_p^\dagger\hat{a}_q|\tilde{\Psi}_J\rangle\,X_{J,m}}_{=\rho_{mn,pq}} = \sum_{pq} d_{pq}\,\rho_{mn,pq}\,. \tag{2.125}$$

The same form of equations for the calculation of properties is also true for the unitary coupled-cluster scheme, which will be discussed in Section 3.7 (page 83).

2.6 Coupled-Cluster Theory

The ground-state wave function in coupled-cluster theory[9–11,15,70,98,99] is given by the exponential ansatz of Eq. (2.62), $|\Psi_0^{\mathrm{CC}}\rangle = \exp(\hat{T})|\Phi_0\rangle$, with the cluster operators $\hat{T} = \hat{T}_1 + \hat{T}_2 + \ldots + \hat{T}_N$ given by Eqs. (2.60) and (2.61). The exponential of the cluster operator is defined via its Taylor series as

$$e^{\hat{T}} = \sum_{k=0}^{\infty} \frac{1}{k!}\hat{T}^k = 1 + \hat{T} + \frac{1}{2!}\hat{T}^2 + \frac{1}{3!}\hat{T}^3 + \ldots . \tag{2.126}$$

If the cluster operator is not truncated, the exact wave function within the one-electron basis set is obtained, which is equivalent to FCI, just the parametrization is more complicated. Truncation of $\hat{T}$ at a certain excitation level leads to a hierarchy of approximate CC methods, for example if $\hat{T} = \hat{T}_2$ the *coupled cluster doubles* (CCD) model is obtained, whereas if $\hat{T} = \hat{T}_1 + \hat{T}_2$ the scheme is referred to as *coupled cluster singles and doubles* (CCSD).[9] The advantage of the more complicated wave-function parametrization compared to CI is that truncated CC schemes are also size consistent, or more precisely, **size extensive**, which means results obtained with CC wave functions scale properly with the system size.[11]

In CI theory, the wave function ansatz (2.57) is optimized by minimizing the expectation value of the Hamiltonian $\hat{H}$ with respect to the linear expansion coefficients,

$$E_0^{\mathrm{CI}} = \min_{c_\mu} \frac{\langle \Psi_0^{\mathrm{CI}} | \hat{H} | \Psi_0^{\mathrm{CI}} \rangle}{\langle \Psi_0^{\mathrm{CI}} | \Psi_0^{\mathrm{CI}} \rangle} . \tag{2.127}$$

The CC ground-state energy can in principle be obtained analogously to CI by plugging the wave function $|\Psi_0^{\mathrm{CC}}\rangle$ into the electronic Schrödinger equation and employing the variational principle, meaning the energy is minimized with respect to the amplitudes t_μ,

$$E_0^{\mathrm{CC}} = \min_{t_\mu} \frac{\langle \Psi_0^{\mathrm{CC}} | \hat{H} | \Psi_0^{\mathrm{CC}} \rangle}{\langle \Psi_0^{\mathrm{CC}} | \Psi_0^{\mathrm{CC}} \rangle} = \min_{t_\mu} \frac{\langle \Phi_0 | e^{\hat{T}^\dagger} \hat{H} e^{\hat{T}} | \Phi_0 \rangle}{\langle \Phi_0 | e^{\hat{T}^\dagger} e^{\hat{T}} | \Phi_0 \rangle} , \tag{2.128}$$

where $\hat{T}^\dagger$ acts as an excitation operator to the left and $\langle \Psi_0^{\mathrm{CC}}| = \langle \Phi_0 | \exp(\hat{T})^\dagger = \langle \Phi_0 | \exp(\hat{T}^\dagger)$. However, due to the *nonlinear ansatz* of CC theory, this leads to intractable set of non-linear equations for the amplitudes, since there is no natural truncation of its power series expansion before the N-electron limit,

$$\langle \Phi_0 | e^{\hat{T}^\dagger} \hat{H} e^{\hat{T}} | \Phi_0 \rangle = \langle \Phi_0 | (1 + \hat{T}^\dagger + \frac{1}{2}(\hat{T}^\dagger)^2 + \ldots) \hat{H} (1 + \hat{T} + \frac{1}{2}\hat{T}^2 + \ldots) | \Phi_0 \rangle . \tag{2.129}$$

As such, even the simplest coupled cluster singles (CCS) model would have the same computational effort as FCI. Therefore, the CC equations are usually solved in a different way in practice, namely by projective techniques that are discussed in the

following. Alternative ansätze like the variational one (2.128) are presented in more detail in Section 2.6.9 (page 55).

2.6.1 The Projected Coupled-Cluster Equations

The CC wave function $|\Psi_0^{\mathrm{CC}}\rangle = e^{\hat{T}}|\Phi_0\rangle$ in a given orbital basis is used to solve the electronic Schrödinger equation

$$\hat{H}e^{\hat{T}}|\Phi_0\rangle = E_0^{\mathrm{CC}}e^{\hat{T}}|\Phi_0\rangle\,. \tag{2.130}$$

By *projecting* Eq. (2.130) onto the HF ground state $\langle\Phi_0|$ and the corresponding excited determinant manifold $\langle\Phi_I|$, equations for the CC energy and amplitudes are obtained,

$$\langle\Phi_0|\hat{H}e^{\hat{T}}|\Phi_0\rangle = E_0^{\mathrm{CC}} \tag{2.131}$$

$$\langle\Phi_I|\hat{H}e^{\hat{T}}|\Phi_0\rangle = E_0^{\mathrm{CC}}\langle\Phi_I|e^{\hat{T}}|\Phi_0\rangle\,, \tag{2.132}$$

where again intermediate normalization is used, $\langle\Phi_0|\Psi_0^{\mathrm{CC}}\rangle = 1$. It is convenient to express the projected CC equations in a slightly different form, where the Schrödinger equation (2.130) is multiplied from the left by $e^{-\hat{T}}$ to obtain[9]

$$e^{-\hat{T}}\hat{H}e^{\hat{T}}|\Phi_0\rangle = E_0^{\mathrm{CC}}|\Phi_0\rangle \tag{2.133}$$

which can be seen as a Schrödinger equation with a so-called **similarity-transformed Hamiltonian**,

$$\bar{H} = e^{-\hat{T}}\hat{H}e^{\hat{T}} \tag{2.134}$$

that is not Hermitian anymore, as can be seen by

$$(e^{-\hat{T}}\hat{H}e^{\hat{T}})^\dagger = (e^{\hat{T}})^\dagger\hat{H}^\dagger(e^{-\hat{T}})^\dagger = e^{\hat{T}^\dagger}\hat{H}e^{-\hat{T}^\dagger} \neq e^{-\hat{T}}\hat{H}e^{\hat{T}}\,. \tag{2.135}$$

Hence, its matrix representation is *non-symmetric* in contrast to the CI or ADC matrix. Projecting the similarity-transformed Schrödinger equation (2.133) onto the same determinants as before, the following set of equations for the CC energy and amplitudes is obtained:

$$\langle\Phi_0|e^{-\hat{T}}\hat{H}e^{\hat{T}}|\Phi_0\rangle = E_0^{\mathrm{CC}} \tag{2.136}$$

$$\langle\Phi_I|e^{-\hat{T}}\hat{H}e^{\hat{T}}|\Phi_0\rangle = 0\,. \tag{2.137}$$

These equations can be shown to be equivalent to the ones before,[33] but the amplitude equations are now decoupled from the energy equation. For example, the

energy equation (2.136) can easily be simplified in the following way:

$$E_0^{\mathrm{CC}} = \langle\Phi_0|e^{-\hat{T}}\hat{H}e^{\hat{T}}|\Phi_0\rangle = \langle\Phi_0|\hat{H}e^{\hat{T}}|\Phi_0\rangle\,, \tag{2.138}$$

since $\hat{T}$ acts as a deexcitation operator to the left and thus $\langle\Phi_0|e^{-\hat{T}} = \langle\Phi_0|(1-\hat{T}+\ldots) = \langle\Phi_0|$. For diagrammatic reasons, Eq. (2.132) is referred to as the *unlinked* and (2.137) as the *linked coupled-cluster equations.*[33] Expanding the exponential function in Eq. (2.138) and inserting $\hat{T} = \hat{T}_1 + \hat{T}_2 + \ldots$, one obtains

$$E_0^{\mathrm{CC}} = \langle\Phi_0|\hat{H}(1+\hat{T}+\frac{1}{2}\hat{T}^2+\ldots)|\Phi_0\rangle = \langle\Phi_0|\hat{H}(1+\hat{T}_1+\hat{T}_2+\frac{1}{2}\hat{T}_1^2)|\Phi_0\rangle\,, \tag{2.139}$$

where cluster operators higher than doubles do not contribute due to the Slater–Condon rules.[24] Furthermore, $\hat{T}_1$ does not contribute as long as Brillouin's theorem (2.75) is valid, i.e. for any converged HF solution. Hence, irrespective of the truncation level of the cluster operator, only single and double amplitudes contribute directly to the CC energy. However, higher-order excitations contribute indirectly since all amplitudes are coupled by the projected equations (2.137).[9] Unlike the variational ansatz (2.128) the projected form of the CC equations truncates naturally. Eq. (2.139) also reveals that there are two different types of contributions to the energy as well as amplitude equations arising from the linear and nonlinear parts of the cluster operator. The simple $\hat{T}_2$ operator generates doubly-excited determinants such as $|\Phi_{ij}^{ab}\rangle$ with corresponding amplitudes t_{ij}^{ab}, that are referred to as **connected cluster amplitudes**, whereas $\hat{T}_1^2$ generates the same doubly-excited determinants, but with products of amplitudes such as $t_i^a t_j^b$ that are referred to as **disconnected cluster amplitudes**.[33]

In order to further evaluate the linked projected CC equations (2.137), the Baker–Campbell–Hausdorff (BCH) expansion is exploited. For two matrices $\mathbf{A}$ and $\mathbf{B}$ the BCH expansion is given as

$$\exp(-\mathbf{A})\mathbf{B}\exp(\mathbf{A}) = \mathbf{B} + [\mathbf{B},\mathbf{A}] + \frac{1}{2!}[[\mathbf{B},\mathbf{A}],\mathbf{A}] + \frac{1}{3!}[[[\mathbf{B},\mathbf{A}],\mathbf{A}],\mathbf{A}] + \ldots\,, \tag{2.140}$$

which can be derived by inserting the Taylor expansions of the exponentials. Since the Hamiltonian is at most a two-particle operator, the cluster operators commute among each other and each commutator of $\hat{H}$ with $\hat{T}$ eliminates one general-orbital index of $\hat{H}$, the BCH expansion of the similarity-transformed Hamiltonian $\bar{H}$ is not higher than quartic in the amplitudes,[9,33]

$$e^{-\hat{T}}\hat{H}e^{\hat{T}} = \hat{H} + [\hat{H},\hat{T}\,] + \frac{1}{2}[[\hat{H},\hat{T}\,],\hat{T}\,] + \frac{1}{6}[[[\hat{H},\hat{T}\,],\hat{T}\,],\hat{T}\,] + \frac{1}{24}[[[[\hat{H},\hat{T}\,],\hat{T}\,],\hat{T}\,],\hat{T}\,]\,. \tag{2.141}$$

2.6.2 The Coupled-Cluster Hamiltonian

As is shown in Ref. 9, by employing anticommutation relations and Wick's theorem, the electronic Hamiltonian (2.74) can be rewritten as

$$\begin{aligned}\hat{H} = &\sum_{pq} h_{pq}\{\hat{a}_p^\dagger \hat{a}_q\} + \sum_{pqi}\langle pi||qi\rangle\{\hat{a}_p^\dagger \hat{a}_q\} + \frac{1}{4}\sum_{pqrs}\langle pq||rs\rangle\{\hat{a}_p^\dagger \hat{a}_q^\dagger \hat{a}_s \hat{a}_r\} \\ &+ \sum_i h_{ii} + \frac{1}{2}\sum_{ij}\langle ij||ij\rangle\,,\end{aligned} \tag{2.142}$$

where the first and second terms are identified as the normal-ordered Fock operator $\hat{F}_\mathrm{N}$, the last two terms correspond to the the HF energy $E_0^\mathrm{HF} = \langle\Phi_0|\hat{H}|\Phi_0\rangle$, and the third term is thus defined as the normal-ordered fluctuation potential $\hat{V}_\mathrm{N}$. Hence, the Hamiltonian can be written as $\hat{H} = \hat{F}_\mathrm{N} + \hat{V}_\mathrm{N} + \langle\Phi_0|\hat{H}|\Phi_0\rangle$, such that the normal-ordered Hamiltonian is simply[9]

$$\hat{H}_\mathrm{N} = \hat{H} - \langle\Phi_0|\hat{H}|\Phi_0\rangle = \hat{F}_\mathrm{N} + \hat{V}_\mathrm{N} = \sum_{pq} f_{pq}\{\hat{a}_p^\dagger \hat{a}_q\} + \frac{1}{4}\sum_{pqrs}\langle pq||rs\rangle\{\hat{a}_p^\dagger \hat{a}_q^\dagger \hat{a}_s \hat{a}_r\}\,. \tag{2.143}$$

This result can easily be generalized, meaning that the normal-ordered form of any operator is the operator itself minus its reference expectation value.

The concepts of normal ordering and Wick's theorem in combination with the BCH expansion (2.141) are in principle enough to derive programmable CC equations from the formal equations (2.136) and (2.137). For example, truncating the cluster operator as $\hat{T} \equiv \hat{T}_1 + \hat{T}_2$ corresponding to the CCSD model and inserting it into the similarity-transformed normal-ordered Hamiltonian $\bar{H} \equiv e^{-\hat{T}}\hat{H}_\mathrm{N}e^{\hat{T}}$, one obtains

$$\bar{H} = \hat{H}_\mathrm{N} + [\hat{H}_\mathrm{N}, \hat{T}_1] + [\hat{H}_\mathrm{N}, \hat{T}_2] + \frac{1}{2}[[[\hat{H}_\mathrm{N}, \hat{T}_1], \hat{T}_1] + \frac{1}{2}[[\hat{H}_\mathrm{N}, \hat{T}_2], \hat{T}_2] + [[\hat{H}_\mathrm{N}, \hat{T}_1], \hat{T}_2] + \dots\,, \tag{2.144}$$

where the BCH expansion truncates naturally after quadruply nested commutators as described before. It should be noted that the cluster operators (2.60) and (2.61) are already in normal-ordered form. By employing Wick's theorem on the commutators of $\hat{F}_\mathrm{N}$ and $\hat{V}_\mathrm{N}$ with $\hat{T}_1$ and $\hat{T}_2$, one notices that the second part of the commutator always cancels the part of the first commutator term, where the Hamiltonian fragment shares no contraction indices with the cluster operators.[9] This leads to a significant simplification of coupled-cluster theory: *The only nonzero terms in the BCH expansion are those in which the Hamiltonian $\hat{H}_N$ has at least one contraction with every cluster operator $\hat{T}_n$ on its right.*[9] This means that $\hat{H}_\mathrm{N}$ is always **connected** to the cluster operator $\hat{T}$, which can be written schematically as

$$e^{-\hat{T}}\hat{H}_\mathrm{N}e^{\hat{T}} = (\hat{H}_\mathrm{N}e^{\hat{T}})_\mathrm{c}\,, \tag{2.145}$$

where the subscript "c" stands for connected.

2.6.3 The CC Energy Equation

With the simplifications from Section 2.6.2, the CCSD energy equation can be derived rather straightforward using Wick's theorem. According to Eqs. (2.139) and (2.145), the CC correlation energy is given by

$$E_0^{\mathrm{CC}} - E_0^{\mathrm{HF}} = \langle\Phi_0|\bar{H}|\Phi_0\rangle = \langle\Phi_0|(\hat{H}_{\mathrm{N}}\hat{T}_1)_{\mathrm{c}} + (\hat{H}_{\mathrm{N}}\hat{T}_2)_{\mathrm{c}} + \frac{1}{2}(\hat{H}_{\mathrm{N}}\hat{T}_1^2)_{\mathrm{c}}|\Phi_0\rangle\,, \tag{2.146}$$

where no other terms can contribute since no fully connected terms can be generated from three or more pairs of excitation operators with the Hamiltonian. Inserting the definition of the normal-ordered Hamiltonian, $\hat{H}_{\mathrm{N}} = \hat{F}_{\mathrm{N}} + \hat{V}_{\mathrm{N}}$, the first term involving the Fock operator and $\hat{T}_1$ can be evaluated as

$$\begin{aligned}
\langle\Phi_0|(\hat{F}_{\mathrm{N}}\hat{T}_1)_{\mathrm{c}}|\Phi_0\rangle &= \sum_{pq}\sum_{ia} f_{pq}t_i^a \langle\Phi_0|\{\hat{a}_p^\dagger\hat{a}_q\}\{\hat{a}_a^\dagger\hat{a}_i\}|\Phi_0\rangle \\
&= \sum_{pq}\sum_{ia} f_{pq}t_i^a \langle\Phi_0|\{\hat{a}_p^\dagger\hat{a}_q\hat{a}_a^\dagger\hat{a}_i\}|\Phi_0\rangle \\
&= \sum_{pq}\sum_{ia} f_{pq}t_i^a\, \delta_{pi}\delta_{qa} = \sum_{ia} f_{ia}t_i^a\,,
\end{aligned} \tag{2.147}$$

which is zero if Brillouin's theorem is fulfilled, whereas the part with the fluctuation potential vanishes, $\langle\Phi_0|(\hat{V}_{\mathrm{N}}\hat{T}_1)_{\mathrm{c}}|\Phi_0\rangle = 0$, since no fully contracted terms can be generated from it.[9] An analogous argument holds for the Fock operator part and the $\hat{T}_2$ operator, $\langle\Phi_0|(\hat{F}_{\mathrm{N}}\hat{T}_2)_{\mathrm{c}}|\Phi_0\rangle = 0$, where no fully contracted terms can be generated. The two-electron component, on the other hand, does not vanish but produces four equivalent terms,

$$\begin{aligned}
\langle\Phi_0|(\hat{V}_{\mathrm{N}}\hat{T}_2)_{\mathrm{c}}|\Phi_0\rangle &= \frac{1}{16}\sum_{pqrs}\sum_{ijab}\langle pq||rs\rangle t_{ij}^{ab}\langle\Phi_0|\{\hat{a}_p^\dagger\hat{a}_q^\dagger\hat{a}_s\hat{a}_r\}\{\hat{a}_a^\dagger\hat{a}_b^\dagger\hat{a}_j\hat{a}_i\}|\Phi_0\rangle \\
&= \frac{1}{16}\sum_{pqrs}\sum_{ijab}\langle pq||rs\rangle t_{ij}^{ab}\langle\Phi_0|\{\hat{a}_p^\dagger\hat{a}_q^\dagger\hat{a}_s\hat{a}_r\hat{a}_a^\dagger\hat{a}_b^\dagger\hat{a}_j\hat{a}_i\} + \{\hat{a}_p^\dagger\hat{a}_q^\dagger\hat{a}_s\hat{a}_r\hat{a}_a^\dagger\hat{a}_b^\dagger\hat{a}_j\hat{a}_i\} \\
&\quad + \{\hat{a}_p^\dagger\hat{a}_q^\dagger\hat{a}_s\hat{a}_r\hat{a}_a^\dagger\hat{a}_b^\dagger\hat{a}_j\hat{a}_i\} + \{\hat{a}_p^\dagger\hat{a}_q^\dagger\hat{a}_s\hat{a}_r\hat{a}_a^\dagger\hat{a}_b^\dagger\hat{a}_j\hat{a}_i\}|\Phi_0\rangle \\
&= \frac{1}{16}\sum_{pqrs}\sum_{ijab}\langle pq||rs\rangle t_{ij}^{ab}(\delta_{pi}\delta_{qj}\delta_{ra}\delta_{sb} + \delta_{pj}\delta_{qi}\delta_{rb}\delta_{sa} \\
&\quad - \delta_{pj}\delta_{qi}\delta_{ra}\delta_{sb} - \delta_{pi}\delta_{qj}\delta_{rb}\delta_{sa}) \\
&= \frac{1}{4}\sum_{ijab}\langle ij||ab\rangle t_{ij}^{ab}\,,
\end{aligned} \tag{2.148}$$

where the factor of $\frac{1}{16}$ in the first three equalities arises from the product of $\frac{1}{4}$ that appear in the definitions of $\hat{V}_{\mathrm{N}}$ and $\hat{T}_2$, and the final factor of $\frac{1}{4}$ results from combining the last four terms by employing the permutational symmetry of the two-electron integrals. The same contraction scheme occurs in the last term of Eq. (2.146), where the square of the

$\hat{T}_1$ operator occurs. This term thus evaluates to

$$\begin{aligned}\frac{1}{2}\langle\Phi_0|(\hat{V}_\mathrm{N}\hat{T}_1^2)_\mathrm{c}|\Phi_0\rangle &= \frac{1}{8}\sum_{pqrs}\sum_{ia}\sum_{jb}\langle pq||rs\rangle t_i^a t_j^b \langle\Phi_0|\{\hat{a}_p^\dagger\hat{a}_q^\dagger\hat{a}_s\hat{a}_r\hat{a}_a^\dagger\hat{a}_i\hat{a}_b^\dagger\hat{a}_j\}|\Phi_0\rangle \\ &= \frac{1}{2}\sum_{ijab}\langle ij||ab\rangle t_i^a t_j^b\,,\end{aligned} \tag{2.149}$$

where the factor of $\frac{1}{2}$ from the BCH expansion and $\frac{1}{4}$ from the definition of $\hat{V}_\mathrm{N}$ yield $\frac{1}{8}$, but the resulting four identical terms give back the factor of $\frac{1}{2}$.[9]

With this, all contributions to the CCSD energy have been derived, which can be summarized as

$$E_0^\mathrm{CC} = E_0^\mathrm{HF} + \sum_{ia} f_{ia}t_i^a + \frac{1}{4}\sum_{ijab}\langle ij||ab\rangle t_{ij}^{ab} + \frac{1}{2}\sum_{ijab}\langle ij||ab\rangle t_i^a t_j^b\,. \tag{2.150}$$

In fact, this equation is not restricted to the CCSD approximation, but is valid also for more complicated methods such as CCSDT or CCSDTQ, since cluster operators like $\hat{T}_3$ or $\hat{T}_4$ cannot produce fully contracted terms and thus do not contribute directly to the energy.[9] The CCD energy expression is obtained by neglecting the terms involving the $\hat{T}_1$ operator and is thus formally identical to the MP2 energy contribution (2.84), only with different correlation amplitudes.

An analogous derivation employing Wick's theorem can be carried out for the amplitude equations, as is demonstrated in Ref. 9. This, however, is very tedious and thus omitted here. Instead, I want to restrict myself to a diagrammatic approach, which will prove to be more convenient and useful also for the UCC scheme in Chapter 3.

The expression for the CC energy is often written in terms of a Lagrange functional

$$E_0^\mathrm{CC} - E_0^\mathrm{HF} = \langle\Phi_0|(1+\hat{\Lambda})e^{-\hat{T}}\hat{H}_\mathrm{N}e^{\hat{T}}|\Phi_0\rangle\,, \tag{2.151}$$

where $\hat{\Lambda}$ is a deexcitation operator defined similarly to the adjoint of the CI operator as

$$\hat{\Lambda} = \hat{\Lambda}_1 + \hat{\Lambda}_2 + \ldots = \sum_{ia}\lambda_a^i\,\hat{a}_i^\dagger\hat{a}_a + \frac{1}{4}\sum_{ijab}\lambda_{ab}^{ij}\,\hat{a}_i^\dagger\hat{a}_j^\dagger\hat{a}_b\hat{a}_a + \ldots \tag{2.152}$$

and that is used to ensure stationarity of the CC energy with respect to the $\hat{T}$ amplitudes in order to faciliate the calculation of analytical gradients and properties.[18,100,101]

2.6.4 Introducing CC Diagrams

In this section, I want to introduce a simple diagrammatic formalism made popular by Kucharski and Bartlett,[102] by which the CC energy and amplitude equations can be derived significantly faster than by direct application of Wick's theorem. The presentation follows closely the one in Ref. 9, for more details the reader is also referred to Ref. 11.

After describing some of the general features, I explain how diagrams can be connected to form operator products in a manner analogous to Wick's theorem. While different types of diagrams have been employed in the literature, I restrict myself to the use of so-called antisymmetrized Goldstone diagrams.[11,103]

By making use of the particle-hole formalism, upward- and downward-directed lines are drawn to identify the orbitals that differ from those in the reference $|\Phi_0\rangle$, as shown in Figure 2.2. Downward-directed lines represent hole states, upward-directed lines particle states. Combining these one may represent exicted determinants like $|\Phi_i^a\rangle$, no lines thus stand for the HF reference $|\Phi_0\rangle$.

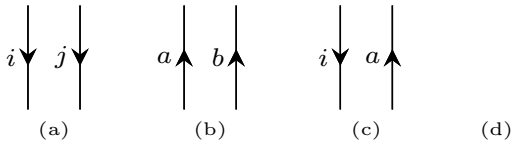

FIGURE 2.2: Some basic components of CC diagrams: (a) hole lines; (b) particle lines; (c) a singly-excited determinant $|\Phi_i^a\rangle$; (d) the reference $|\Phi_0\rangle$ represented by empty space.

Dynamical operators like the one- and two-electron part of $\hat{H}_\mathrm{N}$ and the cluster operators $\hat{T}_n$ are depicted by horizontal "interaction lines" that have a number of interaction *vertices* (represented as dots) according to their electron number, and the vertical lines from Figure 2.2 represent the creation and annihilation operators. Different interaction lines represent different operators, dashed lines will be used for the electronic Hamiltonian, whereas solid lines will be used for the cluster operators. The directed lines emerge from the aforementioned vertices on the interaction line where each vertex represents the action of the operator on an individual electron.[9] Hence, one-electron operators have one vertex, two-electron operators two vertices, and so on, each of them have two directed lines, one ingoing and one outgoing, associated to the annihilation and creation operators from the operator's normal-ordered string. Since two-electron operators contain four quasi-particle construction operators, their diagrammatic representation contains four directed lines.[9] The direction of these lines indicates the orbital subspace in which the second-quantized operators act: q-creation operators lie above the interaction line, and q-annihilation operators lie below.

For instance, the normal-ordered Fock operator $\hat{F}_\mathrm{N}$ is denoted by a dashed interaction line capped by an "$\times$". The operator is written in four fragments as shown in Figure 2.3, The first fragment has only operators in the unoccupied (particle) space, one q-creation line above the interaction line that corresponds to the $\hat{a}_a^\dagger$ operator, and one q-annihilation line below the interaction line corresponding to the $\hat{a}_b$ operator.[9] An analogous description holds for the second fragment in the occupied (hole) space. Both fragments do not change the excitation level relative to $|\Phi_0\rangle$, which is why their total excitation level is 0. The third fragment contains only q-annihilation lines below the interaction line, which corresponds to the operator string $\{\hat{a}_i^\dagger \hat{a}_a\}$ of a deexcitation, which is why it has the excitation level

$$\hat{F}_{\mathrm{N}} = \sum_{ab} f_{ab}\{\hat{a}_a^\dagger \hat{a}_b\} + \sum_{ij} f_{ij}\{\hat{a}_i^\dagger \hat{a}_j\} + \sum_{ia} f_{ia}\{\hat{a}_i^\dagger \hat{a}_a\} + \sum_{ia} f_{ai}\{\hat{a}_a^\dagger \hat{a}_i\}$$

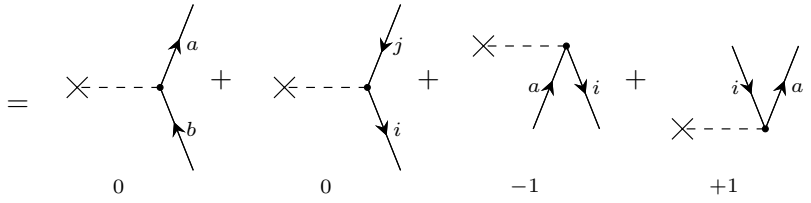

FIGURE 2.3: Diagrammatic representation of each fragment of the normal-ordered Fock operator $\hat{F}_{\mathrm{N}}$. The excitation level of each fragment is given below the diagram itself.

-1. The fourth $\hat{F}_{\mathrm{N}}$ fragment contains only q-creation lines above the interaction line representing the $\{\hat{a}_a^\dagger \hat{a}_i\}$ string of a single excitation, thus the excitation level of $+1$.

The two-electron fluctuation potential $\hat{V}_{\mathrm{N}}$ may be partitioned in an analogous manner as shown in Figure 2.4, where the antisymmetry with respect to a permutation of the lines leaving and entering the vertices is implicit. For example, the third diagram, corresponding to the sum over $\langle ia||bj\rangle\{\hat{a}_i^\dagger \hat{a}_a^\dagger \hat{a}_j \hat{a}_b\}$ fragments, may also be mirrored in the middle or drawn like one of the first two diagrams with the arrow direction of one side inversed, but the result is still the same, with the exception of a possible sign change.[9]

The cluster operators $\hat{T}$ and their Hermitian conjugates $\hat{T}^\dagger$ are represented diagrammatically as shown in Figure 2.5, where the interaction lines are depicted as solid horizontal bars. Since $\hat{T}$ contains only q-creation operators, which means it generates excited determinants from $|\Phi_0\rangle$, it contains no lines below the horizontal interaction line.[9] The opposite holds for its Hermitian conjugate $\hat{T}^\dagger$, which is a deexcitation operator. They are also fully antisymmetric in the sense that the sign changed when any pair of outgoing or ingoing lines is exchanged, as will be explained in the rules of algebraic interpretation of the diagrams.

For the rest of this thesis, the diagrams will mostly be interpreted as matrix elements of operators or operator products between determinants. The energy and amplitude equations of the coupled-cluster ground state always contain the reference determinant $|\Phi_0\rangle$ on the right and either $\langle\Phi_0|$ or excited determinant such as $\langle\Phi_i^a|$ and $\langle\Phi_{ij}^{ab}|$ on the left. Diagrams are particularly convenient for the construction of such matrix elements as they provide a straightforward way to evaluate the types of determinants they may be applied to or what determinants they produce.[9] For example, considering the fourth $\hat{F}_{\mathrm{N}}$ fragment in Figure 2.3, which contains two lines above and none below the operator interaction line. Since $|\Phi_0\rangle$ is represented by empty space and a singly-excited determinant $|\Phi_i^a\rangle$ by a pair of directed lines such as those in Figure 2.2(c), the diagram may be interpreted as the matrix element[9]

$$\langle\Phi_i^a|\hat{F}_{\mathrm{N}}|\Phi_0\rangle =$$

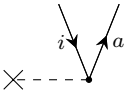

. (2.153)

$$\hat{V}_{\mathrm{N}} = \frac{1}{4}\sum_{abcd}\langle ab||cd\rangle\{\hat{a}_a^\dagger\hat{a}_b^\dagger\hat{a}_d\hat{a}_c\} + \frac{1}{4}\sum_{ijkl}\langle ij||kl\rangle\{\hat{a}_i^\dagger\hat{a}_j^\dagger\hat{a}_l\hat{a}_k\} + \sum_{ijab}\langle ia||bj\rangle\{\hat{a}_i^\dagger\hat{a}_a^\dagger\hat{a}_j\hat{a}_b\}$$
$$+ \frac{1}{2}\sum_{iabc}\langle ai||bc\rangle\{\hat{a}_a^\dagger\hat{a}_i^\dagger\hat{a}_c\hat{a}_b\} + \frac{1}{2}\sum_{ijka}\langle ij||ka\rangle\{\hat{a}_i^\dagger\hat{a}_j^\dagger\hat{a}_a\hat{a}_k\} + \frac{1}{2}\sum_{iabc}\langle ab||ci\rangle\{\hat{a}_a^\dagger\hat{a}_b^\dagger\hat{a}_i\hat{a}_c\}$$
$$+ \frac{1}{2}\sum_{ijka}\langle ia||jk\rangle\{\hat{a}_i^\dagger\hat{a}_a^\dagger\hat{a}_k\hat{a}_j\} + \frac{1}{4}\sum_{ijab}\langle ab||ij\rangle\{\hat{a}_a^\dagger\hat{a}_b^\dagger\hat{a}_j\hat{a}_i\} + \frac{1}{4}\sum_{ijab}\langle ij||ab\rangle\{\hat{a}_i^\dagger\hat{a}_j^\dagger\hat{a}_b\hat{a}_a\}$$

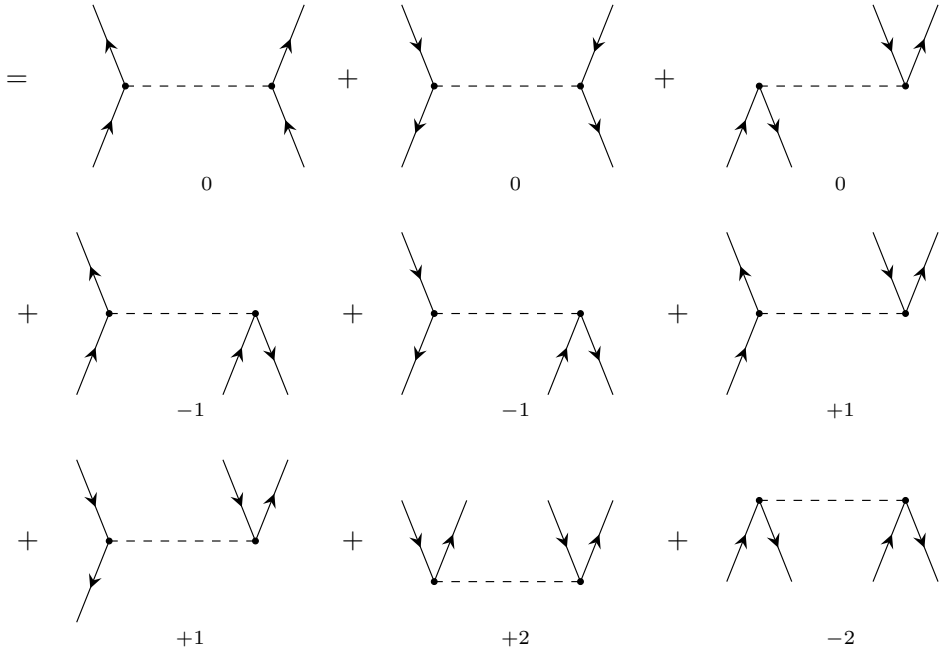

FIGURE 2.4: Diagrammatic representation of each fragment of the normal-ordered fluctuation potential $\hat{V}_{\mathrm{N}}$. The excitation level of each fragment is given below the diagram itself.

$$\hat{T}_1 = \sum_{ia} t_i^a\{\hat{a}_a^\dagger\hat{a}_i\} =$$

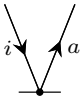

$$+1$$

$$\hat{T}_1^\dagger = \sum_{ia} t_i^{a*}\{\hat{a}_i^\dagger\hat{a}_a\} =$$

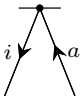

$$-1$$

$$\hat{T}_2 = \frac{1}{4}\sum_{ijab} t_{ij}^{ab}\{\hat{a}_a^\dagger\hat{a}_b^\dagger\hat{a}_j\hat{a}_i\} =$$

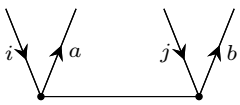

$$+2$$

$$\hat{T}_2^\dagger = \frac{1}{4}\sum_{ijab} t_{ij}^{ab*}\{\hat{a}_i^\dagger\hat{a}_j^\dagger\hat{a}_b\hat{a}_a\} =$$

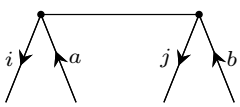

$$-2$$

FIGURE 2.5: Diagrammatic representation of the cluster operators $\hat{T}_1$ and $\hat{T}_2$ and their Hermitian conjugates $\hat{T}_1^\dagger$ and $\hat{T}_2^\dagger$. The excitation level of each fragment is given on its right.

A similar analysis can be applied to the third diagram fragment of $\hat{V}_\mathrm{N}$ in Figure 2.4, which contains pairs of particle-hole lines both above and below the interaction line which may be interpreted as singly-excited determinants and thus as the general matrix element $\langle\Phi_i^a|\hat{V}_\mathrm{N}|\Phi_j^b\rangle$.[9] Matrix elements like these play an important role for excited-state theories such as EOM-CC or UCC and will be discussed in more detail later. As in Ref. 9, I make use of the "excitation level" bookkeeping system[102] that is determined by half of the difference between the number of q-creation and q-annihilation lines. If one line is above and one is below a certain vertex in an interaction line, no net exctation or deexcitation is produced and the excitation level for this vertex is thus 0, whereas if both lines are above or below the interaction line the excitation level for this vertex is $+1$ or -1, respectively. To get the total excitation level of an operator fragment, all corresponding vertex excitation levels must be summed.

2.6.5 Diagrammatic Representation of the CC Energy Equation

As was seen earlier, many of the contractions resulting from the application of Wick's theorem generate mathematically redundant terms that can be combined after tedious manipulations to eventually give a much simpler result. Diagrams provide a straightforward way to eliminate these redundancies.[9] The CCSD energy equation was previously derived using Wick's theorem to yield Eq. (2.150). Each term of the general expression (2.146) is a matrix element of a component of $\bar{H} = e^{-\hat{T}}\hat{H}_\mathrm{N}e^{\hat{T}}$ with the HF determinant on both sides. Since $|\Phi_0\rangle$ is depicted diagrammatically by empty space, the diagrams involved in the energy equation must not contain directed lines above or below the first (lowest) or last (highest) operator interaction lines, which means that the diagrams contain no so-called "external lines". Obviously, no fragment of $\hat{H}_\mathrm{N}$ as shown in Figures 2.3 and 2.4 satisfies this criterion, and therefore they do not contribute to the CCSD correlation energy $E_0^\mathrm{CC} - E_0^\mathrm{HF}$, as expected, since all diagrams represent normal-ordered operators whose expectation value with the reference is zero, by construction.[9]

Next I consider the linear term in $\hat{T}_1$ from Eq. (2.146), $E_0^\mathrm{CC} \leftarrow \langle\Phi_0|(\hat{H}_\mathrm{N}\hat{T}_1)_\mathrm{c}|\Phi_0\rangle$, which was already evaluated by employing Wick's theorem in Eq. (2.147). The arrow indicates that the term to its right is only one of several contributions to E_0^CC to its left. The rightmost operator here is $\hat{T}_1$, so its interaction line must be the lowest one in the final diagram. By making use of the excitation levels associated with each operator fragment, the total excitation level of the final diagram must be 0 since the reference is found on both sides of the matrix element. As $\hat{T}_1$ has an excitation level of $+1$, the only fragments of the Hamiltonian that can possibly contribute are the ones with an excitation level of -1 and contain the reference at the top of the diagram. Of the $\hat{F}_\mathrm{N}$ and $\hat{V}_\mathrm{N}$ diagrams given before, only the third diagram of Figure 2.3 meets these criteria.

TABLE 2.1: Rules for the algebraic interpretation of coupled-cluster diagrams.[9]

1. All directed lines are labeled with appropriate indices, $i, j, k, l, \ldots$ for hole indices, $a, b, c, d, \ldots$ for particle indices.
2. Fock operator fragments contribute $f_{pq} = \langle \texttt{out}|\hat{F}|\texttt{in}\rangle$, where `out` indicates the index of the outgoing line and `in` the ingoing line at the interaction line's vertex.
3. Fluctuation potential fragments contribute an integral constructed by the rule $\langle pq||rs\rangle = \langle \texttt{left-out, right-out}||\texttt{left-in, right-in}\rangle$.
4. Cluster operators contribute amplitudes constructed using the hole and particle indices in left-to-right order from the diagram.
5. Summation over all internal indices, i.e. all indices of lines that start and end at an operator vertex.
6. The sign is determined from $(-1)^{h+l}$, where h is the number of hole lines in the diagram and l is the number of "loops", i.e. a route along a series of directed lines that either returns to its beginning or starts at one external line and ends at another.
7. Factor of $\frac{1}{2}$ for each pair of equivalent lines, i.e. lines that start at the same interaction line and end at the same interaction line. More generally, a factor of $\frac{1}{n!}$ for n equivalent lines needs to be included.
8. Factor of $\frac{1}{n!}$ for n equivalent vertices, i.e. vertices of equivalent cluster fragments that are connected to the same interaction line in the same manner.
9. Permutation function $\hat{\mathcal{P}}(pq) = 1 - \hat{P}_{pq}$ for each pair of unique external hole or particle lines, to ensure antisymmetry of the final expression.

Thus, the $\hat{T}_1$ diagram may be connected with this $\hat{F}_\mathrm{N}$ fragment to obtain

$$\langle \Phi_0|(\hat{F}_\mathrm{N}\hat{T}_1)_\mathrm{c}|\Phi_0\rangle =$$ 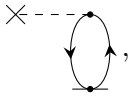 , (2.154)

where all lines from the $\hat{T}_1$ fragment must be connected to each line from the $\hat{F}_\mathrm{N}$ fragment in order to avoid open lines.

The set of rules to interpret the CC diagrams algebraically are summarized in Table 2.1.[9] According to rule 1, the downward-directed hole line gets the index i whereas the upward-directed particle line gets the index a. Rules number 2 and 4 thus say that the Fock operator contributes the matrix element f_{ia} and the cluster operator the amplitude t_i^a. Since both lines are internal lines, rule 5 states that one must sum over both indices. The last rule necessary here is number 6, which says that the sign is positive since there is one loop and one hole line i and thus $(-1)^{h+l} = (-1)^{1+1} = +1$. Hence, he final algebraic

interpretation of the diagram is

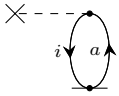

$$= \sum_{ia} f_{ia}\, t_i^a \,, \tag{2.155}$$

which is identical to the result in Eq. (2.147) obtained earlier using Wick's theorem.

Now consider the term linear in $\hat{T}_2$ of Eq. (2.146), $E_0^{\mathrm{CC}} \leftarrow \langle\Phi_0|(\hat{H}_{\mathrm{N}}\hat{T}_2)_{\mathrm{c}}|\Phi_0\rangle$, which was evaluated in Eq. (2.148). The cluster operator is at the bottom of the diagram since it is the rightmost operator in the expression, and since it produces an excitation level of +2, a Hamiltonian fragment with an excitation level of −2 with no open lines above the interaction bar is needed in order to obtain a total excitation level of 0. The only $\hat{H}_{\mathrm{N}}$ diagram fulfilling these criteria is the last diagram of Figure 2.4 that contains four q-annihilation lines.[9] The most straightforward way to connect these two diagrams without leaving any open lines is

$\langle\Phi_0|(\hat{V}_{\mathrm{N}}\hat{T}_2)_{\mathrm{c}}|\Phi_0\rangle =$

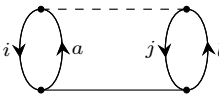

$$= \frac{1}{4}\sum_{ijab}\langle ij||ab\rangle\, t_{ij}^{ab} \,, \tag{2.156}$$

where the algebraic interpretation proceeded as follows. According to rule 7, the diagram has two pairs of equivalent lines, since i and j as well as a and b start and end at the same interaction line, giving a factor of $\frac{1}{2}$ each, thus yielding a total prefactor of $\frac{1}{4}$. All four lines are internal lines, thus one must sum over all of them (rule 5). Rule 3 states that the fluctuation potential contributes and integral $\langle ij||ab\rangle$ and rule 4 that the cluster operator contributes an amplitude t_{ij}^{ab}. Since there are two loops and two hole lines (i and j), according to rule 6 the total sign of the final expression is positive. Hence, the final result is again identical to the one obtained in Eq. (2.148). The lines could in principle also be connected in a different way, with two lines crossing each other in the middle, but since all operators are antisymmetric and due to slight changes in the interpretation of rule 6, the final expression is equivalent to the above way of drawing the diagram.[9]

The last contribution to the energy in Eq. (2.146) is the one quadratic in $\hat{T}_1$, which reads $E_0^{\mathrm{CC}} \leftarrow \frac{1}{2}\langle\Phi_0|(\hat{H}_{\mathrm{N}}\hat{T}_1^2)_{\mathrm{c}}|\Phi_0\rangle$. The same obersvations concerning the excitation levels hold as in the previous matrix elements, since $\hat{T}_1^2$ also excites two electrons. The cluster operators act before the Hamiltonian, thus they are placed at the bottom of the diagram, but since they commute, their vertical alignment is not of importance.[9] The diagram is thus given as

$\frac{1}{2}\langle\Phi_0|(\hat{V}_{\mathrm{N}}\hat{T}_1^2)_{\mathrm{c}}|\Phi_0\rangle =$

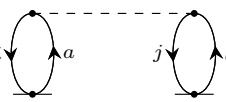

$$= \frac{1}{2}\sum_{ijab}\langle ij||ab\rangle\, t_i^a\, t_j^b \,, \tag{2.157}$$

where the algebraic interpretation is analogous to the previous diagram with the exception of the prefactor. There are two particle and two hole indices, which are all summation indices, and two loops, making the overall sign positive. The two-electron integral

stemming from $\hat{V}_\mathrm{N}$ is again $\langle ij||ab\rangle$, but now there are two amplitude fragments, one providing an amplitude t_i^a and the other t_j^b. However, the two pairs of particle and hole lines are no longer equivalent as in Eq. (2.156), but according to rule 8 the two $\hat{T}_1$ vertices are connected to the same $\hat{V}_\mathrm{N}$ interaction line in exactly the same manner, by a hole and a particle line each, thus the prefactor is $\frac{1}{2}$.[9] The result is again identical to the one obtained in Eq. (2.149). From this diagrammatic point of view it is also clearer that no higher-order terms of the BCH expansion can contribute to the CC energy, since all remaining terms contain cluster operators or operator products that produce excitation levels higher than +2, which cannot be cancelled by $\hat{H}_\mathrm{N}$ fragments to yield the required total excitation level of 0.[9] A diagrammatic summation of Eqs. (2.155), (2.156) and (2.157) thus yields the same result for the CC energy as Eq. (2.150) derived by using Wick's theorem.

2.6.6 The CCSD Amplitude Equations

By employing the same concepts as in Section 2.6.5, explicit expressions for the CCSD amplitude equations may be obtained. The corresponding matrix elements of $\bar{H}$ always contain $|\Phi_0\rangle$ on the right and an excited determinant, $\langle\Phi_i^a|$ for the $\hat{T}_1$ and $\langle\Phi_{ij}^{ab}|$ for the $\hat{T}_2$ equations, on the left. Hence, the corresponding diagrams have no q-annihilation lines below the diagram but either one or two pairs of q-creation lines above to match the total excitation level of +1 or +2 for the respective excited determinants.[9]

The leading term of $\bar{H}$ is just the bare electronic Hamiltonian $\hat{H}_\mathrm{N}$ itself. For the $\hat{T}_1$ amplitude equation, the matrix element $\langle\Phi_i^a|\hat{F}_\mathrm{N}+\hat{V}_\mathrm{N}|\Phi_0\rangle$ must be evaluated. Since the reference determinant is on the right and a singly-excited determinant on the left, those fragments of $\hat{H}_\mathrm{N}$ with an excitation level of +1 and no lines below the interaction line are required. The only diagram from Figures 2.3 and 2.4 is the fourth fragment of the Fock operator $\hat{F}_\mathrm{N}$, while $\hat{V}_\mathrm{N}$ cannot contribute in this case. The algebraic interpretation of the diagram proceeds as follows. The two lines are labeled using i and a to be consistent with the singly excited determinant $\langle\Phi_i^a|$ on the left of the matrix element. There is no summation since there are no internal lines; $\hat{F}_\mathrm{N}$ contributes the corresponding matrix element f_{ai}. There is one loop that starts at one external line and ends at the other, and one hole line, so the overall sign is positive. This finally gives[9]

$$\langle\Phi_i^a|\hat{F}_\mathrm{N}|\Phi_0\rangle =$$ 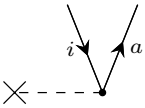 $$= f_{ai}\,. \tag{2.158}$$

For the contribution of $\hat{H}_\mathrm{N}$ to the $\hat{T}_2$ amplitude equation the matrix element $\langle\Phi_{ij}^{ab}|\hat{F}_\mathrm{N}+\hat{V}_\mathrm{N}|\Phi_0\rangle$ must be evaluated, which contains the reference determinant on the right and a doubly-excited determinant on the left, which means a Hamiltonian fragment with an excitation level of +2 and without q-annihilation operators is required. This requirement is only fulfilled by the eighth diagram in Figure 2.4, the algebraic interpretation of

which is analogous:[9] the lines are labeled in the order i, a, j, b to be consistent with the doubly-excited determinant, there are no internal lines and thus no summation indices, the fluctuation potential contributes the corresponding integral $\langle ab||ij\rangle$ and since there are two loops and two hole lines, the sign of the final expression is positive. Hence, the matrix element may be written as

$$\langle \Phi_{ij}^{ab}|\hat{V}_\mathrm{N}|\Phi_0\rangle = \quad = \langle ab||ij\rangle \tag{2.159}$$

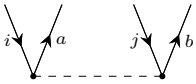

The next term considered here is the matrix element $\langle \Phi_i^a|((\hat{F}_\mathrm{N} + \hat{V}_\mathrm{N})\hat{T}_1)_\mathrm{c}|\Phi_0\rangle$, where Hamiltonian fragments with an excitation level of 0 are required. While both fragments of the Fock operator in Figure 2.3 can contribute, the first two possible fragments of the fluctuation potential in Figure 2.4 cannot contribute because they would leave an open line below the diagram, which violates the condition that empty space for $|\Phi_0\rangle$ must be beneath the diagram. Thus, only the third fragment with an excitation level of 0 from $\hat{V}_\mathrm{N}$ can contribute. The two diagrams including the Fock operator and their algebraic interpretation are given as

$$\langle \Phi_i^a|(\hat{F}_\mathrm{N}\hat{T}_1)_\mathrm{c}|\Phi_0\rangle = \quad + \quad = \sum_b f_{ab}\, t_i^b - \sum_j f_{ji}\, t_j^a\,, \tag{2.160}$$

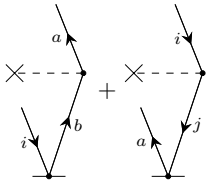

where the first diagram has a positive sign since it has one loop and one hole line, the second one a negative sign because it has one loop and two hole lines. The corresponding diagram including $\hat{V}_\mathrm{N}$ and its interpretation are given as

$$\langle \Phi_i^a|(\hat{V}_\mathrm{N}\hat{T}_1)_\mathrm{c}|\Phi_0\rangle = \quad = \sum_{jb}\langle ja||bi\rangle\, t_j^b\,, \tag{2.161}$$

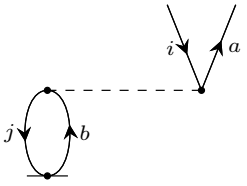

where the sign is positive because there are two loops and two hole lines.

Next, consider the contribution of the corresponding term linear in $\hat{T}_1$ to the doubles equation, $\langle \Phi_{ij}^{ab}|(\hat{H}_\mathrm{N}\hat{T}_1)_\mathrm{c}|\Phi_0\rangle$. Due to the doubly-excited determinant on the left, an overall excitation level of +2 is needed. Since the $\hat{T}_1$ fragment produces a +1 excitation, Hamiltonian fragments with an excitation level of +1 are needed to fulfill the requirement. In principle, there is a +1 Fock operator fragment in Figure 2.3, but this cannot be connected to the $\hat{T}_1$ operator from below and this thus violates the "connected cluster" form of $e^{-\hat{T}}\hat{H}_\mathrm{N}e^{\hat{T}} = (\hat{H}_\mathrm{N}e^{\hat{T}})_\mathrm{c}$.[9] The only contributions come from the two +1 fragments of Figure 2.4, both of which produce diagrams with a pair of unique external particle or hole lines, thus a permutation function needs to be included according to rule 9 (Table 2.1

on page 44) to maintain the antisymmetry of the entire equation.[9] The two final diagrams and their algebraic interpretations are given as

$$\langle \Phi_{ij}^{ab} | (\hat{V}_\mathrm{N} \hat{T}_1)_\mathrm{c} | \Phi_0 \rangle = \quad + \tag{2.162}$$

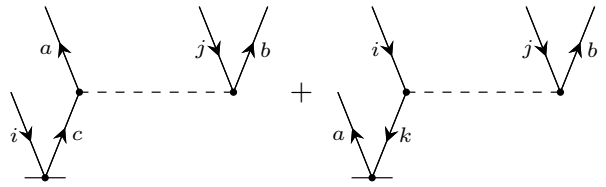

$$= \hat{\mathcal{P}}(ij) \sum_c \langle ab||cj\rangle \, t_i^c \qquad - \; \hat{\mathcal{P}}(ab) \sum_k \langle kb||ij\rangle \, t_k^a \,,$$

where the first term has two loops and two hole lines and thus a positive sign, whereas the second term has two loops and three hole lines and thus an overall negative sign.

The above procedure can be carried out for the remaining terms of the CCSD amplitude equations,[9,11] but this is rather lengthy and thus omitted here. The final equation for the $\hat{T}_1$ amplitudes are given as[9]

$$\begin{aligned}
0 = {} & f_{ai} + \sum_c f_{ac} t_i^c - \sum_k f_{ki} t_k^a + \sum_{kc} \langle ka||ci\rangle t_k^c + \sum_{kc} f_{kc} t_{ik}^{ac} \\
& + \frac{1}{2} \sum_{kcd} \langle ka||cd\rangle t_{ki}^{cd} - \frac{1}{2} \sum_{klc} \langle kl||ci\rangle t_{kl}^{ca} - \sum_{kc} f_{kc} t_i^c t_k^a \\
& - \sum_{klc} \langle kl||ci\rangle t_k^c t_l^a - \sum_{kcd} \langle ka||cd\rangle t_k^c t_i^d - \sum_{klcd} \langle kl||cd\rangle t_k^c t_i^d t_l^a \\
& + \sum_{klcd} \langle kl||cd\rangle t_k^c t_{li}^{da} - \frac{1}{2} \sum_{klcd} \langle kl||cd\rangle t_{ki}^{cd} t_l^a - \frac{1}{2} \sum_{klcd} \langle kl||cd\rangle t_{kl}^{ca} t_i^d \,,
\end{aligned} \tag{2.163}$$

and for the $\hat{T}_2$ amplitudes, showing only the leading terms[9]

$$\begin{aligned}
0 = {} & \langle ab||ij\rangle + \sum_c (f_{bc} t_{ij}^{ac} - f_{ac} t_{ij}^{bc}) - \sum_k (f_{kj} t_{ik}^{ab} - f_{ki} t_{jk}^{ab}) + \frac{1}{2} \sum_{kl} \langle kl||ij\rangle t_{kl}^{ab} \\
& + \frac{1}{2} \sum_{cd} \langle ab||cd\rangle t_{ij}^{ab} + \hat{\mathcal{P}}(ij) \hat{\mathcal{P}}(ab) \sum_{kc} \langle kb||cj\rangle t_{ik}^{ac} + \hat{\mathcal{P}}(ij) \sum_c \langle ab||cj\rangle t_i^c \\
& - \hat{\mathcal{P}}(ab) \sum_k \langle kb||ij\rangle t_k^a + \frac{1}{2} \hat{\mathcal{P}}(ij) \hat{\mathcal{P}}(ab) \sum_{klcd} \langle kl||cd\rangle t_{ik}^{ac} t_{lj}^{db} + \frac{1}{4} \sum_{klcd} \langle kl||cd\rangle t_{ij}^{cd} t_{kl}^{ab} \\
& - \frac{1}{2} \hat{\mathcal{P}}(ab) \sum_{klcd} \langle kl||cd\rangle t_{ij}^{ac} t_{kl}^{bd} - \frac{1}{2} \hat{\mathcal{P}}(ij) \sum_{klcd} \langle kl||cd\rangle t_{ik}^{ab} t_{jl}^{cd} + \dots \,.
\end{aligned} \tag{2.164}$$

2.6.7 Connection to MP Perturbation Theory

As originally pointed out by Bartlett,[70,104] coupled-cluster theory is closely connected to Møller–Plesset perturbation theory in the sense that one may obtain finite-order perturbation theory energies and wave functions via the iterations of the CC equations.[9] For this, the normal-ordered electronic Hamiltonian is again split into the zeroth-order component taken as the Fock operator, and the perturbation as the remaining two-electron

operator, $\hat{H}_\mathrm{N} = \hat{F}_\mathrm{N} + \hat{V}_\mathrm{N}$, and each perturbed wave function $|\Psi_0^{(k)}\rangle$ is expanded in a CI-like fashion according to Eq. (2.79). As mentioned in Section 2.4, in low orders of perturbation theory only modest excitation levels are needed for the wave-function expansion. The first-order correction $|\Psi_0^{(1)}\rangle$, for example, only contains doubly-excited determinants and can be used to calculate the second- and third-order energy corrections, whereas the second-order wave function $|\Psi_0^{(2)}\rangle$ contains from singly- up to quadruply-excited determinants and contributes to the fourth- and fifth-order energy corrections.[9] This determinant-based expansion of $|\Psi_0^{(k)}\rangle$ suggests that also the cluster operators $\hat{T}_n$ may be decomposed by order of perturbation theory as

$$\hat{T}_n = \hat{T}_n^{(1)} + \hat{T}_n^{(2)} + \hat{T}_n^{(3)} + \dots \,, \tag{2.165}$$

where the low-order terms for certain excitation levels are naturally zero.[9] By employing the partitioning of $\hat{H}_\mathrm{N}$ and the expansion of the cluster operators (2.165), the CC Hamiltonian $\bar{H}$ may analogously expanded in orders of perturbation theory through the BCH expansion, $\bar{H} = \bar{H}^{(0)} + \bar{H}^{(1)} + \bar{H}^{(2)} + \dots$, where the lowest orders are given as[9]

$$\bar{H}^{(0)} = \hat{F}_\mathrm{N} \tag{2.166a}$$

$$\bar{H}^{(1)} = \hat{V}_\mathrm{N} + (\hat{F}_\mathrm{N}\hat{T}_2^{(1)})_\mathrm{c} \tag{2.166b}$$

$$\bar{H}^{(2)} = (\hat{F}_\mathrm{N}\hat{T}_1^{(2)} + \hat{V}_\mathrm{N}\hat{T}_2^{(1)} + \frac{1}{2}\hat{F}_\mathrm{N}(\hat{T}_2^{(1)})^2)_\mathrm{c} \,, \tag{2.166c}$$

which is simply constructed by assigning the appropriate perturbational order to each cluster operator in Eq. (2.144) and retaining only the terms of the desired order n.[9] The n-th order Schrödinger equation may then be constructed from the respective $\bar{H}^{(n)}$ as

$$\bar{H}^{(n)}|\Phi_0\rangle = E_0^{(n)}|\Phi_0\rangle \,, \tag{2.167}$$

from which the n-th order MP energy contribution may be calculated via projection on the HF reference, $E_0^{(n)} = \langle\Phi_0|\bar{H}^{(n)}|\Phi_0\rangle$. The n-th order cluster amplitudes are obtained by projecting the n-th order Schrödinger equation onto the respective excited determinants.[9] For instance, the first-order $\hat{T}_2$ amplitudes are obtained by projecting the first-order variant of Eq. (2.167) onto a doubly-excited determinant, analogous to the CC amplitude equations,

$$0 = \langle\Phi_{ij}^{ab}|\bar{H}^{(1)}|\Phi_0\rangle = \langle\Phi_{ij}^{ab}|\hat{V}_\mathrm{N}|\Phi_0\rangle + \langle\Phi_{ij}^{ab}|(\hat{F}_\mathrm{N}\hat{T}_2^{(1)})_\mathrm{c}|\Phi_0\rangle \,, \tag{2.168}$$

which may also be evaluated diagrammatically[9] to obtain the identical amplitudes $t_{ijab}^{(1)}$ as in Eq. (2.82). Another way to obtain the lowest-order cluster amplitudes is directly from the CCSD amplitude equations. Assuming a canonical HF reference, the Fock matrix is diagonal with orbital energies as diagonal elements, $f_{ij} = \delta_{ij}\varepsilon_i$ and $f_{ab} = \delta_{ab}\varepsilon_a$. The amplitude equations (2.163) and (2.164) may thus be rewritten by taking the terms

involving orbital energies on the other side as

$$\begin{aligned}(\varepsilon_i - \varepsilon_a) t_i^a &= f_{ai} + \sum_{kc} \langle ka||ci\rangle t_k^c + \sum_{kc} f_{kc} t_{ik}^{ac} \\ &\quad + \frac{1}{2}\sum_{kcd} \langle ka||cd\rangle t_{ki}^{cd} - \frac{1}{2}\sum_{klc} \langle kl||ci\rangle t_{kl}^{ca} + \dots \end{aligned} \tag{2.169a}$$

$$\begin{aligned}(\varepsilon_i + \varepsilon_j - \varepsilon_a - \varepsilon_b) t_{ij}^{ab} &= \langle ab||ij\rangle + \frac{1}{2}\sum_{kl} \langle kl||ij\rangle t_{kl}^{ab} \\ &\quad + \frac{1}{2}\sum_{cd} \langle ab||cd\rangle t_{ij}^{ab} + \hat{\mathcal{P}}(ij)\hat{\mathcal{P}}(ab) \sum_{kc} \langle kb||cj\rangle t_{ik}^{ac} \\ &\quad + \hat{\mathcal{P}}(ij) \sum_{c} \langle ab||cj\rangle t_i^c - \hat{\mathcal{P}}(ab) \sum_{k} \langle kb||ij\rangle t_k^a + \dots \end{aligned} \tag{2.169b}$$

By setting all amplitudes on the RHS of the above equations initially to zero, successive division by the orbital-energy differences yields the first-order amplitudes as

$$t_{ia}^{(1)} = \frac{f_{ai}}{\varepsilon_i - \varepsilon_a} \tag{2.170a}$$

$$t_{ijab}^{(1)} = \frac{\langle ab||ij\rangle}{\varepsilon_i + \varepsilon_j - \varepsilon_a - \varepsilon_b}\,, \tag{2.170b}$$

where the first-order singles $t_{ia}^{(1)} = 0$ as long as Brillouin's theorem holds, and $t_{ijab}^{(1)}$ is again identical to Eq. (2.82). Plugging these first-order amplitudes into the linear terms in Eqs. (2.169a) and (2.169b), the second-order amplitudes are obtained as

$$\begin{aligned} t_{ia}^{(2)} &= \frac{1}{\varepsilon_i - \varepsilon_a}\Big[\sum_{kc} \langle ka||ci\rangle t_{kc}^{(1)} + \sum_{kc} f_{kc} t_{ikac}^{(1)} \\ &\quad + \frac{1}{2}\sum_{kcd} \langle ka||cd\rangle t_{kicd}^{(1)} - \frac{1}{2}\sum_{klc} \langle kl||ci\rangle t_{klca}^{(1)} \Big] \end{aligned} \tag{2.171a}$$

$$\begin{aligned} t_{ijab}^{(2)} &= \frac{1}{\varepsilon_i + \varepsilon_j - \varepsilon_a - \varepsilon_b}\Big[\frac{1}{2}\sum_{kl} \langle kl||ij\rangle t_{klab}^{(1)} + \frac{1}{2}\sum_{cd} \langle ab||cd\rangle t_{ijab}^{(1)} \\ &\quad + \hat{\mathcal{P}}(ij)\hat{\mathcal{P}}(ab) \sum_{kc} \langle kb||cj\rangle t_{ikac}^{(1)} \\ &\quad + \hat{\mathcal{P}}(ij) \sum_{c} \langle ab||cj\rangle t_{ic}^{(1)} - \hat{\mathcal{P}}(ab) \sum_{k} \langle kb||ij\rangle t_{ka}^{(1)} \Big]\,, \end{aligned} \tag{2.171b}$$

where the first two terms in brackets of Eq. (2.171a) and the last two terms of Eq. (2.171b) are zero for a HF reference.

2.6.8 Equation-of-Motion Coupled-Cluster Theory

Let me turn the attention to the calculation of excited electronic states with coupled-cluster theory. Several schemes have been developed over the last decades, the most prominent being **equation-of-motion coupled-cluster** (EOM-CC)[12–15] and **coupled-cluster**

linear response (CCLR) theory.[16–19] Despite their conceptual differences, EOM-CC and CCLR yield identical results for excitation energies and may be viewed as **biorthogonal representations** (BCC) of the (shifted) Hamiltonian in terms of correlated excited states obtained from the CC ground state and an associated set of biorthogonal states, which correspond essentially to excited determinants used in CI theory.[20,21] I restrict myself to a more detailed discussion of EOM-CC in the following.

In equation-of-motion theory, the wave function $|\Psi_n\rangle$ of the n-th excited state is written as

$$|\Psi_n\rangle = \hat{R}|\Psi_0\rangle\,, \tag{2.172}$$

where $|\Psi_0\rangle$ is the ground-state wave function and $\hat{R}$ is an excitation operator that transforms the ground-state into the excited-state wave function and thus describes differences in orbitals, correlation, etc. upon excitation. In EOM-CC, the ground state is taken as Eq. (2.62), $|\Psi_0^{\mathrm{CC}}\rangle = e^{\hat{T}}|\Phi_0\rangle$, and the excitation operator is parameterized the same way as the cluster operator, as a linear combination of excitation operators

$$\hat{R} = \hat{R}_0 + \hat{R}_1 + \hat{R}_2 + \ldots \tag{2.173}$$

$$\hat{R}_0 = r_0 \tag{2.174}$$

$$\hat{R}_1 = \sum_{ia} r_i^a\, \hat{a}_a^\dagger \hat{a}_i \tag{2.175}$$

$$\hat{R}_2 = \frac{1}{4}\sum_{ijab} r_{ij}^{ab}\, \hat{a}_a^\dagger \hat{a}_b^\dagger \hat{a}_j \hat{a}_i\,, \tag{2.176}$$

and so on, where the unknown parameters are the amplitudes of $\hat{R}$. If no approximations are introduced, this corresponds to an exact parametrization of the excited-state wave function.

In order to obtain equations for $\hat{R}$, the EOM-CC ansatz is plugged into the electronic Schrödinger equation for some excited state with energy E_{exc}

$$\hat{H}\hat{R}\, e^{\hat{T}}|\Phi_0\rangle = E_{\mathrm{exc}}\, \hat{R}\, e^{\hat{T}}|\Phi_0\rangle\,, \tag{2.177}$$

exploit that the physical excitation operators $\hat{R}$ and $\hat{T}$ commute and multiply from the left by $e^{-\hat{T}}$ to obtain

$$e^{-\hat{T}}\hat{H}e^{\hat{T}}\, \hat{R}|\Phi_0\rangle = E_{\mathrm{exc}}\, \hat{R}|\Phi_0\rangle\,, \tag{2.178}$$

which can be seen as an eigenvalue problem for the similarity-transformed Hamiltonian $\bar{H} = e^{-\hat{T}}\hat{H}e^{\hat{T}}$ with eigenvalue E_{exc} and eigenfunction $\hat{R}|\Phi_0\rangle$. The eigenvalue equation (2.178) can further be rewritten by applying $\hat{R}$ to the ground-state CC equation (2.133)

$$\hat{R}\, e^{-\hat{T}}\hat{H}e^{\hat{T}}|\Phi_0\rangle = \hat{R}E_0^{\mathrm{CC}}|\Phi_0\rangle \tag{2.179}$$

and subtract the two equations to obtain an equation directly for the excitation energy $\omega = E_{\text{exc}} - E_0^{\text{CC}}$ as

$$\big(e^{-\hat{T}}\hat{H}e^{\hat{T}}\hat{R} - \hat{R}e^{-\hat{T}}\hat{H}e^{\hat{T}}\big)|\Phi_0\rangle = \omega\hat{R}|\Phi_0\rangle\,, \tag{2.180}$$

which can be written more compactly as

$$\big[\bar{H},\hat{R}\big]|\Phi_0\rangle = \omega\hat{R}|\Phi_0\rangle\,. \tag{2.181}$$

By expanding the commutator to $(\bar{H}\hat{R} - \hat{R}\bar{H})$ and inserting the **resolution of the identity** (RI) $1 = |\Phi_0\rangle\langle\Phi_0| + \sum_I |\Phi_I\rangle\langle\Phi_I|$ between $\hat{R}$ and $\bar{H}$, one obtains

$$\big[\bar{H}\hat{R} - \hat{R}\big(|\Phi_0\rangle\langle\Phi_0| + \sum_I |\Phi_I\rangle\langle\Phi_I|\big)\bar{H}\big]|\Phi_0\rangle = \omega\hat{R}|\Phi_0\rangle \tag{2.182}$$

$$\bar{H}\hat{R}|\Phi_0\rangle - \hat{R}|\Phi_0\rangle\langle\Phi_0|\bar{H}|\Phi_0\rangle - \sum_I \hat{R}|\Phi_I\rangle\langle\Phi_I|\bar{H}|\Phi_0\rangle = \omega\hat{R}|\Phi_0\rangle \tag{2.183}$$

$$\big(\bar{H} - \langle\Phi_0|\bar{H}|\Phi_0\rangle\big)\hat{R}|\Phi_0\rangle - \sum_I \hat{R}|\Phi_I\rangle \underbrace{\langle\Phi_I|\bar{H}|\Phi_0\rangle}_{=0} = \omega\hat{R}|\Phi_0\rangle\,, \tag{2.184}$$

where the sum vanishes due to the CC amplitude equations (2.137). By defining the normal-ordered similarity-transformed Hamiltonian as $\bar{H}_{\text{N}} = \bar{H} - \langle\Phi_0|\bar{H}|\Phi_0\rangle$, an eigenvalue problem directly for the excitation energy is obtained,

$$\bar{H}_{\text{N}}\hat{R}|\Phi_0\rangle = \omega\hat{R}|\Phi_0\rangle\,, \tag{2.185}$$

which is equivalent to FCI if no further approximations are introduced, since the effective Hamiltonian $\bar{H}$ used in EOM-CC is defined via similarity transformation that preserves the eigenvalues of the original operator. However, since it is not Hermitian anymore, the left eigenvectors are different from the right ones. The LHS eigenvalue problem of EOM-CC reads

$$\langle\Phi_0|\hat{L}\bar{H} = \langle\Phi_0|\hat{L}E_{\text{exc}}\,, \tag{2.186}$$

where $\hat{L}$ is a **deexcitation operator** defined as

$$\begin{aligned}
\hat{L} &= \hat{L}_0 + \hat{L}_1 + \hat{L}_2 + \ldots \\
\hat{L}_0 &= l_0 \\
\hat{L}_1 &= \sum_{ia} l_i^a\, \hat{a}_i^\dagger \hat{a}_a \\
\hat{L}_2 &= \frac{1}{4}\sum_{ijab} l_{ij}^{ab}\, \hat{a}_i^\dagger \hat{a}_j^\dagger \hat{a}_b \hat{a}_a\,,
\end{aligned} \tag{2.187}$$

and so on, where the amplitudes of the $\hat{R}$ and $\hat{L}$ operators are different, $r_I \neq l_I$. They are usually chosen to be **biorthogonal**,

$$\langle \Phi_0 | \hat{L}^m \hat{R}^n | \Phi_0 \rangle = \delta_{mn} \,, \tag{2.188}$$

where m and n are **state labels**. Orthogonality, on the ther hand, does not hold, $\langle \Phi_0 | (\hat{R}^m)^\dagger \hat{R}^n | \Phi_0 \rangle \neq \delta_{mn}$. The EOM-CC energy expression is thus a generalized expectation value of the form

$$E_{\text{exc}} = \langle \Phi_0 | \hat{L} \bar{H} \hat{R} | \Phi_0 \rangle = E_0^{\text{CC}} + \langle \Phi_0 | \hat{L} \bar{H}_{\text{N}} \hat{R} | \Phi_0 \rangle \,. \tag{2.189}$$

In order to obtain a **matrix representation** of EOM-CC, the corresponding eigenvalue equation $\bar{H}\hat{R}|\Phi_0\rangle = E_{\text{exc}}\,\hat{R}|\Phi_0\rangle$ is projected onto the determinant manifold $\langle \Phi_I|$ (including the HF state)

$$\langle \Phi_I | \bar{H} \hat{R} | \Phi_0 \rangle = E_{\text{exc}} \langle \Phi_I | \hat{R} | \Phi_0 \rangle \tag{2.190}$$

and insert the resolution of the identity between the operators on the left-hand side to obtain

$$\sum_J \langle \Phi_I | \bar{H} | \Phi_J \rangle \langle \Phi_J | \hat{R} | \Phi_0 \rangle = E_{\text{exc}} \langle \Phi_I | \hat{R} | \Phi_0 \rangle \,, \tag{2.191}$$

which can be written in matrix form as

$$\bar{\mathbf{H}}\,\mathbf{r} = E_{\text{exc}}\,\mathbf{r} \,, \tag{2.192}$$

where the elements of the matrix $\bar{\mathbf{H}}$ and the eigenvector $\mathbf{r}$ are given as

$$\bar{H}_{IJ} = \langle \Phi_I | \bar{H} | \Phi_J \rangle \qquad\qquad r_I = \langle \Phi_I | \hat{R} | \Phi_0 \rangle \,. \tag{2.193}$$

The corresponding LHS eigenvalue problem reads

$$\mathbf{l}^{\text{T}}\,\bar{\mathbf{H}} = \mathbf{l}^{\text{T}} E_{\text{exc}} \tag{2.194}$$

and the biorthogonality can be written as $(\mathbf{l}^m)^{\text{T}}\,\mathbf{r}^n = \delta_{mn}$ where m and n again are state labels and the expression for the energy then simply is $E_{\text{exc}} = \mathbf{l}^{\text{T}}\bar{\mathbf{H}}\mathbf{r}$.

By looking again at the eigenvalue equation (2.192) and the definition of the corresponding matrix elements in Eq. (2.193), it is immediately obvious that EOM-CC can be regarded as a CI approach with $\mathbf{H}$ replaced by $\bar{\mathbf{H}}$. Furthermore, it can be shown that excitation energies obtained with EOM-CC are **size intensive**,[11] which means they do not depend on the system size.[19] This is in contrast to other properties such as the ground-state energy, which was shown to be **size extensive**,[11] meaning it scales linearly with the size of the system.[105] The related term **size consistency** denotes that a quantum-chemical energy calculation on a system consisting of two fragments yields the sum of two individual calculations on the separate fragments.[68]

Due to the biorthogonality, the left- and right-hand **transition moments** differ in EOM-CC, and one can show that one of the two terms violates the size-consistency condition.[11,21,106] Transition moments obtained with CCLR theory, on the other hand, yield size-intensive results.[21,106]

As mentioned at the beginning of this section, both EOM-CC and CCLR can be regarded as a biorthogonal representation of the (shifted) Hamiltonian,[20] and thus an analogy to the intermediate state representation of Section 2.5.1 (page 25) can be established. Within BCC representations, the correlated excited states take the form[20]

$$|\bar{\Psi}_J^0\rangle = \hat{C}_J|\Psi_0^{\mathrm{CC}}\rangle = \hat{C}_J e^{\hat{T}}|\Phi_0\rangle = e^{\hat{T}}\hat{C}_J|\Phi_0\rangle\,, \tag{2.195}$$

where the physical excitation operators $\hat{C}_J$ are given by Eq. (2.89a). Unlike the ADC-ISR procedure, the CES of Eq. (2.195) are not orthogonalized, but instead a set of biorthogonal states $\langle\Psi_I^{\perp}|$ is introduced that obey the relation

$$\langle\Psi_I^{\perp}|\bar{\Psi}_J^0\rangle = \delta_{IJ}\,. \tag{2.196}$$

The CC form of $|\bar{\Psi}_J^0\rangle$ in Eq. (2.195) allows one to write the bra states explicitly as[20]

$$\langle\Psi_I^{\perp}| = \langle\Phi_0|\hat{C}_I^{\dagger}e^{-\hat{T}}\,. \tag{2.197}$$

The "mixed" representation of $\hat{H} - E_0$ defined with respect to the biorthogonal sets of states leads to the non-Hermitian secular matrix $\bar{\mathbf{M}}$, with the matrix elements

$$\bar{M}_{IJ} = \langle\Psi_I^{\perp}|\hat{H} - E_0|\bar{\Psi}_J^0\rangle = \langle\Phi_0|\hat{C}_I^{\dagger}e^{-\hat{T}}[\hat{H},\hat{C}_J]e^{\hat{T}}|\Phi_0\rangle\,, \tag{2.198}$$

where the ground-state energy is no longer explicit in the last equation. The resulting secular equation

$$\bar{\mathbf{M}}\mathbf{X} = \mathbf{X}\boldsymbol{\Omega} \tag{2.199}$$

is used both in the CCLR[18] and EOM-CC methods.[13] Here, $\boldsymbol{\Omega}$ is the diagonal matrix of excitation energies and $\mathbf{X}$ is the matrix of right-hand eigenvectors. Due to the non-Hermitian nature of the secular matrix, an analogous equation arises for the matrix $\mathbf{Y}$ of the left-hand eigenvectors $\mathbf{Y}^{\dagger}\bar{\mathbf{M}} = \boldsymbol{\Omega}\mathbf{Y}^{\dagger}$. Both equations can be combined to

$$\mathbf{Y}^{\dagger}\bar{\mathbf{M}}\mathbf{X} = \boldsymbol{\Omega}\,, \quad \mathbf{Y}^{\dagger}\mathbf{X} = \mathbf{1}\,, \tag{2.200}$$

where it should be noted that the left-hand and right-hand eigenvectors are biorthogonal but in general not normalized.[20] The CI-like definition of the matrix $\bar{\mathbf{H}}$ and the ISR approach described here can be shown to be equivalent via

$$\bar{H}_{IJ} = \langle\Phi_I|\bar{H}|\Phi_J\rangle = \langle\Phi_0|\hat{C}_I^{\dagger}e^{-\hat{T}}\hat{H}e^{\hat{T}}\hat{C}_I|\Phi_0\rangle = \langle\Psi_I^{\perp}|\hat{H}|\bar{\Psi}_J^0\rangle = \bar{M}_{IJ} + E_0^{\mathrm{CC}}\delta_{IJ}\,. \tag{2.201}$$

By choosing the excitation operators $\hat{C}_J$ in Eqs. (2.195) and (2.197) as the ones from Eq. (2.89b) or (2.89c), or by adapting the respective $\hat{R}$ and $\hat{L}$ operators, the EOM approach can also be applied to obtain ionization potentials and electron affinities, for instance, giving rise to the EOM-IP-CC and EOM-EA-CC methods, respectively.[107–112]

Another closely related scheme is the **symmetry-adapted-cluster configuration interaction** (SAC-CI) method[113–115] that is based on the mixed representation

$$M_{IJ}^{\mathrm{SAC}} = \langle \Phi_I | \hat{H} - E_0 | \bar{\Psi}_J^0 \rangle \,, \tag{2.202}$$

where CI configurations $\langle \Phi_I | = \langle \Phi_0 | \hat{C}_I^\dagger$ and the CC correlated excited states (2.195) are used on the left- and right-hand sides, respectively. The overlap matrix $S_{IJ} = \langle \Phi_I | \bar{\Psi}_J^0 \rangle$ of the left- and right-hand basis functions is of lower triangular form. The right-hand form of the SAC-CI secular equations read[20]

$$\mathbf{M}^{\mathrm{SAC}}\mathbf{X} = \mathbf{S}\mathbf{X}\boldsymbol{\Omega} \,, \tag{2.203}$$

where $\boldsymbol{\Omega}$ is the diagonal matrix of excitation energies and $\mathbf{X}$ denotes the matrix of right-hand eigenvectors. An analogous equation applies to the matrix $\mathbf{Y}$ of left-hand eigenvectors. A mutual orthogonalization is obtained via $\mathbf{Y}^\dagger\mathbf{S}\mathbf{X} = \mathbf{1}$. If the configuration spaces extend to the same excitation class and $\exp(\hat{T})$ is treated in the same way, the SAC-CI and BCC treatments give the same results for the energies, even though the equations differ.[20]

2.6.9 Alternative Coupled-Cluster Ansätze

Although it is the most commonly used, the standard formulation of the CC equations according to Eqs. (2.136) and (2.137), it is only one possible formulation for the correlation problem built upon an exponential wave-function ansatz. Several other formulations exist and have been discussed by Bartlett and co-workers.[34,35,37,116,117]

The first one, that has already been mentioned is the variational **expectation-value coupled-cluster** (XCC) method,[34,117] that uses an energy functional as given in Eq. (2.128). It has been shown that this expression can be written in a fully linked (connected) and extensive form as[118,119]

$$E_0^{\mathrm{XCC}} = \langle \Phi_0 | (e^{\hat{T}^\dagger} \hat{H} e^{\hat{T}})_{\mathrm{c}} | \Phi_0 \rangle \,, \tag{2.204}$$

which is the starting point for finite-order XCC(n) approaches[34,117] and noniterative corrections to lower-order CC methods.[120] Eq. (2.204) is an exact energy expression, but the finite character of Eq. (2.128) is lost.[35,116]

The linear nature of the $\hat{\Lambda}$ operator in the CC energy functional (2.151) is the reason why effects of higher excitations are lost compared to XCC,[35] and also why transition moments in EOM-CC are not size consistent. Replacing $1 + \hat{\Lambda}$ by $e^{\hat{\Sigma}}$, where $\hat{\Sigma}$ is a

connected deexcitation operator that establishes the same relationship between $\hat{\Lambda}$ and $\hat{\Sigma}$ as between $\hat{C}^{\mathrm{CI}}$ and $\hat{T}$,[35] the resulting energy functional reads

$$E_0^{\mathrm{ECC}} = \langle \Phi_0 | (e^{\hat{\Sigma}} (\hat{H} e^{\hat{T}})_{\mathrm{c}})_{\mathrm{c}} | \Phi_0 \rangle \,, \tag{2.205}$$

which defines the **extended coupled-cluster** (ECC) energy.[121–127] The energy expression has a similar structure as XCC, but it should be noted that $\hat{\Sigma}$ is different from $\hat{T}^{\dagger}$.[35] Other methods include **symmetric expectation coupled-cluster** (SXCC),[117] **strongly-connected expectation-value coupled cluster** (SC-XCC),[35] nonvariational expectation-value coupled cluster[41] and, finally, **unitary coupled cluster** (UCC),[37,39,93,117,128–138] which will be discussed in great detail in Chapter 3.

Alternative excited-state approaches comprise **similarity-transformed equation-of-motion coupled cluster** (STEOM-CC),[139–143] where the CC Hamiltonian is similarity-transformed a second time with a transformation operator $\hat{\mathcal{S}}$ as $\bar{\bar{H}} = \{e^{\hat{\mathcal{S}}}\}^{-1} \bar{H} \{e^{\hat{\mathcal{S}}}\}$, **equation-of-motion expectation-value coupled cluster** (EOM-XCC),[144] and time-dependent variational (TD-VCC)[49] or unitary coupled cluster (TD-UCC).[50]

2.7 Molecular Properties

In order to set the stage for Chapter 7 (page 143), a brief review of the notions of molecular properties shall be given, following closely the one in Ref. 57. Having a molecular system with an electronic charge distribution $\rho(\mathbf{r})$ with an electric potential $\phi(\mathbf{r})$ gives an energy contribution $\mathcal{E}$

$$\mathcal{E} = \int \rho(\mathbf{r}) \phi(\mathbf{r}) \mathrm{d}\mathbf{r} \,. \tag{2.206}$$

Since the electric field $\boldsymbol{\mathcal{F}} = \partial\phi/\partial\mathbf{r}$ is normally uniform at the molecular level, $\mathcal{E}$ is written as a *multipole expansion*

$$\mathcal{E} = q\phi + \boldsymbol{\mu}\boldsymbol{\mathcal{F}} + \frac{1}{2}\mathbf{Q}\boldsymbol{\mathcal{F}}' + \dots \,, \tag{2.207}$$

where q is the net charge (monopole), $\boldsymbol{\mu}$ is the electric **dipole moment**, $\mathbf{Q}$ the **quadrupole moment** and $\boldsymbol{\mathcal{F}}' = \partial\boldsymbol{\mathcal{F}}/\partial\mathbf{r}$ the electric **field gradient**.[57] In the absence of an external field, the *unperturbed* dipole (and quadrupole) moments may be calculated from the electronic wave function $|\Psi_n\rangle$ as **expectation values** according to $\boldsymbol{\mu} = \langle \Psi_n | \hat{\mu} | \Psi_n \rangle$, where $\hat{\mu}$ is the dipole operator in second quantization. The presence of a field influences the wave function and leads to *induced* moments, which for the dipole moment $\boldsymbol{\mu}$ may be written as

$$\boldsymbol{\mu} = \boldsymbol{\mu}_0 + \boldsymbol{\alpha}\boldsymbol{\mathcal{F}} + \frac{1}{2}\boldsymbol{\beta}\boldsymbol{\mathcal{F}}^2 + \frac{1}{6}\boldsymbol{\gamma}\boldsymbol{\mathcal{F}}^3 + \dots \,, \tag{2.208}$$

where $\boldsymbol{\mu}_0$ is the permanent dipole moment, $\boldsymbol{\alpha}$ the dipole polarizability, $\boldsymbol{\beta}$ the first hyperpolarizability, $\boldsymbol{\gamma}$ the second hyperpolarizability, and so on.[57] For a *homogeneous field* $\boldsymbol{\mathcal{F}}$, where the derivatives of the field are zero, the total energy E of a neutral molecule

can be written as a Taylor series around $\boldsymbol{\mathcal{F}} = 0$ as

$$E(\boldsymbol{\mathcal{F}}) = E(0) + \left.\frac{\partial E}{\partial \boldsymbol{\mathcal{F}}}\right|_{\boldsymbol{\mathcal{F}}=0} \boldsymbol{\mathcal{F}} + \frac{1}{2} \left.\frac{\partial^2 E}{\partial \boldsymbol{\mathcal{F}}^2}\right|_{\boldsymbol{\mathcal{F}}=0} \boldsymbol{\mathcal{F}}^2 + \frac{1}{6} \left.\frac{\partial^3 E}{\partial \boldsymbol{\mathcal{F}}^3}\right|_{\boldsymbol{\mathcal{F}}=0} \boldsymbol{\mathcal{F}}^3 + \dots \tag{2.209}$$

From the multipole expansion (2.207) it can be seen that $\partial E/\partial \boldsymbol{\mathcal{F}} = \boldsymbol{\mu}$. Differentiating the above equation w.r.t. $\boldsymbol{\mathcal{F}}$ thus gives

$$\boldsymbol{\mu} = \left.\frac{\partial E}{\partial \boldsymbol{\mathcal{F}}}\right|_{\boldsymbol{\mathcal{F}}=0} + \left.\frac{\partial^2 E}{\partial \boldsymbol{\mathcal{F}}^2}\right|_{\boldsymbol{\mathcal{F}}=0} \boldsymbol{\mathcal{F}} + \frac{1}{2} \left.\frac{\partial^3 E}{\partial \boldsymbol{\mathcal{F}}^3}\right|_{\boldsymbol{\mathcal{F}}=0} \boldsymbol{\mathcal{F}}^2 + \dots , \tag{2.210}$$

from which by comparison with Eq. (2.208) it follows that

$$\boldsymbol{\mu}_0 = \left.\frac{\partial E}{\partial \boldsymbol{\mathcal{F}}}\right|_{\boldsymbol{\mathcal{F}}=0} \qquad \boldsymbol{\alpha} = \left.\frac{\partial^2 E}{\partial \boldsymbol{\mathcal{F}}^2}\right|_{\boldsymbol{\mathcal{F}}=0} \qquad \boldsymbol{\beta} = \frac{1}{2} \left.\frac{\partial^3 E}{\partial \boldsymbol{\mathcal{F}}^3}\right|_{\boldsymbol{\mathcal{F}}=0} . \tag{2.211}$$

An analogous analysis can be carried out for the influence of an external *magnetic* field.[57] Hence, it may be stated generally that when a molecular system is perturbed by some perturbation η, its total energy E changes according to

$$E(\eta) = E^{(0)} + E^{(1)}\eta + \frac{1}{2} E^{(2)} \eta^2 + \dots , \tag{2.212}$$

where the expansion coefficients are referred to as **molecular properties**, which are characteristic of the molecule and its quantum state.[145] For a *static* perturbation, the properties are said to be *time-independent* and may be calculated by differentiation

$$E^{(1)} = \left.\frac{\mathrm{d}E}{\mathrm{d}\eta}\right|_{\eta=0} \qquad E^{(2)} = \left.\frac{\mathrm{d}^2 E}{\mathrm{d}\eta^2}\right|_{\eta=0} . \tag{2.213}$$

Examples of such properties include responses to geometrical perturbations, from which one obtains forces and force constants as well as spectroscopic constants, responses to external electromagnetic fields, which yield permanent and induced moments, polarizabilities and magnetizabilities, responses to external magnetic fields and nuclear magnetic moments, which yield NMR shielding and spin-spin coupling constants as well as EPR hyperfine coupling constants and g values.[57]

The derivatives themselves can be calculated either numerically or analytically. In the former case, one employs finite differences in combination with polynomial fitting, meaning one chooses a small $\eta > 0$, and then the first derivative is given as

$$E^{(1)} \approx \frac{E(\eta) - E(-\eta)}{2\eta} , \tag{2.214}$$

which is usually simple to implement, but its numerical accuracy and computational efficiency are rather low.[57] Analytical differentiation requires considerable programming effort, but it has much greater speed, precision and convenience. Assuming that the

electronic Hamiltonian $\hat{H}$ is augmented by linear terms only in the perturbation, $\hat{\mathcal{H}}(\eta) = \hat{H} + \eta\hat{P}$, then the energy E may be written as

$$E(\eta) = \langle\Psi(\eta)|\hat{\mathcal{H}}(\eta)|\Psi(\eta)\rangle\,, \tag{2.215}$$

where $\hat{\mathcal{H}}$ has an *explicit* dependence on η, whereas the one of $|\Psi\rangle$ is only *implicit* via its parameterization and possibly also basis functions.[57] The first derivative of the energy at $\eta = 0$ for real wave functions is given as

$$\begin{aligned}\left.\frac{\mathrm{d}E}{\mathrm{d}\eta}\right|_{\eta=0} &= \left\langle\Psi\middle|\frac{\mathrm{d}\hat{\mathcal{H}}}{\mathrm{d}\eta}\middle|\Psi\right\rangle + 2\left\langle\frac{\mathrm{d}\Psi}{\mathrm{d}\eta}\middle|\hat{H}+\eta\hat{P}\middle|\Psi\right\rangle\Big|_{\eta=0} \\ &= \langle\Psi|\hat{P}|\Psi\rangle + 2\left\langle\frac{\mathrm{d}\Psi}{\mathrm{d}\eta}\middle|\hat{H}\middle|\Psi\right\rangle.\end{aligned} \tag{2.216}$$

The wave function depends *indirectly* on the perturbation, namely via the wave-function parameters $\boldsymbol{\Lambda}$ and possibly also via the basis functions $\boldsymbol{\chi}$, such that its total derivative is given as

$$\frac{\mathrm{d}\Psi}{\mathrm{d}\eta} = \frac{\partial\Psi}{\partial\boldsymbol{\Lambda}}\frac{\mathrm{d}\boldsymbol{\Lambda}}{\mathrm{d}\eta} + \frac{\partial\Psi}{\partial\boldsymbol{\chi}}\frac{\mathrm{d}\boldsymbol{\chi}}{\mathrm{d}\eta}\,, \tag{2.217}$$

where the partial derivative vanishes since there is no explicit dependence on the perturbation. Assuming the basis functions are independent of the perturbation, $\mathrm{d}\boldsymbol{\chi}/\mathrm{d}\eta = 0$, the derivative may be written as[57]

$$\left.\frac{\mathrm{d}E}{\mathrm{d}\eta}\right|_{\eta=0} = \langle\Psi|\hat{P}|\Psi\rangle + 2\frac{\mathrm{d}\boldsymbol{\Lambda}}{\mathrm{d}\eta}\left\langle\frac{\partial\Psi}{\partial\boldsymbol{\Lambda}}\middle|\hat{H}\middle|\Psi\right\rangle. \tag{2.218}$$

If $|\Psi\rangle$ is variationally optimized w.r.t. to the parameters $\boldsymbol{\Lambda}$, the last term of the derivative disappears since E is stationary w.r.t. $\boldsymbol{\Lambda}$,

$$\left.\frac{\partial E}{\partial\boldsymbol{\Lambda}}\right|_{\eta=0} = 2\left\langle\frac{\partial\Psi}{\partial\boldsymbol{\Lambda}}\middle|\hat{H}\middle|\Psi\right\rangle = 0\,, \tag{2.219}$$

which means that *variational wave functions* obey the so-called **Hellmann–Feynman theorem**[57,146,147]

$$\frac{\mathrm{d}E}{\mathrm{d}\eta} = \left\langle\Psi\middle|\frac{\mathrm{d}\hat{\mathcal{H}}}{\mathrm{d}\eta}\middle|\Psi\right\rangle. \tag{2.220}$$

Chapter 3

Unitary Coupled-Cluster Theory

In Section 2.6, the standard formulation of coupled-cluster theory was discussed, which corresponds to a non-Hermitian, biorthogonal representation of the Hamiltonian. A related, yet Hermitian approach is the so-called **unitary coupled-cluster** (UCC) method,[20,35,37,39,93,116,117,128–138] which I want to describe in detail in the following. Furthermore, it is closely related to the algebraic-diagrammatic construction scheme presented in Section 2.5. Several methods based on the UCC ansatz have been derived and implemented within this thesis, which is why I want to discuss it in great detail. In particular, first-time ever explicit derivations by employing diagrammatic techniques of the so-called UCC2 and UCC3 schemes are given.

3.1 Intermediate State Representation Approach to UCC

An ISR scheme based on the UCC approach was initially considered by Prasad *et al.*[92] and by Mukherjee and Kutzelnigg[93] and was later reviewed by Mertins and Schirmer.[20] In UCC theory, the ground-state wave function is expressed in an exponential CC form as

$$|\Psi_0^{\mathrm{UCC}}\rangle = e^{\hat{\sigma}}|\Phi_0\rangle\,, \tag{3.1}$$

where the UCC cluster operator is chosen to be anti-Hermitian, $\hat{\sigma}^\dagger = -\hat{\sigma}$, such that $e^{\hat{\sigma}}$ is unitary. Usually, $\hat{\sigma}$ is written as

$$\hat{\sigma} = \hat{S} - \hat{S}^\dagger\,, \tag{3.2}$$

where the operator $\hat{S}$ (like $\hat{T}$) is given by a linear combination of physical excitation operators

$$\hat{S} = \sum_{n=1}^{N} \hat{S}_n = \sum_{ia} \sigma_i^a\, \hat{a}_a^\dagger \hat{a}_i + \frac{1}{4} \sum_{ijab} \sigma_{ij}^{ab}\, \hat{a}_a^\dagger \hat{a}_b^\dagger \hat{a}_j \hat{a}_i + \dots\,. \tag{3.3}$$

Since $\hat{S}^\dagger$ contains only "unphysical" deexcitation operators, $\hat{S}^\dagger|\Phi_0\rangle = 0$. In contrast to the normal cluster operator $\hat{T}$, the UCC operator $\hat{\sigma}$ does not commute with physical

excitation operators. The UCC intermediate states $|\tilde{\tilde{\Psi}}_J\rangle$ are obtained by applying so-called consistent operators $e^{\hat{\sigma}}\hat{C}_J e^{-\hat{\sigma}}$ to the UCC ground state,

$$|\tilde{\tilde{\Psi}}_J\rangle = e^{\hat{\sigma}}\hat{C}_J e^{-\hat{\sigma}}|\Psi_0^{\mathrm{UCC}}\rangle = e^{\hat{\sigma}}\hat{C}_J|\Phi_0\rangle\,, \tag{3.4}$$

which corresponds to a unitary transformation of the CI configurations and thus the UCC states form a complete and orthonormal set.[20] The UCC representation $\tilde{\tilde{\mathbf{H}}}$ of the Hamiltonian is thus given by the matrix elements

$$\tilde{\tilde{H}}_{IJ} = \langle\tilde{\tilde{\Psi}}_I|\hat{H}|\tilde{\tilde{\Psi}}_J\rangle = \langle\Phi_0|\hat{C}_I^\dagger e^{-\hat{\sigma}}\hat{H}e^{\hat{\sigma}}\hat{C}_J|\Phi_0\rangle = \langle\Phi_I|\bar{H}|\Phi_J\rangle\,, \tag{3.5}$$

which can also be viewed as a representation of the UCC transformed Hamiltonian

$$\bar{H} = e^{\hat{\sigma}^\dagger}\hat{H}e^{\hat{\sigma}} = e^{-\hat{\sigma}}\hat{H}e^{\hat{\sigma}} \tag{3.6}$$

within the basis of CI configurations, analogous to EOM-CC. Due to the similarity transformation, $\bar{H}$ can also be written in the connected form $e^{-\hat{\sigma}}\hat{H}e^{\hat{\sigma}} = (\hat{H}e^{\hat{\sigma}})_{\mathrm{c}}$. In fact, the UCC states $|\tilde{\tilde{\Psi}}_I\rangle$ and the ECO intermediate states $|\tilde{\Psi}_J\rangle$ that are used in ADC are related by a unitary transformation $\mathbf{U}$ with $U_{IJ} = \langle\tilde{\tilde{\Psi}}_I|\tilde{\Psi}_J\rangle$, and the matrix representations of the Hamiltonian are thus related by $\tilde{\tilde{\mathbf{H}}} = \mathbf{U}\tilde{\mathbf{H}}\mathbf{U}^\dagger$, which means that the same canonical order relations hold for the UCC representation as for the ECO representation as well as the compactness property.[20] Furthermore, the UCC representation is separable, which means that it yields size consistent properties.[20]

In analogy to traditional coupled-cluster theory, the UCC ground-state energy E_0^{UCC} is obtained via

$$E_0^{\mathrm{UCC}} = \langle\Phi_0|\bar{H}|\Phi_0\rangle\,, \tag{3.7}$$

and the UCC amplitudes are the solution of the projection equations

$$\langle\Phi_I|\bar{H}|\Phi_0\rangle = 0\,. \tag{3.8}$$

The UCCSD Hamiltonian matrix $\tilde{\tilde{\mathbf{H}}}$ thus has the following form

$$\tilde{\tilde{\mathbf{H}}} = \begin{pmatrix} E_0^{\mathrm{UCC}} & \mathbf{0} & \mathbf{0} \\ \mathbf{0} & \tilde{\tilde{\mathbf{H}}}_{\mathrm{SS}} & \tilde{\tilde{\mathbf{H}}}_{\mathrm{SD}} \\ \mathbf{0} & \tilde{\tilde{\mathbf{H}}}_{\mathrm{DS}} & \tilde{\tilde{\mathbf{H}}}_{\mathrm{DD}} \end{pmatrix}, \tag{3.9}$$

which can be compared to the CISD and EOM-CCSD matrices $\mathbf{H}$ and $\bar{\mathbf{H}}$, respectively,

$$\mathbf{H} = \begin{pmatrix} E_0^{\mathrm{HF}} & \mathbf{0} & \mathbf{H}_{\mathrm{0D}} \\ \mathbf{0} & \mathbf{H}_{\mathrm{SS}} & \mathbf{H}_{\mathrm{SD}} \\ \mathbf{H}_{\mathrm{D0}} & \mathbf{H}_{\mathrm{DS}} & \mathbf{H}_{\mathrm{DD}} \end{pmatrix}, \qquad \bar{\mathbf{H}} = \begin{pmatrix} E_0^{\mathrm{CC}} & \bar{\mathbf{H}}_{\mathrm{0S}} & \bar{\mathbf{H}}_{\mathrm{0D}} \\ \mathbf{0} & \bar{\mathbf{H}}_{\mathrm{SS}} & \bar{\mathbf{H}}_{\mathrm{SD}} \\ \mathbf{0} & \bar{\mathbf{H}}_{\mathrm{DS}} & \bar{\mathbf{H}}_{\mathrm{DD}} \end{pmatrix}, \tag{3.10}$$

where $E_0^{\mathrm{HF}} = \langle\Phi_0|\hat{H}|\Phi_0\rangle$ is the HF ground-state energy, $\mathbf{H}_{\mathrm{S0}} = \mathbf{H}_{\mathrm{0S}} = \mathbf{0}$ due to Brillouin's theorem, $\bar{\mathbf{H}}_{\mathrm{S0}} = \bar{\mathbf{H}}_{\mathrm{D0}} = \mathbf{0}$ because of the amplitude equations (2.137), $\bar{\mathbf{H}}_{\mathrm{0S}} \neq \mathbf{0}$ in spite of Brillouin's theorem because of higher-order terms (products of $\hat{H}$ with $\hat{T}$) in $\bar{H}$, and $\bar{\mathbf{H}}_{\mathrm{SD}} \neq \bar{\mathbf{H}}_{\mathrm{DS}}$, since the similarity-transformed Hamiltonian $\bar{H} = e^{-\hat{T}}\hat{H}e^{\hat{T}}$ of traditional CC is not Hermitian.

The representation of the Hamiltonian (3.5), or rather its shifted version defined as $\tilde{\tilde{\mathbf{M}}} = \tilde{\tilde{\mathbf{H}}} - E_0^{\mathrm{UCC}}\mathbf{1}$, gives rise to a Hermitian eigenvalue equation

$$\tilde{\tilde{\mathbf{M}}}\mathbf{X} = \mathbf{X}\boldsymbol{\Omega}\,, \tag{3.11}$$

which yields vertical excitation energies as eigenvalues in $\boldsymbol{\Omega}$ and the corresponding excitation vectors as eigenvectors collected in $\mathbf{X}$. It should be noted that the same secular equation has also been obtained in UCC-based self-consistent polarization propagator theory.[51,92]

3.2 Bernoulli Expansion for the Transformed Hamiltonian

A complication of UCC compared to traditional CC theory is the **non-terminating Baker–Campbell–Hausdorff** expansion of $\bar{H}$ in Eq. (3.6),

$$\bar{H} = \hat{H} + [\hat{H},\hat{\sigma}] + \frac{1}{2!}[[\hat{H},\hat{\sigma}],\hat{\sigma}] + \frac{1}{3!}[[[\hat{H},\hat{\sigma}],\hat{\sigma}],\hat{\sigma}] + \dots\,, \tag{3.12}$$

due to the presence of both excitation and deexcitation operators in $\hat{\sigma}$. As discussed in Section 2.6, the BCH expansion truncates at the quartic commutator in traditional CC theory. Thus, a practical truncation scheme is a mandatory prerequisite for a useful UCC-based method. Several truncation schemes have been proposed and studied in the literature.[37,39,131,137] Major cancellations between commutators involving the Fock operator $\hat{F}_{\mathrm{N}}$ and those involving the fluctuation potential $\hat{V}_{\mathrm{N}}$ has been observed in the derivation for the perturbative expansion of the ground-state energy expression in the UCC(4) approach.[37] The cancellation of the commutators involving $\hat{F}_{\mathrm{N}}$ and those involving $\hat{V}_{\mathrm{N}}$ has also been explored in the context of a non-perturbative treatment, where the resulting formalism retains only a single commutator involving $\hat{F}_{\mathrm{N}}$ and has so-called **Bernoulli numbers** as the expansion coefficients of the commutators involving $\hat{V}_{\mathrm{N}}$.[130,131] In the following, a different derivation for this "Bernoulli expansion" of $\bar{H}$ according to Ref. 51 is presented.

The normal-ordered Hamiltonian $\hat{H}_{\mathrm{N}}$ is again split like in MP perturbation theory according to $\hat{H}_{\mathrm{N}} = \hat{F}_{\mathrm{N}} + \hat{V}_{\mathrm{N}}$. For any converged HF solution, the Fock operator is (block-)diagonal and thus "rank-preserving", which means that the commutator $[\hat{F}_{\mathrm{N}},\hat{A}]$

has the same number of holes and particles as the original operator $\hat{A}$,

$$\hat{F}_{\mathrm{N}} = \sum_{ij} f_{ij} \{\hat{a}_i^\dagger \hat{a}_j\} + \sum_{ab} f_{ab} \{\hat{a}_a^\dagger \hat{a}_b\}\,, \tag{3.13}$$

whereas the fluctuation potential

$$\hat{V}_{\mathrm{N}} = \frac{1}{4} \sum_{pqrs} \langle pq||rs\rangle \{\hat{a}_p^\dagger \hat{a}_q^\dagger \hat{a}_s \hat{a}_r\} \tag{3.14}$$

contains various types of rank-changing and rank-preserving operators,[51] as can also be seen in Figure 2.4 (page 42).

In the following, the definition of a so-called **superoperator** is useful. The operation of a superoperator $\widehat{B}$ on an arbitrary operator $\hat{A}$ yields the commutator between the standard operators $\hat{B}$ and $\hat{A}$,

$$\widehat{B}\hat{A} = [\hat{A}, \hat{B}] = \hat{A}\hat{B} - \hat{B}\hat{A}\,, \tag{3.15}$$

while the identity superoperator $\widehat{I}$ is defined as $\widehat{I}\hat{A} = \hat{A}$. With the definition (3.15), the transformed Hamiltonian $\bar{H}_{\mathrm{N}}$ can be rewritten as

$$\bar{H}_{\mathrm{N}} = e^{\widehat{\sigma}} \hat{H}_{\mathrm{N}}\,, \tag{3.16}$$

where the equivalence to the standard BCH expansion of $\bar{H}$ in Eq. (3.12) can be seen via

$$e^{\widehat{\sigma}}\hat{H} = \sum_{k=0}^{\infty} \frac{1}{k!} \widehat{\sigma}^k \hat{H} = \hat{H} + \widehat{\sigma}\hat{H} + \frac{1}{2}\widehat{\sigma}^2\hat{H} + \ldots = \hat{H} + [\hat{H}, \hat{\sigma}] + \frac{1}{2}[[\hat{H}, \hat{\sigma}], \hat{\sigma}] + \ldots\,. \tag{3.17}$$

The transformed Hamiltonian can be reorganized by separating terms involving $\hat{F}_{\mathrm{N}}$ and $\hat{V}_{\mathrm{N}}$ as

$$\begin{aligned} \bar{H}_{\mathrm{N}} &= e^{\widehat{\sigma}} \hat{F}_{\mathrm{N}} + e^{\widehat{\sigma}} \hat{V}_{\mathrm{N}} \\ &= \hat{F}_{\mathrm{N}} + \hat{X}(\widehat{\sigma})\widehat{\sigma}\hat{F}_{\mathrm{N}} + e^{\widehat{\sigma}} \hat{V}_{\mathrm{N}}\,, \end{aligned} \tag{3.18}$$

where $\hat{X}$ is a **polynomial function** of the superoperator $\widehat{\sigma}$,[51]

$$\hat{X}(\widehat{\sigma}) = \sum_{N=1}^{\infty} \frac{1}{N!} \widehat{\sigma}^{N-1} = 1 + \frac{1}{2}\widehat{\sigma} + \frac{1}{6}\widehat{\sigma}^2 + \frac{1}{24}\widehat{\sigma}^3 + \frac{1}{120}\widehat{\sigma}^4 + \ldots\,. \tag{3.19}$$

In order to derive the "Bernoulli expansion" of the transformed Hamiltonian, the derivatives of $\hat{X}$ as well as its inverse function are required for its Taylor expansion, which shall be derived explicitly in the following. The first few derivatives of this function with

respect to $\widehat{\sigma}$ are given as

$$\hat{X}'(\widehat{\sigma}) = \frac{1}{2} + \frac{1}{3}\widehat{\sigma} + \frac{1}{8}\widehat{\sigma}^2 + \frac{1}{30}\widehat{\sigma}^3 + \dots \tag{3.20a}$$

$$\hat{X}''(\widehat{\sigma}) = \frac{1}{3} + \frac{1}{4}\widehat{\sigma} + \frac{1}{10}\widehat{\sigma}^2 + \dots \tag{3.20b}$$

$$\hat{X}'''(\widehat{\sigma}) = \frac{1}{4} + \frac{1}{5}\widehat{\sigma} + \dots \tag{3.20c}$$

$$\hat{X}''''(\widehat{\sigma}) = \frac{1}{5} + \dots , \tag{3.20d}$$

where in general the value at $\widehat{\sigma} = 0$ is $\hat{X}^{(n)}(0) = \frac{1}{n+1}$ for the n-th derivative.[1]

The **inverse function** $\hat{X}^{-1}(\widehat{\sigma}) = (1 + \frac{1}{2}\widehat{\sigma} + \frac{1}{6}\widehat{\sigma}^2 + \frac{1}{24}\widehat{\sigma}^3 + \frac{1}{120}\widehat{\sigma}^4 + \dots)^{-1}$, also denoted by $\hat{X}_{-1}$ for the sake of notational brevity in the following, can be expanded in a Taylor series around $\widehat{\sigma} = 0$ according to

$$T(\widehat{\sigma}) = \sum_{k=0}^{\infty} \frac{1}{k!} \hat{X}_{-1}^{(k)}(0) \cdot \widehat{\sigma}^k = \hat{X}_{-1}(0) + \hat{X}'_{-1}(0) \cdot \widehat{\sigma} + \frac{1}{2}\hat{X}''_{-1}(0) \cdot \widehat{\sigma}^2 + \frac{1}{6}\hat{X}'''_{-1}(0) \cdot \widehat{\sigma}^3 + \dots \tag{3.21}$$

The first few derivatives of $\hat{X}_{-1}$ are given as

$$\hat{X}'_{-1}(\widehat{\sigma}) = -(1 + \frac{1}{2}\widehat{\sigma} + \frac{1}{6}\widehat{\sigma}^2 + \dots)^{-2} \cdot (\frac{1}{2} + \frac{1}{3}\widehat{\sigma} + \frac{1}{8}\widehat{\sigma}^2 + \dots) \tag{3.22a}$$

$$\begin{aligned} \hat{X}''_{-1}(\widehat{\sigma}) = {} & +2 \cdot (1 + \frac{1}{2}\widehat{\sigma} + \frac{1}{6}\widehat{\sigma}^2 + \dots)^{-3} \cdot (\frac{1}{2} + \frac{1}{3}\widehat{\sigma} + \frac{1}{8}\widehat{\sigma}^2 + \dots)^2 \\ & - (1 + \frac{1}{2}\widehat{\sigma} + \frac{1}{6}\widehat{\sigma}^2 + \dots)^{-2} \cdot (\frac{1}{3} + \frac{1}{4}\widehat{\sigma} + \dots) \end{aligned} \tag{3.22b}$$

$$\begin{aligned} \hat{X}'''_{-1}(\widehat{\sigma}) = {} & -6 \cdot (1 + \frac{1}{2}\widehat{\sigma} + \frac{1}{6}\widehat{\sigma}^2 + \dots)^{-4} \cdot (\frac{1}{2} + \frac{1}{3}\widehat{\sigma} + \frac{1}{8}\widehat{\sigma}^2 + \dots)^3 \\ & + 2 \cdot (1 + \frac{1}{2}\widehat{\sigma} + \frac{1}{6}\widehat{\sigma}^2 + \dots)^{-3} \cdot 2 \cdot (\frac{1}{2} + \frac{1}{3}\widehat{\sigma} + \dots)(\frac{1}{3} + \frac{1}{4}\widehat{\sigma} + \dots) \\ & + 2 \cdot (1 + \frac{1}{2}\widehat{\sigma} + \frac{1}{6}\widehat{\sigma}^2 + \dots)^{-3} \cdot (\frac{1}{2} + \frac{1}{3}\widehat{\sigma} + \dots)(\frac{1}{3} + \frac{1}{4}\widehat{\sigma} + \dots) \\ & - (1 + \frac{1}{2}\widehat{\sigma} + \frac{1}{6}\widehat{\sigma}^2 + \dots)^{-2} \cdot (\frac{1}{4} + \frac{1}{5}\widehat{\sigma} + \dots) \end{aligned} \tag{3.22c}$$

[1] The values of the first few derivatives at $\widehat{\sigma} = 0$ are thus $\hat{X}(0) = 1; \hat{X}'(0) = \frac{1}{2}; \hat{X}''(0) = \frac{1}{3}; \hat{X}'''(0) = \frac{1}{4}; \hat{X}''''(0) = \frac{1}{5}$.

$$
\begin{aligned}
\hat{X}_{-1}''''(\widehat{\sigma}) = {} & 24 \cdot (1 + \frac{1}{2}\widehat{\sigma} + \frac{1}{6}\widehat{\sigma}^2 + \ldots)^{-5} \cdot (\frac{1}{2} + \frac{1}{3}\widehat{\sigma} + \frac{1}{8}\widehat{\sigma}^2 + \ldots)^4 \\
& - 6 \cdot (1 + \frac{1}{2}\widehat{\sigma} + \frac{1}{6}\widehat{\sigma}^2 + \ldots)^{-4} \cdot 3 \cdot (\frac{1}{2} + \frac{1}{3}\widehat{\sigma} + \frac{1}{8}\widehat{\sigma}^2 + \ldots)^2 \cdot (\frac{1}{3} + \frac{1}{4}\widehat{\sigma} + \ldots) \\
& - 6 \cdot (1 + \frac{1}{2}\widehat{\sigma} + \frac{1}{6}\widehat{\sigma}^2 + \ldots)^{-4} \cdot 2 \cdot (\frac{1}{2} + \frac{1}{3}\widehat{\sigma} + \frac{1}{8}\widehat{\sigma}^2 + \ldots)^2 \cdot (\frac{1}{3} + \frac{1}{4}\widehat{\sigma} + \frac{1}{10}\widehat{\sigma}^2 + \ldots) \\
& + 2 \cdot (1 + \frac{1}{2}\widehat{\sigma} + \frac{1}{6}\widehat{\sigma}^2 + \ldots)^{-3} \cdot 2 \cdot (\frac{1}{3} + \frac{1}{4}\widehat{\sigma} + \ldots)(\frac{1}{3} + \frac{1}{4}\widehat{\sigma} + \frac{1}{10}\widehat{\sigma}^2 + \ldots) \\
& + 2 \cdot (1 + \frac{1}{2}\widehat{\sigma} + \frac{1}{6}\widehat{\sigma}^2 + \ldots)^{-3} \cdot 2 \cdot (\frac{1}{2} + \frac{1}{3}\widehat{\sigma} + \frac{1}{8}\widehat{\sigma}^2 + \ldots) \cdot (\frac{1}{4} + \frac{1}{5}\widehat{\sigma} + \ldots) \\
& - 6 \cdot (1 + \frac{1}{2}\widehat{\sigma} + \frac{1}{6}\widehat{\sigma}^2 + \ldots)^{-4} \cdot (\frac{1}{2} + \frac{1}{3}\widehat{\sigma} + \frac{1}{8}\widehat{\sigma}^2 + \ldots)^2 \cdot (\frac{1}{3} + \frac{1}{4}\widehat{\sigma} + \frac{1}{10}\widehat{\sigma}^2 + \ldots) \\
& - 6 \cdot (1 + \frac{1}{2}\widehat{\sigma} + \frac{1}{6}\widehat{\sigma}^2 + \ldots)^{-4} \cdot (\frac{1}{2} + \frac{1}{3}\widehat{\sigma} + \frac{1}{8}\widehat{\sigma}^2 + \ldots)^2 \cdot (\frac{1}{3} + \frac{1}{4}\widehat{\sigma} + \frac{1}{10}\widehat{\sigma}^2 + \ldots) \\
& + 2 \cdot (1 + \frac{1}{2}\widehat{\sigma} + \frac{1}{6}\widehat{\sigma}^2 + \ldots)^{-3} \cdot (\frac{1}{3} + \frac{1}{4}\widehat{\sigma} + \ldots)(\frac{1}{3} + \frac{1}{4}\widehat{\sigma} + \frac{1}{10}\widehat{\sigma}^2 + \ldots) \\
& + 2 \cdot (1 + \frac{1}{2}\widehat{\sigma} + \frac{1}{6}\widehat{\sigma}^2 + \ldots)^{-3} \cdot (\frac{1}{2} + \frac{1}{3}\widehat{\sigma} + \frac{1}{8}\widehat{\sigma}^2 + \ldots) \cdot (\frac{1}{4} + \frac{1}{5}\widehat{\sigma} + \ldots) \\
& + 2 \cdot (1 + \frac{1}{2}\widehat{\sigma} + \frac{1}{6}\widehat{\sigma}^2 + \ldots)^{-3} \cdot (\frac{1}{2} + \frac{1}{3}\widehat{\sigma} + \frac{1}{8}\widehat{\sigma}^2 + \ldots) \cdot (\frac{1}{4} + \frac{1}{5}\widehat{\sigma} + \frac{1}{12}\widehat{\sigma}^2 + \ldots) \\
& - (1 + \frac{1}{2}\widehat{\sigma} + \frac{1}{6}\widehat{\sigma}^2 + \ldots)^{-2} \cdot (\frac{1}{5} + \frac{1}{6}\widehat{\sigma} + \ldots) \,.
\end{aligned}
\tag{3.22d}
$$

With this,[2] one obtains for the Taylor expansion

$$
\hat{X}^{-1}(\widehat{\sigma}) \approx T(\widehat{\sigma}) = 1 - \frac{1}{2}\widehat{\sigma} + \frac{1}{2!} \cdot \frac{1}{6}\widehat{\sigma}^2 + \frac{1}{3!} \cdot 0 \cdot \widehat{\sigma}^3 - \frac{1}{4!} \cdot \frac{1}{30}\widehat{\sigma}^4 + \ldots \,. \tag{3.23}
$$

Multiplying the second line of Eq. (3.18) with $\hat{X}^{-1}$ from the left, one obtains

$$
\hat{X}^{-1}(\widehat{\sigma})(\bar{H}_{\mathrm{N}} - \hat{F}_{\mathrm{N}}) = \widehat{\sigma}\hat{F}_{\mathrm{N}} + \hat{X}^{-1}(\widehat{\sigma})e^{\widehat{\sigma}}\hat{V}_{\mathrm{N}} \tag{3.24}
$$

Hence, from Eq. (3.23) it can be seen that the inverse function $\hat{X}^{-1}$ contains **Bernoulli numbers** as the **expansion coefficients**,[51]

$$
\hat{X}^{-1}(\widehat{\sigma}) = 1 + \sum_{n>0} B_n \widehat{\sigma}^n \tag{3.25}
$$

$$
B_1 = -\frac{1}{2}, B_2 = \frac{1}{12}, B_3 = 0, B_4 = -\frac{1}{720}, \ldots \tag{3.26}
$$

In the following, the subscript "N" for normal ordering is dropped for better readability, but normal-ordered operators are still assumed throughout. Thus, a suitable expression

[2] The values of $\hat{X}_{-1}^{(n)}$ at $\widehat{\sigma} = 0$ are thus $\hat{X}_{-1}'(0) = -1$; $\hat{X}_{-1}''(0) = \frac{1}{2} - \frac{1}{3} = \frac{1}{6}$; $\hat{X}_{-1}'''(0) = -\frac{3}{4} + \frac{1}{3} + \frac{2}{3} - \frac{1}{4} = 0$; $\hat{X}_{-1}''''(0) = 24 \cdot \frac{1}{16} - 6 \cdot 3 \cdot \frac{1}{4} \cdot \frac{1}{3} - 6 \cdot 2 \cdot \frac{1}{4} \cdot \frac{1}{3} + 2 \cdot 2 \cdot \frac{1}{3} \cdot \frac{1}{3} + 2 \cdot 2 \cdot \frac{1}{8} - 6 \cdot \frac{1}{4} \cdot \frac{1}{3} + 2 \cdot \frac{1}{9} + 2 \cdot \frac{1}{8} + 2 \cdot \frac{1}{8} - \frac{1}{5} = -\frac{1}{30}$.

for the **iterative generation** of $\bar{H}$ is obtained

$$\bar{H} = \hat{F} + \bar{V} \tag{3.27}$$

$$\bar{V} = \widehat{\sigma}\hat{F} + \hat{X}^{-1}(\widehat{\sigma})e^{\widehat{\sigma}}\hat{V} - \sum_{n>0} B_n \widehat{\sigma}^n \bar{V}\,, \tag{3.28}$$

where the last equation is obtained from Eq. (3.18) by multiplying $\bar{V} = \hat{X}(\widehat{\sigma})\widehat{\sigma}\hat{F} + e^{\widehat{\sigma}}\hat{V}$ with $1 = \hat{X}^{-1}(\widehat{\sigma}) - \sum_{n>0} B_n \widehat{\sigma}^n$:

$$1 \cdot \bar{V} = (\hat{X}^{-1}(\widehat{\sigma}) - \sum_{n>0} B_n \widehat{\sigma}^n) \cdot (\hat{X}(\widehat{\sigma})\widehat{\sigma}\hat{F} + e^{\widehat{\sigma}}\hat{V}) \tag{3.29}$$

$$\begin{aligned} \bar{V} &= \hat{X}^{-1}(\widehat{\sigma})\hat{X}(\widehat{\sigma})\widehat{\sigma}\hat{F} + \hat{X}^{-1}(\widehat{\sigma})e^{\widehat{\sigma}}\hat{V} - \sum_{n>0} B_n \widehat{\sigma}^n \bar{V} \\ &= \widehat{\sigma}\hat{F} + \hat{X}^{-1}(\widehat{\sigma})e^{\widehat{\sigma}}\hat{V} - \sum_{n>0} B_n \widehat{\sigma}^n \bar{V} \end{aligned} \tag{3.30}$$

Now $\hat{O}_{\mathrm{ND}}$ is defined as the "nondiagonal" part of an arbitrary operator $\hat{O}$ containing all the excitation and deexcitation operators in $\hat{O}$. For instance, the last two diagrams with excitation levels of -1 and $+1$ of the Fock operator in Figure 2.3 (page 41) and the last two diagrams with excitation levels of $+2$ and -2 of the fluctuation potential in Figure 2.4 (page 42) are the respective nondiagonal parts, whereas cluster operators from Figure 2.5 are purely nondiagonal. Defining furthermore the "rest" part $\hat{O}_{\mathrm{R}}$ as $\hat{O}_{\mathrm{R}} = \hat{O} - \hat{O}_{\mathrm{ND}}$, the UCC amplitude equation can be written as

$$0 = \langle \Phi_I | \bar{H}_{\mathrm{ND}} | \Phi_0 \rangle = \underbrace{\langle \Phi_I | \hat{F}_{\mathrm{ND}} | \Phi_0 \rangle}_{=0} + \langle \Phi_I | \bar{V}_{\mathrm{ND}} | \Phi_0 \rangle\,, \tag{3.31}$$

where only $\bar{H}_{\mathrm{ND}}$ needs to be considered since otherwise $|\Phi_0\rangle$ does not couple to excited determinants and $\hat{F}_{\mathrm{ND}} = 0$ since the Fock operator is block diagonal according to Eq. (3.13). Thus, the amplitude equation can be equivalently written as

$$\bar{V}_{\mathrm{ND}} = 0\,, \tag{3.32}$$

and after having solved this equation only $\bar{V}_{\mathrm{R}}$ needs to be included in the iterative procedure for the generation of $\bar{V}$,[51]

$$\bar{V}^{\{k+1\}} = \widehat{\sigma}\hat{F} + \hat{X}^{-1}(\widehat{\sigma})e^{\widehat{\sigma}}\hat{V} - \sum_{n>0} B_n \widehat{\sigma}^n \bar{V}_{\mathrm{R}}^{\{k\}}\,. \tag{3.33}$$

If one starts with $\bar{V}_\mathrm{R}^{\{0\}} = \hat{V}_\mathrm{R}$, then $\bar{H}$ can be generated as a **power series** of $\widehat{\sigma}$. Plugging all expansions into Eq. (3.33), one obtains in the first round

$$\begin{aligned}
\bar{V}_\mathrm{R}^{\{1\}} &= \widehat{\sigma}\hat{F} + \Big(1 - \frac{1}{2}\widehat{\sigma} + \frac{1}{12}\widehat{\sigma}^2 + \dots\Big)\Big(1 + \widehat{\sigma} + \frac{1}{2}\widehat{\sigma}^2 + \dots\Big)\hat{V} - \Big(-\frac{1}{2}\widehat{\sigma} + \frac{1}{12}\widehat{\sigma}^2 + \dots\Big)\hat{V}_\mathrm{R} \\
&= \Big(\widehat{\sigma}\hat{F} + \hat{V} + \widehat{\sigma}\hat{V} + \frac{1}{2}\widehat{\sigma}^2\hat{V} + \dots\Big) + \Big(-\frac{1}{2}\widehat{\sigma}\hat{V} - \frac{1}{2}\widehat{\sigma}^2\hat{V} - \frac{1}{4}\widehat{\sigma}^3\hat{V} - \dots\Big) \\
&\quad + \Big(\frac{1}{12}\widehat{\sigma}^2\hat{V} + \frac{1}{12}\widehat{\sigma}^3\hat{V} + \frac{1}{24}\widehat{\sigma}^4\hat{V} + \dots\Big) + \Big(\frac{1}{2}\widehat{\sigma}\hat{V}_\mathrm{R} - \frac{1}{12}\widehat{\sigma}^2\hat{V}_\mathrm{R} - \dots\Big) \\
&= \widehat{\sigma}\hat{F} + \hat{V} + \widehat{\sigma}\hat{V} - \frac{1}{2}\widehat{\sigma}\hat{V} + \frac{1}{2}\widehat{\sigma}\hat{V}_\mathrm{R} + \frac{1}{2}\widehat{\sigma}^2\hat{V} - \frac{1}{2}\widehat{\sigma}^2\hat{V} + \frac{1}{12}\widehat{\sigma}^2\hat{V} - \frac{1}{12}\widehat{\sigma}^2\hat{V}_\mathrm{R} + \dots \\
&= \widehat{\sigma}\hat{F} + \hat{V} + \frac{1}{2}\widehat{\sigma}\hat{V} + \frac{1}{2}\widehat{\sigma}\hat{V}_\mathrm{R} + \frac{1}{12}\widehat{\sigma}^2\hat{V}_\mathrm{ND} + \dots\,,
\end{aligned} \tag{3.34}$$

the result of which can again be plugged into Eq. (3.33) to obtain $\bar{V}_\mathrm{R}^{\{2\}}$, and so on. The lowest-order terms, which are the most important ones, converge rather rapidly. Eventually, the expressions for $\bar{H}$ are obtained, which up to cubic commutators are given by[51]

$$\bar{H} = \bar{H}_0 + \bar{H}_1 + \bar{H}_2 + \bar{H}_3 \tag{3.35a}$$

$$\bar{H}_0 = \hat{F} + \hat{V} \tag{3.35b}$$

$$\bar{H}_1 = [\hat{F}, \hat{\sigma}] + \frac{1}{2}[\hat{V}, \hat{\sigma}] + \frac{1}{2}[\hat{V}_\mathrm{R}, \hat{\sigma}] \tag{3.35c}$$

$$\bar{H}_2 = \frac{1}{12}[[\hat{V}_\mathrm{ND}, \hat{\sigma}], \hat{\sigma}] + \frac{1}{4}[[\hat{V}, \hat{\sigma}]_\mathrm{R}, \hat{\sigma}] + \frac{1}{4}[[\hat{V}_\mathrm{R}, \hat{\sigma}]_\mathrm{R}, \hat{\sigma}] \tag{3.35d}$$

$$\begin{aligned}
\bar{H}_3 = {} & \frac{1}{24}[[[\hat{V}_\mathrm{ND}, \hat{\sigma}], \hat{\sigma}]_\mathrm{R}, \hat{\sigma}] + \frac{1}{8}[[[\hat{V}_\mathrm{R}, \hat{\sigma}]_\mathrm{R}, \hat{\sigma}]_\mathrm{R}, \hat{\sigma}] + \frac{1}{8}[[[\hat{V}, \hat{\sigma}]_\mathrm{R}, \hat{\sigma}]_\mathrm{R}, \hat{\sigma}] \\
& - \frac{1}{24}[[[\hat{V}, \hat{\sigma}]_\mathrm{R}, \hat{\sigma}], \hat{\sigma}] - \frac{1}{24}[[[\hat{V}_\mathrm{R}, \hat{\sigma}]_\mathrm{R}, \hat{\sigma}], \hat{\sigma}]\,,
\end{aligned} \tag{3.35e}$$

where the terms of $\bar{H}$ that involve $\hat{F}$ now truncate to the **first power** of $\hat{\sigma}$, which constitutes a significant simplification compared to the original BCH expansion (3.12). In order to differentiate approaches using the BCH or the Bernoulli (Bn) expansion for $\bar{H}$, the methods will sometimes be donoted by BCH-UCC or Bn-UCC, respectively.

As stated previously, for an efficient UCC theory, not only the excitation manifold, but also the expansion of $\bar{H}$ needs to be truncated in a certain manner. In the following, the excitation manifold will include single and double excitations (and deexcitations) only, which corresponds to the UCCSD scheme. For the truncation of $\bar{H}$, several possibilities have already been studied in the literature, for instance a truncation based on the order of commutators,[137] the requirement for the method to be exact for a given number of electrons,[39] or more often arguments from perturbation theory have been used to obtain the UCC ground-state energy E_0^UCC consistent through a certain order.[37,38,131] The aim of the method presented in the following is to obtain excitation energies of predominantly singly-excited states correct through second or third order in MP perturbation theory.

As was shown in Section 2.6.7 (page 48), doubly-excited configurations appear in first order of perturbation theory, whereas single excitations occur only in second order for the first time (assuming that Brillouin's theorem holds). Thus, for the derivation of approximate UCCSD amplitude equations, the $\hat{\sigma}_2$ amplitudes will be regarded to be of first order, whereas $\hat{\sigma}_1$ amplitudes to be of second order. For a consistent second-order scheme, apart from the commutator with $\hat{F}$, only one commutator of $\hat{\sigma}_2$ with $\hat{V}$ needs to be taken into account for the matrix elements of $\bar{H}$, whereas with the BCH expansion also the double commutator of $\hat{\sigma}_2$ with $\hat{F}$ needs to be included. For a consistent third-order scheme one commutator of $\hat{\sigma}_1$ with $\hat{V}$ and two commutators of $\hat{\sigma}_2$ have to be considered. This will be carried out for two approximate UCC schemes termed UCC2 and UCC3, where the matrix elements of $\bar{H}$ are consistent through second and third order, respectively. For the UCCSD scheme, the amplitude equations (3.8) can be equivalently written as the matrix elements

$$\begin{aligned} \bar{H}_{ai} &= \langle \Phi_i^a | \bar{H} | \Phi_0 \rangle = 0 \\ \bar{H}_{ab,ij} &= \langle \Phi_{ij}^{ab} | \bar{H} | \Phi_0 \rangle = 0 \end{aligned} \tag{3.36}$$

3.3 The Second-Order UCC2 Scheme

In this section, a consistent second-order scheme based on UCC theory is presented. First, the ground-state amplitude equations will be derived, followed by the secular matrix elements for the calculation of excitation energies, which will be seen to be equivalent to ADC(2), but depend on how the transformed Hamiltonian $\bar{H}$ is treated. The terms from the Bernoulli expansion of $\bar{H}$ that need to be considered in the UCC2 scheme are given as

$$\bar{H}^{\mathrm{UCC2}} = \hat{F} + \hat{V} + [\hat{F}, \hat{\sigma}_1 + \hat{\sigma}_2] + \frac{1}{2}[\hat{V}, \hat{\sigma}_2] + \frac{1}{2}[\hat{V}_{\mathrm{R}}, \hat{\sigma}_2]\,, \tag{3.37}$$

where the leading term of $\bar{H}$ is the (normal-ordered) Hamiltonian $\hat{H} = \hat{F} + \hat{V}$ itself, Eq. (3.35b). All commutators involving $\hat{\sigma} = \hat{S} - \hat{S}^\dagger$ can be written as two commutators, one involving the excitation and one the deexcitation operator part as $[\hat{V}, \hat{\sigma}] = [\hat{V}, \hat{S}] + [\hat{S}^\dagger, \hat{V}]$, such that in principle always two possible contributions need to be considered.

3.3.1 Derivation of the UCC2 Amplitude Equations

In the following, the UCC2 amplitude equations shall be derived using the diagrammatic techniques presented in Section 2.6. For the $\hat{S}$ and $\hat{S}^\dagger$ operators the same diagrams are used as for $\hat{T}$ and $\hat{T}^\dagger$ in Figure 2.5 (page 42). The only two contributions of $\hat{H}$ to the amplitude equations are the same as for CCSD and have already been derived in Section 2.6.6. The Fock operator contributes Eq. (2.158) to the singles equation, $\langle \Phi_i^a | \hat{F} | \Phi_0 \rangle = f_{ai}$, which vanishes if Brillouin's theorem is fulfilled, and the fluctuation potential contributes the integral from Eq. (2.159) to the doubles equation, $\langle \Phi_{ij}^{ab} | \hat{V} | \Phi_0 \rangle = \langle ab || ij \rangle$.

Due to the connectedness of the transformed Hamiltonian $\bar{H}$, often only the (physical) excitation part $\hat{S}_2$ of $\hat{\sigma}_2$ contributes to the amplitude equations, making the linear contributions almost identical to the CCSD ones (Section 2.6.6), for instance

$$\langle \Phi_i^a | (\hat{F}\hat{\sigma}_1)_\mathrm{c} | \Phi_0 \rangle = \langle \Phi_i^a | (\hat{F}\hat{S}_1)_\mathrm{c} | \Phi_0 \rangle + \underbrace{\langle \Phi_i^a | (\hat{S}_1^\dagger \hat{F})_\mathrm{c} | \Phi_0 \rangle}_{=0} = \sum_b f_{ab}\, \sigma_i^b - \sum_j f_{ji}\, \sigma_j^a \,, \quad (3.38)$$

as shown in Eq. (2.160). Another example is the contribution of the $[\hat{F}, \hat{\sigma}_2]$ commutator to the singles equation, that turns to vanish for a block-diagonal Fock matrix. Since only the $\hat{S}_2$ part of $\hat{\sigma}_2$ can contribute, the matrix element can be evaluated as

$$\langle \Phi_i^a | (\hat{F}\hat{\sigma}_2)_\mathrm{c} | \Phi_0 \rangle =$$

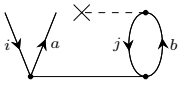

$$= \sum_{jb} f_{jb}\, \sigma_{ij}^{ab} \,, \quad (3.39)$$

which vanishes if Brillouin's theorem holds. The only remaining term for the singles equation is the contribution of $[\hat{V}, \hat{\sigma}_2]$, where again only the $\hat{S}_2$ part can contribute, making it identical to the CCSD contribution,

$$\langle \Phi_i^a | (\hat{V}\hat{\sigma}_2)_\mathrm{c} | \Phi_0 \rangle =$$

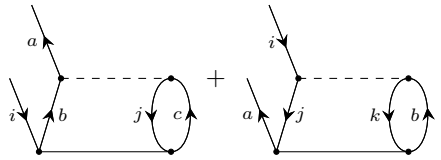

$$= \frac{1}{2} \sum_{jbc} \langle aj||bc\rangle \sigma_{ij}^{bc} \; - \; \frac{1}{2} \sum_{jkb} \langle jk||ib\rangle \sigma_{jk}^{ab} \,, \quad (3.40)$$

where the factor of $\frac{1}{2}$ arises from the pair of equivalent lines (b and c, j and k, respectively), and the signs come from two loops each but two or three hole lines, respectively.

Going on with the doubles equation, the contribution of $[\hat{F}, \hat{\sigma}_2]$ can be evaluated as

$$\langle \Phi_{ij}^{ab} | (\hat{F}\hat{\sigma}_2)_\mathrm{c} | \Phi_0 \rangle =$$

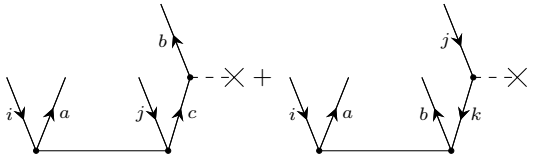

$$= \hat{\mathcal{P}}(ab) \sum_c f_{bc}\, \sigma_{ij}^{ac} \qquad - \; \hat{\mathcal{P}}(ij) \sum_k f_{kj}\, \sigma_{ik}^{ab} \,, \quad (3.41)$$

where the permutation operator had to be included because of the pair of unique external particle (a and b) or hole lines (i and j), respectively. The last contribution to the UCC2 amplitude equations comes from the $[\hat{V}, \hat{\sigma}_2]$ commutator, which gives rise to three distinct contributions coming from the fragments of $\hat{V}$ with excitation level 0 and the excitation

part $\hat{S}_2$, which are given as

$$\langle \Phi_{ij}^{ab} | (\hat{V}\hat{S}_2)_\mathrm{c} | \Phi_0 \rangle = \quad + \quad + \quad$$

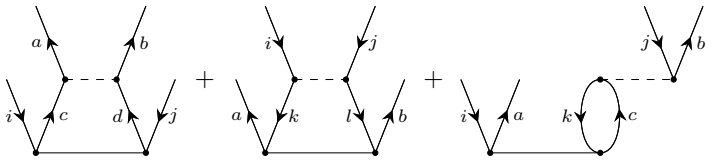

$$\begin{aligned} &= \frac{1}{2}\sum_{cd}\langle ab||cd\rangle\, \sigma_{ij}^{cd} + \frac{1}{2}\sum_{kl}\langle kl||ij\rangle\, \sigma_{kl}^{ab} \\ &\quad + \hat{\mathcal{P}}(ij)\hat{\mathcal{P}}(ab)\sum_{kc}\langle kb||cj\rangle\, \sigma_{ik}^{ac}\,. \end{aligned} \tag{3.42}$$

With this, the UCC2 amplitude equations can be summarized as

$$\begin{aligned} 0 = \bar{H}_{ai}^{\mathrm{UCC2}} &= f_{ai} + \sum_b f_{ab}\,\sigma_i^b - \sum_j f_{ji}\,\sigma_j^a + \sum_{jb} f_{jb}\,\sigma_{ij}^{ab} \\ &\quad + \frac{1}{2}\sum_{jbc}\langle aj||bc\rangle\sigma_{ij}^{bc} - \frac{1}{2}\sum_{jkb}\langle jk||ib\rangle\sigma_{jk}^{ab} \end{aligned} \tag{3.43a}$$

$$\begin{aligned} 0 = \bar{H}_{ab,ij}^{\mathrm{UCC2}} &= \langle ab||ij\rangle + \hat{\mathcal{P}}(ab)\sum_c f_{bc}\,\sigma_{ij}^{ac} - \hat{\mathcal{P}}(ij)\sum_k f_{kj}\,\sigma_{ik}^{ab} \\ &\quad + \frac{1}{2}\sum_{cd}\langle ab||cd\rangle\,\sigma_{ij}^{cd} + \frac{1}{2}\sum_{kl}\langle kl||ij\rangle\,\sigma_{kl}^{ab} + \hat{\mathcal{P}}(ij)\hat{\mathcal{P}}(ab)\sum_{kc}\langle kb||cj\rangle\,\sigma_{ik}^{ac}\,. \end{aligned} \tag{3.43b}$$

Assuming a diagonal Fock matrix, $f_{pq} = \varepsilon_p\delta_{pq}$, the equations can be simplified to

$$0 = \bar{H}_{ai}^{\mathrm{UCC2}} = (\varepsilon_a - \varepsilon_i)\sigma_i^a + \frac{1}{2}\sum_{jbc}\langle aj||bc\rangle\sigma_{ij}^{bc} - \frac{1}{2}\sum_{jkb}\langle jk||ib\rangle\sigma_{jk}^{ab} \tag{3.44a}$$

$$\begin{aligned} 0 = \bar{H}_{ab,ij}^{\mathrm{UCC2}} &= \langle ab||ij\rangle + (\varepsilon_a + \varepsilon_b - \varepsilon_i - \varepsilon_j)\sigma_{ij}^{ab} \\ &\quad + \frac{1}{2}\sum_{cd}\langle ab||cd\rangle\,\sigma_{ij}^{cd} + \frac{1}{2}\sum_{kl}\langle kl||ij\rangle\,\sigma_{kl}^{ab} + \hat{\mathcal{P}}(ij)\hat{\mathcal{P}}(ab)\sum_{kc}\langle kb||cj\rangle\,\sigma_{ik}^{ac}\,, \end{aligned} \tag{3.44b}$$

from which the doubles equation can be seen to be equivalent to the one of the **linearized coupled-cluster doubles** (LCCD) method,[37,70,148–150] which can be obtained from the CCSD doubles equation (2.164) by omitting all terms involving $\hat{T}_1$ amplitudes and the quadratic terms in $\hat{T}_2$. LCCD is also known under other names in the literature such as D-MBPT(∞)[104,151] or CEPA-0.[129,152] The ground-state energy obtained with these amplitudes is correct through third order in perturbation theory, and is also equivalent to the third-order expectation-value coupled-cluster method, XCC(3).[34] The singles equation, on the other hand, is formally identical to the second-order singles $t_{ai}^{(2)}$, see Eq. (2.171a), and since the singles amplitudes do not couple to the doubles, the LCCD equations can be iterated alone and the converged amplitudes can then be plugged into the singles equation.

3.3.2 Derivation of the UCC2 Secular Matrix Elements

In order to obtain excitation energies within the UCC scheme, the secular matrix $\tilde{\tilde{\mathbf{M}}}$ within the space of singles and doubles has to be diagonalized, which looks like

$$\begin{pmatrix} \tilde{\tilde{\mathbf{M}}}_{\mathrm{SS}} & \tilde{\tilde{\mathbf{M}}}_{\mathrm{SD}} \\ \tilde{\tilde{\mathbf{M}}}_{\mathrm{DS}} & \tilde{\tilde{\mathbf{M}}}_{\mathrm{DD}} \end{pmatrix} = \begin{pmatrix} \{\langle \Phi_i^a | \bar{H} - E_0^{\mathrm{UCC}} | \Phi_j^b \rangle\} & \{\langle \Phi_i^a | \bar{H} - E_0^{\mathrm{UCC}} | \Phi_{jk}^{bc} \rangle\} \\ \{\langle \Phi_{ij}^{ab} | \bar{H} - E_0^{\mathrm{UCC}} | \Phi_k^c \rangle\} & \{\langle \Phi_{ij}^{ab} | \bar{H} - E_0^{\mathrm{UCC}} | \Phi_{kl}^{cd} \rangle\} \end{pmatrix}, \tag{3.45}$$

where for the same arguments as discussed for ADC in Section 2.5.2 (page 27), only the singles-singles block needs to be expanded through second order, the coupling blocks through first order and the doubles-doubles block in zeroth order.

Starting with the $\tilde{\tilde{\mathbf{H}}}_{\mathrm{SS}}$ block and the bare Hamiltonian, the matrix elements $\langle \Phi_i^a | \hat{H} | \Phi_j^b \rangle$ can be evaluated diagrammatically as follows. Since there is a singly-excited determinant both on the left and on the right side of the operators, a pair of open particle and hole lines is required above and below the operator interaction line, respectively. The Fock operator can only couple two lines, which means the other pair of particle or hole indices needs to be identical, which is indicated by the additional separate line with two indices (counting as one), which gives rise to the Kronecker delta,

$\langle \Phi_i^a | \hat{F} + \hat{V} | \Phi_j^b \rangle =$

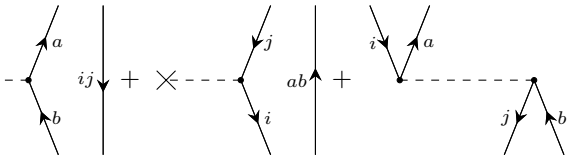

$$= f_{ab}\,\delta_{ij} - f_{ij}\,\delta_{ab} + \langle aj||ib\rangle\,, \tag{3.46}$$

where the first two diagrams have only one loop, since the separate open lines can be thought to form a loop with the other open lines by going towards infinity and come back again with another open line.[11] For non-HF references there might also be a contribution from the $[\hat{F}, \hat{\sigma}_1]$ commutator, that itself has contributions from both the $\hat{S}_1$ and the $\hat{S}_1^\dagger$ part of $\hat{\sigma}_1$,

$\langle \Phi_i^a | (\hat{F}\hat{S}_1 + \hat{S}_1^\dagger \hat{F})_{\mathrm{c}} | \Phi_j^b \rangle =$

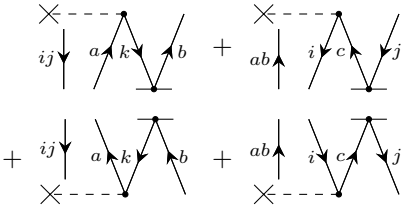

$$\begin{aligned} &= \delta_{ij} \sum_k f_{ka}\,\sigma_k^b + \delta_{ab} \sum_c f_{ic}\,\sigma_j^c \\ &\quad + \delta_{ij} \sum_k f_{ak}\,\sigma_k^{b*} + \delta_{ab} \sum_c f_{ci}\,\sigma_j^{c*}\,. \end{aligned} \tag{3.47}$$

The $[\hat{F}, \hat{\sigma}_2]$ commutator cannot contribute to the singles-singles block, hence the only remaining term in the singles-singles block is the second-order contribution $[\hat{V}, \hat{\sigma}_2]$, which

gives rise to three distinct contributions including their Hermitian conjugates, where the diagram is mirrored horizontally and thus the indices of the amplitude and two-electron integral are exchanged. Thus, only the part involving $\hat{S}_2$ is discussed. Since $\hat{S}_2$ has an excitation level of $+2$, but the total excitation of the commutator has to be zero, only the -2 fragment of $\hat{V}$ comes into play, but again this is only present in the $[\hat{V}, \hat{\sigma}_2]$ commutator of Eq. (3.37), but not in $[\hat{V}_\mathrm{R}, \hat{\sigma}_2]$, which is why the final equations will get an additional factor of $\frac{1}{2}$. The diagrams and their algebraic interpretation are given as

$\langle \Phi_i^a | (\hat{V}\hat{S}_2)_\mathrm{c} | \Phi_j^b \rangle =$ 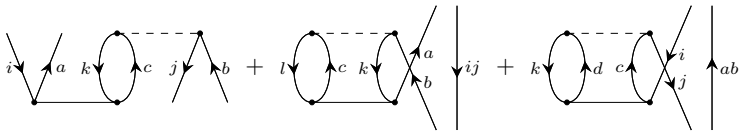

$$= \sum_{kc} \langle kj||cd\rangle \sigma_{ik}^{ac} - \frac{1}{2}\delta_{ij} \sum_{klc} \langle lk||cb\rangle \sigma_{lk}^{ca} - \frac{1}{2}\delta_{ab} \sum_{kcd} \langle kj||dc\rangle \sigma_{ki}^{dc} \,, \tag{3.48}$$

where the first term has three loops and three hole lines and thus a positive sign, whereas the other two have a negative sign because of two loops and three hole lines. By taking the missing factor of $\frac{1}{2}$ and the Hermitian conjugate part $\langle \Phi_i^a | (\hat{S}_2^\dagger \hat{V})_\mathrm{c} | \Phi_j^b \rangle$ into account, the resulting second-order part of the matrix element

$$\begin{aligned} \frac{1}{2}\langle \Phi_i^a | [\hat{V}, \hat{\sigma}_2] | \Phi_j^b \rangle = \frac{1}{2} \sum_{kc} \left[\langle kj||cd\rangle \sigma_{ik}^{ac} + \langle ac||ik\rangle \sigma_{kj}^{cd*} \right] \\ - \frac{1}{4}\delta_{ij} \sum_{klc} \left[\langle lk||cb\rangle \sigma_{lk}^{ca} + \langle ca||lk\rangle \sigma_{lk}^{cb*} \right] \\ - \frac{1}{4}\delta_{ab} \sum_{kcd} \left[\langle kj||dc\rangle \sigma_{ki}^{dc} + \langle dc||ki\rangle \sigma_{kj}^{dc*} \right] \end{aligned} \tag{3.49}$$

is seen to be equivalent to the corresponding contribution of the ADC(2) matrix, Eq. (2.119). As will be discussed in Chapter 4 (page 91), this equivalence does not hold if the BCH expansion is used for $\bar{H}$, but the matrix elements will be equivalent to a second-order ISR approach based on a CCD ground state.

Going on to the singles-doubles coupling block, only the first-order contribution from $\hat{V}$ contributes for a canonical HF reference, which corresponds to the identical contribution as in the CI matrix $\mathbf{H}_\mathrm{SD} = \mathbf{H}_\mathrm{DS}^\dagger$, but also to the corresponding first-order term of the ADC matrix $\mathbf{M}^{(1)}$. The matrix element can be evaluated diagramatically as

$\langle \Phi_i^a | \hat{V} | \Phi_{jk}^{bc} \rangle =$ 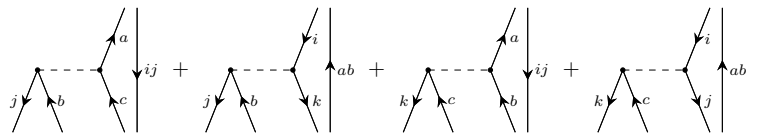

$$= \delta_{ik}\langle ja||bc\rangle - \delta_{ac}\langle jk||bi\rangle + \delta_{ij}\langle ka||cb\rangle - \delta_{ab}\langle kj||ci\rangle \,, \tag{3.50}$$

where the signs differ because each diagram has two loops but a different number of hole lines. The other coupling block $\tilde{\tilde{\mathbf{M}}}_{\mathrm{DS}} = \tilde{\tilde{\mathbf{M}}}_{\mathrm{SD}}^{\dagger}$ can analogously be evaluated as

$$\langle \Phi_{ij}^{ab} | \hat{V} | \Phi_k^c \rangle = \delta_{ik} \langle ab||cj\rangle - \delta_{ac} \langle kb||ij\rangle + \delta_{jk} \langle ba||ci\rangle - \delta_{bc} \langle ka||ji\rangle \,. \tag{3.51}$$

The only missing term is the zeroth-order contribution in the doubles-doubles block, $\langle \Phi_{ij}^{ab} | \hat{F} | \Phi_{kl}^{cd} \rangle$, which of course is identical to the corresponding CI or ADC matrix element given as the orbital-energy differences on the diagonal. The UCC2 matrix elements for a canonical HF reference can thus be summarized as

$$\begin{aligned} \bar{H}_{ia,bj}^{\mathrm{UCC2}} &= (\varepsilon_a - \varepsilon_i)\delta_{ab}\delta_{ij} + \langle aj||ib\rangle + \frac{1}{2}\sum_{kc}\left[\langle kj||cd\rangle \sigma_{ik}^{ac} + \langle ac||ik\rangle \sigma_{kj}^{cd*}\right] \\ &\quad - \frac{1}{4}\delta_{ij}\sum_{klc}\left[\langle lk||cb\rangle \sigma_{lk}^{ca} + \langle ca||lk\rangle \sigma_{lk}^{cd*}\right] \\ &\quad - \frac{1}{4}\delta_{ab}\sum_{kcd}\left[\langle kj||dc\rangle \sigma_{ki}^{dc} + \langle dc||ki\rangle \sigma_{kj}^{dc*}\right] \end{aligned} \tag{3.52a}$$

$$\bar{H}_{ijba,ck}^{\mathrm{UCC2}} = \delta_{ik}\langle ja||bc\rangle - \delta_{ac}\langle jk||bi\rangle + \delta_{ij}\langle ka||cb\rangle - \delta_{ab}\langle kj||ci\rangle \tag{3.52b}$$

$$\bar{H}_{ia,bckj}^{\mathrm{UCC2}} = \delta_{ik}\langle ab||cj\rangle - \delta_{ac}\langle kb||ij\rangle + \delta_{jk}\langle ba||ci\rangle - \delta_{bc}\langle ka||ji\rangle \tag{3.52c}$$

$$\bar{H}_{ijba,cdlk}^{\mathrm{UCC2}} = (\varepsilon_a + \varepsilon_b - \varepsilon_i - \varepsilon_j)\delta_{ik}\delta_{jl}\delta_{ac}\delta_{bd} \,. \tag{3.52d}$$

It should be noted that apart from the terms given in Eq. (3.47), there will also be contributions from matrix elements like $\langle \Phi_i^a | \hat{F} | \Phi_{jk}^{bc} \rangle$, $\langle \Phi_{ij}^{ab} | \hat{F} | \Phi_k^c \rangle$, $\langle \Phi_i^a | (\hat{F}\hat{\sigma}_1)_{\mathrm{c}} | \Phi_{jk}^{bc} \rangle$ and $\langle \Phi_{ij}^{ab} | (\hat{F}\hat{\sigma}_1)_{\mathrm{c}} | \Phi_k^c \rangle$ for a non-HF reference, since Brillouin's theorem does not hold, $f_{ai} \neq 0$, and the $\hat{\sigma}_1$ amplitudes then already appear in first order.

3.4 The Third-Order UCC3 Scheme

Now, the approach presented in Section 3.3 will be extended to third order. For this, the commutators with $\hat{\sigma}_1$ need to be included in Eq. (3.35c) as well as the double commutators with $\hat{\sigma}_2$ in Eq. (3.35d) to take all third-order terms into account. The UCC3 Hamiltonian is thus given as

$$\begin{aligned} \bar{H}^{\mathrm{UCC3}} &= \hat{F} + \hat{V} + [\hat{F}, \hat{\sigma}_1 + \hat{\sigma}_2] + \frac{1}{2}[\hat{V}, \hat{\sigma}_1 + \hat{\sigma}_2] + \frac{1}{2}[\hat{V}_{\mathrm{R}}, \hat{\sigma}_1 + \hat{\sigma}_2] \\ &\quad + \frac{1}{12}[[\hat{V}_{\mathrm{ND}}, \hat{\sigma}_2], \hat{\sigma}_2] + \frac{1}{4}[[\hat{V}, \hat{\sigma}_2]_{\mathrm{R}}, \hat{\sigma}_2] + \frac{1}{4}[[\hat{V}_{\mathrm{R}}, \hat{\sigma}_2]_{\mathrm{R}}, \hat{\sigma}_2] \\ &= \bar{H}^{\mathrm{UCC2}} + \frac{1}{2}[\hat{V}, \hat{\sigma}_1] + \frac{1}{2}[\hat{V}_{\mathrm{R}}, \hat{\sigma}_1] \\ &\quad + \frac{1}{12}[[\hat{V}_{\mathrm{ND}}, \hat{\sigma}_2], \hat{\sigma}_2] + \frac{1}{4}[[\hat{V}, \hat{\sigma}_2]_{\mathrm{R}}, \hat{\sigma}_2] + \frac{1}{4}[[\hat{V}_{\mathrm{R}}, \hat{\sigma}_2]_{\mathrm{R}}, \hat{\sigma}_2] \,, \end{aligned} \tag{3.53}$$

where for the first time double commutators occur and the "rest" part needs to be taken after a commutator, which will be explained at a later point.

3.4.1 Derivation of the UCC3 Amplitude Equations

The UCC3 amplitude equations correspond to the UCC2 ones plus the additional third-order terms arising from the single commutators of $\hat{V}$ with $\hat{\sigma}_1$ and the double commutators of $\hat{V}$ with $\hat{\sigma}_2$, as can be seen in Eq. (3.53). Let me first discuss the contributions of $\hat{\sigma}_1$ to the singles equation, where two different terms need to be distinguished. The first one contains the excitation operator $\hat{S}_1$ and thus needs a fragment of the fluctuation potential with an excitation level of 0 and a pair of particle and hole lines above the interaction line, such that the only possibility is the one already given for the CCSD case in Eq. (2.161),

$$\langle \Phi_i^a | (\hat{V}\hat{S}_1)_\mathrm{c} | \Phi_0 \rangle = \sum_{jb} \langle aj||ib\rangle \, \sigma_j^b \,, \tag{3.54}$$

which occurs also in $\hat{V}_\mathrm{R}$, and thus no additional factor of $\frac{1}{2}$ needs to be included. However, the deexcitation operator $\hat{S}_1^\dagger$ can also contribute here by including the fragment of the fluctuation potential with an excitation level of +2,

$$\langle \Phi_i^a | (\hat{S}_1^\dagger \hat{V})_\mathrm{c} | \Phi_0 \rangle = \quad$$

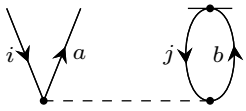

$$= \sum_{jb} \langle ab||ij\rangle \, \sigma_j^{b*} \,, \tag{3.55}$$

where the final contribution will get a factor of $\frac{1}{2}$ since the required fragment of the fluctuation potential is not included in the commutator involving $\hat{V}_\mathrm{R}$ in Eq. (3.53). No such differentiation needs to be done for the contribution of $\hat{\sigma}_1$ to the doubles equation, since only $\hat{S}_1$ can contribute with a +1 fragment of the fluctuation potential. The deexcitation part $\hat{S}_1^\dagger$ would require an excitation level +3, which is not present in $\hat{V}$. The $[\hat{V}, \hat{S}_1]$ commutator has already been evaluated in Eq. (2.162) for the CCSD case, but is equivalent to the one here, and thus

$$\langle \Phi_{ij}^{ab} | (\hat{V}\hat{S}_1)_\mathrm{c} | \Phi_0 \rangle = \hat{\mathcal{P}}(ij) \sum_c \langle ab||cj\rangle \, \sigma_i^c - \hat{\mathcal{P}}(ab) \sum_k \langle kb||ij\rangle \, \sigma_k^a \,. \tag{3.56}$$

Special care needs to be taken for double commutators involving $\hat{\sigma}$, since they can be rewritten in terms of four commutators involving $\hat{S}$ and $\hat{S}^\dagger$. In the most general case, this can be written as

$$[[\hat{O}, \hat{\sigma}_m], \hat{\sigma}_n] = [[\hat{O}, \hat{S}_m], \hat{S}_n] + [\hat{S}_n^\dagger, [\hat{S}_m^\dagger, \hat{O}]] + [\hat{S}_n^\dagger, [\hat{O}, \hat{S}_m]] + [[\hat{S}_n^\dagger, \hat{O}], \hat{S}_m] \,, \tag{3.57}$$

for an arbitrary operator $\hat{O}$. The only double commutators (DC) occurring in the UCC3 scheme are the ones involving $\hat{\sigma}_2$ in Eq. (3.53),

$$\bar{H}_\mathrm{DC}^\mathrm{UCC3} = \frac{1}{12}[[\hat{V}_\mathrm{ND}, \hat{\sigma}_2], \hat{\sigma}_2] + \frac{1}{4}[[\hat{V}, \hat{\sigma}_2]_\mathrm{R}, \hat{\sigma}_2] + \frac{1}{4}[[\hat{V}_\mathrm{R}, \hat{\sigma}_2]_\mathrm{R}, \hat{\sigma}_2] \,, \tag{3.58}$$

for which Eq. (3.57) can be written as $[[\hat{H}, \hat{\sigma}_2], \hat{\sigma}_2] = [[\hat{H}, \hat{S}_2], \hat{S}_2] + [\hat{S}_2^\dagger, [\hat{S}_2^\dagger, \hat{H}]] +$

$[\hat{S}_2^\dagger,[\hat{H},\hat{S}_2]]+[[\hat{S}_2^\dagger,\hat{H}],\hat{S}_2]$. Starting with the singles equation of Eq. (3.36), $\langle\Phi_i^a|\bar{H}|\Phi_0\rangle = 0$, the two double commutators that involve only $\hat{S}_2$ or $\hat{S}_2^\dagger$ do not contribute because the excitation levels cannot match. Hence, only the mixed commutators involving both $\hat{S}_2$ and $\hat{S}_2^\dagger$ make a contribution. For this, only the +1 fragments of the fluctuation potential are required, which is why the first commutator in Eq. (3.58) involving $\hat{V}_{\mathrm{ND}}$ does not contribute. Thus, only the other two double commutators can possibly contribute to the singles equation. In order to derive the explicit terms, a prior look at the operator fragments seems advantageous. In the middle is a +1 fragment from the fluctuation potential, Figure 2.4 (page 42), on top of that is a $\hat{S}_2^\dagger$ and below a $\hat{S}_2$ fragment, see the cluster operators in Figure 2.5 (page 42). According to the matrix element, the target indices (i and a) can either be both from the $\hat{V}$ fragment, both from the $\hat{S}_2$ operator, or one on $\hat{V}$ and the other one on $\hat{S}_2$. The task now is to find all possible, *uniquely connected* diagrams.

The most straightforward possibility is the first one with both target indices on the $\hat{V}$ fragment, which gives rise to two contributions as

$$\langle\Phi_i^a|(\hat{S}_2^\dagger\hat{V}\hat{S}_2)_{\mathrm{c}}|\Phi_0\rangle \leftarrow$$

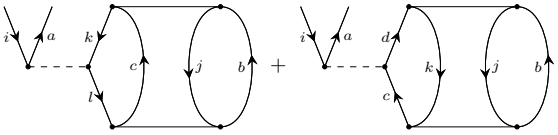

$$= -\frac{1}{2}\sum_{jklbc}\langle al||ik\rangle\,\sigma_{lj}^{cb}\sigma_{kj}^{cb*} + \frac{1}{2}\sum_{jkbcd}\langle ad||ic\rangle\,\sigma_{kj}^{cb}\sigma_{kj}^{db*}\,, \tag{3.59}$$

where the left arrow again indicates that it is only one of several contributions to the matrix element. The prefactors arise from a pair of equivalent particle or hole indices and the signs differ because both diagrams have three loops, but four or three hole lines, respectively. The most difficult contribution is when one target index (one open line) comes from $\hat{V}$ and the other one from $\hat{S}_2$. In order to find only uniquely connected diagrams, the procedure developed by Kucharski and Bartlett is useful.[9,11,102] Here, as a first step, + symbols are assigned to particle lines and − symbols to hole lines between the interaction lines. These signs are combined in all unique ways in order to produce only unique connectivities of the operator diagrams. Since the $\hat{V}$ fragment has one open line and the $\hat{S}_2$ fragment the other one, the $\hat{S}_2^\dagger$ fragment has two connections with $\hat{V}$, whereas $\hat{S}_2$ has only one, which are the only relevant connections to define the uniqueness. For example, choosing one + and one − connection with $\hat{S}_2^\dagger$ and one − connection with $\hat{S}_2$, this "sign sequence" will be denoted as $+-|-$, where the first pair of signs belongs to the $\hat{S}_2^\dagger$ operator, and the one after the vertical bar to $\hat{S}_2$. Thus, there are only four unique ways to combine them: (1) $++|+$, (2) $--|-$, (3) $+-|+$, and (4) $+-|-$. The

four corresponding diagrams and their algebraic interpretation are given as (in order)

$$\langle \Phi_i^a | (\hat{S}_2^\dagger \hat{V} \hat{S}_2)_\mathrm{c} | \Phi_0 \rangle \leftarrow$$

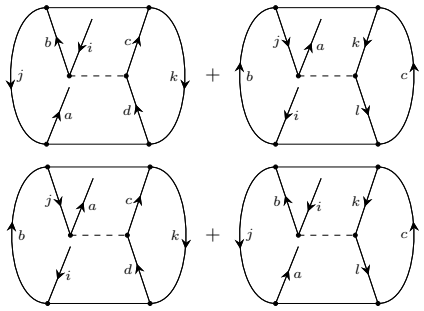

$$= -\frac{1}{4} \sum_{jkbcd} \langle bc||id\rangle \, \sigma_{jk}^{ad} \sigma_{jk}^{bc*} + \frac{1}{4} \sum_{jklbc} \langle al||jk\rangle \, \sigma_{il}^{bc} \sigma_{jk}^{bc*} - \sum_{jkbcd} \langle ac||jd\rangle \, \sigma_{ik}^{bd} \sigma_{jk}^{bc*} + \sum_{jklbc} \langle bl||ik\rangle \, \sigma_{jl}^{ac} \sigma_{jk}^{bc*} \,, \tag{3.60}$$

where the factor of $\frac{1}{4}$ in the first two diagrams comes from two pairs of equivalent lines. The last contribution to the singles equation comes from the part where both target indices i and a are on the $\hat{S}_2$ fragment. However, in this case the order of the commutators in Eq. (3.57) is of importance. If the inner part is $[\hat{S}_2^\dagger, \hat{V}]$, this commutator forms an intermediate of the form 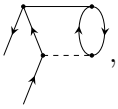 , which corresponds to a single deexcitation (the direction of the arrows is not important here), and this term is vanished by the "R" operation after the second and third commutator of Eq. (3.58). The other possibility, where the inner commutator corresponds to $[\hat{V}, \hat{S}_2]$, generates an intermediate of the form 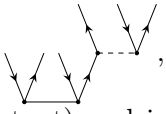 , which corresponds to a triple excitation (the arrow direction is not important) and is **not vanished** by the "R" operation, since the UCCSD amplitude equations as written in Eq. (3.32) only guarantee that the nondiagonal part of $\bar{V}$ vanishes for single and double (de)excitations, but not necessarily for triples. Hence, only half of the corresponding terms contribute and the final matrix elements will get an additional factor of $\frac{1}{2}$. Neglecting this subtlety for a moment, the final diagrams are obtained by adding the missing $\hat{S}_2$ or $\hat{S}_2^\dagger$ fragment to obtain

$$\langle \Phi_i^a | (\hat{S}_2^\dagger \hat{V} \hat{S}_2)_\mathrm{c} | \Phi_0 \rangle \leftarrow$$

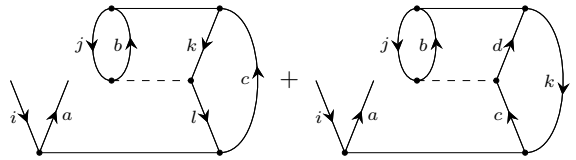

$$= -\frac{1}{2} \sum_{jklbc} \langle bl||jk\rangle \, \sigma_{il}^{ac} \sigma_{jk}^{bc*} + \frac{1}{2} \sum_{jkbcd} \langle bd||jc\rangle \, \sigma_{ik}^{ac} \sigma_{jk}^{bd*} \,, \tag{3.61}$$

where this factor of $\frac{1}{2}$ comes from a pair of equivalent hole or particle lines. Hence, the final contributions of Eq. (3.61) will have a prefactor of $\frac{1}{4}$.

Let me go on with the third-order contributions to the doubles equation, $\langle \Phi_{ij}^{ab} | \bar{H} | \Phi_0 \rangle = 0$. The simple commutator of the fluctation potential with $\hat{\sigma}_1$ gives only a contribution for the $\hat{S}_1$ part, since otherwise the excitation levels do not match. This commutator is thus identical to the corresponding CCSD term, which has already been derived in Eq. (2.162). The only remaining part is again the double commutator with $\hat{\sigma}_2$. Here, in addition to the mixed commutators involving both $\hat{S}_2$ and $\hat{S}_2^\dagger$, also the part of Eq. (3.57) with two $\hat{S}_2$ fragments contributes, which actually corresponds to an analogous contribution to the CCSD doubles equation. The +4 excitation level from the two $\hat{S}_2$ operators is met by the -2 part of the fluctuation potential to yield a total excitation level of +2, matching the doubly-excited determinant on the left of the matrix element. Since only the -2 fragment of $\hat{V}$ is used, the third commutator involving $\hat{V}_\mathrm{R}$ in Eq. (3.58) does not contribute. The second commutator, on the other hand, is not vanished by the "R" operation, since the intermediates are no pure excitations or deexcitations.

Employing again the Kucharski–Bartlett sign sequences, there are four unique connectivity patterns of the cluster operators to the fluctation potential: (1) $+-|+-$, (2) $++|--$, (3) $++-|-$, and (4) $+--|+$, where the order of the parts left and right of the vertical bar does not matter since the $\hat{S}_2$ operators commute. The resulting diagrams and their algebraic interpretation are given as (in order)

$$\begin{aligned}
\frac{1}{3}\langle \Phi_{ij}^{ab} | (\hat{V}\hat{S}_2^2)_\mathrm{c} | \Phi_0 \rangle = {} & \\
& + \\
& + \\
= {} & \frac{1}{3}\hat{\mathcal{P}}(ij)\hat{\mathcal{P}}(ab) \sum_{klcd} \langle kl||cd\rangle \, \sigma_{ik}^{ac} \sigma_{lj}^{db} + \frac{1}{6} \sum_{klcd} \langle kl||cd\rangle \, \sigma_{ij}^{cd} \sigma_{kl}^{ab} \\
& - \frac{1}{3}\hat{\mathcal{P}}(ab) \sum_{klcd} \langle kl||cd\rangle \, \sigma_{ij}^{ac} \sigma_{kl}^{bd} - \frac{1}{3}\hat{\mathcal{P}}(ij) \sum_{klcd} \langle kl||cd\rangle \, \sigma_{ik}^{ab} \sigma_{jl}^{cd} \, ,
\end{aligned} \tag{3.62}$$

where the first diagram has the prefactor because of a pair of equivalent vertices (that would correspond to $\frac{1}{2}$ in CCSD[9] and differs here because of the Bernoulli expansion for $\bar{H}$), the third and fourth diagram have one pair of equivalent lines each, and the second diagram has an additional factor of $\frac{1}{2}$ because it has two pairs of equivalent lines.

The last contributions to the doubles equation comes from the double commutators in Eq. (3.58) involving one $\hat{S}_2$ and one $\hat{S}_2^\dagger$ fragment in combination with the +2 fragment of $\hat{V}$. The same conclusions whether the double commutators of Eq. (3.58) contribute or not hold as previously for the $\hat{S}_2^2$ case. However, more care has to be taken here since the operator fragments do not commute with each other, which gives rise to seven unique Kucharski–Bartlett sign sequences: (1) $+-|+-$, (2) $++|--$, (3) $--|++$, (4) $++-|-$, (5) $+--|+$, (6) $+|+--$, and (7) $-|++-$, where only the first one is symmetric. The

corresponding diagrams (in order) and their algebraic interpretations are given as

$$
\begin{aligned}
&\frac{1}{3}\langle\Phi_{ij}^{ab}|(\hat{S}_2^\dagger \hat{V} \hat{S}_2)_\mathrm{c}|\Phi_0\rangle = \\
&\quad + \\
&\quad + \\
&\quad + \\
&= \frac{1}{3}\hat{\mathcal{P}}(ij)\hat{\mathcal{P}}(ab)\sum_{klcd}\langle ac||ik\rangle\, \sigma_{lj}^{db}\sigma_{kl}^{cd*} \\
&\quad + \frac{1}{12}\sum_{klcd}\langle cd||ij\rangle\, \sigma_{kl}^{ab}\sigma_{kl}^{cd*} + \frac{1}{12}\sum_{klcd}\langle ab||kl\rangle\, \sigma_{ij}^{cd}\sigma_{kl}^{cd*} \\
&\quad - \frac{1}{6}\hat{\mathcal{P}}(ij)\sum_{klcd}\langle cd||ki\rangle\, \sigma_{lj}^{ab}\sigma_{kl}^{cd*} - \frac{1}{6}\hat{\mathcal{P}}(ab)\sum_{klcd}\langle ca||kl\rangle\, \sigma_{ij}^{db}\sigma_{kl}^{cd*} \\
&\quad - \frac{1}{6}\hat{\mathcal{P}}(ab)\sum_{klcd}\langle ac||ij\rangle\, \sigma_{kl}^{bd}\sigma_{kl}^{cd*} - \frac{1}{6}\hat{\mathcal{P}}(ij)\sum_{klcd}\langle ab||ik\rangle\, \sigma_{jl}^{cd}\sigma_{kl}^{cd*}\,,
\end{aligned}
\tag{3.63}
$$

where the first diagram has a pair of equivalent vertices but is the only term that actually occurs twice in the double commutator for symmetry reasons, the last four diagrams have one pair of equivalent particle or hole lines each but are unique (meaning they occur only once), and the second and third diagram also occur only once but have two pairs of equivalent lines, thus explaining the different prefactors.

It should be noted that in the original publication the terms in the amplitude equations stemming from the bare Hamiltonian $\hat{H}$ were not shown.[51]

The final UCC3 amplitude equations[51] can thus be summarized in the following:

$$
\begin{aligned}
0 = \bar{H}^{\mathrm{UCC3}}_{ai} &= f_{ai} + \sum_{b} f_{ab}\,\sigma^{b}_{i} - \sum_{j} f_{ji}\,\sigma^{a}_{j} + \sum_{jb} f_{jb}\,\sigma^{ab}_{ij} \\
&+ \frac{1}{2}\sum_{jbc}\langle aj||bc\rangle\sigma^{bc}_{ij} - \frac{1}{2}\sum_{jkb}\langle jk||ib\rangle\sigma^{ab}_{jk} + \sum_{jb}\langle aj||ib\rangle\,\sigma^{b}_{j} + \frac{1}{2}\sum_{jb}\langle ab||ij\rangle\,\sigma^{b*}_{j} \\
&- \frac{1}{2}\sum_{jklbc}\langle al||ik\rangle\,\sigma^{cb}_{lj}\sigma^{cb*}_{kj} + \frac{1}{2}\sum_{jkbcd}\langle ad||ic\rangle\,\sigma^{cb}_{kj}\sigma^{db*}_{kj} \\
&- \frac{1}{4}\sum_{jkbcd}\langle bc||id\rangle\,\sigma^{ad}_{jk}\sigma^{bc*}_{jk} + \frac{1}{4}\sum_{jklbc}\langle al||jk\rangle\,\sigma^{bc}_{il}\sigma^{bc*}_{jk} \\
&- \sum_{jkbcd}\langle ac||jd\rangle\,\sigma^{bd}_{ik}\sigma^{bc*}_{jk} + \sum_{jklbc}\langle bl||ik\rangle\,\sigma^{ac}_{jl}\sigma^{bc*}_{jk} \\
&- \frac{1}{4}\sum_{jklbc}\langle bl||jk\rangle\,\sigma^{ac}_{il}\sigma^{bc*}_{jk} + \frac{1}{4}\sum_{jkbcd}\langle bd||jc\rangle\,\sigma^{ac}_{ik}\sigma^{bd*}_{jk}
\end{aligned}
\tag{3.64a}
$$

$$
\begin{aligned}
0 = \bar{H}^{\mathrm{UCC3}}_{ab,ij} &= \langle ab||ij\rangle + \hat{\mathcal{P}}(ab)\sum_{c} f_{bc}\,\sigma^{ac}_{ij} - \hat{\mathcal{P}}(ij)\sum_{k} f_{kj}\,\sigma^{ab}_{ik} \\
&+ \frac{1}{2}\sum_{cd}\langle ab||cd\rangle\,\sigma^{cd}_{ij} + \frac{1}{2}\sum_{kl}\langle kl||ij\rangle\,\sigma^{ab}_{kl} + \hat{\mathcal{P}}(ij)\hat{\mathcal{P}}(ab)\sum_{kc}\langle kb||cj\rangle\,\sigma^{ac}_{ik} \\
&+ \hat{\mathcal{P}}(ij)\sum_{c}\langle ab||cj\rangle\,\sigma^{c}_{i} - \hat{\mathcal{P}}(ab)\sum_{k}\langle kb||ij\rangle\,\sigma^{a}_{k} \\
&+ \frac{1}{3}\hat{\mathcal{P}}(ij)\hat{\mathcal{P}}(ab)\sum_{klcd}\langle kl||cd\rangle\,\sigma^{ac}_{ik}\sigma^{db}_{lj} + \frac{1}{6}\sum_{klcd}\langle kl||cd\rangle\,\sigma^{cd}_{ij}\sigma^{ab}_{kl} \\
&- \frac{1}{3}\hat{\mathcal{P}}(ab)\sum_{klcd}\langle kl||cd\rangle\,\sigma^{ac}_{ij}\sigma^{bd}_{kl} - \frac{1}{3}\hat{\mathcal{P}}(ij)\sum_{klcd}\langle kl||cd\rangle\,\sigma^{ab}_{ik}\sigma^{cd}_{jl} \\
&+ \frac{1}{3}\hat{\mathcal{P}}(ij)\hat{\mathcal{P}}(ab)\sum_{klcd}\langle ac||ik\rangle\,\sigma^{db}_{lj}\sigma^{cd*}_{kl} \\
&+ \frac{1}{12}\sum_{klcd}\langle cd||ij\rangle\,\sigma^{ab}_{kl}\sigma^{cd*}_{kl} + \frac{1}{12}\sum_{klcd}\langle ab||kl\rangle\,\sigma^{cd}_{ij}\sigma^{cd*}_{kl} \\
&- \frac{1}{6}\hat{\mathcal{P}}(ij)\sum_{klcd}\langle cd||ki\rangle\,\sigma^{ab}_{lj}\sigma^{cd*}_{kl} - \frac{1}{6}\hat{\mathcal{P}}(ab)\sum_{klcd}\langle ca||kl\rangle\,\sigma^{db}_{ij}\sigma^{cd*}_{kl} \\
&- \frac{1}{6}\hat{\mathcal{P}}(ab)\sum_{klcd}\langle ac||ij\rangle\,\sigma^{bd}_{kl}\sigma^{cd*}_{kl} - \frac{1}{6}\hat{\mathcal{P}}(ij)\sum_{klcd}\langle ab||ik\rangle\,\sigma^{cd}_{jl}\sigma^{cd*}_{kl}\,.
\end{aligned}
\tag{3.64b}
$$

3.4.2 The UCC3 Secular Matrix Elements

In order to obtain electronic excitation energies with the UCC3 scheme, also the elements of the secular matrix (3.45) need to be expanded one order higher, respectively. This means $\tilde{\tilde{\mathbf{M}}}_{\mathrm{SS}}$ needs to be expanded through third order, $\tilde{\tilde{\mathbf{M}}}_{\mathrm{SD}}$ and $\tilde{\tilde{\mathbf{M}}}_{\mathrm{DS}}$ through second order and $\tilde{\tilde{\mathbf{M}}}_{\mathrm{DD}}$ through first order. Their derivation is very lengthy and thus omitted here, only the final results are presented.

There are two distinct third-order contributions in the singles-singles block, one from the single commutator of $\hat{V}$ with $\hat{\sigma}_1$, and one from the double commutator with $\hat{\sigma}_2$. The former is given as[51]

$$\begin{aligned}\langle\Phi_i^a|(\hat{V}\hat{S}_1+\hat{S}_1^\dagger\hat{V})_\mathrm{c}|\Phi_j^b\rangle = \big(&\delta_{ab}\sum_{kc}\langle ik||jc\rangle\,\sigma_k^c+\delta_{ij}\sum_{kc}\langle ak||bc\rangle\,\sigma_k^c\\&+\sum_c\langle ai||cb\rangle\,\sigma_j^c-\sum_k\langle ki||jb\rangle\,\sigma_k^a\big)+\mathrm{h.c.}\,,\end{aligned}\tag{3.65}$$

where "h.c." stands for Hermitian conjugate.

The third-order terms arising from the double commutator with $\hat{\sigma}_2$ are given as[51]

$$\begin{aligned}\langle\Phi_i^a|(\hat{S}_2^\dagger\hat{V}\hat{S}_2)_\mathrm{c}|\Phi_j^b\rangle = &\big(\big(\frac{1}{2}\delta_{ab}\sum_{klcde}\langle ie||cl\rangle\,\sigma_{jk}^{cd}\sigma_{kl}^{de*}\\&+\frac{1}{8}\delta_{ab}\sum_{klmcd}\langle im||kl\rangle\,\sigma_{jm}^{cd}\sigma_{kl}^{ab*}\big)+\mathrm{h.c.}\big)\\&-\frac{1}{2}\delta_{ab}\sum_{klmcd}\langle im||jl\rangle\,\sigma_{kl}^{cd*}\sigma_{km}^{cd}+\frac{1}{2}\delta_{ab}\sum_{klcde}\langle ie||jd\rangle\,\sigma_{kl}^{cd}\sigma_{kl}^{ce*}\\&-\big(\big(\frac{1}{2}\delta_{ij}\sum_{klmcd}\langle md||bl\rangle\,\sigma_{km}^{ca}\sigma_{kl}^{cd*}\\&+\frac{1}{8}\delta_{ij}\sum_{klcde}\langle de||bc\rangle\,\sigma_{kl}^{ac}\sigma_{kl}^{ed*}\big)+\mathrm{h.c.}\big)\\&+\frac{1}{2}\delta_{ij}\sum_{klcde}\langle ad||bc\rangle\,\sigma_{kl}^{ec}\sigma_{kl}^{ed*}-\frac{1}{2}\delta_{ij}\sum_{klmcd}\langle ma||lb\rangle\,\sigma_{km}^{cd}\sigma_{kl}^{cd*}\\&+\big(\big(\frac{1}{4}\sum_{klmc}\langle im||kl\rangle\sigma_{kl}^{bc*}\sigma_{jm}^{ac}+\frac{1}{4}\sum_{kcde}\langle ce||bd\rangle\,\sigma_{ik}^{ce*}\sigma_{jk}^{ad}\\&-\frac{1}{2}\sum_{klcd}\langle lc||kb\rangle\,\sigma_{jl}^{ad}\sigma_{ik}^{cd*}-\frac{1}{2}\sum_{klcd}\langle id||kc\rangle\,\sigma_{jl}^{ac}\sigma_{kl}^{bd*}\\&-\frac{1}{4}\sum_{klcd}\langle id||bj\rangle\,\sigma_{kl}^{ca}\sigma_{kl}^{cd*}-\frac{1}{4}\sum_{klcd}\langle ia||bl\rangle\,\sigma_{jk}^{dc}\sigma_{kl}^{cd*}\\&-\sum_{klcd}\langle ia||kc\rangle\,\sigma_{jl}^{cd}\sigma_{kl}^{bd*}\big)+\mathrm{h.c.}\big)\\&+\sum_{klmc}\langle ik||lj\rangle\,\sigma_{km}^{ac}\sigma_{lm}^{bc*}+\sum_{kcde}\langle ad||cb\rangle\,\sigma_{jk}^{ce}\sigma_{ik}^{de*}\\&+\frac{1}{2}\sum_{klcd}\langle ka||bl\rangle\,\sigma_{kj}^{cd}\sigma_{il}^{cd*}+\frac{1}{2}\sum_{klcd}\langle ic||dj\rangle\,\sigma_{kl}^{cb*}\sigma_{kl}^{ad}\,.\end{aligned}\tag{3.66}$$

The second-order terms in the coupling blocks come from the commutator of $\hat{V}$ with $\hat{\sigma}_2$, where depending on the block only one cluster fragment ($\hat{S}_2$ or $\hat{S}_2^\dagger$) can contribute,

and the singles-doubles block is given as[51]

$$\begin{aligned}\langle\Phi_i^a|(\hat{S}_2^\dagger\hat{V})_\mathrm{c}|\Phi_{jk}^{bc}\rangle &= \delta_{ij}\hat{\mathcal{P}}(bc)\hat{\mathcal{P}}(jk)\sum_{lc}\langle ac||bl\rangle\,\sigma_{kl}^{bc*} + \frac{1}{2}\delta_{ij}\hat{\mathcal{P}}(jk)\sum_{lm}\langle ak||lm\rangle\,\sigma_{lm}^{bc*} \\ &\quad - \delta_{ab}\hat{\mathcal{P}}(bc)\hat{\mathcal{P}}(jk)\sum_{ld}\langle jd||il\rangle\,\sigma_{kl}^{cd*} - \frac{1}{2}\delta_{ab}\hat{\mathcal{P}}(bc)\sum_{de}\langle de||ic\rangle\,\sigma_{jk}^{de*} \\ &\quad - \hat{\mathcal{P}}(jk)\sum_{l}\langle ak||il\rangle\,\sigma_{jl}^{bc*} + \hat{\mathcal{P}}(bc)\sum_{d}\langle ad||ib\rangle\,\sigma_{jk}^{dc*}\,,\end{aligned} \tag{3.67}$$

and the other coupling block is the Hermitian conjugate of this one. The first-order contribution to the doubles-doubles block is given as[51]

$$\begin{aligned}\langle\Phi_{ij}^{ab}|\hat{V}|\Phi_{kl}^{cd}\rangle &= \delta_{ik}\delta_{jl}\langle ab||cd\rangle + \delta_{ac}\delta_{bd}\langle kl||ij\rangle - \hat{\mathcal{P}}(cd)\hat{\mathcal{P}}(kl)\big(\delta_{bd}\delta_{jl}\langle ak||ci\rangle \\ &\quad + \delta_{bd}\delta_{ik}\langle al||cj\rangle + \delta_{ac}\delta_{jl}\langle bk||di\rangle + \delta_{ac}\delta_{ik}\langle bl||dj\rangle\big)\,.\end{aligned} \tag{3.68}$$

3.5 Strict UCC Variants and Connection to ADC

In the following, the "**strict**" versions of UCCn ($n = 2, 3$) , denoted UCCn-s, are referred to as the ones that contain the *minimum number of terms* required for obtaining excitation energies of predominantly singly-excited states correct to order n.[51] This corresponds to a perturbation expansion of the matrix elements of $\tilde{\tilde{\mathbf{H}}}$ that uses amplitudes derived from standard perturbation theory, as discussed for traditional CC in Section 2.6.7 (page 48). In low order, the perturbation expansion of $\hat{T}$ is the same as for $\hat{\sigma}$, such that the first- and second-order amplitudes required for UCC2 and UCC3 are the same as the ones given in Eqs. (2.170) and (2.171), where the first-order singles amplitudes vanish, $\sigma_i^{a(1)} = 0$. The UCC3-s Hamiltonian is thus given as

$$\bar{H}^{\text{UCC3-s}} = \bar{H}^{(0)} + \bar{H}^{(1)} + \bar{H}^{(2)} + \bar{H}^{(3)}\,, \tag{3.69}$$

where the individual terms are given as[51]

$$\bar{H}^{(0)} = \hat{F} \tag{3.70a}$$

$$\bar{H}^{(1)} = [\hat{F}, \hat{\sigma}_2^{(1)}] + \hat{V} \tag{3.70b}$$

$$\bar{H}^{(2)} = [\hat{F}, \hat{\sigma}_1^{(2)} + \hat{\sigma}_2^{(2)}] + \frac{1}{2}[\hat{V}, \hat{\sigma}_2^{(1)}] + \frac{1}{2}[\hat{V}_\mathrm{R}, \hat{\sigma}_2^{(1)}] \tag{3.70c}$$

$$\begin{aligned}\bar{H}^{(3)} &= [\hat{F}, \hat{\sigma}_1^{(3)} + \hat{\sigma}_2^{(3)}] + \frac{1}{2}[\hat{V}, \hat{\sigma}_2^{(2)}] + \frac{1}{2}[\hat{V}_\mathrm{R}, \hat{\sigma}_2^{(2)}] \\ &\quad + \frac{1}{12}[[\hat{V}_\mathrm{ND}, \hat{\sigma}_2^{(1)}], \hat{\sigma}_2^{(1)}] + \frac{1}{4}[[\hat{V}, \hat{\sigma}_2^{(1)}]_\mathrm{R}, \hat{\sigma}_2^{(1)}] + \frac{1}{4}[[\hat{V}_\mathrm{R}, \hat{\sigma}_2^{(1)}]_\mathrm{R}, \hat{\sigma}_2^{(1)}]\,,\end{aligned} \tag{3.70d}$$

which differs from the expansion of standard CC in Eq. (2.166) due to the Bernoulli expansion. The perturbation expansion is simpler than the corresponding one using the BCH expansion for $\bar{H}$, since at most single commutators are needed for $\bar{H}^{(2)}$ and double commutators for $\bar{H}^{(3)}$. The UCC secular matrix elements thus still have the same form

as derived in previous sections, only the converged amplitudes need to be replaced by the n-th order ones. Plugging the first-order doubles amplitudes $t_{ijab}^{(1)} = \sigma_{ij}^{ab(1)} = \frac{\langle ab||ij\rangle}{\varepsilon_i+\varepsilon_j-\varepsilon_a-\varepsilon_b}$ into the UCC2 secular matrix elements (3.52), the identical terms as for the ADC(2) matrix (2.119) are obtained, thus establishing the equivalence of UCC2-s and ADC(2) for excitation energies. The same equivalence can be shown for the strict UCC3 and ADC(3) schemes,[51] since the UCC2 amplitude equations are exactly contained in CCSD, the second-order amplitudes from UCC are identical to the ones obtained in the iterations of standard CC theory, $\hat{\sigma}_1^{(2)} = \hat{T}_1^{(2)}$ and $\hat{\sigma}_2^{(2)} = \hat{T}_2^{(2)}$, which correspond to the MP amplitudes used in ADC. However, the UCC3 amplitude equations differ from traditional CC, since contributions from $\hat{S}_2^\dagger$ occur for the first time, and hence the third-order doubles amplitudes will differ, $\hat{\sigma}_2^{(3)} \neq \hat{T}_2^{(3)}$. Together with the fluctation potential $\hat{V}$, these amplitudes occur for instance as a fourth-order term in the p-h/p-h block of the UCC secular matrix, $\langle\Phi_i^a|[\hat{V}, \hat{\sigma}_2^{(3)}]|\Phi_j^b\rangle$, which means that the strict version of UCC4 will differ from ADC(4).

3.6 The UCC Ground-State Energy

Employing the standard Taylor expansions for the exponentials, the UCC ground-state energy has already been expanded through fifth order, which has been termed UCC(5).[37] Here, E_0^{UCC} will be developed using the Bernoulli expansion of $\bar{H}$. For the UCC ground-state energy (3.7) to be consistent through at least second order, the terms of $\bar{H}$ in Eq. (3.37) need to be taken into account, but for the correlation energy only the commutators $[\hat{F}, \hat{\sigma}_1]$ and $[\hat{V}, \hat{\sigma}_2]$ can contribute. The commutator involving the Fock operator contains the same matrix element as in the CCSD equations, Eq. (2.155), but additionally the diagram mirrored horizontally in the middle contributes, which yields the total matrix element

$$\langle\Phi_i^a|(\hat{F}\hat{\sigma}_1)_{\mathrm{c}}|\Phi_0\rangle = \langle\Phi_i^a|(\hat{F}\hat{S}_1)_{\mathrm{c}}|\Phi_0\rangle + \langle\Phi_i^a|(\hat{S}_1^\dagger\hat{F})_{\mathrm{c}}|\Phi_0\rangle = \sum_{ia} f_{ia}\,\sigma_i^a + \sum_{ia} f_{ai}\,\sigma_i^{a*}\,, \quad (3.71)$$

which vanishes, of course, as long as Brillouin's theorem holds. The commutator involving the fluctuation potential and $\hat{\sigma}_2$ also contains the same matrix element as CCSD, Eq. (2.156), but also the same diagram mirrored horizontally. However, only the first commutator involving $\hat{V}$ in Eq. (3.37) contributes, the second commutator involving $\hat{V}_{\mathrm{R}}$ does not contribute since the required operator fragments having excitation levels of $+2$ or -2 (see Figure 2.4) are contained in $\hat{V}_{\mathrm{ND}}$, not in $\hat{V}_{\mathrm{R}}$. Thus, an additional factor of $\frac{1}{2}$ has to be included before the matrix elements and the UCC2 ground-state energy is given as

$$E_0^{\mathrm{UCC2}} - E_0^{\mathrm{HF}} = \sum_{ia} f_{ia}\,\sigma_i^a + \sum_{ia} f_{ai}\,\sigma_i^{a*} + \frac{1}{8}\sum_{ijab}\langle ij||ab\rangle\,\sigma_{ij}^{ab} + \frac{1}{8}\sum_{ijab}\langle ab||ij\rangle\,\sigma_{ij}^{ab*}\,, \quad (3.72)$$

which simply yields the same formula as CCD (or MP2) for real orbitals,

$$E_0^{\mathrm{UCC2}} - E_0^{\mathrm{HF}} = \frac{1}{4} \sum_{ijab} \langle ij||ab\rangle \, \sigma_{ij}^{ab} \,, \tag{3.73}$$

i.e. when $\sigma_{ij}^{ab} = \sigma_{ij}^{ab*}$ holds. Actually, this equation is correct through **third order**, since the MP3 energy contribution can be written in the same way with the cluster amplitudes replaced by the second-order doubles $t_{ijab}^{(2)}$ from Eq. (2.171b). Hence, Eq. (3.72) or (3.73) would also be correct for E_0^{UCC3}. However, by using an approximate UCCSD ansatz, like for CCSD, the ground-state energy can never be made consistent through fourth order, since the third-order doubles $t_{ijab}^{(3)}$ required for the MP4 correlation energy contain contributions from triple excitations, that are not included in (U)CCSD.[11,153,154] Yet, a comparison to fourth-order perturbation theory including only singles, doubles and quadruples, MP4(SDQ),[104,153] seems possible since the quadruples can be factorized into products of doubles.[11,153]

Nonetheless, the UCC3 ground-state energy can be made "more consistent" by including higher-order terms from the Bernoulli expansion (3.35a). Hence, the double commutators (3.35d) involving $\hat{\sigma}_1$ and $\hat{\sigma}_2$ shall be investigated. From the four possible contributions of Eq. (3.57), two different cases have to be differentiated, either only $\hat{S}_1$ or $\hat{S}_1^\dagger$ are involved, or both of them in the mixed commutators. In the first case, an excitation level of $+2$ or -2 is generated by the cluster fragments, which has to be cancelled by the fluctuation potential. This means that the term involving $\hat{V}_{\mathrm{R}}$ from the double commutators (3.35d) cannot contribute, but also the second term does not contribute, since the inner commutator produces a single excitation or deexcitation, which is vanished by the "R" operation after the commutator. Hence, only the first double commutator involving $\hat{V}_{\mathrm{ND}}$ contributes to the energy as

$$\begin{aligned}
\frac{1}{12}\langle\Phi_0|[[\hat{V}_{\mathrm{ND}},\hat{\sigma}_1],\hat{\sigma}_1]|\Phi_0\rangle &= \frac{1}{12}\big[\langle\Phi_0|(\hat{V}_{\mathrm{ND}}\hat{S}_1^2)_{\mathrm{c}}|\Phi_0\rangle + \langle\Phi_0|((\hat{S}_1^\dagger)^2\hat{V}_{\mathrm{ND}})_{\mathrm{c}}|\Phi_0\rangle\big] \\
&= \frac{1}{12} \times \Bigg[\quad + \quad \Bigg] \\
&= \frac{1}{12} \sum_{ijab} \big[\langle ij||ab\rangle \, \sigma_i^a \sigma_j^b + \langle ab||ij\rangle \, \sigma_i^{a*} \sigma_j^{b*}\big] \,,
\end{aligned} \tag{3.74}$$

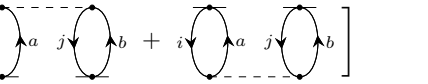

where the first term is equivalent to the corresponding contribution in the CC case (in contrast to the second one that is typical for UCC), but the prefactor comes purely from the Bernoulli expansion and thus differs from the corresponding factor occurring in the BCH expansion. The mixed commutators, i.e. the ones involving one $\hat{S}_1$ and one $\hat{S}_1^\dagger$, cannot contribute because the required fragment of $\hat{V}$ with excitation level 0 is not present in $\hat{V}_{\mathrm{ND}}$, and for the the other two double commutators it is vanished by the "R" operation because the inner commutator produces a single excitation or deexcitation.

A similar conclusion holds for the $[[\hat{V},\hat{\sigma}_2],\hat{\sigma}_2]$ commutators. The terms involving

only $\hat{S}_2$ or $\hat{S}_2^\dagger$ cannot contribute, because the excitation level of ± 4 generated by the cluster operators cannot be cancelled by $\hat{V}$, and the mixed terms need a fragment of the fluctuation potential with an excitation level of 0, which is not present in $\hat{V}_{\mathrm{ND}}$, and the inner commutators generate intermediates that correspond to double excitations or deexcitations which are then vanished by the "R" operation. This lack of contributions from $\hat{\sigma}_2^2$ is a major difference of Bn-UCC compared to BCH-UCC. Mixed commutators such as $[[\hat{V}, \hat{\sigma}_1], \hat{\sigma}_2]$ cannot contribute either, since the pure excitation or deexcitation terms generate an excitation level of ± 3 that cannot be neutralized by the fluctuation potential and the mixed commutators require fragments of $\hat{V}$ with an excitation level of ± 1, which is not present if $\hat{V}_{\mathrm{ND}}$. Furthermore, the inner commutators generate intermediates that correspond to single or double (de)excitations and are thus vanished by the "R" operation. Hence, the only contribution from double commutators is the fifth-order term given in Eq. (3.74).

The next contributions to the ground-state energy would arise from triple commutators. There are, however, many terms and they are computationally rather expensive and have not been implemented in the present work. In order to give an example, one fourth-order contribution coming from $\frac{1}{12}[[[\hat{V}_{\mathrm{ND}}, \hat{\sigma}_2], \hat{\sigma}_2], \hat{\sigma}_2]$ which correpsonds to an expectation value like $\langle \Phi_0 | (\hat{S}_2^\dagger \hat{V} \hat{S}_2^2)_{\mathrm{c}} | \Phi_0 \rangle$ can be represented diagrammatically and evaluated as

$\frac{1}{12} \times$ 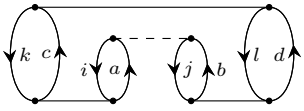

$= -\frac{1}{12} \sum_{ijklabcd} \langle ij||ab\rangle \, \sigma_{ki}^{ca} \, \sigma_{jl}^{bd} \, \sigma_{kl}^{cd*} \, . \qquad (3.75)$

3.7 Calculation of Properties with UCC

Molecular properties other than the energy can be calculated as expectation values of the corresponding operator with the wave function.[57,155] For an arbitrary one-electron operator $\hat{D}$ with

$$\hat{D} = \sum_{pq} d_{pq} \, \hat{a}_p^\dagger \hat{a}_q \, , \qquad (3.76)$$

where d_{pq} are the single-particle matrix elements according to Eq. (2.20), the expectation value with the wave function $|\Psi_n\rangle$ of electronic state n is given as

$$D_n = \langle \Psi_n | \hat{D} | \Psi_n \rangle \, . \qquad (3.77)$$

Transition moments between different states can be calculated in an analogous manner as the off-diagonal elements of the operator, i.e. by choosing different $m \neq n$ on the LHS and RHS of the expectation value in Eq. (3.77). In order to derive explicit equations for the UCC scheme, one needs to differentiate between **ground-state properties**, ground- to excited-state **transition moments**, and **excited-state properties**, where the latter

also includes state-to-state transition moments. All of these will be discussed in the following sections.

Another approach to molecular properties is to calculate the derivative of the energy E_n with respect to a perturbation connected to the observable. This approach will be discussed in more detail and compared to the expectation value in Chapter 7 (page 143).

3.7.1 Ground-State Properties

By employing the exponential UCC ansatz for the ground-state wave function (3.1), the expectation value of $\hat{D}$ can be written as

$$D_0 = \langle \Psi_0^{\mathrm{UCC}} | \hat{D} | \Psi_0^{\mathrm{UCC}} \rangle = \langle \Phi_0 | e^{-\hat{\sigma}} \hat{D} e^{\hat{\sigma}} | \Phi_0 \rangle = \langle \Phi_0 | \bar{D} | \Phi_0 \rangle \,, \tag{3.78}$$

where the similarity-transformed operator $\bar{D}$ is defined via its BCH expansion as

$$\bar{D} = e^{-\hat{\sigma}} \hat{D} e^{\hat{\sigma}} = \hat{D} + [\hat{D}, \hat{\sigma}] + \frac{1}{2!}[[\hat{D}, \hat{\sigma}], \hat{\sigma}] + \frac{1}{3!}[[[\hat{D}, \hat{\sigma}], \hat{\sigma}], \hat{\sigma}] + \dots \tag{3.79}$$

The zeroth-order term is of course the Hartree–Fock contribution,

$$\langle \Phi_0 | \hat{D} | \Phi_0 \rangle = \sum_{pq} d_{pq} \langle \Phi_0 | \hat{a}_p^\dagger \hat{a}_q | \Phi_0 \rangle = \sum_i d_{ii} \,, \tag{3.80}$$

which is trivial and vanishes for the normal-ordered operator form. In the following all diagrams have to be closed, since an expectation value including the HF state $|\Phi_0\rangle$ on both sides is calculated. The first-order contribution would come from the commutator of $\hat{D}$ with $\hat{\sigma}_2$, but this term vanishes since a one-electron operator cannot cancel the ± 2 excitation level of $\hat{\sigma}_2$. The single commutator involving $\hat{\sigma}_1$ survives, however, and yields the second-order contributions

$$\langle \Phi_0 | (\hat{S}_1^\dagger \hat{D} + \hat{D} \hat{S}_1)_{\mathrm{c}} | \Phi_0 \rangle =$$

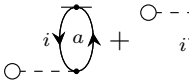

$+$

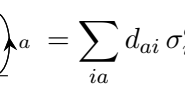

$$= \sum_{ia} d_{ai}\, \sigma_i^{a*} + \sum_{ia} d_{ia}\, \sigma_i^a \,, \tag{3.81}$$

where the circle is used for the one-electron operator $\hat{D}$ to distinguish it from the Fock operator $\hat{F}$. Another second-order term comes from the double commutator involving $\hat{\sigma}_2$, where the two "mixed" commutators including both $\hat{S}_2$ and $\hat{S}_2^\dagger$ give a contribution as

$$\begin{aligned} \langle \Phi_0 | (\hat{S}_2^\dagger \hat{D} \hat{S}_2)_{\mathrm{c}} | \Phi_0 \rangle &= \\ &= -\frac{1}{2} \sum_{ijkab} d_{ji}\, \sigma_{jk}^{ab} \sigma_{ik}^{ab*} + \frac{1}{2} \sum_{ijabc} d_{ab}\, \sigma_{ij}^{bc} \sigma_{ij}^{ac*} \,, \end{aligned} \tag{3.82}$$

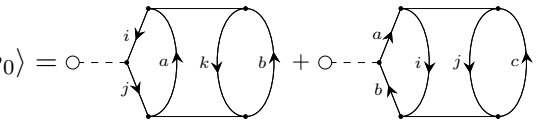

where the factor of $\frac{1}{2}$ comes from a pair of equivalent lines, respectively.

Third-order contributions come from the mixed double commutator involving both $\hat{\sigma}_1$ and $\hat{\sigma}_2$, which gives two pairs of double commutators involving either $\hat{S}_1$ and $\hat{S}_2^\dagger$ or $\hat{S}_2$ and $\hat{S}_1^\dagger$. The corresponding diagrams and algebraic interpretations are given as

$$\begin{aligned}\langle\Phi_0|(\hat{S}_1^\dagger\hat{D}\hat{S}_2 + \hat{S}_2^\dagger\hat{D}\hat{S}_1)_\mathrm{c}|\Phi_0\rangle = {}& \\ &= \sum_{ijab} d_{ia}\,\sigma_j^{b*}\sigma_{ij}^{ab} + \sum_{ijab} d_{ai}\,\sigma_{ij}^{ab*}\sigma_j^a\,,\end{aligned} \tag{3.83}$$

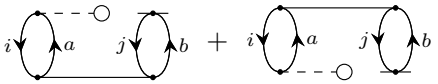

while a fourth-order contribution comes from the double commutator with $\hat{\sigma}_1$, which is given as

$$\begin{aligned}\langle\Phi_0|(\hat{S}_1^\dagger\hat{D}\hat{S}_1)_\mathrm{c}|\Phi_0\rangle = {}& \\ &= -\sum_{ija} d_{ji}\,\sigma_i^{a*}\sigma_j^a + \sum_{iab} d_{ab}\,\sigma_i^{a*}\sigma_i^b\,.\end{aligned} \tag{3.84}$$

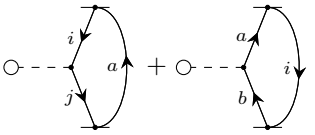

Higher-order contributions can be included by taking triple and higher commutators into account, which is not done here.

3.7.2 Ground- to Excited-State Transition Moments

The strength of a peak in an optical absorption or emission spectrum depends on the strength of the coupling between the electronic ground and respective excited state via a suitable transition operator, usually the dipole operator. In general, this can be written as

$$x_n = \langle\Psi_n|\hat{D}|\Psi_0\rangle\,, \tag{3.85}$$

while for UCC the effective transition moments are defined by using the intermediate states from Eq. (3.4), $\langle\tilde{\tilde{\Psi}}_I| = \langle\Phi_0|\hat{C}_I^\dagger e^{-\hat{\sigma}}$, as

$$\tilde{\tilde{F}}_I = \langle\tilde{\tilde{\Psi}}_I|\hat{D}|\Psi_0^\mathrm{UCC}\rangle = \langle\Phi_0|\hat{C}_I^\dagger e^{-\hat{\sigma}}\hat{D}e^{\hat{\sigma}}|\Phi_0\rangle = \langle\Phi_I|\bar{D}|\Phi_0\rangle\,, \tag{3.86}$$

which can also be seen as off-diagonal matrix elements of $\bar{D}$ including the HF reference on the right side. Thus, the effective transition moments can be written in a diagrammatic form like the UCC amplitude equations. The true transition moments (3.85) can then be obtained by contracting the corresponding eigenvector $\mathbf{X}_n$ with the effective transition moments $\tilde{\tilde{\mathbf{F}}}$ according to $x_n = \mathbf{X}_n^\dagger\,\tilde{\tilde{\mathbf{F}}} = \sum_I X_{I,n}^*\,\tilde{\tilde{F}}_I$.

Starting with the singles part of $\tilde{\tilde{F}}_I$, the zeroth-order term is simply given by an open diagram with the same form as the one in Eq. (2.158), such that $\langle\Phi_i^a|\hat{D}|\Phi_0\rangle = d_{ai}$. The first-order contribution comes from the commutator with $\hat{\sigma}_2$, where only the physical excitation part does not vanish, yielding a contribution analogous to Eq. (3.39), such

that the term is given by

$$\langle \Phi_i^a | (\hat{D}\hat{S}_2)_\mathrm{c} | \Phi_0 \rangle = \sum_{jb} d_{jb}\, \sigma_{ij}^{ab} \,. \tag{3.87}$$

The first second-order contribution comes from the single commutator with $\hat{\sigma}_1$ that is analogous to Eq. (2.160), such that it is given as

$$\langle \Phi_i^a | (\hat{D}\hat{S}_1)_\mathrm{c} | \Phi_0 \rangle = \sum_{b} d_{ab}\, \sigma_{i}^{b} - \sum_{j} d_{ji}\, \sigma_{j}^{a} \,, \tag{3.88}$$

while another second-order contribution comes from the double commutator with $\hat{\sigma}_2$ that gives rise to three distinct terms which are given as

$$\begin{aligned} \frac{1}{2}\langle \Phi_i^a | (\hat{S}_2^\dagger \hat{D}\hat{S}_2)_\mathrm{c} | \Phi_0 \rangle = {} & \\ &= \frac{1}{2} \sum_{jkbc} d_{ck}\, \sigma_{jk}^{bc*} \sigma_{ij}^{ab} - \frac{1}{4} \sum_{jkbc} d_{aj}\, \sigma_{jk}^{bc*} \sigma_{ik}^{bc} - \frac{1}{4} \sum_{jkbc} d_{bi}\, \sigma_{jk}^{bc*} \sigma_{jk}^{ac} \,, \end{aligned} \tag{3.89}$$

where the different signs come from a different number of loops and the additional factor of $\frac{1}{2}$ comes from the fact that connected contributions can only arise when the inner commutator is $[\hat{S}_2^\dagger, \hat{D}]$, since the $\hat{S}_2$ fragment cannot be connected to the $+1$ fragments of $\hat{D}$ and $[\hat{D}, \hat{S}_2]$ as the inner commutator hence does not contribute.

The third-order contribution comes from the mixed commutator involving both $\hat{\sigma}_1$ and $\hat{\sigma}_2$, where only those terms involving $\hat{S}_2$ in combination with $\hat{S}_1^\dagger$ can survive, since otherwise the total excitation level does not match. The resulting possible diagrams and their algebraic interpretations are given as

$$\begin{aligned} \langle \Phi_i^a | (\hat{S}_1^\dagger \hat{D}\hat{S}_2)_\mathrm{c} | \Phi_0 \rangle = {} & \\ &= \frac{1}{2} \sum_{jbc} d_{ab}\, \sigma_{j}^{c*} \sigma_{ij}^{bc} - \frac{1}{2} \sum_{jkb} d_{ji}\, \sigma_{k}^{b*} \sigma_{jk}^{ab} \\ &\quad + \sum_{jbc} d_{bc}\, \sigma_{j}^{b*} \sigma_{ik}^{ab} - \sum_{jkb} d_{kj}\, \sigma_{j}^{b*} \sigma_{ik}^{ab*} \,, \end{aligned} \tag{3.90}$$

where the different signs are due to a different number of hole lines and the first two terms get an additional factor of $\frac{1}{2}$ for the same reason as before, since in those the $\hat{S}_1^\dagger$ fragment is not connected to $\hat{D}$.

The fourth-order contribution is given by the double commutator involving $\hat{\sigma}_1$, with the corresponding diagrams and interpretations given as

$$\langle \Phi_i^a | (\hat{S}_1^\dagger \hat{D} \hat{S}_1)_\mathrm{c} | \Phi_0 \rangle = \quad (3.91)$$

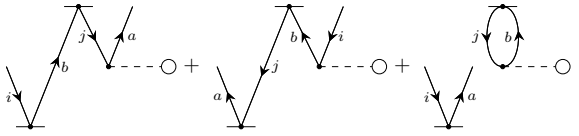

$$= -\frac{1}{2} \sum_{jb} d_{aj}\, \sigma_j^{b*} \sigma_i^b - \frac{1}{2} \sum_{jb} d_{bi}\, \sigma_j^{b*} \sigma_j^a + \sum_{jb} d_{bj}\, \sigma_j^{b*} \sigma_i^a \,,$$

where for the first time a partially disconnected contribution arises because both target indices (i and a) are on the $\hat{S}_1$ fragment.

The doubles part of $\tilde{\bar{F}}_I$ has no zeroth-order contributions, but a first-order contribution analogous to Eq. (3.41), such that the corresponding term is given as

$$\langle \Phi_{ij}^{ab} | (\hat{D} \hat{S}_2)_\mathrm{c} | \Phi_0 \rangle = \hat{\mathcal{P}}(ab) \sum_c d_{bc}\, \sigma_{ij}^{ac} - \hat{\mathcal{P}}(ij) \sum_k d_{kj}\, \sigma_{ik}^{ab} \,, \quad (3.92)$$

which are the only terms needed for a consistent second-order scheme such as UCC2.

Second-order terms arising from the commutator with $\hat{\sigma}_1$ and the double commutator with $\hat{\sigma}_2$ do not contribute because the operator fragments cannot be connected at all or the total excitation levels cannot match the doubly-excited determinant on the left. In the strict UCC versions, a second-order contribution arises from the single commutator with $\hat{\sigma}_2^{(2)}$, that is of course equivalent to Eq. (3.92). Analogous contributions are given by replacing $\hat{\sigma}$ by the corresponding n-th order operator $\hat{\sigma}^{(n)}$. A third-order contribution from the mixed commutator involving both $\hat{\sigma}_1$ and $\hat{\sigma}_2$ is given as

$$\frac{1}{2} \langle \Phi_{ij}^{ab} | (\hat{S}_1^\dagger \hat{D} \hat{S}_2)_\mathrm{c} | \Phi_0 \rangle = \quad (3.93)$$

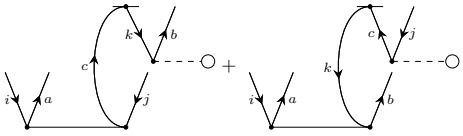

$$= -\frac{1}{2} \hat{\mathcal{P}}(ab) \sum_{kc} d_{bk}\, \sigma_k^{c*} \sigma_{ij}^{ac} - \frac{1}{2} \hat{\mathcal{P}}(ij) \sum_{kc} d_{cj}\, \sigma_k^{c*} \sigma_{ik}^{ab} \,,$$

where the factor of $\frac{1}{2}$ arises again because the $\hat{S}_2$ fragment is not connected to $\hat{D}$.

3.7.3 Excited-State Properties and State-to-State Transition Moments

Analogous to the ADC scheme in Eq. (2.121), excited-state properties can be calculated in UCC by contracting the eigenvector with the (shifted) "UCC-ISR" matrix $\tilde{\tilde{\mathbf{B}}}$, where

$$\tilde{\tilde{B}}_{IJ} + D_0 \delta_{IJ} = \langle \tilde{\tilde{\Psi}}_I | \hat{D} | \tilde{\tilde{\Psi}}_J \rangle = \langle \Phi_0 | \hat{C}_I^\dagger e^{-\hat{\sigma}} \hat{D} e^{\hat{\sigma}} \hat{C}_J | \Phi_0 \rangle = \langle \Phi_I | \bar{D} | \Phi_J \rangle \,, \quad (3.94)$$

that can also be viewed as a general matrix element of $\bar{D}$ within the basis of excited determinants. The ground-state property D_0 is subtracted on the diagonal in order to

obtain only the excited-state contribution, which corresponds to neglecting closed $\bar{D}$ diagrams.

Starting with the singles-singles block $\langle\Phi_i^a|\bar{D}|\Phi_j^b\rangle$, the zeroth-order contribution is analogous to the one-particle operator part of Eq. (3.46), giving the general matrix element $\langle\Phi_i^a|\hat{D}|\Phi_j^b\rangle = d_{ab}\,\delta_{ij} - d_{ij}\,\delta_{ab}$. There is no first-order contribution since the total excitation level of the $[\hat{D},\hat{\sigma}_2]$ commutator cannot be 0, as it would be required for the corresponding matrix element. The second-order contribution from the $\hat{\sigma}_1$ commutator is in fact equivalent to the non-HF term in the secular matrix, Eq. (3.47), such that it is given as

$$\begin{aligned}\langle\Phi_i^a|(\hat{D}\hat{S}_1 + \hat{S}_1^\dagger\hat{D})_\mathrm{c}|\Phi_j^b\rangle = \delta_{ij}\sum_k d_{ka}\,\sigma_k^b + \delta_{ab}\sum_c d_{ic}\,\sigma_j^c \\ + \delta_{ij}\sum_k d_{ak}\,\sigma_k^{b*} + \delta_{ab}\sum_c d_{ci}\,\sigma_j^{c*}\,.\end{aligned} \tag{3.95}$$

The most complicated second-order contribution comes from the double commutator involving $\hat{\sigma}_2$. The analysis is faciliated by considering on which operator fragments the target indices (i,j,a,b) can be located and generate all unique combinations thereof with the remaining parts. The most straightforward way is when $\hat{D}$ has no target indices, which means $\hat{S}_2$ has two (i and a) and $\hat{S}_2^\dagger$ the other two (j and b), which gives rise to two contributions depending on how $\hat{D}$ is connected to the other operator fragments. The are four unique possibilities where $\hat{D}$ has one of the target indices and the other three are on either the $\hat{S}_2$ or the $\hat{S}_2^\dagger$ fragment. The remaining contributions arise when two of the target indices are not given by one of the operator fragments, which gives rise to terms involving one Kronecker delta, either δ_{ij} or δ_{ab}, but not both since that would correspond to a closed $\bar{D}$ diagram and thus a ground-state contribution. The resulting diagrams with

their algebraic interpretation are given as

$$\langle \Phi_i^a | (\hat{S}_2^\dagger \hat{D} \hat{S}_2)_\mathrm{c} | \Phi_j^b \rangle =$$

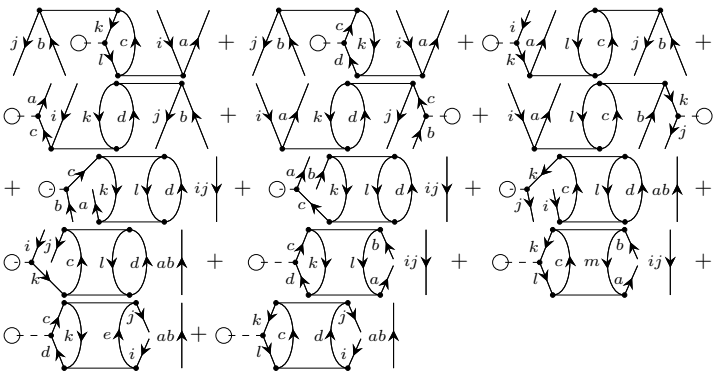

$$\begin{aligned}
&= -\sum_{klc} d_{lk}\, \sigma_{jk}^{bc*} \sigma_{li}^{ca} + \sum_{kcd} d_{cd}\, \sigma_{jk}^{bc*} \sigma_{ki}^{da} - \frac{1}{2} \sum_{klc} d_{ki}\, \sigma_{lj}^{cb*} \sigma_{kl}^{ac} \\
&\quad + \frac{1}{2} \sum_{kcd} d_{ac}\, \sigma_{kj}^{db*} \sigma_{ik}^{cd} + \frac{1}{2} \sum_{kcd} d_{cb}\, \sigma_{kj}^{dc*} \sigma_{ik}^{ad} - \frac{1}{2} \sum_{klc} d_{jk}\, \sigma_{lk}^{cb*} \sigma_{il}^{ac} \\
&\quad - \frac{1}{4} \delta_{ij} \sum_{klcd} d_{cb}\, \sigma_{kl}^{cd*} \sigma_{kl}^{ad} - \frac{1}{4} \delta_{ij} \sum_{klcd} d_{ac}\, \sigma_{kl}^{bd*} \sigma_{kl}^{cd} \\
&\quad + \frac{1}{4} \delta_{ab} \sum_{klcd} d_{jk}\, \sigma_{kl}^{cd*} \sigma_{il}^{cd} + \frac{1}{4} \delta_{ab} \sum_{klcd} d_{ki}\, \sigma_{jl}^{cd*} \sigma_{kl}^{cd} \\
&\quad - \frac{1}{2} \delta_{ij} \sum_{klcd} d_{cd}\, \sigma_{kl}^{cb*} \sigma_{kl}^{da} + \delta_{ij} \sum_{klmc} d_{lk}\, \sigma_{km}^{cb*} \sigma_{lm}^{ca} \\
&\quad - \delta_{ab} \sum_{kcde} d_{cd}\, \sigma_{kj}^{ce*} \sigma_{ki}^{de} + \frac{1}{2} \delta_{ab} \sum_{klcd} d_{lk}\, \sigma_{kj}^{cd*} \sigma_{li}^{cd} \,,
\end{aligned} \tag{3.96}$$

where factors of $\frac{1}{2}$ arise because of a pair of equivalent lines or because the inner commutator is not connected to $\hat{D}$.

In the coupling blocks the zeroth- and first-order contributions need to be considered. I restrict myself to the presentation of the singles-doubles block, but the doubles-singles block is just its Hermitian conjugate, $\mathbf{D}_\mathrm{DS} = \mathbf{D}_\mathrm{SD}^\dagger$. The zeroth-order contribution is given by

$$\langle \Phi_i^a | \hat{D} | \Phi_{jk}^{bc} \rangle =$$

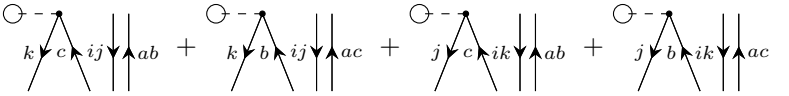

$$= \delta_{ab}\delta_{ij}\, d_{kc} - \delta_{ac}\delta_{ij}\, d_{kb} - \delta_{ab}\delta_{ik}\, d_{jc} + \delta_{ac}\delta_{ik}\, d_{jb} \,, \tag{3.97}$$

where different signs occur because of different numbers of permutations that need to be done before the contractions of the corresponding operator can be carried out. In first order, only the $\hat{S}_2^\dagger$ part of the $[\hat{D}, \hat{\sigma}_2]$ commutator contributes, which gives rise to eight

distinct terms as

$$\langle \Phi_i^a | (\hat{S}_2^\dagger \hat{D})_\mathrm{c} | \Phi_{jk}^{bc} \rangle =$$

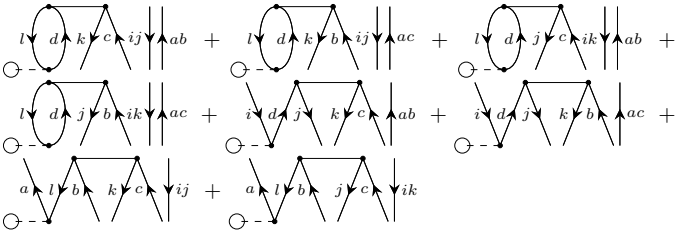

$$\begin{aligned}
&= -\delta_{ab}\delta_{ij} \sum_{ld} d_{dl}\, \sigma_{lk}^{dc*} + \delta_{ac}\delta_{ij} \sum_{ld} d_{dl}\, \sigma_{lk}^{db*} \\
&\quad + \delta_{ab}\delta_{ik} \sum_{ld} d_{dl}\, \sigma_{lj}^{dc*} - \delta_{ac}\delta_{ik} \sum_{ld} d_{jb}\, \sigma_{lj}^{db*} \\
&\quad - \delta_{ab} \sum_{d} d_{di}\, \sigma_{jk}^{dc*} + \delta_{ac} \sum_{d} d_{di}\, \sigma_{jk}^{db*} \\
&\quad - \delta_{ij} \sum_{l} d_{al}\, \sigma_{lk}^{bc*} + \delta_{ik} \sum_{l} d_{al}\, \sigma_{lj}^{bc*} \,,
\end{aligned} \tag{3.98}$$

where it should be mentioned that equivalent contributions would also arise in the coupling blocks of the secular matrix $\tilde{\tilde{\mathbf{M}}}$ if Brillouin's theorem is not fulfilled, i.e. if $f_{ia} = f_{ai} \neq 0$, for instance in an implementation of arbitrary-orbital ADC or UCC.

For the doubles-doubles block only the zeroth-order contribution is needed, which represents mostly a combinatorial problem. By taking all possible index combinations into account, eight distinct contributions arise with different signs which are given as

$$\begin{aligned}
\langle \Phi_{ij}^{ab} | \hat{D} | \Phi_{kl}^{cd} \rangle = {} & \delta_{bd}\delta_{ik}\delta_{jl}\, d_{ac} - \delta_{bc}\delta_{ik}\delta_{jl}\, d_{ad} + \delta_{ac}\delta_{ik}\delta_{jl}\, d_{bd} - \delta_{ad}\delta_{ik}\delta_{jl}\, d_{bc} \\
& - \delta_{ac}\delta_{bd}\delta_{jl}\, d_{ki} + \delta_{ac}\delta_{bd}\delta_{jk}\, d_{li} - \delta_{ac}\delta_{bd}\delta_{ik}\, d_{lj} + \delta_{ac}\delta_{bd}\delta_{il}\, d_{kj} \,.
\end{aligned} \tag{3.99}$$

Excited-state properties are obtained by contracting the matrix $\tilde{\tilde{\mathbf{B}}}$ with the same vector on the left and right, $D_n = D_0 + \mathbf{X}_n^\dagger\, \tilde{\tilde{\mathbf{B}}}\, \mathbf{X}_n$, whereas transition moments between excited states are obtained by taking two different vectors, $T_{mn} = \mathbf{X}_m^\dagger\, \tilde{\tilde{\mathbf{B}}}\, \mathbf{X}_n$, where $m \neq n$. It should be noted that this property matrix $\tilde{\tilde{\mathbf{B}}}$ through second order is again equivalent to $\mathbf{B}$ from Section 2.5.3 (page 32) as derived in the ADC framework.[30] Ground- and excited-state properties as well as oscillator strengths derived from the transition moments correct through second order will be presented in Chapter 6.

Chapter 4

Comparison and Benchmark of Hermitian Second-Order Methods for Excited States

4.1 Introduction

In this chapter, the time-independent approach to excitation energies via UCC theory as presented in Section 3.3 is further investigated, for which the resulting secular equation has been shown to be equivalent to an ISR approach employing a so-called self-consistent operator manifold for the generation of the correlated excited states.[20,51,92,93] The aim is to examine the exact relationship between the second-order ADC-ISR approach and an analogous UCC2 scheme based on unitary coupled-cluster theory as well as the related hybrid CC-ADC(2) approaches. It will be shown that the working equations of the UCC2 method differ depending on how the similarity-transformed Hamiltonian is treated, and that the same difference occurs between the CC-ADC(2) method and a second-order ISR approach based on traditional CC ground state. In a strict perturbation-theoretical framework, however, all investigated methods turn out to be identical. Excitation energies of the different methods will be compared and benchmarked on a set of small molecules.

Parts of this chapter have already been published in

- M. Hodecker, A. L. Dempwolff, D. R. Rehn, A. Dreuw, "Algebraic-Diagrammatic Construction Scheme for the Polarization Propagator Including Ground-State Coupled-Cluster Amplitudes. I. Excitation Energies", *The Journal of Chemical Physics*, **2019**, *150*, 174104.
- M. Hodecker, A. Dreuw, "Hermitian Second-Order Methods for Excited Electronic States: Unitary Coupled Cluster in Comparison with Algebraic-Diagrammatic Construction Schemes", *The Journal of Chemical Physics*, **2020**, *152*, 094106.

The CC-ADC(2) schemes have initially been motivated by something similar that has been done before for the related second-order polarization propagator approximation (SOPPA) method.[54–56,156,157] Geertsen and Oddershede developed a variant of SOPPA called the coupled-cluster polarization propagator approximation (CCPPA) where they essentially replaced Rayleigh–Schrödinger (RS) correlation coefficients by CC amplitudes.[54,55] With this and similar modifications of SOPPA significantly improved results for excitation energies, polarizabilities and other properties in systems like Li^-, Be, BH and CH^+ among others were obtained.[54,158–164] In this chapter, excitation energies obtained with the CC-ADC(2) schemes are thoroughly benchmarked and compared to standard second-order ADC, while a further benchmark of UCC schemes is postponed to Chapter 6 (page 129), where the results are directly compared to the third-order variant. It should be noted that in my master thesis only a part of the amplitudes had been replaced.

This chapter is organized as follows. In the theoretical analysis, the ISR procedure is carried out more explicitly to derive the second-order terms of ADC(2), which have been given in Section 2.5.2. Subsequently, the hybrid CC-ADC and unitary CC schemes are compared to ADC. Computational details and results for excitation energies on several small molecules are given for all considered methods, while the CC-ADC schemes are benchmarked on an extensive set of medium-sized organic molecules. Finally a short summary will be given.

4.2 Theoretical Analysis

4.2.1 Algebraic-Diagrammatic Construction

General aspects of the ISR have been given in Section 2.5.1 and the procedure has been applied explicitly through first order for the algebraic-diagrammatic construction scheme for the polarization propagator in Section 2.5.2, where also the required terms of the overlap matrix have been given. Here, the derivation of the second-order terms in the p-h/p-h block shall be sketched, for a successive comparison with CC-ADC and UCC. In order to derive $\mathbf{M}^{(2)}$, the second-order precursor matrix from Eq. (2.113c) need to be evaluated, where the second-order overlap matrix $\mathbf{S}^{(2)}$ is given in Eq. (2.107). Thus, the three terms involving matrix elements of the Hamiltonian in Eq. (2.113c) need to be evaluated, which can be done using Wick's theorem,[94] then all terms can be plugged in

and collected, which yields

$$\begin{aligned}
M^{\#(2)}_{ia,jb} = {} & \delta_{ab}\delta_{ij}E^{(2)}_0 + \frac{1}{2}\delta_{ij}\sum_{klc}\left(t^{(1)*}_{klbc}\langle ac||kl\rangle + t^{(1)}_{klac}\langle kl||bc\rangle\right) \\
& + \frac{1}{2}\delta_{ab}\sum_{kcd}\left(t^{(1)*}_{jkcd}\langle cd||ik\rangle + t^{(1)}_{ikcd}\langle jk||cd\rangle\right) \\
& - \sum_{kc}\left(t^{(1)*}_{jkbc}\langle ac||ik\rangle + t^{(1)}_{ikac}\langle jk||bc\rangle\right) \\
& + \frac{1}{4}\delta_{ab}\delta_{ij}\sum_{klcd}|t^{(1)}_{klcd}|^2(\varepsilon_a+\varepsilon_c+\varepsilon_d-\varepsilon_i-\varepsilon_k-\varepsilon_l) \\
& - \frac{1}{2}\delta_{ab}\sum_{kcd}t^{(1)*}_{ikcd}t^{(1)}_{jkcd}(\varepsilon_a+\varepsilon_c+\varepsilon_d-\varepsilon_i-\varepsilon_j-\varepsilon_k) \\
& - \frac{1}{2}\delta_{ij}\sum_{klc}t^{(1)*}_{klac}t^{(1)}_{klbc}(\varepsilon_a+\varepsilon_b+\varepsilon_c-\varepsilon_i-\varepsilon_k-\varepsilon_l) \\
& + \sum_{kc}t^{(1)*}_{ikac}t^{(1)}_{jkbc}(\varepsilon_a+\varepsilon_b+\varepsilon_c-\varepsilon_i-\varepsilon_j-\varepsilon_k)\,,
\end{aligned} \tag{4.1}$$

where Eq. (2.84) was used for $E^{(2)}_0$ in the matrix elements of $\hat{H}_1$. The last four terms involving orbital-energy differences can be reordered and shown to cancel terms in the matrix element

$$M^{(2)}_{ia,jb} = -\frac{1}{2}S^{(2)}_{ia,jb}(\varepsilon_a-\varepsilon_i) - \frac{1}{2}S^{(2)}_{ia,jb}(\varepsilon_b-\varepsilon_j) + M^{\#(2)}_{ia,jb} \tag{4.2}$$

involving the overlap matrix $\mathbf{S}^{(2)}$, such that the matrix element is given as[94]

$$\begin{aligned}
M^{(2)}_{ia,jb} = {} & \delta_{ab}\delta_{ij}E^{(2)}_0 + \frac{1}{2}\delta_{ij}\sum_{klc}\left[t^{(1)*}_{klbc}\langle ac||kl\rangle + t^{(1)}_{klac}\langle kl||bc\rangle\right] \\
& + \frac{1}{2}\delta_{ab}\sum_{kcd}\left[t^{(1)*}_{jkcd}\langle cd||ik\rangle + t^{(1)}_{ikcd}\langle jk||cd\rangle\right] \\
& - \sum_{kc}\left[t^{(1)*}_{jkbc}\langle ac||ik\rangle + t^{(1)}_{ikac}\langle jk||bc\rangle\right] \\
& + \frac{1}{4}\delta_{ab}\delta_{ij}\sum_{klcd}|t^{(1)}_{klcd}|^2(\varepsilon_c+\varepsilon_d-\varepsilon_k-\varepsilon_l) \\
& - \frac{1}{4}\delta_{ab}\sum_{kcd}\left[t^{(1)*}_{ikcd}t^{(1)}_{jkcd}(\varepsilon_c+\varepsilon_d-\varepsilon_i-\varepsilon_k) + t^{(1)*}_{ikcd}t^{(1)}_{jkcd}(\varepsilon_c+\varepsilon_d-\varepsilon_j-\varepsilon_k)\right] \\
& - \frac{1}{4}\delta_{ij}\sum_{klc}\left[t^{(1)*}_{klac}t^{(1)}_{klbc}(\varepsilon_a+\varepsilon_c-\varepsilon_k-\varepsilon_l) + t^{(1)*}_{klac}t^{(1)}_{klbc}(\varepsilon_b+\varepsilon_c-\varepsilon_k-\varepsilon_l)\right] \\
& + \frac{1}{2}\sum_{kc}\left[t^{(1)*}_{ikac}t^{(1)}_{jkbc}(\varepsilon_a+\varepsilon_c-\varepsilon_i-\varepsilon_k) + t^{(1)*}_{ikac}t^{(1)}_{jkbc}(\varepsilon_b+\varepsilon_c-\varepsilon_j-\varepsilon_k)\right].
\end{aligned} \tag{4.3}$$

Exploiting the form of the first-order doubles amplitudes (2.82), several simplifications occur. Since the orbital-energy differences cancel the denominators of the first-order

doubles amplitudes, the first term involving $E_0^{(2)}$ cancels with the fifth term involving the square of the same amplitudes, and last six terms partially cancel the ones with the same summation indices, yielding the final ADC(2) matrix elements of Eq. (2.119).[94]

As will be discussed in the following, these terms in Eq. (4.3) do not cancel for other than first-order MP amplitudes, and hence one obtains ground-state energy contributions on the diagonal of $\mathbf{M}$. However, the latter point is of minor importance for the discussion here since it does not change the excitation energies, it just shifts the total energies.

4.2.2 Traditional Coupled-Cluster Theory

Before discussing the unitary ansatz for coupled-cluster (CC) theory, the traditional CC ground-state aspresentedd in Section 2.6 is considered.[9–11,70] As explained there, the representation of the Hamiltonian is not Hermitian since it has different left- and right-hand basis states in this ISR (or since $e^{\hat{T}}$ is not unitary), it is not topic of this work. Nonetheless, one can derive a Hermitian second-order approach to excited states from a CC ground state, in a similar spirit to the coupled-cluster polarization propagator approximation (CCPPA) by Geertsen and Oddershede.[54,55,156,165] For this it is noted that the ground-state wave function was only needed up to first order wihin the ADC-ISR approach presented in Section 2.5.2, which can be written as

$$|\Psi_0\rangle \equiv |\Phi_0\rangle + |\Psi_0^{(1)}\rangle = (1 + \hat{T}_2^{(1)})|\Phi_0\rangle\,, \tag{4.4}$$

where the first-order doubles excitation operator $\hat{T}_2^{(1)}$ is given by Eq. (2.61), but the CC doubles amplitudes t_{ij}^{ab} are replaced by the first-order MP ones $t_{ijab}^{(1)}$ from Eq. (2.82). If one was to insert the CC ground-state parameterization from Eq. (2.62) together with its Hermitian conjugate $\langle\Phi_0|e^{\hat{T}^\dagger}$ into the ISR procedure, this would lead to a nonterminating series, which is why a truncation at a certain power of the cluster operator must be applied. A reasonable way to do so is to require that the standard ADC method must be obtained in the first iteration of the cluster equations, analogous to CCPPA.[55] This leads to essentially the same ansatz for the ground-state wave function correct through at least first order, but replacing the MP correlation coefficients with the cluster operator from Eq. (2.61),

$$|\Psi_0\rangle \equiv (1 + \hat{T}_2)|\Phi_0\rangle\,. \tag{4.5}$$

An analogous second-order ISR procedure can be carried out like in Section 2.5, which is now referred to as CCD-ISR(2), and the resulting equations will be of the same form as for the standard ADC procedure, just the first-order MP amplitudes $t_{ijab}^{(1)}$ in Eq. (4.3) are replaced by the CC ones t_{ij}^{ab} as obtained from Eq. (2.137), that are formally of infinite order. It is important to note that the truncation of the ground-state wave function in Eq. (4.5) only applies to the ISR derivation or propagator calculation, analogous to the CCPPA method,[54,55] but not to the determination of the ground-state cluster

amplitudes themselves. The inclusion of double excitations only can further be justified since effects of single excitations from $|\Psi_0^{(2)}\rangle$ do not appear in the secular matrix $\mathbf{M}$ in a consistent second-order method, only in the equations for the transition moments $\tilde{\mathbf{F}}$, which are not considered in this chapter.

Only one complication arises in the derivation of the matrix elements due to the different choice of the reference function, as mentioned at the end of Section 4.2.1. The terms in $M^{(2)}_{ia,jb}$ arising from $\langle\Phi_0|\hat{T}_2^\dagger\hat{a}_i^\dagger\hat{a}_a\hat{H}_0\hat{a}_b^\dagger\hat{a}_j\hat{T}_2|\Phi_0\rangle \equiv \langle\Psi_0^{(1)}|\hat{a}_i^\dagger\hat{a}_a\hat{H}_0\hat{a}_b^\dagger\hat{a}_j|\Psi_0^{(1)}\rangle$ do not cancel (parts of) the ones from $\langle\Psi_0^{(1)}|\hat{a}_i^\dagger\hat{a}_a\hat{H}_1\hat{a}_b^\dagger\hat{a}_j|\Phi_0\rangle$ and $\langle\Phi_0|\hat{a}_i^\dagger\hat{a}_a\hat{H}_1\hat{a}_b^\dagger\hat{a}_j|\Psi_0^{(1)}\rangle$, since the orbital-energy difference cannot cancel the denominators of the t_{ij}^{ab} amplitudes and thus cannot be simplified further than in Eq. (4.3). Using CC amplitudes within the simplified ADC(2) equations (2.119) in an *ad hoc* modification is termed CC-ADC(2).

4.2.3 Unitary Coupled Cluster

Unitary coupled-cluster (UCC) theory has been discussed in detail in the previous Chapter 3. It has also been shown that when using the so-called Bernoulli (Bn) expansion (Section 3.2) for the similarity-transformed Hamiltonian $\bar{H}$, which up to second order is given by Eq. (3.37) the resulting matrix elements of the second-order scheme UCC2 (Section 3.3) are equivalent to those of ADC(2), compare Eqs. (2.119) and (3.49).

However, when using the standard BCH expansion for $\bar{H}$, the following commutators need to be included for a second-order scheme within the singles and doubles space of the cluster operator:

$$\bar{H} = \hat{F} + \hat{V} + [\hat{F}, \hat{\sigma}_1 + \hat{\sigma}_2] + [\hat{V}, \hat{\sigma}_2] + \frac{1}{2}[[\hat{F}, \hat{\sigma}_2], \hat{\sigma}_2] + \mathcal{O}(3)\,, \tag{4.6}$$

where the differences to the Bn expansion are thus the missing splitting of $\hat{V}$ into $\hat{V}_{\mathrm{ND}}$ and $\hat{V}_{\mathrm{R}}$ and, in particular the double commutator of $\hat{F}$ with $\hat{\sigma}_2$. The contributions arising from $[\hat{V}, \hat{\sigma}_2]$ in the singles-singles block are $\langle\Phi_i^a|(\hat{V}\hat{S}_2)_{\mathrm{c}}|\Phi_j^b\rangle$ and $\langle\Phi_i^a|(\hat{S}_2^\dagger\hat{V})_{\mathrm{c}}|\Phi_j^b\rangle$, which are given by Eq. (3.48) and its Hermitian conjugate, respectively. The double commutator of $\hat{F}$ with $\hat{\sigma}_2$ is in fact equivalent to the second-order contribution of a general one-particle operator for the calculation of excited-state properties, as given in Eq. (3.96). By replacing the general matrix elements d_{pq} with those of the diagonal Fock operator, $f_{pq} = \varepsilon_p\delta_{pq}$, and renaming some of the dummy indices, the terms can be rewritten as follows for the example where no Kronecker delta appears,

$$\begin{aligned}
\langle\Phi_i^a|(\hat{S}_2^\dagger\hat{F}\hat{S}_2)_{\mathrm{c}}|\Phi_j^b\rangle &\leftarrow \sum_{kc} \sigma_{jk}^{bc*}\sigma_{ik}^{ac}\big(\varepsilon_c + \frac{1}{2}\varepsilon_a + \frac{1}{2}\varepsilon_b - \varepsilon_k - \frac{1}{2}\varepsilon_i - \frac{1}{2}\varepsilon_j\big) \\
&= \sum_{kc} \sigma_{jk}^{bc*}\sigma_{ik}^{ac}\big(\varepsilon_b + \varepsilon_c - \varepsilon_j - \varepsilon_k + \frac{1}{2}\varepsilon_a - \frac{1}{2}\varepsilon_b - \frac{1}{2}\varepsilon_i + \frac{1}{2}\varepsilon_j\big) \\
&= \sum_{kc} \sigma_{jk}^{bc*}\sigma_{ik}^{ac}\big(\varepsilon_a + \varepsilon_c - \varepsilon_i - \varepsilon_k - \frac{1}{2}\varepsilon_a + \frac{1}{2}\varepsilon_b + \frac{1}{2}\varepsilon_i - \frac{1}{2}\varepsilon_j\big)\,,
\end{aligned} \tag{4.7}$$

where half of the last two forms each can be added to obtain

$$\frac{1}{2}\sum_{kc}\sigma_{jk}^{bc*}\sigma_{ik}^{ac}\left[(\varepsilon_b+\varepsilon_c-\varepsilon_j-\varepsilon_k)+(\varepsilon_a+\varepsilon_c-\varepsilon_i-\varepsilon_k)\right], \tag{4.8}$$

which means that the final matrix elements of BCH-UCC2 are equivalent to those of Eq. (4.3), which cannot be simplified to Eq. (2.119) if the converged UCC2 (LCCD) amplitudes from Eq. (3.44b) are used (the subtracted ground-state reference energy is ignored from now on). Thus, the UCC2 secular matrix elements are identical to the CCD-based ISR procedure from Section 4.2.2, as shown in Eq. (4.3), that again cannot be simplified like in the ADC(2) case. The difference lies again only in the correlation amplitudes. In this case, LCCD amplitudes are used, in contrast to the full CCD ones in the CCD-ISR(2) procedure or first-order MP ones in ADC(2). Yet, if one uses the first-order $\sigma_{ij}^{ab(1)}$ amplitudes, the orbital-energy differences cancel and also this "strict" UCC2 approach is again exactly identical to ADC(2), which means one includes the minimal amount of terms to be consistent through second order.[51]

To summarize, basically three different Hermitian second-order approaches to excited electronic states have been discussed, that are all identical in a strict perturbation-theoretical framework, but not when different coupled-cluster based references are used. Employing the algebraic derivation via the excitation-class orthogonalized or intermediate state representation framework based on a wave function that is correct through first order, essentially three terms contribute to the final secular matrix elements, two including the perturbation operator $\hat{H}_1$ and one the Fock operator $\hat{H}_0$. If the first-order correction to the ground-state wave function according to MP perturbation theory is used, i.e. the first-order doubles amplitudes $t_{ijab}^{(1)}$, the terms originating from $\hat{H}_0$ cancel parts of the other terms, simplifying the equations. If, on the other hand, the ground-state wave function includes higher-order or (infinite order) CC doubles amplitudes t_{ij}^{ab}, this cancellation does not occur. Another approach, based on an expectation-value or unitary coupled-cluster ansatz yields formally the same secular equations up to second order as the ISR approach. However, the ground-state amplitude equations correspond to the LCCD model in this case and a subtlety occurs in the secular matrix depending on how the UCC similarity-transformed Hamiltonian $\bar{H}$ is treated. Employing the standard BCH expansion, the same matrix elements as in the CCD-ISR(2) scheme are obtained, whereas the "simplified" matrix elements without contributions from the Fock operator of the MP-based ADC(2) scheme are obtained if one uses the so-called Bernoulli expansion for $\bar{H}$.

4.3 Computational Details and Implementation

The CCD-ADC(2), CCD-ISR(2), BCH-UCC2 and Bn-UCC2 approaches have been implemented in a development version of the Q-Chem 5.2 program package,[53] employing

utilities of the `ccman2` and `adcman` modules.[52] Calculations of vertical excitation energies of 66 states of H_2O, HF, N_2, Ne, CH_2 and BH have been performed with the same basis sets and geometrical parameters as in previous FCI, CC and ADC studies.[166–170] In practice, this means that for HF, BH and N_2 the internuclear distances are 1.7328795 a_0, 2.3289 a_0 and 2.068 a_0, respectively. For the triatomic molecules C_{2v} symmetry was used with the following coordinates (in a_0): O(0, 0, 0) and H(0, ±1.429937284, −1.107175113) for water and for methylene C(0, 0, 0) and H(±1.644403, 0, 1.32213) for the *singlet* excitations and C(0, 0, 0) and H(±1.644403, 0, 1.32313) for the *triplet* excitations. For the Ne, BH and CH_2 singlet excitations the entire molecular orbital space was used in the correlated calculations, whereas for all other cases the 1s orbitals of the first-row elements were kept frozen. For N_2, Dunning's cc-pVDZ basis set[171] was used. For the *singlet* excitations of Ne one s function with exponent 0.04 and one p function with exponent 0.03 was added. For BH, two s, two p and two d functions with exponents of 0.03105, 0.009244, 0.02378, 0.005129, 0.0904 and 0.02383, respectively, were added to the standard cc-pVDZ basis of B, respectively.[166] For H, two s and two p functions were added with exponents 0.0297, 0.00725, 0.141 and 0.02735. For CH_2, the basis of C was augmented with one s function of exponent 0.015 and for H one s function with exponent 0.025 was added. For H_2O the oxygen basis was augmented with one s function of exponent 0.07896 and one p function of exponent 0.06856, and for H one s function with exponent 0.02974 was added. For HF and the *triplet* excitations of Ne the aug-cc-pVDZ basis set was used.[168]

The consistency of the input data with the ones used in previous FCI calculations was checked by comparing the HF, MP2 and CCSD ground-state energies, as well as the EOM-CCSD, ADC(1) and ADC(2) excitation energies, as far as they were available.[170] For HF and the Ne and BH triplets the CIS energies were compared.[168] The Hartree–Fock ground-state energy of −38.884254 E_h reported in Ref. 169 could not be reproduced, but the same value as in Ref. 170 (−38.884244 E_h) was obtained. All calculations have been carried out with the Q-CHEM program package[53] interfaced to a development version of the `adcman` module. Also the standard-ADC excitation energies have been calculated again, where sometimes discrepancies in the order of 0.01 eV compared to literature[170] occur, which have been accounted to round-off errors.

Furthermore, 102 vertical excitation energies for states of different characters (such as valence, Rydberg, n-π^*, π-π^*, singlet, triplet, ...) for 18 small molecules of the benchmark set introduced by Jacquemin and co-workers[172] have been calculated with CCD-ADC(2), CCD-ISR(2), BCH-UCC2 and Bn-UCC2 employing the standard aug-cc-pVTZ basis set[171,173,174] and compared to the standard ADC(2) approach,[25,27] the perturbative doubles correction to configuration interaction singles, CIS(D),[175,176] as well as the non-Hermitian iterative second-order methods CIS(D_∞),[177] and CC2.[178] The geometries, originally optimized at the CC3/aug-cc-pVTZ level of theory, were taken from literature.[172] The excitation energies with the standard ADC(2) method have been recalculated in order to check the consistency of the input data.

In order to check the performance of CCD-ADC(2) on unsaturated organic molecules, vertical excitation energies of the benchmark set established by Thiel and co-workers [179–181] were calculated. For this, the standard TZVP basis set was employed and geometries employing Abelian point-group symmetry were taken from the literature, which had been optimized at the MP2/6-31G* level of theory.

4.4 Results and Discussion

4.4.1 Atoms, Diatomic and Triatomic Molecules

In Table 4.1, vertical excitation energies for water, hydrogen fluoride, neon, and nitrogen calculated with ADC(2), CCD-ADC(2), CCD-ISR(2), and the two different UCC2 variants are shown in comparison to full configuration interaction (FCI) results from the literature. [166–169] These are regular systems that are well described by means of perturbation theory, where MP2 recovers already a large amount of the electron correlation. [166,167] Correspondingly, all five methods yield in general rather similar results. In particular, the deviation of the mean absolute error from the standard ADC(2) one for H_2O, HF and Ne is only in the range of about 0.05 eV. Interestingly, the largest difference can here be observed between the BCH-UCC2 and Bn-UCC2 methods. The former yields results that are almost identical to CCD-ISR(2), whereas the latter is, as expected, more similar to CCD-ADC(2), with the difference between the respective two methods being only the ground-state amplitudes (CCD vs. LCCD). If MP2 already recovers most of the correlation energy, the difference between the full CCD variant and its linearized version becomes rather negligible. The largest discrepancies can here be observed for the nitrogen molecule, where CCD-ISR(2) and in particular BCH-UCC2 yield the best results with a mean absolute error of only about 0.2 eV. While Bn-UCC2 has the smallest mean absolute error for the other three systems, it has the largest one for N_2 of about 0.5 eV.

TABLE 4.1: Results for vertical excitation energies (in eV) of H_2O, HF, Ne, and N_2 computed with ADC(2), CCD-ADC(2), CCD-ISR(2), BCH-UCC2 and Bn-UCC2, given relative to FCI.[a] The last two lines for each system give the mean absolute error ($\overline{\Delta}_{\mathrm{abs}}$) and the maximum absolute error (Δ_{max}).

Transition	FCI[a]	ADC(2)	CCD-ADC(2)	CCD-ISR(2)	BCH-UCC2	Bn-UCC2
H_2O $1\,{}^1A_1 \rightarrow$						
$2\,{}^1A_1$	9.87	−0.50	−0.45	−0.54	−0.56	−0.42
$1\,{}^1B_1$	7.45	−0.50	−0.47	−0.54	−0.55	−0.45
$1\,{}^1B_2$	11.61	−0.64	−0.61	−0.68	−0.69	−0.58
$1\,{}^1A_2$	9.21	−0.63	−0.61	−0.66	−0.67	−0.59
$1\,{}^3B_1$	7.06	−0.45	−0.42	−0.49	−0.51	−0.40
$1\,{}^3A_2$	9.04	−0.58	−0.56	−0.62	−0.63	−0.54
$1\,{}^3A_1$	9.44	−0.44	−0.39	−0.49	−0.50	−0.37
$2\,{}^3A_1$	10.83	−0.36	−0.37	−0.40	−0.40	−0.35

TABLE 4.1: (*Continued.*)

Transition	FCI[a]	ADC(2)	CCD-ADC(2)	CCD-ISR(2)	BCH-UCC2	Bn-UCC2
$2\ ^3B_1$	11.05	−0.48	−0.47	−0.52	−0.52	−0.45
$1\ ^3B_2$	11.32	−0.55	−0.52	−0.60	−0.61	−0.49
$\overline{\Delta}_{\mathrm{abs}}$		0.51	0.49	0.55	0.57	0.47
Δ_{max}		0.64	0.61	0.68	0.69	0.59
HF $1\ ^1\Sigma^+ \rightarrow$						
$1\ ^1\Pi$	10.44	−0.81	−0.80	−0.84	−0.85	−0.78
$2\ ^1\Pi$	14.21	−0.86	−0.86	−0.89	−0.90	−0.84
$2\ ^1\Sigma^+$	14.58	−0.67	−0.65	−0.70	−0.71	−0.62
$1\ ^1\Delta$	15.2	−0.74	−0.76	−0.77	−0.78	−0.74
$1\ ^1\Sigma^-$	15.28	−0.74	−0.76	−0.77	−0.78	−0.74
$3\ ^1\Pi$	15.77	−0.85	−0.85	−0.88	−0.89	−0.84
$3\ ^1\Sigma^+$	16.43	−1.11	−1.08	−1.14	−1.14	−1.07
$1\ ^3\Pi$	10.04	−0.74	−0.74	−0.78	−0.79	−0.72
$1\ ^3\Sigma^+$	13.54	−0.49	−0.48	−0.53	−0.55	−0.45
$2\ ^3\Pi$	14.01	−0.87	−0.87	−0.90	−0.91	−0.85
$2\ ^3\Sigma^+$	14.46	−0.66	−0.70	−0.69	−0.70	−0.68
$1\ ^3\Delta$	14.93	−0.71	−0.73	−0.74	−0.75	−0.71
$1\ ^3\Sigma^-$	15.25	−0.74	−0.75	−0.77	−0.77	−0.74
$3\ ^3\Pi$	15.57	−0.85	−0.85	−0.88	−0.89	−0.84
$\overline{\Delta}_{\mathrm{abs}}$		0.77	0.78	0.81	0.81	0.76
Δ_{max}		1.11	1.08	1.14	1.14	1.07
Ne $1\ ^1S \rightarrow$						
$1\ ^1P$	16.40	−0.78	−0.76	−0.80	−0.80	−0.76
$1\ ^1D$	18.21	−0.91	−0.90	−0.93	−0.93	−0.89
$2\ ^1P$	18.26	−0.92	−0.91	−0.93	−0.94	−0.90
$2\ ^1S$	18.48	−1.05	−1.03	−1.06	−1.06	−1.02
$3\ ^1S$	44.05	−0.48	−0.45	−0.50	−0.50	−0.45
$1\ ^3P$	18.70	−0.71	−0.70	−0.73	−0.73	−0.69
$1\ ^3S$	19.96	−0.74	−0.76	−0.76	−0.76	−0.75
$1\ ^3D$	20.62	−0.79	−0.79	−0.81	−0.81	−0.78
$2\ ^3P$	20.97	−0.82	−0.82	−0.84	−0.84	−0.81
$2\ ^3S$	45.43	−0.32	−0.30	−0.34	−0.34	−0.30
$\overline{\Delta}_{\mathrm{abs}}$		0.75	0.74	0.77	0.77	0.73
Δ_{max}		1.05	1.03	1.06	1.06	1.02
$N_2\ 1\ ^1\Sigma_g^+ \rightarrow$						
$1\ ^1\Pi_g$	9.58	0.18	0.19	0.03	−0.06	0.29
$1\ ^1\Sigma_u^-$	10.33	0.29	0.28	0.13	0.02	0.49
$1\ ^1\Delta_u$	10.72	0.45	0.44	0.33	0.25	0.65
$1\ ^1\Pi_u$	13.61	0.95	1.03	0.81	0.72	1.13
$1\ ^3\Sigma_u^+$	7.90	0.41	0.11	0.26	0.20	0.17
$1\ ^3\Pi_g$	8.16	0.18	0.18	0.02	−0.08	0.29
$1\ ^3\Delta_u$	9.19	0.33	0.20	0.12	−0.03	0.35
$1\ ^3\Sigma_u^-$	10.00	0.54	0.47	0.33	0.17	0.63
$1\ ^3\Pi_u$	11.44	0.29	0.37	0.14	0.04	0.49

TABLE 4.1: (*Continued.*)

Transition	FCI[a]	ADC(2)	CCD-ADC(2)	CCD-ISR(2)	BCH-UCC2	Bn-UCC2
$\overline{\Delta}_{\text{abs}}$		0.40	0.36	0.24	0.17	0.50
Δ_{max}		0.95	1.03	0.81	0.72	1.13

[a] Results from the literature.[166–170]

In Table 4.2, the results for CH_2 and BH are shown, which can be considered to be of quasi-open-shell type, since they only possess are very small gap between occupied and virtual orbitals.[170] Thus, perturbation theory is not well suited for these systems and second-order methods are not accurate enough. An improved description of excited states of such systems is rather expected at the third-order level.[51,170] Nonetheless, their comparison gives some insight into the differences between the various second-order methods discussed here. Although the results are still rather similar, the mean abolute errors of the CCD-ADC(2) and Bn-UCC2 methods differ now by slightly more than 0.1 eV for CH_2 and BH, and they both yield worse results than the standard ADC(2) variants. However, the results of the CCD-ISR(2) and BCH-UCC2 schemes are even worse and they differ significantly more than for the previous systems. In particular BCH-UCC2 has a relatively large mean absolute error of about 1 eV. While ADC(2) tends to underestimate the excitation energies of these two systems, CCD-ADC(2) and Bn-UCC2 systematically overestimate them by about 0.2–0.4 eV, whereas CCD-ISR(2) and BCH-UCC2 underestimate them even more strongly. This is probably a consequence of the small orbital-energy differences, that are directly present in the singles-singles block of the respective secular matrix. But also the ground-state amplitudes themselves have a significantly larger influence. The full CCD scheme in CCD-ISR(2) improves the mean absolute error of CH_2 for instance by almost 0.6 eV in comparison to BCH-UCC2, where the LCCD ground state is used in an otherwise identical scheme.

TABLE 4.2: Results for vertical excitation energies (in eV) of CH_2 and BH computed with ADC(2), CCD-ADC(2), CCD-ISR(2), BCH-UCC2 and Bn-UCC2, given relative to FCI. The last two lines for each system give the mean absolute error ($\overline{\Delta}_{\text{abs}}$) and the maximum absolute error (Δ_{max}) in eV, respectively, relative to FCI.

Transition	FCI[a]	ADC(2)	CCD-ADC(2)	CCD-ISR(2)	BCH-UCC2	Bn-UCC2
CH_2 $1\ ^1A_1 \rightarrow$						
$3\ ^1A_1$	6.51	−0.08	0.23	−0.45	−1.04	0.35
$4\ ^1A_1$	8.48	−0.20	0.11	−0.56	−1.14	0.22
$1\ ^1B_2$	7.70	−0.11	0.20	−0.48	−1.06	0.31
$1\ ^1B_1$	1.79	−0.14	0.28	−0.55	−1.15	0.40
$1\ ^1A_2$	5.85	0.04	0.47	−0.36	−0.92	0.59
$1\ ^3A_1$	6.39	−0.12	0.20	−0.47	−1.06	0.31
$2\ ^3A_1$	8.23	−0.17	0.15	−0.52	−1.12	0.27

TABLE 4.2: (*Continued.*)

Transition	FCI[a]	ADC(2)	CCD-ADC(2)	CCD-ISR(2)	BCH-UCC2	Bn-UCC2
$3\ ^3A_1$	9.84	−0.11	0.20	−0.46	−1.05	0.32
$2\ ^3B_2$	7.70	−0.18	0.13	−0.54	−1.13	0.25
$1\ ^3B_1$	−0.01	−0.16	0.22	−0.56	−1.17	0.34
$2\ ^3B_1$	8.38	−0.08	0.22	−0.44	−1.02	0.34
$1\ ^3A_2$	4.79	−0.00	0.40	−0.38	−0.94	0.52
$\overline{\Delta}_{abs}$		0.12	0.23	0.48	1.07	0.35
Δ_{max}		0.20	0.47	0.56	1.17	0.59
BH $1\ ^1\Sigma^+ \rightarrow$						
$1\ ^1\Pi$	2.94	−0.09	0.42	−0.58	−0.93	0.54
$2\ ^1\Sigma^+$	6.38	−0.08	0.35	−0.54	−0.89	0.47
$2\ ^1\Pi$	7.47	−0.12	0.32	−0.67	−0.93	0.44
$4\ ^1\Sigma^+$	7.56	−0.20	0.24	−0.66	−1.01	0.36
$3\ ^1\Pi$	8.24	−0.13	0.30	−0.60	−0.95	0.42
$1\ ^3\Pi$	1.31	−0.29	0.22	−0.81	−1.18	0.35
$1\ ^3\Sigma^+$	6.26	−0.12	0.31	−0.59	−0.93	0.43
$2\ ^3\Sigma^+$	7.20	−0.20	0.24	−0.66	−1.01	0.36
$2\ ^3\Pi$	7.43	−0.17	0.27	−0.63	−0.98	0.38
$3\ ^3\Sigma^+$	7.62	−0.08	0.35	−0.55	−0.89	0.47
$3\ ^3\Pi$	7.92	0.00	0.41	−0.43	−0.76	0.52
$\overline{\Delta}_{abs}$		0.13	0.31	0.61	0.95	0.43
Δ_{max}		0.29	0.42	0.81	1.18	0.54

[a] Results from the literature.[166–170]

In order to further include a challenging case, the lowest excited states of the ozone molecule have been calculated, which exhibits a complicated ground-state electronic structure and has thus been used as a benchmark molecule in the development especially of multi-reference methodologies,[182–192] and the results are compared to available experimental data.[193,194] Improving the ground-state electronic structure by going from MP2 to LCCD or CCD should thus improve the accuracy of the excitation energies. Therefore, vertical excitation energies have been calculated with ADC(2), CCD-ADC(2), CCD-ISR(2), BCH-UCC2 and Bn-UCC2 in combination with the cc-pVTZ basis set[171] using the experimental C_{2v} geometry of the $^1A_1$ ground state,[195] where the bond length and angle are 1.272 Å and 116.8°, respectively. I focus the discussion on the comparison of ADC(2) and CCD-ADC(2), since the latter generally yields the best results in this case. From the results shown in Table 4.3 it can be seen that for the first excited singlet state $^1A_2$, ADC(2) overestimates the excitation energy by more than 0.5 eV compared to experiment, whereas the CCD-ADC(2) variant is on spot. For the next state, $^1B_1$, ADC(2) yields a better result than CCD-ADC(2), but for the third excited state $^1B_2$, that is actually the only one here with a non-vanishing oscillator strength, standard ADC(2) again overestimates the excitation energy by almost 0.5 eV, whereas the CCD-ADC(2) result agrees within less than 0.1 eV with experiment. The comparison of the triplet states

TABLE 4.3: Vertical excitation energies (in eV) for the lowest excited singlet and triplet states of the O_3 molecule calculated with the cc-pVTZ basis set compared to experimental results.

State	ADC(2)	CCD-ADC(2)	CCD-ISR(2)	BCH-UCC2	Bn-UCC2	Exp.[a]
$^1A_2$	2.14	1.59	1.88	1.10	2.28	1.6
$^1B_1$	2.24	1.67	1.96	1.16	2.37	2.1
$^1B_2$	5.38	4.82	5.15	4.71	5.83	4.9
$^3A_2$	1.83	1.25	1.53	0.69	1.92	1.18
$^3B_2$	1.73	1.13	1.67	0.67	1.70	1.30
$^3B_1$	2.07	1.13	1.428	0.58	1.80	1.45

[a] Experimental results for singlet states from Ref. 193, for triplet states from Ref. 194.

with experiment has to be done with care. Since they were determined via photoelectron spectroscopy of the O_3^- anion,[194] they can be regarded as adiabatic excitation energies rather than vertical ones.[188] However, disregarding these issues for a moment, indeed a clear improvement can be observed when going from ADC(2) to CCD-ADC(2), especially for the lowest triplet state $^3A_2$, where ADC(2) again overestimates the excitation energy significantly by more than 0.6 eV, whereas CCD-ADC(2) agrees within less than 0.1 eV with experiment.

While CCD-ISR(2) yields results of a similar quality as CCD-ADC(2), BCH-UCC2 underestimates the excitation energies consistently, whereas Bn-UCC2 tends to overestimate them slightly. This is an indicator that the UCC2 (LCCD) ground-state description is not sufficient for a system exhibiting strong multi-reference character such as ozone.

4.4.2 Small Organic and Inorganic Molecules

Now I briefly want to discuss the benchmark set of Jacquemin *et al.*[172] The results for the vertical excitation energies are compiled in the Table A.1 in the appendix (page 193), the statistical error analysis with respect to the theoretical best estimates (TBE) is shown in Table 4.4. As expected, for regular systems well described by means of perturbation theory, the results of all methods are rather similar, as in Table 4.1. The mean abolute error of all shown methods lies between 0.2 and 0.3 eV, similar conclusions hold for the root mean square deviation (RMS). Interestingly, the Bn-UCC2 approach has the largest RMS value of 0.32 eV, similar to the CIS(D) method, whereas the CCD-ISR(2) and BCH-UCC2 have the smallest RMS of about 0.26 and 0.25 eV, respectively, and thus perform even slightly better than CC2, which has a RMS of 0.28 eV. Whether this is a general trend or only owed to the small size of the compounds remains to be seen, since it has also been observed that the ADC(3) scheme tends to overcorrect its second-order variant and thus performs significantly worse than CC3 for these systems,[172] whereas for larger organic compounds of the Thiel benchmark set no real difference between ADC(3) and CC3 could be observed, but rather a significant improvement when going

TABLE 4.4: Mean signed error (MSE), mean abolute error (MAE), root mean square deviation (RMS), as well as positive (Max) and negative (Min) maximal deviations with respect to the TBE(FC) values.[172] All values are given in eV.

Method	No. of States	MSE	MAE	RMS	Max	Min
ADC(2)	102	−0.022	0.219	0.293	0.570	−0.760
CCD-ADC(2)	102	−0.035	0.210	0.286	0.511	−0.768
CCD-ISR(2)	102	−0.123	0.202	0.259	0.368	−0.809
BCH-UCC2	102	−0.212	0.253	0.253	0.277	−0.838
Bn-UCC2	102	0.104	0.284	0.324	0.653	−0.722
CIS(D)[a]	106	0.10	0.25	0.32	1.06	−0.63
CIS(D_∞)[a]	106	−0.01	0.21	0.28	0.57	−0.76
CC2[a]	106	0.03	0.22	0.28	0.63	−0.71

[a] Taken from Ref. 172.

from ADC(2) to ADC(3).[196] How this turns out for the third-order approach based on UCC theory[51] will be investigated in a future contribution.

4.4.3 Medium-Sized Organic Molecules

In this subsection the performance of CCD-ADC(2) and CCD-ADC(2)-x for unsaturated organic compounds is investigated, using the benchmark set introduced by Thiel and co-workers.[179–181] The evaluation of UCC-based methods on the same set of molecules is reported in Chapter 6. The 28 molecules used for this study are shown in Figure 4.1. It comprises unsaturated aliphatic hydrocarbons, aromatic hydrocarbons and heterocycles, carbonyl compounds and nucleobases, which are all standard chromophores in organic photochemistry. An extensive comparison of standard ADC methods with CC2, CCSD and CC3 results has been given before.[196] Here, I want to focus on the difference between standard ADC(2) variants and the hybrid CCD-ADC(2) ones and evaluate them with respect to the theoretical best estimates (TBE).[179] Furthermore, a variety of SOPPA-based methods including SOPPA(CCSD) has been tested on the same benchmark set,[197] where it was shown that standard ADC(2) clearly outperforms standard SOPPA. For SOPPA(CCSD) a deterioration compared to its standard version could even be observed.[197]

For consistency, all geometries have been optimized at the MP2/6-31G* level of theory and the standard TZVP basis set has been used for the excited-state calculations.[179,198–200] As discussed before,[179,196] excited states which are spatially extended, such as Rydberg states, are not well described since this basis set does not include diffuse functions.[198,199] Both the electronic structure as well as the symmetries and assignments of the individual transitions of the molecules in the benchmark set have already been discussed in detail[179] and are here not given again. 134 singlet and 71 triplet states have been computed and compared at the CCD-ADC(2) and CCD-ADC(2)-x levels.

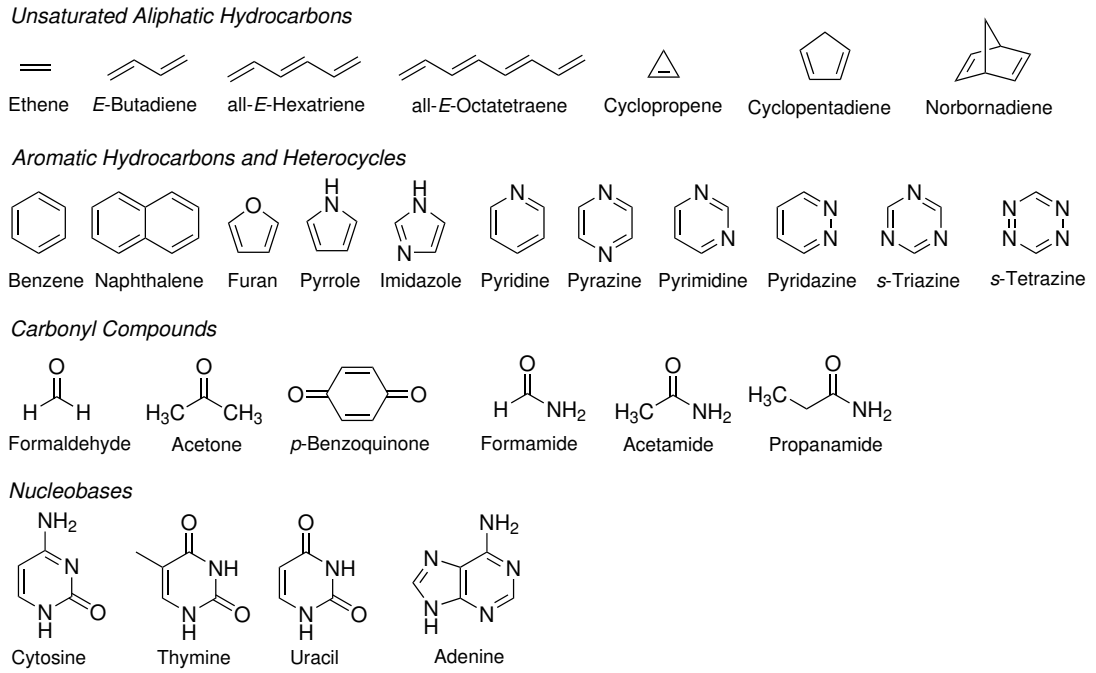

FIGURE 4.1: Thiel's benchmark set of molecules considered for testing CCD-ADC(2) and CCD-ADC(2)-x as well as UCC2 and UCC3 (see Chapter 6).

4.4.3.1 Singlet Excited States

The calculated vertical excitation energies of singlet states of the benchmark set are compiled in Table A.2 in the appendix (page 196). The results for CCD-ADC(2) and CCD-ADC(2)-x are compared with the ones from standard ADC(2) and ADC(2)-x and, most importantly, with the theoretical best estimates (TBE). For the different ADC(2) variants also the amount of doubly excited configurations ($\%R_2$) contained in the ADC excitation vector is given as the sum of the squared doubles amplitudes.

Prior to a thorough discussion of the accuracy of the (CCD-)ADC methods, a brief look at their performance for different substance classes is taken. For *unsaturated aliphatic hydrocarbons*, standard ADC(2) overestimates excitation energies on average by about 0.5 eV whereas ADC(2)-x tends to underestimate them strongly (about 0.6 eV on average). Similar to what has been observed in Section 4.4.1, the use of CCD amplitudes generally increases excitation energies here, thus increasing also the error for ADC(2) while for ADC(2)-x it becomes slightly smaller. However, the description of states with large double-excitation character such as the $^1\mathrm{A_g}$ states of linear polyenes is in general difficult for single-reference methods,[196,201] because of its large $\%R_2$ values in the ADC excitation vectors at the ADC(2)-x and CCD-ADC(2)-x levels (Table A.2). For these states, both ADC(2) and ADC(2)-x have significantly larger errors compared to the TBE values than for states with smaller $\%R_2$ fractions, however with different signs. It can also be seen that the difference between standard ADC(2) and CCD-ADC(2) becomes negligibly small for doubly-excited states, because the correlation amplitudes occur only in the p-h block

of the ADC matrix. Hence for pure doubly-excited states both ADC(2) and CCD-ADC(2) schemes will yield exactly the same excitation energies.

Going to *aromatic hydrocarbons and heterocycles*, ADC(2) performs somewhat better, slightly overestimating excitation energies in most cases. While for aromatic systems with one heteroatom such as furan, pyrrole or pyridine the overestimation lies mostly in the range between 0.2 and 0.5 eV, for the six-membered rings containing two or three nitrogens (with the exception of pyrazine), the error is always below 0.2 eV. ADC(2)-x shows the same trend as before, strongly underestimating excitation energies up to about 1 eV, on average between 0.3 and 0.7 eV. The use of CCD amplitudes within ADC(2), however, now has the opposite effect, as it tends to lower the excitation energies. For ADC(2) this has a positive effect and decreases the errors, whereas for ADC(2)-x the magnitude of the error becomes somewhat bigger. Only for states where ADC(2) already slightly underestimates the TBE value, the lowering of the excitation energy in CCD-ADC(2) has a negative effect compared to the reference.

The *carbonyl compounds* in the benchmark set (aldehydes, ketones and amides) possess different excited-state structures which can be classified as $\pi\pi^*$, $n\pi^*$, and $\sigma\pi^*$ transitions.[196] The accuracy and trends for ADC(2) and ADC(2)-x as well as CCD-ADC(2) and CCD-ADC(2)-x are very similar to the ones of the previous compound classes. The use of CCD amplitudes does not seem to have a significant impact on the results, but mostly lower the excitation energies slightly.

For the last set of molecules considered in the benchmark set, the *nucleobases*, ADC(2) shows only very small negative deviations of less than 0.1 eV on average, which is due to the fact that no CC3 values were available for these molecules and hence also CC2 was taken into consideration for the TBE values.[179,196] Due to the surprisingly good results of standard ADC(2), the use of CCD amplitudes makes the error slightly larger in most cases, again by lowering the excitation energies. For ADC(2)-x and CCD-ADC(2)-x the same conclusions hold as before.

The *statistical analysis* of the obtained data is presented in Table 4.5 and Figure 4.2. In the former, both TBE and ADC(3) values from Ref. 196 were taken as reference in order to evaluate the accuracy of the CCD-ADC(2) approaches. Starting with the TBE reference, one can see that the mean error can be significantly improved by using CCD amplitudes within ADC(2). The mean error of CCD-ADC(2) is with 0.15 eV almost as good as ADC(3), which has a mean error of 0.12 eV, whereas the one of standard ADC(2) is 0.22 eV. However, the mean absolute error is very similar for all three methods, ranging from 0.23 eV for ADC(3) to 0.26 eV for ADC(2), while CCD-ADC(2) lies in between with 0.25 eV. Concerning the standard deviation, on the other hand, CCD-ADC(2) has a larger value of 0.34 eV than standard ADC(2) with 0.30 eV, indicating a slightly higher variation of the results when using CCD amplitudes. This is also indicated by the about 0.2 eV larger range between the minimal and maximal error of CCD-ADC(2) compared to ADC(2). Going to the extended version CCD-ADC(2)-x, the underestimation of excitation

TABLE 4.5: Statistical error analysis of the calculated excitation energies (in eV) of the excited singlet states of Thiel's benchmark set at the ADC(2), CCD-ADC(2), ADC(2)-x, CCD-ADC(2)-x and ADC(3) levels of theory.[a] The theoretical best estimates (TBE) were used as reference data as well as the ADC(3) values.

	TBE as reference				
	ADC(2)[a]	CCD-ADC(2)	ADC(2)-x[a]	CCD-ADC(2)-x	ADC(3)[a]
Count[b]	103	103	103	103	103
Min	−0.32	−0.42	−1.83	−1.37	−0.78
Max	1.63	1.71	0.20	0.38	0.90
Mean	0.22	0.15	−0.70	−0.76	0.12
Mean Absolute	0.26	0.25	0.71	0.76	0.23
Standard Deviation	0.30	0.34	0.32	0.33	0.27
	ADC(3) as reference				
	ADC(2)[a]	CCD-ADC(2)	ADC(2)-x[a]	CCD-ADC(2)-x	ADC(3)[a]
Count[b]	134	134	134	134	...
Min	−1.00	−1.06	−1.79	−1.79	...
Max	2.20	2.28	−0.13	0.04	...
Mean	0.09	0.03	−0.83	−0.89	...
Mean Absolute	0.33	0.34	0.83	0.89	...
Standard Deviation	0.48	0.51	0.37	0.38	...

[a] For ADC(2), ADC(2)-x, and ADC(3) results see Ref. 196.

[b] Total number of considered states.

energies by the *ad hoc* extension of the 2p-2h block to first order cannot be corrected by using CCD amplitudes, on the opposite, it gets slightly worse. The mean error is with −0.76 eV slightly larger than for ADC(2)-x with −0.70 eV. This underestimation, however, is very consistent, since the mean absolute error has exactly the same numerical value, just the opposite sign. The standard deviation of CCD-ADC(2)-x is with 0.33 eV almost identical to the one for ADC(2)-x with 0.32 eV. Only the range between the minimal and maximal error is slightly improved, which amounts to 2.03 eV for standard ADC(2)-x and only 1.75 eV for CCD-ADC(2)-x. Taking ADC(3) as a reference, a similar picture is obtained. The mean error of 0.09 eV of ADC(2) can be reduced by using CCD amplitudes to only 0.03 eV for CCD-ADC(2), whereas the mean absolute error stays almost the same and the standard deviation increases slightly from 0.48 eV for ADC(2) to 0.51 eV for CCD-ADC(2). The range between minimal and maximal error is again increased by about 0.14 eV. The mean (absolute) error for CCD-ADC(2)-x is again slightly larger in magnitude than for ADC(2)-x, whereas the standard deviation remains virtually unchanged. However, the range between minimal and maximal deviation becomes slightly larger in this case when CCD amplitudes are employed.

4.4.3.2 Triplet Excited States

For a further evaluation of the accuracy of the CCD-ADC(2) methods, 71 excited triplet states of 20 molecules of the benchmark set (Figure 4.1) have been calculated and compared to available TBE and ADC(2) and ADC(2)-x values. No benchmark data are

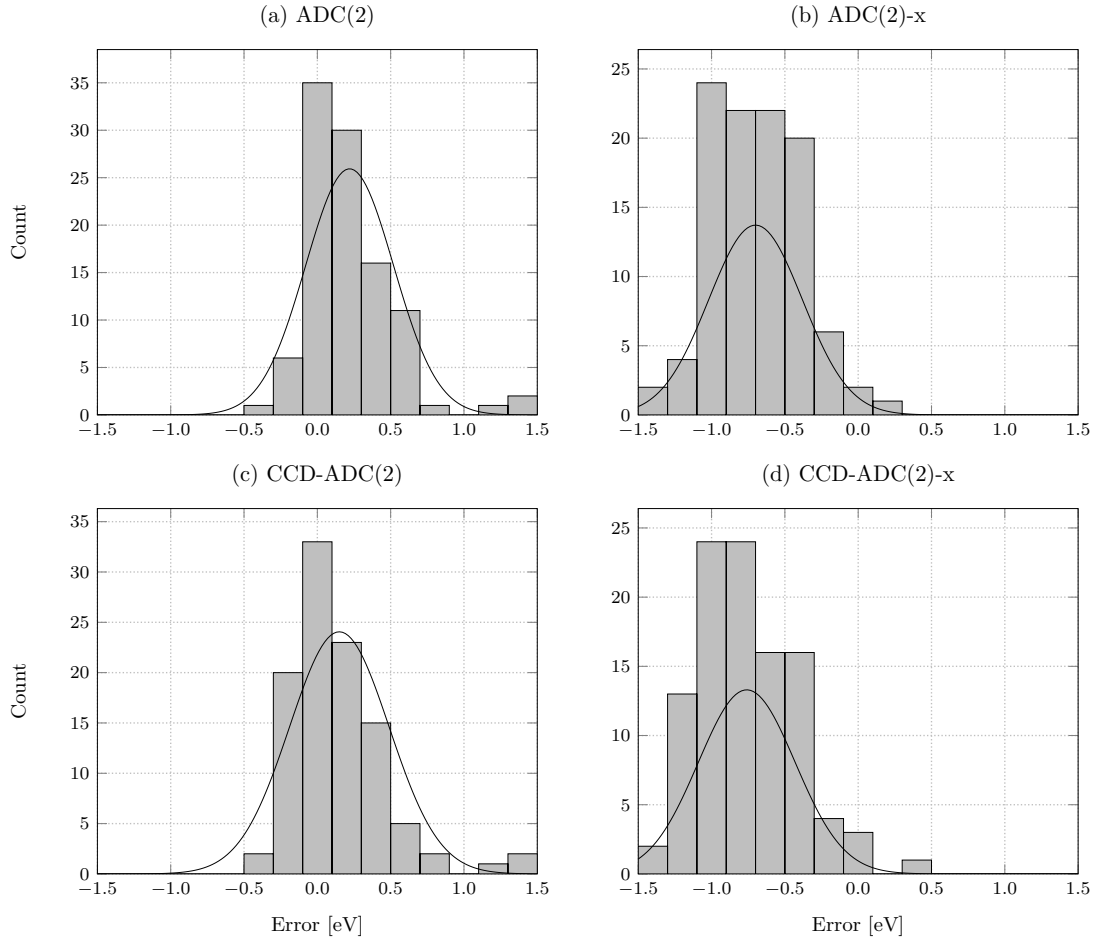

FIGURE 4.2: Histograms of the error distribution of all calculated excited singlet states with respect to the theoretical best estimates at the theoretical levels of (a) ADC(2), (b) ADC(2)-x, (c) CCD-ADC(2), and (d) CCD-ADC(2)-x.

available for the triplet states of the molecules pyrazine, pyrimidine, pyridazine, *s*-triazine as well as the nucleobases cytosine, thymine, uracil and adenine. The results are compiled in Table A.3 in the appendix (page 200). Since the results are rather similar for all considered substance classes, an individual discussion is omitted at this point and the statistical analysis presented in Table 4.6 and Figure 4.3 is discussed immediately.

The error of the second-order ADC methods is generally smaller for triplet than for singlet excited states. Compared to the TBE values, standard ADC(2) has a mean error of 0.12 eV with a standard deviation of only 0.17 eV. The largest improvement, however, can be seen for the CCD-ADC(2) variant with a vanishing mean error of 0.00 eV and almost the same small standard deviation as standard ADC(2). This can be seen in the histogram in Figure 4.3 (c), where the Gaussian curve is centered exactly at 0.0 eV. The mean absolute error, on the other hand, is of course larger than zero, but with 0.13 eV still smaller than the one of ADC(2) with 0.17 eV.

The mean (absolute) errors of ADC(2)-x and CCD-ADC(2)-x are also smaller in

TABLE 4.6: Statistical error analysis of the calculated excitation energies (in eV) of the excited triplet states of the benchmark set at the ADC(2), CCD-ADC(2), ADC(2)-x, CCD-ADC(2)-x and ADC(3) levels of theory.[a] The theoretical best estimates (TBE) were used as reference data as well as the ADC(3) values.

	TBE as reference				
	ADC(2)[a]	CCD-ADC(2)	ADC(2)-x[a]	CCD-ADC(2)-x	ADC(3)[a]
Count[b]	63	63	63	63	63
Min	−0.27	−0.38	−0.96	−1.06	−0.49
Max	0.48	0.35	−0.24	−0.23	0.44
Mean	0.12	0.00	−0.55	−0.67	−0.18
Mean Absolute	0.17	0.13	0.55	0.67	0.21
Standard Deviation	0.16	0.17	0.20	0.22	0.16
	ADC(3) as reference				
	ADC(2)[a]	CCD-ADC(2)	ADC(2)-x[a]	CCD-ADC(2)-x	ADC(3)[a]
Count[b]	71	71	71	71	...
Min	−0.38	−0.42	−1.41	−1.44	...
Max	1.52	1.32	0.08	−0.01	...
Mean	0.32	0.20	−0.40	−0.51	...
Mean Abolute	0.38	0.29	0.41	0.51	...
Standard Deviation	0.30	0.29	0.33	0.32	...

[a] For ADC(2), ADC(2)-x, and ADC(3) results see Ref. 196.

[b] Total number of considered states.

magnitude for the triplet than for the singlet excited states, but both still underestimate excitation energies by more than 0.5 eV on average. The mean error of CCD-ADC(2)-x is 0.12 eV smaller than the one of the standard version, exactly the same amount as for ADC(2), although here this represents a deterioration. The lowering of the excitation energies when using CCD amplitudes in ADC(2) thus seems to be rather consistent. Yet, one has to keep in mind that these are numbers averaged over the employed benchmark set and not rigorous trends that are valid for all individual excitation energies. Still, both mean error as well as mean absolute error compared to TBE values are significantly smaller for CCD-ADC(2) than for ADC(3).

Taking now ADC(3) values as reference, CCD-ADC(2) still outperforms ADC(2) significantly. Both the mean error with 0.20 eV as well as the mean absolute error with 0.29 eV are more than 0.1 eV smaller than for ADC(2). It can thus be said that by the use of CCD instead of Møller–Plesset amplitudes, the ground-state energy is consistently lowered which may lead to the on average improved numerical results.

The trend for CCD-ADC(2)-x compared to standard ADC(2)-x is the same as with respect to the TBE reference, both mean error and mean absolute error are about 0.1 eV larger in magnitude when CCD amplitudes are employed. The range between minimal and maximal deviation from the reference, however, decreases both for CCD-ADC(2) and for CCD-ADC(2)-x with respect to the ADC(3) reference, for CCD-ADC(2) significantly by 0.18 eV.

A subset of the molecules considered in Sections 4.4.1 and 4.4.3 has also been

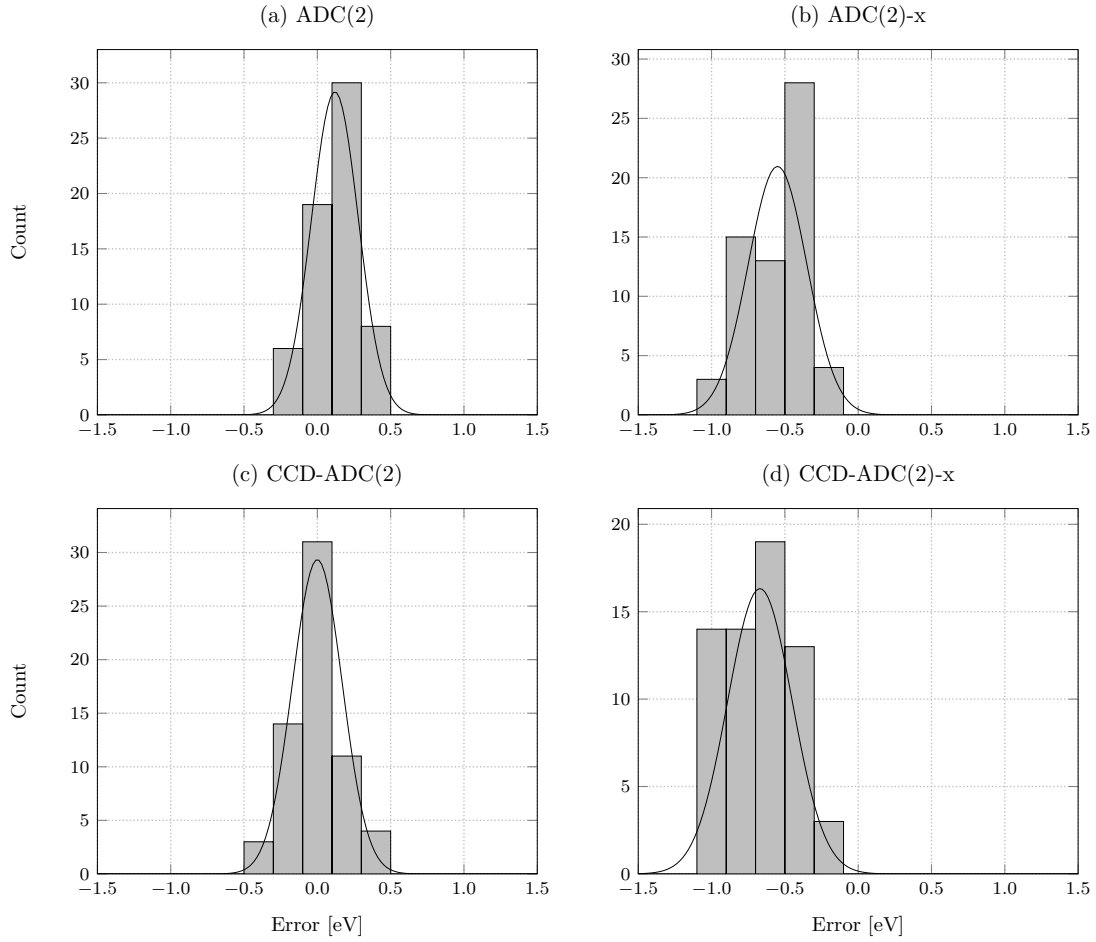

FIGURE 4.3: Histograms of the error distribution of all calculated excited triplet states with respect to the theoretical best estimates at the theoretical levels of (a) ADC(2), (b) ADC(2)-x, (c) CCD-ADC(2), and (d) CCD-ADC(2)-x.

calculated with the CCSD-ADC(2) variant, the results of which can be found in Table A.4 in the appendix (page 202). As can be seen there, for the small molecules the difference in excitation energies between the variants using CCD or CCSD doubles amplitudes is usually only up to 0.02 eV. For the organic molecules this difference is sligtly larger, although no improvement can be observed when using CCSD amplitudes. Rather, the results of CCSD-ADC(2) are in general closer to standard ADC(2) than the ones of CCD-ADC(2).

4.4.4 Excited-State Potential Energy Curves Along N_2 Dissociation

The failure of standard perturbation theory at points away from the equilibrium geometry due to static correlation has been known for a long time.[24] Along a bond dissocation coordinate any MPn model fails to give the correct asymptotic behavior. Single-reference coupled-cluster models, on the other hand, tend to be more stable and break down at a later point along the dissociation coordinate.[202] Several approaches exist which

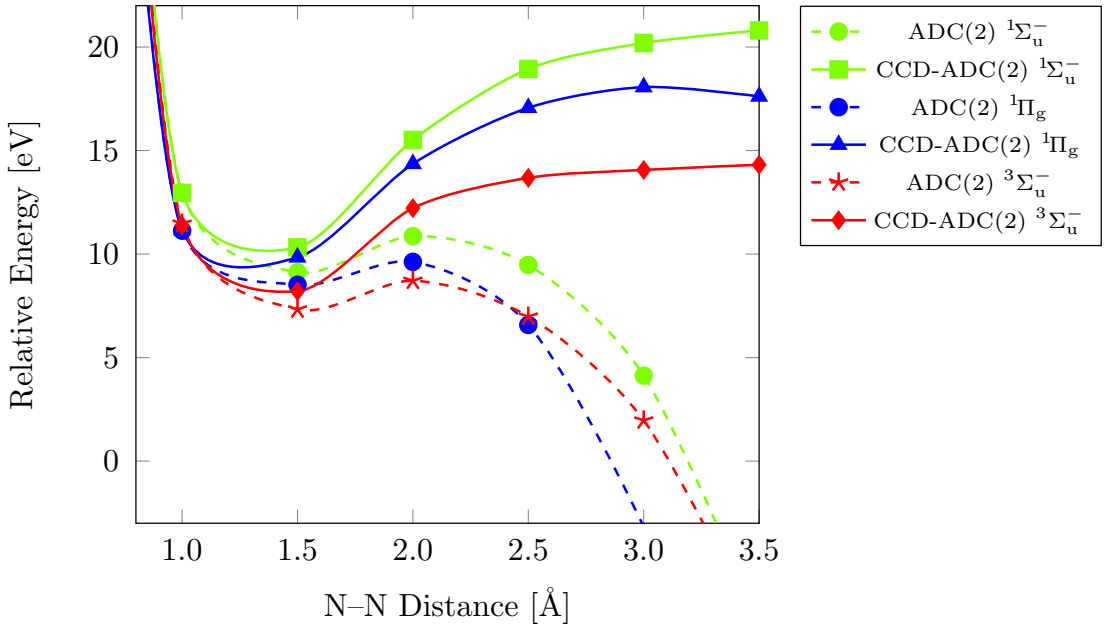

FIGURE 4.4: Excited-state potential energy curves along the dissociation of N_2 calculated with standard ADC(2) (dashed lines) and CCD-ADC(2) (solid lines) using the cc-pVTZ basis set.

describe dissociation processes correctly, for instance multi-reference (MR) methods such as MR-CI or MR-CC,[202–204] and also the so-called spin-flip (SF) methods starting from an open-shell triplet ground state.[205–212]

Here, the conceptually simple approach of CCD-ADC(2) is tested, thus staying within a closed-shell single-reference description. Since standard ADC methods can generally not be applied for cases where the MP ground-state description breaks down, it is investigated whether the higher stability of the CCD ground state can be transferred to the excited states. The potential energy curves of the HF molecule with standard ADC as well as SF-ADC were presented before.[209] In order to choose a different, non-trivial example, the dissociation of the triple bond in the N_2 molecule is investigated here. The MP2 curve breaks down already at about 1.7 Å, while the CCSD one for instance stays stable also beyond 2 Å.[202]

Figure 4.4 shows that the increased stability of CCD along the dissociation coordinate can indeed be transferred to the ADC excited states. Exemplarily, the energy curves of the first excited singlet and triplet states of the nitrogen molecule are shown, i.e. the first $^1\Sigma_u^-$, $^1\Pi_g$ and $^3\Sigma_u^-$ states. As can be seen in Figure 4.4, the energy curves obtained at the ADC(2) level start to break down at around 2 Å, similar to the MP2 curve, and eventually even become lower in energy than the ground state. The CCD-ADC(2) curves, on the other hand, do not show this unphysical behavior that early and remain reasonable throughout almost the entire range up to 3.5 Å, as shown here. As a cosequence, chemical reactions in the excited state might be modeled qualitatively more correctly at the CCD-ADC(2) level as well as excited-state equilibrium geometries which are spatially far away

from the ground-state geometry may be obtained with higher accuracy. As mentioned before, this is achievable by staying within a single-reference framework and with a closed-shell RHF determinant, in contrast to SF-ADC where one necessarily starts from an open-shell reference. Of course, it remains restricted to within the area of applications where single-reference coupled cluster remains stable.

4.5 Summary and Conclusions

In this chapter, the working equations of the second-order algebraic-diagrammatic construction scheme for the polarization propagator ADC(2) have been derived using an intermediate-state representation (ISR) approach. The resulting equations have been compared to analogous schemes based on a coupled-cluster (CC) reference function and two methods based on a unitary coupled-cluster (UCC) parameterization of the ground state. While the standard ADC(2) method uses the first-order doubles amplitudes $t_{ijab}^{(1)}$ from MP perturbation theory, converged cluster amplitudes are used in the CCD-ADC(2), CCD-ISR(2), and UCC2 schemes. The latter uses converged amplitudes from the linearized coupled-cluster doubles (LCCD) method, whereas the full coupled-cluster doubles (CCD) amplitudes are used in the CCD-ADC(2) and CCD-ISR(2) schemes. Furthermore, while the standard ADC(2) equations employing $t_{ijab}^{(1)}$ can be simplified such that no more Fock matrix elements occur in second-order part of the singles-singles block of the secular matrix, no such simplification is possible with a CCD ground-state wave function, thus resulting in the CCD-ISR(2) scheme. If the amplitude substitution is done only after this simplification, one ends up with the CCD-ADC(2) method. The same sublety occurs in the second-order UCC scheme, depending on whether one uses the Baker–Campbell–Hausdorff (BCH) or the so-called Bernoulli (Bn) expansion for the similarity-transformed Hamiltonian $\bar{H}$. While no Fock matrix elements occur in second order for Bn-UCC2 analogous to CCD-ADC(2), the same working equations as for CCD-ISR(2) are obtained in the BCH-UCC2 scheme. In a strict perturbation-theoretical framework, however (i.e., using the first-order amplitudes $t_{ijab}^{(1)}$), all methods are identical to the standard ADC(2) method.

All different variants have been implemented and tested on a set of small molecules. For systems that are well described by perturbation theory, no significant differences occur in the excitation energies for the various schemes. For systems like CH_2 and BH, for instance, that are of quasi-open-shell type, larger differences could be observed, where the methods that include orbital-energy differences in their second-order terms (CCD-ISR(2) and BCH-UCC2) generally perform worse than their counterparts. The opposite trend has been observed for the benchmark set introduced by Jacquemin *et al.*[172] Here, the BCH-UCC2 scheme showed a slightly better performance than its Bn-UCC2 counterpart.

The development of the CCD-ADC(2) and CCD-ISR(2) schemes was motivated by similar work on the related SOPPA method.[54,55] Apart from the small molecules and the

benchmark set by Jacquemin and co-workers, they were tested on the benchmark set of medium-sized organic molecules by Thiel *et al.*[179] as well as applied to the dissociation of the nitrogen molecule. Concerning the Thiel benchmark set, no significant difference could be observed in the mean signed and mean absolute errors as well as standard deviation for the investigated singlet excited states. For triplet excited states, however, the mean error and standard deviation exhibited by ADC(2) of 0.12 ± 0.16 eV could be lowered to 0.00 ± 0.17 eV for CCD-ADC(2) at the same time leading to a worse description in the (CCD-)ADC(2)-x case. These results are in contrast to SOPPA-based methods,[197] where, on the one hand, standard ADC(2) outperforms standard SOPPA and the use of coupled-cluster amplitudes like in SOPPA(CCSD) reduced the quality of the results in the statistical analysis. On the other hand, CCD-ADC(2) did not significantly change or rather slightly improved the results.

The most impressive improvement apart from the ozone molecule, however, was observed for the excited-state potential energy curves of N_2. Since the MP2 ground state breaks down at a distance of only about 1.7 Å, so do the excited states described by ADC(2). Using a CCD ground-state description that remains stable up to more than 3 Å of interatomic distance, also the corresponding excited states calculated with CCD-ADC(2) remain stable over this range.

Chapter 5

Influence of the Ground-State Correlation Amplitudes on ADC Static Dipole Polarizabilities

5.1 Introduction

The algebraic-diagrammatic construction scheme (ADC) for the polarization propagator is not only a versatile and reliable tool for the calculation of excitation energies and transition moments,[25,52,84–86,170,196] but has also been applied successfully to static and dynamic polarizabilities,[213,214] X-ray absorption spectroscopy,[215–217] two-photon absorption,[218] and C_6 dispersion coefficients,[214] particularly exploiting the formalism of the intermediate state representation (ISR).[30,213] In a recent work on static polarizabilities and C_6 dispersion coefficients,[214] aromatic systems like benzene have proven difficult cases for standard ADC approaches, yielding rather poor results compared to other theoretical approaches or experiment. Thus, the previous implementation of second-order ADC with ground-state coupled-cluster (CC) amplitudes (see Chapter 4) has been extended to the calculation of molecular properties and tested its performance on static polarizabilities of several small to medium-sized molecules, which is presented in this chapter. This approach has again been inspired by similar work on the related second-order polarization propagator approximation (SOPPA) method by Geertsen, Oddershede and Sauer.[54–56] Furthermore, a variant of the implementation relevant for molecular properties has been made by replacing the amplitudes in the transition moment vectors only, but not in the

Parts of this chapter have already been published in

- M. Hodecker, D. R. Rehn, P. Norman A. Dreuw, "Algebraic-Diagrammatic Construction Scheme for the Polarization Propagator Including Ground-State Coupled-Cluster Amplitudes. II. Static Polarizabilities", *The Journal of Chemical Physics*, **2019**, *150*, 174105.

ADC secular matrix itself. This variant has also been implemented for the ADC(3/2) method, in which the eigenvectors (and response vectors) of the third-order ADC matrix are used to calculate properties with second-order dipole matrices. The implementation allows for the use of CC with double excitations (CCD) as underlying coupled-cluster model as well as CC with single and double excitations (CCSD), where the singles amplitudes replace a part of the second-order density-matrix correction as described in the following section.

Experimentally, static polarizabilities can for instance be obtained by considering the relative dielectric permittivity or the refractive index,[219] for which a comprehensive work exists, where experimental data for 174 molecules are compiled.[220] Alternatively, static polarizabilities and other properties such as inelastic scattering cross sections of charged particles, Lamb shifts or dipole-dipole dispersion coefficients can be estimated using the so-called dipole oscillator strength distribution (DOSD), which is constructed using various pieces of experimental information such as photoabsorption spectra, refractivity, and electron scattering as well as constraints from quantum mechanics.[214,221,222]

As an example of the performance of the CC-ADC variants on molecular properties, static dipole polarizabilities of several small to medium-sized atomic and molecular systems are reinvestigated. In general, care has to be taken when comparing with experiment, in particular due to vibrational or environmental effects. For example, the compilation of Ref. 220 often includes estimates of vibrational contributions to the static polarizability, but such effects are not considered in the present computational study.[126,223] DOSD estimates, on the other hand, often include zero-point vibrational effects, and a previous study on methane reported an increase of its static polarizability by about 5% when including zero-point vibrational averaging (ZPVA).[224] While, in the static limit, pure vibrational contributions can be of the same order of magnitude as the electronic contributions for some molecules, ZPVA has been observed to change polarizabilities in general by only a few percent.[126,225]

5.2 Theoretical Methodology and Implementation

The underlying theory and the ADC formalism for calculating polarizabilities has been discussed in detail elsewhere.[213,214] Here, only a brief outline of the basic equations and principles for the calculation of dipole polarizabilities within the intermediate state representation shall be given.

Apart from the classical derivation of the ADC equations with the propagator approach,[25,28] an alternative exists via the so-called intermediate state representation (ISR).[27–30] The ISR does not only give direct access to excited states and transition properties, but also offers a straightforward way to transform expressions from time-dependent response theory into closed-form matrix expressions.[213,218] The components of the frequency-dependent molecular dipole polarizability $\alpha_{AB}(\omega)$ (with $A, B \in \{x, y, z\}$)

as a response function are given as

$$\begin{aligned}\alpha_{AB}(\omega) = &- \langle\Psi_0|\hat{\mu}_A(\hbar\omega - \hat{H} + E_0)^{-1}\hat{\mu}_B|\Psi_0\rangle \\ &+ \langle\Psi_0|\hat{\mu}_B(\hbar\omega + \hat{H} - E_0)^{-1}\hat{\mu}_A|\Psi_0\rangle\,,\end{aligned} \tag{5.1}$$

with the electric dipole operator $\hat{\mu} = \sum_{pq}\mu_{pq}\hat{a}_p^\dagger\hat{a}_q$. The exact sum-over-states expression is obtained by inserting the resolution of the identity of *exact* states, $1 = \sum_n |\Psi_n\rangle\langle\Psi_n|$.[213] If instead the resolution of the identity of *intermediate* states, $1 = |\Psi_0\rangle\langle\Psi_0| + \sum_I |\tilde{\Psi}_I\rangle\langle\tilde{\Psi}_I|$ is inserted, one arrives at the ADC formulation of the polarizability.[214] For a static perturbation ($\omega = 0$), it is given by

$$\alpha_{AB}(0) = \mathbf{F}_A^\dagger\,\mathbf{M}^{-1}\,\mathbf{F}_B + \mathbf{F}_B^\dagger\,\mathbf{M}^{-1}\,\mathbf{F}_A\,, \tag{5.2}$$

where the vectors of modified transition moments $\mathbf{F}$ were introduced with elements

$$F_I = \langle\tilde{\Psi}_I|\hat{\mu}|\Psi_0\rangle = \sum_{pq}\mu_{pq}\langle\tilde{\Psi}_I|\hat{a}_p^\dagger\hat{a}_q|\Psi_0\rangle = \sum_{pq}\mu_{pq}f_{pq}^I \tag{5.3}$$

and used the definition of the modified transition amplitudes, $f_{pq}^I = \langle\tilde{\Psi}_I|\hat{a}_p^\dagger\hat{a}_q|\Psi_0\rangle$. In order to obtain ADC expressions, the intermediate states are constructed as described in Section 2.5 and the exact ground-state wave function and energy are replaced by the Møller–Plesset (MP) perturbation series expansions from Section 2.4.

The first-order MP doubles amplitudes which are defined in Eq. (2.82) occur for the first time in the second-order contribution to the p-h/p-h block of the ADC matrix. In the previous Chapter 4 they have already been replaced here for the calculation of excitation energies by CCD amplitudes, which are calculated in an iterative manner according to the CC amplitude equations as described in Section 2.6.

The MP amplitudes also occur in the first- and second-order contribution to the modified transition amplitudes f_{pq}^I,[25] where they were replaced by CCD or CCSD doubles amplitudes as well. Furthermore, in a similar spirit to the work of Sauer,[56] the p-h part of the second-order one-particle density matrix correction $\rho_{ia}^{(2)} = t_{ia}^{(2)}$, see Eq. (2.171a), was replaced by the corresponding CCSD singles amplitudes. Since $\rho_{ia}^{(2)}$ corresponds precisely to the second-order contribution of $\hat{T}_1$, i.e. the lowest order where the singles occur in the MP wave-function expansion, CCSD was considered to an equal extent as CCD here, in contrast to the previous work on excitation energies. These singles amplitudes are not replaced when CCD is chosen as coupled-cluster model, but $\rho_{ia}^{(2)}$ is calculated instead with the CCD $\hat{T}_2$ amplitudes.

It is worth mentioning that the CC-ADC approach presented here is still size consistent (size intensive), since on the one hand in the ISR the ground state is completely decoupled from the excited configurations, and on the other hand, the form of the ADC equations is still the same in the CC-ADC variants, which means that local and non-local excitations

are exactly decoupled as well.

The CCD and CCSD amplitudes were combined with ADC(2) to yield the variants termed CCD-ADC(2) and CCSD-ADC(2). Furthermore, in order to check for the importance of the amplitudes in different parts of the calculation, more variants of ADC(2) as well as ADC(3/2) have been implemented, in which the amplitudes are replaced in the modified transition moments **F**, but not in the ADC matrix **M**. These variants are then referred to as F/CC-ADC(2) and F/CC-ADC(3/2), where CC stands for either CCD or CCSD.

5.3 Results and Discussion

In the following, static dipole polarizabilities of a series of small and medium-sized atomic and molecular systems are calculated using different ADC and CC-ADC variants and the results are compared to full configuration interaction (FCI), CC3 or experimental values. In a previous study[213] it was shown that double-zeta basis sets are clearly insufficient for the calculation of polarizabilites at the correlated wave-function level. Furthermore, one set of diffuse functions is crucial, whereas adding further sets of diffuse functions seemed to be of minor importance at the triple-zeta level. Thus, a basis set like aug-cc-pVTZ can be seen as a good compromise between basis-set size and accuracy.[213] Since the purpose of this study is to compare different CC-ADC variants with other methods, in particular standard ADC, no attempt was made to optimize the employed one-particle basis set. Instead, the basis sets of previous studies were employed for comparability. Most of the geometries were taken from literature as well.[213]

5.3.1 Comparison with FCI

5.3.1.1 The Case of Li^-

As first step, the case of the lithium anion, Li^- is reinvestigated, which has been a prominent test case for the calculation of dipole polarizabilities with many correlated methods.[159,226–229] Sauer chose to investigate this anion first as an "ideal test case" for his SOPPA variant referred to as SOPPA(CCSD),[56] where he replaced MP by CCSD amplitudes, based on earlier work by Geertsen *et al.*[54,55] Thus, it was chosen as first test case for the CC-ADC approaches using the same uncontracted (16s12p4d) Gaussian one-electron basis set.[56]

The values for the static dipole polarizability calculated with different ADC- and SOPPA-based methods compared to FCI are shown in Table 5.1. A graphical representation of the relative error defined as $\frac{\alpha(X)-\alpha(\mathrm{FCI})}{\alpha(\mathrm{FCI})}$, where X is the corresponding method, is depicted in Figure 5.1. As can be seen, both standard second-order methods, ADC(2) and SOPPA, show only a small improvement compared to the first-order random-phase approximation (RPA) which has a relative error of about 50% (corresponding to 400 a.u.).

TABLE 5.1: Static dipole polarizability (in a.u.) of Li^- calculated with different methods.

Method	α
RPA[a]	1198.39
SOPPA[a]	1061.70
CCSDPPA[a]	620.80
SOPPA(CCSD)[a]	732.60
ADC(2)	1039.17
CCD-ADC(2)	601.66
F/CCD-ADC(2)	747.59
CCSD-ADC(2)	448.38
F/CCSD-ADC(2)	558.30
FCI[1]	797.77

[a] Taken from literaure.[56]

They still overestimate the static polarizability significantly by more than 30% (about 250 a.u.). The use of coupled-cluster amplitudes within these methods lowers the value of the polarizability in all cases, but the magnitude of the effect varies strongly for the different variants. While SOPPA(CCSD) yields better results than Geertsen's coupled-cluster polarization propagator approximation (CCSDPPA) variant,[56] this also holds true for the ADC(2) variant with CCD, but not for the one with CCSD amplitudes. In the latter case the polarizability is underestimated by more than 40% or 350 a.u. With CCD amplitudes the underestimation is less than 25% (200 a.u.). A further improvement can be observed for the variants in which the amplitudes are only substituted in the modified transition moments **F**. While for the F/CCSD-ADC(2) the error is still −30% (about 240 a.u.), the best result of all compared methods could be obtained with F/CCD-ADC(2), where the underestimation is with 6% (50 a.u.) even smaller than for SOPPA(CCSD) with 8% (65 a.u.). It can already be seen in this system that the amplitudes in the **F** vectors play a larger role than the ones in the secular matrix, since the change in

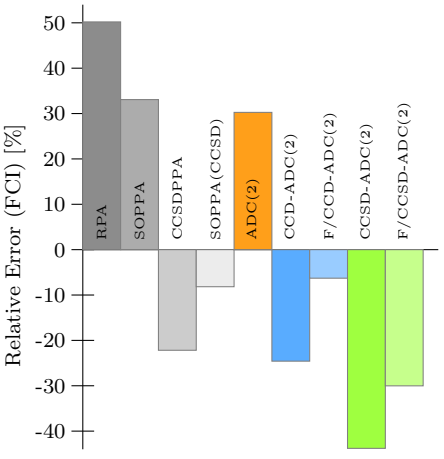

FIGURE 5.1: The relative error of the static dipole polarizability α for Li^- of results presented in Table 5.1 with respect to FCI.

TABLE 5.2: Static dipole polarizability (in a.u.) of Ne (d-aug-cc-pVDZ basis set) and HF (aug-cc-pVDZ basis set) obtained with different variants of the ADC scheme compared to FCI.

	Ne	HF		
Method	α	α_{xx}	α_{zz}	$\bar{\alpha}$
ADC(2)	2.83	4.55	6.71	5.27
CCD-ADC(2)	2.78	4.43	6.47	5.11
F/CCD-ADC(2)	2.78	4.43	6.48	5.11
CCSD-ADC(2)	2.83	4.53	6.58	5.21
F/CCSD-ADC(2)	2.83	4.53	6.59	5.22
ADC(3/2)	2.70	4.29	6.32	4.97
F/CCD-ADC(3/2)	2.65	4.19	6.12	4.84
F/CCSD-ADC(3/2)	2.70	4.28	6.21	4.93
FCI[a]	2.67	4.29	6.21	4.93

[a] Taken from literaure.[213,230]

going from standard ADC(2) to F/CCD-ADC(2) is already almost 300 a.u., and when the amplitudes are additionally substituted in the secular matrix in CCD-ADC(2), the polarizability decreases by another 145 a.u. For CCSD amplitudes, this trend is even more pronounced: the difference between ADC(2) and F/CCSD-ADC(2) amounts to 480 a.u., and between F/CCSD-ADC(2) and 'full' CCSD-ADC(2) only 110 a.u.

However, the results obtained with the different methods do not appear to be very systematic, and especially the best result obtained with the F/CCD-ADC(2) variant seems rather fortuitous. Since the lithium anion is a system with a diffuse charge cloud that is easily polarizable, it is understandable that the computed polarizability is very sensitive to small changes in the parameters. This makes it, however, questionable whether the Li^- ion is really an ideal test case and whether the observed improvements were obtained for the right reasons and not fortuitously. Furthermore, Li^- is isoelectronic to the beryllium atom that in turn is known to be a strongly correlated system and therefore perturbation theories at low order and even single-reference coupled-cluster approaches may not be appropriate, such that in this case a real multi-reference treatment would be needed.

In order to further investigate the CC-ADC methods and deduce some general trends when using different t-amplitudes within ADC, more calculations on rather standard chemical systems have been carried out and analyzed as shall be discussed in the following.

5.3.1.2 Neon and Hydrogen Fluoride

Two more small systems are discussed now, namely neon and hydrogen fluoride. The static dipole polarizabilities of Ne and HF have been calculated with various ADC methods and the results are compared to FCI. The basis sets used here are only of double-zeta quality, but since the reference FCI values were calculated in the same one-particle basis, the deviations from FCI stem solely from the approximations in the respective ADC

method. Table 5.2 shows the static dipole polarizability of the Ne atom calculated with the d-aug-cc-pVDZ basis set,[171,231] and the relative error is depicted in Figure 5.2. The deviation of the standard ADC(2) result from FCI of 6% (0.16 a.u.) are improved by 0.05 a.u. when using CCD amplitudes, such that the deviation is only 4% or 0.11 a.u. When CCSD doubles amplitudes are employed, the polarizability increases again to the same value as standard ADC(2) and hence no improvement is observed. It can be seen, however, that the results for both CCD-ADC(2) and F/CCD-ADC(2) as well as for CCSD-ADC(2) and F/CCSD-ADC(2) are the same, underlining the greater importance of the amplitudes in the modified transition moments **F** compared to the ones in the secular matrix **M** for the calculation of the polarizability. The same trend as for ADC(2) is observed for the third-order variants, where standard ADC(3/2) slightly overestimates the static polarizability by 1.0% compared to FCI. The use of CCD amplitudes within the second-order modified transition moments **F** lowers the obtained value and improves it slightly with a relative error of −0.7%, whereas with F/CCSD-ADC(3/2) the same value as for standard ADC(3/2) is obtained.

The dipole polarizability of hydrogen fluoride was calculated with the aug-cc-pVDZ basis set,[173] and the results can also be found in Table 5.2 and Figure 5.2. Again, the results for the CC-ADC and F/CC-ADC variants are almost identical. Focusing first on the isotropic polarizability of HF $\bar{\alpha} = \frac{1}{3}(\alpha_{xx} + \alpha_{yy} + \alpha_{zz})$, with $\alpha_{xx} = \alpha_{yy}$ for symmetry reasons, standard ADC(2) overestimates its value by 6.9% or 0.34 a.u. As before, the use of CC amplitudes in ADC lowers the static polarizability and thus improves its value compared to standard ADC. CCD amplitudes again yield a better result in ADC(2) than CCSD ones, with the error of the former being only 3.7% (0.18 a.u.) compared to about 5.8% (0.28 a.u.) of the latter. So again, when CCSD amplitudes are employed the polarizability is raised compared to CCD ones, making the result more similar to standard ADC(2). A similar trend is observed for the ADC(3/2) method. Here, however, F/CCD-ADC(3/2) underestimates the polarizability by 1.9% or 0.09 a.u. due to the

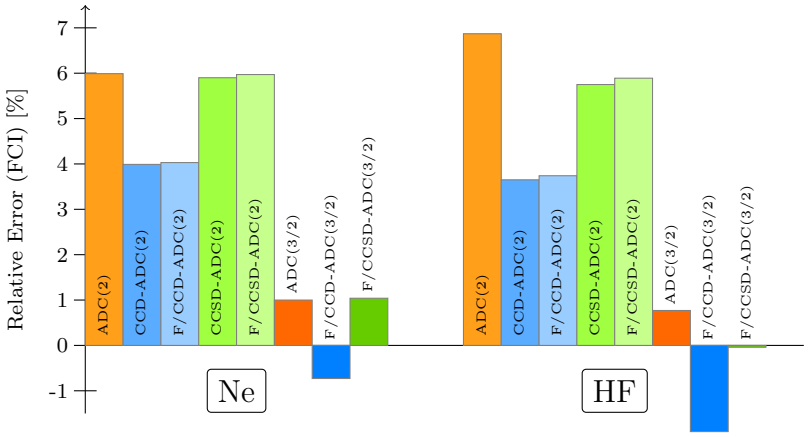

FIGURE 5.2: Relative error of the isotropic polarizability $\bar{\alpha}$ for Ne and HF of results presented in Table 5.2 with respect to FCI.

already very good result of standard ADC(3/2), having an error of only 0.8% or 0.04 a.u. The F/CCSD-ADC(3/2) method again raises the value of the polarizability to some extent compared to F/CCD-ADC(3/2) and is in this case in almost perfect agreement (relative error $< 0.1\%$) with the FCI result of 4.93 a.u. for the isotropic polarizability.

Having a look at the individual values of the polarizability tensor, all ADC(2) variants describe the components of the polarizability perpendicular to the molecular axis (that is, α_{xx} and α_{yy}) better than the component parallel to the axis, α_{zz}. The relative improvement when using CCD amplitudes, however, is larger for the parallel z component than for the perpendicular ones. A similar observation holds for the ADC(3/2) method. Here, however, the standard version is already in agreement with FCI for the diagonal x and y components of the polarizability, whereas the error of the z component amounts to 0.11 a.u. When using CCSD amplitudes in the **F** vectors, the perpendicular components remain virtually unchanged, whereas the parallel z component is lowered to be in perfect agreement with the FCI value as well.

5.3.2 Comparison with Experiment

In the following, the accuracy of the CC-ADC methods for molecular systems of increasing size and with larger basis sets will be evaluated and the results will be compared to the ones obtained in experiments, often by means of the dipole oscillator strength distribution (DOSD).[222] Since no FCI results are available for these systems, results of the third-order approximate coupled cluster (CC3) method[232] were taken as a theoretical reference when they were available. Additionally, the polarizability anisotropy defined as

$$\Delta\alpha = \sqrt{\frac{(\alpha_{xx} - \alpha_{yy})^2 + (\alpha_{yy} - \alpha_{zz})^2 + (\alpha_{zz} - \alpha_{xx})^2}{2}} \tag{5.4}$$

is compared. Previous studies have shown that ADC(2) yields in general rather large discrepancies in the anisotropies due to a poor reproduction of longitudinal polarizability components.[213,214]

5.3.2.1 Water and Carbon Monoxide

Let me start with the investigation of the water molecule, using the rather large d-aug-cc-pVTZ basis set[231] in order to allow for a proper comparison of theory and experiment.[213] The results obtained for H_2O are shown in Table 5.3 and the relative error with respect to CC3 is depicted in Figure 5.3. Compared to CC3, the standard ADC(2) variant overestimates the polarizability by almost 5%. This can be significantly improved to almost 1% by using CCD amplitudes, independent of whether they are used everywhere or only in the **F** vectors. When using CCSD amplitudes the results are with a relative error of about 3.5% worse, but still better than for the standard ADC(2) variant. ADC(3/2), however, yields a result very similar to CC3, having a relative error

TABLE 5.3: Static dipole polarizability (in a.u.) of H_2O and CO calculated with different ADC variants (d-aug-cc-pVTZ basis set) compared to CC3 and experiment.

	H_2O					CO			
Method	α_{xx}	α_{yy}	α_{zz}	$\bar{\alpha}$	$\Delta\alpha$	α_{xx}	α_{zz}	$\bar{\alpha}$	$\Delta\alpha$
ADC(2)	9.79	10.41	10.17	10.13	0.54	11.88	17.32	13.70	5.43
CCD-ADC(2)	9.48	9.97	9.83	9.76	0.44	11.45	16.92	13.27	5.47
F/CCD-ADC(2)	9.48	9.97	9.85	9.77	0.45	11.47	17.07	13.34	5.61
CCSD-ADC(2)	9.81	10.11	10.05	9.99	0.28	11.51	17.14	13.38	5.63
F/CCSD-ADC(2)	9.81	10.12	10.06	10.00	0.28	11.55	17.27	13.46	5.72
ADC(3/2)	9.30	10.09	9.71	9.70	0.69	12.07	16.35	13.50	4.29
F/CCD-ADC(3/2)	9.03	9.70	9.43	9.39	0.58	11.68	16.28	13.21	4.59
F/CCSD-ADC(3/2)	9.33	9.82	9.63	9.59	0.43	11.78	16.45	13.33	4.67
CC3[a]	9.38	9.96	9.61	9.65	0.51	11.95	15.57	13.16	3.62
Experiment[a]				9.83	0.67			13.08	3.59

[a] Taken from literature.[213,233–237]

of only 0.5%. The trend of using CCD or CCSD amplitudes within ADC(3/2) is the same as for the pure second-order method. Here, however, this means a deterioration in the case of CCD amplitudes, since the polarizability is underestimated by about 2.7%. F/CCSD-ADC(3/2) has rougly the same relative error compared to CC3 as the standard variant, just with the opposite sign.

When taking the experimental value as reference, which was obtained using refractive index data,[234,236] similar trends are observed. ADC(2) overestimates the polarizability by 3% or 0.3 a.u., the use of CC amplitudes again lowers the obtained values, thus generally improving the results. As for Ne and HF, CCD amplitudes yield better results than CCSD ones and the difference between the CC- and F/CC-ADC variants is negligible. CCSD-ADC(2), however, still overestimates the static polarizability by about 1.6% (0.16 a.u.), whereas the variants with CCD amplitudes now *underestimate* its value by

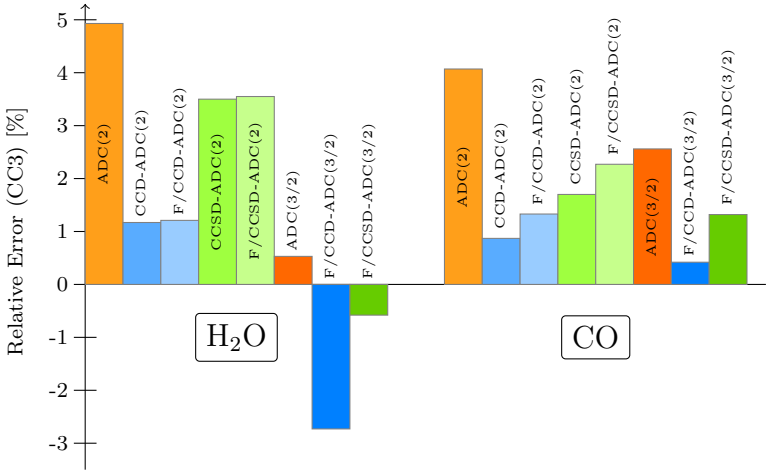

FIGURE 5.3: Relative error of the isotropic polarizability $\bar{\alpha}$ of H_2O and CO of results presented in Table 5.3 with respect to CC3.

0.06 a.u. Overall, (F/)CCD-ADC(2) yields the best results of all compared methods with a relative error of only about −0.65%. In fact, the result with CCD-ADC(2) agrees even better with experiment than the CC3 one, which for the previously studied systems yielded results almost identical to FCI, but here underestimates the polarizability by 1.8% (0.18 a.u.) compared to experiment.[213,230] A significant difference to previous results is observed for the third-order ADC scheme. The effect of the CC amplitudes of lowering the values is still the same, but since standard ADC(3/2) already underestimates the polarizability compared to experiment by 1.3% (0.13 a.u., thus being still more accurate than CC3), in this case the results deviate stronger when using CCD or CCSD amplitudes within the second-order **F** vectors. Deviations from experiment of −0.44 and −0.24 a.u. corresponding to relative errors of −4.5% and −2.4% were obtained for F/CCD-ADC(3/2) and F/CCSD-ADC(3/2), respectively.

Having a look at the polarizability anisotropy $\Delta\alpha$ as defined in Eq. (5.4), standard ADC(2) yields the best result of 0.54 a.u. with respect to CC3 or experiment compared to all other second-order methods. CCD amplitudes lower this value only by 0.1 a.u., but with CCSD amplitudes the result is with 0.28 a.u. the worst of all. Standard ADC(3/2) yields the best result of all with respect to experiment, even better than CC3. Taking CC3 as a reference, on the other hand, the ADC(3/2) value can be slightly improved by using CC amplitudes.

Another molecular system under investigation here is carbon monoxide, which was also calculated using the d-aug-cc-pVTZ basis set. As can be seen from the results for the isotropic polarizability shown in Table 5.3 and the relative error with respect to CC3 depicted in Figure 5.3, standard ADC(2) overestimates its value significantly by 4.1% or 0.34 a.u. The use of CCD amplitudes in both the **F** vectors and the secular matrix **M** of ADC(2) lowers this error significantly to 0.11 a.u., yielding again the best result of all ADC(2) variants compared to CC3 with a relative error of only about 0.9%. With CCSD amplitudes, the deviation is 1.7% (0.22 a.u.), which is still less than half as large as for standard ADC(2). The difference between the CC-ADC(2) and F/CC-ADC(2) variants is for CO larger than for Ne or HF, but the trend is the same as for Li^-: employing CC amplitudes only in the modified transition moments has the largest influence and lowers the value of the dipole polarizability significantly, with F/CCD-ADC(2) and F/CCSD-ADC(2) resulting in a relative error of about 1.3% and 2.3%, respectively, while the additional substitution in the secular matrix **M** has the same effect, but to a smaller extent. Going to the third-order description in the secular matrix only yields a small improvement compared to pure second-order; the error of standard ADC(3/2) still amounts to 2.6% or 0.34 a.u. Replacing the MP amplitudes in the second-order transition moment vectors by CC ones gives an improvement both for CCD and CCSD doubles amplitudes. In this case, however, the variant with CCD amplitudes yields better result than with CCSD ones. While F/CCSD-ADC(3/2) still deviates from experiment by 1.3% (0.17 a.u.), F/CCD-ADC(3/2) yields the best result of all presented ADC variants with

a deviation of only 0.05 a.u., corresponding to a relative error of about 0.4%. It is also remarkable at this point that all "hybrid" CC-ADC variants, even the pure second-order ones, yield better results than the (third-order) standard ADC(3/2) method. For example, the relative error of F/CCD-ADC(3/2) is only one third of the standard ADC(3/2) one, and the relative error of CCD-ADC(2) is about half as large as the one of standard ADC(3/2) and only one third of the standard ADC(2) one. All observed trends and results hold as well when taking experiment[213,235] as a reference for the isotropic polarizability, just that the absolute deviation is 0.08 a.u. larger for all ADC variants.

A different picture is observed for the individual components of the polarizability tensor. For the two components perpendicular to the molecular axis, α_{xx} and α_{yy}, the standard ADC approaches with MP amplitudes have a smaller deviation from the CC3 results than the ones with CC amplitudes, the order of magnitude of the deviation for the former being about 0.1 a.u., whereas for the latter it is up to 0.5 a.u. However, for the component along the molecular axis, α_{zz}, the largest difference can be observed between the pure second-order ADC variants and the ADC(3/2) ones. The third-order description of the secular matrix $\mathbf{M}$ significantly improves the description of α_{zz} by about 1.0 a.u. for the standard ADC approaches. The influence of the chosen amplitudes in the $\mathbf{F}$ vectors on the ADC(3/2) results is rather negligible. At the ADC(2) level, this influence is somewhat larger, and the largest improvement is again obtained with CCD amplitudes replacing the MP ones everywhere; with the error of CCD-ADC(2) being 0.4 a.u. smaller than the one of the standard ADC(2) variant. These differences, of course, explain the changes in the polarizability anisotropy. While all ADC variants overestimate its value compared to experiment[213,237] or also CC3,[233] the use of CC amplitudes within ADC generally raises $\Delta\alpha$, thus worsening the results. For CCSD amplitudes the effect is more pronounced than for CCD ones.

5.3.2.2 Aromatic Systems

Finally, I turn the attention to some larger chemical systems: aromatic and heteroaromatic compounds. Due to the lack of CC3 or similar values in the literaure for the systems, they are compared to experimental values only. The prototype of aromatic systems is, of course, the benzene molecule, which is computed as a first example using the Sadlej-pVTZ basis set.[238] Experimental values in the literature were obtained by applying ultraviolet Stark spectroscopy[239] or through a series of experimental and theoretical data using the DOSD technique.[240] For standard ADC methods the benzene molecule has proven to be a difficult case,[214] which can be seen in the results shown in Table 5.4 and Figure 5.4 on the left. Compared to the DOSD value, standard ADC(2) overestimates the static polarizability significantly by 5.14 a.u., corresponding to a relative error of 7.6%. Expanding the secular matrix $\mathbf{M}$ to third order in standard ADC(3/2) improves the result only slightly and still overestimates $\bar{\alpha}$ notably by 6.1% or absolutely by 4.13 a.u. Using CC amplitudes within ADC again improves the values for the polarizability significantly by

TABLE 5.4: Static dipole polarizability (in a.u.) of the benzene, pyridine and naphthalene molecules calculated with different ADC variants (Sadlej-pVTZ basis set) compared to DOSD values.

	Benzene				Pyridine					Naphthalene				
Method	α_{xx}	α_{zz}	$\bar{\alpha}$	$\Delta\alpha$	α_{xx}	α_{yy}	α_{zz}	$\bar{\alpha}$	$\Delta\alpha$	α_{xx}	α_{yy}	α_{zz}	$\bar{\alpha}$	$\Delta\alpha$
ADC(2)	86.32	46.14	72.93	40.18	82.64	42.21	78.49	67.78	38.53	182.3	134.4	69.2	128.6	98.3
CCD-ADC(2)	81.68	45.99	69.78	35.69	78.41	42.09	74.67	65.05	34.60	172.8	128.5	69.4	123.6	89.8
F/CCD-ADC(2)	81.90	46.08	69.96	35.82	78.51	42.14	74.88	65.18	34.69	171.0	128.7	69.6	123.1	88.2
CCSD-ADC(2)	81.79	45.57	69.72	36.22	78.70	41.83	75.20	65.24	35.26	172.9	129.0	68.9	123.6	90.4
F/CCSD-ADC(2)	82.14	45.75	70.01	36.39	78.96	41.97	75.54	65.49	35.41	171.6	129.5	69.3	123.4	89.1
ADC(3/2)	84.89	45.97	71.92	38.92	80.91	41.95	76.59	66.48	36.99	178.1	130.7	68.6	125.8	95.2
F/CCD-ADC(3/2)	80.91	46.08	69.30	34.82	77.27	42.07	73.46	64.27	33.46	168.3	126.0	69.3	121.2	86.1
F/CCSD-ADC(3/2)	81.12	45.75	69.33	35.37	77.67	41.87	74.05	64.53	34.13	168.8	126.6	68.9	121.4	86.8
Experiment[a]			67.79	31.5				62.88					117.4	86.8

[a] Taken from literature.[222,239–241]

lowering the computed values. Here, the difference between CCD and CCSD amplitudes is replacing the MP ones either only in the **F** vectors or both in **F** and the secular matrix **M** is rather negligible, with the difference between the two corresponding CC-ADC(2) and F/CC-ADC(2) variants being $\leq$0.1%. Using CC amplitudes within ADC(2) in the modified transition moment vectors only yields a deviation from experiment of about 3.2% (2.2 a.u.), whereas the error is about 2.9% (less than 2.0 a.u.) when the amplitudes are replaced everywhere in CC-ADC(2). A significant improvement is also observed when using CC amplitudes in the **F** vectors of the ADC(3/2) variant, with the deviation from experiment being merely about 2.2% (1.5 a.u.), thus yielding the best results for all compared ADC variants. Hence, the improvement obtained when using CC amplitudes within ADC for the calculation of the static polarizability lies in the order of 63%, which is the most significant one of all systems compared so far. Again, all CC-ADC variants show a substantial improvement over the standard ones with the relative error of CC-ADC(2) methods being only about half as large as the one for standard ADC(3/2). A possible explanation for the better performance of the CC-ADC variants compared to the standard ADC ones is the better description of excitation energies, especially for the lowest ones, as shown in Chapter 4. Yet, the transition moments seem to be a more important factor. They are, however, hard to compare with literature or especially experiment. In literature,[196] only oscillator strengths were compared, but those depend also linearly on the excitation energy.

But not only the isotropic polarizability, also its anisotropy is improved significantly compared to the experimental value[239] when using CC amplitudes in ADC. While it does not seem to play a significant role whether they are employed both in the secular matrix and the modified transition moments, CCD amplitudes again yield slightly better results than the corresponding versions with CCSD amplitudes. Other experimental results give the polarizability anisotropy of benzene as 35.02 a.u.,[241,242] which is in almost perfect agreement with CCD-ADC(2) or F/CCSD-ADC(3/2) results, for instance.

Another system closely related to benzene is the six-membered heteroaromatic compound pyridine, the geometry of which has been optimized using the Gaussian 09

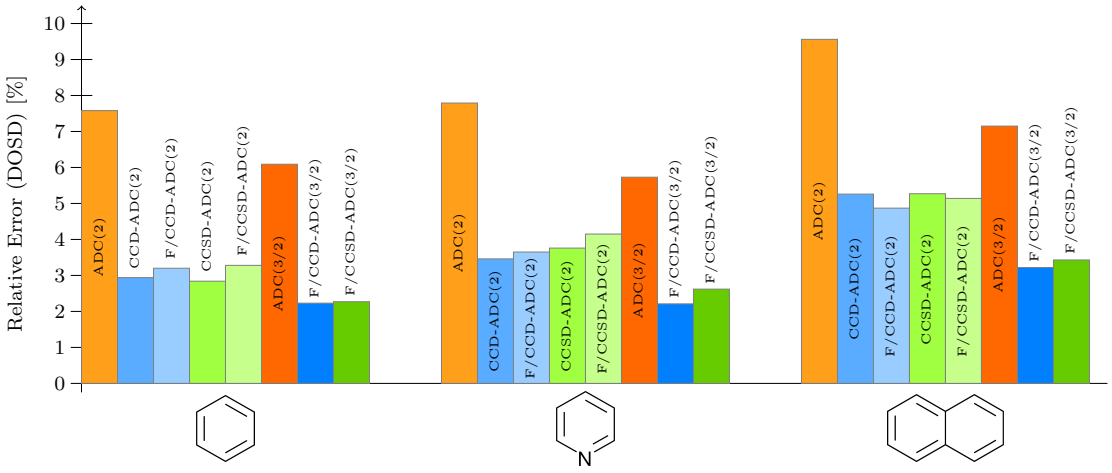

FIGURE 5.4: Relative error of the isotropic polarizability $\bar{\alpha}$ for benzene, pyridine and naphthalene of results presented in Table 5.4 with respect to DOSD values.

program package[243] at the MP2/cc-pVTZ level of theory. For the calculation of the static polarizability again the Sadlej-pVTZ basis set was used, the results are shown next to the ones for benzene in Table 5.4 and the relative errors are depicted in Figure 5.4. The experimental value of its isotropic polarizability was obtained using the DOSD method.[222] However, no value for the individual components or its anisotropy could be found in the literature. The deviation of the standard ADC(2) method from the DOSD value is with 7.8% or 4.9 a.u. very similar to the one for the benzene molecule, while the deviation of the standard ADC(3/2) variant is with 5.7% (3.6 a.u.) slightly smaller (0.5 a.u. in absolute numbers) for pyridine than for benzene. However, a clear improvement is observed again for all ADC variants when using CC instead of MP amplitudes. The difference between the individual variants is slightly larger in this case than for benzene, though all variants are still very similar. The best result for the pure second-order ADC method is again obtained when CCD amplitudes are used throughout, i.e. CCD-ADC(2). Here, the error amounts to 3.46% (2.17 a.u.), as compared to 3.76% (2.36 a.u.) when CCSD amplitudes are used, or 3.65% and 4.15% corresponding to 2.30 and 2.61 a.u. when CCD or CCSD amplitudes are used in the **F** vectors only, respectively. This corresponds to an improvement of up to 55% compared to the relative error of the standard ADC(2) method. Another significant improvement is observed when F/CCD-ADC(3/2) is employed. With a deviation from experiment of 2.21% (1.39 a.u.), the F/CCD-ADC(3/2) variant again yields the best result, which corresponds to an improvement of 61% as compared to the standard ADC(3/2) variant. The F/CCSD-ADC(3/2) variant yields a comparable result with a relative error of 2.62%. Again, the results obtained with all hybrid CC-ADC variants show a significant improvement over the standard ones, even CC-ADC(2) over standard ADC(3/2), at a lower overall computational cost.

The results for the last and largest system discussed here, the naphthalene molecule, are summarized in Table 5.4 and Figure 5.4, as well calculated with the Sadlej-pVTZ basis

set. As noted by Millefiori and Alparone,[241] experimental results of the polarizability and its anisotropy were obtained from the Cotton–Mouton effect,[244] molar Kerr constants and refractions[245,246] as well as from laser Stark spectroscopy.[247,248] Concerning the isotropic polarizability, the standard ADC(2) variant has an even larger deviation from experiment than for benzene and pyridine, the relative overestimation amounting to 9.6%, its absolute error being 11.22 a.u. As previously, significant improvement is obtained when CC amplitudes are used. For CCD-ADC(2), CCSD-ADC(2) and F/CCSD-ADC(2) the relative error lies between 5.1% and 5.3%, with the absolute error between 6.0 and 6.2 a.u. In this case, the F/CCD-ADC(2) variant again stands somewhat out, having the smallest error of all compared methods with 4.9% or 5.72 a.u. Thus, the improvement obtained when using CC amplitudes is up to almost 50% compared to the standard ADC(2) variant. The standard third-order ADC(3/2) method again shows no significant improvement compared to standard ADC(2) and has an error of 7.2% corresponding to 8.4 a.u. The use of CC amplitudes within the second-order $\mathbf{F}$ vectors improves notably upon this value, yielding the best result of all compared methods with 3.2% corresponding to 3.8 a.u. As for the aromatic systems studied before, all CC-ADC variants yield better results compared to experiment than the standard ones, especially CC-ADC(2) yields better results than standard ADC(3/2) while the computational cost remains significantly lower. On the other hand, an improvement in the relative error of more than 50% is obtained when going from standard ADC(3/2) to F/CCD-ADC(3/2) at a higher computational cost that only amounts to about 1% in this case. Again, a possible explanation for the improved description of the polarizability is the improvement in excitation energies. Even more pronounced than for benzene, significantly improved results for the polarizability anisotropy $\Delta\alpha$ compared to experiment are obtained when using CC amplitudes within ADC, especially in the ADC(3/2) scheme where the F/CCSD-ADC(3/2) variant is in perfect agreement with the experimental value.

Two more related aromatic systems, quinoline and isoquinoline, have been calculated as well (see Appendix B on page 209), and the results show the same trends and improvements for the CC-ADC methods, underlining the consistency of the improvement for this class of molecules.

5.4 Summary

In this chapter, the existing implementation of the algebraic-diagrammatic construction scheme for the polarization propagator with coupled-cluster amplitudes (Chapter 4) has been extended to molecular properties, and in this special case tested for dipole polarizabilities recently implemented for standard ADC using the damped response formalism.[214] Furthermore, in addition to CCD, CCSD amplitudes can be used as well, also in the second-order transition moments of the ADC(3/2) method. This new approach is inspired by similar work done on the SOPPA method by Geertsen, Oddershede and

Sauer.[54,56] In the new CC-ADC(2) variants, the Møller–Plesset correlation coefficients that occur in ADC are replaced by either CCD or CCSD amplitudes, in the F/CC-ADC(2) and F/CC-ADC(3/2) variants they are replaced only in the second-order modified transition moments **F**, but not in the secular matrix **M**. In order to test the performance of the new CC-ADC variants, the static dipole polarizabilities of several small to medium-sized chemical systems have been calculated and compared to FCI, CC3, DOSD or experimental reference values. As a first test case the Li^- ion was chosen, since it served previously as reference.[56] In my opinion, however, this is not a good test case since the results are very sensitive with respect to the amplitudes employed in the calculation and hence the values vary very strongly and unsystematically. Although the result obtained with the F/CCD-ADC(2) variant is very close to FCI, this seems to be rather fortuitous than systematic and hence does not allow for many general conclusions regarding the use of CC amplitudes within ADC, except that the polarizability becomes smaller when using CC amplitudes. For the ten-electron systems neon and hydrogen fluoride the standard ADC methods show a relatively large deviation from FCI that could be improved when employing CCD amplitudes. Since, however, the third-order ADC(3/2) scheme already provided very good results with relative errors $\leq$1%, no significant improvement was obtained with CC amplitudes in the **F** vectors. A slightly different picture is obtained when experimental values are used as reference. While for the water molecule notable improvements, especially with CCD amplitudes, could be observed for the second-order ADC method, an increased deviation is observed for ADC(3/2) because the standard variant already underestimates the static polarizability by about 1%, and the use of CC amplitudes in the **F** vectors generally lower its absolute value even more. For carbon monoxide and in particular the aromatic systems benzene, pyridine and naphthalene, which have proven to be very problematic cases for standard ADC,[214] very consistent improvements for all CC-ADC variants compared to the standard schemes are obtained. The CCD-ADC(2) results for instance even exhibit a notably smaller relative error than the considerably more expensive ADC(3/2) method. For benzene the relative errors of both the CC-ADC(2) and F/CC-ADC(3/2) variants amounted only to about 35–50% to the one of standard ADC(3/2).

Due to the less favorable scaling of CCD/CCSD compared to MP2, the CC-ADC(2) variants are of course computationally somewhat more demanding than standard ADC(2), but still significantly cheaper than the standard third-order ADC(3/2) or EOM-CC methods. At this point it seems appropriate to consider some computational efficiency aspects of the different standard ADC, CC-ADC and standard (EOM-)CC aproaches in terms of their formal scaling with system size a bit more in detail. Both MP2 and ADC(2) scale as $\mathcal{O}(N^5)$ (the latter in an iterative manner, however), whereas ADC(3) and both (EOM-)CCSD and CCD scale as $\mathcal{O}(N^6)$, where N is the number of basis functions. The price that has thus to be paid for the improvement of the results for the static polarizability with CC-ADC(2) is the $\mathcal{O}(N^6)$ iterative ground-state calculation with

CCD or CCSD instead of just the single $\mathcal{O}(N^5)$ MP2 one. The successive excited-state calculation, however, scales more favorably for ADC(2) than for ADC(3) or CCSD. Thus, while the ground-state calculation has become one order of magnitude more expensive compared to MP2, the excited-state calculation still scales as $\mathcal{O}(N^5)$ and the results obtained with the CC-ADC(2) variants are notably better than the ones for standard ADC(3/2). In this way, one obtains very good results at an overall lower cost than standard third-order ADC or CCSD methods which are sometimes even comparable to the very accurate iterative CC3 method, that however scales very unfavorably as $\mathcal{O}(N^7)$. As an example, in the ADC(2) and CC-ADC(2) computations of the aromatic systems the CPU time needed for the ADC (and CC) calculations only amounts to about 1% compared to ADC(3/2). On the other hand, the additional time needed for the CC calculation in F/CC-ADC(3/2) also amounts only to about 1% of the total time, and the improvement in the results is remarkable.

Especially the CC-ADC(2) variants might become useful and versatile alternatives to standard ADC in the calculation of molecular properties such as polarizabilities, since it combines a reliable iterated CC ground state and retains the advantageous features of ADC with its Hermitian eigenvalue problem and low computational cost.

Chapter 6

Third-Order Unitary Coupled Cluster for Electronic Excitation and Molecular Properties

In this chapter, the third-order unitary coupled-cluster approach, as described in Section 3.4 (page 72) based on the Bernoulli expansion of the similarity-transformed Hamiltonian (Section 3.2), is discussed in more detail, in particular its implementation within the `adcman` module[52] of the Q-Chem 5.2 program package.[53] For this, the general block tensor library `libtensor` is used throughout,[249] which also means that the implementations are parallelized via shared memory and exploit permutation, spin, and Abelian point-group symmetry. First, the implementation of the UCC3 amplitude equations (3.64) for the electronic ground state is described, exploiting the similarity to standard coupled-cluster approaches, then the eigenvalue problem to obtain excitation energies and ionization potentials, where the relationship to the ADC schemes as described in Section 3.5 is exploited. The UCC3 scheme is then benchmarked on the same set of molecules as the second-order methods in Chapter 4. Apart from electronic excitation energies, also transition moments, as well as dipole moments in the ground and excited states, have been calculated with the approach described in Section 3.7. Furthermore, the first-ever implementation of UCC-based self-consistent electron propagator theory (IP-UCC) through third order as well as results of ionization potentials for selected amino acids calculated with IP-UCC2 and IP-UCC3 are reported.

6.1 Implementation

6.1.1 Amplitude Equations

Since the UCC3 amplitude equations (3.64) are coupled and nonlinear, they need to be solved in an iterative manner analogous to standard CC amplitude equations.[9] For

this, they are rewritten analogous to Eqs. (2.169) in Section 2.6.7 by taking the terms involving $f_{ii} = \varepsilon_i$ and $f_{aa} = \varepsilon_a$ on the LHS. Then, all amplitudes on the RHS are set to zero and one divides by the orbital-energy differences. As the initial guess, the first-order amplitudes $t^{(1)}_{ijab}$ from MP are used. Through the second iteration, i.e., up to second-order, the perturbation expansion of the amplitudes is identical to the ones of CCSD.

However, in order to efficiently implement the UCC3 amplitude equations, it is useful to factorize some terms that include products of $\hat{\sigma}_2$ amplitudes and introduce intermediates, which are stored in memory. All intermediates are listed in the following. First, for the singles equations (3.64a), two intermediates denoted as $I^{(1)}_{\mathtt{ovvv}}$ and $I^{(2)}_{\mathtt{ooov}}$ are presented below, where `o` stands for "occupied" and `v` for "virtual" orbitals. The first line of each equation represents the way the terms occur in the original equation,[51] the second line includes index renaming and the third line shows the intermediate as implemented, possibly with further index permutations. The index renaming and permutation is necessary since only the canonical blocks `oooo`, `ooov`, `oovv`, `ovov`, `ovvv` and `vvvv` of the electron repulsion tensor are available. The first two intermediates are given as

$$
\begin{aligned}
&-\frac{1}{2}\sum_{jkb}\langle kj||ib\rangle\sigma^{ba}_{jk} - \sum_{jklbc}\langle bl||ji\rangle\sigma^{bc*}_{jk}\sigma^{ca}_{kl} + \frac{1}{4}\sum_{jkbcd}\langle bd||ic\rangle\sigma^{bd*}_{jk}\sigma^{ca}_{jk} \\
&\quad= -\frac{1}{2}\sum_{jkb}\langle kj||ib\rangle\sigma^{ba}_{jk} - \sum_{jklbc}\langle ck||li\rangle\sigma^{cb*}_{lj}\sigma^{ba}_{jk} + \frac{1}{4}\sum_{jkbcd}\langle cd||ib\rangle\sigma^{cd*}_{jk}\sigma^{ba}_{jk} \\
&\quad= \sum_{jkb}\Big[-\frac{1}{2}\langle kj||ib\rangle - \sum_{c}\Big(\sum_{l}\langle il||kc\rangle\sigma^{bc*}_{jl} - \frac{1}{4}\sum_{d}\langle ib||cd\rangle\sigma^{cd*}_{jk}\Big)\Big]\sigma^{ba}_{jk} \\
&\quad= \sum_{jkb}\Big[I^{(1)}_{kj,ib}\Big]\sigma^{ba}_{jk}
\end{aligned}
\tag{6.1}
$$

$$
\begin{aligned}
&\frac{1}{2}\sum_{jbc}\langle aj||cb\rangle\sigma^{cb}_{ij} + \sum_{jkbcd}\langle ab||dj\rangle\sigma^{bc*}_{jk}\sigma^{cd}_{ki} - \frac{1}{4}\sum_{jklbc}\langle al||jk\rangle\sigma^{bc*}_{jk}\sigma^{cb}_{il} \\
&\quad= \frac{1}{2}\sum_{jbc}\langle aj||cb\rangle\sigma^{cb}_{ij} + \sum_{jklbc}\langle ad||bk\rangle\sigma^{dc*}_{kj}\sigma^{cb}_{ji} - \frac{1}{4}\sum_{jkbcd}\langle aj||kl\rangle\sigma^{bc*}_{kl}\sigma^{cb}_{ij} \\
&\quad= \sum_{jbc}\Big[\frac{1}{2}\langle ja||bc\rangle - \sum_{k}\Big(\sum_{d}\langle kb||ad\rangle\sigma^{dc*}_{kj} - \frac{1}{4}\sum_{l}\langle kl||ja\rangle\sigma^{bc*}_{kl}\Big)\Big]\sigma^{cb}_{ij} \\
&\quad= \sum_{jbc}\Big[I^{(2)}_{ja,bc}\Big]\sigma^{cb}_{ij}\,.
\end{aligned}
\tag{6.2}
$$

For the doubles equation (3.64b) three intermediates are introduced. For the first two, $I^{(3)}_{\mathtt{oooo}}$ and $I^{(4)}_{\mathtt{vvvv}}$, no index renaming is necessary. Thus the second line immediately

represents the intermediate as implemented, if required with index permutations,

$$\begin{aligned}
&\frac{1}{2}\sum_{kl}\langle kl||ij\rangle\sigma_{kl}^{ab} + \frac{1}{6}\sum_{klcd}\langle kl||cd\rangle\sigma_{ij}^{cd}\sigma_{kl}^{ab} + \frac{1}{12}\sum_{klcd}\langle cd||ij\rangle\sigma_{kl}^{cd*}\sigma_{kl}^{ab} \\
&\quad= \sum_{kl}\Big[\frac{1}{2}\langle ij||kl\rangle + \frac{1}{6}\sum_{cd}\Big(\langle kl||cd\rangle\sigma_{ij}^{cd} + \frac{1}{2}\langle ij||cd\rangle\sigma_{kl}^{cd*}\Big)\Big]\sigma_{kl}^{ab} \\
&\quad= \sum_{kl}\Big[I_{kl,ij}^{(3)}\Big]\sigma_{kl}^{ab} \\
&\frac{1}{2}\sum_{cd}\langle ab||cd\rangle\sigma_{ij}^{cd} + \frac{1}{12}\sum_{klcd}\langle ab||kl\rangle\sigma_{kl}^{cd*}\sigma_{ij}^{cd} \\
&\quad= \sum_{cd}\Big[\frac{1}{2}\langle ab||cd\rangle + \frac{1}{12}\sum_{kl}\langle ab||kl\rangle\sigma_{kl}^{cd*}\Big]\sigma_{ij}^{cd} \\
&\quad= \sum_{cd}\Big[I_{ab,cd}^{(4)}\Big]\sigma_{ij}^{cd}\,,
\end{aligned} \tag{6.3, 6.4}$$

where the choice to include the term with a prefactor of $\frac{1}{6}$ into the $I^{(3)}_{\mathtt{oooo}}$ intermediate instead of $I^{(4)}_{\mathtt{vvvv}}$ was arbitrary. The last intermediate, $I^{(5)}_{\mathtt{ovov}}$, needs index renaming and is given as

$$\begin{aligned}
&\hat{\mathcal{P}}(ij)\hat{\mathcal{P}}(ab)\Big(\sum_{kc}\langle ak||ic\rangle\sigma_{jk}^{bc} + \frac{1}{3}\sum_{klcd}\langle kl||cd\rangle\sigma_{ik}^{ac}\sigma_{jl}^{bd} + \frac{1}{3}\sum_{klcd}\langle ad||il\rangle\sigma_{kl}^{cd*}\sigma_{jk}^{bc}\Big) \\
&= \hat{\mathcal{P}}(ij)\hat{\mathcal{P}}(ab)\Big(\sum_{kc}\langle ak||ic\rangle\sigma_{jk}^{bc} + \frac{1}{3}\sum_{ld}\langle lk||dc\rangle\sigma_{il}^{ad}\sigma_{jk}^{bc} + \frac{1}{3}\sum_{ld}\langle ad||il\rangle\sigma_{kl}^{cd*}\sigma_{jk}^{bc}\Big) \\
&= \hat{\mathcal{P}}(ij)\hat{\mathcal{P}}(ab)\Big(\sum_{kc}\Big[-\langle ka||ic\rangle + \frac{1}{3}\sum_{ld}\Big(\langle kl||cd\rangle\sigma_{il}^{ad} + \langle il||ad\rangle\sigma_{kl}^{cd*}\Big)\Big]\sigma_{jk}^{bc}\Big) \\
&= \hat{\mathcal{P}}(ij)\hat{\mathcal{P}}(ab)\Big(\sum_{kc}\Big[I_{ka,ic}^{(5)}\Big]\sigma_{jk}^{bc}\Big)\,.
\end{aligned} \tag{6.5}$$

The convergence of the iterative solution of Eqs. (3.64) is accelerated analogous to SCF or standard CC by using Pulay's *direct inversion in the iterative subspace* (DIIS) method.[250–252] The converged amplitudes and the ground-state energy E_0^{UCC} (see Section 3.6) are saved in the context for further use, and the ground-state density matrix $\boldsymbol{\rho}$ is calculated and stored as well. Up to now, the ground-state energy is strictly correct through third order in perturbation theory, and properties obtained with this density matrix are correct through second order (see Section 3.7.1). In the future, both E_0^{UCC} and $\boldsymbol{\rho}$ will be extended to include higher-order terms. The density-matrix contributions are obtained from the equations for the property, which can be interpreted as the trace of the matrix product between the density matrix and the one-particle integrals, $D_0 = \mathrm{Tr}(\boldsymbol{\rho}\mathbf{D})$. For instance, the second-order density matrix elements obtained from Eqs. (3.81) and

(3.82) are given by

$$\rho_{ij}^{(2)} = -\frac{1}{2}\sum_{kab} \sigma_{ik}^{ab}\, \sigma_{jk}^{ab*} \tag{6.6a}$$

$$\rho_{ab}^{(2)} = \frac{1}{2}\sum_{ijc} \sigma_{ij}^{ac}\, \sigma_{ij}^{bc*} \tag{6.6b}$$

$$\rho_{ia}^{(2)} = \sigma_i^a\,, \tag{6.6c}$$

and $\rho_{ai}^{(2)} = \sigma_i^{a*}$, which is equal to $\rho_{ia}^{(2)}$ for real orbitals, making the density matrix symmetric.

6.1.2 Excitation Energies and Transition Moments

After the solution of the amplitude equations, the eigenvalue problem has been implemented within `adcman`. This has been done by exploiting the close relationship between ADC and UCC as described in Section 3.5. For the second-order variants, the only difference between ADC(2) and UCC2 comes from the second commutator of $\bar{H}^{(2)}$ in Eq. (3.70c), where the first-order doubles amplitudes appear $\frac{1}{2}[\hat{V}, \hat{\sigma}_2^{(1)}]$, which have to be replaced by the converged ones for UCC2, corresponding to the contribution of $\frac{1}{2}[\hat{V}, \hat{\sigma}_2]$. This has been done by replacing the reference in the context used by ADC calculations from the MP2 ground-state energy and amplitudes to the corresponding UCC2 contributions. The implementation of excitation energies via UCC3 proceeded analogously. The contributions of the double commutators part in $\bar{H}^{(3)}$, Eq. (3.70d), needed the same change of replacing $t_{ijab}^{(1)}$ by converged σ_{ij}^{ab} amplitudes. However, one further change had to be done, since ADC(3) or UCC3-s has an additional third-order contribution in the singles-singles block arising from the $\frac{1}{2}[\hat{V}, \hat{\sigma}_2^{(2)}]$ commutator involving the second-order doubles amplitudes $t_{ijab}^{(2)}$. These do not occur in a non-perturbative treatment of UCC, and hence the corresponding contribution was set to zero. The resulting equations are implemented in matrix-vector-product form and the eigenvalue problem is solved numerically by using the Davidson algorithm.[253]

The same changes described above for the ADC matrix are also valid for the ground- to excited-state transition moments through second order (see Section 3.7.2). Thus, the first-order doubles amplitudes are replaced by the converged UCC ones, whereas the second-order doubles are set to zero, and $\rho_{ia}^{(2)}$ from the MP2 ground-state density matrix is replaced by the UCC singles amplitudes σ_i^a.

Analogously, a UCC-based scheme for the calculation of ionization potentials (IP) or electron attachment (EA) energies could be implemented by employing the existing IP-ADC code.[89,90,254–256] The resulting schemes are referred to as IP-UCC2 and IP-UCC3.

6.1.3 Program Invocation and Control

In the Q-Chem input file, the METHOD keyword in the `$rem` section can be set to UCC2, UCC2-x or UCC3 in order to carry out UCC calculations for the ground and excited states at several levels of theory. The same keywords from standard CC theory can be used to specify the parameters of the ground-state DIIS run, such as CC_CONVERGENCE, CC_E_CONV, CC_T_CONV, to set the convergence criteria or CC_MAX_ITER to set the maximum number of iterations.

Concerning excited-state calculations, the same keywords from ADC calculations apply. EE_STATES sets the number of excited states to calculate; by setting ADC_PROP_ES = TRUE excited-state properties are calculated, and ADC_PROP_ES2ES controls the calculation of transition properties between excited states (transition dipole moments and oscillator strengths). ADC_DAVIDSON_MAXSUBSPACE, ADC_DAVIDSON_MAXITER, and ADC_DAVIDSON_CONV control the maximum subspace size, the maximum number of iterations, and the convergence criterion of the Davidson procedure, respectively.

6.2 Vertical Electronic Excitations

In order to test the performance of the UCC3 scheme, apart from the pilot applications published in Ref. 51, calculations were performed on the benchmark sets of Jacquemin *et al.*[172] as well as Thiel and co-workers,[179–181] analogous to the other methods compared in Chapter 4. All the input data is thus identical to the ones described there. I want to acknowledge that the calculations of the Thiel benchmark set were carried out under my guidance by Sebastian M. Thielen. The results of the vertical excitation energies for the Jacquemin benchmark set are given in Table A.1 in Appendix A (page 193). The results of the Bernoulli variant of UCC2 as well as UCC3 are given in Table A.2 for singlet excited states and Table A.3 for triplet excited states.

6.2.1 Small Inorganic and Organic Molecules

Let me start with a brief discussion of the benchmark set introduced by Jacquemin and co-workers.[172] The ADC(3) values were recomputed to check the consistency of the input data, but the fluorescence energies were not calculated and thus not taken into account for the statistical error evaluation presented in Table 6.1, where also the results of the third-order methods CCSDR(3), CCSDT-3 and CC3 are shown. CCSDT-3 is an iterative third-order approximation to the full CCSDT model[257] similar to CC3,[232,258] while CCSDR(3) can be seen as the non-iterative analog of CC3.[259] While all methods based on standard CC theory have tiny errors and RMS deviations (< 0.1 eV), these values are significantly larger for both ADC(3) and UCC3. The iterative ground state of UCC3 improves the mean absolute error and RMS deviation slightly compared to ADC(3), but it does not come close to the other CC methods. However, one should keep in mind that

the theoretical best estimates were obtained by extrapolating CC schemes towards the FCI limit, and they are based on CC3 geometries.[172]

TABLE 6.1: Mean signed error (MSE), mean absolute error (MAE), root mean square deviations (RMS), as well as positive (Max) and negative (Min) maximal deviations with respect to the TBE(FC) values.[a] All values are given in eV.

Method	No. of States	MSE	MAE	RMS	Max	Min
ADC(3)	102	−0.120	0.227	0.244	0.740	−0.560
UCC3	102	−0.128	0.223	0.234	0.594	−0.634
CCSDR(3) [a]	59	0.01	0.04	0.05	0.25	−0.07
CCSDT-3 [a]	58	0.01	0.03	0.05	0.24	−0.07
CC3 [a]	106	−0.01	0.03	0.04	0.19	−0.09

[a] Taken from Ref. 172.

6.2.2 Singlet Excited States

Going on with the Thiel benchmark set, I will only focus on the statistical error evaluation in order to keep the discussion concise, which is presented in Table 6.2 and Figure 6.1 for the singlet excited states. At first, the UCC excitation energies are compared against the TBE values as reference. While UCC2 exhibits a mean error of 0.36 eV and a standard deviation of 0.41 eV, its third-order variant UCC3 significantly improves upon this decreasing the mean error to 0.07 eV and the standard deviation to 0.30 eV. Concerning the second-order methods, UCC2 performs worse than CC2 and ADC(2). Both the mean error, mean absolute error, and the standard deviation are about 0.1 eV larger for UCC2 than for the other two methods.

Compared to the other third-order methods, the mean error of UCC3 is significantly smaller than those of ADC(3) and CC3, while the standard deviation of UCC3 is slightly larger than for ADC(3). In the histograms in Figure 6.1, the distribution of the UCC methods seems somewhat more narrow; however, they have an outlier each that is not present in the ADC schemes. Taking ADC(3) as a reference in Table 6.2, UCC2 performs very similar to CC2 but worse than ADC(2), as may not be surprising considering the similarity to the reference. With CC3 as the reference, UCC2 again performs slightly worse than ADC(2) and CC2, whereas UCC3 yields very similar results as ADC(3).

TABLE 6.2: Statistical error analysis of the calculated excitation energies (in eV) of the excited singlet states of Thiel's benchmark set at the ADC(2), ADC(3), UCC2, UCC3 and CC3 levels of theory. The theoretical best estimates (TBE) were used as reference data as well as the ADC(3) and CC3 values.

	TBE as reference				
	ADC(2)[a]	UCC2	ADC(3)[a]	UCC3	CC3[a]
Count[b]	103	103	103	103	84
Min	−0.32	−1.38	−0.78	−0.77	−0.11
Max	1.63	2.03	0.90	1.43	1.15
Mean	0.22	0.36	0.12	0.07	0.23
Mean Absolute	0.26	0.41	0.23	0.23	0.24
Standard Deviation	0.30	0.41	0.27	0.30	0.21
	ADC(3) as reference				
	ADC(2)[a]	UCC2	ADC(3)[a]	UCC3	CC3[a]
Count[b]	134	134	...	132	111
Min	−1.29	−0.92	...	−0.68	−1.10
Max	2.19	2.62	...	1.03	2.41
Mean	0.07	0.24	...	−0.04	0.18
Mean Absolute	0.33	0.42	...	0.11	0.27
Standard Deviation	0.49	0.54	...	0.16	0.42
	CC3 as reference				
	ADC(2)[a]	UCC2	ADC(3)[a]	UCC3	CC3[a]
Count[b]	109	109	109	108	...
Min	−1.51	−1.02	−1.24	−1.41	...
Max	2.16	2.45	1.10	1.11	...
Mean	0.02	0.22	−0.14	−0.17	...
Mean Absolute	0.21	1.08	0.23	0.26	...
Standard Deviation	0.38	0.40	0.32	0.35	...

[a] Taken from the literature.[179,196]

[b] Total number of considered states.

6.2.3 Triplet Excited States

The statistical error evaluation of the triplet excited states is presented in Table 6.3 and Figure 6.2. Starting again with TBE as the reference, UCC2 performs worst of all second-order methods, having a mean error and standard deviation of 0.22 ± 0.21 eV, whereas ADC(2) has 0.12 ± 0.17 eV and CC2 0.17 ± 0.13 eV. Concerning the third-order methods, CC3 outperforms all other methods, having errors < 0.1 eV. The ADC(3) and UCC3 results, on the other hand, are rather similar, the former having a mean error and standard deviation of -0.18 ± 0.16 eV, whereas -0.22 ± 0.15 eV is obtained for the latter. Taking ADC(3) as the reference, UCC3 has very small errors of -0.04 ± 0.08 eV, thereby clearly outperforming CC3 with 0.23 ± 0.20 eV, which demonstrates the similarity of the two approaches. This similarity is further underlined by taking CC3 as the reference,

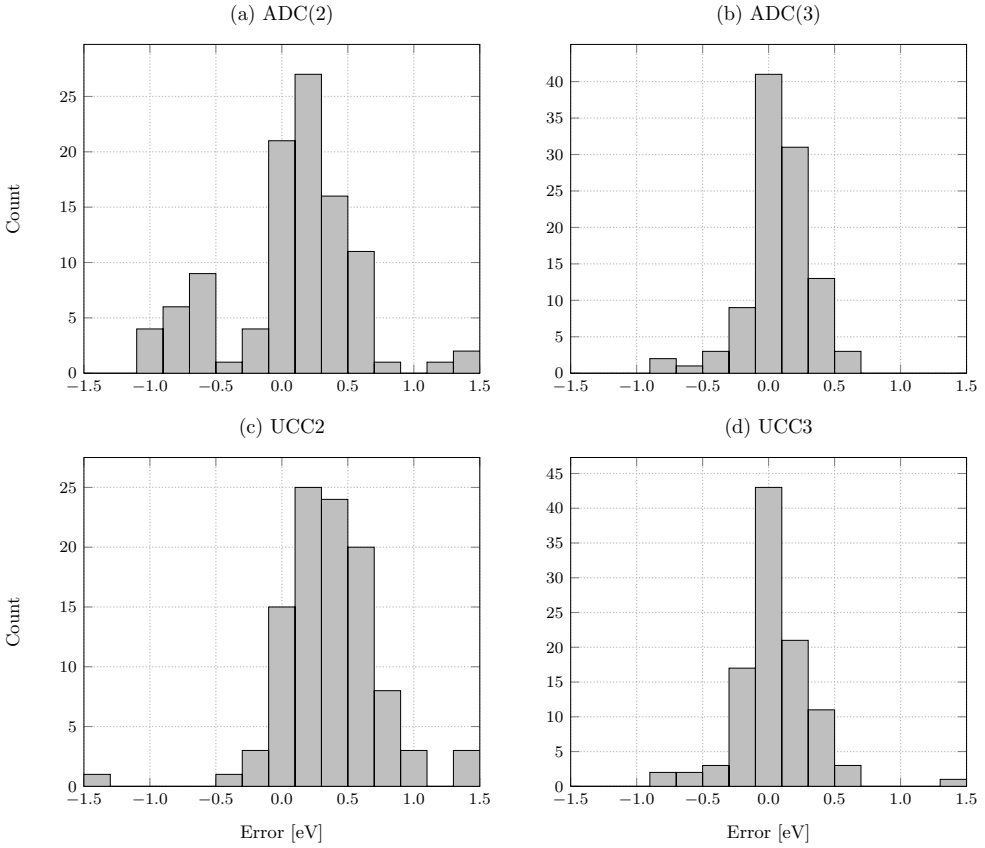

FIGURE 6.1: Histograms of the error distribution of all calculated excited singlet states with respect to the theoretical best estimates at the theoretical levels of (a) ADC(2), (b) ADC(3), (c) UCC2, and (d) UCC3.

where ADC(3) and UCC3 again have very similar mean errors and standard deviations of -0.23 ± 0.20 eV and -0.27 ± 0.19 eV, respectively.

6.2.4 Oscillator Strengths

Apart from the computation of excitation energies, another vital aspect of the theoretical investigation of excited electronic states is the prediction of spectral intensities. The latter is usually given in terms of oscillator strengths, which are calculated from the excitation energies and the transition dipole moments from the ground to the respective excited states. The results for oscillator strengths of selected transitions of the Thiel benchmark set are compiled in Table A.5 in the appendix. Values obtained from calculations using ADC(2) and ADC(3/2), as well as reference literature data, are given for comparison.[179,196] In analogy to the ADC(3/2) scheme,[196] oscillator strengths are computed using the third-order UCC3 excitation vectors contracted with the second-order effective transition moments (see Section 3.7.2) to produce transition matrix elements which are referred to as UCC(3/2). Using UCC3 excitation energies, one then obtains UCC(3/2) oscillator strengths. UCC2 and UCC(3/2) oscillator strengths are for almost every considered state

TABLE 6.3: Statistical error analysis of the calculated excitation energies (in eV) of the excited triplet states of Thiel's benchmark set at the ADC(2), ADC(3), UCC2, UCC3 and CC3 levels of theory. The theoretical best estimates (TBE) were used as reference data as well as the ADC(3) and CC3 values.

	TBE as reference					
	ADC(2)[a]	UCC2	CC2[a]	ADC(3)[a]	UCC3	CC3[a]
States	63	63	63	63	63	63
Min	−0.27	−0.27	−0.09	−0.49	−0.49	−0.04
Max	0.48	0.63	0.48	0.44	0.43	0.32
Mean	0.12	0.22	0.17	−0.18	−0.22	0.04
Std. dev.	0.17	0.21	0.13	0.16	0.15	0.08
Abs. mean	0.17	0.25	0.18	0.21	0.24	0.04
	ADC(3) as reference					
	ADC(2)[a]	UCC2	CC2[a]	ADC(3)[a]	UCC3	CC3[a]
States	71	71	71	...	71	71
Min	−0.38	−0.31	−0.37	...	−0.24	−0.26
Max	1.52	1.76	1.58	...	0.17	1.29
Mean	0.32	0.42	0.37	...	−0.04	0.23
Std. dev.	0.30	0.33	0.29	...	0.08	0.20
Abs. mean	0.38	0.45	0.40	...	0.07	0.25
	CC3 as reference					
	ADC(2)[a]	UCC2	CC2[a]	ADC(3)[a]	UCC3	CC3[a]
States	71	71	71	71	71	...
Min	−0.27	−0.27	−0.11	−1.29	−1.29	...
Max	0.48	0.70	0.56	0.26	0.29	...
Mean	0.10	0.19	0.14	−0.23	−0.27	...
Std. dev.	0.15	0.19	0.14	0.20	0.19	...
Abs. mean	0.14	0.23	0.15	0.25	0.28	...

[a] Taken from the literature.[179,196]

in good accordance with the literature data. However, since these values are in most cases given in a relatively big interval, not many values disagree with the literature in the first place. As can be seen there, the UCC2 oscillator strengths are usually quite similar to the ADC(2) ones, whereas UCC(3/2) is very similar to ADC(3/2). The good agreement of essentially all values with the results from the literature thus underlines the reliability of the UCC approaches for spectral intensities.

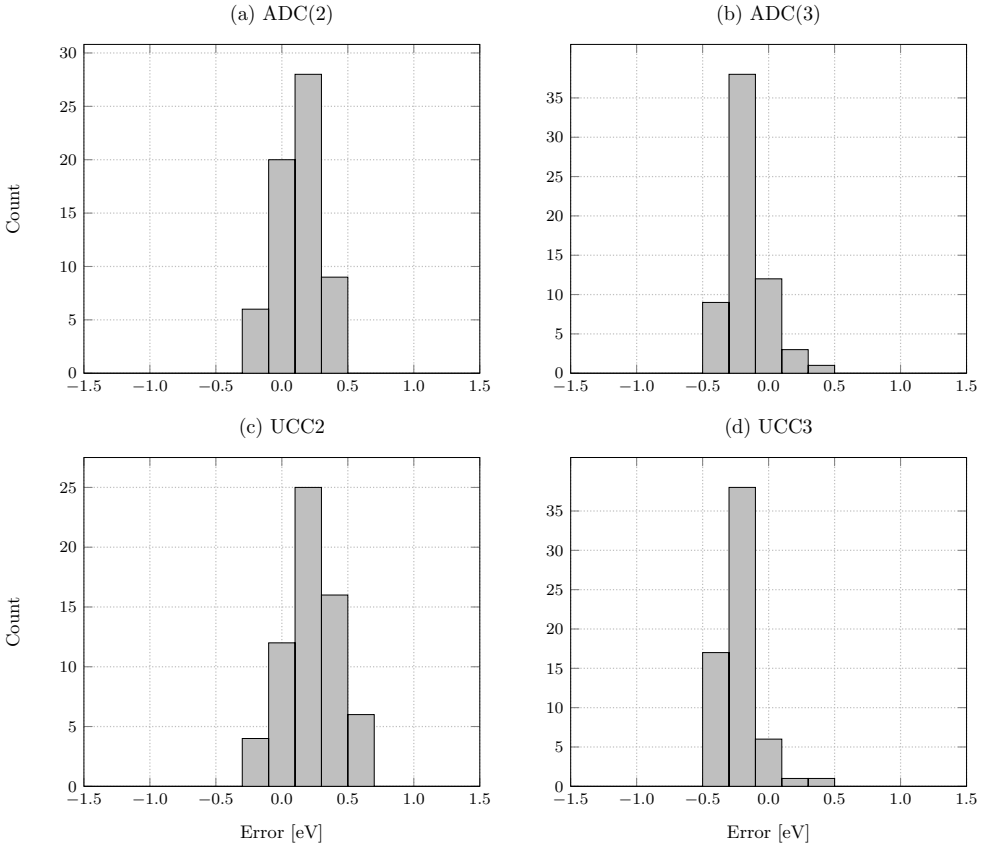

FIGURE 6.2: Histograms of the error distribution of all calculated excited triplet states with respect to the theoretical best estimates at the theoretical levels of (a) ADC(2), (b) ADC(3), (c) UCC2, and (d) UCC3.

6.3 Ground- and Excited-State Dipole Moments

One-particle properties such as the electric dipole moment can be calculated in UCC via an expectation-value approach, as described in Section 3.7. The implementation of ground- and excited-state properties through second order was analogous to the excitation energies and transition moments by replacing the first-order doubles and second-order singles amplitudes from MP by the converged UCC2 or UCC3 ones. As a first test and validation of the present development, I performed UCC computations of dipole moments for the H_2O and HF molecules within the small 3-21G basis set [260] and compared them to FCI and ADC results. [30] The same geometrical parameters were used as in Ref. 30 ($R_{OH} = 0.957$ Å, $\angle(HOH) = 104.5°$, $R_{HF} = 0.917$ Å), and the 1s core orbitals were kept frozen in all correlated calculations. The Hartree–Fock and MP2 dipole moments were recalculated in order to check the consistency of the input data. In the present implementation, both the ground- and effective excited-state densities ($\boldsymbol{\rho}$ and $\tilde{\tilde{\mathbf{B}}}$, respectively) are correct through second order in perturbation theory, higher-order terms will be included in future work. The dipole moments obtained with UCC3 amplitudes

(and excitation vectors) and the second-order densities are denoted UCC(3/2), analogously to ADC(3/2).[26,30]

As can be seen in the results for the ground-state dipole moments in Table 6.4, the values are getting closer to the FCI reference, starting from HF over MP2 and UCC2 to UCC(3/2) for both the H_2O and HF molecules. Especially UCC(3/2) is in excellent agreement with the FCI value.

TABLE 6.4: Ground-state dipole moments $\mu = |\boldsymbol{\mu}|$ (in Debye) of the H_2O and HF molecules calculated at the FCI, HF, MP2, UCC2 and UCC(3/2) levels of theory in combination with the 3-21G basis set.

System	FCI[a]	HF	MP2	UCC2	UCC(3/2)
H_2O	2.30	2.44	2.36	2.34	2.30
HF	2.03	2.16	2.08	2.05	2.02

[a] FCI results from Ref. 30.

In general, however, strict second-order schemes will be less satisfactory than in these cases. For instance, for the CO molecule ($R_{CO} = 1.128$ Å) within the minimal STO-3G basis set[260] the ground-state dipole moment is 0.63 D at the FCI level. Here, MP2 yields 1.30 D, and UCC2 improves only slightly with 1.16 D. Using third-order amplitudes in UCC(3/2), the result is improved significantly to 0.70 D.

Going with dipole moments in excited electronic states for H_2O and HF molecules using the same input parameters, the results at the FCI, ADC(1), ADC(2), ADC(3/2), UCC2 and UCC(3/2) levels of theory are presented in Table 6.5. It should be noted that excitation energies and excited-state properties obtained with ADC(1) are identical to the values obtained by configuration interaction singles (CIS) and a hypothetical UCC1 scheme since no ground-state correlation treatment enters the ADC(1) and UCC1 secular or property matrices. Assuming that the UCC amplitudes are also correct through first order, ground- to excited-state transition moments are identical in ADC(1) and UCC1 as well. However, they differ from CIS, since they are only correct in zeroth order in the latter. As can be seen in Table 6.5, the dipole moments obtained with the second-order schemes ADC(2) and UCC2 are very similar and a significant improvement upon the first-order ADC(1) results, but they still deviate relatively strongly. By combining the second-order property matrix with the eigenvectors of the third-order secular matrix, the results can be significantly improved in both the ADC(3/2) and UCC(3/2) schemes, where both again yield very similar results. For the lowest excited singlet states of water, UCC(3/2) is 0.01–0.02 D further off than ADC(3/2), but for the 2 $^1B_2$ and the higher triplet states as well as most states in hydrogen fluoride, the UCC(3/2) results are closer to the FCI reference than ADC(3/2). These results are very promising and will be further investigated by including higher-order terms to the effective density matrix in the future.

TABLE 6.5: Excited-state dipole moments $\mu = |\boldsymbol{\mu}|$ (in Debye) of the H_2O and HF molecules calculated at the FCI, ADC(1), ADC(2), ADC(3/2), UCC2 and UCC(3/2) levels of theory in combination with the 3-21G basis set.

State	FCI[a]	ADC(1)[a]	ADC(2)[a]	ADC(3/2)[a]	UCC2	UCC(3/2)
H_2O $1\,{}^1A_1 \rightarrow$						
$1\,{}^1B_1$	0.17	0.76	0.35	0.24	0.38	0.26
$1\,{}^1A_2$	0.19	0.27	0.01	0.15	0.03	0.13
$2\,{}^1A_1$	0.50	1.15	0.72	0.60	0.74	0.61
$1\,{}^1B_2$	0.24	0.64	0.45	0.26	0.47	0.27
$2\,{}^1B_2$	0.54	0.24	0.44	0.52	0.43	0.54
$1\,{}^3B_1$	0.15	0.69	0.32	0.22	0.35	0.24
$1\,{}^3A_1$	0.59	0.80	0.68	0.61	0.70	0.62
$1\,{}^3A_2$	0.12	0.22	0.03	0.08	0.05	0.06
$1\,{}^3B_2$	0.37	0.32	0.42	0.39	0.44	0.39
HF $1\,{}^1\Sigma^+ \rightarrow$						
$1\,{}^1\Pi$	1.80	2.42	2.07	1.84	2.09	1.85
$2\,{}^1\Sigma^+$	1.28	2.13	1.66	1.31	1.66	1.28
$1\,{}^3\Pi$	1.82	2.34	2.06	1.87	2.08	1.88
$1\,{}^3\Sigma^+$	1.65	1.54	1.68	1.65	1.68	1.65

[a] FCI and ADC results from Ref. 30.

6.4 Vertical Ionization Potentials

Apart from electronic excitation energies, where the total number of electrons N in the system remains unchanged, also processes where one or several electrons are removed from or attached to the system can be described by theories such as EOM-CC, ADC, and UCC. For this, the "physical" excitation operators $\hat{C}_J$ are not chosen to be the particle-number conserving ones of Eq. (2.89a), but those from Eq. (2.89b) for the IP case of (2.89c) for the EA case. Considering only IP for now, this means that the Hamiltonian is represented within the basis of intermediate states with $N-1$ electrons, $|\tilde{\hat{\Psi}}_J^{N-1}\rangle = e^{\hat{\sigma}}\hat{C}_J|\Phi_0\rangle$, which corresponds to the transformed Hamiltonian $\bar{H}$ being represented within the basis of "ionized" determinants, $|\Phi_J^{N-1}\rangle$, i.e., determinants having one electron less than the HF reference,

$$\tilde{\bar{H}}_{IJ}^{N-1} = \langle\tilde{\hat{\Psi}}_I^{N-1}|\hat{H}|\tilde{\hat{\Psi}}_J^{N-1}\rangle = \langle\Phi_I^{N-1}|\bar{H}|\Phi_J^{N-1}\rangle\,. \tag{6.7}$$

By diagonalizing the above matrix and subtracting the energy of the N-electron ground state E_0^{UCC}, vertical ionization potentials are obtained. It can be shown that the resulting IP-UCC scheme is equivalent to IP-ADC through third order. The matrix elements of IP-UCC2 and IP-UCC3 thus correspond to those of IP-ADC(2) and IP-ADC(3), respectively.[254] For instance, the zeroth-order element is given as the downward-directed fragment of the Fock operator (see Figure 2.3), $\langle\Phi_i|\hat{F}_{\mathrm{N}}|\Phi_j\rangle = -f_{ji} = -\varepsilon_i\,\delta_{ij}$, which corresponds to Koopmans' theorem.[24,65] The first-order contribution vanishes since there are no fragments of the normal-ordered fluctuation potential with only two

open lines, $\langle\Phi_i|\hat{V}_\mathrm{N}|\Phi_j\rangle = 0$. Hence, Koopmans' theorem is correct through first order in perturbation theory. The second-order part of the 1h/1h block is given as

$$\begin{aligned}\frac{1}{2}\langle\Phi_i|[\hat{V}_\mathrm{N},\hat{\sigma}_2]|\Phi_j\rangle &= \frac{1}{2}\times\Bigg[\quad + \quad\Bigg] \\ &= -\frac{1}{4}\sum_{kab}\langle kj||ab\rangle\,\sigma_{ki}^{ab} - \frac{1}{4}\sum_{kab}\langle ab||ki\rangle\,\sigma_{kj}^{ab*}\,,\end{aligned} \tag{6.8}$$

where the additional factor of $\frac{1}{2}$ comes from the Bernoulli expansion of $\bar{H}$, see Eq. (3.37), since the $\hat{V}_\mathrm{R}$ part does not contribute.

As some preliminary results, the ionization energies of the amino acids glycine, alanine, and serine have been calculated with IP-UCC2 and IP-UCC3. They are compared to IP-ADC and experimental results[261] in Table 6.6, where the same basis set (cc-pVTZ) and geometries as in the IP-ADC study were used.[254] As can be seen in Table 6.6, both second-order methods consistently underestimate the IPs compared to the experiment. However, the IP-UCC2 values tend to be closer to the reference than its IP-ADC(2) counterpart. For the third-order variants, the opposite is true. IP-ADC(3) tends to overestimate ionization potentials slightly compared to the experiment. At the same time, for IP-UCC3, this overestimation is sometimes more pronounced, in particular for the first ionized state, but in general, the results are well comparable. However, more tests and calculations need to be carried out for a thorough investigation of the performance and capabilities of the IP-UCC schemes.

TABLE 6.6: Computed IP-UCC values for the lowest vertical ionization energies of selected amino acids compared to IP-ADC and experimental data. All values in eV.

System	State	Exp.[a]	IP-ADC(2)[b]	IP-ADC(3)[b]	IP-UCC2	IP-UCC3
Glycine	1	10.0	9.44	10.11	9.50	10.26
	2	11.1	9.95	11.37	9.95	11.34
	3	12.2	11.46	12.28	11.44	12.27
	4	13.6	13.19	13.57	13.30	13.81
	5	14.4	13.50	14.70	13.51	14.82
Alanine	1	9.85	9.24	9.95	9.29	10.10
	2	11.0	9.77	11.16	9.76	11.14
	3	12.1	11.31	12.14	11.30	12.14
	4	12.8	12.40	12.85	12.50	13.11
	5	13.4	12.90	13.50	12.97	13.73
Serine	1	10.0	9.39	10.28	9.42	10.39
	2	11.0	10.00	10.99	10.05	11.03
	3	11.25	10.09	11.44	10.09	11.43
	4	12.4	11.41	12.24	11.42	12.27
	5	12.6	11.81	12.77	11.83	12.84

[a] Experimental data from Ref. 261. The stated values refer to band maxima.

[b] IP-ADC results from Ref. 254.

Chapter 7

Analysis and Comparison of Expectation-Value and Derivative-Based Molecular Properties

7.1 Introduction

The quantum-chemical calculation of molecular properties is an every-day task of modern computational chemistry. It is for example needed to predict properties for a rational design of functional materials, to guide synthesis or to help identifying molecular species with spectroscopic techniques. In principle, most (time-independent) molecular properties can be calculated in two different ways, which are in general not equivalent for approximate wave functions, since the Hellmann–Feynman theorem[146,147] may not be fulfilled. It is therefore of great interest to understand the accuracy, advantages and drawbacks of these two approaches.[262–264]

The first approach is based on the expectation value of the corresponding operator for the physical observable with the wave function and the second one on derivatives of the energy with respect to (w.r.t.) a perturbation connected with the observable. For instance, as described in Section 2.7, in case of the electric dipole moment $\boldsymbol{\mu}$, the expectation value

---

Parts of this chapter have already been published in

- M. Hodecker, D. R. Rehn, A. Dreuw, S. Höfener, "Similarities and differences of the Lagrange formalism and the intermediate state representation in the treatment of molecular properties", *The Journal of Chemical Physics*, **2019**, *150*, 164125.

is given as

$$\boldsymbol{\mu} = \langle \Psi_n | \hat{\mu} | \Psi_n \rangle \,, \tag{7.1}$$

where $\hat{\mu}$ is the dipole operator and $|\Psi_n\rangle$ is the wave function of electronic state n. Alternatively, the dipole moment can be computed as derivative of the energy w.r.t. an external electric field $\boldsymbol{\mathcal{F}}$ according to

$$\boldsymbol{\mu} = \frac{\mathrm{d}}{\mathrm{d}\boldsymbol{\mathcal{F}}} E_n[\hat{H} + \hat{\mu} \cdot \boldsymbol{\mathcal{F}}] \,, \tag{7.2}$$

evaluated at zero field strength. Here, $E_n[\hat{H} + \hat{\mu} \cdot \boldsymbol{\mathcal{F}}]$ denotes the general energy expression of the electronic state n in the presence of the perturbation, which does not necessarily need to also correspond to an expectation value. Formally, for exact energies and wave functions, the two approaches in Eqs. (7.1) and (7.2) are equivalent, as well as whenever the Hellmann–Feynman theorem is fulfilled. For approximate wave functions, however, the two approaches can and usually do yield different results and for some properties even only one of the approaches is applicable. For example, analytical nuclear gradients can only be calculated as derivatives, unless Pulay forces are neglected.[265,266]

Following the postulates of quantum mechanics,[77] properties or observables are associated with eigenvalues of the corresponding operator. Expectation values are averages over such observables according to Eq. (7.1), which are identical to the eigenvalues if the system is in an eigenstate of the operator. Eq. (7.1) yields the formally correct value for a property within a given quantum-chemical model defined by approximations in the Hamiltonian or the wave function. Comparing this value with an experimental reference or the exact value may reveal substantial deviations due to the approximations in the model. In fact, a value for the observable obtained as derivative of the approximate energy defined by the same approximate level of theory according to Eq. (7.2) may yield a better agreement, because additional contributions are taken into account, e.g. orbital and amplitude relaxations, which may not be properly accounted for in the approximate wave function used to compute the expectation value, and the derivative value may thus be closer to the exact value.[57,96] On the other hand, one can argue that it lies conceptually "outside" the model chemistry defined by the approximate quantum-chemical method. It is generally ambiguous as to which approach can be called more "correct" and therefore, both computational pathways to molecular properties should not be seen as exclusive, but rather complementary, since they can provide a measurement on how important orbital or amplitude relaxation effects are for the respective property.

Generally, the description of molecular properties using approximate wave functions requires additional considerations compared to exact-state theory. This applies not only for ground-state but also for excited-state properties.[267] For example, the evaluation of derivatives is generally more involved because the Hellmann–Feynman theorem[146,147] does not apply for nonvariational approximate wave functions (see Ref. 265 and references therein). For non-Hermitian approaches, such as coupled-cluster theory, it is assumed

that generalized expressions are employed, e.g. by obtaining the real part as a sum of the value and its complex conjugate.[13]

When computing molecular properties of excited states as expectation values, in particular in connection with the algebraic-diagrammatic construction (ADC) scheme for the polarization propagator[25,27,28] as described in Section 2.5, the algebraic approach used is denoted intermediate state representation (ISR) formalism.[21,29,30] In general, propagator methods are usually limited to the calculation of excitation energies and transition moments from the ground state without having access to the corresponding wave functions. Within the alternative formulation of the ADC equations via the ISR formalism this limitation is overcome, because the Hamiltonian shifted by the ground state energy represented in a complete basis of known, so-called correlated excited states or intermediate states also yields the ADC equations, and together with the excitation vectors, the ISR provides thus access to the excited-state wave functions. The ISR formalism can be used to calculate arbitrary excited-state properties and transition properties between different excited states as formally correct expectation values within a given ADC model.[28,30]

When computing molecular properties as derivatives w.r.t. the perturbation strength, changes of the wave function parameters w.r.t. the perturbation are taken into account,

$$\langle \boldsymbol{\mu} \rangle_{\mathrm{rel}} = \frac{\mathrm{d}E[\boldsymbol{\kappa}, \boldsymbol{\lambda}]}{\mathrm{d}\boldsymbol{\mathcal{F}}} = \frac{\partial E}{\partial \boldsymbol{\mathcal{F}}} + \frac{\partial E}{\partial \boldsymbol{\kappa}} \frac{\mathrm{d}\boldsymbol{\kappa}}{\mathrm{d}\boldsymbol{\mathcal{F}}} + \frac{\partial E}{\partial \boldsymbol{\lambda}} \frac{\mathrm{d}\boldsymbol{\lambda}}{\mathrm{d}\boldsymbol{\mathcal{F}}} \,, \tag{7.3}$$

where $\boldsymbol{\kappa}$ and $\boldsymbol{\lambda}$ represent the SCF coefficients and the correlated wave function parameters such as amplitudes, respectively. In practice, a number of (coupled) response equations have thus to be solved and their solution is then used to evaluate the derivative expression Eq. (7.3). While such a treatment is in principle straightforward and numerically correct, the derivation of the necessary equations is often cumbersome, even for basic correlation methods such as second-order Møller–Plesset perturbation theory.[268] Here, the Lagrange formalism can be employed, which provides a simple recipe to include all perturbations as Lagrange multipliers $\bar{\boldsymbol{\kappa}}$ and $\bar{\boldsymbol{\lambda}}$ representing orbital rotations and correlated amplitude parameters, respectively,

$$L_{\mathrm{rel}}[\boldsymbol{\kappa}, \boldsymbol{\lambda}, \bar{\boldsymbol{\kappa}}, \bar{\boldsymbol{\lambda}}] = E[\boldsymbol{\kappa}, \boldsymbol{\lambda}] + \bar{\boldsymbol{\kappa}} \cdot \boldsymbol{e}_{\boldsymbol{\kappa}} + \bar{\boldsymbol{\lambda}} \cdot \boldsymbol{e}_{\boldsymbol{\lambda}} = E[\boldsymbol{\kappa}, \boldsymbol{\lambda}] \text{ “} + 0\text{”} \,. \tag{7.4}$$

The Lagrange functional is by construction stationary w.r.t. all parameters using the constraints $\mathbf{e}_\kappa = 0$ and $\mathbf{e}_\lambda = 0$ for the multipliers $\bar{\boldsymbol{\kappa}}$ and $\bar{\boldsymbol{\lambda}}$, respectively, i.e. by fulfilling the set of equations

$$\frac{\partial L_{\mathrm{rel}}}{\partial \bar{\boldsymbol{\kappa}}} = \boldsymbol{e}_{\boldsymbol{\kappa}} = 0 \qquad \frac{\partial L_{\mathrm{rel}}}{\partial \boldsymbol{\kappa}} = \frac{\partial E}{\partial \boldsymbol{\kappa}} + \bar{\boldsymbol{\kappa}} \frac{\partial \boldsymbol{e}_{\boldsymbol{\kappa}}}{\partial \boldsymbol{\kappa}} \overset{!}{=} 0 \tag{7.5a}$$

$$\frac{\partial L_{\mathrm{rel}}}{\partial \bar{\boldsymbol{\lambda}}} = \boldsymbol{e}_{\boldsymbol{\lambda}} = 0 \qquad \frac{\partial L_{\mathrm{rel}}}{\partial \boldsymbol{\lambda}} = \frac{\partial E}{\partial \boldsymbol{\lambda}} + \bar{\boldsymbol{\lambda}} \frac{\partial \boldsymbol{e}_{\boldsymbol{\lambda}}}{\partial \boldsymbol{\lambda}} \overset{!}{=} 0 \,, \tag{7.5b}$$

which means that the Lagrange multipliers contain the same information as the perturbed wave function parameters and are computed in a strict mathematical framework with a clear-cut derivation.[19,269–275] Once the multipliers have been determined by solving Eqs. (7.5), the desired property can then be computed as a *partial* derivative:

$$\langle \boldsymbol{\mu} \rangle_{\mathrm{rel}} = \frac{\mathrm{d}L_{\mathrm{rel}}}{\mathrm{d}\boldsymbol{\mathcal{F}}} = \frac{\partial L_{\mathrm{rel}}}{\partial \boldsymbol{\mathcal{F}}} = \frac{\partial E}{\partial \boldsymbol{\mathcal{F}}} + \bar{\boldsymbol{\kappa}} \frac{\partial \boldsymbol{e}_{\boldsymbol{\kappa}}}{\partial \boldsymbol{\mathcal{F}}} + \bar{\boldsymbol{\lambda}} \frac{\partial \boldsymbol{e}_{\boldsymbol{\lambda}}}{\partial \boldsymbol{\mathcal{F}}} \,, \tag{7.6}$$

which has the advantage compared to the original expression (7.3) that only one set of Lagrange multipliers need to determined independent of the perturbation, and no perturbation-dependent orbital response need to be solved.[57] If all terms in Eqs. (7.3) and (7.4) are taken into account, the final property is denoted "orbital relaxed" because also the response of the molecular orbitals onto the perturbation is included. Neglecting this response of the orbitals w.r.t. the perturbation,

$$\langle \boldsymbol{\mu} \rangle_{\mathrm{unrel}} = \frac{\partial L_{\mathrm{unrel}}}{\partial \boldsymbol{\mathcal{F}}} = \frac{\partial E}{\partial \boldsymbol{\mathcal{F}}} + \bar{\boldsymbol{\lambda}} \frac{\partial \boldsymbol{e}_{\boldsymbol{\lambda}}}{\partial \boldsymbol{\mathcal{F}}} \,, \tag{7.7}$$

leads to so-called "orbital unrelaxed" molecular properties. While the relaxed treatment employs a "fully" perturbed Hamiltonian, the unrelaxed case corresponds to a perturbation of the Hamiltonian in the correlation treatment only and can be regarded as an *ad hoc* approximation, which has the advantage of being computationally less demanding since the response of the orbital coefficients $\boldsymbol{\kappa}$ does not need to be determined. However, the computation of both unrelaxed and relaxed properties have become standard in computational chemistry and the differences of unrelaxed and relaxed properties have been subject of detailed studies, see Ref. 276 for instance. It should further be pointed out that in particular cases the unrelaxed approach can yield better results than the relaxed approach. For example, in case of indirect spin-spin coupling constants computed using coupled-cluster theory the unrelaxed results do not suffer from the poor orbital response of Hartree–Fock to triplet perturbations.[277,278]

Using diagrammatic techniques, Bartlett and co-workers already discussed the connection between the relaxed density matrix and the one obtained with the expectation-value approach (referred to as ISR in this chapter) in MP2.[96] In addition, they also investigated orbital relaxation effects in the ground-state CCSD method,[276] and similar diagrammatic analyses were performed for second-order properties by other groups.[279,280]

While the above-mentioned works focus on the electronic ground state, this chapter aims to address these questions for excited states and therefore choose a slightly different perspective. It is well understood that the singly-excited determinants correspond to orbital-relaxation effects in case of ground-state methods.[33] Similarly, one can argue that it is necessary to include at least doubly excited determinants in the wave function to account for orbital-relaxation effects for singly excited states. While such a perspective is straightforward for configuration-interaction (CI) methods, it is not clear to which

extent orbital-relaxation is included in methods based on perturbation theory such as ADC in case of excited states.

The goal of the present work is to fill this gap and analyze to which extend contributions can be associated with orbital-relaxation contributions with an emphasis on the algebraic-diagrammatic construction scheme for the polarization propagator. In the theory Section 7.2, working equations of both the Lagrange formalism and the ISR approach are presented and similarities and differences are worked out. First, the MP2 expectation value is formulated and then the scheme is transferred to ADC for excited states. In the results Section 7.4, numerical examples are given to illustrate the conclusions drawn from the theoretical analysis. Eventually, a short summary is given. I would like to mention that the work presented here is the result of a close collaboration with Dr. Dirk R. Rehn and Dr. Sebastian Höfener from the Karlsruhe Institute of Technology.

7.2 Theoretical Analysis

In this section, working equations for both the Lagrange formalism and the expectation-value/ISR approach are presented for one-particle operators. I start with an analysis of the HF/DFT and MP2 method for ground states, and highlight the origin of different terms in the expectation-value (ISR) and Lagrange formalism, which are further used to identify similarities and differences. This is followed by an analogous analysis of the excited-state methods CI, ADC(1) and ADC(2) pinpointing the presence and absence of different algebraic expression in the calculation of excited-state properties using the ISR or Lagrange formalism.

7.2.1 Self-Consistent Field Methods

In self-consistent field (SCF) methods, i.e. Hartree–Fock and DFT,[57] the expectation value (EV) is given by Eq. (3.80),

$$\langle \boldsymbol{\mu} \rangle_{\mathrm{EV}}^{\mathrm{HF}} = \langle \Phi_0 | \hat{\mu} | \Phi_0 \rangle = \sum_{pq} \mu_{qp} \underbrace{\langle \Phi_0 | \hat{a}_p^\dagger \hat{a}_q | \Phi_0 \rangle}_{=D_{pq}^{\mathrm{HF}}} = \sum_i \mu_{ii} \,, \tag{7.8}$$

where $\mathbf{D}^{\mathrm{HF}}$ is the HF density matrix in the MO basis, that corresponds to the unit matrix in the occupied–occupied block and is zero everywhere else. The energy derivative is obtained by replacing the Hamiltonian with $\hat{\mathcal{H}} = \hat{H} + \hat{\mu}\boldsymbol{\mathcal{F}}$ and differentiating according to

$$\begin{aligned} \langle \boldsymbol{\mu} \rangle_{\mathrm{rel}}^{\mathrm{HF}} &= \frac{\mathrm{d}E_0^{\mathrm{HF}}[\boldsymbol{\kappa}]}{\mathrm{d}\boldsymbol{\mathcal{F}}} = \frac{\mathrm{d}}{\mathrm{d}\boldsymbol{\mathcal{F}}} \langle \Phi_0 | \hat{\mathcal{H}} | \Phi_0 \rangle \\ &= \langle \Phi_0 | \hat{\mu} | \Phi_0 \rangle + \underbrace{\frac{\partial E_0^{\mathrm{HF}}}{\partial \boldsymbol{\kappa}}}_{=0} \frac{\mathrm{d}\boldsymbol{\kappa}}{\mathrm{d}\boldsymbol{\mathcal{F}}} = \langle \boldsymbol{\mu} \rangle_{\mathrm{EV}}^{\mathrm{HF}} \,, \end{aligned} \tag{7.9}$$

where the derivative of E_0^{HF} w.r.t. the SCF coefficients $\boldsymbol{\kappa}$ is identified as the electronic gradient (2.45) that vanishes for a converged HF solution and thus the derivative is identical to the expectation value. This can also be explained by the fact that the method is fully variational and thus the Hellmann–Feynman theorem is fulfilled.

7.2.2 Second-Order Møller–Plesset Perturbation Theory

As discussed in Section 2.4.2, in Møller–Plesset (MP) perturbation theory,[24,32,33] the electronic Hamiltonian $\hat{H}$ is split into the Fock operator $\hat{F}$ and the fluctuation potential $\hat{V}$ representing electron correlation. The exact ground-state energy E_0 and the exact ground-state wave function $|\Psi_0\rangle$ are expanded in a series according to Eqs. (2.67) and (2.68). The Hartree–Fock (HF) determinant $|\Psi_0^{(0)}\rangle = |\Phi_0\rangle$ fulfills the zeroth-order equation

$$\hat{F}|\Phi_0\rangle = E_0^{(0)}|\Phi_0\rangle\,, \tag{7.10}$$

where the energy $E_0^{(0)}$ is given by Eq. (2.80), while the first-order wave function correction $|\Psi_0^{(1)}\rangle$ contains only doubly-excited configurations according to Eq. (2.83) due to Brillouin's theorem. The equation to obtain the first-order doubles amplitudes $t_{\mu_2}^{(1)}$ can be written as

$$\langle\mu_2|\hat{H} + [\hat{F}, \hat{T}_2^{(1)}]|\Phi_0\rangle = 0\,, \tag{7.11}$$

in which $|\mu_2\rangle$ represents doubly-excited determinants, yielding the well-known expression of Eq. (2.82) in the canonical case. Orbitals and wave functions are assumed to be real-valued throughout, and the superscript "(1)" for first order will be dropped in the remainder of this chapter for better readability. Finally, the MP2 energy is given as the sum of zeroth and first order, the Hartree–Fock energy ($E_0^{\mathrm{HF}} = E_0^{(0)} + E_0^{(1)}$) as given in Eq. (2.53), and the second-order contribution $E_0^{(2)}$ given by Eq. (2.84), such that $E_0^{\mathrm{MP2}} = E_0^{\mathrm{HF}} + E_0^{(2)}$.

7.2.2.1 Orbital-Unrelaxed Lagrange Formalism for MP2 Properties

The unrelaxed MP2 Lagrange functional combines MP2 ground-state energy, i.e. the Hartree–Fock energy and the MP2 correlation energy, with the equations defining the doubles amplitudes t_{μ_2}, Eq. (7.11),

$$L_{\mathrm{unrel}}^{\mathrm{MP2}} = E_0^{\mathrm{HF}} + \langle\Phi_0|[\hat{H}, \hat{T}_2]|\Phi_0\rangle + \sum_{\mu_2} \bar{t}_{\mu_2}^{(0)} \langle\mu_2|\hat{H} + [\hat{F}, \hat{T}_2]|\Phi_0\rangle\,, \tag{7.12}$$

where $\bar{\mathbf{t}}^{(0)}$ are the Lagrange multipliers to ensure stationarity of the Lagrangian w.r.t. the amplitude parameters and the superscript "(0)" refers to the electronic ground state. The

Lagrange multipliers are chosen such that they fulfill the stationarity condition

$$\frac{\partial}{\partial t_{\nu_2}} L^{\mathrm{MP2}}_{\mathrm{unrel}} = \langle \Phi_0 | [\hat{F}, \hat{\tau}_{\nu_2}] | \Phi_0 \rangle + \sum_{\mu_2} \bar{t}^{(0)}_{\mu_2} \langle \mu_2 | [\hat{F}, \hat{\tau}_{\nu_2}] | \Phi_0 \rangle \stackrel{!}{=} 0 \,, \tag{7.13}$$

the solution of which reveals the amplitudes and multipliers to be identical in the case of MP2, $\bar{t}^{(0)}_{\mu_2} = t_{\mu_2}$. In the Lagrange framework, unrelaxed dipole moments are obtained from a perturbed Hamiltonian, $\hat{\mathcal{H}} = \hat{H} + \hat{\mu}\boldsymbol{\mathcal{F}}$, in the Lagrange expression (7.12) followed by differentiation:

$$\begin{aligned} \langle \boldsymbol{\mu} \rangle^{\mathrm{MP2}}_{\mathrm{unrel}} &= \frac{\partial}{\partial \boldsymbol{\mathcal{F}}} L^{\mathrm{MP2}}_{\mathrm{unrel}}[\hat{\mathcal{H}}] \\ &= \frac{\partial}{\partial \boldsymbol{\mathcal{F}}} \Big(\langle \Phi_0 | \hat{\mathcal{H}} + [\hat{\mathcal{H}}, \hat{T}_2] | \Phi_0 \rangle + \sum_{\mu_2} \bar{t}^{(0)}_{\mu_2} \langle \mu_2 | \hat{\mathcal{H}} + [\hat{\mathcal{H}}, \hat{T}_2] | \Phi_0 \rangle \Big) \\ &= \mu_0^{\mathrm{HF}} + \sum_{ij} D^{\mathrm{F}}_{ij}(\bar{\mathbf{t}}^{(0)})\, \mu_{ji} + \sum_{ab} D^{\mathrm{F}}_{ab}(\bar{\mathbf{t}}^{(0)})\, \mu_{ba} \,, \end{aligned} \tag{7.14}$$

where μ_{pq} are the one-particle matrix elements of the dipole operator in the MO basis, and $\mu_0^{\mathrm{HF}} = \langle \Phi_0 | \hat{\mu} | \Phi_0 \rangle$ is the Hartree–Fock dipole moment. The density $\mathbf{D}^{\mathrm{F}}$ defined as

$$D^{\mathrm{F}}_{ij}(\bar{\mathbf{t}}^{(0)}) = -\frac{1}{2} \sum_{kab} \bar{t}^{(0)}_{ikab} t_{jkab} \tag{7.15a}$$

$$D^{\mathrm{F}}_{ab}(\bar{\mathbf{t}}^{(0)}) = \frac{1}{2} \sum_{ijc} \bar{t}^{(0)}_{ijac} t_{ijbc} \,, \tag{7.15b}$$

thus describes the contribution of the MP2 amplitudes to the dipole moment, which consists of two blocks, occupied–occupied and virtual–virtual. It should be noted that there are no occupied–virtual contributions to $\mathbf{D}^{\mathrm{F}}$ since no singles amplitudes are present in canonical MP2.

7.2.2.2 Orbital-Relaxed Lagrange Formalism for MP2 Properties

In Eq. (7.14) the change of the orbitals due to the perturbation is not taken into account. Including, however, the Brillouin condition, i.e. a vanishing occupied–virtual block of the Fock matrix ($f_{ia} = 0$), in the Lagrange functional ensures that the HF solution is also independent of the perturbation. The relaxed MP2 Lagrange functional then reads

$$L^{\mathrm{MP2}}_{\mathrm{rel}} = L^{\mathrm{MP2}}_{\mathrm{unrel}} + \sum_{ia} \bar{\kappa}^{(0)}_{ai} f_{ia} \tag{7.16}$$

and a new term enters the calculation of the dipole moment

$$\langle \boldsymbol{\mu} \rangle^{\mathrm{MP2}}_{\mathrm{rel}} = \frac{\partial}{\partial \boldsymbol{\mathcal{F}}} L^{\mathrm{MP2}}_{\mathrm{rel}}[\hat{\mathcal{H}}] = \langle \boldsymbol{\mu} \rangle^{\mathrm{MP2}}_{\mathrm{unrel}} + \sum_{ia} \bar{\kappa}^{(0)}_{ai} \mu_{ia} \,. \tag{7.17}$$

In the calculation of unrelaxed MP2 properties the occupied–virtual block of the dipole operator μ_{ia} does not contribute, for relaxed properties it does due to orbital relaxation. Similar to the multipliers $\bar{\mathbf{t}}^{(0)}$, the new orbital rotation multipliers $\bar{\boldsymbol{\kappa}}^{(0)}$ have to be computed before the dipole moment can be evaluated. Requesting that the derivative of the relaxed Lagrange functional w.r.t. the orbital rotation parameters is zero,

$$\begin{aligned} 0 &\stackrel{!}{=} \frac{\partial}{\partial \kappa_{bj}} L_{\mathrm{rel}}^{\mathrm{MP2}} \\ &= \frac{\partial}{\partial \kappa_{bj}} \langle \Phi_0 | [\hat{H}, \hat{T}_2] | \Phi_0 \rangle + \frac{\partial}{\partial \kappa_{bj}} \sum_{\mu_2} \bar{t}_{\mu_2}^{(0)} \langle \mu_2 | [\hat{F}, \hat{T}_2] | \Phi_0 \rangle + \sum_{ia} \bar{\kappa}_{ai}^{(0)} \frac{\partial}{\partial \kappa_{bj}} f_{ia} \,, \end{aligned} \tag{7.18}$$

yields the well-known Z-vector equations[269,281] determining the multipliers $\bar{\boldsymbol{\kappa}}^{(0)}$:

$$-\sum_{ia} \bar{\kappa}_{ai}^{(0)} \frac{\partial}{\partial \kappa_{bj}} f_{ia} = \frac{\partial}{\partial \kappa_{bj}} \langle \Phi_0 | [\hat{H}, \hat{T}_2] | \Phi_0 \rangle + \frac{\partial}{\partial \kappa_{bj}} \sum_{\mu_2} \bar{t}_{\mu_2}^{(0)} \langle \mu_2 | [\hat{F}, \hat{T}_2] | \Phi_0 \rangle \,. \tag{7.19}$$

The derivative of the relevant occupied–virtual block of the Fock matrix w.r.t. the orbital rotation parameters, i.e. a part of the electronic Hessian (2.46), is given as[33]

$$\frac{\partial}{\partial \kappa_{bj}} f_{ia} = \delta_{ab} \delta_{ij} (\varepsilon_a - \varepsilon_i) + A_{iajb}^{\kappa} \,, \tag{7.20}$$

where the elements of the supermatrix $\mathbf{A}^{\kappa}$ are given as $A_{pqrs}^{\kappa} = \langle pq || rs \rangle + \langle ps || rq \rangle$. The Z-vector equations for occupied–virtual rotations are thus given as

$$-\sum_{ia} \left(\delta_{ab} \delta_{ij} (\varepsilon_a - \varepsilon_i) + A_{iajb}^{\kappa} \right) \bar{\kappa}_{ai}^{(0)} = Z_{bj}^{\mathrm{MP2}} (\bar{\mathbf{t}}^{(0)}) \,, \tag{7.21}$$

where for convenience $\mathbf{Z}^{\mathrm{MP2}}$ was introduced for the RHS of Eq. (7.19) as

$$Z_{bj}^{\mathrm{MP2}} = \frac{\partial}{\partial \kappa_{bj}} \langle \Phi_0 | [\hat{H}, \hat{T}_2] | \Phi_0 \rangle + \frac{\partial}{\partial \kappa_{bj}} \sum_{\mu_2} \bar{t}_{\mu_2}^{(0)} \langle \mu_2 | [\hat{F}, \hat{T}_2] | \Phi_0 \rangle \,. \tag{7.22}$$

Note that for occupied–virtual rotations the multipliers $\bar{\kappa}_{ai}^{(0)}$ of the Z-vector equation (7.21) cannot be computed directly due to the nondiagonal matrix $\mathbf{A}^{\kappa}$. $\mathbf{Z}^{\mathrm{MP2}}$ of Eq. (7.22) can be evaluated as

$$\begin{aligned} Z_{ai}^{\mathrm{MP2}} (\bar{\mathbf{t}}^{(0)}) = \frac{1}{2} \sum_{jbc} t_{ijcb} \langle bc || ja \rangle - \frac{1}{2} \sum_{jkb} t_{kjcb} \langle jk || bi \rangle \\ - \frac{1}{4} \sum_{pq} \left(D_{pq}^{\mathrm{F}} (\bar{\mathbf{t}}^{(0)}) + D_{qp}^{\mathrm{F}} (\bar{\mathbf{t}}^{(0)}) \right) A_{pqia}^{\kappa} \,. \end{aligned} \tag{7.23}$$

The final orbital-relaxed one-particle MP2 density matrix is then given as

$$D_{pq}^{\mathrm{MP2}} = D_{pq}^{\mathrm{F}} (\bar{\mathbf{t}}^{(0)}) + \frac{1}{2} (\delta_{pi} \delta_{qa} + \delta_{qi} \delta_{pa}) \bar{\kappa}_{ai}^{(0)} \,. \tag{7.24}$$

7.2.2.3 Expectation-Value Formalism for MP2 Properties

Dipole moments, as any one-particle operator, can be computed using the expectation value according to Eq. (3.77), which can also be written as

$$\langle \boldsymbol{\mu} \rangle = \langle \Psi_0 | \hat{\mu} | \Psi_0 \rangle = \sum_{pq} \underbrace{\langle \Psi_0 | \hat{a}_p^\dagger \hat{a}_q | \Psi_0 \rangle}_{=\rho_{pq}} \mu_{qp} = \sum_{pq} \rho_{pq} \, \mu_{qp} \,, \tag{7.25}$$

where $\boldsymbol{\rho}$ denotes the exact one-particle density matrix of the ground state. In case of MP2, the wave function $|\Psi_0\rangle$ is expanded according to Eq. (2.68) and all terms up to only second order of the general expectation value (7.25) are considered in $\boldsymbol{\rho}$,[95,96]

$$\langle \mu \rangle_{\mathrm{EV}}^{\mathrm{MP2}} = \langle \Phi_0 | \hat{\mu} | \Phi_0 \rangle + 2 \langle \Phi_0 | \hat{\mu} | \Psi_0^{(1)} \rangle + \langle \Psi_0^{(1)} | \hat{\mu} | \Psi_0^{(1)} \rangle + 2 \langle \Phi_0 | \hat{\mu} | \Psi_0^{(2)} \rangle \,, \tag{7.26}$$

yielding the following nonvanishing elements of the symmetric density matrix[52] for the first three terms:

$$\rho_{ij}^{(0)} = \delta_{ij} \tag{7.27a}$$

$$\rho_{ij}^{(2)} = -\frac{1}{2} \sum_{kab} t_{ikab} t_{jkab} \tag{7.27b}$$

$$\rho_{ab}^{(2)} = \frac{1}{2} \sum_{ijc} t_{ijac} t_{ijbc} \,. \tag{7.27c}$$

The contribution in Eq. (7.27a) originates from the first term on the RHS of Eq. (7.25), i.e. $\boldsymbol{\rho}^{(0)}$ corresponds to the Hartree–Fock density matrix $\mathbf{D}^{\mathrm{HF}}$, the second term vanishes for a canonical HF reference, meaning the first-order density matrix correction is zero $\rho_{pq}^{(1)} = 0$, and the terms in Eqs. (7.27b) and (7.27c) originate from the third term. The last term of Eq. (7.26) contains the second-order correction to the wave function,

$$\langle \Phi_0 | \hat{\mu} | \Psi_0^{(2)} \rangle = \sum_{ia} \rho_{ai}^{(2)} \, \mu_{ia} \,, \tag{7.28}$$

in which the second-order density is given as the second-order singles amplitudes (2.171a), which for a canonical reference are given as

$$\rho_{ai}^{(2)} = t_{ai}^{(2)} = \frac{1}{2(\varepsilon_i - \varepsilon_a)} \Big[\sum_{jbc} t_{ijbc} \langle ja || bc \rangle + \sum_{jkb} t_{jkab} \langle jk || ib \rangle \Big] \,, \tag{7.29}$$

where as before t_{ijab} are to be understood as first-order amplitudes $t_{ijab}^{(1)}$. These contributions to the one-electron density matrix represent that part of relaxation effects contained in the MP2 expectation value. Since the MP2 ground state corresponds to the reference ground state employed in the construction of the ISR representation for the ADC(2) scheme, *vide infra*, the computation of an MP2 ground-state expectation value is formally identical to the ISR formalism applied later within the ADC schemes.

7.2.2.4 Comparison of Lagrange and Expectation-Value Formalism for MP2

Comparing the expectation-value formalism with the derivative approach, first the occupied–occupied and virtual–virtual contributions are found to be identical for the expectation value, unrelaxed and relaxed properties at the MP2 level

$$\rho_{ij}^{(2)} = -\frac{1}{2}\sum_{kab} t_{ikab}t_{jkab} = D_{ij}^{\mathrm{F}}(\mathbf{t}) \tag{7.30a}$$

$$\rho_{ab}^{(2)} = \frac{1}{2}\sum_{ijc} t_{ijac}t_{ijbc} = D_{ab}^{\mathrm{F}}(\mathbf{t})\,. \tag{7.30b}$$

The only difference is located in the occupied–virtual block of the density matrix, which is zero in the unrelaxed Lagrangian and nonzero in the other two approaches. In order to analyze the connection between the latter two approaches, I need to turn back to the Z-vector equation. Neglecting the (non-diagonal) supermatrix $\mathbf{A}^{\kappa}$ in Eq. (7.21) and the contributions containing the Lagrange multipliers, yields a diagonal Z-vector equation of the form

$$-\bar{\kappa}_{ai}^{(0)}(\varepsilon_a - \varepsilon_i) = \frac{1}{2}\sum_{jbc} t_{ijcb}\langle bc||ja\rangle + \frac{1}{2}\sum_{jkb} t_{kjab}\langle jk||ib\rangle\,, \tag{7.31}$$

which can directly be inverted to yield

$$\bar{\kappa}_{ai}^{(0)} = \frac{1}{2(\varepsilon_i - \varepsilon_a)}\Big[\sum_{jbc} t_{ijcb}\langle bc||ja\rangle + \sum_{jkb} t_{kjab}\langle jk||ib\rangle\Big]\,. \tag{7.32}$$

Comparison with the identical Eq. (7.29) reveals the differences between the relaxed and expectation-value approach in the case of MP2 to originate from the neglected contribution of the nondiagonal part $\mathbf{A}^{\kappa}$ of the electronic Hessian in the Z-vector equation.

7.2.3 Coupled Cluster

In the case of coupled-cluster (CC) theory (Section 2.6), the ground state is usually parameterized by two different left- and right-hand wave functions, $|\Psi_0^{\mathrm{CC}}\rangle = e^{\hat{T}}|\Phi_0\rangle$ and $\langle\Psi_0^{\perp}| = \langle\Phi_0|(1+\hat{\Lambda})e^{-\hat{T}}$, respectively, where $\hat{T}$ is the cluster (excitation) operator and $\hat{\Lambda}$ is the de-excitation operator that ensures stationarity of the CC energy functional (2.151) w.r.t. to the cluster amplitudes, while the cluster amplitudes themselves ensure stationarity w.r.t. the $\hat{\Lambda}$ amplitudes,

$$E_0^{\mathrm{CC}} = \langle\Psi_0^{\perp}|\hat{H}|\Psi_0^{\mathrm{CC}}\rangle = \langle\Phi_0|(1+\hat{\Lambda})e^{-\hat{T}}\hat{H}e^{\hat{T}}|\Phi_0\rangle\,. \tag{7.33}$$

The expectation-value dipole moment is thus given as

$$\langle\boldsymbol{\mu}\rangle_{\mathrm{EV}}^{\mathrm{CC}} = \langle\Psi_0^{\perp}|\hat{\mu}|\Psi_0^{\mathrm{CC}}\rangle = \langle\Phi_0|(1+\hat{\Lambda})e^{-\hat{T}}\hat{\mu}e^{\hat{T}}|\Phi_0\rangle\,, \tag{7.34}$$

and the orbital-unrelaxed dipole moment can be evaluated to be identical to the expectation value,

$$\langle\boldsymbol{\mu}\rangle^{\mathrm{CC}}_{\mathrm{unrel}} = \frac{\partial E^{\mathrm{CC}}_0}{\partial\boldsymbol{\mathcal{F}}} = \left\langle \Psi^{\perp}_0 \middle| \frac{\partial\hat{\mathcal{H}}}{\partial\boldsymbol{\mathcal{F}}} \middle| \Psi^{\mathrm{CC}}_0 \right\rangle = \langle\Phi_0|(1+\hat{\Lambda})e^{-\hat{T}}\hat{\mu}e^{\hat{T}}|\Phi_0\rangle = \langle\boldsymbol{\mu}\rangle^{\mathrm{CC}}_{\mathrm{EV}}\,, \tag{7.35}$$

since E^{CC}_0 in Eq. (7.33) is stationary w.r.t. both $\hat{T}$ and $\hat{\Lambda}$. The orbital-relaxed CC dipole moment can be calculated by differentiating the relaxed Lagrangian $L^{\mathrm{CC}}_{\mathrm{rel}} = E^{\mathrm{CC}}_0 + \sum_{ia}\bar{\kappa}_{ai}f_{ia}$ after having solved $\partial L^{\mathrm{CC}}_{\mathrm{rel}}/\partial\kappa_{ai} = 0$ for $\bar{\boldsymbol{\kappa}}$.

7.2.4 Configuration Interaction

As discussed in Section 2.3.1 (page 18), in configuration interaction (CI) the electronic Hamiltonian $\hat{H}$ is represented in the orthonormal basis of excited determinants $|\Phi_J\rangle$, which leads to a Hermitian eigenvalue problem $\mathbf{H}\mathbf{C}_n = E^{\mathrm{CI}}_n\mathbf{C}_n$, where $H_{IJ} = \langle\Phi_I|\hat{H}|\Phi_J\rangle$ and $\mathbf{C}^{\dagger}_n\mathbf{C}_n = 1$. The diagonalization of $\mathbf{H}$ thus yields eigenvectors $\mathbf{C}_n$ and state energies $E^{\mathrm{CI}}_n = \mathbf{C}^{\dagger}_n\mathbf{H}\mathbf{C}_n$, and the wave function of electronic state n can be written as

$$|\Psi^{\mathrm{CI}}_n\rangle = \sum_J C_{n,J}|\Phi_J\rangle\,, \tag{7.36}$$

where n can refer to either the ground or some excited state. The dipole moment can be calculated as an expectation value by plugging Eq. (7.36) twice into Eq. (3.77),

$$\langle\boldsymbol{\mu}\rangle^{\mathrm{CI}}_{\mathrm{EV}} = \langle\Psi^{\mathrm{CI}}_n|\hat{\mu}|\Psi^{\mathrm{CI}}_n\rangle = \sum_{IJ} C^{*}_{n,I}\underbrace{\langle\Phi_I|\hat{\mu}|\Phi_J\rangle}_{=\tilde{B}^{(0)}_{IJ}}C_{n,J} = \mathbf{C}^{\dagger}_n\tilde{\mathbf{B}}^{(0)}\mathbf{C}_n\,, \tag{7.37}$$

where $\tilde{\mathbf{B}}^{(0)}$ is the representation of the dipole operator in the CI determinant basis. The *unrelaxed* dipole moment is obtained by using $L^{\mathrm{CI}}_{n,\mathrm{unrel}} = E^{\mathrm{CI}}_n$ and $\hat{\mathcal{H}} = \hat{H} + \hat{\mu}\boldsymbol{\mathcal{F}}$, and differentiating the expression to obtain

$$\begin{aligned}\langle\boldsymbol{\mu}\rangle^{\mathrm{CI}}_{\mathrm{unrel}} &= \frac{\mathrm{d}}{\mathrm{d}\boldsymbol{\mathcal{F}}}E^{\mathrm{CI}}_n[\boldsymbol{\kappa},\mathbf{C}_n] = \frac{\partial E^{\mathrm{CI}}_n}{\partial\boldsymbol{\mathcal{F}}} + \underbrace{\frac{\partial E^{\mathrm{CI}}_n}{\partial\mathbf{C}_n}}_{=0}\frac{\mathrm{d}\mathbf{C}_n}{\mathrm{d}\boldsymbol{\mathcal{F}}} + \underbrace{\frac{\partial E^{\mathrm{CI}}_n}{\partial\boldsymbol{\kappa}}\frac{\mathrm{d}\boldsymbol{\kappa}}{\mathrm{d}\boldsymbol{\mathcal{F}}}}_{\text{neglected}} \\ &= \frac{\partial}{\partial\boldsymbol{\mathcal{F}}}\langle\Psi^{\mathrm{CI}}_n|\hat{H} + \hat{\mu}\boldsymbol{\mathcal{F}}|\Psi^{\mathrm{CI}}_n\rangle = \langle\Psi^{\mathrm{CI}}_n|\hat{\mu}|\Psi^{\mathrm{CI}}_n\rangle = \langle\boldsymbol{\mu}\rangle^{\mathrm{CI}}_{\mathrm{EV}}\,,\end{aligned} \tag{7.38}$$

which means that the *unrelaxed* property is identical to the expectation value, since the CI energy E^{CI}_n is variational w.r.t. the eigenvectors $\mathbf{C}_n$, but not w.r.t. to the orbital coefficients $\boldsymbol{\kappa}$. The *relaxed* dipole moment is obtained from the Lagrangian

$$L^{\mathrm{CI}}_{n,\mathrm{rel}} = E^{\mathrm{CI}}_n + \sum_{ia}\bar{\kappa}_{ai}\,f_{ia}\,, \tag{7.39}$$

where the orbital rotation multipliers $\bar{\boldsymbol{\kappa}}$ need to be determined analogous to Section 7.2.2.2. Using again the perturbed Hamiltonian $\hat{\mathcal{H}}$ and differentiating, the relaxed CI dipole

moment is given

$$\langle \boldsymbol{\mu} \rangle_{\mathrm{rel}}^{\mathrm{CI}} = \frac{\partial}{\partial \boldsymbol{\mathcal{F}}} L_{n,\mathrm{rel}}^{\mathrm{CI}} = \langle \boldsymbol{\mu} \rangle_{\mathrm{unrel}}^{\mathrm{CI}} + \sum_{ia} \bar{\kappa}_{ai}\, \mu_{ia} \,. \tag{7.40}$$

7.2.5 Algebraic-Diagrammatic Construction Scheme for the Polarization Propagator

The analysis in the previous sections has shown that orbital-relaxation effects are not included in the CI or CC expectation value in their standard parameterization, and neither are they in MP2 using the first-order wave function but arise only in the second-order contributions. In these second-order contributions of MP2 the orbital-relaxation effects are given due to singles contributions in the second-order wave function. As will be discussed in the present section, a similar argument holds also for excited states. For example, in the CI picture doubly-excited configurations are needed to account for orbital-relaxation effects in p-h states, triply-excited configurations for 2p-2h states and so on. However, in the ADC scheme, which combines a CI approach with perturbation theory, this is not as straightforward since relaxation effects could be included via the perturbation expansion of the expectation value similar to MP2. In the following, this shall be investigated for the ADC scheme of first and second order in more detail.

The total energy of state n in ADC can be written as $E_n = E_0 + \omega_n$, where E_0 is the MP ground-state energy and the excitation energy is given as $\omega_n = \mathbf{X}_n^\dagger \mathbf{M} \mathbf{X}_n$. However, in the following it is assumed that only one excitation vector is treated and thus the index "n" is dropped. The property calculation within the intermediate state representation approach was discussed briefly in Section 2.5.3 (page 32). The ISR matrix $\mathbf{B}$ is available up to second order, where the elements are equivalent to the ones presented in Section 3.7.3 (page 87), i.e. the strict version of the UCC property matrix $\tilde{\tilde{\mathbf{B}}}$ through second order is identical to the ADC variant $\mathbf{B}$. The excitation vectors obtained with the ADC(3) scheme, which is currently the highest available order of the ADC scheme for the polarization propagator, can be combined with the second-order $\mathbf{B}$ to obtain excited-state one-particle properties in the expectation-value approach at the theoretical level referred to as ADC(3/2). Analytical gradients are available up to third order,[282] such that fully relaxed properties are available through ADC(3).

7.2.5.1 ADC(1) Excited-State Properties

The elements of the ADC(1) matrix are identical to the configuration interaction singles (CIS) ones and are given as the sum of Eqs. (2.115a) and (2.117),[25] i.e. $M_{ia,jb}^{\mathrm{ADC(1)}} = M_{ia,jb}^{(0)} + M_{ia,jb}^{(1)} = \delta_{ab}\delta_{ij}(\varepsilon_a - \varepsilon_i) - \langle aj||bi\rangle$. The explicit equations for the excited-state

contributions $\mathbf{B}$ up to first order are[30]

$$B^{(0)}_{ia,jb} = \delta_{ij}\mu_{ab} - \delta_{ab}\mu_{ji} \tag{7.41a}$$

$$B^{(1)}_{ia,jb} = 0\,, \tag{7.41b}$$

which can be inserted into Eq. (2.121) to obtain the dipole moment as

$$\langle \boldsymbol{\mu} \rangle^{\mathrm{ADC(1)}}_{n,\mathrm{ISR}} = \mu_0^{\mathrm{HF}} + \sum_{pq} \gamma_{pq}\,\mu_{qp}\,, \tag{7.42}$$

where the only nonzero contributions to the density $\boldsymbol{\gamma}$ are given as

$$\gamma_{ij} = -\sum_a X^a_i X^a_j \tag{7.43a}$$

$$\gamma_{ab} = \sum_i X^a_i X^b_i\,. \tag{7.43b}$$

At this point it should be mentioned that the ADC(1) and CIS schemes provide not only identical excitation energies, but also the identical excited-state properties. However, this analysis does not hold for transition moments from the ground to the excited state, which differ from ADC(1) and CIS. At ADC(1) transition properties are correct up to first order, while they are only given at zeroth order in CIS, where the respective terms are equivalent to those in Section 3.7.2 (page 85). Hence, since ADC excitation energies are stationary w.r.t. the ADC eigenvectors, analogous to CI, and in first order no parameters from the MP perturbation treatment enter the ADC matrix, the unrelaxed Lagrangian requires no multipliers and the dipole moments are thus identical to the ISR values

$$\langle \boldsymbol{\mu} \rangle^{\mathrm{ADC(1)}}_{n,\mathrm{unrel}} = \frac{\partial}{\partial \boldsymbol{\mathcal{F}}} E^{\mathrm{ADC(1)}}_n[\hat{\mathcal{H}}] = \langle \boldsymbol{\mu} \rangle^{\mathrm{ADC(1)}}_{n,\mathrm{ISR}}\,, \tag{7.44}$$

cf. Eq. (7.42). Similar to MP2 or CI/CC, in case of relaxed properties the ADC(1) energy expression is augmented with the constraint of the Brillouin condition to be fulfilled at all times. Relaxed properties are thus obtained from the Lagrangian

$$L^{\mathrm{ADC(1)}}_n = E^{\mathrm{ADC(1)}}_n + \sum_{ia} \bar{\kappa}^{(n)}_{ai} f_{ia}\,, \tag{7.45}$$

which gives rise to a new term to be added to the unrelaxed dipole moment. The Lagrange multipliers $\bar{\boldsymbol{\kappa}}^{(n)}$, where the superscript "(n)" refers to the excited state n, have to be computed first and are chosen such that they ensure stationarity of the Lagrange function w.r.t. orbital rotations.

From the analysis so far, I have shown that while for MP2 orbital-relaxation effects are included partially in an expectation value of the electronic ground state, for ADC(1) and CI approaches in general no orbital-relaxation effects are included in an expectation value of p-h states.

7.2.5.2 Orbital-Unrelaxed Lagrange Formalism for ADC(2) Excited-State Properties

For excited states, an unrelaxed excited-state Lagrange function is used which includes the MP2 ground-state energy, the equations defining the doubles amplitudes as well as the ADC(2) excitation energy and which is given as

$$L_{n,\mathrm{unrel}}^{\mathrm{ADC(2)}} = E_0^{\mathrm{MP2}} + \sum_{\mu_2} \bar{t}_{\mu_2} \langle \mu_2 | \hat{H} + [\hat{F}, \hat{T}_2] | \Phi_0 \rangle + \omega_n \,, \tag{7.46}$$

where the excitation energy ω_n was defined above. It should be noted that the Lagrange multipliers $\bar{\mathbf{t}}$ are solved in the presence of an excited-state contribution, but the explicit dependence is dropped in Eq. (7.46) and the following for better readability similar to the excitation vectors. Excited-state contributions to the one-particle density without Lagrange multipliers can be collected in the matrix $\mathbf{D}^{\mathrm{A}}$ with

$$D_{ij}^{\mathrm{A}} = \gamma_{ij}^{(0)} \tag{7.47a}$$

$$D_{ia}^{\mathrm{A}} = -\frac{1}{2}\gamma_{ia}^{(0)} - \sum_b \big(\sum_{jkc} X_{kj}^{bc} t_{kjac} \big) X_i^b - \sum_j \big(\sum_{kbc} X_{jk}^{cb} t_{ikcb} \big) X_j^a \tag{7.47b}$$

$$D_{ab}^{\mathrm{A}} = \gamma_{ab}^{(0)} \,. \tag{7.47c}$$

where the contributions to the density matrix $\boldsymbol{\gamma}^{(0)}$ are defined as

$$\gamma_{ij}^{(0)} = \gamma_{ij} - \sum_{kab} X_{jk}^{ab} X_{ik}^{ab} \tag{7.48a}$$

$$\gamma_{ia}^{(0)} = -2 \sum_{jb} X_j^b X_{ij}^{ab} \tag{7.48b}$$

$$\gamma_{ab}^{(0)} = \gamma_{ab} + \sum_{ijc} X_{ij}^{ac} X_{ij}^{bc} \,, \tag{7.48c}$$

see also Eqs. (7.43). The unrelaxed dipole moment can therefore be computed as

$$\langle \boldsymbol{\mu} \rangle_{n,\mathrm{unrel}}^{\mathrm{ADC(2)}} = \frac{\partial}{\partial \boldsymbol{\mathcal{F}}} L_{n,\mathrm{unrel}}^{\mathrm{ADC(2)}} [\hat{\mathcal{H}}] = \sum_{pq} D_{pq}^{\mathrm{ADC(2)}} \, \mu_{qp} \tag{7.49}$$

$$D_{pq}^{\mathrm{ADC(2)}} = D_{pq}^{\mathrm{HF}} + D_{pq}^{\mathrm{F}}(\bar{\mathbf{t}}) + D_{pq}^{\mathrm{A}} \,, \tag{7.50}$$

where it should be noted that the only explicit excited-state contribution is given by $\mathbf{D}^{\mathrm{A}}$, while implicitly also contributions are included in $\mathbf{D}^{\mathrm{F}}(\bar{\mathbf{t}})$ due to different Lagrange multipliers. In order to compute these excited-state contributions to $\mathbf{D}^{\mathrm{F}}$, stationarity of the Lagrangian is enforced w.r.t. the ground-state amplitudes[267,283]

$$\frac{\partial}{\partial t_{\nu_2}} L_{n,\mathrm{unrel}}^{\mathrm{ADC(2)}} = \eta_{\nu_2}^{(0)} + \sum_{\mu_2} \bar{t}_{\mu_2} \langle \mu_2 | [\hat{F}, \hat{\tau}_{\nu_2}] | \Phi_0 \rangle + \frac{\partial}{\partial t_{\nu_2}} \omega_n \overset{!}{=} 0 \,, \tag{7.51}$$

where $\eta^{(0)}_{\nu_2} = \partial E_0^{\mathrm{MP2}}/\partial t_{\nu_2}$ was used. The last contribution, i.e. the derivative of the excitation energy with respect to the amplitudes, is given as[282]

$$\begin{aligned}\frac{\partial}{\partial t_{ijab}}\omega_n = &- \hat{\mathcal{P}}(ab)\sum_c \langle ij||bc\rangle\gamma_{ac} - \hat{\mathcal{P}}(ij)\sum_k \langle jk||ab\rangle\gamma_{ik} \\ &- \hat{\mathcal{P}}(ij)\hat{\mathcal{P}}(ab)X_i^a\sum_{ck}\langle jk||bc\rangle X_k^c\,,\end{aligned} \tag{7.52}$$

where the antisymmetrization operator $\hat{\mathcal{P}}(pq) = 1 - \hat{P}_{pq}$ is used as before. Rearranging Eq. (7.51) with respect to the Lagrange multipliers yields the explicit contribution in case of ADC(2) including the excited-state contributions

$$\bar{t}_{ijab} = -\frac{\eta^{(0)}_{ijab} + \frac{\partial\omega_n}{\partial t_{ijab}}}{\varepsilon_a + \varepsilon_b - \varepsilon_i - \varepsilon_j} = t_{ijab} + \bar{n}_{ijab}\,. \tag{7.53}$$

For ADC(2), the excited-state contribution $\bar{\mathbf{n}}$ in Eq. (7.53) is explicitly given as

$$\begin{aligned}\bar{n}_{ijab} = &- \hat{\mathcal{P}}(ab)\sum_c \frac{\langle ij||bc\rangle}{\varepsilon_a + \varepsilon_b - \varepsilon_i - \varepsilon_j}\gamma_{ac} \\ &- \hat{\mathcal{P}}(ij)\sum_k \frac{\langle jk||ab\rangle}{\varepsilon_a + \varepsilon_b - \varepsilon_i - \varepsilon_j}\gamma_{ik} \\ &- \hat{\mathcal{P}}(ij)\hat{\mathcal{P}}(ab)X_i^a\sum_{ck}\frac{\langle jk||bc\rangle}{\varepsilon_a + \varepsilon_b - \varepsilon_i - \varepsilon_j}X_k^c\,.\end{aligned} \tag{7.54}$$

Combining the density $\mathbf{D}^{\mathrm{A}}$ and the amplitude-relaxed contributions containing $\bar{\mathbf{n}}$ thus yield the explicit excited-state contributions to the ADC(2) density matrix:

$$D_{ij}^{\Delta\mathrm{ADC(2)}} = \gamma_{ij}^{(0)} + D_{ij}^{\mathrm{F}}(\bar{\mathbf{n}}) \tag{7.55a}$$

$$D_{ab}^{\Delta\mathrm{ADC(2)}} = \gamma_{ab}^{(0)} + D_{ab}^{\mathrm{F}}(\bar{\mathbf{n}})\,. \tag{7.55b}$$

7.2.5.3 ISR Formalism for ADC(2) Excited-State Properties

For the second-order intermediate state representation, the configuration space has to be expanded to doubly-excited configurations and hence the ADC matrix consists of the p-h/p-h block, the diagonal 2p-2h/2p-2h block, and the p-h/2p-2h and 2p-2h/p-h coupling blocks. Plugging the resulting equations,[30] which are again equivalent to those in Section 3.7.3, into Eq. (2.121) yields several terms, sorted by order of perturbation theory,

$$\langle\boldsymbol{\mu}\rangle_{n,\mathrm{ISR}}^{\mathrm{ADC(2)}} = \langle\boldsymbol{\mu}\rangle_{\mathrm{EV}}^{\mathrm{MP2}} + \langle\boldsymbol{\mu}\rangle_{n,\mathrm{ISR}}^{(0)} + \langle\boldsymbol{\mu}\rangle_{n,\mathrm{ISR}}^{(1)} + \langle\boldsymbol{\mu}\rangle_{n,\mathrm{ISR}}^{(2)}\,, \tag{7.56}$$

where each excited-state term represents a contraction of a density $\boldsymbol{\gamma}$ with the one-particle elements μ_{qp}, analogously to the ground state of Eq. (7.25). While the first-order contributions $\boldsymbol{\gamma}^{(1)}$ vanish for the excited state (similar to the ground state), a set of

effective (ISR) densities can be found in zeroth and second order. Explicit expressions for the ISR densities have been published in Ref. 52. The zeroth-order density $\boldsymbol{\gamma}^{(0)}$ is closely related to the unrelaxed Lagrange density $\mathbf{D}^{\mathrm{A}}$ of Eq. (7.47). Together with the second-order density $\boldsymbol{\gamma}^{(2)}$, the excited-state dipole moment is thus given up to second order as

$$\langle \boldsymbol{\mu} \rangle_{n,\mathrm{ISR}}^{\Delta\mathrm{ADC(2)}} = \sum_{pq} \gamma_{pq}^{(0)}\, \mu_{qp} + \sum_{pq} \gamma_{pq}^{(2)}\, \mu_{qp}\,. \tag{7.57}$$

7.2.5.4 Comparison of the ADC(2) Lagrange and ISR Formalism

The comparison of Lagrange and ISR can be split into a discussion of the occupied–occupied, virtual–virtual and occupied–virtual blocks. Concerning the diagonal blocks, only the virtual–virtual part is discussed explicitly but an analogous comparison is also obtained for the occupied–occupied part.

In the case of MP2, the virtual–virtual and also the occupied–occupied blocks are identical for the derivative and the ISR approach. For ADC(2) only the zeroth order contributions to the expectation value $\gamma_{ab}^{(0)}$ and $\gamma_{ij}^{(0)}$ are identical to the unrelaxed density, see Eq. (7.47). However, also the second-order contributions to the ISR densities are very similar to the unrelaxed densities. This can be seen after some rewriting of the ISR expressions found in the appendix of Ref. 52. The result shows that for each term in the ISR densities a corresponding one can be found in the unrelaxed densities. An example is given as

$$D_{ab}^{\mathrm{ADC(2)}} \leftarrow -\frac{1}{4}\left(1+\hat{P}_{ab}\right) \sum_{jkcd} \frac{\langle jk||cd\rangle}{\varepsilon_c + \varepsilon_a - \varepsilon_j - \varepsilon_k} \gamma_{ad} t_{jk}^{bc} \tag{7.58}$$

$$\gamma_{ab}^{(2)} \leftarrow -\frac{1}{4}\left(1+\hat{P}_{ab}\right) \sum_{jkcd} \frac{\langle jk||cd\rangle}{\varepsilon_c + \varepsilon_d - \varepsilon_j - \varepsilon_k} \gamma_{ad} t_{jk}^{bc}\,, \tag{7.59}$$

where the arrow again indicates that it is only one of several contributing terms of the quantity on the left. The only difference between the terms in the ISR part and the unrelaxed density is represented by the indices of the orbital energy denominator. In the ISR case the indices refer to internal summation indices of the two-electron integral only, while in the other case one index refers to the external index a of the unrelaxed density $D_{ab}^{\mathrm{ADC(2)}}$. The analogous comparison can be done for the remaining contributions to the virtual–virtual block of the ISR density as well as the occupied–occupied part. In all cases the only difference is found in one index of the orbital energy denominator.

Now I turn the discussion to the occupied–virtual block, for which more pronounced differences can be found. In case of ADC(2), the differences are even further increased as

compared to MP2. In the ISR framework, the occupied–virtual block is given as[52]

$$\begin{aligned}\gamma_{ia}^{(2)} = &-\sum_{bj} t_{ij}^{ab}\gamma_{jb}^{(0)} - \sum_{klcd} t_{klad} X_{kl}^{cd} X_i^c - \sum_{jkcd} X_j^a X_{jk}^{cd} t_{ikcd} \\ &- \sum_b \rho_{bi}^{(2)}\gamma_{ab} - \sum_j \gamma_{ij}\rho_{aj}^{(2)}\end{aligned} \tag{7.60}$$

where $\rho_{ai}^{(2)}$ is the second-order correction to the occupied–virtual block of the ground-state density matrix, cf. Eq. (7.29).

The relaxed excited-state Lagrange function used is given, similarly to the relaxed MP2 and ADC(1) Lagrange functions, as the sum of the unrelaxed Lagrangian and the Brillouin condition:

$$L_{n,\mathrm{rel}}^{\mathrm{ADC(2)}} = L_{n,\mathrm{unrel}}^{\mathrm{ADC(2)}} + \sum_{ia} \bar{\kappa}_{ai}^{(n)} f_{ia}\,, \tag{7.61}$$

which again gives a contribution to the occupied–virtual block of the density matrix. In order to ensure stationarity of the Lagrangian w.r.t. orbital rotations, Eq. (7.61) is differentiated w.r.t. the orbital rotations and set to zero

$$\frac{\partial}{\partial\kappa_{bj}} L_{n,\mathrm{rel}}^{\mathrm{ADC(2)}} = \frac{\partial}{\partial\kappa_{bj}} L_{n,\mathrm{unrel}}^{\mathrm{ADC(2)}} + \sum_{ia} \bar{\kappa}_{ai}^{(n)} \frac{\partial}{\partial\kappa_{bj}} f_{ia} \stackrel{!}{=} 0\,. \tag{7.62}$$

Rearranging Eq. (7.62) yields the Z-vector equation, from which the orbital rotation multipliers $\bar{\boldsymbol{\kappa}}^{(n)}$ are obtained. Neglecting the nondiagonal supermatrix $\mathbf{A}^{\kappa}$ on the left-hand side the multipliers can directly be computed,

$$\bar{\kappa}_{ai}^{(n)} = -\frac{1}{\varepsilon_a - \varepsilon_i}\Big(\frac{\partial}{\partial\kappa_{bj}} L_{n,\mathrm{unrel}}^{\mathrm{ADC(2)}}\Big)\,. \tag{7.63}$$

Similarly to the ground-state MP2 method, the right-hand side leads to two contributions originating from the (nonseparable) two-electron density matrix of ADC(2). The relevant block of the (nonseparable) two-particle density matrix has the contributions given as[284]

$$d_{ijab}^{\mathrm{A}} \leftarrow (1 + \hat{P}_{ab}\hat{P}_{ij})\Big(\sum_k \gamma_{jk}\, t_{ikab} - \sum_c \gamma_{bc}\, t_{ijac}\Big)\,, \tag{7.64}$$

which yields two terms which include the ground-state density $\rho_{ai}^{(2)}$, corresponding in the derivative approach to terms which are contained also in the ISR

$$\begin{aligned}\bar{\kappa}_{ai}^{(n)} &\leftarrow -\frac{1}{\varepsilon_a - \varepsilon_i}\Big(\sum_{jkb} d_{jkab}^{\mathrm{A}}\langle ij||kb\rangle + \sum_{jbc} d_{ijbc}^{\mathrm{A}}\langle aj||bc\rangle\Big) \\ &= -\sum_b \gamma_{ab}\,\rho_{bi}^{(2)} - \sum_j \gamma_{ij}\,\rho_{aj}^{(2)}\,.\end{aligned} \tag{7.65}$$

The comparison so far leads to a number of conclusions. First, while for the ground-state MP2 method a clear match of the individual terms in the ISR and Lagrange

formalism can be achieved, such a one-to-one mapping is not straightforward to realize for ADC(2) excited-state properties. Second, the occupied–occupied and virtual–virtual blocks of the unrelaxed and ISR density matrices are very similar. Third, major deviations can only be found in the occupied–virtual block of the orbital-relaxed and the ISR density matrix. However, the terms occurring in the occupied–virtual block of the ISR matrix can be found in the Z-vector equation of the orbital-relaxed derivative approach, which leads to the conclusion that the ISR at ADC(2) level captures a small fraction of the orbital relaxation, but the missing terms will still lead to a significant deviation of ISR and relaxed excited-state properties.

Going to higher-order ADC(3), the 2p-2h/2p-2h block is expanded to first order and is no longer diagonal. Thereby, the doubly excited configurations are now fully coupled and are able to describe first-order orbital relaxation effects of the primary p-h states via the diagonalization of the ADC(3) matrix, analogous to the case of CI methods. As a result, more orbital relaxation effects of the p-h states will be captured via the ADC(3) vectors, and consequently, the expectation value computed via the ISR formalism will get closer to the relaxed value obtained from the Lagrangian formalism. Also, relaxed and unrelaxed properties of p-h states will lie closer together at ADC(3) level than at ADC(2) level, at which orbital relaxation effects are not yet sufficiently contained in the ADC vectors. For 2p-2h states, however, this conclusion does not hold, as will be shown in Section 7.4.2.3.

7.3 Computational Details

Geometries of the test molecules were either taken from literature (where stated) or optimized at the MP2/cc-pVTZ level of theory with the Q-Chem 5.0 program package.[53] Calculations with different coupled-cluster (CC) and equation-of-motion (EOM) CC models were carried out with the Cfour program.[285] LR-CC calculations and Lagrangian-based RI-MP2 and RI-ADC(2) calculations, in particular using the modified Z-vector equations, were carried out by Dr. Sebastian Höfener with the Koala program.[286] ISR (expectation-value based) ADC calculations were carried out with the Q-Chem program package, analytic gradient calculations of ADC with a locally modified version thereof. Calculations using the resolution-of-the-identity (RI) approximation were done throughout with the corresponding auxiliary basis set and the 1s core orbitals were kept frozen, in all other calculations all electrons and orbitals were correlated.

Different correlation-consistent basis sets by Dunning and co-workers[171,287] were used throughout, although no attempt was made in order to optimize the one-particle basis set for the calculation of molecular properties. Rather, the effect of increasing ζ-quality on the difference between relaxed and unrelaxed properties is investigated.

TABLE 7.1: FCI results for dipole moments $\mu = |\boldsymbol{\mu}|$ (in milli a.u.) in the first excited state of the H atom and the HHe^+ molecule calculated with increasing basis sets. For the H atom, an external electric field with a field strength of 1.0 a.u. was employed. An interatomic distance of 0.774 Å was used for the HHe^+ molecule.

	H atom ($2\,^2S$)			HHe^+ ($2\,^1\Sigma^+$)		
	FCI		ADC(1)	FCI		ADC(3/2)
Basis set	μ_{unrel}	μ_{rel}	μ_{ISR}	μ_{unrel}	μ_{rel}	μ_{ISR}
cc-pVDZ	0.529	0.529	0.529	402.027	402.027	602.990
cc-pVTZ	139.523	139.523	139.523	294.470	294.470	493.362
cc-pVQZ	383.240	383.240	383.241	264.044	264.043	462.973
cc-pV5Z	589.898	589.898	589.898	249.305	249.304	448.251
cc-pV6Z	1149.967	1149.967	1149.967	248.114	248.113	447.014

7.4 Numerical Studies

In this section the theoretical analysis is illustrated with numerical results. First, orbital-unrelaxed and orbital-relaxed approaches are compared, followed by an analysis of the ISR approach. In order to emphasize the influence of the excitation level of the excited state vectors, the chapter closes with a discussion of states with pronounced double-excitation character.

7.4.1 Orbital-Unrelaxed and Orbital-Relaxed Properties

7.4.1.1 Full Configuration Interaction

I start the numerical investigations with an analysis of excited-state dipole moments computed at the full configuration interaction (FCI) level of theory for two small model systems, the hydrogen atom and the HHe^+ molecule. In order to induce a dipole moment, a static external electric field of 1 a.u. (in z direction) was applied for the hydrogen atom. Due to practical issues, both systems were computed using an EOM-CCSD implementation which corresponds to FCI for one- and two-electron systems like these two. The results are compiled in Table 7.1, revealing that in both cases relaxed and unrelaxed FCI results are identical, independent of the basis used. In particular for the excited-state dipole moment of the hydrogen atom, the strong electric field has a significant impact upon the basis set requirements, leading to a dipole moment that is far from being converged to the complete basis set (CBS) limit even for large basis sets. Highly augmented basis sets would be needed for a proper description of the excited-state dipole moment with the external electric field. Table 7.1 thus illustrates nicely that at the FCI level orbital relaxation is already fully included in the wave-function expansion, independent of the quality of the one-particle basis set.

For one-electron systems such as the hydrogen atom, the ADC(1) method also corresponds to a full CI treatment, so that the ISR approach yields identical results compared to FCI. For two-electron systems like HHe^+, however, the ADC(3/2) method

TABLE 7.2: Results for the ground-state dipole moment $\mu = |\boldsymbol{\mu}|$ (in milli a.u.) of the HF molecule calculated at the CC2, CCSD, CC3, and CCSDT levels with increasing basis sets. The relaxed dipole moment is obtained as $\mu_{\text{rel}} = \mu_{\text{unrel}} + \Delta_{\text{rel}}$.

	CC2		CCSD		CC3		CCSDT	
Basis set	μ_{unrel}	Δ_{rel}	μ_{unrel}	Δ_{rel}	μ_{unrel}	Δ_{rel}	μ_{unrel}	Δ_{rel}
cc-pVDZ	715.31	+5.99	717.13	+3.17	715.76	+0.08	715.50	+0.28
cc-pVTZ	705.14	+7.01	714.55	+3.80	711.12	+0.13	711.32	+0.62
cc-pVQZ	702.84	+7.30	715.93	+3.97	711.99	+0.08	712.36	+0.77
cc-pV5Z	703.51	+7.43	717.38	+3.92	713.24	+0.09	713.70	+0.81
cc-pV6Z	700.99	+7.44	715.56	+3.99	711.24	+0.07	711.76	+0.85

is not equivalent to FCI and thus yields different results. The deviation of the FCI and ADC(3/2) results which amounts approximately 200 milli a.u. is rooted in missing terms in the second-order treatment of the ISR of the dipole operator. In addition, also the ground-state contribution to the dipole moment is described at the the MP2 level only in the ADC(3/2) method.

7.4.1.2 Ground-State Properties

In order to further investigate the convergence of relaxed and unrelaxed dipole moments in more detail, the hydrogen fluoride (HF) molecule in its ground state is computed using a hierarchy of coupled-cluster models with increasing basis sets. As shown in Section 7.2.3, for ground-state coupled cluster the unrelaxed value corresponds to the expectation value. The results, displayed in Table 7.2 and graphically represented with the example of the cc-pVTZ basis set in Figure 7.1, show that the difference between the relaxed and unrelaxed dipole moment Δ_{rel} becomes significantly smaller with increasing excitation level, i.e. from CC2 *via* CCSD to CC3, independent of the size of the one-particle basis set. In case of CCSDT the difference increases slightly compared to CC3, but it is nevertheless

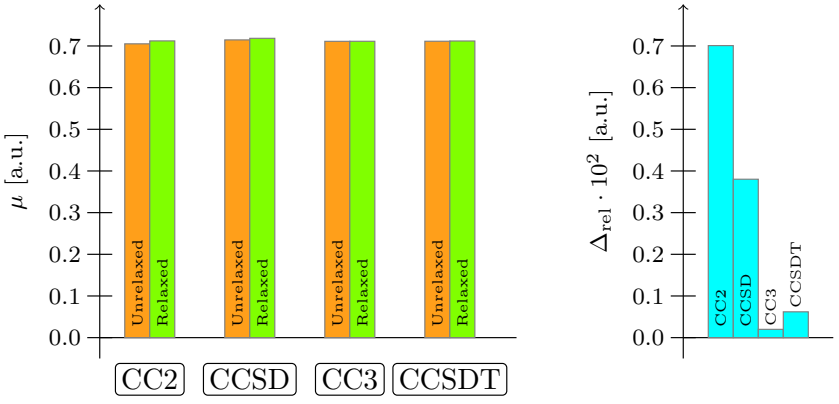

FIGURE 7.1: Relaxed and unrelaxed ground-state dipole moments $\mu = |\boldsymbol{\mu}|$ and their difference Δ_{rel} of hydrogen fluoride calculated with a hierarchy of coupled-cluster models and the cc-pVTZ basis set.

TABLE 7.3: Results for the first excited-state dipole moment $\mu = |\boldsymbol{\mu}|$ (in milli a.u.) of the HF molecule calculated at different levels of theory with increasing basis sets. The relaxed dipole moment is obtained as $\mu_{\text{rel}} = \mu_{\text{unrel}} + \Delta_{\text{rel}}$.

	LR-CCS		EOM-CC2		EOM-CCSD		EOM-CCSDT	
Basis set	μ_{unrel}	Δ_{rel}	μ_{unrel}	Δ_{rel}	μ_{unrel}	Δ_{rel}	μ_{unrel}	Δ_{rel}
cc-pVDZ	943.94	−92.42	946.55	−59.76	914.22	−27.54	895.02	−0.76
cc-pVTZ	991.42	−90.07	1021.67	−58.14	973.23	−31.13	954.33	−2.20
cc-pVQZ	1049.10	−88.02	1098.15	−56.09	1034.39	−31.75	1017.20	−2.81

smaller by one order of magnitude compared to CCSD. If the excitation level is further increased, the difference will decrease further until it vanishes in the limit of FCI.

Table 7.2 also shows results for increasing basis sets with fixed methods, for which the difference between relaxed and unrelaxed dipole moments in general increases slightly with increasing basis-set size. This observation is probably rooted in the higher flexibility with increasing basis-set size, resulting in overall larger orbital relaxation effects. The effect is therefore particularly pronounced for the CC2 model, which is the most approximate scheme in Table 7.2, so that relaxation has the largest effect. The results of which are depicted schematically in Figure 7.2. Similarly, the largest increase of relaxation contribution can be observed between the two smallest basis sets employed, i.e. cc-pVDZ and cc-pVTZ. While for the CC3 model the differences with increasing basis set are almost negligible, in case of the more accurate CCSDT model the effect is more pronounced. Stated differently, the slightly increasing differences with basis-set size are obtained because the relaxed dipole moment does not decrease as much as the unrelaxed dipole moment. However, these dipole moments show no clear convergence towards the CBS limit which is most likely rooted in an imbalance of the basis sets.

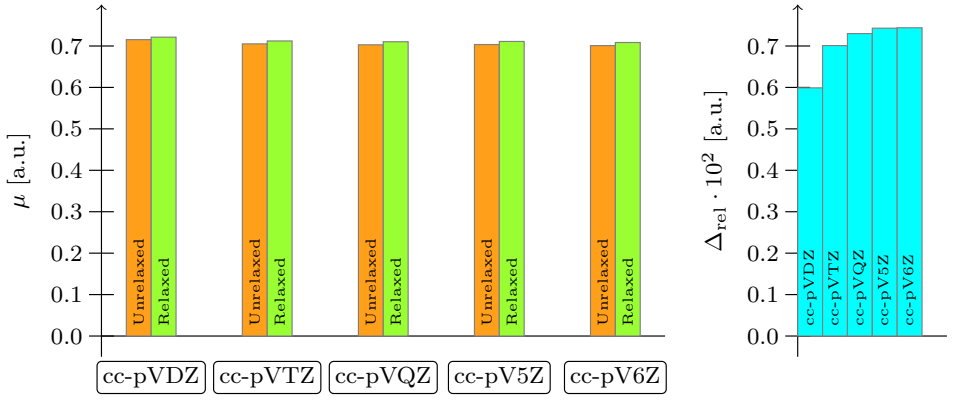

FIGURE 7.2: Relaxed and unrelaxed ground-state dipole moments $\mu = |\boldsymbol{\mu}|$ and their difference Δ_{rel} of hydrogen fluoride calculated with CC2 and increasing basis-set size.

7.4.1.3 Excited-State Properties

In analogy to the ground state, the dipole moment of the first excited state is analyzed for the HF molecule using different coupled-cluster models and basis sets. It should be noted that both the equation-of-motion (EOM) and linear-response (LR) coupled-cluster approaches yield not only identical excitation energies, but also the same first-order properties such as dipole moments.[288–290] The results are compiled in Table 7.3, showing that the relaxed and unrelaxed values exhibit a more pronounced difference for excited states as compared to the ground state.

Table 7.3 confirms that the difference between relaxed and unrelaxed dipole moments becomes significantly smaller with increasing excitation level in the coupled-cluster hierarchy from CCS to CCSDT. At the LR-CCS level, no orbital relaxation is included, leading to large differences of unrelaxed and relaxed dipole moments. Including doubly-excited determinants in zeroth order as in EOM-CC2 leads to the inclusion of some orbital-relaxation effects and thus decreases Δ_{rel} already significantly, but a difference of about 50 milli a.u. remains. Including doubly-excited determinants to first order in EOM-CCSD decreases the difference between relaxed and unrelaxed dipole moments further by about 50%. The EOM-CCSDT method reduces Δ_{rel} significantly to a few milli a.u., where missing orbital-relaxation effects are included by virtue of the the higher excited determinants.

TABLE 7.4: Results for dipole moments $\mu = |\boldsymbol{\mu}|$ and first excitation energies of different molecules calculated at the RI-MP2/cc-pVTZ and RI-ADC(2)/cc-pVTZ level of theory. All values in milli a.u. The frozen-core approximation was employed.

	RI-MP2				RI-ADC(2)			
Molecule	$E_0^{(2)}$ [a]	μ_{unrel}	μ_{rel}	μ_{EV}	ω_1 [b]	μ_{unrel}	μ_{rel}	μ_{ISR}
H_2O	−261.94	788.83	760.25	759.13	289.74	409.08	264.05	338.26
HF	−272.50	760.48	726.54	719.31	376.72	1133.06	947.95	1060.77
HCN	−346.20	1253.34	1169.49	1160.74	315.40	852.17	949.43	830.03
H_2CO	−395.92	1057.44	892.46	872.02	146.87	268.81	623.88	287.87
Acetone	−741.25	1266.10	1094.23	1073.93	161.80	251.34	690.18	292.26
Ethanol	−555.64	411.47	510.56	522.19	116.03	391.24	368.76	398.33
Serine	−1420.86	825.67	855.58	831.30	214.76	1507.41	1186.05	1400.63
Aniline	−1161.62	573.43	593.94	592.71	177.26	1243.03	1001.04	1182.52
DMABN	−2187.97	2998.53	2717.22	2858.91	136.71	1689.06	1974.53	1739.52

[a] MP2 correlation energy.
[b] First excitation energy.

7.4.2 The Expectation-Value Approach

7.4.2.1 MP2 and ADC(2)

In order to further study the behavior of the molecular properties with different computational schemes numerically, the ground-state and first excited-state dipole moments for a series of small to medium-sized molecules are compared in the unrelaxed, relaxed, and the expectation-value (ISR) approach using RI-MP2 and RI-ADC(2), respectively. The results for nine molecules of different size using the cc-pVTZ basis set are compiled in Table 7.4.

A general observation is that for the small molecules H_2O, HF, HCN, H_2CO, acetone and for dimethylamino benzonitrile (DMABN), including orbital relaxation decreases the absolute value of the ground-state dipole moment, while for the other molecules ethanol, aniline and serine orbital relaxation increases its value. Similarly, while for the small molecules the RI-MP2 expectation-value results are always somewhat smaller than the relaxed ones, this is not necessarily the case for the larger molecules. However, such effects might be related to the basis set which does not include diffuse functions and are thus not of importance here.

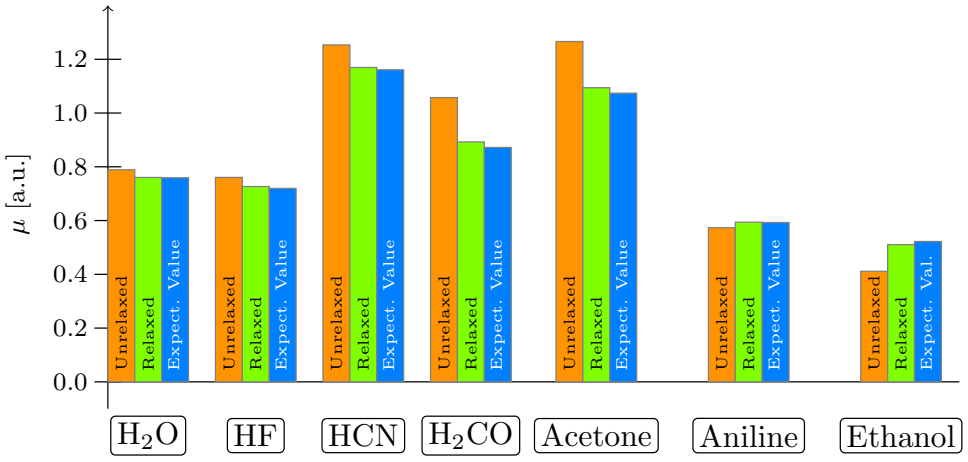

FIGURE 7.3: Relaxed, unrelaxed and expectation-value dipole moments $\mu = |\boldsymbol{\mu}|$ of different molecules calculated at the RI-MP2/cc-pVTZ level of theory.

In case of the RI-MP2 ground-state dipole moments, the expectation values show a small deviation to the relaxed dipole moments while exhibiting an increased deviation to the unrelaxed dipole moments, which can be seen for a few example molecules in Figure 7.3. An exception is serine, but in this case the difference between the relaxed and unrelaxed dipole moment is smaller than in most other molecules. However, the numerical results nicely support the theoretical analysis in Section 7.2.2, showing that in the average MP2 density a significant amount of orbital relaxation is included.

Concerning dipole moments in the first excited state computed at the RI-ADC(2)/cc-pVTZ level of theory, Table 7.4 reveals that the numerical ISR results are in fact close to

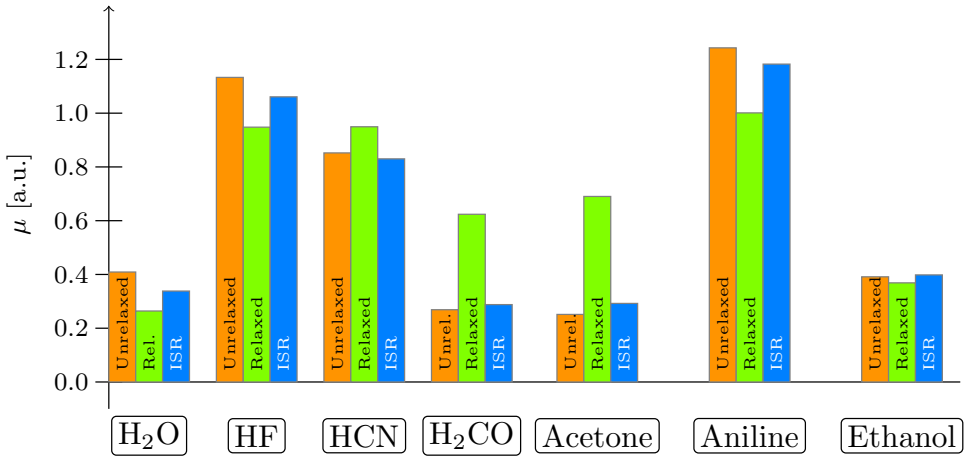

FIGURE 7.4: Relaxed and unrelaxed as well as expectation-value dipole moments $\mu = |\boldsymbol{\mu}|$ in the first excited state of different molecules calculated at the RI-ADC(2)/cc-pVTZ level of theory.

the unrelaxed dipole moments and increased deviations to the relaxed dipole moments are obtained, as shown graphically for a few examples in Figure 7.4. This effect is very pronounced for H_2CO and acetone for both unrelaxed and ISR dipole moments deviate from the relaxed dipole moments by a factor of 2. As numerically illustrated in Table 7.3, the zeroth-order doubles block is not able to account for orbital relaxation. Therefore, the second-order densities that occur additionally in the ISR approach cannot sufficiently recover these relaxation effects, resulting in the observation that the ISR dipole moments are numerically close to the unrelaxed dipole moments. Stated differently, the expectation value is the formally correct value within the ADC(2) model, but its deviation from the relaxed value reveals a generally incomplete description of orbital relaxation of that particular state at the ADC(2) level.

7.4.2.2 Assessment of ADC(n)

In order to study the behavior of ADC expectation values of the dipole operator when going to higher order in perturbation theory as well as to larger basis-sets of double- to quadruple-ζ quality, they are compared to the values obtained with the orbital-relaxed Lagrangian formalism. Therefore, the same molecules (except for DMABN) are studied as before in Table 7.4. The results for the first excited-state relaxed and ISR dipole moments calculated with ADC(1), ADC(2), ADC(2)-x and ADC(3) with the cc-pVDZ, cc-pVTZ and cc-pVQZ basis sets are compiled in Table 7.5. ADC(2)-x is an *ad hoc* extension of the standard ADC(2) scheme, where the first order terms in the 2p-2h/2p-2h block are included that would naturally arise only at the ADC(3) level. As discussed in Section 7.2.5.1, the ISR properties at ADC(1) level are equivalent to the unrelaxed values, and hence the differences between relaxed and ISR dipole moments in ADC(1) are rather large. Furthermore, the difference remains almost constant with increasing basis, although

TABLE 7.5: Results for ADC first excited-state dipole moments $\mu = |\boldsymbol{\mu}|$ (in milli a.u.) with increasing basis. The calculation of serine and aniline excited-state dipole moments employing the cc-pVQZ basis set was not feasible with ADC(2)-x and ADC(3).

	ADC(1)						ADC(2)					
Basis	cc-pVDZ		cc-pVTZ		cc-pVQZ		cc-pVDZ		cc-pVTZ		cc-pVQZ	
Molecule	μ_{rel}	μ_{ISR}	μ_{rel}	μ_{ISR}	μ_{rel}	μ_{ISR}	μ_{rel}	μ_{ISR}	μ_{rel}	μ_{ISR}	μ_{rel}	μ_{ISR}
H_2O	194.92	478.90	243.48	524.81	297.72	575.96	216.54	300.16	263.08	337.23	319.63	388.10
HF	835.38	1119.81	886.55	1181.50	945.58	1240.73	866.63	989.64	947.20	1059.98	1025.45	1130.85
HCN	953.65	866.97	932.43	835.14	909.29	809.22	956.43	854.69	950.80	831.90	931.69	806.61
H_2CO	553.10	237.75	555.53	254.51	549.35	253.53	613.16	280.76	626.17	290.31	627.89	289.40
Acetone	653.98	277.37	673.00	316.28	689.11	342.02	652.38	255.67	692.79	294.67	728.72	327.26
Ethanol	247.25	370.97	237.73	356.05	228.94	345.04	247.25	370.97	237.73	356.05	346.99	378.77
Serine	1325.29	1598.80	1300.40	1554.17	1298.93	1543.16	1213.00	1430.82	1188.13	1403.15		1397.47
Aniline	832.86	981.70	802.75	941.08	781.47	913.43	982.26	1178.22	919.61	1122.83	889.83	1095.44
	ADC(2)-x						ADC(3)[a]					
Basis	cc-pVDZ		cc-pVTZ		cc-pVQZ		cc-pVDZ		cc-pVTZ		cc-pVQZ	
Molecule	μ_{rel}	μ_{ISR}	μ_{rel}	μ_{ISR}	μ_{rel}	μ_{ISR}	μ_{rel}	μ_{ISR}	μ_{rel}	μ_{ISR}	μ_{rel}	μ_{ISR}
H_2O	230.19	235.88	268.93	281.92	318.35	334.79	223.59	262.53	251.94	308.87	293.61	357.85
HF	889.07	921.24	956.09	995.31	1021.52	1062.64	869.72	907.62	914.87	974.52	969.04	1035.27
HCN	984.30	946.56	977.37	932.50	958.07	910.39	928.76	959.79	919.81	944.27	898.54	921.84
H_2CO	539.53	403.25	549.20	410.96	551.86	412.89	503.07	475.72	519.31	490.44	522.02	496.25
Acetone	577.00	417.73	610.83	455.51	643.57	488.96	573.51	539.78	617.25	589.36	648.37	627.98
Ethanol	431.16	460.12	389.43	421.44	368.39	403.72	372.11	361.44	331.84	325.48	313.84	307.95
Serine	1258.51	1340.62	1240.20	1313.43			1239.68	1246.02	1218.95	1209.73		
Aniline	865.70	912.84	794.98	864.39			835.45	861.79	794.98	818.65		

[a] ISR values obtained with ADC(3/2).

in most cases it becomes somewhat smaller, similar to what was observed for the LR-CCS model in Table 7.3. Parts of the ADC(2) results have already been included in Table 7.4, but neither the RI nor frozen-core approximation was used here and additionally the influence of the basis-set size and the comparison to other ADC orders can be made in Table 7.5. Exemplarily, the results for hyrdogen fluoride, acetone and aniline with the cc-pVTZ basis set are depicted graphically in Figure 7.5. Again, the difference between ISR and relaxed dipole moment is not largely affected by the basis set, but in most cases it becomes slightly larger, indicating that larger orbital relaxation contributions from bigger basis set are generally not recovered in the intermediate state representation approach at the ADC(2) level. An unclear trend is observed when comparing the ISR/relaxed

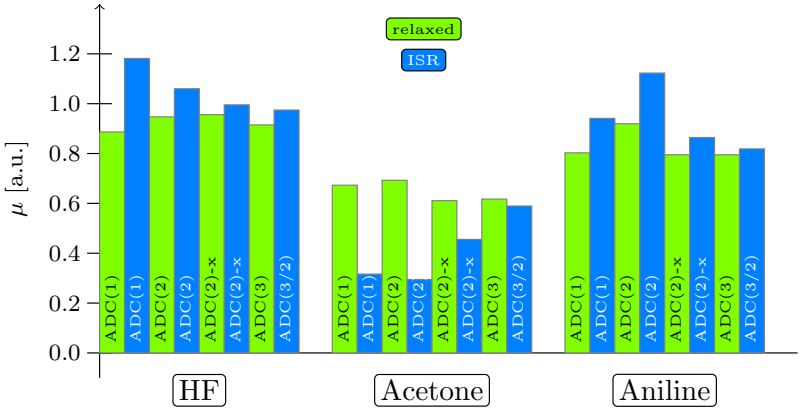

FIGURE 7.5: Relaxed and ISR dipole moments $\mu = |\boldsymbol{\mu}|$ in the first excited state of hydrogen fluoride, acetone, and aniline calculated with different ADC(n) schemes and the cc-pVTZ basis set.

differences between ADC(1) and ADC(2). While for half of the considered molecules (water, hydrogen fluoride, ethanol and serine) the ISR/relaxed difference becomes smaller at second-order ADC, for the other half (hydrogen cyanide, formaldehyde, acetone and aniline) the difference becomes somewhat larger. This is due to the fact that the absolute values for the relaxed dipole moments always increase, while the ISR dipole moments decrease when going from ADC(1) to ADC(2), respectively, but for the first set of molecules the relaxed values are smaller in magnitude than the ISR ones, while for the second set the ISR values are smaller than the relaxed ones.

The effect of the inclusion of the first-order terms in the 2p-2h/2p-2h block in ADC(2)-x compared to ADC(2) is more revealing. Here, the difference between ISR and relaxed dipole moments becomes significantly smaller in all cases (except ethanol), independent of the employed basis set. Hence, the description through first order in perturbation theory of doubly excited states in ADC already leads to a better description of orbital relaxation effects through the ADC(2)-x vectors, similar to what has been observed for EOM-CCSD in the previous section. This is also identical to configuration interaction schemes, in which the doubly excited configurations are known to be needed to capture orbital relaxation effects of primary p-h states. Except for the two small molecules H_2O and HF, the difference between relaxed and ISR dipole moments is further reduced when going to the ADC(3) level of theory. Thus, the expansion up to third order of the p-h/p-h block and in particular to second order of the p-h/2p-2h and 2p-2h/p-h coupling blocks recovers most of the remaining orbital relaxation effects.

However, one has to keep in mind that while for ADC(1) and ADC(2) the matrix and ISR equations are both consistent in first and second order of perturbation theory, respectively, the ADC(2)-x matrix is inconsistent since the 2p-2h/2p-2h block is expanded to first order in an *ad hoc* manner. In the calculation of the ADC(3/2) ISR expectation values, only the ADC(3) vectors are consistently third order, while the ISR used to represent the dipole operator is only of second order. The relaxed ADC(3) dipole moment is on the other hand consistent through third order as derivative of the third-order ADC energy. This somewhat limits the direct comparability of the ISR value at ADC(3/2) level and the relaxed ADC(3) value. Yet, it is seen that the additional ISR equations in ADC(2) have little influence compared to the unrelaxed values, and hence orbital relaxation has to be included already with the excitation vectors. Disregarding these limitations for the moment, one can clearly see that for the primary singly excited states considered here doubly-excited configurations are needed in order to describe their orbital relaxation. If doubles are included only at zeroth order as in ADC(2), only little orbital relaxation is recovered, but including them to first order as in ADC(2)-x or ADC(3) significantly improves upon this.

However, combining the ADC(3) eigenvectors with the property matrix through second order to obtain ADC(3/2) properties is not the only possible way to combine different orders of perturbation theory for $\mathbf{M}$ and $\mathbf{B}$. In order to to investigate the

TABLE 7.6: Results for dipole moments $\mu = |\boldsymbol{\mu}|$ (in milli a.u.) of different molecules calculated at the ADC(1/2), ADC(2/0), ADC(2/0)-x and ADC(3/0) level of theory employing the cc-pVTZ basis set.

	ADC(1)		ADC(1/2)	ADC(2)		ADC(2/0)
Molecule	μ_{rel}	μ_{ISR}	μ_{ISR}	μ_{rel}	μ_{ISR}	μ_{ISR}
H_2O	243.48	524.81	509.38	263.08	337.23	255.21
HF	886.55	1181.50	1158.07	947.20	1059.98	966.79
HCN	932.43	835.14	893.56	950.80	831.90	805.59
H_2CO	555.53	254.51	376.81	626.17	290.31	275.10
Acetone	672.10	316.28	446.88	692.79	294.67	298.04

	ADC(2)-x		ADC(2/0)-x	ADC(3)	ADC(3/2)	ADC(3/0)
Molecule	μ_{rel}	μ_{ISR}	μ_{ISR}	μ_{rel}	μ_{ISR}	μ_{ISR}
H_2O	268.93	281.92	183.69	251.94	308.87	235.21
HF	956.09	995.31	888.34	914.87	974.52	893.80
HCN	977.37	932.50	923.04	919.81	944.27	927.35
H_2CO	549.20	410.96	454.60	519.31	490.44	501.64
Acetone	610.84	455.51	515.14	617.25	589.36	604.05

importance of relaxation effects through the excitation vectors and the property matrix, the combinations of the first-order ADC matrix with the second-order ISR matrix in the singles space, denoted ADC(1/2), as well the second- and third-order eigenvectors with the zeroth-order ISR matrix in the singles and doubles space have been implemented, the latter are denoted by ADC(2/0), ADC(2/0)-x and ADC(3/0). A similar strategy has been employed for the properties of electron-detached states via the ADC scheme for the electron propagator.[254–256]

As can be seen in the results in Table 7.6, a clear trend is observed for the first-order scheme where the ISR value obtained with ADC(1/2) is still close to the one of ADC(1), but the second-order **B** matrix captures a small fraction of the orbital relaxation, such that it goes towards the relaxed ADC(1) result. This is nicely in line with the conclusions drawn in the previous sections. However, for the other schemes involving the zeroth-order ISR matrix, no clear trend can be observed.

7.4.2.3 States with Double-Excitation Character

In order to analyze the effect of the excitation level of the calculated excited state upon the description of its orbital relaxation effects, all-*trans* linear polyenes (butadiene, hexatriene, octatetraene) are investigated, which are known to have low-lying doubly excited states.[201] In the present work, the lowest totally-symmetric excited state $2\ ^1A_g$ (assuming C_{2h} point-group symmetry) and the third excited state $2\ ^1B_u$ are considered. Geometries were taken from the benchmark set introduced by Thiel and co-workers.[179] In order to induce a dipole moment, an external electric field in z direction coinciding with the C_2 axis of symmetry was applied with a of strength of 0.0001 a.u. Additionally, the $3\ ^1A'$

TABLE 7.7: Results for excited-state dipole moments $\mu = |\boldsymbol{\mu}|$ (in milli a.u.) of the linear polyenes butadiene, hexatriene, and octatetraene as well as pentadieniminium calculated with different orders of ADC and the cc-pVTZ basis set. For the linear polyenes an external electric field of 0.0001 a.u. was applied perpendicular to the molecular plane. The amount of doubly-excited configurations ($\%R_2$) in the ADC excitation vectors is given as well.

	ADC(1)		ADC(2)			ADC(2)-x			ADC(3)[a]		
Molecule (State)	μ_{rel}	μ_{ISR}	μ_{rel}	μ_{ISR}	$\%R_2$	μ_{rel}	μ_{ISR}	$\%R_2$	μ_{rel}	μ_{ISR}	$\%R_2$
Butadiene ($2\ ^1A_g$)	2.11	2.36	0.60	0.43	10.9	2.02	1.43	57.6	2.33	1.55	67.6
Butadiene ($2\ ^1B_u$)	1.92	2.08	0.87	0.69	6.8	0.41	0.44	22.7	0.39	0.27	37.7
Hexatriene ($2\ ^1A_g$)	9.34	10.78	3.56	3.11	12.3	27.84	24.46	65.3	29.95	26.00	76.0
Hexatriene ($2\ ^1B_u$)	4.29	4.80	9.49	9.61	11.1	22.03	18.99	52.0	21.80	18.08	60.2
Octatetraene ($2\ ^1A_g$)	7.36	6.84	5.95	5.27	13.1	5.39	5.88	68.6	4.80	5.85	79.3
Octatetraene ($2\ ^1B_u$)	5.65	5.64	4.20	4.02	12.8	4.48	4.93	61.0	4.28	5.23	72.1
Pentadieniminium ($3\ ^1A'$)	922.0	782.2	634.3	599.0	11.2	2229.1	1892.1	52.1	2472.2	1824.9	60.9

[a] ISR values obtained with ADC(3/2).

state of the protonated Schiff-base penta-2,4-dieniminium cation *cis*-$C_5H_6NH_2^+$, denoted "pentadieniminium" in the following, exhibiting C_s symmetry was considered.[291,292]

Results for these states with significant double-excitation character are compiled in Table 7.7. In the following, I focus on the differences of the relaxed and ISR dipole moments while the absolute values are of minor importance for our discussion. The trends observed in Table 7.7 are quite the opposite of the ones observed previously in Table 7.5. While no clear trend can be observed when going from ADC(1) to ADC(2), the difference between relaxed and ISR becomes bigger for most states when going from strict ADC(2) to the extended version ADC(2)-x, with the exception of the B_u state in butadiene and A_g in octatetraene. For the states considered here, however, the clearest trend is observed when going from second-order ADC, i.e. either ADC(2) or ADC(2)-x, to the third-order method ADC(3), where the difference of relaxed and ISR increases in all cases.

The pentadieniminium cation exhibits a static dipole moment and shall serve as an example to illustrate the trends. For this molecule, relaxation effects seem to play a huge role in the first-order treatment, since there is a difference of about 140 milli a.u. between the relaxed and ISR approach. In case of strict second-order ADC(2), a difference of 35 milli a.u. is observed which is smaller by approximately a factor of 5, but the amount of doubly-excited configurations in the state vector is only about 11%. The description of the doubly-excited state is therefore not accurately accounted for. Employing the extended ADC(2)-x method, the double-excitation character increases to about 52%, so that the first-order description of the doubles block is no longer sufficient to recover orbital relaxation, yielding a difference of about 337 milli a.u. between ISR and relaxed dipole moment. This effect becomes even more pronounced at the third-order ADC level. The doubly-excited configurations in the excitation vector amount for 61% in this case and the difference between relaxed and ISR dipole moments becomes as large as 647 milli a.u.

The results in Table 7.7 illustrate that for excited states with significant double-excitation character the first-order description of doubly-excited configurations is not sufficient to account for orbital relaxation effects, because additional single excitations are required on top of the leading doubly-excited configuration to describe their orbital relaxation. Hence, the explicit inclusion of triply-excited configurations is required to account for a proper description of orbital relaxation effects of predominantly doubly excited states. In case of ADC, however, no triply-excited configurations are present in the ADC(2) or ADC(3) matrix, which would arise only at the ADC(4) level. This is in contrast to third-order coupled-cluster schemes like EOM-CCSDT-3 or CC3,[232,257,258,293] where triple excitations are explicitly included. Furthermore, the ISR values are not strict third order, but rather calculated with the ADC(3/2) method, in which the ADC(3) excitation vectors are contracted with the second-order ISR equations. Thus it may be speculated that the missing terms in the occupied–virtual block of the ISR density matrix are relevant for these states, and that a full third-order ISR representation might slightly improve the results. However, this remains to be shown in future work.

7.5 Summary

In this chapter, the expectation-value or intermediate state representation (ISR) formalism is compared to the Lagrange formalism, which are both frequently used to compute molecular properties, by analysis of the explicit algebraic equations as well as by numerical results. The analysis reveals that in the Lagrange formalism higher-order terms enter *via* the orbital-rotation multipliers in case of all methods. In the ISR formalism, however, which amounts to the computation of an expectation value within a given ADC model, these higher-order orbital relaxation terms are included in some cases only, namely when they enter via the corresponding ADC vector, or in other words, when they are contained within the ADC model. For example, in case of ground-state MP2 a large faction is contained yielding expectation-value dipole moments close to orbital-relaxed dipole moments, while in case of ADC(1) no higher-order orbital relaxation contributions are included at all, resulting in a one-to-one mapping to unrelaxed properties in analogy to CIS. Formally this is correct, as in CI models orbital relaxation is not included, and relaxed CIS values thus go formally beyond the CIS model. Relaxed properties, however, may lie closer to the "exact" values computed at higher level or determined experimentally.[57]

Due to the inclusion of a few higher-order contributions, ADC(2) ISR expectation values are numerically close but slightly different from unrelaxed ADC(2) properties, while explicit inclusion of doubly-excited configurations in the **M** matrix of ADC(2)-x and ADC(3), similar to going from CIS to CISD, leads to a drastic improvement of orbital relaxation effects of singly excited states. Then, ISR expectation values tend to lie closer to the relaxed Lagrangian values. Eventually, in case of full configuration action (FCI) no

differences of relaxed and unrelaxed and ISR values are obtained, as full orbital relaxation is contained in the FCI vectors.

The present work allows for an identification of terms which are responsible for higher-order contributions. It might be worthwile to introduce further approximate ADC schemes, for example, at the ADC(2) level, in which the rigorous ISR expectation value is augmented with terms providing a significant fraction of higher-order contributions, possibly based on semi-empirical evaluation of numerical results. Furthermore, it was shown that most of the excited-state orbital relaxation is included *via* the excitation vector going from ADC(2) to ADC(2)-x and ADC(3), and that the extension of the ISR representation to higher orders had only little effect on the expectation values. Last but not least, the amount of orbital relaxation included in an approximate excited-state calculation does not only depend on the approximation level of the method but also on the excitation level of the investigated excited state. The majority of orbital relaxation effects of typical p-h states are captured when doubly-excited configurations are explicitly included, while for 2p-2h states triply excited configurations are explicitly needed to describe the same level of orbital relaxation.

Chapter 8

Investigating Fluorescence Quenching in Azaacenes Bearing Five-Membered Rings

In this chapter, the topic takes a drastic turn, from theoretical analyses to applied computational chemistry. It is included as an expample of my collaborations with experimental organic chemists.

8.1 Introduction

Azaacenes and their derivatives have been widely investigated due to their unique properties and employed in optoelectronic devices, e.g. as emitters in organic light-emitting diodes or in organic field-effect transistors.[294–306]

Recently, the synthesis of processible (dihydro-)pyracyclene- and acenaphthylene-substituted azaacenes was described, and the targets were characterized experimentally via cyclic voltammetry, X-ray crystallography as well as UV/Vis absorption and fluorescence spectroscopy.[307] Surprisingly, formal dehydrogenation of the annulated five-membered ring significantly altered the emission properties of the substances, turning them from strongly fluorescent to non-fluorescent at all. It was argued that this is because of a modulation of the aromaticity, as indicated by nucleus-independent chemical shift (NICS) calculations.[308,309]

Furthermore, preliminary computational investigations indicated the formal inclusion of the unsaturated C_2-bridge not only to lower the energy gap between the electronic

This chapter has already been published in

- M. Hodecker, M. Ganschow, M. Abu-Odeh, U. H. F. Bunz, A. Dreuw, "Optical Spectra and Fluorescence Quenching in Azaacenes Bearing Five-Membered Rings", *ChemPhotoChem*, **2019**, *3*, 755–762.

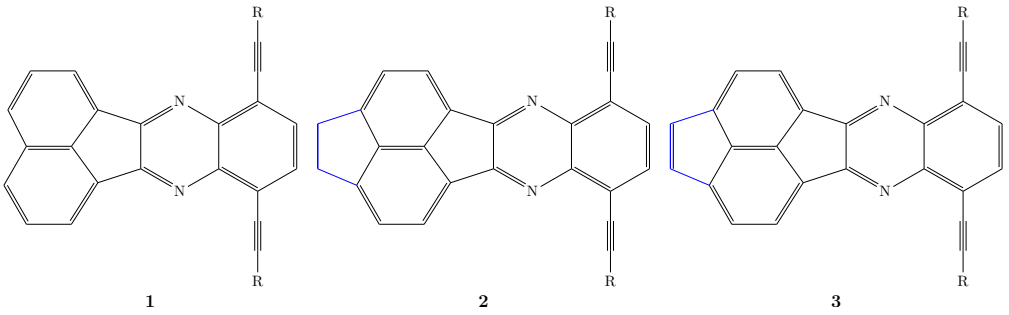

FIGURE 8.1: Structures of the molecules considered in this study. R = TIPS for the synthesized molecules (Ref. 307), whereas R = Me for the ones investigated computationally.

ground state S_0 and the first excited state S_1 at the equilibrium geometry of the latter. Moreover, also the oscillator strength decreases, turning the $S_0 \leftarrow S_1$ transition into a dark one. This usually leads to longer fluorescence lifetimes of excited states, which gives thus more time for fluorescence quenching, i.e. a radiationless decay into S_0.[307] The purpose of this work is to explain the optical spectra of the azaacenes shown in Figure 8.1, especially the different emission properties of the structurally similar azaacenes beyond a qualitative level using state-of-the-art electronic structure methods.

This chapter is organized as follows. First, the computational strategy employed in this work is described. Next, a suitable molecular model chemistry is derived by decreasing the size of the system and by benchmarking different density functionals and basis sets. Then the excited electronic states of the individual molecules are investigated, followed by the investigation of possible intersystem crossing. Finally, vibrationally-resolved electronic absorption and emission spectra are simulated and compared to experiment. The chapter closes with a short summary. I would like to mention that many of the initial computations were performed under my supervision by Mahmud Abu-Odeh and the experimental spectra were measured and provided by Michael Ganschow from the group of Prof. Dr. Uwe H. F. Bunz at the Institute of Organic Chemisty at Heidelberg University.

8.2 Computational Strategy

Due to the relatively large size of the synthesized molecules in Ref. 307, in particular because of the triisopropylsilyl (TIPS) groups, a compromise between accuracy and computational cost has to be made. Here, the group of molecules **1**–**3** is investigated, which are shown in Figure 8.1. First, a time-dependent density functional theory (TDDFT) methodology in conjunction with medium-sized basis sets is validated by benchmarking against a high-level *ab initio* method as well as against experimental results. For the sake of computational efficiency, the size of the moieties (R = TIPS in Figure 8.1) is successively reduced: R is replaced by trimethylsilyl (TMS) or methyl (Me), and the acetylene group

is replaced entirely by Me. As will be seen below, the first two simplifications can be done without significant loss of accuracy. The chosen functional and basis set will then be used to simulate optical absorption and emission spectra using the appropriate size-reduced molecules.

Calculations were carried out using the GAUSSIAN09 and Q-CHEM 5 program packages.[53,243] The standard density functionals BLYP,[310–312] B3LYP,[313] BHandHLYP (here called BHLYP in the following),[314] CAM-B3LYP,[315] ωB97X[316] and ωB97X-D[317] as implemented in GAUSSIAN were employed in combination with the standard basis sets by Ahlrichs and co-workers in their "def2" form up to quadruple-ζ quality (specifically, def2-SVP, def2-SVPP, def2-TZVP, def2-TZVPP, def2-QZVP and def2-QZVPP).[198–200] The polarizable continuum model (PCM)[318–320] in its integral-equation formalism (IEF-PCM)[321] was used to account for solvation effects of *n*-hexane. Excited-state calculations were carried out with linear-response TDDFT[6–8,322] using the functionals mentioned before as well as with the algebraic-diagrammatic construction (ADC) scheme for the polarization propagator of second order, ADC(2),[25,27,28,52] as benchmark method. Calculations of spin-orbit couplings (SOC)[323,324] in the TDDFT framework[325,326] were carried out with the Q-CHEM program package.

First, the gas-phase ground-state equilibrium geometry of molecule **1** with different moieties R was optimized at the B3LYP/def2-TZVP level of theory (Section 8.3.1). The chosen model molecule was then used for the basis set and functional benchmark of vertical excitation energies at the TDDFT and ADC(2) levels (Section 8.3.2). Having chosen a suitable functional and basis set, excited electronic states were calculated in solution employing the PCM, for which the molecules were re-optimized in the ground state S_0 as well as optimized in the first excited singlet state S_1 (Section 8.3.3).

Since the experimental optical spectra, in particular the fluorescence spectra, show a significant vibrational broadening, vibrationally-resolved electronic (vibronic) spectra were simulated with different vibronic models in a time-independent framework,[327–330] assuming the validity of the harmonic oscillator approximation (Section 8.3.5). The vertical Hessian (VH) and vertical gradient (VG) models employ the same reference geometry for both the initial and final state (the equilibrium geometry of the ground state for absorption spectra), while the equilibrium geometry of the final state is extrapolated. Within the adiabatic Hessian (AH) and adiabatic shift (AS) models the equilibrium geometry of both the initial and the final state is optimized. It is noteworthy that the computation times of the vibronic part are similar for all models, so the computational cost is determined by the electronic-structure level used to describe the potential energy surface (PES) of the excited state.[330] The most demanding approaches are thus in general the VH and AH models, which require the Hessians of excited states. Concerning electronic transition moments, the so-called Franck–Condon (FC) approximation was employed,[331–333] which assumes that they keep their equilibrium values during the transition.

In order to obtain spectral line shapes from the calculated stick spectra that are comparable to the experimental ones, all relevant electronic or vibronic transitions have been convoluted by means of Lorentzian functions with a full width at half maximum (FWHM) of 0.2 eV for vibronic absorption spectra and 0.06 eV for vibronic emission spectra.

8.3 Results and Discussion

8.3.1 Size-Reduced Model Molecules

First, smaller model molecules shall be found by replacing the original ones as shown in Figure 8.1 with R = TIPS. This is done exemplarily with molecule **1**, where the TIPS groups are replaced by TMS or Me ones. As further simplification, the ethynyl groups (R—C≡C) were completely replaced by methyl groups. The resulting molecules **1a**–**d** are shown in Figure C.1 in Appendix C (page 211) and were optimized at the B3LYP/def2-TZVP level of theory. Frequency calculations were carried out to verify the stationary points to be minima. As can be seen from the results in Table C.1 and Figure C.2 in the Appendix, the excitation energies of the first ten excited singlet states calculated in gas phase at the CAM-B3LYP/def2-TZVP level of theory do not change significantly when going from R = TIPS (**1a**) via R = TMS (**1b**) to R = Me (**1c**), whereas both the excitation energies and the order of the excited states change when the entire ethynyl group is substituted by Me (**1d**). Similar conclusions hold for the resulting spectral line shapes. Especially in the lower energy region, all important spectral features are well reproduced for **1a**–**c** and in good agreement with experiment, while the first peak after 3 eV is missing for **1d**. Thus, in the following computational study only the molecules **1**, **2** and **3** of Figure 8.1 with R = Me were considered.

8.3.2 Choosing Functional and Basis Set

To identify a suitable TDDFT-based methodology, vertical singlet excitation energies of molecule **1** (Figure 8.1, with R = Me) have been computed with different electronic structure methods and basis sets. First, different exchange-correlation functionals (specifically, BLYP, B3LYP, BHLYP, CAM-B3LYP, ωB97X and ωB97X-D) are compared against ADC(2) using the def2-SVP basis set.[200] The results for the lowest excited singlet states are shown schematically in Figure 8.2, where it can be seen that the BHLYP and CAM-B3LYP functionals have by far the best agreement with the benchmark method. The pure functional BLYP underestimates all excitations significantly, underlining the necessity of exact exchange in TDDFT. The global hybrid B3LYP performs somewhat better than BLYP, but still underestimates the excitation energies strongly. The range-separated hybrid ωB97X performs clearly better than B3LYP, but not as good as CAM-B3LYP, as it overestimates most excitation energies slightly. The additional dispersion correction

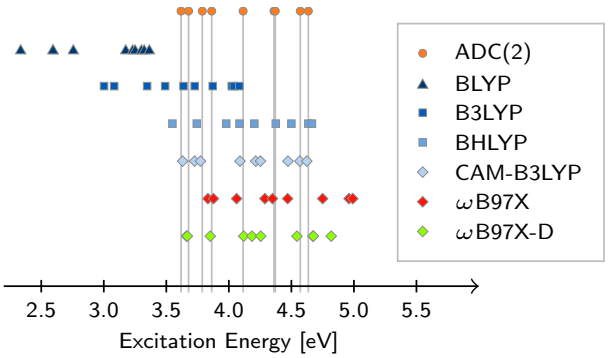

FIGURE 8.2: Vertical excitation energies of molecule **1** (Figure 8.1, with R = Me) calculated with ADC(2) and different density functionals in combination with the def2-SVP basis set.

in ωB97X-D improves the results slightly, but they are still not as good as those of BHLYP and CAM-B3LYP. Hence, since range-separated exchange-correlation functionals are often superior to global hybrids, the CAM-B3LYP functional was chosen over the BHLYP one for all further investigations. An analogous benchmark has been carried out for vertical triplet excitation energies, the results of which are shown in Figure C.3 in Appendix C. Here, no functional proved to be clearly superior over the others. However, TDDFT seems to underestimate the triplet excitation energies rather strongly compared to ADC(2), which has to be kept in mind in the following.

Next, various basis sets from double- to quadruple-ζ quality as well as the influence of additional sets of polarization functions on excitation energies and oscillator strengths were investigated. As can be seen in the results shown in Figure 8.3, while the double-ζ basis set def2-SVP is not sufficiently large, neither excitation energies nor oscillator strengths change significantly when going from triple-ζ def2-TZVP to quadruple-ζ def2-QZVP basis sets, indicating basis-set convergence at triple-ζ level. Furthermore, the influence of additional sets of polarization functions in def2-SVPP, def2-TZVPP and def2-QZVPP seems to be negligible, since no significant change in excitation energies or oscillator strengths can be observed. Since no Rydberg or similarly diffuse states are considered in this work, diffuse functions are not expected to play a significant role. It is thus safe to assume that the error in the one-particle basis will be negligible with def2-TZVP and therefore this basis set was chosen for all further investigations.

8.3.3 Electronic Excitations

Having chosen a suitable model chemistry, in this section we start with the investigation of purely electronically excited singlet and triplet states of the molecules **1**–**3** (Figure 8.1, with R = Me) and compare the resulting spectra to the experimental ones. From now on, a PCM was applied to account for solvent effects of *n*-hexane ($\varepsilon = 1.8819$). The molecules were thus re-optimized in the ground state using the PCM and CAM-B3LYP/def2-TZVP

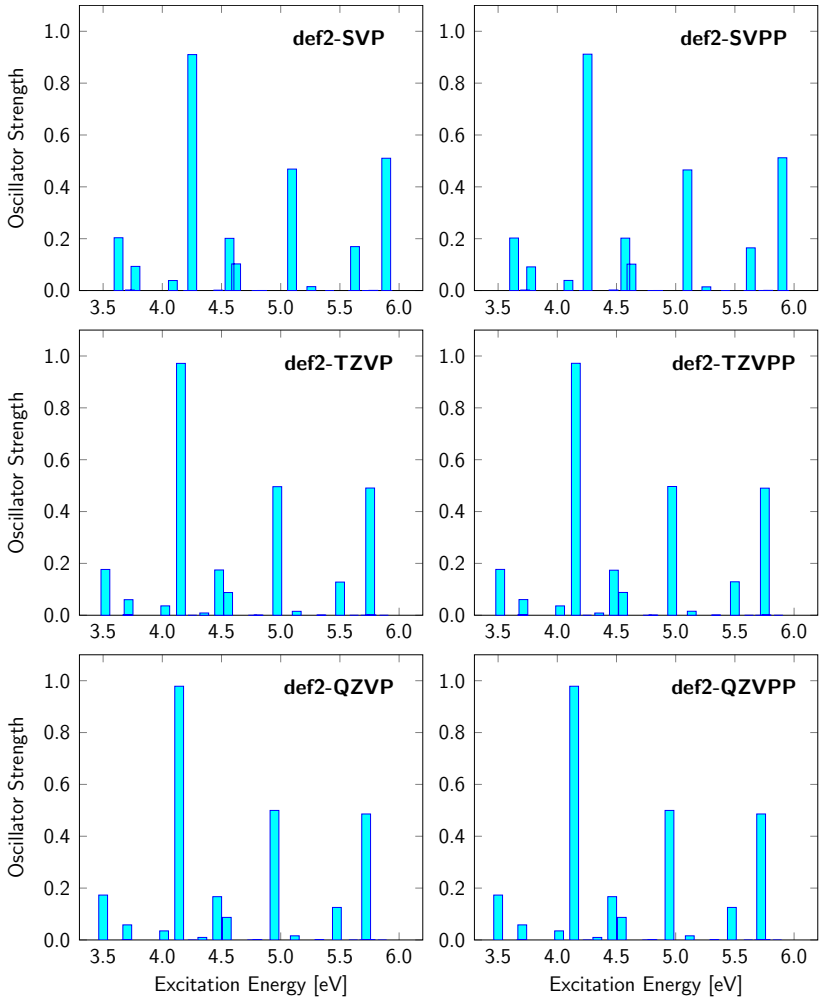

FIGURE 8.3: Vertical excitation energies and oscillator strengths of molecule **1** (Figure 8.1, with R = Me) calculated with CAM-B3LYP and different one-particle basis sets.

as well as optimized in the first excited singlet state S_1, the state from which emission should occur according to Kasha's rule.[334–336]

Results for excitation energies and oscillator strengths as well as the resulting electronic absorption spectra compared to the experimental ones are given in Tables C.2 and C.3 and Figure C.4 in the Appendix. By comparing the corresponding results for the excitation energies in Tables C.1 and C.2 of molecule **1** (with R = Me), one can also estimate the influence of solvent effects introduced by the PCM, which are seen to be usually smaller than 0.1 eV and thus do not play a significant role. Purely electronic emission spectra have not been simulated, since the experimental ones show are prounced vibrational fine structure that could not be resolved this way.[307]

The findings are summarized in terms of simple Jablonski diagrams[337,338] in Figure 8.4, where it can be seen that both for molecule **1** and **2** the transition between S_0 and S_1 is bright with a non-vanishing oscillator strength f, at the equilibrium geometries

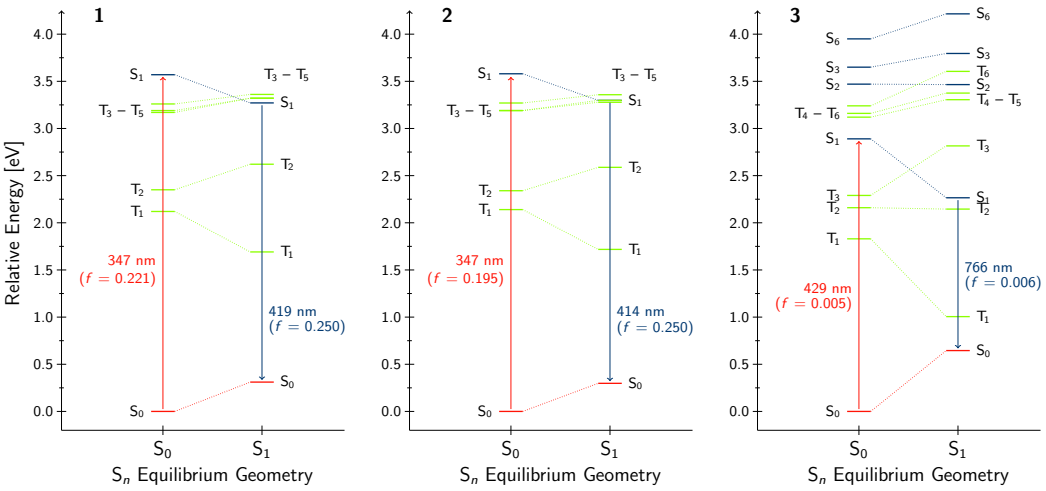

FIGURE 8.4: Simplified Jablonski diagrams of the molecules **1**–**3** (Figure 8.1, with R = Me) considering the equilibrium geometries of the S_0 and S_1 states, respectively. The energy of the S_0 state in its equilibrium geometry was set to zero in each case.

of both states. After excitation and internal conversion, the S_1 state relaxes about 0.3 eV in both molecules, but it is still about 3 eV above the ground state. The large energy gap and oscillator strength indicate a fast radiative decay of the S_1 state and thus explain the experimentally observed fluorescence around 450 nm in accordance with Kasha's rule.[307]

In the case of molecule **3**, however, the situation is not that simple. Concerning absorption, the $S_0 \rightarrow S_1$ transition has an almost vanishing oscillator strength and is thus not a bright one, and the same holds true for the $S_0 \leftarrow S_1$ transition in the emission case. This means that the molecule relaxes into the equilibrium geometry of the S_1 state only after excitation to the brighter S_2 state and internal conversion. Due to the lower energy gap and the small oscillator strength of S_1, the molecule remains longer in this state, which may open the possibility for fluorescence quenching via non-radiative decay. According to Fermi's golden rule,[339–342] the transition rate from one state to another is proportional to the square of the transition dipole moment or "dipole strength", which also corresponds to the oscillator strength divided by the excitation energy (ignoring prefactors). Using this assumptions, the fluorescence rates of molecules **1** and **2** are estimated to be more than 20 times faster than for molecule **3**. Another striking difference between molecule **3** and the other two is the extremely low-lying triplet state T_1 at the S_1 equilibrium geometry (see Figure 8.4), that lies only 0.36 eV above the S_0 state, ignoring the assumed underestimation of triplet excitation energies at the TDDFT level for the moment. A possible explanation for the missing fluorescence in case of molecule **3** would thus be an intersystem crossing into the triplet manifold after excitation, relaxation into the equilibrium geometry of the T_1 state, and phosphorescence from there in the infrared region. This route will be further investigated in the next Section 8.3.4.

Since the Stokes shift of all molecules is rather large, changes of the bond distances

between equilibrium geometries of the S_0 and the S_1 states were investigated exemplarily for molecule **3**. The results are shown in Table C.4 in the Appendix, where it can be seen that the structural changes due to relaxation in the first excited state are rather small and thus are not expected to affect the fluorescence behavior significantly.

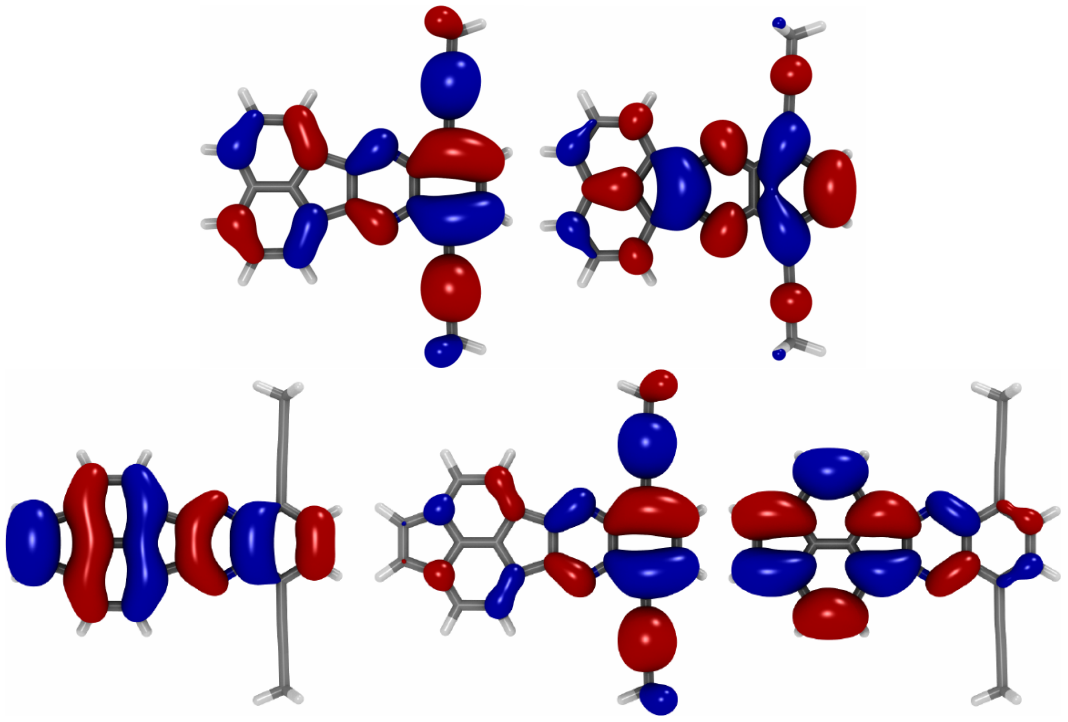

FIGURE 8.5: Frontier molecular orbitals of molecule **1** (top left: HOMO, top right: LUMO) and **3** (bottom left: HOMO–1, bottom middle: HOMO, bottom right: LUMO).

In the single-particle or molecular orbital (MO) picture, the S_1 and T_1 states of molecules **1** and **2** can be described as a transition from the highest occupied molecular orbital (HOMO) to the lowest unoccupied molecular orbital (LUMO). For molecule **3**, however, both the S_1 and T_1 states correspond to transitions from the HOMO–1 to the LUMO, while the S_2 corresponds to the HOMO→LUMO transition. These so-called frontier molecular orbitals are shown in Figure 8.5 for molecules **1** and **3**. The MOs and transitions of molecule **2** are analogous to the ones of molecule **1** (see also Figure 7 in Ref. 307). The HOMO–1 and LUMO of molecule **3** are both located mostly on the pyracyclene unit of the molecule, whereas the HOMO itself is located more on the diethynylbenzene part. Thus, the S_2 state might have some charge-transfer character in contrast to S_1 and T_1, but it still has a larger oscillator strength than the local HOMO→LUMO transition. While this picture is only qualitative, it underlines the different nature of the S_1 state of molecule **3** in contrast to molecules **1** and **2**.

8.3.4 Fluorescence Quenching via an Intersystem Crossing?

In order for intersystem crossing (ISC) to occur efficiently, significant spin-orbit coupling between the involved states is needed in molecule **3**, while they should not necessarily be present in molecules **1** and **2**. Hence, spin-orbit coupling (SOC) calculations were carried out for all three molecules at their ground-state equilibrium geometry at the TDDFT/PCM/CAM-B3LYP/def2-TZVP level of theory with the Q-Chem 5 program package[53]. However, as can be seen from the results in Tables C.6–C.8 in Appendix C, no significant SOC element between the singlet ground state or an excited singlet state and an excited triplet state could be found for any of the molecules. Analogous SOC calculations were also carried out at the equilibrium geometry of the S_1 state, but no significant coupling element was obtained at this geometry, either. Hence, the low-lying triplet state in Figure 8.4 for molecule **3** seems unlikely to play a role in the fluorescence quenching mechanism, but can at this stage also not definitely be excluded. However, the strong underestimation of triplet excitation energies at the TDDFT level as shown in Figure C.3 in the Appendix makes triplet states more unlikely to play a significant role in the fluorescence quenching mechanism of the considered molecules. Due to the high energy gap between the S_0 and S_1 states, a radiationless decay via a conical intersection is also very unlikely. Yet, for a thorough investigation of the absorption and emission properties of the three molecules, vibrationally-resolved electronic spectra shall be discussed in the next section.

8.3.5 Vibrationally-Resolved Electronic Spectra

At first, the vibrationally-resolved electronic absorption spectra shall be discussed. Only excited states with an oscillator strength larger than zero at the ground-state equilibrium geometry were considered for the generation of the "stick spectra" in a general time-independent framework.[329] The stick spectra of the different excited states were

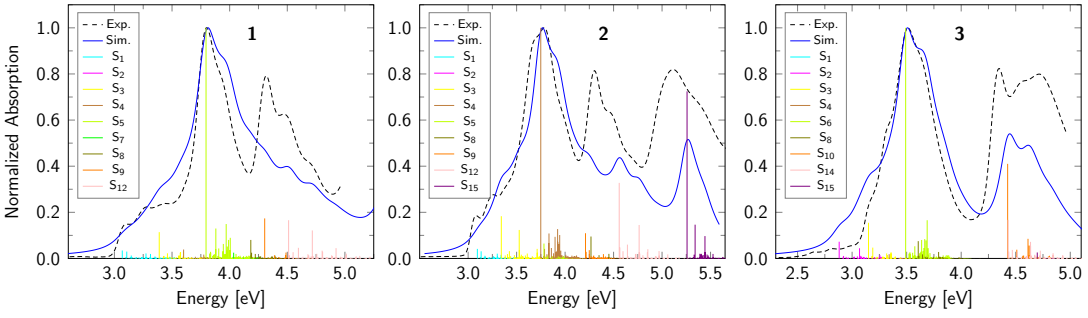

Figure 8.6: Vibrationally-resolved electronic absorption spectra of molecules **1**–**3** (Figure 8.1, with R = Me) calculated with the AS model and shifted by −0.2 eV for molecules **1** and **2**, and with the VG model shifted by −0.32 eV for molecule **3**, to match the most intense peak, respectively. Lorentzian functions with a FWHM of 0.2 eV were used to convolute the calculated stick spectra, which are shown in different colors for the individual excited states.

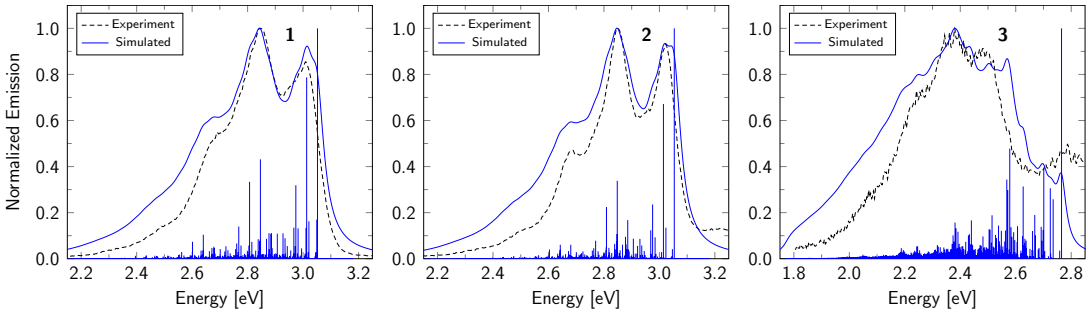

FIGURE 8.7: Vibrationally-resolved electronic $S_0 \leftarrow S_1$ emission spectrum of molecules **1**, **2** and **3** (Figure 8.1, with R = Me) calculated with the AH model and shifted by −0.11, −0.13 and +0.55 eV, respectively, to match the most intense peak. Lorentzian functions with a FWHM of 0.06 eV were used to convolute the calculated stick spectra.

added and convoluted with Lorentzian functions with a FWHM of 0.2 eV. For both the experimental and the simulated spectrum, the most intense peak has been normalized to unity. The Franck–Condon (FC) approximation for the electronic transition moment was used throughout for the vibronic spectra. Concerning vibronic transitions, the adiabatic shift (AS) model was employed for molecules **1** and **2**, whereas for molecule **3** the vertical gradient (VG) model was used, since no minimum of the S_6 state could be found. The VG model has also been applied to the first two molecules, and the results are very similar to the AS model. Effects of anharmonicity and a finite temperature ("hot bands") have been neglected throughout. The vibrationally-resolved electronic absorption spectra for molecules **1**–**3** are shown in Figure 8.6, where the simulated spectra of molecules **1** and **2** have been shifted by −0.2 eV, and by −0.32 eV for molecule **3** in order to match the most intense peak. The shift can possibly be explained by the fact that both in the AS and the VG model the normal modes and vibrational frequencies of the final excited states are ignored and assumed to be the same as the ones of the initial ground state. As can be seen in Figure 8.6, the general shape of the absorption spectra is quite well reproduced for molecules **1** and **2**, whereas the relative intensity of the highest peak compared to the second highest is not. However, in particular for molecule **2**, the distance and shape of the three most intense peaks is significantly better reproduced than in the purely electronic case (see Figure C.4 in the Appendix). Although the shift is slightly larger for molecule **3** than for the other two, the experimental spectral line shape is remarkably well reproduced in this case, and a significant improvement can be observed here as well compared to the purely electronic spectrum. Furthermore, it should be noted that the absorption spectra are not only broadened by vibronic progressions, but many electronic states contribute and overlap in general.

For the vibrationally-resolved electronic $S_0 \leftarrow S_1$ emission spectra of molecules **1**–**3** the same approximations as for the absorption spectra were used, except that the adiabatic Hessian (AH) model was employed for the vibronic transition. The fluorescence spectrum of molecule **3** has a very low measured emission intensity compared to the other two

systems. Again, the most intense peaks have been normalized to unity in each case. However, one has to keep in mind that the experimental emission intensity of molecule **3** only amounts to about 1–5% compared to molecules **1** or **2** and is thus significantly weaker (see also Figure 5 in Ref. 307), an effect that is not properly seen anymore in the results shown in Figure 8.7 because of the normalization. The simulated spectra were shifted by −0.11 eV for molecule **1**, −0.13 eV for molecule **2** and +0.55 eV for molecule **3**, respectively, and the stick spectra have been convoluted with Lorentzian functions with a FWHM of 0.06 eV. As can be seen in the results shown in Figure 8.7, the shapes of the computed spectra are in very good agreement with the experimental ones. Both the energetic distance and the relative intensity of the two most intense peaks in the very similar spectra of molecules **1** and **2** around 2.8 and 3.0 eV perfectly match experiment, and also the "shoulder" between 2.6 and 2.7 eV is nicely reproduced. The agreement with experiment is thus even significantly better than for the absorption spectra, but one has to keep in mind that here only one excited electronic state had to be considered, in contrast to about ten in the absorption case.

The emission of molecule **3** is a more difficult case. As stated before, no fluorescence can be observed with the naked eye and the measured emission is very weak. In principle, the spectrum on the right in Figure 8.7 shows a similar structure as the other two molecules, just that the absolute intensity is two orders of magnitude lower and the energy of the maximum peak is shifted by about 0.4 eV. The calculated energy difference between the S_0 and the S_1 state in the equilibrium geometry of the latter (see Figure 8.4) indicates a transition wavelength of 766 nm, which would be in the near infrared. However, the experimentally observed emission takes place between about 2.0 and 2.6 eV or 475 and 620 nm, which is still in the visible region. Due to the large underestimation of the electronic energy gap between the ground and first excited state in the equilibrium geometry of the latter, the calculated spectrum had to be shifted by 0.55 eV. Yet, it can be seen that molecule **3** does indeed fluoresce, albeit just very weakly, and that its emission spectrum possesses a similar vibrational fine structure as the other two molecules.

8.4 Summary

In this work, the optical absorption and emission spectra as well as fluorescence quenching of the azaacenes **1**–**3** (Figure 8.1) that bear five-membered rings have been investigated computationally. While two of three structurally very similar azaacenes highly fluorescent, a third class with an additional unsaturated C_2 group did not show any visible emission at all.[307] To this end, TDDFT computations employing the CAM-B3LYP functional and the def2-TZVP basis set on somewhat smaller model molecules were validated with reference to ADC(2) vertical excitation energies and experimental results. Purely vertical electronic excitation proved not to be accurate enough for a proper description of the experimental absorption and, in particular, emission spectra. Thus, vibrationally-resolved

electronic spectra of the model molecules were calculated that were in very good to excellent agreement with the experimental ones. Geometry optimizations in the first excited singlet state indicated that an energetically very low-lying triplet state is present in the non-fluorescent molecule in contrast to the other two molecules, and that a fluorescence quenching might occur via an intersystem crossing and successive phosphorescence in the infrared region. However, calculations of spin-orbit coupling elements showed that this is probably not the case. Rather, the computations have shown that the S_1 state has a different character for the non-fluorescent molecule as compared to the other two. While for the emitting molecules the first excited state corresponds to a transition from the HOMO to the LUMO with a significant oscillator strength, the S_1 state of the non-emitting molecule corresponds to a transition from the HOMO–1 to the LUMO with an almost vanishing oscillator strength. The corresponding bright HOMO→LUMO transition corresponds to the S_2 state in this case. Thus, the additional double bond of the C_2 unit changes the character of the first two excited singlet states in the molecules, making the S_1 a dark one with a very low oscillator strenth. This gives this excited species a long lifetime and a low fluorescence rate, such that the emission cannot be seen anymore with the naked eye.

Chapter 9

Conclusions and Outlook

In this thesis, I have presented the theory, implementation, and results of several methodologies for the calculation of excited electronic states based on unitary coupled cluster (UCC) or the algebraic-diagrammatic construction (ADC) scheme. Due to the particular kind of basis states used to represent the electronic Hamiltonian, these schemes have very beneficial properties such as separability and compactness. Separability is a sufficient condition that the method under consideration treats electronic excitation in a size-consistent or, more specifically, size-intensive manner. Compactness means that only modest configuration spaces need to be taken into account in order to be correct through a specific order in perturbation theory. While ADC is strictly based on Møller–Plesset perturbation theory (MP), UCC is, in principle, a nonperturbative ansatz. However, in contrast to traditional coupled-cluster (CC) theory, its expansion does not truncate naturally, and hence the working equations cannot be cast into closed-form expressions. Thus, the disadvantage of UCC is that it needs to be truncated manually, usually by employing arguments from MP perturbation theory.

My work consisted of a theoretical analysis of the different methods, their implementation into an existing program package, and their evaluation by comparing my results to the ones from established methods. After presenting the basics of quantum-chemical methods such as Hartree–Fock, configuration interaction, MP, ADC and traditional CC in Chapter 2, I presented the UCC scheme for the calculation of ground-state energies, electronic excitation energies and molecular properties by deriving most of the equations using diagrammatic techniques explicitly through third order in perturbation theory in Chapter 3. Furthermore, I gave an explicit derivation of the "Bernoulli expansion" (Bn) of the similarity-transformed Hamiltonian $\bar{H}$, which bears several advantages over the traditional Baker–Campbell–Hausdorff expansion (BCH) such as cancellation of many terms and the Fock operator occurring only up to a single commutator with the cluster operator. Using the intermediate state representation (ISR), I explicitly derived the ADC(2) equations, which uses the first-order correction to the wave function from MP. Due to the form of the first-order correlation amplitudes, simplifications in the matrix

elements occur due to partial cancellation of terms.

An analogous ISR procedure can be carried out starting from a different reference function that is correct through first order. However, if other amplitudes such as from a converged CC calculation are used, this cancellation of terms involving cluster amplitudes and orbital-energy differences does not occur anymore. Taking coupled cluster doubles (CCD) as the reference, I implemented the scheme termed CCD-ISR(2) as well as CCD-ADC(2), where the MP amplitudes are replaced by CCD ones in the simplified matrix version. Concerning UCC, I showed that matrix elements equivalent through second order, but that the same subtlety arises depending on whether the BCH or Bernoulli expansion is used for $\bar{H}$. The BCH-UCC2 matrix elements are equivalent to those of CCD-ISR(2), while the "simplified" version occurs for the Bn-UCC2 scheme. The difference lies again in the ground-state cluster amplitudes, which for UCC2 essentially correspond to those from linearized coupled-cluster doubles (LCCD). In a strict perturbation-theoretical framework, however, where the ground-state amplitudes are only required to be correct to first order, all variants are identical.

All schemes discussed above have been implemented as modifications of the standard ADC(2) variant and tested on a set of small molecules. While for systems well described by means of perturbation theory, the results for vertical excitation energies do not differ significantly, larger deviations could be observed for systems of "quasi open-shell type." For the ozone molecule as an example, the first excitation energy was obtained experimentally to be 1.6 eV. Standard ADC(2) yields 2.14 eV, CCD-ISR(2) 1.88 eV and CCD-ADC(2) 1.59 eV. A benchmark on a set of small organic and inorganic molecules did not reveal major differences between the methods.

Focussing on the CCD-ADC variants, an extensive benchmark on small to medium-sized unsaturated organic molecules revealed a mean error and standard deviation for singlet excited states of 0.15 ± 0.34 eV for CCD-ADC(2), whereas for standard ADC(2) 0.22 ± 0.30 eV was obtained compared to the theoretical best estimates (TBE). For triplet excited states, ADC(2) has a mean error and standard deviation of 0.12 ± 0.16 eV, CCD-ADC(2) improves significantly upon this with 0.00 ± 0.17 eV. The same benchmark has also been carried out for the extended variants ADC(2)-x and CCD-ADC(2)-x, where the doubles block of the secular matrix is expanded through first order in an *ad hoc* manner, but no improvements were observed when employing CCD amplitudes in this case.

Another case where MP perturbation theory is known to fail, whereas CC is more stable, is the stretching of bonds. The failure of MP has immediate consequences to the excited-state potential energy surfaces calculated via ADC. When stretching the triple bond of the N_2 molecule, MP2 starts to break down at around 2 Å, and so do the ADC(2) excited states. On the other hand, CCD is more stable, and so are the potential energy surfaces of CCD-ADC(2), which I could show to be reasonable towards the dissociation limit up to about 3.5 Å. This behavior can have significant consequences for the theoretical

description of photochemical reactions via excited-state geometry optimizations.

In order to test CC-ADC schemes for a more complex property other than excitation energies, I calculated static dipole polarizabilities of several small to medium-sized systems, presented in Chapter 5. In particular aromatic molecules like benzene had proven difficult cases for standard ADC approaches. For this, I extended and modified the previous implementation to allow for calculations where the amplitudes are only replaced in the transition moments, but not in the secular matrix, denoted F/CC-ADC(2). This includes the F/CC-ADC(3/2) scheme, where the second-order transition moments are combined with the third-order ADC matrix. Furthermore, both CCD and CCSD reference functions were considered, where, in the latter case, the converged CC singles amplitudes replaced a part of the second-order correction to the ground-state density matrix. The amplitudes in the transition moments turned out to be more important than the ones in the secular matrix itself, and consistent improvements for static polarizabilities were observed compared to standard ADC schemes, in particular for aromatic systems like benzene and pyridine. Here, both CCD-ADC(2) and CCSD-ADC(2) had a significantly smaller relative error compared to experimental results than standard ADC(3/2), at a computational cost amounting to only about 1% of the latter. The results are thus very encouraging, such that in future projects also dynamic polarizabilities or other properties like C_6 dispersion coefficients could be calculated in order to further test and validate the CC-ADC(2) schemes.

Turning back the attention to unitary coupled cluster in Chapter 6, the third-order scheme UCC3 has been implemented, in which the amplitude equations and excited states dominated by single excitations are correct through third order in perturbation theory. The current implementation allows for the computation of the ground state and excitation energies, vertical ionization potentials as well as properties and transition properties of the ground and excited states. Both the second-order scheme UCC2 and UCC3 have been benchmarked on the same set of unsaturated organic molecules as the CC-ADC(2) schemes. Here, the performance of UCC2 was somewhat worse with a mean error and standard deviation of 0.36 ± 0.41 eV as compared to standard ADC(2) with 0.22 ± 0.30 eV for singlet excited states compared to the TBE values. Concerning the third-order variants, the performance of UCC3 with 0.07 ± 0.30 eV is slightly better than ADC(3) with 0.12 ± 0.27 eV. Oscillator strengths calculated with UCC2 and UCC(3/2), which is analogous to ADC(3/2) described above, appear to be very reliable and sometimes agree better with other literature values than those calculated with ADC.

The dipole moments calculated with UCC gave very promising results; for the H_2O and HF molecules, the UCC(3/2) result agreed almost perfectly with full configuration interaction (FCI). For the more difficult CO molecule, FCI predicts a dipole moment of 0.63 D, whereas the second-order methods deviate severely. MP2 predicts 1.30 D, UCC2 improves slightly upon this with 1.16 D. However, using third-order amplitudes in UCC(3/2), the result is very close to FCI with 0.70 D. These results suggest that it may

be very rewarding to include higher-order terms in the expansion of the ground-state energy expression, the one-particle densities of the ground and excited states as well as the transition moments. Some of these expressions have already been derived, but still need to be implemented. Another possible extension that will be tested in the future is the perturbative inclusion of triple excitations, analogous to corrections to CCSD, such as CCSD[T] or CCSD(T). In this manner, the ground-state energy can be made consistent through fourth order as well as the density matrix through third order in perturbation theory.

In general, the second- and third-order UCC schemes can be expanded into many different directions. Apart from a more thorough investigation of ionization potentials via the IP-UCC methods, unitary coupled-cluster schemes can furthermore be adapted to the calculation of electron affinities (EA-UCC). Environment effects can be included via the frozen density embedding approach (FDE-UCC) or the polarizable embedding scheme (PE-UCC) in order to be able to calculate excited states in biologically relevant systems. The spin-flip ansatz (SF-UCC) can be exploited for the calculation of systems with a multi-reference character. The calculation of core-excited states and X-ray spectra can be achieved by employing the so-called core-valence separation (CVS-UCC), everything analogous to the work done on the ADC schemes. To check for the computational efficiency of the implementations, the general timings of all UCC schemes need to be investigated, and the performance could be improved by employing the resolution-of-the-identity approximation (RI-UCC) for the two-electron integrals. All of the aforementioned approaches can then be used to calculate optical spectra of molecular systems, such as UV/Vis absorption or electronic circular dichroism (ECD). For the latter, not only the electric transition dipole or oscillator strength but also the magnetic transition dipole moment or rotatory strength is required. By developing analytical gradients for the ground and excited states, geometry optimizations can be performed, and more complex response properties for other spectroscopies calculated.

Analytic gradients, i.e., derivatives of the energy, constitute the second standard approach for the calculation of molecular properties, besides the expectation value of the respective operator with the wave function. In Chapter 7, the relationship between the two approaches is investigated, which are not equivalent for nonvariational wave functions, for all standard quantum-chemical methods, with a focus on the inclusion of orbital relaxation in the expectation-value approach. While for fully variational SCF methods like HF and DFT, the Hellmann–Feynman theorem is fulfilled, and the two approaches are equivalent, no orbital relaxation is included by definition in the (ground-state) CC and CI methods. For methods based on perturbation theory, i.e., MP and ADC, the situation is not that clear. In MP2, orbital relaxation is partially included in the expectation value by virtue of the singly-excited determinants in the second-order correction to the wave function, which is exactly obtained in the first iteration of the Z vector equations, the solution of which yields the full orbital relaxation.

ADC(1), being essentially equivalent to the CIS method, contains no orbital relaxation. An analogous analysis as for MP2 has been carried out for ADC(2), and even though a one-to-one mapping like for MP2 is not possible in this case, it was shown that the expectation value contains some orbital-relaxation terms, but is more similar to the orbital unrelaxed expression. Numerical studies confirmed the conclusions from the theoretical analysis. Concerning ground-state dipole moments, the MP2 expectation value was very close to the relaxed one, while for ADC(2), the opposite trend was observed. This behavior can also be explained by the fact that the doubles block of ADC(2) is diagonal in zeroth order, and hence singles on top of single excitations cannot account for orbital relaxation in singly-excited states. By taking the excitation vectors from the ADC(3) method, in which doubly-excited configurations are fully coupled, in combination with the second-order effective density, the expectation value results came closer to the relaxed dipole moments. However, this is only true for excited states dominated by single excitations. For doubly-excited states, both the ADC(2) and ADC(3/2) expectation values were far from the relaxed value, showing that in this case, triply-excited configurations are needed to account for orbital-relaxation effects.

Apart from my work on theoretical methods and development, I have been involved in several projects in collaboration with experimental organic chemists. As an example, the work resulting from one of these projects has been presented in Chapter 8. Here, the optical absorption and emission spectra as well as fluorescence quenching of three similar azaacenes bearing five-membered rings has been investigated computationally. While two of the three structurally very similar compounds are highly fluorescent, the third class with an additional unsaturated C_2 group did not show any visible emission at all. TDDFT calculations on somewhat smaller model molecules were validated against ADC(2) excitation energies and experimental results. As the purely vertical electronic excitations proved not to be accurate enough, in particular for a proper description of the experimental emission spectra, vibrationally-resolved electronic spectra were calculated and turned out to be in excellent agreement with the experimental ones.

An energetically very low-lying triplet state and a possible fluorescence quenching via an intersystem crossing followed by phosphorescence in the infrared region were ruled out as the spin-orbit coupling elements were very small. Rather, the first excited singlet state S_1 of the nonfluorescent molecule has a different character as compared to the other two. While for the emitting molecules, the S_1 state has a high oscillator strength and can be described by a HOMO-LUMO transition, the S_1 of the non-emissive molecule has an almost vanishing oscillator strength and different involved orbitals. The bright HOMO-LUMO transition corresponds to the second excited state S_2 in this case. Thus, the additional double bond of the C_2 unit alters the character of the first two excited singlet states and turns the S_1 into a dark one with an almost negligible oscillator strength. This property gives the excited species a long lifetime and a low fluorescence rate, such that the emission cannot be seen anymore with the naked eye.

Appendices

Appendix A

Vertical Excitation Energies and Oscillator Strengths of the Benchmark Sets

Table A.1 contains the results of the vertical excitaion energies calculated at the theoretical levels of ADC(2), CCD-ADC(2), CCD-ISR(2), BCH-UCC2, Bn-UCC2 and UCC3 with the aug-cc-pVTZ basis set in comparison with the theoretical best estimates (TBE) of the benchmark set introduced by Jacquemin *et al.*[172] Tables A.2 and A.3 contain those of the Thiel benchmark set[179] calculated at the ADC(2), CCD-ADC(2), ADC(2)-x and CCD-ADC(2)-x levels in combination with the TZVP basis set. Table A.4 contains results for selected molecules calculated with CCSD-ADC(2) compared to standard ADC(2) and CCD-ADC(2). Table A.5 contains results for oscillator strengths at the theoretical levels of ADC(2), ADC(3/2), UCC2 and UCC(3/2) in comparison with literature data.

A.1 Jacquemin Benchmark Set

TABLE A.1: Vertical excitation energies (in eV) of the considered molecules in the benchmark set at the theoretical levels of ADC(2), CCD-ADC(2), CCD-ISR(2), BCH-UCC2, Bn-UCC2, and Bn-UCC3 calculated with the aug-cc-pVTZ basis set in comparison with the theoretical best estimates (TBE).[a]

Molecule	State	TBE[a]	CCD-ADC(2)	CCD-ISR(2)	BCH-UCC2	Bn-UCC2	Bn-UCC3
Acetaldehyde	$^1A''$	4.31	4.20	4.12	4.05	4.35	4.09
	$^3A''$	3.97	3.77	3.70	3.62	3.93	3.72
Acetylene	$^1\Sigma_u^-$	7.10	7.27	7.10	6.97	7.50	6.82
	$^1\Delta_u$	7.44	7.60	7.46	7.36	7.82	7.17
	$^3\Sigma_u^+$	5.53	5.56	5.65	5.60	5.65	5.26
	$^3\Delta_u$	6.40	6.53	6.41	6.25	6.71	6.11
	$^3\Sigma_u^-$	7.08	7.26	7.11	6.94	7.46	6.80

TABLE A.1: (*Continued.*)

Molecule	State	TBE[a]	CCD-ADC(2)	CCD-ISR(2)	BCH-UCC2	Bn-UCC2	Bn-UCC3
Ammonia	$^1A_2$	6.59	6.47	6.37	6.35	6.52	6.64
	^1E	8.16	7.92	7.84	7.82	7.97	8.23
	$^1A_1$	9.33	9.11	9.02	9.01	9.16	9.39
	$^1A_2$	9.96	9.74	9.64	9.62	9.79	10.02
	$^3A_2$	6.31	6.22	6.12	6.10	6.28	6.33
Carbon monoxide	$^1\Pi$	8.49	8.72	8.53	8.43	8.85	8.44
	$^1\Sigma^-$	9.92	9.93	9.89	9.82	10.10	9.53
	$^1\Delta$	10.06	10.20	10.18	10.12	10.37	9.60
	$^1\Sigma^+$	10.95	11.45	11.22	11.14	11.53	11.05
	$^1\Sigma^+$	11.52	11.98	11.73	11.66	12.05	11.57
	$^1\Pi$	11.72	12.17	11.93	11.85	12.25	11.77
	$^3\Pi$	6.28	6.53	6.28	6.18	6.66	6.18
	$^3\Sigma^+$	8.45	8.31	8.39	8.34	8.41	8.10
	$^3\Delta$	9.27	9.18	9.17	9.10	9.32	8.87
	$^3\Sigma^-$	9.80	9.88	9.85	9.77	10.03	9.35
	$^3\Sigma^+$	10.47	10.97	10.73	10.65	11.05	10.50
Cyclopropene	$^1B_1$	6.68	6.82	6.64	6.50	7.01	6.54
	$^1B_2$	6.79	6.84	6.66	6.53	7.04	6.60
	$^3B_2$	4.38	4.39	4.32	4.18	4.56	4.07
	$^3B_1$	6.45	6.52	6.33	6.19	6.71	6.23
Diazomethane	$^1A_2$	3.14	3.23	3.17	3.00	3.54	2.65
	$^1B_1$	5.54	5.57	5.56	5.46	5.76	5.18
	$^1A_1$	5.90	5.84	5.86	5.75	6.08	5.28
	$^3A_2$	2.79	2.87	2.83	2.65	3.17	2.45
	$^3A_1$	4.05	3.95	4.04	3.92	4.19	3.42
	$^3B_1$	5.35	5.44	5.43	5.33	5.63	5.02
	$^3A_1$	6.82	6.84	6.91	6.80	7.02	6.67
Dinitrogen	$^1\Pi_g$	9.34	9.41	9.33	9.23	9.56	9.20
	$^1\Sigma_u^-$	9.88	10.13	10.08	9.96	10.40	9.52
	$^1\Delta_u$	10.29	10.66	10.66	10.57	10.93	9.95
	$^1\Sigma_g^+$	12.98	12.99	12.93	12.90	13.04	13.11
	$^1\Pi_u$	13.03	13.34	13.27	13.24	13.39	12.87
	$^1\Sigma_u^+$	13.09	13.08	13.02	12.98	13.13	13.20
	$^1\Pi_u$	13.46	13.97	13.83	13.73	14.11	13.49
	$^3\Sigma_u^+$	7.70	7.77	7.97	7.91	7.87	7.36
	$^3\Pi_g$	8.01	8.14	8.04	7.94	8.28	7.84
	$^3\Delta_u$	8.87	9.02	9.04	8.88	9.22	8.51
	$^3\Sigma_u^-$	9.66	10.06	10.02	9.85	10.28	9.33
Ethylene	$^1B_{3u}$	7.39	7.41	7.25	7.10	7.57	7.29
	$^1B_{1u}$	7.93	8.04	7.82	7.68	8.24	7.76
	$^1B_{1g}$	8.08	8.06	7.90	7.75	8.22	7.96
	$^3B_{1u}$	4.54	4.60	4.46	4.31	4.77	4.27
	$^3B_{3u}$	7.23	7.30	7.14	6.99	7.46	7.18
	$^3B_{1g}$	7.98	8.02	7.85	7.70	8.18	7.90
Formaldehyde	$^1A_2$	3.98	3.92	3.80	3.71	4.08	3.74

Table A.1: (*Continued.*)

Molecule	State	TBE[a]	CCD-ADC(2)	CCD-ISR(2)	BCH-UCC2	Bn-UCC2	Bn-UCC3
	$^1B_2$	7.23	6.50	6.45	6.43	6.55	7.53
	$^1B_2$	8.13	7.53	7.48	7.46	7.57	8.37
	$^1A_1$	8.23	7.46	7.42	7.40	7.51	8.52
	$^1A_2$	8.67	7.98	7.94	7.92	8.03	8.92
	$^1B_1$	9.22	9.14	9.06	8.97	9.29	9.03
	$^1A_1$	9.43	9.45	9.40	9.36	9.53	8.97
	$^3A_2$	3.58	3.44	3.32	3.22	3.60	3.34
	$^3A_1$	6.06	6.01	6.05	5.94	6.16	5.62
	$^3B_2$	7.06	6.40	6.34	6.32	6.45	7.37
	$^3B_2$	7.94	7.40	7.36	7.34	7.45	8.17
	$^3A_1$	8.10	7.39	7.34	7.32	7.44	8.38
	$^3B_1$	8.42	8.34	8.26	8.17	8.49	8.19
Formamide	$^1A''$	5.65	5.34	5.35	5.31	5.48	5.49
	$^1A'$	6.77	6.20	6.21	6.19	6.26	7.06
	$^1A'$	7.63	7.32	7.31	7.24	7.31	7.66
	$^1A'$	7.38	7.25	7.26	7.28	7.45	7.97
	$^3A''$	5.38	5.03	5.04	4.99	5.16	5.20
	$^3A'$	5.81	5.70	5.77	5.72	5.84	5.48
Hydrogen chloride	$^1\Pi$	7.84	8.01	7.89	7.86	8.18	7.76
Hydrogen sulfide	$^1A_2$	6.18	6.57	6.27	6.21	6.69	6.03
	$^1B_1$	6.24	6.46	6.26	6.22	6.55	6.16
	$^3A_2$	5.81	6.11	5.81	5.75	6.22	5.66
	$^3B_1$	5.88	6.10	5.88	5.84	6.19	5.79
Ketene	$^1A_2$	3.86	4.04	3.99	3.90	4.24	3.66
	$^1B_1$	6.01	6.02	5.97	5.92	6.15	5.96
	$^1A_2$	7.18	7.17	7.13	7.07	7.29	7.18
	$^3A_2$	3.77	3.85	3.80	3.71	4.04	3.57
	$^3A_1$	5.61	5.55	5.55	5.48	5.71	5.37
	$^3B_1$	5.79	5.85	5.80	5.74	5.98	5.76
	$^3A_2$	7.12	7.14	7.10	7.04	7.26	7.14
Methanamine	$^1A''$	5.23	5.39	5.16	5.02	5.57	4.98
	$^3A''$	4.65	4.70	4.47	4.32	4.88	4.38
Nitrosomethane	$^1A''$	1.96	1.85	1.70	1.30	2.13	1.63
	$^1A'$	6.40	5.86	5.79	5.56	5.96	6.56
	$^3A''$	1.16	0.98	0.84	0.43	1.24	0.81
	$^3A'$	5.60	5.47	5.52	5.47	5.71	4.97
Streptocyanine	$^1B_2$	7.13	6.99	6.93	6.89	7.13	7.07
	$^3B_2$	5.47	5.49	5.46	5.41	5.63	5.16
Thioformaldehyde	$^1A_2$	2.22	2.40	2.08	1.87	2.64	1.90
	$^1B_2$	5.96	5.88	5.71	5.67	5.97	6.01
	$^1A_1$	6.38	6.68	6.46	6.28	6.91	6.58
	$^3A_2$	1.94	2.01	1.70	1.49	2.25	1.58
	$^3A_1$	3.43	3.43	3.30	3.09	3.64	2.96
	$^3B_2$	5.72	5.71	5.53	5.49	5.79	5.80
Water	$^1B_1$	7.62	7.19	7.15	7.14	7.23	7.75

TABLE A.1: (*Continued.*)

Molecule	State	TBE[a]	CCD-ADC(2)	CCD-ISR(2)	BCH-UCC2	Bn-UCC2	Bn-UCC3
	$^1A_2$	9.41	8.84	8.81	8.80	8.88	9.55
	$^1A_1$	9.99	9.54	9.48	9.47	9.59	10.14
	$^3B_1$	7.25	6.86	6.83	6.81	6.91	7.34
	$^3A_2$	9.24	8.72	8.69	8.68	8.76	9.36
	$^3A_1$	9.54	9.17	9.11	9.09	9.21	9.65

[a] Taken from literature.[172]

A.2 Thiel Benchmark Set

TABLE A.2: Vertical excitation energies (EE in eV) of the lowest excited singlet states of the considered molecules in the Thiel benchmark set at the theoretical levels of CCD-ADC(2), CCD-ADC(2)-x, Bernoulli UCC2 and UCC3 calculated with the TZVP basis set in comparison with the theoretical best estimates (TBE). The amount of doubly-excited configurations ($\%R_2$) in the ADC excitation vectors is given as well.

Molecule	State	TBE[a]	CCD-ADC(2)		CCD-ADC(2)-x		UCC2		UCC3	
			EE	$\%R_2$	EE	$\%R_2$	EE	$\%R_2$	EE	$\%R_2$
Ethene	1 $^1B_{1u}$	7.80	8.55	3	8.18	5	8.73	3	8.26	4
E-Butadiene	1 ^1B_u	6.18	6.58	6	6.08	10	6.88	6	6.45	7
	2 ^1A_g	6.55	7.79	10	5.18	60	8.04	10	5.78	69
all-*E*-	1 ^1B_u	5.10	5.46	7	4.96	11	5.85	7	5.42	9
Hexatriene	2 ^1A_g	5.09	6.80	12	4.05	67	7.12	12	4.51	77
all-*E*-	2 ^1A_g	4.47	5.98	13	3.32	70	6.35	13	3.71	80
Octatetraene	1 ^1B_u	4.66	4.73	8	4.24	12	5.20	8	4.75	10
Cyclopropene	1 $^1B_1$	6.76	7.09	6	6.32	10	7.26	6	6.77	8
	1 $^1B_2$	7.06	7.27	5	6.74	8	7.46	4	6.99	6
Cyclo-	1 $^1B_2$	5.55	5.74	6	5.24	9	6.05	6	5.60	7
pentadiene	2 $^1A_1$	6.31	7.14	10	5.14	54	7.39	10	5.78	68
	3 $^1A_1$		8.94	5	7.49	61	9.14	5	7.80	48
Norborna-	1 $^1A_2$	5.34	5.61	7	5.02	11	5.90	7	5.56	8
diene	1 $^1B_2$	6.11	6.43	8	5.74	13	6.68	8	6.48	10
	2 $^1B_2$		7.69	6	7.14	10	7.91	7	7.62	8
	2 $^1A_2$		7.71	7	7.11	11	7.94	7	7.67	9
Benzene	1 $^1B_{2u}$	5.08	5.14	9	4.11	18	5.40	9	5.01	15
	1 $^1B_{1u}$	6.54	6.58	6	6.14	9	6.91	6	6.54	6
	1 $^1E_{1u}$	7.13	7.42	8	6.75	13	7.63	8	7.38	9
	2 $^1E_{2g}$	8.41	9.05	15	7.10	40	9.24	15	8.46	45
Naphtha-	1 $^1B_{3u}$	4.24	4.23	10	3.25	20	4.55	10	4.08	17
lene	1 $^1B_{2u}$	4.77	4.82	10	4.23	16	5.22	9	4.90	11
	2 ^1A_g	5.90	6.05	11	4.82	34	6.32	11	5.47	65

Table A.2: (*Continued.*)

Molecule	State	TBE[a]	CCD-ADC(2)		CCD-ADC(2)-x		UCC2		UCC3	
			EE	$\%R_2$	EE	$\%R_2$	EE	$\%R_2$	EE	$\%R_2$
	$1\ ^1B_{1g}$	6.00	6.11	12	4.99	29	6.43	12	5.97	32
	$2\ ^1B_{3u}$	6.07	6.10	10	5.47	15	6.37	10	6.25	11
	$2\ ^1B_{2u}$	6.33	6.40	9	5.78	14	6.69	9	6.47	12
	$2\ ^1B_{1g}$	6.48	6.71	8	6.13	12	7.02	8	6.64	11
	$3\ ^1A_g$	6.71	7.29	16	5.60	44	7.56	16	6.43	51
Furan	$1\ ^1B_2$	6.32	6.73	6	6.13	10	7.01	6	6.54	8
	$2\ ^1A_1$	6.57	6.78	10	5.48	26	7.02	10	6.50	25
	$3\ ^1A_1$	8.13	8.75	6	7.67	35	8.94	6	8.16	40
Pyrrole	$2\ ^1A_1$	6.37	6.52	10	5.40	21	6.74	10	6.36	17
	$1\ ^1B_2$	6.57	6.84	6	6.15	13	7.09	6	6.58	10
	$3\ ^1A_1$	7.91	8.43	6	7.41	26	8.61	6	7.90	25
Imidazole	$2\ ^1A'$	6.19	6.63	9	5.58	20	6.86	9	6.52	15
	$1\ ^1A''$	6.81	6.69	7	6.00	13	6.86	7	6.56	11
	$3\ ^1A'$	6.93	7.18	7	6.38	14	7.42	7	6.99	13
	$2\ ^1A''$		7.70	8	7.04	14	7.81	8	7.76	11
	$4\ ^1A'$		8.55	8	7.61	22	8.73	8	8.08	23
Pyridine	$1\ ^1B_1$	4.59	5.03	9	4.14	18	5.23	9	4.85	15
	$1\ ^1B_2$	4.85	5.16	10	4.13	17	5.42	10	5.10	14
	$2\ ^1A_2$	5.11	5.34	11	4.42	17	5.52	11	5.80	13
	$2\ ^1A_1$	6.26	6.75	6	6.21	12	7.07	7	6.60	11
	$3\ ^1A_1$	7.18	7.66	8	6.96	14	7.87	9	7.62	12
	$2\ ^1B_2$	7.27	7.53	8	6.70	19	7.75	8	7.47	15
	$4\ ^1A_1$		7.99	12	7.24	37	8.06	12	8.61	43
	$3\ ^1B_2$		8.84	12	7.49	35	8.89	12	8.91	48
Pyrazine	$1\ ^1B_{3u}$	3.95	4.19	9	3.36	16	4.42	9	4.12	12
	$1\ ^1B_{2u}$	4.64	4.97	10	3.92	18	5.26	10	4.91	14
	$1\ ^1A_u$	4.81	4.94	10	4.03	17	5.13	10	5.20	13
	$1\ ^1B_{2g}$	5.56	5.84	9	4.71	24	6.06	10	5.50	23
	$1\ ^1B_{1u}$	6.58	6.97	6	6.52	9	7.32	6	6.94	7
	$1\ ^1B_{1g}$	6.60	6.68	12	5.52	23	6.86	13	7.04	23
	$2\ ^1B_{2u}$	7.60	7.97	9	7.19	15	8.20	9	8.05	11
	$2\ ^1B_{1u}$	7.72	8.03	8	7.32	14	8.30	8	7.99	11
	$1\ ^1B_{3g}$		9.38	14	7.36	43	9.45	11	8.65	68
	$2\ ^1A_g$		8.11	11	7.13	41	8.17	11	7.52	100
Pyrimidine	$1\ ^1B_1$	4.55	4.36	10	3.51	16	4.55	10	4.39	14
	$1\ ^1A_2$	4.91	4.73	10	3.86	16	4.92	10	5.06	14
	$1\ ^1B_2$	5.44	5.29	10	4.29	18	5.55	10	5.39	14
	$2\ ^1A_1$	6.95	6.92	7	6.28	15	7.23	7	6.56	17
	$2\ ^1B_2$		7.84	10	7.14	17	7.95	11	7.91	15
	$3\ ^1A_1$		7.61	9	6.73	20	7.83	9	7.51	18
Pyridazine	$1\ ^1B_1$	3.78	3.81	10	2.93	17	4.05	10	3.83	13

TABLE A.2: (*Continued.*)

Molecule	State	TBE[a]	CCD-ADC(2)		CCD-ADC(2)-x		UCC2		UCC3	
			EE	$\%R_2$	EE	$\%R_2$	EE	$\%R_2$	EE	$\%R_2$
	$1\ ^1A_2$	4.32	4.37	11	3.36	19	4.57	11	4.57	17
	$2\ ^1A_1$	5.18	5.16	11	4.06	19	5.47	10	5.11	16
	$2\ ^1A_2$	5.77	5.73	10	4.65	24	5.98	10	5.58	23
	$2\ ^1B_1$		6.36	11	5.29	21	6.55	11	6.53	16
	$1\ ^1B_2$		6.84	7	6.17	18	7.22	7	6.80	9
	$2\ ^1B_2$		7.32	13	6.62	18	7.40	14	7.46	12
s-Triazine	$1\ ^1A_1''$	4.60	4.53	10	3.64	15	4.70	10	5.27	12
	$1\ ^1A_2''$	4.66	4.64	10	3.78	16	4.82	10	4.52	14
	$1\ ^1E''$	4.71	4.61	10	3.75	16	4.78	10	4.89	13
	$1\ ^1A_2'$	5.79	5.53	11	4.56	18	5.77	10	5.83	14
	$2\ ^1A_1'$		7.69	8	6.45	17	7.48	8	6.60	20
	$2\ ^1E''$		7.93	11	6.68	24	8.09	11	8.03	19
	$1\ ^1E'$		7.82	9	6.98	19	8.03	9	7.87	17
	$2\ ^1E'$		8.61	10	8.00	15	8.66	10	9.45	10
s-Tetrazine	$1\ ^1B_{3u}$	2.24	2.34	10	1.46	16	2.66	10	2.40	12
	$1\ ^1A_u$	3.48	3.65	11	2.65	18	3.88	11	3.91	15
	$1\ ^1B_{1g}$	4.73	5.00	11	3.70	26	5.31	11	4.88	20
	$1\ ^1B_{2u}$	4.91	4.91	11	3.80	20	5.29	11	5.00	16
	$1\ ^1B_{2g}$	5.18	5.42	11	3.99	33	5.72	11	4.78	41
	$2\ ^1A_u$	5.47	5.38	10	4.35	20	5.69	10	5.31	17
	$2\ ^1B_{2g}$		6.33	12	4.86	30	6.55	12	6.43	29
	$2\ ^1B_{1g}$		6.87	12	5.46	38	7.08	12	6.52	83
	$2\ ^1B_{3u}$		6.66	11	5.56	21	6.88	11	6.76	17
	$3\ ^1B_{1g}$		7.69	14	5.91	35	7.84	14	7.04	22
	$1\ ^1B_{1u}$		7.35	7	6.74	15	7.82	7	7.29	10
	$2\ ^1B_{1u}$		7.61	9	6.92	11	7.94	10	7.71	13
	$2\ ^1B_{3g}$		8.83	12	7.13	16	8.90	12	8.08	57
	$2\ ^1B_{2u}$		8.57	12	7.58	48	8.64	12	7.78	97
Formaldehyde	$1\ ^1A_2$	3.88	3.93	6	3.13	11	4.07	6	3.70	10
	$1\ ^1B_1$	9.10	9.17	6	8.39	11	9.30	6	9.01	10
	$2\ ^1A_1$	9.30	9.37	9	8.72	20	9.43	10	9.04	31
Acetone	$1\ ^1A_2$	4.40	4.26	7	3.50	11	4.39	7	4.18	10
	$1\ ^1B_1$	9.10	9.08	7	8.37	9	9.22	7	9.04	9
	$2\ ^1A_1$	9.40	9.45	8	8.71	15	9.59	7	9.99	12
p-Benzo-	$1\ ^1B_{1g}$	2.78	2.58	10	1.66	21	2.86	10	2.64	19
quinone	$1\ ^1A_u$	2.80	2.65	11	1.72	22	2.93	11	2.73	20
	$1\ ^1B_{3g}$	4.25	4.75	9	3.69	24	5.16	9	4.55	19
	$1\ ^1B_{1u}$	5.29	5.34	10	4.61	16	5.75	11	5.40	17
	$1\ ^1B_{3u}$	5.60	5.63	14	4.41	46	5.78	14	5.30	89
	$2\ ^1B_{3g}$	6.98	7.23	10	6.15	27	7.56	11	6.80	44
Formamide	$1\ ^1A''$	5.63	5.38	7	4.69	11	5.49	7	5.47	9
	$2\ ^1A'$	7.44	7.79	10	7.23	14	7.86	10	7.41	12

Table A.2: (*Continued.*)

Molecule	State	TBE[a]	CCD-ADC(2)		CCD-ADC(2)-x		UCC2		UCC3	
			EE	$\%R_2$	EE	$\%R_2$	EE	$\%R_2$	EE	$\%R_2$
	$3\ ^1\mathrm{A}'$		7.95	11	7.43	15	8.01	10	8.78	14
Acetamide	$1\ ^1\mathrm{A}''$	5.80	5.38	7	4.71	11	5.49	7	5.54	9
	$2\ ^1\mathrm{A}'$	7.27	7.41	9	6.76	13	7.52	9	7.50	12
	$3\ ^1\mathrm{A}'$		8.29	11	7.73	16	8.34	11	8.04	12
Propanamide	$1\ ^1\mathrm{A}''$	5.72	5.39	7	4.72	11	5.50	7	5.56	9
	$2\ ^1\mathrm{A}'$	7.20	7.33	9	6.70	13	7.23	7	7.25	9
	$3\ ^1\mathrm{A}'$		7.91	11	7.41	15	7.96	11	8.04	11
Cytosine	$2\ ^1\mathrm{A}'$	4.66	4.45	11	3.69	17	4.65	11	4.70	16
	$1\ ^1\mathrm{A}''$	4.87	4.68	14	4.03	18	4.82	14	5.23	13
	$2\ ^1\mathrm{A}''$	5.26	5.14	12	4.37	18	5.29	11	5.75	12
	$3\ ^1\mathrm{A}'$	5.62	5.47	11	4.59	19	5.65	11	5.60	18
	$4\ ^1\mathrm{A}'$		6.29	10	5.60	15	6.45	10	6.51	13
Thymine	$1\ ^1\mathrm{A}''$	4.82	4.54	10	3.81	16	4.69	10	4.89	13
	$2\ ^1\mathrm{A}'$	5.20	5.19	9	4.62	14	5.41	9	5.33	13
	$2\ ^1\mathrm{A}''$	6.16	5.95	10	5.33	14	6.08	10	6.45	10
	$3\ ^1\mathrm{A}'$	6.27	6.17	12	5.23	23	6.36	12	6.37	22
	$4\ ^1\mathrm{A}'$	6.53	6.57	10	5.83	16	6.76	10	6.75	14
	$3\ ^1\mathrm{A}''$		6.44	14	5.80	21	6.58	15	6.61	10
	$4\ ^1\mathrm{A}''$		6.68	7	6.07	12	6.82	8		
Uracil	$1\ ^1\mathrm{A}''$	4.80	4.51	10	3.77	16	4.67	10	4.85	14
	$2\ ^1\mathrm{A}'$	5.35	5.32	9	4.62	15	5.53	9	5.39	15
	$2\ ^1\mathrm{A}''$	6.10	5.88	10	5.24	14	6.00	10	6.39	10
	$3\ ^1\mathrm{A}'$	6.26	6.15	12	5.18	23	6.34	12	6.35	22
	$3\ ^1\mathrm{A}''$	6.56	6.47	15	5.79	21	6.61	15	6.79	11
	$4\ ^1\mathrm{A}'$	6.70	6.75	10	5.97	16	6.93	10	6.88	14
	$4\ ^1\mathrm{A}''$		6.90	7	6.05	17	7.03	7	7.68	25
	$5\ ^1\mathrm{A}'$		7.25	11	6.54	15	7.39	11	7.65	14
Adenine	$1\ ^1\mathrm{A}''$	5.12	5.06	11	4.30	15	5.24	11	5.43	13
	$2\ ^1\mathrm{A}'$	5.25	4.96	11	4.14	17	5.20	11	5.11	14
	$3\ ^1\mathrm{A}'$	5.25	5.12	10	4.46	15	5.38	10	5.22	14
	$2\ ^1\mathrm{A}''$	5.75	5.68	10	4.92	15	5.85	10	5.97	13
	$4\ ^1\mathrm{A}'$		6.31	11	5.51	19	6.53	11	6.47	16
	$5\ ^1\mathrm{A}'$		6.63	11	5.64	24	6.86	11	6.60	25

[a] Taken from literature.[179,196]

TABLE A.3: Vertical excitation energies (EE in eV) of the lowest excited triplet states of the considered molecules in the benchmark set at the theoretical levels of CCD-ADC(2), CCD-ADC(2)-x, Bernoulli UCC2 and UCC3 calculated with the TZVP basis set in comparison with the theoretical best estimates (TBE). The amount of double excited configurations ($\%R_2$) in the ADC excitation vectors is given as well.

Molecule	State	TBE[a]	CCD-ADC(2)		CCD-ADC(2)-x		UCC2		UCC3	
			EE	$\%R_2$	EE	$\%R_2$	EE	$\%R_2$	EE	$\%R_2$
Ethene	1 $^3B_{1u}$	4.50	4.56	2	4.21	4	4.69	2	4.27	3
E-Butadiene	1 ^3B_u	3.20	3.37	3	2.82	9	3.53	3	3.05	7
	1 ^3A_g	5.08	5.28	3	4.85	5	5.50	3	4.91	5
all-*E*-	1 ^3B_u	2.40	2.71	4	2.07	12	2.88	4	2.37	10
Hexatriene	1 ^3A_g	4.15	4.38	3	3.84	10	4.64	3	4.01	8
all-*E*-	1 ^3B_u	2.20	2.29	5	1.61	14	2.47	4	1.94	13
Octatetraene	1 ^3A_g	3.55	3.71	4	3.09	12	3.99	4	3.33	10
Cyclopropene	1 $^3B_2$	4.34	4.41	3	3.99	5	4.55	3	4.11	4
	1 $^3B_1$	6.62	6.77	5	6.07	9	6.94	5	6.48	7
Cyclo-	1 $^3B_2$	3.25	3.27	4	2.73	9	3.44	3	2.97	7
pentadiene	1 $^3A_1$	5.09	5.18	3	4.71	6	5.41	3	4.83	5
Norborna-	1 $^3A_2$	3.72	3.67	4	3.23	6	3.86	4	3.49	5
diene	1 $^3B_2$	4.16	4.14	4	3.73	5	4.30	3	3.92	4
Benzene	1 $^3B_{1u}$	4.15	4.01	4	3.52	7	4.08	3	3.88	5
	1 $^3E_{1u}$	4.86	5.02	7	4.23	14	5.32	7	4.58	12
	1 $^3B_{2u}$	5.88	6.00	5	5.38	8	6.33	5	5.79	7
	1 $^3E_{2g}$	7.51	7.85	7	7.22	12	8.02	7	7.78	9
Naphtha-	1 $^3B_{2u}$	3.11	2.95	5	2.38	11	3.08	5	2.80	8
lene	1 $^3B_{3u}$	4.18	4.16	8	3.39	16	4.52	8	3.84	15
	1 $^3B_{1g}$	4.47	4.44	5	3.84	10	4.69	5	4.17	8
	2 $^3B_{2u}$	4.64	4.57	7	3.86	14	4.87	8	4.31	13
	2 $^3B_{3u}$	5.11	4.92	7	4.30	11	5.32	7	4.84	8
	1 ^3A_g	5.52	5.59	6	4.90	13	5.88	6	5.22	11
	2 $^3B_{1g}$	6.48	6.33	12	5.47	22	6.65	12	6.13	41
	2 ^3A_g	6.47	6.68	8	5.55	32	6.97	8	6.04	36
	3 $^3B_{1g}$	6.76	7.11	7	5.82	36	7.36	7	6.45	21
	3 ^3A_g	6.79	6.82	9	5.99	14	7.11	9	6.60	11
Furan	1 $^3B_2$	4.17	4.18	3	3.61	9	4.35	3	3.89	7
	1 $^3A_1$	5.48	5.50	4	4.94	8	5.73	4	5.31	7
Pyrrole	1 $^3B_2$	4.48	4.49	4	3.93	9	4.65	4	4.21	7
	1 $^3A_1$	5.51	5.58	5	4.94	10	5.80	5	5.31	9
Imidazole	1 $^3A'$	4.69	4.68	4	4.10	9	4.85	4	4.40	7
	2 $^3A'$	5.79	5.84	5	5.21	10	6.07	5	5.59	8
	1 $^3A''$	6.37	6.31	7	5.52	13	6.48	7	6.22	9
	3 $^3A'$	6.55	6.56	5	5.87	10	6.77	5	6.23	8
	4 $^3A'$		7.59	13	6.70	14	7.64	13	7.09	12

Table A.3: (*Continued.*)

Molecule	State	TBE[a]	CCD-ADC(2)		CCD-ADC(2)-x		UCC2		UCC3	
			EE	$\%R_2$	EE	$\%R_2$	EE	$\%R_2$	EE	$\%R_2$
	$2\ ^3A''$		7.50	9	6.87	13	7.61	8	7.54	11
Pyridine	$1\ ^3A_1$	4.06	4.13	4	3.62	7	4.20	4	3.94	5
	$1\ ^3B_1$	4.25	4.45	8	3.73	13	4.65	8	4.25	10
	$1\ ^3B_2$	4.64	4.92	6	4.14	13	5.24	7	4.52	11
	$2\ ^3A_1$	4.91	5.15	7	4.35	11	5.46	7	4.73	12
	$1\ ^3A_2$	5.28	5.30	10	4.40	17	5.48	10	5.71	13
	$2\ ^3B_2$	6.08	6.38	6	5.67	10	6.71	6	6.13	9
	$3\ ^3B_2$		8.32	6	6.96	31	8.53	6	7.27	31
	$3\ ^3A_1$		7.87	12	6.89	30	7.92	12	7.11	27
s-Tetrazine	$1\ ^3B_{3u}$	1.89	1.71	9	0.95	13	2.02	8	1.72	10
	$1\ ^3A_u$	3.52	3.39	10	2.49	17	3.62	10	3.55	12
	$1\ ^3B_{1g}$	4.21	4.17	8	3.30	16	4.47	8	3.99	11
	$1\ ^3B_{1u}$	4.33	4.07	4	3.49	8	4.15	4	3.96	6
	$1\ ^3B_{2u}$	4.54	4.52	7	3.69	13	4.98	7	4.05	11
	$1\ ^3B_{2g}$	4.93	4.88	8	3.92	20	5.18	8	4.58	24
	$2\ ^3A_u$	5.03	4.91	9	4.04	15	5.22	9	4.93	12
	$2\ ^3B_{1u}$	5.38	5.38	8	4.43	16	5.79	8	4.98	15
	$2\ ^3B_{2g}$		6.06	12	4.68	28	6.28	12	6.04	53
	$2\ ^3B_{1g}$		6.69	12	5.34	55	6.89	12	6.36	87
	$2\ ^3B_{3u}$		6.48	10	5.47	19	6.70	10	6.59	15
	$2\ ^3B_{2u}$		7.39	7	6.07	100	7.83	7	6.07	100
Formaldehyde	$1\ ^3A_2$	3.50	3.42	5	2.79	7	3.55	5	3.32	7
	$1\ ^3A_1$	5.87	5.79	2	5.38	4	5.91	2	5.43	3
Acetone	$1\ ^3A_2$	4.05	3.83	6	3.20	9	3.96	6	3.82	8
	$1\ ^3A_1$	6.03	5.93	3	5.46	5	6.05	3	5.58	4
p-Benzo-	$1\ ^3B_{1g}$	2.51	2.25	9	1.49	17	2.52	9	2.39	13
quinone	$1\ ^3A_u$	2.62	2.33	9	1.56	18	2.60	9	2.48	14
	$1\ ^3B_{1u}$	2.96	2.83	5	2.15	13	3.03	5	2.56	9
	$1\ ^3B_{3g}$	3.41	3.41	6	2.76	11	3.72	5	3.23	7
Formamide	$1\ ^3A''$	5.36	5.03	6	4.44	9	5.14	6	5.18	7
	$1\ ^3A'$	5.74	5.64	5	5.05	7	5.75	5	5.41	6
Acetamide	$1\ ^3A''$	5.42	5.06	7	4.46	9	5.16	6	5.24	8
	$1\ ^3A'$	5.88	5.74	5	5.16	8	5.86	5	5.55	6
Propanamide	$1\ ^3A''$	5.45	5.07	7	4.48	9	5.18	7	5.27	8
	$1\ ^3A'$	5.90	5.75	5	5.16	8	5.86	5	5.56	6

[a] Taken from literature.[179,196]

TABLE A.4: ADC(2), CCD-ADC(2) and CCSD-ADC(2) results for vertical excitation energies (in eV) of H_2O, HF, Ne, CH_2, and selected examples of the medium-sized organic molecules (Figure 4.1).

Molecule	State	ADC(2)[a]	CCD-ADC(2)	CCSD-ADC(2)
H_2O	$2\ ^1A_1$	9.37	9.42	9.43
	$1\ ^1B_1$	6.95	6.98	6.99
	$1\ ^1B_2$	10.97	11.01	11.02
	$1\ ^1A_2$	8.58	8.60	8.61
	$1\ ^3B_1$	6.61	6.64	6.65
	$1\ ^3A_2$	8.46	8.48	8.49
	$1\ ^3A_1$	9.00	9.05	9.06
	$2\ ^3A_1$	10.47	10.46	10.48
	$2\ ^3B_1$	10.57	10.58	10.60
	$1\ ^3B_2$	10.77	10.80	10.81
HF	$1\ ^1\Pi$	9.63	9.64	9.66
	$2\ ^1\Pi$	13.35	13.35	13.37
	$2\ ^1\Sigma^+$	13.91	13.94	13.95
	$1\ ^1\Delta$	14.46	14.44	14.47
	$1\ ^1\Sigma^-$	14.54	14.52	14.55
	$3\ ^1\Pi$	14.92	14.92	14.93
	$3\ ^1\Sigma^+$	15.32	15.34	15.35
	$1\ ^3\Pi$	9.30	9.30	9.32
	$1\ ^3\Sigma^+$	13.05	13.06	13.08
	$2\ ^3\Pi$	13.14	13.14	13.15
	$2\ ^3\Sigma^+$	13.80	13.76	13.79
	$1\ ^3\Delta$	14.22	14.20	14.22
	$1\ ^3\Sigma^-$	14.52	14.50	14.52
	$3\ ^3\Pi$	14.72	14.72	14.73
Ne	$1\ ^1P$	15.62	15.64	15.64
	$1\ ^1D$	17.30	17.31	17.31
	$2\ ^1P$	17.34	17.35	17.35
	$2\ ^1S$	17.43	17.45	17.45
	$3\ ^1S$	43.57	43.60	43.60
	$1\ ^3P$	17.99	18.00	18.01
	$1\ ^3S$	19.22	19.20	19.21
	$1\ ^3D$	19.83	19.83	19.85
	$2\ ^3P$	20.15	20.15	20.17
	$2\ ^3S$	45.11	45.13	45.14
CH_2	$3\ ^1A_1$	6.43	6.74	6.75
	$4\ ^1A_1$	8.28	8.59	8.60
	$1\ ^1B_2$	7.59	7.90	7.91
	$1\ ^1B_1$	1.65	2.07	2.09
	$1\ ^1A_2$	5.89	6.31	6.33
	$1\ ^3A_1$	6.27	6.59	6.53
	$2\ ^3A_1$	8.06	8.37	8.43
Ethene	$1\ ^1B_{1u}$	8.36	8.55	8.60

Table A.4: (*Continued.*)

Molecule	State	ADC(2)[a]	CCD-ADC(2)	CCSD-ADC(2)
	$1\ ^3B_{1u}$	4.52	4.56	4.61
E-Butadiene	$1\ ^1B_u$	6.43	6.58	6.64
	$2\ ^1A_g$	7.68	7.79	7.85
	$1\ ^3B_u$	3.40	3.37	3.43
	$2\ ^3A_g$	5.22	5.28	5.33
Cyclopentadiene	$1\ ^1B_2$	5.66	5.74	5.80
	$2\ ^1A_1$	7.08	7.14	7.19
	$3\ ^1A_1$	8.85	8.94	8.98
	$1\ ^3B_2$	3.35	3.27	3.32
	$1\ ^3A_1$	5.19	5.18	5.23
Furan	$1\ ^1B_2$	6.76	6.73	6.80
	$2\ ^1A_1$	6.85	6.78	6.84
	$3\ ^1A_1$	8.73	8.75	8.80
	$1\ ^3B_2$	4.35	4.18	4.25
	$1\ ^3A_1$	5.59	5.50	5.57
Pyrrole	$2\ ^1A_1$	6.60	6.52	6.57
	$1\ ^1B_2$	6.89	6.84	6.89
	$3\ ^1A_1$	8.43	8.43	8.48
	$1\ ^3B_2$	4.66	4.49	4.54
	$1\ ^3A_1$	5.67	5.58	5.63
Imidazole	$2\ ^1A'$	6.73	6.63	6.69
	$1\ ^1A''$	6.74	6.69	6.73
	$3\ ^1A'$	7.26	7.18	7.23
	$2\ ^1A''$	7.80	7.70	7.74
	$4\ ^1A'$	8.60	8.55	8.60
	$1\ ^3A'$	4.86	4.68	4.73
	$2\ ^3A'$	5.98	5.84	5.91
	$1\ ^3A''$	6.38	6.31	6.36
	$3\ ^3A'$	6.71	6.56	6.62
	$4\ ^3A'$	7.60	7.59	7.61
	$2\ ^3A''$	7.61	7.50	7.65
Pyridine	$1\ ^1B_1$	5.10	5.03	5.08
	$1\ ^1B_2$	5.32	5.16	5.22
	$2\ ^1A_2$	5.37	5.34	5.38
	$2\ ^1A_1$	6.83	6.75	6.80
	$3\ ^1A_1$	7.70	7.66	7.71
	$2\ ^1B_2$	7.59	7.53	7.58
	$4\ ^1A_1$	7.99	7.99	8.02
	$3\ ^1B_2$	8.84	8.84	8.86
	$1\ ^3A_1$	4.46	4.13	4.17
	$1\ ^3B_1$	4.52	4.45	4.49
	$1\ ^3B_2$	5.06	4.92	4.98
	$2\ ^3A_1$	5.30	5.15	5.21

TABLE A.4: (*Continued.*)

Molecule	State	ADC(2)[a]	CCD-ADC(2)	CCSD-ADC(2)
	$1\ ^3A_2$	5.34	5.30	5.32
	$2\ ^3B_2$	6.47	6.38	6.44
	$3\ ^3B_2$	8.14	8.32	8.36
	$3\ ^3A_1$	7.86	7.87	7.89
Formaldehyde	$1\ ^1A_2$	3.91	3.93	4.02
	$1\ ^1B_1$	9.17	9.17	9.17
	$2\ ^1A_1$	9.37	9.37	9.41
	$1\ ^3A_2$	3.41	3.42	3.50
	$1\ ^3A_1$	5.96	5.79	5.89
Formamide	$1\ ^1A''$	5.46	5.38	5.49
	$2\ ^1A'$	7.82	7.79	7.84
	$3\ ^1A'$	7.98	7.95	7.99
	$1\ ^3A''$	5.13	5.03	5.13
	$1\ ^3A'$	5.81	5.64	5.75
Thymine	$1\ ^1A''$	4.67	4.54	4.64
	$2\ ^1A'$	5.30	5.19	5.30
	$2\ ^1A''$	6.09	5.95	6.05
	$3\ ^1A'$	6.29	6.17	6.28
	$4\ ^1A'$	6.72	6.57	6.69
	$3\ ^1A''$	6.58	6.44	6.53
	$4\ ^1A''$	6.74	6.68	6.74

[a] Taken from literature.[196]

TABLE A.5: Oscillator strengths of a selected set of vertical excited singlet states of the benchmark set at the theoretical levels of ADC(2), ADC(3/2), UCC2 and UCC(3/2) in comparison with the literature data.

Molecule	State	Literature[a]	ADC(2)[a]	UCC2	ADC(3/2)[a]	UCC(3/2)
Ethene	$1\ ^1B_{1u}$	0.358−0.494	0.437	0.397	0.423	0.408
E-Butadiene	$1\ ^1B_u$	0.52−0.803	0.811	0.700	0.806	0.784
all-*E*-Hexatriene	$1\ ^1B_u$	0.655−1.154	1.253	1.029	1.257	1.233
all-*E*-Octatetraene	$1\ ^1B_u$	1.382	1.701	1.331	1.724	1.696
Cyclopropene	$1\ ^1B_1$		0.001	0.001	0.001	0.001
	$1\ ^1B_2$		0.094	0.082	0.096	0.092
Cyclopentadiene	$1\ ^1B_2$	0.099−0.157	0.113	0.097	0.101	0.101
	$2\ ^1A_1$	0.001−0.019	0.012	0.009	0.001	0.001
	$3\ ^1A_1$	0.025−0.538	0.695	0.631	0.029	0.034
Norbornadiene	$1\ ^1B_2$		0.028	0.024	0.036	0.035

Table A.5: (*Continued.*)

Molecule	State	Literature[a]	ADC(2)[a]	UCC2	ADC(3/2)[a]	UCC(3/2)
	$2\ ^1B_2$		0.210	0.173	0.221	0.213
	$2\ ^1A_2$		0	0	0	0
Benzene	$1\ ^1E_{1u}$	0.323−1.33	0.748	0.670	0.707	0.699
Naphthalene	$1\ ^1B_{3u}$	0	0	0	0	0
	$1\ ^1B_{2u}$	0.082	0.106	0.081	0.097	0.102
	$2\ ^1B_{3u}$	1.326	1.531	1.327	1.524	1.488
	$2\ ^1B_{2u}$	0.268	0.313	0.279	0.299	0.286
Furan	$1\ ^1B_2$	0.144−0.185	0.176	0.156	0.160	0.172
	$2\ ^1A_1$	0.000−0.011	0.007	0.009	0.000	0
	$3\ ^1A_1$	0.194−0.494	0.546	0.490	0.345	0.300
Pyrrole	$2\ ^1A_1$	0.000−0.036	0.009	0.009	0.004	0.004
	$1\ ^1B_2$	0.099−0.99	0.185	0.166	0.171	0.176
	$3\ ^1A_1$	0.176−0.706	0.574	0.536	0.458	0.411
Imidazole	$2\ ^1A'$	0.08	0.092	0.071	0.112	0.109
	$1\ ^1A''$		0.000	0.000	0.000	0.000
	$3\ ^1A'$	0.07	0.093	0.094	0.064	0.070
	$2\ ^1A''$		0.003	0.003	0.002	0.002
	$4\ ^1A'$		0.435	0.389	0.273	0.264
Pyridine	$1\ ^1B_2$	0.023−0.040	0.025	0.021	0.027	0.026
	$1\ ^1B_1$	0.005−0.01	0.005	0.005	0.005	0.005
	$2\ ^1A_1$	0.006−0.021	0.020	0.016	0.010	0.007
	$3\ ^1A_1$	0.513−0.67	0.611	0.475	0.620	0.614
	$2\ ^1B_2$	0.407−0.65	0.609	0.543	0.538	0.538
Pyrazine	$1\ ^1B_{3u}$	0.01	0.007	0.007	0.007	0.007
	$1\ ^1B_{2u}$	0.08	0.074	0.062	0.077	0.077
	$1\ ^1B_{1u}$	0.06	0.098	0.086	0.070	0.070
	$2\ ^1B_{1u}$	0.37	0.505	0.429	0.496	0.482
	$2\ ^1B_{2u}$	0.33	0.471	0.402	0.446	0.433
Pyrimidine	$1\ ^1B_1$	0.007−0.01	0.006	0.006	0.007	0.009
	$1\ ^1B_2$	0.01−0.026	0.024	0.019	0.028	0.026
	$2\ ^1A_1$	0.017−0.03	0.052	0.045	0.025	0.012
	$2\ ^1B_2$	0.41−0.499	0.213	0.056	0.523	0.518
	$3\ ^1A_1$		0.519	0.468	0.462	0.493
Pyridazine	$1\ ^1B_1$		0.006	0.006	0.007	0.007
	$2\ ^1A_1$		0.016	0.013	0.019	0.019

TABLE A.5: (*Continued.*)

Molecule	State	Literature[a]	ADC(2)[a]	UCC2	ADC(3/2)[a]	UCC(3/2)
	$2\ ^1B_1$		0.005	0.005	0.005	0.005
	$1\ ^1B_2$		0.007	0.007	0.012	0.013
	$2\ ^1B_2$		0.544	0.003	0.492	0.471
	$3\ ^1A_1$		0.541	0.436	0.466	0.453
s-Triazine	$1\ ^1A_2''$	0.02−0.027	0.017	0.017	0.016	0.018
	$1\ ^1E'$	0.92	0.521	0.464	0.443	0.478
	$2\ ^1E'$		0.070	0.072	0.062	0.063
s-Tetrazine	$1\ ^1B_{3u}$	0.007−0.012	0.007	0.007	0.008	0.008
	$1\ ^1B_{2u}$	0.052−0.095	0.055	0.042	0.000	0.058
	$2\ ^1B_{3u}$	0.01−0.018	0.011	0.011	0.011	0.012
	$1\ ^1B_{1u}$	0.00−0.054	0.009	0.041	0.004	0.007
	$2\ ^1B_{1u}$	0.39−0.630	0.448	0.326	0.421	0.383
	$2\ ^1B_{2u}$	0.45−0.755	0.022	0.007	0.013	0.012
Formaldehyde	$1\ ^1B_1$	0.000−0.001	0.068	0.004	0.091	0.003
	$2\ ^1A_1$	0.063−0.100	0.029	0.044	0.096	0.109
Acetone	$1\ ^1B_1$	0.003	0.000	0.000	0.000	0.000
	$2\ ^1A_1$	0.255	0.401	0.376	0.134	0.119
p-Benzoquinone	$1\ ^1B_{3g}$		0	0	0	0
	$1\ ^1B_{1u}$	0.636−0.704	0.621	0.551	0.590	0.638
	$1\ ^1B_{3u}$	0	0	0	0	0
Formamide	$1\ ^1A''$	0.000−0.001	0.001	0.001	0.001	0.001
	$2\ ^1A'$	0.149−0.338	0.373	0.312	0.135	0.137
	$3\ ^1A'$		0.213	0.246	0.299	0.320
Acetamide	$1\ ^1A''$		0.001	0.000	0.001	0.001
	$2\ ^1A'$		0.235	0.223	0.132	0.146
	$3\ ^1A'$		0.281	0.088	0.145	0.144
Propanamide	$1\ ^1A''$		0	0	0	0
	$2\ ^1A'$		0.179	0.165	0.126	0.136
	$3\ ^1A'$		0.098	0.101	0.112	0.114
Cytosine	$2\ ^1A'$	0.052−0.080	0.046	0.043	0.071	0.069
	$1\ ^1A''$	0.001−0.002	0	0	0.002	0.002
	$3\ ^1A'$	0.138−0.181	0.195	0.190	0.143	0.137
	$4\ ^1A'$		0.712	0.689	0.538	0.574
	$2\ ^1A''$	0.001−0.003	0.002	0.002	0.000	0.000
Thymine	$1\ ^1A''$		0	0	0	0

Table A.5: (*Continued.*)

Molecule	State	Literature[a]	ADC(2)[a]	UCC2	ADC(3/2)[a]	UCC(3/2)
	$2\ ^1A'$	0.18	0.23	0.198	0.238	0.263
	$3\ ^1A'$	0.04	0.083	0.097	0.055	0.041
	$2\ ^1A''$		0	0	0	0
	$4\ ^1A'$	0.18	0.284	0.271	0.242	0.255
	$3\ ^1A''$		0	0	0	0
	$4\ ^1A''$		0	0	0.001	
Uracil	$1\ ^1A''$		0	0	0	0
	$2\ ^1A'$	$0.18 - 0.26$	0.235	0.207	0.242	0.266
	$3\ ^1A'$	$0.04 - 0.05$	0.059	0.070	0.04	0.027
	$2\ ^1A''$		0	0	0	0
	$3\ ^1A''$		0	0	0	0
	$4\ ^1A'$	0.035−0.17	0.215	0.205	0.179	0.193
	$4\ ^1A''$		0	0	0.001	0.001
	$5\ ^1A'$	0.51	0.377	0.362	0.471	0.476
Adenine	$1\ ^1A''$	0.001−0.007	0.001	0.001	0.001	0.002
	$2\ ^1A'$	0.004−0.03	0.091	0.036	0.006	0.135
	$3\ ^1A'$	$0.17 - 0.36$	0.244	0.265	0.274	0.136
	$2\ ^1A''$	0.003−0.005	0.002	0.002	0.002	0.002
	$4\ ^1A'$	0.51	0.563	0.519	0.249	0.528
	$5\ ^1A'$		0.044	0.062	0.257	0.052

[a] Taken from literature.[179,196]

Appendix B

Static Dipole Polarizabilities of Quinoline and Isoquinoline

In this appendix, the static polarizabilities of quinoline and isoquinoline calculted with the Sadlej-pVTZ basis set are presented in Table B.1 and Figure B.1.

TABLE B.1: Static dipole polarizability (in a.u.) of quinoline and isoquinoline calculated with different ADC variants (Sadlej-pVTZ basis set) compared to experimental values.

	Quinoline					Isoquinoline				
Method	α_{xx}	α_{yy}	α_{zz}	$\bar{\alpha}$	$\Delta\alpha$	α_{xx}	α_{yy}	α_{zz}	$\bar{\alpha}$	$\Delta\alpha$
ADC(2)	65.64	127.67	176.72	123.34	96.42	65.34	130.24	171.62	122.40	92.79
CCD-ADC(2)	65.85	122.44	168.03	118.77	88.66	65.56	124.63	163.41	117.87	85.35
F/CCD-ADC(2)	66.01	122.71	166.03	118.25	86.88	65.72	124.80	161.68	117.40	83.84
CCSD-ADC(2)	65.49	123.43	168.34	119.09	89.31	65.19	125.46	163.92	118.19	86.19
F/CCSD-ADC(2)	65.79	123.92	166.92	118.88	87.91	65.49	125.86	162.74	118.03	85.04
ADC(3/2)	64.88	123.46	172.43	120.26	93.26	64.62	126.25	167.00	119.29	89.28
F/CCD-ADC(3/2)	65.55	119.45	163.21	116.07	84.73	65.30	121.77	158.54	115.20	81.35
F/CCSD-ADC(3/2)	65.31	120.51	163.98	116.60	85.65	65.04	122.71	159.46	115.74	82.43
Experiment[a]	53.30	111.30	151.10	105.20	85.18	50.60	128.90	134.90	104.90	81.47

[a] Taken from literature.[343]

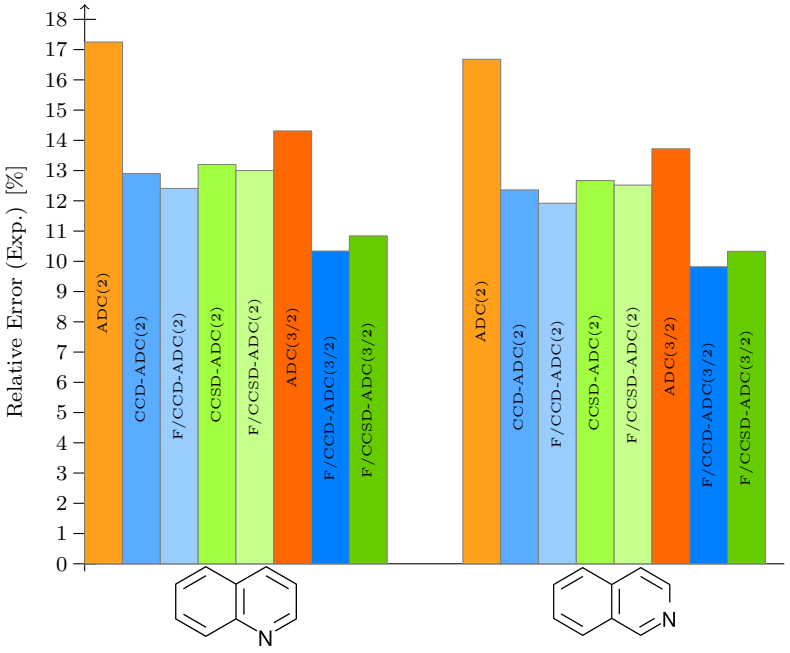

FIGURE B.1: Relative error of the isotropic polarizability $\bar{\alpha}$ for quinoline and isoquinoline of results presented in Table B.1 with respect to experimental values.

Appendix C

Azaacenes Bearing Five-Membered Rings

In this appendix, additional information for Chapter 8 is given.

C.1 Determination of Suitable Model Molecules

The moieties of the original, synthesized molecule **1a** (Figure C.1) was systematically made smaller, in order to reduce the computational cost without affecting relevant photophysical properties. In this manner, the moieties containing the TIPS groups were modified according to Figure C.1. The four molecules shown there were optimized in the gas phase at the B3LYP/def2-TZVP level of theory[200,313] using the GAUSSIAN 09 program package.[243] For molecules **1a**, **1c** and **1d** symmetry of the C_s point group was obtained, for **1b** the C_{2v} point group. The minimum character of the stationary points obtained was confirmed by frequency calculations, yielding all-positive vibrational frequencies. Consecutively, vertical excitation energies and transition moments of the four species in the gas phase were calculated at the linear-response time-dependent density functional theory (TDDFT) level[6–8] using the CAM-B3LYP functional[315] and

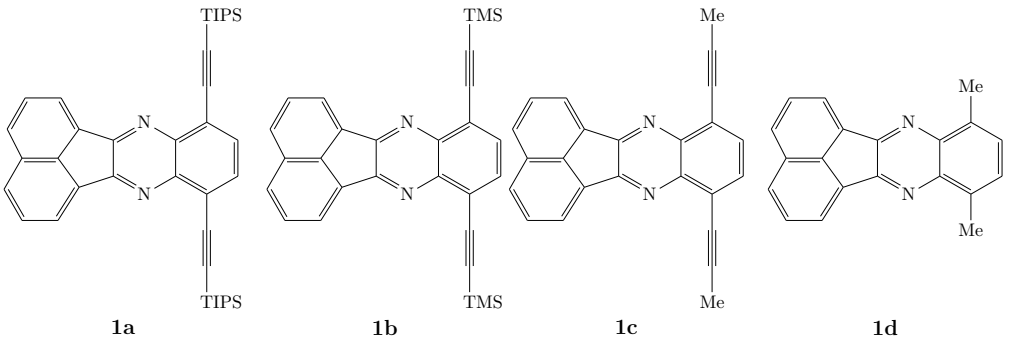

FIGURE C.1: Systematic reduction of the system size for the calculation of excitation energies.

TABLE C.1: Gas-phase vertical excitation energies ΔE (in eV) and oscillator strengths f of the first twenty excited singlet states of the molecules **1a**–**d** (Figure C.1) calculated at the TDDFT/CAM-B3LYP/def2-TZVP level of theory. The symmetry of the state in the respective point group is given as well.

	1a			**1b**			**1c**			**1d**		
State	Sym.	ΔE	f	Sym.	ΔE	f	Sym.	ΔE	f	Sym.	ΔE	f
S_1	A″	3.50	0.373	B_2	3.52	0.308	A″	3.52	0.177	A′	3.75	0.001
S_2	A′	3.69	0.001	B_1	3.68	0.001	A′	3.70	0.002	A″	3.80	0.005
S_3	A′	3.75	0.038	A_1	3.75	0.034	A′	3.72	0.060	A′	3.84	0.054
S_4	A″	4.02	0.089	B_2	4.03	0.079	A″	4.03	0.036	A″	4.12	0.014
S_5	A′	4.11	0.968	A_1	4.11	0.978	A′	4.16	0.972	A′	4.23	0.906
S_6	A″	4.28	0.000	A_2	4.27	0.000	A″	4.25	0.000	A″	4.25	0.000
S_7	A″	4.30	0.035	B_2	4.31	0.033	A″	4.35	0.009	A″	4.42	0.009
S_8	A′	4.51	0.136	A_1	4.53	0.161	A′	4.48	0.175	A″	4.71	0.070
S_9	A″	4.54	0.117	B_2	4.54	0.111	A″	4.56	0.088	A′	4.82	0.388
S_{10}	A″	4.62	0.000	A_2	4.66	0.000	A″	4.76	0.000	A′	5.25	0.003
S_{11}	A′	4.65	0.001	B_1	4.69	0.001	A′	4.81	0.000	A″	5.68	0.000
S_{12}	A″	4.81	0.590	B_2	4.83	0.509	A″	4.97	0.496	A″	5.80	0.706
S_{13}	A′	5.06	0.011	A_1	5.06	0.010	A′	5.14	0.015	A′	5.81	0.054
S_{14}	A′	5.19	0.020	A_1	5.26	0.012	A′	5.34	0.001	A′	6.05	0.097
S_{15}	A′	5.42	0.088	A_1	5.43	0.087	A′	5.51	0.128	A″	6.15	0.012
S_{16}	A″	5.57	0.000	B_1	5.55	0.000	A″	5.62	0.000	A′	6.27	0.461
S_{17}	A′	5.57	0.000	A_2	5.57	0.000	A′	5.71	0.000	A″	6.30	0.000
S_{18}	A′	5.69	0.000	B_1	5.70	0.001	A″	5.76	0.491	A′	6.34	0.000
S_{19}	A′	5.72	0.002	A_2	5.75	0.000	A′	5.77	0.001	A″	6.43	0.081
S_{20}	A″	5.74	0.066	B_2	5.77	0.500	A″	5.87	0.000	A′	6.48	0.000

the def2-TZVP basis set.[200] The results for the first twenty excited singlet states are reported in Table C.1.

Using these results, one-photon absorption spectra were simulated by convoluting the peaks with Lorentzian functions with a full width at half maximum (FWHM) of 0.3 eV. For the sake of a better comparison to experiment, the calculated spectra were normalized to unity and shifted in energy such that the maximum absorption peaks overlap. In practice, this meant a shift of 0.31 eV for molecules **1a** and **1b**, 0.35 eV for **1c** and 0.43 eV for **1d** towards lower energies, respectively. The resulting spectra are shown in Figure C.2. It can be seen that the peaks in the low-energy region between 3.0 and 3.5 eV are still quite well reproduced when the TIPS group is substituted by TMS or Me, but it is missing in the **1d** molecule. Yet, the distance between the most intense peak around 3.8 eV and the next one seem to be best reproduced in the latter case, however, the spectrum had to be shifted the most here. Changes in the spectrum above 5 eV are not relevant, since this region was not measured experimentally. It should be noted that so far vibrational contributions are neglected in the calculations.

C.2 Triplet Excitation Energies

Analogously to the singlet excitation energies benchmarked in the main paper, the same comparison has been made for excitation energies of triplet states. The results are shown

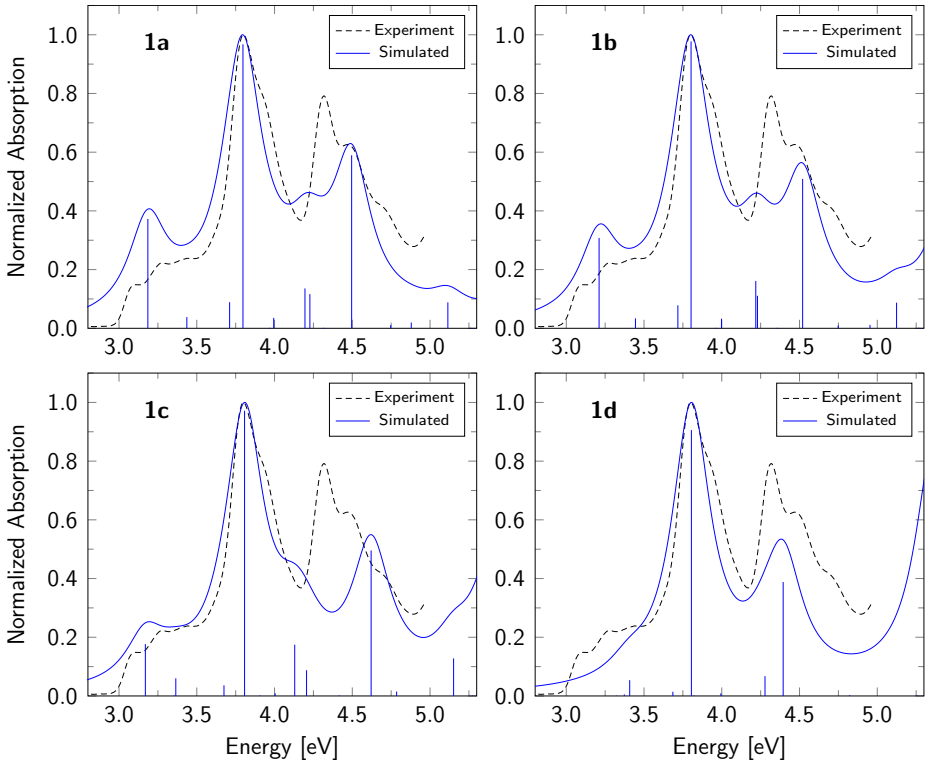

FIGURE C.2: Simulated vacuum absorption spectra of molecules **1a–d** (Figure C.1) at the TDDFT/CAM-B3LYP/def2-TZVP level compared to the experimental one. Lorentzian functions with a FWHM of 0.3 eV were used as a convolution.

schematically in Figure C.3. It can be seen that the lowest TDDFT excitation energies are in general rather strongly underestimated compared to ADC(2), in particular with BHLYP. The other density functionals yield rather similar results for the first triplet excitation energies, such that the choice of CAM-B3LYP as the density functional for the rest of this study was not altered by this benchmark. However, they have to be treated a bit with care.

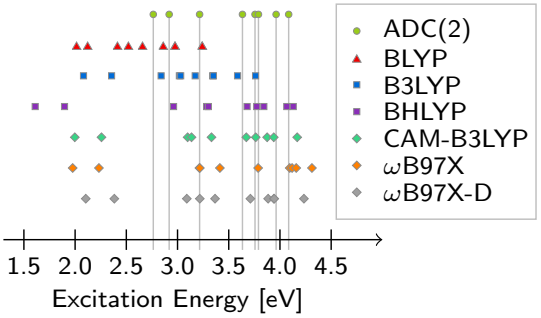

FIGURE C.3: Vertical triplet excitation energies of molecule **1c** calculated with ADC(2) and different density functionals in combination with the def2-SVP basis set.

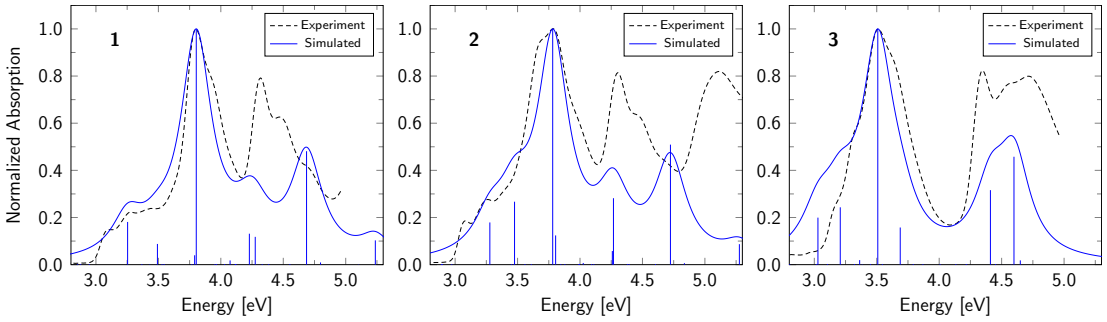

FIGURE C.4: Simulated absorption spectra of molecules **1**–**3** (Figure 8.1) at the TDDFT/PCM/CAM-B3LYP/def2-TZVP level compared to the experimental one. Lorentzian functions with a FWHM of 0.3 eV were used as a convolution.

C.3 Vertical Excitation Energies and Electronic Spectra

In this section, results for the vertical excitation energies of singlet and triplet states of the three molecules **1**, **2** and **3** (Figure 8.1, page 174) in the equilibrium geometry of both the ground state S_0 and the first excited singlet state S_1 are given. The excitation energies were calculated at the TDDFT/CAM-B3LYP/def2-TZVP level of theory using the integral-equation formalism polarizable continuum model (IEF-PCM)[320,321] to account for the solvation effects of *n*-hexane. The ground-state geometries had been re-optimized using the same methodology. The minimum character of the obtained stationary points was again confirmed by means of frequency calculations. In the case of molecule **3**, the C_s point-group symmetry was lost during the optimization in the S_1 state.

The results for vertical excitation energies and oscillator strengths of the lowest excited singlet and triplet states are shown in Table C.2 for the equilibrium geometry of the S_0 state and in Table C.3 for the equilibrium geometry of the S_1 state. The resulting one-photon absorption spectra compared to experiment are shown in Figure C.4, where Lorentzian functions with a FWHM of 0.3 eV were used as a convolution, and the excitation energies have been shifted by −0.32 eV for molecule **1**, −0.30 eV for molecule **2** and −0.44 eV for molecule **3**, respectively.

TABLE C.2: Vertical excitation energies ΔE (in eV) and oscillator strengths f of the 15 lowest excited singlet and triplet states of molecules **1**, **2** and **3** at the TDDFT/PCM/CAM-B3LYP/def2-TZVP level of theory in the equilibrium geometry of the S_0 state.

	1			**2**			**3**		
No.	State	ΔE	f	State	ΔE	f	State	ΔE	f
1	T_1 (A″)	2.12	—	T_1 (B_2)	2.14	—	T_1 (A″)	1.83	—
2	T_2 (A′)	2.35	—	T_2 (A_1)	2.34	—	T_2 (A′)	2.15	—
3	T_3 (A′)	3.17	—	T_3 (B_2)	3.19	—	T_3 (A″)	2.29	—
4	T_4 (A″)	3.19	—	T_4 (B_1)	3.19	—	S_1 (A″)	2.89	0.005
5	T_5 (A′)	3.26	—	T_5 (A_1)	3.27	—	T_4 (A″)	3.12	—
6	S_1 (A″)	3.57	0.221	S_1 (B_2)	3.58	0.195	T_5 (A′)	3.16	—
7	T_6 (A″)	3.68	—	T_6 (B_2)	3.75	—	T_6 (A′)	3.24	—
8	S_2 (A′)	3.75	0.002	S_2 (B_1)	3.77	0.002	T_7 (A″)	3.45	—
9	S_3 (A′)	3.81	0.107	S_3 (A_1)	3.78	0.291	S_2 (A′)	3.47	0.226
10	T_7 (A′)	3.85	—	T_7 (B_2)	3.86	—	T_8 (A′)	3.54	—
11	T_8 (A″)	3.86	—	T_8 (A_1)	3.91	—	S_3 (A″)	3.65	0.275
12	T_9 (A″)	4.08	—	S_4 (A_1)	4.08	1.090	T_9 (A″)	3.76	—
13	S_4 (A″)	4.11	0.049	S_5 (B_2)	4.10	0.135	S_4 (A″)	3.80	0.022
14	S_5 (A′)	4.12	1.222	T_9 (A_2)	4.14	—	S_5 (A′)	3.83	0.002
15	T_{10} (A′)	4.27	—	T_{10} (B_2)	4.17	—	T_{10} (A″)	3.89	—
16	T_{11} (A″)	4.28	—	T_{11} (B_2)	4.29	—	S_6 (A′)	3.95	1.132
17	S_6 (A″)	4.35	0.000	T_{12} (A_1)	4.29	—	S_7 (A″)	3.98	0.000
18	S_7 (A″)	4.39	0.022	S_6 (B_2)	4.33	0.008	S_8 (A′)	4.13	0.178
19	T_{12} (A″)	4.43	—	T_{13} (A_1)	4.39	—	T_{11} (A′)	4.23	—
20	T_{13} (A′)	4.44	—	S_7 (A_2)	4.41	0.000	T_{12} (A′)	4.31	—
21	S_8 (A′)	4.55	0.160	S_8 (B_2)	4.56	0.063	T_{13} (A″)	4.44	—
22	S_9 (A″)	4.60	0.144	S_9 (A_1)	4.57	0.307	T_{14} (A′)	4.57	—
23	T_{14} (A″)	4.65	—	T_{14} (A_2)	4.68	—	T_{15} (A″)	4.65	—
24	T_{15} (A′)	4.70	—	T_{15} (B_2)	4.69	—	S_9 (A″)	4.66	0.001
25	S_{10} (A″)	4.87	0.000	S_{10} (A_2)	4.90	0.000	S_{10} (A″)	4.85	0.358
26	S_{11} (A′)	4.93	0.000	S_{11} (B_1)	4.96	0.000	S_{11} (A″)	4.89	0.000
27	S_{12} (A″)	5.01	0.588	S_{12} (B_2)	5.02	0.555	S_{12} (A′)	4.94	0.000
28	S_{13} (A′)	5.12	0.011	S_{13} (A_1)	5.14	0.007	S_{13} (A′)	5.02	0.002
29	S_{14} (A′)	5.42	0.002	S_{14} (A_1)	5.47	0.000	S_{14} (A″)	5.04	0.518
30	S_{15} (A′)	5.56	0.126	S_{15} (A_1)	5.58	0.095	S_{15} (A′)	5.09	0.021

TABLE C.3: Vertical excitation energies ΔE (in eV) and oscillator strengths f of the 15 lowest excited singlet and triplet states of molecules **1**, **2** and **3** at the TDDFT/PCM/CAM-B3LYP/def2-TZVP level of theory in the equilibrium geometry of the S_1 state.

	1			**2**			**3**		
No.	State	ΔE	f	State	ΔE	f	State	ΔE	f
1	T_1 (A″)	1.38	—	T_1 (B_2)	1.42	—	T_1 (A)	0.36	—
2	T_2 (A′)	2.31	—	T_2 (A_1)	2.29	—	T_2 (A)	1.50	—
3	S_1 (A″)	2.96	0.250	T_3 (B_2)	2.98	—	S_1 (A)	1.62	0.006
4	T_3 (A″)	3.01	—	S_1 (B_2)	3.00	0.250	T_3 (A)	2.17	—
5	T_4 (A′)	3.01	—	T_4 (A_1)	3.00	—	T_4 (A)	2.66	—
6	T_5 (A′)	3.05	—	T_5 (B_1)	3.06	—	T_5 (A)	2.73	—
7	S_2 (A′)	3.56	0.033	S_2 (A_1)	3.58	0.087	S_2 (A)	2.82	0.227
8	T_6 (A′)	3.57	—	T_6 (B_2)	3.62	—	T_6 (A)	2.96	—
9	T_7 (A″)	3.58	—	S_3 (B_1)	3.63	0.002	T_7 (A)	2.97	—
10	S_3 (A′)	3.63	0.002	T_7 (A_1)	3.65	—	S_3 (A)	3.15	0.029
11	T_8 (A″)	3.72	—	T_8 (B_2)	3.78	0.000	T_8 (A)	3.18	—
12	S_4 (A′)	3.92	1.406	S_4 (B_2)	3.83	0.071	T_9 (A)	3.25	—
13	S_5 (A″)	3.97	0.040	S_5 (A_1)	3.87	1.477	S_4 (A)	3.36	0.000
14	T_9 (A″)	4.00	—	T_9 (B_2)	3.93	—	S_5 (A)	3.47	0.098
15	T_{10} (A′)	4.02	—	T_{10} (A_1)	4.05	—	S_6 (A)	3.57	1.236
16	T_{11} (A″)	4.07	—	T_{11} (A_2)	4.11	—	S_7 (A)	3.69	0.230
17	S_6 (A″)	4.20	0.011	T_{12} (B_2)	4.20	—	T_{10} (A)	3.82	—
18	T_{12} (A′)	4.30	—	S_6 (B_2)	4.21	0.000	S_8 (A)	3.84	0.002
19	T_{13} (A′)	4.37	—	T_{13} (B_1)	4.33	—	T_{11} (A)	3.99	—
20	S_7 (A″)	4.39	0.000	T_{14} (A_1)	4.34	—	S_9 (A)	4.13	0.162
21	T_{14} (A″)	4.39	—	S_7 (A_1)	4.36	0.082	T_{12} (A)	4.23	—
22	S_8 (A′)	4.40	0.006	S_8 (A_2)	4.43	0.000	T_{13} (A)	4.28	—
23	T_{15} (A″)	4.45	—	T_{15} (A_2)	4.43	—	T_{14} (A)	4.46	—
24	S_9 (A′)	4.49	0.000	S_9 (B_2)	4.52	0.006	T_{15} (A)	4.55	—
25	S_{10} (A″)	4.55	0.003	S_{10} (B_1)	4.53	0.000	S_{10} (A)	4.66	0.000
26	S_{11} (A″)	4.60	0.000	S_{11} (A_2)	4.65	0.000	S_{11} (A)	4.74	0.000
27	S_{12} (A″)	4.63	0.722	S_{12} (B_2)	4.66	0.631	S_{12} (A)	4.76	0.036
28	S_{13} (A′)	4.86	0.010	S_{13} (A_1)	4.87	0.006	S_{13} (A)	4.78	0.281
29	S_{14} (A′)	5.06	0.020	S_{14} (A_1)	5.12	0.016	S_{14} (A)	4.90	0.000
30	S_{15} (A′)	5.37	0.221	S_{15} (A_1)	5.40	0.206	S_{15} (A)	4.91	0.049

C.4 Geometrical Parameters

Due to the rather large Stokes shift of molecule **3**, the change of different C–C and C–N bond distances was compared between the equilibrium geometries of the S_0 and S_1 states. The bond lengths and their changes are presented in Table C.4, the corresponding bonds are labelled on the right.

TABLE C.4: Bond distances r and their changes (in Å) of molecule **3** in the equilibrium geometries of the S_0 and S_1 states.

Bond	$r(S_0)$	$r(S_1)$	Δr
a	1.2868	1.3086	+0.0218
b	1.4640	1.4778	+0.0138
c	1.4792	1.4371	−0.0421
d	1.4014	1.4033	+0.0019
e	1.3476	1.3431	−0.0044
f	1.3754	1.4166	+0.0411
g	1.3679	1.3426	−0.0252
h	1.4341	1.4342	+0.0001
i	1.3783	1.3783	+0.0000
j	1.4810	1.4810	+0.0000
k	1.3551	1.3551	+0.0000
l	1.3966	1.3965	−0.0001

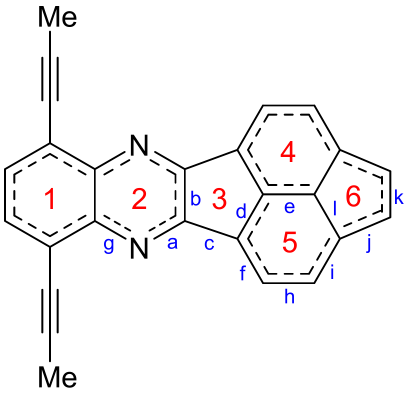

C.5 Spin-Orbit Couplings

In order to test for a possible intersystem crossing (ISC), spin-orbit coupling (SOC) calculations[324] at the TDDFT level of theory[326] were carried out for the three model molecules (Figure 8.1) in their respective ground-state equilibrium geometry (see Section C.3) with the Q-CHEM 5 program package.[53] The results for molecules **1**, **2** and **3** are given in Tables C.6, C.7 and C.8, respectively. The corresponding vertical excitation energies are given in Table C.5.

TABLE C.5: Vertical excitation energies ΔE (in eV) and corresponding wavelength λ (in nm) for the first twenty excited singlet and triplet states of molecules **1**–**3** calculated at the TDDFT/PCM/CAM-B3LYP/def2-TZVP level of theory with the Q-CHEM 5 program package.

	1			**2**			**3**		
No.	State	ΔE	λ	State	ΔE	λ	State	ΔE	λ
1	T_1	2.56	484.5	T_1	2.14	578.9	T_1	2.20	564.4
2	T_2	2.78	446.7	T_2	2.34	529.8	T_2	2.54	488.1
3	T_3	3.25	381.9	T_3	3.19	388.6	T_3	2.67	464.2
4	T_4	3.37	367.8	T_4	3.20	386.9	S_1	2.98	416.2
5	T_5	3.42	362.1	T_5	3.27	379.7	T_4	3.21	386.3
6	S_1	3.72	335.0	S_1	3.58	346.3	T_5	3.27	379.4
7	T_6	3.76	330.0	T_6	3.75	330.8	T_6	3.32	373.8
8	S_2	3.80	325.9	S_2	3.78	328.2	S_2	3.55	349.6
9	S_3	3.89	318.6	S_3	3.78	327.8	T_7	3.60	344.4
10	T_7	3.91	317.1	T_7	3.85	321.7	T_8	3.67	337.4
11	T_8	3.95	313.6	T_8	3.91	316.8	S_3	3.75	330.6
12	T_9	4.14	299.7	S_4	4.08	303.6	T_9	3.80	325.9
13	S_4	4.19	295.9	S_5	4.10	302.2	S_4	3.88	319.7
14	S_5	4.29	288.9	T_9	4.16	298.1	S_5	3.92	315.9
15	S_6	4.38	283.2	T_{10}	4.18	296.7	T_{10}	4.01	309.4
16	T_{10}	4.42	280.7	T_{11}	4.29	288.8	S_6	4.01	309.0
17	S_7	4.45	278.9	T_{12}	4.30	288.3	S_7	4.10	302.5
18	T_{11}	4.45	278.9	S_6	4.33	286.5	S_8	4.24	292.7
19	T_{12}	4.55	272.5	T_{13}	4.39	282.3	T_{11}	4.33	286.3
20	T_{13}	4.55	272.3	S_7	4.43	279.9	T_{12}	4.46	277.9
21	S_8	4.68	265.1	S_8	4.56	271.9	T_{13}	4.55	272.7
22	S_9	4.68	265.1	S_9	4.58	270.9	T_{14}	4.69	264.4
23	T_{14}	4.71	263.1	T_{14}	4.69	264.5	T_{15}	4.72	262.6
24	T_{15}	4.78	259.5	T_{15}	4.70	263.9	S_9	4.74	261.9
25	T_{16}	4.85	255.5	T_{16}	4.73	262.0	T_{16}	4.79	258.9
26	T_{17}	4.86	255.0	T_{17}	4.77	260.2	T_{17}	4.86	255.0
27	S_{10}	4.89	253.6	T_{18}	4.88	254.2	S_{10}	4.91	252.6
28	S_{11}	4.94	250.8	S_{10}	4.91	252.4	S_{11}	4.94	250.9
29	T_{18}	4.98	248.8	S_{11}	4.97	249.5	T_{18}	4.94	250.8
30	S_{12}	5.11	242.6	S_{12}	5.03	246.6	S_{12}	4.96	250.1
31	S_{13}	5.15	240.6	T_{19}	5.11	242.7	T_{19}	5.04	246.1
32	T_{19}	5.15	240.6	S_{13}	5.13	241.6	T_{20}	5.04	245.8
33	T_{20}	5.39	230.2	T_{20}	5.30	233.9	S_{13}	5.06	245.1
34	S_{14}	5.48	226.2	S_{14}	5.47	226.5	S_{14}	5.13	241.8
35	S_{15}	5.62	220.6	S_{15}	5.54	223.9	S_{15}	5.14	241.3
36	S_{16}	5.75	215.6	S_{16}	5.58	222.1	S_{16}	5.39	230.0
37	S_{17}	5.84	212.4	S_{17}	5.73	216.5	S_{17}	5.49	226.0
38	S_{18}	5.83	211.7	S_{18}	5.80	213.7	S_{18}	5.54	223.7
39	S_{19}	5.97	207.6	S_{19}	5.91	209.8	S_{19}	5.66	219.1
40	S_{20}	6.02	206.1	S_{20}	5.93	209.3	S_{20}	5.67	218.5

TABLE C.6: Spin-orbit couplings (in cm^{-1}) between singlet and triplet states for molecule **1** calculated at the TDDFT/PCM/CAM-B3LYP/def2-TZVP level of theory.

	S_0	S_1	S_2	S_3	S_4	S_5	S_6	S_7	S_8	S_9	S_{10}
T_1	0.82	0.00	13.12	1.23	0.01	0.82	0.09	0.01	0.25	0.00	11.10
T_2	0.04	0.19	0.47	0.00	0.84	0.01	10.24	0.92	0.00	2.00	0.64
T_3	4.89	12.09	0.00	1.87	2.84	2.42	0.18	7.81	1.39	4.64	5.47
T_4	2.11	0.00	9.75	0.46	0.00	0.11	1.93	0.00	0.58	0.02	6.94
T_5	0.08	0.75	4.14	0.00	0.18	0.00	1.24	0.12	0.00	0.80	1.14
T_6	1.72	0.00	5.65	0.24	0.00	0.34	1.93	0.00	0.53	0.00	0.53
T_7	0.08	1.16	0.43	0.00	0.14	0.00	8.94	0.14	0.00	0.18	1.67
T_8	0.59	0.00	10.30	0.71	0.01	0.54	1.78	0.00	0.46	0.01	0.95
T_9	48.34	1.77	0.25	10.78	2.05	6.14	0.00	1.25	0.97	0.87	0.05
T_{10}	0.01	0.15	0.45	0.00	0.00	0.00	1.77	0.05	0.00	0.11	0.79
T_{11}	0.34	0.01	7.65	0.52	0.00	0.49	1.96	0.01	0.07	0.02	2.71
T_{12}	1.70	0.00	0.15	0.79	0.01	1.41	0.91	0.01	0.65	0.01	1.35
T_{13}	0.04	0.30	0.64	0.00	0.98	0.00	0.88	0.40	0.00	0.41	0.11
T_{14}	16.47	12.81	5.10	4.62	5.40	0.29	0.02	4.87	0.70	2.82	0.01
T_{15}	13.01	0.24	0.00	1.46	0.25	2.84	0.85	0.28	5.22	0.39	0.16
T_{16}	0.12	0.01	7.51	0.99	0.01	0.48	1.98	0.00	0.60	0.02	6.68
T_{17}	0.02	0.18	0.47	0.01	0.79	0.01	4.36	0.61	0.01	0.48	0.31
T_{18}	0.04	0.18	0.68	0.01	0.01	0.01	4.15	0.12	0.00	0.16	2.83
T_{19}	56.81	5.44	2.25	5.94	3.86	3.92	0.02	3.21	2.46	2.24	0.11
T_{20}	0.11	1.28	0.58	0.02	0.16	0.01	0.61	0.10	0.00	0.60	0.35

	S_{11}	S_{12}	S_{13}	S_{14}	S_{15}	S_{16}	S_{17}	S_{18}	S_{19}	S_{20}
T_1	0.30	0.01	0.54	1.14	0.74	0.01	4.59	2.82	2.09	1.23
T_2	0.45	0.09	0.01	0.00	0.01	0.70	1.99	1.00	1.83	0.70
T_3	0.00	5.01	0.71	1.15	0.73	0.90	0.55	0.00	0.02	0.14
T_4	0.08	0.00	0.82	0.25	0.18	0.01	3.74	5.82	0.15	1.61
T_5	0.29	0.06	0.00	0.00	0.01	0.21	7.45	0.41	0.05	0.66
T_6	0.04	0.00	0.02	0.06	0.08	0.00	0.79	0.88	1.61	0.29
T_7	1.06	0.10	0.01	0.01	0.01	0.29	2.44	5.76	9.20	0.72
T_8	0.05	0.01	0.38	0.05	0.29	0.00	1.43	1.25	2.41	0.34
T_9	0.99	1.03	0.28	0.94	0.96	0.51	0.03	3.86	4.53	0.01
T_{10}	17.69	0.07	0.01	0.00	0.01	0.17	3.25	0.42	0.06	0.62
T_{11}	0.50	0.00	0.57	0.20	0.10	0.02	2.19	4.28	3.45	0.40
T_{12}	0.06	0.00	0.15	0.10	0.26	0.01	0.44	0.27	0.92	0.16
T_{13}	0.57	0.08	0.01	0.00	0.00	0.07	0.15	0.50	0.41	0.11
T_{14}	0.14	10.77	0.08	0.07	2.15	1.09	0.10	1.83	4.17	0.01
T_{15}	0.00	1.04	0.59	21.39	14.11	0.09	0.94	0.00	0.01	0.66
T_{16}	0.61	0.00	0.20	0.03	0.16	0.01	1.63	3.74	1.24	1.10
T_{17}	0.73	0.05	0.01	0.00	0.00	0.22	0.16	1.12	0.80	0.26
T_{18}	3.92	0.50	0.00	0.00	0.00	0.08	4.97	2.35	1.98	0.05
T_{19}	0.54	8.74	0.17	1.31	2.02	0.85	0.03	3.67	1.28	0.00
T_{20}	1.29	0.03	0.01	0.01	0.00	0.20	1.55	2.65	3.83	0.08

TABLE C.7: Spin-orbit couplings (in cm^{-1}) between singlet and triplet states for molecule **2** calculated at the TDDFT/PCM/CAM-B3LYP/def2-TZVP level of theory.

	S_0	S_1	S_2	S_3	S_4	S_5	S_6	S_7	S_8	S_9	S_{10}
T_1	0.85	0.01	13.54	1.07	1.06	0.00	0.00	0.13	0.00	0.29	10.93
T_2	0.02	0.25	0.39	0.00	0.00	0.92	0.01	11.33	2.07	0.00	0.80
T_3	2.57	0.00	11.05	0.55	0.13	0.00	0.00	1.48	0.00	0.64	7.13
T_4	4.61	13.65	0.00	1.49	2.15	5.07	5.61	0.16	2.73	1.22	5.42
T_5	0.02	0.82	3.61	0.00	0.00	0.24	0.12	1.42	0.71	0.01	1.46
T_6	1.35	0.00	7.86	0.32	0.07	0.00	0.00	2.45	0.01	0.06	0.19
T_7	1.21	0.00	5.97	0.84	0.54	0.00	0.01	0.57	0.00	0.46	0.62
T_8	0.00	1.19	0.33	0.00	0.01	0.11	0.30	8.95	0.13	0.00	1.88
T_9	51.01	2.17	0.08	11.68	4.26	1.33	1.47	0.00	0.70	2.94	0.04
T_{10}	1.25	0.00	0.44	1.04	1.22	0.00	0.00	1.01	0.00	0.49	1.04
T_{11}	0.66	0.01	9.00	0.58	0.21	0.00	0.00	1.32	0.00	0.08	2.44
T_{12}	0.01	0.18	0.64	0.00	0.00	0.11	0.09	2.05	0.08	0.00	0.92
T_{13}	0.00	0.41	0.48	0.00	0.00	1.00	0.20	1.00	0.45	0.00	0.23
T_{14}	13.93	11.69	5.15	5.01	0.80	8.73	3.07	0.01	2.05	0.33	0.00
T_{15}	0.32	0.00	6.38	0.78	0.85	0.01	0.00	2.41	0.01	0.47	6.16
T_{16}	12.87	0.12	0.04	1.34	2.03	0.47	0.29	0.78	0.38	5.57	0.22
T_{17}	0.02	0.09	0.19	0.00	0.00	0.43	0.83	5.20	0.16	0.00	0.21
T_{18}	0.04	0.23	0.65	0.00	0.01	0.16	0.08	3.33	0.17	0.01	2.67
T_{19}	56.44	4.64	1.66	6.02	5.17	5.44	1.78	0.01	1.64	2.34	0.09
T_{20}	0.10	0.96	0.77	0.00	0.00	0.49	0.26	2.61	0.96	0.00	0.64

	S_{11}	S_{12}	S_{13}	S_{14}	S_{15}	S_{16}	S_{17}	S_{18}	S_{19}	S_{20}
T_1	0.44	0.00	0.51	1.17	0.00	0.59	4.72	3.48	0.91	0.83
T_2	0.40	0.10	0.00	0.00	0.56	0.00	2.13	0.04	0.00	1.74
T_3	0.10	0.00	0.77	0.24	0.00	0.14	3.63	5.77	0.43	2.55
T_4	0.04	5.27	0.50	1.20	0.84	0.53	0.02	0.01	0.17	0.02
T_5	0.04	0.06	0.01	0.00	0.14	0.01	8.12	0.39	0.00	0.17
T_6	0.04	0.00	0.17	0.01	0.00	0.18	0.82	1.16	0.36	2.29
T_7	0.07	0.00	0.32	0.09	0.00	0.23	0.75	0.61	0.79	1.47
T_8	0.49	0.03	0.00	0.00	0.18	0.00	2.91	1.10	0.00	10.28
T_9	0.92	0.90	0.46	0.79	0.43	0.91	0.00	1.55	4.93	6.17
T_{10}	0.20	0.00	0.29	0.07	0.00	0.28	0.94	2.09	0.80	0.39
T_{11}	0.61	0.00	0.44	0.18	0.00	0.10	1.97	5.77	0.06	1.10
T_{12}	17.62	0.05	0.00	0.01	0.14	0.01	3.27	0.56	0.00	0.46
T_{13}	0.20	0.06	0.00	0.00	0.00	0.00	0.11	0.22	0.00	0.99
T_{14}	0.25	10.64	0.04	0.06	0.76	2.34	0.09	3.37	2.28	3.22
T_{15}	0.61	0.00	0.08	0.03	0.00	0.19	1.84	2.86	0.05	3.28
T_{16}	0.00	1.26	0.26	20.68	0.12	15.72	0.96	0.04	1.54	0.01
T_{17}	1.50	0.13	0.00	0.00	0.12	0.00	1.33	0.95	0.00	1.11
T_{18}	3.57	0.51	0.00	0.00	0.12	0.00	4.96	2.72	0.00	0.87
T_{19}	0.60	8.42	0.08	1.81	0.78	2.42	0.03	2.78	4.95	3.08
T_{20}	0.12	0.14	0.00	0.00	0.36	0.00	1.15	0.29	0.00	2.76

TABLE C.8: Spin-orbit couplings (in cm^{-1}) between singlet and triplet states for molecule **3** calculated at the TDDFT/PCM/CAM-B3LYP/def2-TZVP level of theory.

	S_0	S_1	S_2	S_3	S_4	S_5	S_6	S_7	S_8	S_9	S_{10}
T_1	2.75	0.02	0.19	0.01	0.00	7.69	0.30	0.51	0.57	0.01	0.02
T_2	0.07	0.01	0.01	0.68	0.85	0.26	0.01	11.02	0.02	1.50	0.94
T_3	2.68	0.01	0.76	0.01	0.01	9.23	0.73	0.46	0.21	0.01	0.03
T_4	0.87	0.02	0.49	0.01	0.01	0.78	0.49	1.10	0.51	0.01	0.01
T_5	0.04	0.29	0.00	0.28	0.33	3.12	0.01	2.66	0.01	0.19	0.51
T_6	5.13	2.63	1.23	9.74	3.79	0.01	1.56	0.15	0.80	8.62	8.84
T_7	0.43	0.03	0.55	0.01	0.01	9.28	0.24	2.17	0.49	0.01	0.02
T_8	0.02	0.01	0.01	0.76	0.07	0.62	0.00	8.07	0.00	0.11	0.18
T_9	44.32	0.36	11.68	0.50	1.53	0.33	4.99	0.01	0.89	2.38	1.12
T_{10}	0.63	0.01	0.79	0.01	0.02	14.63	0.25	1.73	0.33	0.02	0.02
T_{11}	0.06	0.77	0.01	0.06	0.43	1.81	0.01	1.31	0.01	0.20	0.01
T_{12}	0.04	0.39	0.01	0.11	0.48	0.31	0.02	0.18	0.01	0.04	0.01
T_{13}	1.53	0.01	0.65	0.01	0.01	3.42	0.09	1.72	0.46	0.01	0.01
T_{14}	0.02	0.49	0.01	0.63	0.66	0.37	0.02	5.16	0.02	0.43	0.08
T_{15}	20.48	0.67	3.12	11.22	8.66	4.86	1.80	0.03	1.69	4.32	5.20
T_{16}	0.56	0.03	0.06	0.01	0.01	4.79	1.20	1.36	0.16	0.02	0.04
T_{17}	13.24	0.32	2.66	0.44	0.35	0.04	1.69	1.53	5.04	0.15	0.39
T_{18}	0.07	0.17	0.01	0.45	0.05	1.01	0.01	0.88	0.00	0.24	0.06
T_{19}	0.08	0.35	0.01	0.74	0.60	0.42	0.01	2.35	0.01	0.23	0.19
T_{20}	0.81	0.00	0.77	0.03	0.00	6.93	0.47	0.59	0.35	0.04	0.02

	S_{11}	S_{12}	S_{13}	S_{14}	S_{15}	S_{16}	S_{17}	S_{18}	S_{19}	S_{20}
T_1	3.75	0.51	0.57	0.01	1.28	3.20	0.13	0.59	0.17	0.43
T_2	0.06	0.80	0.01	0.07	0.01	1.58	0.01	0.14	0.00	0.01
T_3	10.98	0.06	0.55	0.01	0.91	1.68	1.11	0.97	0.22	0.25
T_4	0.44	0.03	0.58	0.00	0.15	0.51	0.10	0.34	0.12	0.13
T_5	1.98	0.81	0.01	0.09	0.02	1.16	0.04	2.57	0.02	0.03
T_6	5.19	0.04	2.04	3.84	0.91	0.03	0.32	0.70	1.38	2.15
T_7	6.30	0.03	0.16	0.01	0.24	2.27	0.40	0.96	0.18	0.42
T_8	1.01	4.47	0.01	0.25	0.02	10.35	0.01	0.19	0.01	0.02
T_9	0.02	1.97	2.18	0.38	0.89	8.47	0.96	0.06	2.97	5.79
T_{10}	1.76	0.31	0.00	0.01	0.45	0.90	0.23	0.49	0.18	0.92
T_{11}	1.46	8.62	0.03	0.07	0.01	1.03	0.01	0.85	0.02	0.01
T_{12}	0.54	13.90	0.01	0.06	0.01	2.97	0.01	0.28	0.00	0.01
T_{13}	1.77	0.70	0.66	0.01	0.18	1.39	0.40	0.54	0.05	0.02
T_{14}	1.05	4.86	0.02	0.19	0.02	0.17	0.01	0.54	0.01	0.03
T_{15}	0.02	0.29	1.37	10.65	1.31	1.71	1.12	0.03	1.29	0.22
T_{16}	5.70	0.10	0.24	0.02	0.03	3.75	0.12	1.99	0.08	0.70
T_{17}	0.20	0.00	0.50	0.98	1.21	0.01	16.27	0.04	20.13	0.24
T_{18}	2.18	4.16	0.01	0.40	0.02	2.13	0.01	1.56	0.00	0.01
T_{19}	0.09	2.15	0.04	0.05	0.00	2.61	0.02	0.11	0.01	0.01
T_{20}	4.71	0.52	0.17	0.01	0.05	0.46	0.02	0.27	0.07	0.31

Bibliography

[1] Bernède, J. C. Organic Photovoltaic Cells: History, Principle and Techniques. *J. Chil. Chem. Soc.* **2008**, *53*, 1549–1564.

[2] Roes, A. L.; Alsema, E. A.; Blok, K.; Patel, M. K. Ex-ante environmental and economic evaluation of polymer photovoltaics. *Prog. Photovoltaics Res. Appl.* **2009**, *17*, 372–393.

[3] Clarke, T. M.; Durrant, J. R. Charge Photogeneration in Organic Solar Cells. *Chem. Rev.* **2010**, *110*, 6736–6767.

[4] Dou, L.; Liu, Y.; Hong, Z.; Li, G.; Yang, Y. Low-Bandgap Near-IR Conjugated Polymers/Molecules for Organic Electronics. *Chem. Rev.* **2015**, *115*, 12633–12665.

[5] Atkins, P.; de Paula, J. *Physical Chemistry*, 10th ed.; Oxford University Press, 2014.

[6] Runge, E.; Gross, E. K. U. Density-Functional Theory for Time-Dependent Systems. *Phys. Rev. Lett.* **1984**, *52*, 997–1000.

[7] Casida, M. E. In *Recent Advances in Density Functional Methods*; Chong, D. P., Ed.; Recent Advances in Computational Chemistry; World Scientific: Singapore, 1995; Chapter 5, pp 155–192.

[8] Dreuw, A.; Head-Gordon, M. Single-Reference ab Initio Methods for the Calculation of Excited States of Large Molecules. *Chem. Rev.* **2005**, *105*, 4009–4037.

[9] Crawford, T. D.; Schaefer III, H. F. An Introduction to Coupled Cluster Theory for Computational Chemists. *Rev. Comput. Chem.* **2000**, *14*, 33–136.

[10] Bartlett, R. J.; Musiał, M. Coupled-Cluster Theory in Quantum Chemistry. *Rev. Mod. Phys.* **2007**, *79*, 291–352.

[11] Shavitt, I.; Bartlett, R. J. *Many-Body Methods in Chemistry and Physics: MBPT and Coupled-Cluster Theory*; Cambridge University Press: Cambridge, 2009.

[12] Geertsen, J.; Rittby, M.; Bartlett, R. J. The Equation-of-Motion Coupled-Cluster Method: Excitation Energies of Be and CO. *Chem. Phys. Lett.* **1989**, *164*, 57–62.

[13] Stanton, J. F.; Bartlett, R. J. The equation of motion coupled-cluster method. A systematic biorthogonal approach to molecular excitation energies, transition probabilities, and excited state properties. *J. Chem. Phys.* **1993**, *98*, 7029–7039.

[14] Krylov, A. I. Equation-of-Motion Coupled-Cluster Methods for Open-Shell and Electronically Excited Species: The Hitchhiker's Guide to Fock Space. *Annu. Rev. Phys. Chem.* **2008**, *59*, 433–462.

[15] Bartlett, R. J. Coupled-cluster theory and its equation-of-motion extensions. *WIREs Comput. Mol. Sci.* **2012**, *2*, 126–138.

[16] Dalgaard, E.; Monkhorst, H. J. Some aspects of the time-dependent coupled-cluster approach to dynamic response functions. *Phys. Rev. A* **1983**, *28*, 1217–1222.

[17] Sekino, H.; Bartlett, R. J. A Linear Response, Coupled-Cluster Theory for Excitation Energy. *Int. J. Quantum Chem. Symp.* **1984**, *18*, 255–265.

[18] Koch, H.; Jørgensen, P. Coupled cluster response functions. *J. Chem. Phys.* **1990**, *93*, 3333–3344.

[19] Koch, H.; Jensen, H. J. A.; Jørgensen, P.; Helgaker, T. Excitation energies from the coupled cluster singles and doubles linear response function (CCSDLR). Applications to Be, CH^+, CO, and H_2O. *J. Chem. Phys.* **1990**, *93*, 3345–3350.

[20] Mertins, F.; Schirmer, J. Algebraic propagator approaches and intermediate-state representations. I. The biorthogonal and unitary coupled-cluster methods. *Phys. Rev. A* **1996**, *53*, 2140–2152.

[21] Schirmer, J.; Mertins, F. Review of biorthogonal coupled cluster representations for electronic excitation. *Theor. Chem. Acc.* **2010**, *125*, 145–172.

[22] Köhn, A.; Tajti, A. Can coupled-cluster theory treat conical intersections? *J. Chem. Phys.* **2007**, *127*, 044105.

[23] Yarkony, D. R. Nonadiabatic Quantum Chemistry—Past, Present, and Future. *Chem. Rev.* **2012**, *112*, 481–498.

[24] Szabo, A.; Ostlund, N. S. *Modern Quantum Chemistry: Introduction to Advanced Electronic Structure Theory*; Dover: Mineola, New York, 1996.

[25] Schirmer, J. Beyond the random-phase approximation: A new approximation scheme for the polarization propagator. *Phys. Rev. A* **1982**, *26*, 2395–2416.

[26] Trofimov, A. B.; Stelter, G.; Schirmer, J. A consistent third-order propagator method for electronic excitation. *J. Chem. Phys.* **1999**, *111*, 9982–9999.

[27] Dreuw, A.; Wormit, M. The algebraic diagrammatic construction scheme for the polarization propagator for the calculation of excited states. *WIREs Comput. Mol. Sci.* **2015**, *5*, 82–95.

[28] Schirmer, J. *Many-Body Methods for Atoms, Molecules and Clusters*; Springer International Publishing, 2018.

[29] Schirmer, J. Closed-form intermediate representations of many-body propagators and resolvent matrices. *Phys. Rev. A* **1991**, *43*, 4647–4659.

[30] Schirmer, J.; Trofimov, A. B. Intermediate state representation approach to physical properties of electronically excited molecules. *J. Chem. Phys.* **2004**, *120*, 11449–11464.

[31] Schirmer, J.; Mertins, F. Size consistency of an algebraic propagator approach. *Int. J. Quantum Chem.* **1996**, *58*, 329–339.

[32] Møller, C.; Plesset, M. S. Note on an Approximation and Treatment for Many-Electron and Systems. *Phys. Rev.* **1934**, *46*, 618–622.

[33] Helgaker, T.; Jørgensen, P.; Olsen, J. *Molecular Electronic-Structure Theory*; John Wiley & Sons, Ltd., 2000.

[34] Bartlett, R. J.; Noga, J. The expectation value coupled-cluster method and analytical energy derivatives. *Chem. Phys. Lett.* **1988**, *150*, 29–36.

[35] Szalay, P. G.; Nooijen, M.; Bartlett, R. J. Alternative ansätze in coupled-cluster theory. III. A critical analysis of different methods. *J. Chem. Phys.* **1995**, *103*, 281–298.

[36] Van Voorhis, T.; Head-Gordon, M. Benchmark variational coupled cluster doubles results. *J. Chem. Phys.* **2000**, *113*, 8873–8879.

[37] Bartlett, R. J.; Kucharski, S. A.; Noga, J. Alternative coupled-cluster ansätze II. The unitary coupled-cluster method. *Chem. Phys. Lett.* **1989**, *155*, 133–140.

[38] Kutzelnigg, W. Error analysis and improvements of coupled-cluster theory. *Theor. Chim. Acta* **1991**, *80*, 349–386.

[39] Taube, A. G.; Bartlett, R. J. New perspectives on unitary coupled-cluster theory. *Int. J. Quantum Chem.* **2006**, *106*, 3393–3401.

[40] Pal, S.; Prasad, M. D.; Mukherjee, D. On certain correspondences among various coupled-cluster theories for closed-shell systems. *Pramana* **1982**, *18*, 261–270.

[41] Jeziorski, B.; Moszynski, R. Explicitly connected expansion for the average value of an observable in the coupled-cluster theory. *Int. J. Quantum Chem.* **1993**, *48*, 161–183.

[42] Cooper, B.; Knowles, P. J. Benchmark studies of variational, unitary and extended coupled cluster methods. *J. Chem. Phys.* **2010**, *133*, 234102.

[43] Moszynski, R.; Żuchowski, P. S.; Jeziorski, B. Time-Independent Coupled-Cluster Theory of the Polarization Propagator. *Collect. Czech. Chem. Commun.* **2005**, *70*, 1109–1132.

[44] Korona, T.; Jeziorski, B. One-electron properties and electrostatic interaction energies from the expectation value expression and wave function of singles and doubles coupled cluster theory. *J. Chem. Phys.* **2006**, *125*, 184109.

[45] Korona, T.; Przybytek, M.; Jeziorski, B. Time-independent coupled cluster theory of the polarization propagator. Implementation and application of the singles and doubles model to dynamic polarizabilities and van der Waals constants. *Mol. Phys.* **2006**, *104*, 2303–2316.

[46] Korona, T. XCC2—a new coupled cluster model for the second-order polarization propagator. *Phys. Chem. Chem. Phys.* **2010**, *12*, 14977–14984.

[47] Robinson, J. B.; Knowles, P. J. Application of the quasi-variational coupled cluster method to the nonlinear optical properties of model hydrogen systems. *J. Chem. Phys.* **2012**, *137*, 054301.

[48] Harsha, G.; Shiozaki, T.; Scuseria, G. E. On the difference between variational and unitary coupled cluster theories. *J. Chem. Phys.* **2018**, *148*, 044107.

[49] Kats, D.; Usvyat, D.; Schütz, M. Second-order variational coupled-cluster linear-response method: A Hermitian time-dependent theory. *Phys. Rev. A* **2011**, *83*, 062503.

[50] Wälz, G.; Kats, D.; Usvyat, D.; Korona, T.; Schütz, M. Application of Hermitian time-dependent coupled-cluster response Ansätze of second order to excitation energies and frequency-dependent dipole polarizabilities. *Phys. Rev. A* **2012**, *86*, 052519.

[51] Liu, J.; Asthana, A.; Cheng, L.; Mukherjee, D. Unitary coupled-cluster based self-consistent polarization propagator theory: A third-order formulation and pilot applications. *J. Chem. Phys.* **2018**, *148*, 244110.

[52] Wormit, M.; Rehn, D. R.; Harbach, P. H. P.; Wenzel, J.; Krauter, C. M.; Epifanovsky, E.; Dreuw, A. Investigating excited electronic states using the algebraic diagrammatic construction (ADC) approach of the polarisation propagator. *Mol. Phys.* **2014**, *112*, 774–784.

[53] Shao, Y.; Gan, Z.; Epifanovsky, E.; Gilbert, A. T.; Wormit, M.; Kussmann, J.; Lange, A. W.; Behn, A.; Deng, J.; Feng, X.; Ghosh, D.; Goldey, M.; Horn, P. R.; Jacobson, L. D.; Kaliman, I.; Khaliullin, R. Z.; Kuś, T.; Landau, A.; Liu, J.; Proynov, E. I.; Rhee, Y. M.; Richard, R. M.; Rohrdanz, M. A.; Steele, R. P.; Sundstrom, E. J.; Woodcock III, H. L.; Zimmerman, P. M.; Zuev, D.; Albrecht, B.; Alguire, E.; Austin, B.; Beran, G. J. O.; Bernard, Y. A.; Berquist, E.; Brandhorst, K.; Bravaya, K. B.; Brown, S. T.; Casanova, D.; Chang, C.-M.; Chen, Y.; Chien, S. H.; Closser, K. D.; Crittenden, D. L.; Diedenhofen, M.; DiStasio Jr., R. A.; Do, H.; Dutoi, A. D.; Edgar, R. G.; Fatehi, S.; Fusti-Molnar, L.; Ghysels, A.; Golubeva-Zadorozhnaya, A.; Gomes, J.; Hanson-Heine, M. W.; Harbach, P. H.; Hauser, A. W.; Hohenstein, E. G.; Holden, Z. C.; Jagau, T.-C.; Ji, H.; Kaduk, B.; Khistyaev, K.; Kim, J.; Kim, J.; King, R. A.; Klunzinger, P.; Kosenkov, D.; Kowalczyk, T.; Krauter, C. M.; Lao, K. U.; Laurent, A. D.; Lawler, K. V.; Levchenko, S. V.; Lin, C. Y.; Liu, F.; Livshits, E.; Lochan, R. C.; Luenser, A.; Manohar, P.; Manzer, S. F.; Mao, S.-P.; Mardirossian, N.; Marenich, A. V.; Maurer, S. A.; Mayhall, N. J.; Neuscamman, E.; Oana, C. M.; Olivares-Amaya, R.; O'Neill, D. P.; Parkhill, J. A.; Perrine, T. M.; Peverati, R.; Prociuk, A.; Rehn, D. R.; Rosta, E.; Russ, N. J.; Sharada, S. M.; Sharma, S.; Small, D. W.; Sodt, A.; Stein, T.; Stück, D.; Su, Y.-C.; Thom, A. J.; Tsuchimochi, T.; Vanovschi, V.; Vogt, L.; Vydrov, O.; Wang, T.; Watson, M. A.; Wenzel, J.; White, A.; Williams, C. F.; Yang, J.; Yeganeh, S.; Yost, S. R.; You, Z.-Q.; Zhang, I. Y.; Zhang, X.; Zhao, Y.; Brooks, B. R.; Chan, G. K.; Chipman, D. M.; Cramer, C. J.; Goddard III, W. A.; Gordon, M. S.; Hehre, W. J.; Klamt, A.; Schaefer III, H. F.; Schmidt, M. W.; Sherrill, C. D.; Truhlar, D. G.; Warshel, A.; Xu, X.; Aspuru-Guzik, A.; Baer, R.; Bell, A. T.; Besley, N. A.; Chai, J.-D.; Dreuw, A.; Dunietz, B. D.; Furlani, T. R.; Gwaltney, S. R.; Hsu, C.-P.; Jung, Y.; Kong, J.; Lambrecht, D. S.; Liang, W.;

Ochsenfeld, C.; Rassolov, V. A.; Slipchenko, L. V.; Subotnik, J. E.; Voorhis, T. V.; Herbert, J. M.; Krylov, A. I.; Gill, P. M.; Head-Gordon, M. Advances in molecular quantum chemistry contained in the Q-Chem 4 program package. *Mol. Phys.* **2015**, *113*, 184–215.

[54] Geertsen, J.; Oddershede, J. A coupled cluster polarization propagator method applied to CH^+. *J. Chem. Phys.* **1986**, *85*, 2112–2118.

[55] Geertsen, J.; Eriksen, S.; Oddershede, J. Some Aspects of the Coupled Cluster Based Polarization Propagator Method. *Adv. Quantum Chem.* **1991**, *22*, 167–209.

[56] Sauer, S. P. A. Second-order polarization propagator approximation with coupled-cluster singles and doubles amplitudes—SOPPA(CCSD): the polarizability and hyperpolarizability of Li^-. *J. Phys. B: At., Mol. Opt. Phys.* **1997**, *30*, 3773–3780.

[57] Jensen, F. *Introduction to Computational Chemistry*, 2nd ed.; John Wiley & Sons: USA, 2006.

[58] Schrödinger, E. Quantisierung als Eigenwertproblem (Erste Mitteilung). *Ann. Phys.* **1926**, *384*, 361–376.

[59] Schrödinger, E. Quantisierung als Eigenwertproblem (Zweite Mitteilung). *Ann. Phys.* **1926**, *384*, 489–527.

[60] Schrödinger, E. Quantisierung als Eigenwertproblem (Dritte Mitteilung). *Ann. Phys.* **1926**, *385*, 437–490.

[61] Schrödinger, E. Quantisierung als Eigenwertproblem (Vierte Mitteilung). *Ann. Phys.* **1926**, *386*, 109–139.

[62] Born, M.; Oppenheimer, J. R. Zur Quantentheorie der Molekeln. *Ann. Phys.* **1927**, *389*, 457–484.

[63] Wick, G.-C. The Evaluation of the Collision Matrix. *Phys. Rev.* **1950**, *80*, 268–272.

[64] Fetter, A. L.; Walecka, J. D. *Quantum Theory of Many-Particle Systems*; McGraw-Hill, 1971.

[65] Koopmans, T. Über die Zuordnung von Wellenfunktionen und Eigenwerten zu den Einzelnen Elektronen Eines Atoms. *Physica* **1934**, *1*, 104–113.

[66] Löwdin, P.-O. Quantum Theory of Many-Particle Systems. III. Extension of the Hartree-Fock Scheme to Include Degenerate Systems and Correlation Effects. *Phys. Rev.* **1955**, *97*, 1509–1520.

[67] Sherrill, C. D.; Schaefer, H. F. The Configuration Interaction Method: Advances in Highly Correlated Approaches. *Adv. Quantum Chem.* **1999**, *34*, 143–269.

[68] Pople, J. A.; Binkley, J. S.; Seeger, R. Theoretical models incorporating electron correlation. *Int. J. Quantum Chem. Symp.* **1976**, *10*, 1–19.

[69] Foresman, J. B.; Head-Gordon, M.; Pople, J. A. Toward a Systematic Molecular Orbital Theory for Excited States. *J. Phys. Chem.* **1992**, *96*, 135–149.

[70] Bartlett, R. J. Many-Body Perturbation Theory and Coupled Cluster Theory for Electron Correlation in Molecules. *Ann. Rev. Phys. Chem.* **1981**, *32*, 359–401.

[71] Parr, R. G.; Yang, W. *Density-Functional Theory of Atoms and Molecules*; Oxford University Press, USA, 1994.

[72] Koch, W.; Holthausen, M. C. *A Chemist's Guide to Density Functional Theory*, 2nd ed.; Wiley-VCH: Weinheim, New York, 2001.

[73] Hohenberg, P.; Kohn, W. Inhomogeneous Electron Gas. *Phys. Rev. B* **1964**, *136*, 864–871.

[74] Kohn, W.; Sham, L. J. Self-Consistent Equations Including Exchange and Correlation Effects. *Phys. Rev. A* **1965**, *140*, 1133–1138.

[75] Scuseria, G. E.; Staroverov, V. N. Progress in the development of exchange-correlation functionals. Theory and Application of Computational Chemistry: The First 40 Years. Amsterdam, 2005; pp 669–724.

[76] Staroverov, V. N. In *A Matter of Density*; Sukumar, N., Ed.; Wiley-Blackwell, 2012; Chapter 6, pp 125–156.

[77] Levine, I. N. *Quantum Chemistry*, 7th ed.; Pearson Education, 2013.

[78] Bartlett, R. J.; Stanton, J. F. Applications of Post-Hartree–Fock Methods: A Tutorial. *Rev. Comput. Chem.* **1994**, *5*, 65–169.

[79] Oddershede, J. Polarization Propagator Calculations. *Adv. Quantum Chem.* **1978**, *11*, 275–352.

[80] Oddershede, J.; Jørgensen, P.; Yeager, D. L. Polarization Propagator Methods in Atomic and Molecular Calculations. *Comput. Phys. Rep.* **1984**, *2*, 33–92.

[81] Oddershede, J. Propagator Methods. *Adv. Chem. Phys.* **1987**, *69*, 201–239.

[82] Schirmer, J.; Cederbaum, L. S.; Walter, O. New approach to the one-particle Green's function for finite Fermi systems. *Phys. Rev. A* **1983**, *28*, 1237–1259.

[83] Ortiz, J. V. Electron propagator theory: an approach to prediction and interpretation in quantum chemistry. *WIREs Comput. Mol. Sci.* **2013**, *3*, 123–142.

[84] Trofimov, A. B.; Schirmer, J. An efficient polarization propagator approach to valence electron excitation spectra. *J. Phys. B: At., Mol. Opt. Phys.* **1995**, *28*, 2299–2324.

[85] Trofimov, A. B.; Schirmer, J. Polarization Propagator Study of Electronic Excitation in Key Heterocyclic Molecules. I. Pyrrole. *Chem. Phys.* **1997**, *214*, 153–170.

[86] Trofimov, A. B.; Schirmer, J. Polarization Propagator Study of Electronic Excitation in Key Heterocyclic Molecules. II. Furan. *Chem. Phys.* **1997**, *224*, 175–190.

[87] Niessen, W. v.; Schirmer, J.; Cederbaum, L. S. Computational Methods for the One-Particle Green's Function. *Comput. Phys. Rep.* **1984**, *1*, 57–125.

[88] Schirmer, J.; Angonoa, G. On Green's function calculations of the static self-energy part, the ground state energy and expectation values. *J. Chem. Phys.* **1989**, *91*, 1754–1761.

[89] Schirmer, J.; Trofimov, A. B.; Stelter, G. A non-Dyson third-order approximation scheme for the electron propagator. *J. Chem. Phys.* **1998**, *109*, 4734–4744.

[90] Trofimov, A. B.; Schirmer, J. Molecular ionization energies and ground- and ionic-state properties using a non-Dyson electron propagator approach. *J. Chem. Phys.* **2005**, *123*, 144115.

[91] Mertins, F.; Schirmer, J.; Tarantelli, A. Algebraic propagator approaches and intermediate-state representations. II. The equation-of-motion methods for N, $N \pm 1$, and $N \pm 2$ electrons. *Phys. Rev. A* **1996**, *53*, 2153–2168.

[92] Prasad, M. D.; Pal, S.; Mukherjee, D. Some aspects of self-consistent propagator theories. *Phys. Rev. A* **1985**, *31*, 1287–1298.

[93] Mukherjee, D.; Kutzelnigg, W. An Effective Liouvillean Formalism for Propagators in Fock Space: Connection with Effective Hamiltonian Approach for Energy Differences. Many-Body Methods in Quantum Chemistry. Springer Berlin, Heidelberg, 1989; pp 257–274.

[94] Rehn, D. R. Development of Quantum-Chemical Methods for Excited-State and Response Properties. Ph.D. thesis, Universität Heidelberg, 2015.

[95] Amos, R. D. Corrections to molecular one-electron properties using Møller-Plesset perturbation theory. *Chem. Phys. Lett.* **1980**, *73*, 602–606.

[96] Trucks, G. W.; Salter, E.; Sosa, C.; Bartlett, R. J. Theory and implementation of the MBPT density matrix. An application to one-electron properties. *Chem. Phys. Lett.* **1988**, *147*, 359 – 366.

[97] Wenzel, J. Development and Implementation of Theoretical Methods for the Description of Electronically Core-Excited States. Ph.D. thesis, Universität Heidelberg, 2016.

[98] Bartlett, R. J. In *Modern Electronic Structure Theory*; Yarkony, D. R., Ed.; World Scientific Publishing Company, 1995; Chapter 16, pp 1047–1131.

[99] Bartlett, R. J. The coupled-cluster revolution. *Mol. Phys.* **2010**, *108*, 2905–2920.

[100] Salter, E. A.; Trucks, G. W.; Bartlett, R. J. Analytic energy derivatives in many-body methods. I. First derivatives. *J. Chem. Phys.* **1989**, *90*, 1752–1766.

[101] Perera, S. A.; Watts, J. D.; Bartlett, R. J. A theoretical study of hyperfine coupling constants. *J. Chem. Phys.* **1994**, *100*, 1425–1434.

[102] Kucharski, S. A.; Bartlett, R. J. Fifth-Order Many-Body Perturbation Theory and Its Relationship to Various Coupled-Cluster Approaches. *Adv. Quantum Chem.* **1986**, *18*, 281–344.

[103] Goldstone, J. Derivation of the Brueckner many-body theory. *Proc. Roy. Soc. A* **1957**, *239*, 267–279.

[104] Bartlett, R. J.; Shavitt, I.; Purvis, G. D. The quartic force field of H_2O determined by many-body methods that include quadruple excitation effects. *J. Chem. Phys.* **1979**, *71*, 281–291.

[105] Bartlett, R. J.; Purvis, G. D. Many-Body Perturbation Theory, Coupled-Pair Many-Electron Theory, and the Importance of Quadruple Excitations for the Correlation Problem. *Int. J. Quantum Chem.* **1978**, *14*, 561–581.

[106] Koch, H.; Kobayashi, R.; Sanchez de Merás, A.; Jørgensen, P. Calculation of size-intensive transition moments from the coupled cluster singles and doubles linear response function. *J. Chem. Phys.* **1994**, *100*, 4393–4400.

[107] Nooijen, M.; Snijders, J. G. Coupled cluster approach to the single-particle Green's function. *Int. J. Quantum Chem. Symp.* **1992**, *44*, 55–83.

[108] Stanton, J. F.; Gauss, J. Analytic energy derivatives for ionized states described by the equation-of-motion coupled cluster method. *J. Chem. Phys.* **1994**, *101*, 8938–8944.

[109] Stanton, J. F.; Gauss, J. A simple scheme for the direct calculation of ionization potentials with coupled-cluster theory that exploits established excitation energy methods. *J. Chem. Phys.* **1999**, *111*, 8785–8788.

[110] Musiał, M.; Kucharski, S. A.; Bartlett, R. J. Equation-of-motion coupled cluster method with full inclusion of the connected triple excitations for ionized states: IP-EOM-CCSDT. *J. Chem. Phys.* **2003**, *118*, 1128–1136.

[111] Manohar, P. U.; Stanton, J. F.; Krylov, A. I. Perturbative triples correction for the equation-of-motion coupled-cluster wave functions with single and double substitutions for ionized states: Theory, implementation, and examples. *J. Chem. Phys.* **2009**, *131*, 114112.

[112] Nooijen, M.; Bartlett, R. J. Equation of motion coupled cluster method for electron attachment. *J. Chem. Phys.* **1995**, *102*, 3629–3647.

[113] Nakatsuji, H.; Hirao, K. Cluster Expansion of the Wavefunction. Pseudo-Orbital Theory Applied to Spin Correlation. *Chem. Phys. Lett.* **1977**, *47*, 569–571.

[114] Nakatsuji, H. Cluster Expansion of the Wavefunction. Electron Correlations in Ground and Excited States by SAC (Symmetry-Adapted-Cluster) and SAC CI Theories. *Chem. Phys. Lett.* **1979**, *67*, 329–333.

[115] Nakatsuji, H. Cluster Expansion of the Wavefunction. Calculation of Electron Correlations in Ground and Excited States by SAC (Symmetry-Adapted-Cluster) and SAC CI Theories. *Chem. Phys. Lett.* **1979**, *67*, 334–342.

[116] Szalay, P. G.; Bartlett, R. J. Alternative ansätze in coupled-cluster theory. IV. Comparison for the two electron problem and the role of exclusion principle violating (EPV) terms. *Int. J. Quantum Chem.* **1992**, *44*, 85–106.

[117] Bartlett, R. J.; Kucharski, S. A.; Noga, J.; Watts, J. D.; Trucks, G. W. Some Consideration of Alternative Ansätze in Coupled-Cluster Theory. Many-Body Methods in Quantum Chemistry. Berlin, Heidelberg, 1989; pp 125–149.

[118] Čížek, J. On the Correlation Problem in Atomic and Molecular Systems. Calculation of Wavefunction Components in Ursell-Type Expansion Using Quantum-Field Theoretical Methods. *J. Chem. Phys.* **1966**, *45*, 4256–4266.

[119] Čížek, J. On the Use of the Cluster Expansion and the Technique of Diagrams in Calculations of Correlation Effects in Atoms and Molecules. *Adv. Chem. Phys.* **1969**, *14*, 35–89.

[120] Bartlett, R. J.; Watts, J. D.; Kucharski, S. A.; Noga, J. Non-iterative fifth-order triple and quadruple excitation energy corrections in correlated methods. *Chem. Phys. Lett.* **1990**, *165*, 513–522.

[121] Arponen, J. Variational principles and linked-cluster exp S expansions for static and dynamic many-body problems. *Ann. Phys.* **1983**, *151*, 311–382.

[122] Arponen, J. S.; Bishop, R. F.; Pajanne, E. Extended coupled-cluster method. I. Generalized coherent bosonization as a mapping of quantum theory into classical Hamiltonian mechanics. *Phys. Rev. A* **1987**, *36*, 2519–2538.

[123] Arponen, J. S.; Bishop, R. F.; Pajanne, E. Extended coupled-cluster method. II. Excited states and generalized random-phase approximation. *Phys. Rev. A* **1987**, *36*, 2539–2549.

[124] Arponen, J.; Bishop, R. F.; Pajanne, E.; Robinson, N. I. Extended coupled-cluster method. III. Zero-temperature hydrodynamics of a condensed Bose fluid. *Phys. Rev. A* **1988**, *37*, 1065–1086.

[125] Robinson, N. I.; Bishop, R. F.; Arponen, J. Extended coupled-cluster method. IV. An excitation energy functional and applications to the Lipkin model. *Phys. Rev. A* **1989**, *40*, 4256–4276.

[126] Bishop, R. F.; Arponen, J. S. Correlations in extended systems: A microscopic multilocal method for describing both local and global properties. *Int. J. Quantum Chem. Symp.* **1990**, *24*, 197–211.

[127] Arponen, J.; Bishop, R. Independent-cluster parametrizations of wave functions in model field theories. I. Introduction to their holomorphic representations. *Ann. Phys.* **1991**, *207*, 171–217.

[128] Kutzelnigg, W. In *Methods of Electronic Structure Theory*; Schaefer, H. F., Ed.; Springer US: Boston, MA, 1977; pp 129–188.

[129] Koch, S.; Kutzelnigg, W. Comparison of CEPA and CP-MET methods. *Theor. Chim. Acta* **1981**, *59*, 387–411.

[130] Kutzelnigg, W. Quantum chemistry in Fock space. I. The universal wave and energy operators. *J. Chem. Phys.* **1982**, *77*, 3081–3097.

[131] Kutzelnigg, W.; Koch, S. Quantum chemistry in Fock space. II. Effective Hamiltonians in Fock space. *J. Chem. Phys.* **1983**, *79*, 4315–4335.

[132] Kutzelnigg, W. Quantum chemistry in Fock space. III. Particle-hole formalism. *J. Chem. Phys.* **1984**, *80*, 822–830.

[133] Pal, S.; Durga Prasad, M.; Mukherjee, D. Use of a size-consistent energy functional in many electron theory for closed shells. *Theor. Chim. Acta* **1983**, *62*, 523–536.

[134] Pal, S.; Prasad, M. D.; Mukherjee, D. Development of a size-consistent energy functional for open shell states. *Theor. Chim. Acta* **1984**, *66*, 311–332.

[135] Tanaka, K.; Terashima, H. A cluster expansion theory with multireference functions using the unitary ansatz. *Chem. Phys. Lett.* **1984**, *106*, 558–562.

[136] Hoffmann, M. R.; Simons, J. Analytical energy gradients for a unitary coupled-cluster theory. *Chem. Phys. Lett.* **1987**, *142*, 451–454.

[137] Hoffmann, M. R.; Simons, J. A unitary multiconfigurational coupled-cluster method: Theory and applications. *J. Chem. Phys.* **1988**, *88*, 993–1002.

[138] Watts, J. D.; Trucks, G. W.; Bartlett, R. J. Coupled-cluster, unitary coupled-cluster and MBPT(4) open-shell analytical gradient methods. *Chem. Phys. Lett.* **1989**, *164*, 502–508.

[139] Nooijen, M.; Bartlett, R. J. A new method for excited states: Similarity transformed equation-of-motion coupled-cluster theory. *J. Chem. Phys.* **1997**, *106*, 6441–6448.

[140] Nooijen, M.; Bartlett, R. J. Similarity transformed equation-of-motion coupled-cluster study of ionized, electron attached, and excited states of free base porphin. *J. Chem. Phys.* **1997**, *106*, 6449–6455.

[141] Nooijen, M.; Bartlett, R. J. Similarity transformed equation-of-motion coupled-cluster theory: Details, examples, and comparisons. *J. Chem. Phys.* **1997**, *107*, 6812–6830.

[142] Nooijen, M. Similarity transformed equation of motion coupled-cluster study of excited states of selected azabenzenes. *Spectrochim. Acta, Part A* **1999**, *55*, 539–559.

[143] Sous, J.; Goel, P.; Nooijen, M. Similarity transformed equation of motion coupled cluster theory revisited: a benchmark study of valence excited states. *Mol. Phys.* **2014**, *112*, 616–638.

[144] Piecuch, P.; Bartlett, R. J. EOMXCC: A New Coupled-Cluster Method for Electronic Excited States. *Adv. Quantum Chem.* **1999**, *34*, 295–380.

[145] Helgaker, T.; Coriani, S.; Jørgensen, P.; Kristensen, K.; Olsen, J.; Ruud, K. Recent Advances in Wave Function-Based Methods of Molecular-Property Calculations. *Chem. Rev.* **2012**, *112*, 543–631.

[146] Hellmann, H. *Einführung in die Quantenchemie*; Deuticke: Leipzig, 1937.

[147] Feynman, R. P. Forces in Molecules. *Phys. Rev.* **1939**, *56*, 340–343.

[148] Taube, A. G.; Bartlett, R. J. Rethinking linearized coupled-cluster theory. *J. Chem. Phys.* **2009**, *130*, 144112.

[149] Bartlett, R. J.; Musiał, M.; Lotrich, V.; Kuś, T. In *Recent Progress in Coupled Cluster Methods: Theory and Applications*; Cársky, P., Paldus, J., Pittner, J., Eds.; Springer Netherlands: Dordrecht, 2010; Chapter 1, pp 1–36.

[150] Rishi, V.; Perera, A.; Bartlett, R. J. Behind the success of modified coupled-cluster methods: addition by subtraction. *Mol. Phys.* **2019**, *117*, 2201–2216.

[151] Bartlett, R. J.; Shavitt, I. Comparison of high-order many-body perturbation theory and configuration interaction for H_2O. *Chem. Phys. Lett.* **1977**, *50*, 190–198.

[152] Ahlrichs, R. Many body perturbation calculations and coupled electron pair models. *Comput. Phys. Commun.* **1979**, *17*, 31–45.

[153] Krishnan, R.; Pople, J. A. Approximate fourth-order perturbation theory of the electron correlation energy. *Int. J. Quantum Chem.* **1978**, *14*, 91–100.

[154] Krishnan, R.; Frisch, M. J.; Pople, J. A. Contribution of triple substitutions to the electron correlation energy in fourth order perturbation theory. *J. Chem. Phys.* **1980**, *72*, 4244–4245.

[155] Atkins, P.; Friedman, R. *Molecular Quantum Mechanics*; OUP Oxford, 2011.

[156] Geertsen, J.; Oddershede, J.; Scuseria, G. E. Calculation of Spectra and Spin-Spin Coupling Constants Using a Coupled-Cluster Polarization Propagator Method. *Int. J. Quantum Chem. Symp.* **1987**, *21*, 475–485.

[157] Geertsen, J. Nuclear Spin-Spin Coupling Constants in a Coupled-Cluster Polarization Propagator Approach. *Chem. Phys. Lett.* **1987**, *134*, 400–402.

[158] Sauer, S. P. A.; Paidarová, I. Calculations of magnetic hyperfine structure constants for the low-lying rovibrational levels of LiH, HF, CH^+, and BH. *Chem. Phys.* **1995**, *201*, 405–425.

[159] Canuto, S.; Duch, W.; Geertsen, J.; Müller-Plathe, F.; Oddershede, J.; Scuseria, G. E. The Dipole Polarizability of Li^-. *Chem. Phys. Lett.* **1988**, *147*, 435–442.

[160] Scuseria, G. E.; Geertsen, J.; Oddershede, J. Electronic spectra and response properties of BH and AlH. *J. Chem. Phys.* **1989**, *90*, 2338–2343.

[161] Sauer, S. P. A.; Oddershede, J.; Geertsen, J. Correlated calculations of the rotational g-tensor and origin independent magnetizability surface of BH. *Mol. Phys.* **1992**, *76*, 445–465.

[162] Sauer, S. P. A.; Enevoldsen, T.; Oddershede, J. Paramagnetism of closed shell diatomic hydrides with six valence electrons. *J. Chem. Phys.* **1993**, *98*, 9748–9757.

[163] Sauer, S. P. A.; Oddershede, J. Correlated Polarization Propagator Calculations of Static Polarizabilities. *Int. J. Quantum Chem.* **1994**, *50*, 317–332.

[164] Sauer, S. P. A.; Ogilvie, J. F. Experimental and Theoretical Estimates of the Rotational g Factor of AlH in the Electronic Ground State $X^1\Sigma^+$. *J. Phys. Chem.* **1994**, *98*, 8617–8621.

[165] Geertsen, J. An Approximate Coupled Cluster Doubles Polarization Propagator Approximation. *Int. J. Quantum Chem. Symp.* **1988**, *22*, 491–495.

[166] Koch, H.; Christiansen, O.; Jørgensen, P.; Olsen, J. Excitation energies of BH, CH_2 and Ne in full configuration Interaction and the Hierarchy CCS, CC2, CCSD and CC3 of coupled cluster models. *Chem. Phys. Lett.* **1995**, *244*, 75–82.

[167] Christiansen, O.; Koch, H.; Jørgensen, P.; Olsen, J. Excitation energies of H_2O, N_2 and C_2 in full configuration Interaction and coupled cluster theory. *Chem. Phys. Lett.* **1996**, *256*, 185–194.

[168] Larsen, H.; Hald, K.; Olsen, J.; Jørgensen, P. Triplet excitation energies in full configuration interaction and coupled-cluster theory. *J. Chem. Phys.* **2001**, *115*, 3015–3020.

[169] Hald, K.; Hättig, C.; Olsen, J.; Jørgensen, P. CC3 triplet excitation energies using an explicit spin coupled excitation space. *J. Chem. Phys.* **2001**, *115*, 3545–3552.

[170] Trofimov, A. B.; Stelter, G.; Schirmer, J. Electron excitation energies using a consistent third-order propagator approach: Comparison with full configuration interaction and coupled cluster results. *J. Chem. Phys.* **2002**, *117*, 6402–6410.

[171] Dunning, T. H. Gaussian basis sets for use in correlated molecular calculations. I. The atoms boron through neon and hydrogen. *J. Chem. Phys.* **1989**, *90*, 1007–1023.

[172] Loos, P.-F.; Scemama, A.; Blondel, A.; Garniron, Y.; Caffarel, M.; Jacquemin, D. A Mountaineering Strategy to Excited States: Highly Accurate Reference Energies and Benchmarks. *J. Chem. Theory Comput.* **2018**, *14*, 4360–4379.

[173] Kendall, R. A.; Dunning Jr., T. H.; Harrison, R. J. Electron affinities of the first-row atoms revisited. Systematic basis sets and wave functions. *J. Chem. Phys.* **1992**, *96*, 6796–6806.

[174] Woon, D. E.; Dunning Jr., T. H. Gaussian basis sets for use in correlated molecular calculations. III. The atoms aluminum through argon. *J. Chem. Phys.* **1993**, *98*, 1358–1371.

[175] Head-Gordon, M.; Rico, R. J.; Oumi, M.; Lee, T. J. A doubles correction to electronic excited states from configuration interaction in the space of single substitutions. *Chem. Phys. Lett.* **1994**, *219*, 21–29.

[176] Head-Gordon, M.; Maurice, D.; Oumi, M. A perturbative correction to restricted open shell configuration interaction with single substitutions for excited states of radicals. *Chem. Phys. Lett.* **1995**, *246*, 114–121.

[177] Head-Gordon, M.; Oumi, M.; Maurice, D. Quasidegenerate second-order perturbation corrections to single-excitation configuration interaction. *Mol. Phys.* **1999**, *96*, 593–602.

[178] Christiansen, O.; Koch, H.; Jørgensen, P. The second-order approximate coupled cluster singles and doubles model CC2. *Chem. Phys. Lett.* **1995**, *243*, 409–418.

[179] Schreiber, M.; Silva-Junior, M. R.; Sauer, S. P. A.; Thiel, W. Benchmarks for electronically excited states: CASPT2, CC2, CCSD, and CC3. *J. Chem. Phys.* **2008**, *128*, 134110.

[180] Silva-Junior, M. R.; Schreiber, M.; Sauer, S. P. A.; Thiel, W. Benchmarks for electronically excited states: Time-dependent density functional theory and density functional theory based multireference configuration interaction. *J. Chem. Phys.* **2008**, *129*, 104103.

[181] Silva-Junior, M. R.; Schreiber, M.; Sauer, S. P. A.; Thiel, W. Benchmarks of electronically excited states: Basis set effects on CASPT2 results. *J. Chem. Phys.* **2010**, *133*, 174318.

[182] Thunemann, K.-H.; Peyerimhoff, S. D.; Buenker, R. J. Configuration interaction calculations for the ground and excited states of ozone and its positive ion: Energy locations and transition probabilities. *J. Mol. Spectrosc.* **1978**, *70*, 432–448.

[183] Nordfors, D.; Ågren, H.; Jensen, H. J. A. MCSCF/MCLR Studies of potential energy surfaces, spectra, and properties of the X^1A_1 and a^3B_2 states of ozone. *Int. J. Quantum Chem.* **1991**, *40*, 475–490.

[184] Barysz, M.; Rittby, M.; Bartlett, R. J. Fock space multi-reference coupled-cluster study of excitation energies and dipole oscillator strengths of ozone. *Chem. Phys. Lett.* **1992**, *193*, 373–379.

[185] Tsuneda, T.; Nakano, H.; Hirao, K. Study of low-lying electronic states of ozone by multireference Møller–Plesset perturbation method. *J. Chem. Phys.* **1995**, *103*, 6520–6528.

[186] Borowski, P.; Fülscher, M.; Åke Malmqvist, P.; Roos, B. O. A theoretical study of the low-lying excited states of ozone. *Chem. Phys. Lett.* **1995**, *237*, 195–203.

[187] McKellar, A. J.; Heryadi, D.; Yeager, D. L.; Nichols, J. A. Complete basis set limit ionization potentials of O_3 and NO_2 using the multiconfigurational spin tensor electron propagator method (MCSTEP). *Chem. Phys.* **1998**, *238*, 1–9.

[188] Vaval, N.; Pal, S. Adiabatic states of ozone using Fock space multireference coupled cluster method. *J. Chem. Phys.* **1999**, *111*, 4051–4055.

[189] Ohtsuka, Y.; ya Hasegawa, J.; Nakatsuji, H. Excited and ionized states of ozone studied by the MEG (multi-exponentially generated)/EX (excited)-MEG method. *Chem. Phys.* **2007**, *332*, 262–270.

[190] Evangelista, F. A.; Allen, W. D.; Schaefer III, H. F. Coupling term derivation and general implementation of state-specific multireference coupled cluster theories. *J. Chem. Phys.* **2007**, *127*, 024102.

[191] Hanauer, M.; Köhn, A. Pilot applications of internally contracted multireference coupled cluster theory, and how to choose the cluster operator properly. *J. Chem. Phys.* **2011**, *134*, 204111.

[192] Jagau, T.-C.; Gauss, J. Linear-response theory for Mukherjee's multireference coupled-cluster method: Excitation energies. *J. Chem. Phys.* **2012**, *137*, 044116.

[193] Steinfeld, J. I.; Adler-Golden, S. M.; Gallagher, J. W. Critical Survey of Data on the Spectroscopy and Kinetics of Ozone in the Mesosphere and Thermosphere. *J. Phys. Chem. Ref. Data* **1987**, *16*, 911–951.

[194] Arnold, D. W.; Xu, C.; Kim, E. H.; Neumark, D. M. Study of low-lying electronic states of ozone by anion photoelectron spectroscopy of O_3^-. *J. Chem. Phys.* **1994**, *101*, 912–922.

[195] Tanaka, T.; Morino, Y. Coriolis interaction and anharmonic potential function of ozone from the microwave spectra in the excited vibrational states. *J. Mol. Spectrosc.* **1970**, *33*, 538–551.

[196] Harbach, P. H. P.; Wormit, M.; Dreuw, A. The third-order algebraic diagrammatic construction method (ADC(3)) for the polarization propagator for closed-shell molecules: Efficient implementation and benchmarking. *J. Chem. Phys.* **2014**, *141*, 064113.

[197] Sauer, S. P. A.; Pitzner-Frydendahl, H. F.; Buse, M.; Jensen, H. J. A.; Thiel, W. Performance of SOPPA-based methods in the calculation of vertical excitation energies and oscillator strengths. *Mol. Phys.* **2015**, *113*, 2026–2045.

[198] Schäfer, A.; Horn, H.; Ahlrichs, R. Fully optimized contracted Gaussian basis sets for atoms Li to Kr. *J. Chem. Phys.* **1992**, *97*, 2571–2577.

[199] Schäfer, A.; Huber, C.; Ahlrichs, R. Fully optimized contracted Gaussian basis sets of triple zeta valence quality for atoms Li to Kr. *J. Chem. Phys.* **1994**, *100*, 5829–5835.

[200] Weigend, F.; Ahlrichs, R. Balanced basis sets of split valence, triple zeta valence and quadruple zeta valence quality for H to Rn: Design and assessment of accuracy. *Phys. Chem. Chem. Phys.* **2005**, *7*, 3297–3305.

[201] Starcke, J. H.; Wormit, M.; Schirmer, J.; Dreuw, A. How much double excitation character do the lowest excited states of linear polyenes have? *Chem. Phys.* **2006**, *329*, 39–49.

[202] Lyakh, D. I.; Musiał, M.; Lotrich, V. F.; Bartlett, R. J. Multireference Nature of Chemistry: The Coupled-Cluster View. *Chem. Rev.* **2012**, *112*, 182–243.

[203] Lindh, R.; Malmqvist, P. Å.; Roos, B. O.; Veryazov, V.; Widmark, P.-O. *Multiconfigurational Quantum Chemistry*; Wiley-Blackwell, 2016.

[204] Köhn, A.; Hanauer, M.; Mück, L. A.; Jagau, T.-C.; Gauss, J. State-specific multireference coupled-cluster theory. *WIREs Comput. Mol. Sci.* **2013**, *3*, 176–197.

[205] Krylov, A. I. Size-consistent wave functions for bond-breaking: the equation-of-motion spin-flip model. *Chem. Phys. Lett.* **2001**, *338*, 375–384.

[206] Krylov, A. I. Spin-Flip Equation-of-Motion Coupled-Cluster Electronic Structure Method for a Description of Excited States, Bond Breaking, Diradicals, and Triradicals. *Acc. Chem. Res.* **2006**, *39*, 83–91.

[207] Casanova, D.; Head-Gordon, M. The spin-flip extended single excitation configuration interaction method. *J. Chem. Phys.* **2008**, *129*, 064104.

[208] Bernard, Y. A.; Shao, Y.; Krylov, A. I. General formulation of spin-flip time-dependent density functional theory using non-collinear kernels: Theory, implementation, and benchmarks. *J. Chem. Phys.* **2012**, *136*, 204103.

[209] Lefrancois, D.; Wormit, M.; Dreuw, A. Adapting algebraic diagrammatic construction schemes for the polarization propagator to problems with multi-reference electronic ground states exploiting the spin-flip ansatz. *J. Chem. Phys.* **2015**, *143*, 124107.

[210] Lefrancois, D.; Rehn, D. R.; Dreuw, A. Accurate adiabatic singlet-triplet gaps in atoms and molecules employing the third-order spin-flip algebraic diagrammatic construction scheme for the polarization propagator. *J. Chem. Phys.* **2016**, *145*, 084102.

[211] Lefrancois, D.; Tuna, D.; Martínez, T. J.; Dreuw, A. The Spin-Flip Variant of the Algebraic-Diagrammatic Construction Yields the Correct Topology of S1/S0 Conical Intersections. *J. Chem. Theory Comput.* **2017**, *13*, 4436–4441.

[212] Gustmann, H.; Lefrancois, D.; Reuss, A. J.; Gophane, D. B.; Braun, M.; Dreuw, A.; Sigurdsson, S. T.; Wachtveitl, J. Spin the light off: rapid internal conversion into a dark doublet state quenches the fluorescence of an RNA spin label. *Phys. Chem. Chem. Phys.* **2017**, *19*, 26255–26264.

[213] Trofimov, A.; Krivdina, I.; Weller, J.; Schirmer, J. Algebraic-diagrammatic construction propagator approach to molecular response properties. *Chem. Phys.* **2006**, *329*, 1–10.

[214] Fransson, T.; Rehn, D. R.; Dreuw, A.; Norman, P. Static polarizabilities and C6 dispersion coefficients using the algebraic-diagrammatic construction scheme for the complex polarization propagator. *J. Chem. Phys.* **2017**, *146*, 094301.

[215] Wenzel, J.; Wormit, M.; Dreuw, A. Calculating X-ray Absorption Spectra of Open-Shell Molecules with the Unrestricted Algebraic-Diagrammatic Construction Scheme for the Polarization Propagator. *J. Chem. Theory Comput.* **2014**, *10*, 4583–4598.

[216] Wenzel, J.; Wormit, M.; Dreuw, A. Calculating core-level excitations and x-ray absorption spectra of medium-sized closed-shell molecules with the algebraic-diagrammatic construction scheme for the polarization propagator. *J. Comput. Chem.* **2014**, *35*, 1900–1915.

[217] Wenzel, J.; Dreuw, A. Physical Properties, Exciton Analysis, and Visualization of Core-Excited States: An Intermediate State Representation Approach. *J. Chem. Theory Comput.* **2016**, *12*, 1314–1330.

[218] Knippenberg, S.; Rehn, D. R.; Wormit, M.; Starcke, J. H.; Rusakova, I. L.; Trofimov, A. B.; Dreuw, A. Calculations of nonlinear response properties using the intermediate state representation and the algebraic-diagrammatic construction polarization propagator approach: Two-photon absorption spectra. *J. Chem. Phys.* **2012**, *136*, 064107.

[219] Bonin, K. D.; Kresin, V. V. *Electric-Dipole Polarizabilities of Atoms, Molecules, and Clusters*; World Scientific, 1997.

[220] Hohm, U. Experimental static dipole–dipole polarizabilities of molecules. *J. Mol. Struct.* **2013**, *1054-1055*, 282–292.

[221] Kumar, A.; Meath, W. J. Isotropic dipole properties for acetone, acetaldehyde and formaldehyde. *Mol. Phys.* **1997**, *90*, 389–398.

[222] Thakkar, A. J. Construction of Constrained Dipole Oscillator Strength Distributions. *Z. Phys. Chem.* **2015**, *230*, 633–650.

[223] Park, K.; Pederson, M. R.; Liu, A. Y. Comparison of vibrational and electronic contributions to van der Waals interactions. *Phys. Rev. B* **2006**, *73*, 205116.

[224] Coriani, S.; Fransson, T.; Christiansen, O.; Norman, P. Asymmetric-Lanczos-Chain-Driven Implementation of Electronic Resonance Convergent Coupled-Cluster Linear Response Theory. *J. Chem. Theory Comput.* **2012**, *8*, 1616–1628.

[225] Kumar, A.; Jhanwar, B. L.; Meath, W. Dipole oscillator strength distributions, properties, and dispersion energies for ethylene, propene, and 1-butene. *Can. J. Chem.* **2007**, *85*, 724–737.

[226] Ågren, H.; Olsen, J.; Jensen, H. J. A.; Jørgensen, P. Accurate static and dynamic polarizabilities of Li^-. *Phys. Rev. A* **1989**, *40*, 2265–2269.

[227] Pouchan, C.; Bishop, D. M. Static dipole polarizability of the lithium atom, cation, and anion. *Phys. Rev. A* **1984**, *29*, 1–5.

[228] Nicolaides, C. A.; Mercouris, T.; Aspromallis, G. Many-electron, many-photon theory of nonlinear polarizabilities. *J. Opt. Soc. Am. B* **1990**, *7*, 494–501.

[229] Archibong, E. F.; Thakkar, A. J. Hyperpolarizabilities and polarizabilities of Li^- and B^+: finite-field coupled-cluster calculations. *Chem. Phys. Lett.* **1990**, *173*, 579–584.

[230] Larsen, H.; Olsen, J.; Hättig, C.; Jørgensen, P.; Christiansen, O.; Gauss, J. Polarizabilities and first hyperpolarizabilities of HF, Ne, and BH from full configuration interaction and coupled cluster calculations. *J. Chem. Phys.* **1999**, *111*, 1917–1925.

[231] Woon, D. E.; Dunning Jr., T. H. Gaussian basis sets for use in correlated molecular calculations. IV. Calculation of static electrical response properties. *J. Chem. Phys.* **1994**, *100*, 2975–2988.

[232] Koch, H.; Christiansen, O.; Jørgensen, P.; Sanchez de Merás, A. M.; Helgaker, T. The CC3 model: An iterative coupled cluster approach including connected triples. *J. Chem. Phys.* **1997**, *106*, 1808–1818.

[233] Christiansen, O.; Gauss, J.; Stanton, J. F. Frequency-dependent polarizabilities and first hyperpolarizabilities of CO and H_2O from coupled cluster calculations. *Chem. Phys. Lett.* **1999**, *305*, 147–155.

[234] Russell, A. J.; Spackman, M. A. Vibrational averaging of electrical properties. *Mol. Phys.* **1995**, *84*, 1239–1255.

[235] Werner, H.-J.; Meyer, W. PNO-CI and PNO-CEPA studies of electron correlation effects. *Mol. Phys.* **1976**, *31*, 855–872.

[236] Murphy, W. F. The Rayleigh depolarization ratio and rotational Raman spectrum of water vapor and the polarizability components for the water molecule. *J. Chem. Phys.* **1977**, *67*, 5877–5882.

[237] Bridge, N. J.; Buckingham, A. D. The polarization of laser light scattered by gases. *Proc. Roy. Soc. A* **1966**, *295*, 334–349.

[238] Sadlej, A. J. Medium-size polarized basis sets for high-level correlated calculations of molecular electric properties. *Collect. Czech. Chem. Commun.* **1988**, *53*, 1995–2016.

[239] Okruss, M.; Müller, R.; Hese, A. High-resolution ultraviolet laser spectroscopy on jet-cooled benzene molecules: Ground and excited electronic state polarizabilities determined from static Stark effect measurements. *J. Chem. Phys.* **1999**, *110*, 10393–10402.

[240] Kumar, A.; Meath, W. J. Dipole oscillator strength properties and dispersion energies for acetylene and benzene. *Mol. Phys.* **1992**, *75*, 311–324.

[241] Millefiori, S.; Alparone, A. Ab initio and density functional theory calculations of the dipole polarizabilities of ethene, benzene and naphthalene. *J. Mol. Struct. THEOCHEM* **1998**, *422*, 179–190.

[242] Alms, G. R.; Burnham, A.; Flygare, W. H. Measurement of the dispersion in polarizability anisotropies. *J. Chem. Phys.* **1975**, *63*, 3321–3326.

[243] Frisch, M. J.; Trucks, G. W.; Schlegel, H. B.; Scuseria, G. E.; Robb, M. A.; Cheeseman, J. R.; Scalmani, G.; Barone, V.; Mennucci, B.; Petersson, G. A.; Nakatsuji, H.; Caricato, M.; Li, X.; Hratchian, H. P.; Izmaylov, A. F.; Bloino, J.; Zheng, G.; Sonnenberg, J. L.; Hada, M.; Ehara, M.; Toyota, K.; Fukuda, R.; Hasegawa, J.; Ishida, M.; Nakajima, T.; Honda, Y.; Kitao, O.; Nakai, H.; Vreven, T.; Montgomery, J. A.; Peralta, J. E.; Ogliaro, F.; Bearpark, M.; Heyd, J. J.; Brothers, E.; Kudin, K. N.; Staroverov, V. N.; Kobayashi, R.; Normand, J.; Raghavachari, K.; Rendell, A.; Burant, J. C.; Iyengar, S. S.; Tomasi, J.; Cossi, M.; Rega, N.; Millam, J. M.; Klene, M.; Knox, J. E.; Cross, J. B.; Bakken, V.; Adamo, C.; Jaramillo, J.; Gomperts, R.; Stratmann, R. E.; Yazyev, O.; Austin, A. J.; Cammi, R.; Pomelli, C.; Ochterski, J. W.; Martin, R. L.; Morokuma, K.; Zakrzewski, V. G.; Voth, G. A.; Salvador, P.; Dannenberg, J. J.; Dapprich, S.; Daniels, A. D.; Farkas,; Foresman, J. B.; Ortiz, J. V.; Cioslowski, J.; Fox, D. J. Gaussian 09, Revision D.01. 2013.

[244] Bogaard, M. P.; Buckingham, A. D.; Pierens, R. K.; White, A. H. Rayleigh scattering depolarization ratio and molecular polarizability anisotropy for gases. *J. Chem. Soc., Faraday Trans. 1* **1978**, *74*, 3008–3015.

[245] Calvert, R. L.; Ritchie, G. L. D. Molecular quadrupole moment of naphtalene. *J. Chem. Soc., Faraday Trans. 2* **1980**, *76*, 1249–1253.

[246] Cheng, L. T.; Tam, W.; Stevenson, S. H.; Meredith, G. R.; Rikken, G.; Marder, S. R. Experimental investigations of organic molecular nonlinear optical polarizabilities. 1. Methods and results on benzene and stilbene derivatives. *J. Phys. Chem.* **1991**, *95*, 10631–10643.

[247] Heitz, S.; Weidauer, D.; Hese, A. On the polarizabilities of centrosymmetric molecules: naphthalene as an example. *Chem. Phys. Lett.* **1991**, *176*, 55 – 60.

[248] Heitz, S.; Weidauer, D.; Rosenow, B.; Hese, A. Measurement of static polarizabilities on $C_{10}H_8$ and $C_{10}D_8$. *J. Chem. Phys.* **1992**, *96*, 976–981.

[249] Epifanovsky, E.; Wormit, M.; Kuś, T.; Landau, A.; Zuev, D.; Khistyaev, K.; Manohar, P.; Kaliman, I.; Dreuw, A.; Krylov, A. I. New implementation of high-level correlated methods using a general block tensor library for high-performance electronic structure calculations. *J. Comput. Chem.* **2013**, *34*, 2293–2309.

[250] Pulay, P. Convergence Acceleration of Iterative Sequences. The Case of SCF Iteration. *Chem. Phys. Lett.* **1980**, *73*, 393–398.

[251] Pulay, P. Improved SCF Convergence Acceleration. *J. Comput. Chem.* **1982**, *3*, 556–560.

[252] Scuseria, G. E.; Lee, T. J.; Schaefer III, H. F. Accelerating the Convergence of the Coupled-Cluster Approach. The Use of the DIIS Method. *Chem. Phys. Lett.* **1986**, *130*, 236–239.

[253] Davidson, E. R. The iterative calculation of a few of the lowest eigenvalues and corresponding eigenvectors of large real-symmetric matrices. *J. Comput. Phys.* **1975**, *17*, 87–94.

[254] Dempwolff, A. L.; Schneider, M.; Hodecker, M.; Dreuw, A. Efficient implementation of the non-Dyson third-order algebraic diagrammatic construction approximation for the electron propagator for closed- and open-shell molecules. *J. Chem. Phys.* **2019**, *150*, 064108.

[255] Dempwolff, A. L.; Paul, A. C.; Belogolova, A. M.; Trofimov, A. B.; Dreuw, A. Intermediate state representation approach to physical properties of molecular electron-detached states. I. Theory and implementation. *J. Chem. Phys.* **2020**, *152*, 024113.

[256] Dempwolff, A. L.; Paul, A. C.; Belogolova, A. M.; Trofimov, A. B.; Dreuw, A. Intermediate state representation approach to physical properties of molecular electron-detached states. II. Benchmarking. *J. Chem. Phys.* **2020**, *152*, 024125.

[257] Watts, J. D.; Bartlett, R. J. Iterative and non-iterative triple excitation corrections in coupled-cluster methods for excited electronic states: the EOM-CCSDT-3 and EOM-CCSD($\tilde{\mathrm{T}}$) methods. *Chem. Phys. Lett.* **1996**, *258*, 581–588.

[258] Christiansen, O.; Koch, H.; Jørgensen, P. Response functions in the CC3 iterative triple excitation model. *J. Chem. Phys.* **1995**, *103*, 7429–7441.

[259] Christiansen, O.; Koch, H.; Jørgensen, P. Perturbative triple excitation corrections to coupled cluster singles and doubles excitation energies. *J. Chem. Phys.* **1996**, *105*, 1451–1459.

[260] Blinkley, J. S.; Pople, J. A.; Hehre, W. J. Self-consistent Molecular and Orbital Methods. 21. Small Split-Valence Basis Sets for First-Row Elements. *J. Am. Chem. Soc.* **1980**, *102*, 939–947.

[261] Cannington, P.; Ham, N. S. He(I) and He(II) photoelectron spectra of glycine and related molecules. *J. Electron Spectrosc. Relat. Phenom.* **1983**, *32*, 139–151.

[262] Hurley, A. C. The electrostatic calculation of molecular energies - II. Approximate wave functions and the electrostatic method. *Proc. Roy. Soc. A* **1954**, *226*, 179–192.

[263] Gerratt, J.; Mills, I. M. Force Constants and Dipole-Moment Derivatives of Molecules from Perturbed Hartree–Fock Calculations. I. *J. Chem. Phys.* **1968**, *49*, 1719–1729.

[264] Diercksen, G. H.; Roos, B. O.; Sadlej, A. J. Legitimate calculation of first-order molecular properties in the case of limited CI functions. Dipole moments. *Chem. Phys.* **1981**, *59*, 29–39.

[265] Pulay, P. Ab initio calculation of force constants and equilibrium geometries in polyatomic molecules. *Mol. Phys.* **1969**, *17*, 197–204.

[266] Bakken, V.; Helgaker, T.; Klopper, W.; Ruud, K. The calculation of molecular geometrical properties in the Hellmann–Feynman approximation. *Mol. Phys.* **1999**, *96*, 653–671.

[267] Christiansen, O.; Jørgensen, P.; Hättig, C. Response functions from Fourier component variational perturbation theory applied to a time-averaged quasienergy. *Int. J. Quantum Chem.* **1998**, *68*, 1–52.

[268] Aikens, C. M.; Webb, S. P.; Bell, R. L.; Fletcher, G. D.; Schmidt, M. W.; Gordon, M. S. A derivation of the frozen-orbital unrestricted open-shell and restricted closed-shell second-order perturbation theory analytic gradient expressions. *Theor. Chem. Acc.* **2003**, *110*, 233–253.

[269] Helgaker, T.; Jørgensen, P. Configuration-interaction energy derivatives in a fully variational formulation. *Theor. Chim. Acta* **1989**, *75*, 111–127.

[270] Jørgensen, P.; Helgaker, T. Møller–Plesset energy derivatives. *J. Chem. Phys.* **1988**, *89*, 1560–1570.

[271] Helgaker, T.; Jørgensen, P.; Handy, N. C. A numerically stable procedure for calculating Møller-Plesset energy derivatives, derived using the theory of Lagrangians. *Theor. Chim. Acta* **1989**, *76*, 227–245.

[272] Hald, K.; Halkier, A.; Jørgensen, P.; Coriani, S.; Hättig, C.; Helgaker, T. A Lagrangian, integral-density direct formulation and implementation of the analytic CCSD and CCSD(T) gradients. *J. Chem. Phys.* **2003**, *118*, 2985–2998.

[273] Furche, F.; Ahlrichs, R. Adiabatic time-dependent density functional methods for excited state properties. *J. Chem. Phys.* **2002**, *117*, 7433–7447.

[274] Hättig, C. Geometry optimizations with the coupled-cluster model CC2 using the resolution-of-the-identity approximation. *J. Chem. Phys.* **2003**, *118*, 7751–7761.

[275] Heuser, J.; Höfener, S. Analytical nuclear excited-state gradients for the Tamm–Dancoff approximation using uncoupled frozen-density embedding. *J. Comput. Chem.* **2017**, *38*, 2316–2325.

[276] Salter, E. A.; Sekino, H.; Bartlett, R. J. Property evaluation and orbital relaxation in coupled cluster methods. *J. Chem. Phys.* **1987**, *87*, 502–509.

[277] Auer, A. A.; Gauss, J. Triple excitation effects in coupled-cluster calculations of indirect spin–spin coupling constants. *J. Chem. Phys.* **2001**, *115*, 1619–1622.

[278] Cheng, C. Y.; Ryley, M. S.; Peach, M. J.; Tozer, D. J.; Helgaker, T.; Teale, A. M. Molecular properties in the Tamm–Dancoff approximation: indirect nuclear spin–spin coupling constants. *Mol. Phys.* **2015**, *113*, 1937–1951.

[279] Caves, T. C.; Karplus, M. Perturbed Hartree–Fock Theory. I. Diagrammatic Double-Perturbation Analysis. *J. Chem. Phys.* **1969**, *50*, 3649–3661.

[280] Sadlej, A. J. Perturbation theory of the electron correlation effects for atomic and molecular properties. *J. Chem. Phys.* **1981**, *75*, 320–331.

[281] Handy, N. C.; Schaefer III, H. F. On the evaluation of analytic energy derivatives for correlated wave functions. *J. Chem. Phys.* **1984**, *81*, 5031–5033.

[282] Rehn, D. R.; Dreuw, A. Analytic nuclear gradients of the algebraic-diagrammatic construction scheme for the polarization propagator up to third order of perturbation theory. *J. Chem. Phys.* **2019**, *150*, 174110.

[283] Hättig, C.; Köhn, A. Transition moments and excited-state first-order properties in the coupled-cluster model CC2 using the resolution-of-the-identity approximation. *J. Chem. Phys.* **2002**, *117*, 6939–6951.

[284] Hättig, C. Structure Optimizations for Excited States with Correlated Second Order Models: CC2 and ADC(2). *Adv. Quantum Chem.* **2005**, *50*, 37–60.

[285] Stanton, J. F.; Gauss, J.; Cheng, L.; Harding, M. E.; Matthews, D. A.; Szalay, P. G. CFOUR, Coupled-Cluster techniques for Computational Chemistry, a quantum-chemical program package. With contributions from A.A. Auer, R.J. Bartlett, U. Benedikt, C. Berger, D.E. Bernholdt, Y.J. Bomble, O. Christiansen, F. Engel, R. Faber, M. Heckert, O. Heun, M. Hilgenberg, C. Huber, T.-C. Jagau, D. Jonsson, J. Jusélius, T. Kirsch, K. Klein, W.J. Lauderdale, F. Lipparini, T. Metzroth, L.A. Mück, D.P. O'Neill, D.R. Price, E. Prochnow, C. Puzzarini, K. Ruud, F. Schiffmann, W. Schwalbach, C. Simmons, S. Stopkowicz, A. Tajti, J. Vázquez, F. Wang, J.D. Watts and the integral packages MOLECULE (J. Almlöf and P.R. Taylor), PROPS (P.R. Taylor), ABACUS (T. Helgaker, H.J. Aa. Jensen, P. Jørgensen, and J. Olsen), and ECP routines by A. V. Mitin and C. van Wüllen. For the current version, see http://www.cfour.de.

[286] Höfener, S. Coupled-cluster frozen-density embedding using resolution of the identity methods. *J. Comput. Chem.* **2014**, *35*, 1716–1724.

[287] Wilson, A. K.; van Mourik, T.; Dunning, T. H. Gaussian basis sets for use in correlated molecular calculations. VI. Sextuple zeta correlation consistent basis sets for boron through neon. *J. Mol. Struct. THEOCHEM* **1996**, *388*, 339–349.

[288] Crawford, T. D.; Sekino, H. In *Advances in the Theory of Atomic and Molecular Systems: Conceptual and Computational Advances in Quantum Chemistry*; Piecuch, P., Maruani, J., Delgado-Barrio, G., Wilson, S., Eds.; Springer Netherlands: Dordrecht, 2009; pp 225–239.

[289] Crawford, T. D. In *Recent Progress in Coupled Cluster Methods: Theory and Applications*; Cársky, P., Paldus, J., Pittner, J., Eds.; Springer Netherlands: Dordrecht, 2010; Chapter 2, pp 37–55.

[290] Watts, J. D. In *Radiation Induced Molecular Phenomena in Nucleic Acids: A Comprehensive Theoretical and Experimental Analysis*; Shukla, M. K., Leszczynski, J., Eds.; Springer Netherlands: Dordrecht, 2008; pp 65–92.

[291] Page, C. S.; Olivucci, M. Ground and excited state CASPT2 geometry optimizations of small organic molecules. *J. Comput. Chem.* **2003**, *24*, 298–309.

[292] Gozem, S.; Melaccio, F.; Valentini, A.; Filatov, M.; Huix-Rotllant, M.; Ferré, N.; Frutos, L. M.; Angeli, C.; Krylov, A. I.; Granovsky, A. A.; Lindh, R.; Olivucci, M. Shape of Multireference, Equation-of-Motion Coupled-Cluster, and Density Functional Theory Potential Energy Surfaces at a Conical Intersection. *J. Chem. Theory Comput.* **2014**, *10*, 3074–3084.

[293] Urban, M.; Noga, J.; Cole, S. J.; Bartlett, R. J. Towards a full CCSDT model for electron correlation. *J. Chem. Phys.* **1985**, *83*, 4041–4046.

[294] Pan, H.; Song, T.; Yin, X.; Jin, P.; Xiao, J. Synthesis, Crystal Analysis, and Optoelectronic Properties of Diazole-Functionalized Acenes and Azaacenes. *Chem. Eur. J.* **2018**, *24*, 6572–6579.

[295] Lindner, B. D.; Engelhart, J. U.; Tverskoy, O.; Appleton, A. L.; Rominger, F.; Peters, A.; Himmel, H.-J.; Bunz, U. H. F. Stable Hexacenes through Nitrogen Substitution. *Angew. Chem. Int. Ed.* **2011**, *50*, 8588–8591.

[296] Tverskoy, O.; Rominger, F.; Peters, A.; Himmel, H.-J.; Bunz, U. H. F. An Efficient Synthesis of Tetraazapentacenes. *Angew. Chem. Int. Ed.* **2011**, *50*, 3557–3560.

[297] Bunz, U. H. F.; Engelhart, J. U.; Lindner, B. D.; Schaffroth, M. Large *N*-Heteroacenes: New Tricks for Very Old Dogs? *Angew. Chem. Int. Ed.* **2013**, *52*, 3810–3821.

[298] Bunz, U. H. F. The Larger Linear *N*-Heteroacenes. *Acc. Chem. Res.* **2015**, *48*, 1676–1686.

[299] Engelhart, J. U.; Lindner, B. D.; Schaffroth, M.; Schrempp, D.; Tverskoy, O.; Bunz, U. H. F. Substituted Tetraaza- and Hexaazahexacenes and their N,N'-Dihydro Derivatives: Syntheses, Properties, and Structures. *Chem. Eur. J.* **2015**, *21*, 8121–8129.

[300] Wang, C.; Wang, J.; Li, P.-Z.; Gao, J.; Tan, S. Y.; Xiong, W.-W.; Hu, B.; Lee, P. S.; Zhao, Y.; Zhang, Q. Synthesis, Characterization, and Non-Volatile Memory Device Application of an *N*-Substituted Heteroacene. *Chem. Asian J.* **2014**, *9*, 779–783.

[301] Li, G.; Wu, Y.; Gao, J.; Li, J.; Zhao, Y.; Zhang, Q. Synthesis, Physical Properties, and Anion Recognition of Two Novel Larger Azaacenes: Benzannelated Hexazaheptacene and Benzannelated N,N'-Dihydrohexazaheptacene. *Chem. Asian J.* **2013**, *8*, 1574–1578.

[302] Zhang, Q.; Xiao, J.; Yin, Z.; Duong, H. M.; Qiao, F.; Boey, F.; Hu, X.; Zhang, H.; Wudl, F. Synthesis, Characterization, and Physical Properties of a Conjugated Heteroacene: 2-Methyl-1,4,6,7,8,9-hexaphenylbenz(g)isoquinolin-3(2H)-one (BIQ). *Chem. Asian J.* **2011**, *6*, 856–862.

[303] Li, G.; Duong, H. M.; Zhang, Z.; Xiao, J.; Liu, L.; Zhao, Y.; Zhang, H.; Huo, F.; Li, S.; Ma, J.; Wudl, F.; Zhang, Q. Approaching a stable, green twisted heteroacene through "clean reaction" strategy. *Chem. Commun.* **2012**, *48*, 5974–5976.

[304] Mateo-Alonso, A. Pyrene-fused pyrazaacenes: from small molecules to nanoribbons. *Chem. Soc. Rev.* **2014**, *43*, 6311–6324.

[305] Cortizo-Lacalle, D.; Pertegás, A.; Melle-Franco, M.; Bolink, H. J.; Mateo-Alonso, A. Pyrene-fused bisphenazinothiadiazoles with red to NIR electroluminescence. *Org. Chem. Front.* **2017**, *4*, 876–881.

[306] Martínez-Abadía, M.; Antonicelli, G.; Zuccatti, E.; Atxabal, A.; Melle-Franco, M.; Hueso, L. E.; Mateo-Alonso, A. Synthesis and Properties of a Twisted and Stable Tetracyano-Substituted Tetrabenzoheptacene. *Org. Lett.* **2017**, *19*, 1718–1721.

[307] Ganschow, M.; Koser, S.; Hodecker, M.; Rominger, F.; Freudenberg, J.; Dreuw, A.; Bunz, U. H. F. Azaacenes Bearing Five-Membered Rings. *Chem. Eur. J.* **2018**, *24*, 13667–13675.

[308] Schleyer, P. v. R.; Maerker, C.; Dransfeld, A.; Jiao, H.; van Eikema Hommes, N. J. R. Nucleus-Independent Chemical Shifts: A Simple and Efficient Aromaticity Probe. *J. Am. Chem. Soc.* **1996**, *118*, 6317–6318.

[309] Chen, Z.; Wannere, C. S.; Corminboeuf, C.; Puchta, R.; Schleyer, P. v. R. Nucleus-Independent Chemical Shifts (NICS) as an Aromaticity Criterion. *Chem. Rev.* **2005**, *105*, 3842–3888.

[310] Becke, A. D. Density-functional exchange-energy approximation with correct asymptotic behavior. *Phys. Rev. A* **1988**, *38*, 3098–3100.

[311] Lee, C.; Yang, W.; Parr, R. G. Development of the Colle-Salvetti correlation-energy formula into a functional of the electron density. *Phys. Rev. B* **1988**, *37*, 785–789.

[312] Miehlich, B.; Savin, A.; Stoll, H.; Preuss, H. Results obtained with the correlation energy density functionals of Becke and Lee, Yang and Parr. *Chem. Phys. Lett.* **1989**, *157*, 200–206.

[313] Becke, A. D. Density-functional thermochemistry. III. The role of exact exchange. *J. Chem. Phys.* **1993**, *98*, 5648–5652.

[314] Becke, A. D. A new mixing of Hartree–Fock and local density-functional theories. *J. Chem. Phys.* **1993**, *98*, 1372–1377.

[315] Yanai, T.; Tew, D. P.; Handy, N. C. A new hybrid exchange-correlation functional using the Coulomb-attenuating method (CAM-B3LYP). *Chem. Phys. Lett.* **2004**, *393*, 51–57.

[316] Chai, J.-D.; Head-Gordon, M. Systematic optimization of long-range corrected hybrid density functionals. *J. Chem. Phys.* **2008**, *128*, 084106.

[317] Chai, J.-D.; Head-Gordon, M. Long-range corrected hybrid density functionals with damped atom-atom dispersion corrections. *Phys. Chem. Chem. Phys.* **2008**, *10*, 6615–6620.

[318] Miertuš, S.; Scrocco, E.; Tomasi, J. Electrostatic interaction of a solute with a continuum. A direct utilizaion of ab initio molecular potentials for the prevision of solvent effects. *Chem. Phys.* **1981**, *55*, 117–129.

[319] Miertuš, S.; Tomasi, J. Approximate evaluations of the electrostatic free energy and internal energy changes in solution processes. *Chem. Phys.* **1982**, *65*, 239–245.

[320] Mennucci, B. Polarizable continuum model. *WIREs Comput. Mol. Sci.* **2012**, *2*, 386–404.

[321] Cancès, E.; Mennucci, B.; Tomasi, J. A new integral equation formalism for the polarizable continuum model: Theoretical background and applications to isotropic and anisotropic dielectrics. *J. Chem. Phys.* **1997**, *107*, 3032–3041.

[322] Neese, F. Prediction of molecular properties and molecular spectroscopy with density functional theory: From fundamental theory to exchange-coupling. *Coord. Chem. Rev.* **2009**, *253*, 526–563.

[323] Marian, C. M. Spin-Orbit Coupling in Molecules. *Rev. Comput. Chem.* **2001**, *17*, 99–204.

[324] Marian, C. M. Spin-orbit coupling and intersystem crossing in molecules. *WIREs Comput. Mol. Sci.* **2012**, *2*, 187–203.

[325] Neese, F. Efficient and accurate approximations to the molecular spin-orbit coupling operator and their use in molecular g-tensor calculations. *J. Chem. Phys.* **2005**, *122*, 034107.

[326] Chiodo, S. G.; Russo, N. DFT spin-orbit coupling between singlet and triplet excited states: A case of psoralen compounds. *Chem. Phys. Lett.* **2010**, *490*, 90–96.

[327] Barone, V.; Bloino, J.; Biczysko, M.; Santoro, F. Fully Integrated Approach to Compute Vibrationally Resolved Optical Spectra: From Small Molecules to Macrosystems. *J. Chem. Theory Comput.* **2009**, *5*, 540–554.

[328] Bloino, J.; Biczysko, M.; Santoro, F.; Barone, V. General Approach to Compute Vibrationally Resolved One-Photon Electronic Spectra. *J. Chem. Theory Comput.* **2010**, *6*, 1256–1274.

[329] Biczysko, M.; Bloino, J.; Santoro, F.; Barone, V. In *Computational Strategies for Spectroscopy: From Small Molecules to Nano Systems*; Barone, V., Ed.; John Wiley & Sons, Ltd, 2012; Chapter 8, pp 361–443.

[330] Hodecker, M.; Biczysko, M.; Dreuw, A.; Barone, V. Simulation of Vacuum UV Absorption and Electronic Circular Dichroism Spectra of Methyl Oxirane: The Role of Vibrational Effects. *J. Chem. Theory Comput.* **2016**, *12*, 2820–2833.

[331] Franck, J. Elementary processes of photochemical reactions. *Trans. Faraday Soc.* **1926**, *21*, 536–542.

[332] Condon, E. A Theory of Intensity Distribution in Band Systems. *Phys. Rev.* **1926**, *28*, 1182–1201.

[333] Condon, E. U. Nuclear Motions Associated with Electron Transitions in Diatomic Molecules. *Phys. Rev.* **1928**, *32*, 858–872.

[334] Kasha, M. Characterization of electronic transitions in complex molecules. *Discuss. Faraday Soc.* **1950**, *9*, 14–19.

[335] Suppan, P. *Chemistry and Light*; The Royal Society of Chemistry, 1994; Chapter 3, pp 27–86.

[336] Klán, P.; Wirz, J. *Photochemistry of Organic Compounds*; John Wiley & Sons, Ltd, 2009; Chapter 2, pp 25–72.

[337] Jablonski, A. Efficiency of Anti-Stokes Fluorescence in Dyes. *Nature* **1933**, *131*, 839–840.

[338] Valeur, B., Brochon, J.-C., Eds. *New Trends in Fluorescence Spectroscopy*; Springer Berlin Heidelberg, 2001.

[339] Dirac, P. A. M. The quantum theory of the emission and absorption of radiation. *Proc. Roy. Soc. A* **1927**, *114*, 243–265.

[340] Fermi, E. *Nuclear Physics*; University of Chicago Press: Chicago, IL, 1950.

[341] Wilson, F. L. Fermi's Theory of Beta Decay. *Am. J. Phys.* **1968**, *36*, 1150–1160.

[342] Zhang, J. M.; Liu, Y. Fermi's golden rule: its derivation and breakdown by an ideal model. *Eur. J. Phys.* **2016**, *37*, 065406.

[343] Hinchliffe, A.; Soscún Machado, H. J. Ab initio studies of the dipole polarizabilities of conjugated molecules: Part 3. One electron properties, dipole polarizability and first hyperpolarizability of quinoline and isoquinoline. *J. Mol. Struct. THEOCHEM* **1994**, *312*, 57–67.

Publication List

- Manuel Hodecker, Malgorzata Biczysko, Andreas Dreuw, Vincenzo Barone, "Simulation of vacuum UV absorption and electronic circular dichroism spectra of methyl oxirane: the role of vibrational effects", *Journal of Chemical Theory and Computation*, **2016**, *12*(6), 2820–2833.

- Sebastian Hahn, Silke Koser, Manuel Hodecker, Olena Tverskoy, Frank Rominger, Andreas Dreuw, Uwe H. F. Bunz, "Alkyne-Substituted N-Heterophenes", *Chemistry—A European Journal*, **2017**, *23*(34), 8148–8151.

- Sebastian Hahn, Silke Koser, Manuel Hodecker, Pascal Seete, Frank Rominger, Ognjen Š. Miljanić, Andreas Dreuw, Uwe H. F. Bunz, "Phenylene Bridged Cyclic Azaacenes: Dimers and Trimers", *Chemistry—A European Journal*, **2018**, *24*(27), 6968–6974.

- Michael Ganschow, Silke Koser, Manuel Hodecker, Frank Rominger, Jan Freudenberg, Andreas Dreuw, Uwe H. F. Bunz, "Azaacenes Bearing Five-Membered Rings", *Chemistry—A European Journal*, **2018**, *24*(51), 13667–13675.

- Adrian L. Dempwolff, Matthias Schneider, Manuel Hodecker, Andreas Dreuw, "Efficient implementation of the non-Dyson third-order algebraic diagrammatic construction approximation for the electron propagator for closed- and open-shell molecules", *The Journal of Chemical Physics*, **2019**, *150*(6), 064108.

- Manuel Hodecker, Dirk R. Rehn, Andreas Dreuw, Sebastian Höfener, "Similarities and differences of the Lagrange formalism and the intermediate state representation in the treatment of molecular properties", *The Journal of Chemical Physics*, **2019**, *150*(16), 164125.

- Manuel Hodecker, Adrian L. Dempwolff, Dirk R. Rehn, Andreas Dreuw, "Algebraic-Diagrammatic Construction Scheme for the Polarization Propagator Including Ground-State Coupled-Cluster Amplitudes. I. Excitation Energies", *The Journal of Chemical Physics*, **2019**, *150*(17), 174104.

- Manuel Hodecker, Dirk R. Rehn, Patrick Norman, Andreas Dreuw, "Algebraic-Diagrammatic Construction Scheme for the Polarization Propagator Including Ground-State Coupled-Cluster Amplitudes. II. Static Polarizabilities", *The Journal of Chemical Physics*, **2019**, *150*(17), 174105.

- Manuel Hodecker, Michael Ganschow, Mahmud Abu-Odeh, Uwe H. F. Bunz, Andreas Dreuw, "Optical Spectra and Fluorescence Quenching in Azaacenes Bearing Five-Membered Rings", *ChemPhotoChem*, **2019**, *3*(9), 755–762.

- Manuel Hodecker, Andreas Dreuw, "Hermitian Second-Order Methods for Excited Electronic States: Unitary Coupled Cluster in Comparison with Algebraic-Diagrammatic Construction Schemes", *The Journal of Chemical Physics*, **2020**, *152*(9), 094106.

Manuscripts Submitted for Publication or in Preparation

- Sebastian N. Intorp, Manuel Hodecker, Matthias Müller, Olena Tverskoy, Marco Rosenkranz, Evgenia Dmitrieva, Alexey A. Popov, Frank Rominger, Jan Freudenberg, Andreas Dreuw, Uwe H. F. Bunz, "Quinoidal Azaacenes: 99% Diradical Character", submitted to *Angewandte Chemie International Edition*, **2020**.

- Victor Brosius, Manuel Hodecker, Hendrik Hoffmann, Sebastian Hahn, Frank Rominger, Andreas Dreuw, Jan Freudenberg, Uwe H. F. Bunz, "Pseudoazulenes Meet Azaacenes: 1H- vs 11H-Indenopyrazines", to be submitted.

- Manuel Hodecker, Yuri Kozhemakin, Frank Rominger, Uwe H. F. Bunz, Andreas Dreuw, "A Doubly Bridged Bis(phenylethynyl)benzene", in preparation.

- Manuel Hodecker, Alexis M. Driscoll, Uwe H. F. Bunz, Andreas Dreuw, "Twist and Bend Photo-Excited Phenylethynylbenzenes – A Theoretical Analysis", to be submitted.

- Manuel Hodecker, Sebastian M. Thielen, Junzi Liu, Dirk R. Rehn, Andreas Dreuw, "Third-Order Unitary Coupled-Cluster (UCC3) for Excited Electronic States: Efficient Implementation and Benchmarking", in preparation.

Danksagung

An erster Stelle möchte ich mich bei Prof. Dr. Andreas Dreuw bedanken. Besonders für die Möglichkeit, meine Doktorarbeit in seiner Gruppe durchzuführen; für die spannende Themenstellung, durch die ich mich auch entsprechend meiner Interessen weiterentwickeln konnte, aber auch für die Freiheit, die er mir bei der Wahl meiner Forschungsinteressieren ließ; für die Möglichkeit, während meiner Doktorarbeit für Forschungsaufenthalte nach Stockholm und Santiago de Chile zu reisen; sowie insbesondere für das Vertrauen, das er während all dieser Zeit in mich gesetzt hat.

Außerdem möchte ich der gesamten Arbeitsgruppe für die angenehme Atmosphäre, zahlreiche sinnvolle und möglicherweise auch sinnlosere, aber erheiternde Gespräche bedanken, sowie für einige andere Aktivitäten (FAB?) außerhalb des IWR, bei allen aktuellen (Adrian, Marvin, Rogo, Sebi, Ben, Max, Dirk, Mikael, Thomas, Jie, Reena, Maximilien) sowie ehemaligen (Michi, Mary, Steffi, Max K., Daniel, Daria, Chong, Tobi, Stefan, Katie, Matze, Tim) Mitgliedern. Manfred danke ich für die Hilfe bei allen möglichen IT-Angelegenheiten sowie die Gespräche über Musik und lustiges J.B.O.-Texteraten.

Für das Korrekturlesen dieser Arbeit bedanke ich mich herzlich bei Maximilian Scheurer, Sebastian Thielen, Marvin Hoffmann und Thomas Fransson.

Des Weiteren wäre das Gelingen dieser Arbeit ohne die hilfreichen Diskussionen im Rahmen der "UCC-Selbsthilfegruppe" sowie mit Prof. Dr. Jochen Schirmer, Dr. Junzi Liu und Adrian L. Dempwolff nicht möglich gewesen. También quiero agradecer al Prof. Dr. Oriol Vendrell por examinar este trabajo.

Tack så mycket an Prof. Dr. Patrick Norman (Stockholm) und *muchas gracias* an Prof. Dr. Alejandro Toro Labbé (Santiago de Chile) für die freundliche Aufnahme in ihrer Arbeitsgruppe bei meinen Auslandsaufenthalten.

Für die Hilfe bei vielen verwaltungstechnischen und organisatorischen Dingen danke ich Ellen Vogel. Der Heidelberg Graduate School of Mathematical and Computational Methods for the Sciences (HGS MathComp) danke ich für mein Promotionsstipendium sowie die Finanzierung einiger Dienstreisen und Sprachkurse, hierbei für die Administration insbesondere Sarah Steinbach und Ria Hillenbrand-Lynott.

Ich bedanke mich auch bei meinen Forschungspraktikanten Christian Busch, Mahmud Abu-Odeh, Felix Zeller, Moritz Schuldt und Alexis Driscoll, die mir durch ihre Unterstützung bei diversen Projekten nicht zu vernachlässigende Hilfestellung geleistet haben.

Natürlich gilt mein Dank auch allen Kommilitonen und Freunden aus der Studienzeit (Julius, Michi, Andy, Thorsten, Hahn, Matze, Chrissi $\times 2$, Giuli, Steffi, ...), für die schönen gemeinsamen Stunden und Frustgespräche. Ohne euch wäre der Weg hierher deutlich langweiliger und vermutlich auch nicht machbar gewesen.

Der allergrößte Dank gilt jedoch meiner Familie, insbesondere meinen Eltern, denen diese Arbeit auch gewidmet ist. Ohne deren nicht zu enden scheinende Unterstützung in jeglicher Hinsicht hätte ich all dies nie erreicht.

Finalmente, me gustaría agradecer a mi pololа por todo el apoyo que me dio durante este tiempo, por entrar a mi vida y permanecer a mi lado.

Eidesstattliche Versicherung gemäß § 8 der Promotionsordnung für die Naturwissenschaftlich-Mathematische Gesamtfakultät der Universität Heidelberg

1. Bei der eingereichten Dissertation zu dem Thema
   "Development and Application of Hermitian Methods for Molecular Properties and Excited Electronic States"
   handelt es sich um meine eigenständig erbrachte Leistung.

2. Ich habe nur die angegebenen Quellen und Hilfsmittel benutzt und mich keiner unzulässigen Hilfe Dritter bedient. Insbesondere habe ich wörtlich oder sinngemäß aus anderen Werken übernommene Inhalte als solche kenntlich gemacht.

3. Die Arbeit oder Teile davon habe ich bislang nicht an einer Hochschule des In- oder Auslands als Bestandteil einer Prüfungs- oder Qualifikationsleistung vorgelegt.

4. Die Richtigkeit der vorstehenden Erklärungen bestätige ich.

5. Die Bedeutung der eidesstattlichen Versicherung und die strafrechtlichen Folgen einer unrichtigen oder unvollständigen eidesstattlichen Versicherung sind mir bekannt.

Ich versichere an Eides statt, dass ich nach bestem Wissen die reine Wahrheit erklärt und nichts verschwiegen habe.

Ort/Datum	Unterschrift